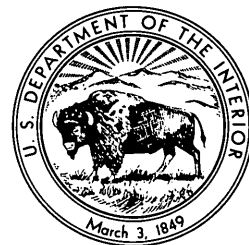# Short Papers in the

Geologic and Hydrologic

Sciences, Articles 1-146

GEOLOGICAL SURVEY RESEARCH 1961

GEOLOGICAL SURVEY PROFESSIONAL PAPER 424-B

Scientific notes and summaries of investigations prepared by members of the Geologic, Water Resources, and Conservation Divisions in the fields of geology, hydrology, and allied sciences

UNITED STATES DEPARTMENT OF THE INTERIOR
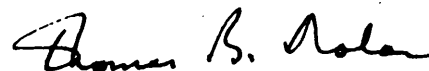
STEWART L. UDALL, *Secretary*

GEOLOGICAL SURVEY

Thomas B. Nolan, *Director*

FOREWORD

The scientific and economic results of work by the United States Geological Survey during the fiscal year 1961, the 12 months ending June 30, 1961, will be summarized in four volumes of which this is the first. This volume includes 146 short papers on a variety of subjects in the fields of geology, hydrology, and related sciences, prepared by members of the Geologic, Water Resources, and Conservation Divisions of the Survey. These papers are of two kinds. Some are announcements of new discoveries or observations on problems of limited scope, which may or may not be described in greater detail subsequently. Others summarize conclusions drawn from more extensive or continuing investigations, which in large part will be described in greater detail in reports to be published at a later date.

Professional Papers 424–C and –D include additional short papers of the same character as those in the present volume. Professional Paper 424–A provides a synopsis of the more important new findings resulting from work during the fiscal year.

THOMAS B. NOLAN

Director.

CONTENTS

CONTENTS

VII

SHORT PAPERS IN THE GEOLOGIC AND HYDROLOGIC SCIENCES, ARTICLES 1–146

GEOLOGY OF METALLIFEROUS DEPOSITS

1. TEMPERATURE OF FORMATION OF A PRECAMBRIAN MASSIVE SULFIDE DEPOSIT, COPPER KING MINE, FRONT RANGE, COLORADO

By P. K. SIMS and PRIESTLEY TOULMIN, 3d, Denver, Colo., and Washington, D. C.

The Copper King mine, at Prairie Divide in Larimer County, Colo., contains ore deposits of two types and ages—massive sulfide-magnetite deposits of Precambrian age and a vein uranium deposit of early Tertiary age. The ore deposits and the geologic setting of the mine have been described previously (Sims, Phair, and Moench, 1958). This report presents some new data concerning the temperature of formation of coexisting sphalerite, pyrrhotite, and pyrite from one of the massive sulfide deposits in the mine.

The sulfide-magnetite deposit is a small, elongate, roughly tabular body that is mainly in cummingtonite-anthophyllite skarn. The ore minerals form massive layers and lenses a few feet in maximum breadth and width and a few tens of feet in length that conform to the foliation and lineation of the host rock. The deposit consists, in order of decreasing abundance, of pyrite, sphalerite, pyrrhotite, chalcopyrite, magnetite, and molybdenite. The relation of the ore minerals to the host rock clearly indicates that they formed mainly by replacement of amphiboles. The deposit and its host rock are enclosed entirely within a biotite-muscovite granite of Precambrian age, which has been called Silver Plume granite (Lovering and Goddard, 1950, pl. 1). Magnetite from the deposit and monazite from a pegmatite in the granite have both been dated as late Precambrian (Phair and Sims, 1954).

Except for molybdenite, the ore minerals are closely associated and commonly intergrown, although the quantities and proportions of the separate mineral phases differ from one ore-bearing layer or lens to another. The close spatial association of the ore minerals and the textural relations observed in the field and in polished sections indicate that they were deposited during a single stage. The minerals crystallized in the commonly observed paragenetic order: magnetite, pyrrhotite, pyrite, sphalerite, and chalcopyrite. The sphalerite is dark reddish-brown and apparently homogeneous. It contains oriented blebs and blades of chalcopyrite and sparse randomly distributed blebs of pyrrhotite, which are interpreted to have formed from exsolution on cooling.

The temperature of formation of the deposit can be estimated by use of the sphalerite and pyrrhotite geothermometers (Kullerud, 1953; Arnold, 1958). Barton and Kullerud (1958) have extended the earlier work of Kullerud (1953) to show that if sphalerite formed in equilibrium with pyrrhotite (with or without pyrite) below a temperature of 600°C., the temperature of formation can be determined from the FeS content of the sphalerite, using the solvus curve determined for the binary systems FeS–ZnS. The sphalerite at the Copper King mine is in contact with both pyrrhotite and pyrite and contains exsolved blebs of pyrrhotite, and therefore probably crystallized in equilibrium with these minerals. The sphalerite in five samples from various parts of the deposit exposed in the mine workings contains 13.6 to 15.6 formula percent FeS, as shown in table 1, which corresponds to a range in temperature of crystallization from 440°C. to 490°C. (Barton and Kullerud, 1958, fig. 33). The low amounts of manganese, copper, and cadmium in solid solution in the sphalerite would have little effect on the solubility of FeS in ZnS.

TABLE 1.1.—*Spectrochemical analyses of sphalerite and estimated temperatures of crystallization*

[Analyses by R. G. Havens, U.S. Geological Survey]

Samples		Analyses (percent)						Estimated temperature of formation (degrees centigrade) [2]
Serial No.	Field No.	Fe	FeS [1]	Mn	Cu	Cd	Zn	
E-1860	A	9.1	15.6	0.13	0.63	0.26	0.015	490±10
1861	B	8.6	14.8	.13	1.1	.28	.014	480±10
1858	CK-69	8.2	14.1	.12	.95	.28	.013	455±10
1857	CK-201	7.9	13.6	.13	.52	.26	.012	440±10
1859	UG-20	7.9	13.6	.13	.69	.26	.011	440±10

[1] Formula percent.
[2] Not corrected for total rock pressure. If the rock cover at the time of mineralization was 5 miles, the sphalerite temperatures would be raised about 50° C.

Compositions of pyrrhotite from two samples (CK–64 and CK–3) collected from the same part of the mine as the sphalerite samples have been determined from measurements of $d_{(102)}$ (Arnold and Reichen, 1959). Pyrrhotite CK–64, associated with pyrite, sphalerite, and chalcopyrite, has $d_{(102)}$ equal to 2.063A, corresponding to 47.03 atomic percent metals. Assuming Fe to be the only metal present, we may apply the solvus curve in the system FeS–FeS$_2$ to find a temperature of 400°C. This temperature is somewhat lower than that indicated by the composition of the associated sphalerite. A similar relationship between "pyrrhotite temperatures" and "sphalerite temperatures" has been found in several other studies (for example: Stone, 1959; Skinner, 1958) and probably is a consequence of different reaction rates in the two systems.

Comparison of the reaction-rate data on sphalerite in the system FeS–ZnS (Kullerud, 1953, p. 98) and on pyrrhotite in the system FeS–FeS$_2$ [1] shows that pyrrhotite equilibrates with pyrite at 325°C. as rapidly as sphalerite equilibrates with FeS at 750°C. Thus as a pyrite–pyrrhotite–sphalerite assemblage cools slowly in nature, one would expect the pyrrhotite to continue to react at temperatures below that at which the sphalerite composition had been effectively "quenched in" by decreasing reaction rates.

Pyrrhotite CK–3 is also associated with pyrite, sphalerite, and chalcopyrite, and is cut by a late generation of pyrite probably related to the Tertiary uranium mineralization. Its (102) peak is much

[1] Pyrrhotite-pyrite equilibrium relations between 325° C. and 743° C. by Ralph G. Arnold, unpublished Ph.D. thesis, Princeton Univ., 1958, p. 41.

broader than that of pyrrhotite CK–64, presumably reflecting a range of composition. The mean value of $d_{(102)}$ is approximately 2.066A, corresponding to a composition of 47.3 atomic percent metals. Both this higher mean metal content and the greater spread in composition of pyrrhotite CK–3 probably reflect partial reaction with the late pyrite. Pyrrhotite that has a composition of 47.3 atomic percent metals is in equilibrium with pyrite at about 325°C.

If the massive sulfide deposit is genetically related to the granite, as seems probable from their close spatial association and their similar absolute ages (Sims, Phair, and Moench, 1958, p. 200), the deposit necessarily formed after the adjacent granite had crystallized and cooled to about 500°C. On this assumption, it is unlikely that the ore-forming solutions could have come from a source near the sulfide body; instead they must have been derived from a more distant source, possibly subjacent crystallizing magma.

REFERENCES

Arnold, R. G., 1958, The Fe-S system: Annual report of the Director of the Geophysical Laboratory, 1957–58, Carnegie Inst. Washington Year Book 57, p. 218–222.

Arnold, R. G., and Reichen, Laura, 1959, Application of the pyrrhotite X-ray determinative curve to natural pyrrhotites: Annual report of the Director of the Geophysical Laboratory, 1957–58, Carnegie Inst. Washington, Year Book 58, p. 155–156.

Barton, P. B., Jr., and Kullerud, Gunnar, 1958, The Fe-Zn-S System: Annual report of the Director of the Geophysical Laboratory 1957–58, Carnegie Inst. Washington Year Book 57, p. 227–229.

Kullerud, Gunnar, 1953, The FeS-ZnS system, a geological thermometer: Norsk geol. tidsskr., v. 32, p. 61–147.

Lovering, T. S., and Goddard, E. N., 1950, Geology and ore deposits of the Front Range, Colorado; U.S. Geol. Survey Prof. Paper 223, 319 p.

Phair, George, and Sims, P. K., 1954, Paragenesis and age of the uranium minerals in the Copper King mine, Larimer County, Colo. [abs.]: Geol. Soc. America Bull., v. 65, p. 1385.

Sims, P. K., Phair, George, and Moench, R. H., 1958, Geology of the Copper King uranium mine, Larimer County, Colo.: U.S. Geol. Survey Bull. 1032–D, p. 171–221.

Skinner, B. J., 1958, The Geology and metamorphism of the Nairne pyritic formation, a sedimentary sulfide deposit in South Australia: Econ. Geology, v. 53, p. 546–562.

Stone, J. G., 1959, Ore genesis in the Naica district, Chihuahua, Mexico: Econ. Geology, v. 54, p. 1002–1034.

2.   COFFINITE IN URANIUM VEIN DEPOSITS OF THE FRONT RANGE, COLORADO

By P. K. SIMS, E. J. YOUNG, and W. N. SHARP, Denver, Colo.

Coffinite, a uranous silicate with hydroxyl substitution, is associated with pitchblende in some hydrothermal vein deposits in the Front Range, and locally is an important ore mineral. Previously reported occurrences of the mineral in the United States (Stieff, Stern, and Sherwood, 1956; Frondel, 1958) have been mainly from the black, unoxidized vanadium-uranium ores of the Colorado Plateau.

The known occurrences of coffinite in the Front Range are listed in table 1. At the Copper King, Fair Day, and Foothills mines, and possibly also the Schwartzwalder mine, coffinite constitutes a substantial part of the uranium ore; at the other localities it is sparse.

TABLE 1.—*Known occurrences of coffinite in the Front Range*

Mine	District or area	County	Principal associated minerals	Source of data
Blue Jay	Jamestown	Boulder	Fluorite, uraninite, and uranothorite	Identified by X-ray powder photographs, this report.
Copper King	Prairie Divide	Larimer	Pitchblende, siderite, pyrite, sphalerite, marcasite, quartz	Reported by Sims, Phair, and Moench (1958).
Fair Day	Jamestown	Boulder	Pitchblende, pyrite, quartz, sphalerite, chalcopyrite	Identified by X-ray powder photographs and in polished and thin sections, this report.
Foothills	Idledale	Jefferson	Pitchblende, pyrite, quartz, potassium feldspar, carbonates	Identified by X-ray powder photographs, this report.
Old Leyden coal	Leyden	Jefferson	Meta-tyuyamunite, autunite, uranophane, and pyrite	Reported by A. J. Gude, 3rd; see also Gude and McKeown (1953).
Schwartzwalder	Ralston Buttes	Jefferson	Pitchblende, pyrite, quartz, carbonate minerals, potassium feldspar	Reported by J. D. Schlottman, U. S. Atomic Energy Commission (oral communication, 1960).
Stanley	Idaho Springs	Clear Creek	Pitchblende, pyrite, sphalerite, and a carbonate mineral	Reported by R. H. Moench, (oral communication, 1961).

Coffinite typically occurs in the Front Range in veins that are characterized by abundant open cavities and conspicuous crustification, features generally considered diagnostic of epithermal veins (Lindgren, 1933, p. 444–445). It is associated with pitchblende, pyrite, and sparse sulfides that rarely are visible megascopically, chiefly sphalerite (nearly pure ZnS), chalcopyrite, and marcasite. Quartz—or quartz, ankerite, and potassium feldspar—is the principal gangue mineral in most deposits, but siderite is dominant in one, the Copper King deposit. Two exceptions to this mode of occurrence are known. At the Stanley mine, coffinite fills fractures that cut sulfide and gangue minerals of a mesothermal vein; at the Old Leyden coal mine, coffinite is associated with fractured and silicified coal.

The coffinite is black in hand specimen and gen-

erally cannot be distinguished megascopically from pitchblende. It can be identified with certainty, however, by X-ray powder photographs, and in some ores at least can be recognized in thin and polished sections. Polished thin sections are particularly useful for study of the coffinite ores.

In transmitted light, the coffinite is brown or yellowish brown, translucent to different degrees, and mostly isotropic. It occurs predominantly as aggregates of extremely small particles that form spheroidal or other rotund forms. Rarely, the aggregates have a visible fibrous structure, with the fibers oriented perpendicular to the colloform bands. The fibrous aggregates show a generally weak but conspicuous dichroism (darker color perpendicular to fibers). In general, the optical properties agree with well crystallized coffinite from the Woodrow mine,

Laguna district, New Mexico (R. H. Moench, written communication, 1961).

Refractive indices, reflectivity, and unit cell sizes of coffinite from two mines are listed below:

Locality	Coffinite		
	Refractive index	Reflectivity [1] (percent)	Unit cell size (A)
Fair Day mine..............	1.77 ± 0.005	7.8–9.8	$A_o = 6.93_5$
			$C_o = 6.21_2$
Copper King mine............	([2])	8.2–8.6	$A_o = 6.97_1$
			$C_o = 6.28_6$

[1] Determined in orange light with a Hallimond visual microphotometer, according to the method described by Leonard (1960).
[2] Coffinite is finely admixed with siderite and other minerals, and a reliable refractive index was not determined. Index is known to be lower than for coffinite from the Fair Day mine.

The pitchblende associated with coffinite from the Fair Day mine has a reflectivity of 13 in orange light. As the coffinite from both the Fair Day and Copper King mines contains some finely intergrown pitchblende, the measured reflectivities are slightly higher than would be obtained from homogeneous coffinite.

In reflected light, coffinite resembles pitchblende in its optical and physical properties and in having rotund forms and ubiquitous shrinkage cracks. It is gray and isotropic, and has a hardness similar to that of pitchblende. It can be distinguished from pitchblende because it has (a) weak internal reflections, (b) a lower reflectivity, and (c) a local radial-fibrous structure in colloform aggregates, which can be seen most clearly under oil immersion.

Metallographic studies of the black uranium ores from the Fair Day mine, which have a delicate colloform structure, indicate that coffinite formed later than pitchblende. In all sections examined, coffinite embays and veins pitchblende, in a manner such as that illustrated in figure 2.1. The upper photomicrograph shows a spheroidal grain of pitchblende that is almost surrounded by coffinite. The coffinite embays the host irregularly and has replaced much of the outer part of the original sphere. One veinlet extends completely across the sphere. Replacement clearly preceded complete solidification of the host, for shrinkage cracks in the pitchblende in part extend outward into the coffinite, suggesting that shrinkage was partly simultaneous in both minerals. If the pitchblende had completely crystallized and shrunk before it was replaced, the coffinite should occur preferably in and along the shrinkage cracks. In detail, the contacts between pitchblende and coffinite are sharp, even when observed under high magnification, and are commonly bulbous or mammillary
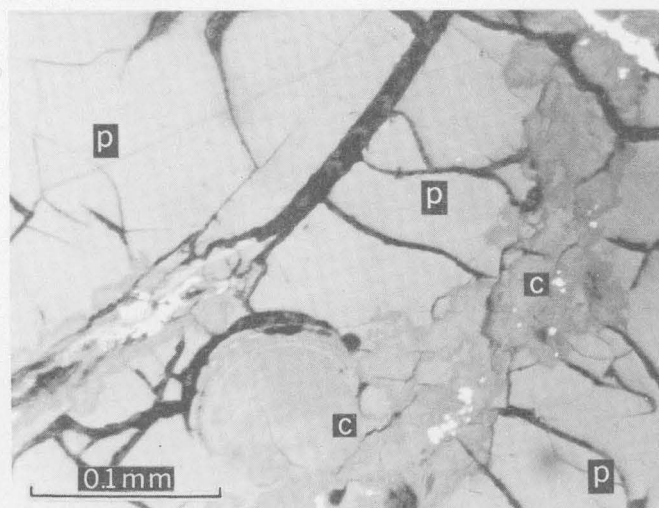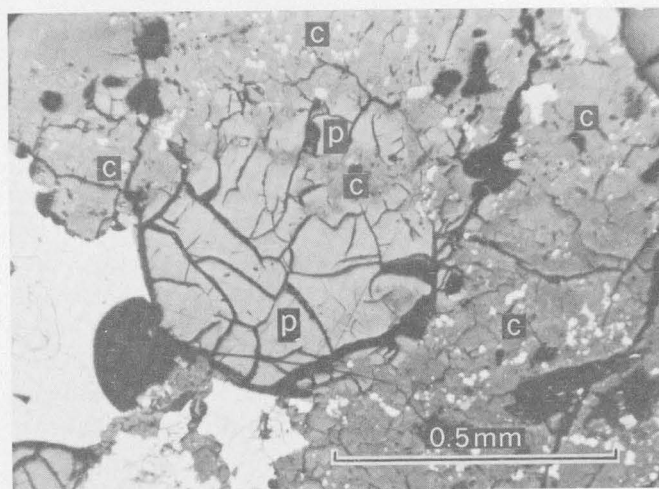
FIGURE 2.1.—Photomicrographs of polished sections of ore from Fair Day mine (c, coffinite; p, pitchblende).

in outline. In the lower photomicrograph, of part of a coffinite veinlet that transects a spheroidal grain of pitchblende, it can be seen that the veinlet is highly irregular and consists of coalescing aggregates of individual rotund forms that are smoothly convex toward the host. The largest node has conspicuous growth bands. This photomicrograph shows also a small veinlet of coffinite that appears to follow a shrinkage crack in pitchblende; this relation is rare in the ores.

Paragenetic studies of the black uranium ores from the Copper King mine are less definitive. Typically, tiny rotund forms of pitchblende, at most a few microns in diameter, occur in dominantly colloform coffinite. Even under magnification of several hundred diameters, there is no evidence that the pitchblende is corroded by coffinite.

The occurrences of coffinite in the Front Range indicate that the mineral characteristically forms in veins in a low temperature-pressure environment. Coffinite has not been identified from the uranium-bearing mesothermal sulfide veins of the Front Range mineral belt (Sims, 1956), except at the Stanley mine (table 1), where coffinite is clearly later than the dominant vein minerals and therefore could have formed under considerably lower temperatures than the main mineral assemblage.

REFERENCES

Frondel, Clifford, 1958, Systematic mineralogy of uranium and thorium: U.S. Geol. Survey Bull. 1064, 400 p.

Gude, A. J., 3d. and McKeown, F. A., 1953, Results of exploration at the Old Leyden coal mine, Jefferson County, Colorado: U.S. Geol. Survey open-file report.

Leonard, B. F., 1960, Reflectivity measurements with a Hallimond visual microphotometer: Econ. Geology, v. 55, p. 1306-1312.

Lindgren, Waldemar, 1933, Mineral deposits, 4th ed.: New York, McGraw-Hill, 930 p.

Sims, P. K., 1956, Paragenesis and structure of pitchblende-bearing veins, Central City district, Colorado: Econ. Geology, v. 51, p. 739-756.

Sims, P. K., Phair, George, and Moench, R. H., 1958, Geology of the Copper King uranium mine, Larimer County, Colorado: U.S. Geol. Survey Bull. 1032-D, p. 171-221.

Stieff, L. R., Stern, T. W., and Sherwood, A. M., 1956, Coffinite, a uranous silicate with hydroxyl substitution: A new mineral: Am. Mineralogist, v. 41, p. 675-688.

---

3. STRUCTURAL CONTROL OF EPIGENETIC URANIUM DEPOSITS IN CARBONATE ROCKS OF NORTHWESTERN NEW MEXICO

By LOWELL S. HILPERT, Salt Lake City, Utah

Work done in cooperation with the U.S. Atomic Energy Commission

A compilation of data on more than 100 uranium deposits in carbonate rocks in northwestern New Mexico shows that the deposits are generally associated with tectonic structures. The deposits occur mostly in the Colorado Plateaus Province in the Todilto limestone of Jurassic age; and a few occur in the Basin and Range Province in the San Andres and Madera limestones of Permian and Pennsylvanian ages, respectively (fig. 3.1). All the deposits are considered to be of epigenetic origin—that is, they were emplaced some time after the host rocks were deposited.

In the Todilto limestone the uranium minerals are of primary and secondary origin. The primary minerals, which are finely disseminated, are uraninite and coffinite, accompanied by the vanadium oxides häggite and paramontroseite (Truesdell and Weeks, 1959, p. 1689-1960). These minerals fill pore spaces, and replace limestone along silty layers. They are accompanied by the accessory minerals pyrite, hematite, fluorite, and barite (Laverty and Gross, 1956, p. 195-201). The secondary uranium minerals, generally closely associated with the primary minerals

above the water table, are yellow and yellow-green uranyl vanadates and silicates, which coat the walls of fractures and the pore spaces along silty layers in the limestone.

The Todilto deposits are roughly tabular with irregular outline, thus resembling many uranium deposits in sandstone in the Colorado Plateaus Province and elsewhere. They generally conform to the bedding but in detail cut across it. More than 50 deposits have been mined, and individual deposits have yielded from a few tons to as much as 100,000 tons of uranium ore.

Control of the uranium deposits in the Todilto limestone has been ascribed to diagenetic folds and larger scale fold and fault structures (Gabelman, 1956, p. 389, 391-392). The diagenetic folds are referred to hereafter as intraformational folds. However, a close spatial relation between the deposits and the larger scale structures is difficult to establish. In fact, these structures may be younger than the primary uranium minerals (Hilpert and Moench, 1960, p. 443-444) as they probably are related to a system of large-scale structures that has

COLORADO
NEW MEXICO

Shiprock

Farmington

Tierra Amarilla

RIO ARRIBA

ARIZONA

SAN JUAN

ROCKY MOUNTAIN PROVINCE

TAOS

PROVINCE

SOUTHERN

SANDOVAL

LOS ALAMOS

Santa Fe

MC KINLEY

Gallup

PLATEAU PROVINCE

SANTA FE

RANGE

Grants

Laguna

Albuquerque

VALENCIA

BERNALILLO

COLORADO AND

EXPLANATION

△

Uranium deposit or group of deposits in Todilto limestone

▲ (outline)

Uranium deposit in San Andres limestone

▲

Uranium deposit in Madera limestone

TORRANCE

BASIN

CATRON

SOCORRO

0 5 10 15 20 25 MILES

Socorro

FIGURE 3.1.—Map of northwestern New Mexico showing uranium deposits in the Todilto, San Andres, and Madera limestones.

been interpreted to be later than early Eocene in age (Hunt, 1938, p. 74-75). On the other hand, the deposits are closely related to the intraformational folds because they generally occur along the flanks and in some places along the axes of the folds.

The intraformational folds are of many types. Some are broad and open, some are recumbent, others are parts of larger intraformational folds, and still others are associated with intraformational faults that have displacements of only a few inches or more. In size the folds range from a few inches to about 30 feet in width and amplitude, and from a few feet to hundreds of feet in length. They are generally confined to the Todilto limestone, but some extend a few feet into the overlying or underlying formations. Many occur in clusters and if so the axes of individual folds may be parallel or subparallel. These structures are developed best in McKinley and Valencia Counties and a few occur in western San Juan and Rio Arriba Counties (fig. 3.1).

These intraformational folds are apparently tectonic in origin, as they are related to tectonic folding (Hilpert and Moench, 1960, p. 437-444). They are probably of Jurassic or Early Cretaceous age; and the associated primary ore minerals are probably of Late Cretaceous or early Tertiary age (Hilpert and Moench, 1960, p. 450).

Deposits in the San Andres and Madera limestones also occur where the rocks have been deformed. These deposits may be wholly secondary in origin, as only secondary minerals have been identified—but it is possible that primary minerals will ultimately be revealed by further exploration or study.

In the San Andres limestone the uranium is in conspicuous yellow vanadates that coat fracture surfaces, bedding surfaces, and fill open space in the rock where it has been broken by faulting. Two deposits in north-central Socorro County (fig. 3.1) are in a sandy zone in the limestone where it is broken by a north-trending high-angle fault. The largest mineralized zone, from which some ore has been mined, is about 50 feet in diameter and 35 feet thick. A deposit also occurs in the San Andres limestone in Valencia County, but the geologic relations are not clear. At this locality a yellow uranium mineral has been reported to occur in fractures in the San Andres limestone near igneous intrusive rocks.

Two uranium deposits also occur in a sandy zone in the Madera limestone in north-central Socorro

County (fig. 3.1) where the limestone has been brecciated along a north-trending high-angle fault. In these deposits also the uranium occurs in yellow vanadates and possibly in silicates that coat the fracture surfaces. The largest mineralized zone is about 100 feet in diameter where exposed at the surface, and is several feet thick. The highest grade material is near the fault and some ore has been mined.

The deposits in the San Andres and Madera limestones are probably of late Tertiary age or younger because the faults that apparently control the deposits displace the Datil formation (Wilpolt and Wanek, 1951), which is probably of late Tertiary age.

In summary, the uranium deposits in carbonate rocks in northwestern New Mexico are almost entirely associated with folds, faults, and minor fractures. These deposits are of epigenetic origin; they occur in two geologic provinces in formations of three geologic ages, and they probably represent two different periods of mineralization. Because they were formed under diverse geologic conditions in which the tectonic structures are the only features common to all, it must be concluded that localization of the uranium deposits is controlled by the tectonic structures. A brief review of the geologic literature reveals that most epigenetic uranium deposits in carbonate rock are controlled by tectonic structures. Therefore, it is concluded that only deformed carbonate rocks are good host rocks for epigenetic uranium deposits.

REFERENCES

Gabelman, J. W., 1956, Uranium deposits in limestone, *in* Page, L. R., and others, compilers, Contributions to the geology of uranium and thorium by the United States Geological Survey and Atomic Energy Commission for the United Nations International Conference on peaceful uses of atomic energy, Geneva, Switzerland, 1955: U.S. Geol. Survey Prof. Paper 300, p. 387-404.

Hilpert, L. S., and Moench, R. H., 1960, Uranium deposits of the southern part of the San Juan Basin, New Mexico: Econ. Geology, v. 55, p. 429-464.

Hunt, C. B., 1938, Igneous geology and structure of the Mount Taylor volcanic field, New Mexico: U.S. Geol. Survey Prof. Paper 189-B, p. 51-80.

Laverty, R. A., and Gross, E. B., 1956, Paragenetic studies of uranium deposits of the Colorado Plateau, *in* Page, L. R., and others, compilers, Contributions to the geology of uranium and thorium by the United States Geological Survey and Atomic Energy Commission for the United Nations International Conference on peaceful uses of atomic energy, Geneva, Switzerland, 1955: U.S. Geol. Survey Prof. Paper 300, p. 195-201.

Truesdell, A. H., and Weeks, A. D., 1959, Relation of the Todilto limestone uranium deposits to Colorado Plateau uranium deposits in sandstone [abs.]: Geol. Soc. America Bull., v. 70, no. 12, pt. 2, p. 1689–1690.

Wilpolt, R. H., and Wanek, A. A., 1951, Geology of the region from Socorro and San Antonio east to Chupadera Mesa, Socorro County, New Mexico: U.S. Geol. Survey Oil and Gas Inv. Map OM–121.

4. ORIGIN OF URANIUM AND GOLD IN THE QUARTZ ITE-CONGLOMERATE OF THE SERRA DE JACOBINA, BRAZIL

By Max G. White, Washington, D. C.

The Serra de Jacobina is in the north-central part of the State of Bahia, northeast Brazil. It is a narrow prominent range that stands out in sharp relief over adjacent plains. The mountainous country rises generally to altitudes of 600 to 800 meters with peaks of approximately 1,100 meters. The adjacent plains have an average altitude of about 450 meters. The principal town in the area is Jacobina, about 360 kilometers, by road, west of the port city of Salvador, Bahia.

The gold deposits of the region have been known since the latter part of the 17th century. Lode and placer deposits have been mined on a small scale. Currently only the Canavieiras gold mine is operating in the district.

Uranium discovered in the pyritic gold ores of Jacobina in early 1954 (White, 1956) has been described in fair detail at the Canavieiras mine (White, 1957; Bateman, 1958). The gold-uranium mineralized quartzite-conglomerates have been traced in discontinuous outcrops from about 3 kilometers north of Jacobina southward to the Rio do Almoco, a distance of 23 kilometers. The conglomerates are known to extend an additional 6 kilometers southward into an area that has not yet been investigated for uranium.

Fieldwork on the gold- and uranium-bearing conglomerates at Morro do Vento, 2 kilometers south of the Canavieiras mine, constitutes the basis for the present report.

GEOLOGIC SETTING AND STRUCTURE

Rocks exposed in the Serra de Jacobina (Branner, 1910) in the vicinity of the town of Jacobina consist of white quartzite that in the upper part has some nonconglomeratic sandstone, and in the lower part numerous conglomerate beds that contain pyritic gold-uranium deposits. The conglomerates are restricted to the western flank of the Serra, where they lie in contact with weathered granitic rocks. On the eastern border of the Serra the white quartzite is overlain by slate and phyllite. Scattered pockets of high-grade manganese oxides are found in the quartzite.

The rocks in the Serra de Jacobina dip easterly at high angles (45° to 70°), and strike northerly, parallel to the trend of the range. Details of the structure are not well known, but considering the steep dip of the rocks and the relatively narrow width (6 km) of the Serra, any divergence in strike of the quartzite from the trend of the Serra would carry the basal conglomerate away from the Serra at some short distance north of Jacobina. Many high-angle faults cut the Serra de Jacobina and many of the morros (hills) that make up the range are fault blocks. The conglomerates may have been removed by faulting north of Jacobina. In a few places highly weathered dark-colored dikes of what probably was an ultramafic rock (possibly pyroxenite) cut across the quartzite-conglomerate. No preferred orientation of the dikes has been observed, but many of them lie in the north-trending faults. A similarity of these rocks and their ore deposits to the well-known gold-bearing conglomerates of South Africa has been noted by earlier writers (Oliveira and Leonardos, 1943).

ORIGIN OF DEPOSITS

The uranium mineral in the Serra de Jacobina conglomerates has been identified by X-ray diffraction as uraninite. It occurs in close association with gold and pyrite in silicified quartzite-conglomerate. The mineralized rock is green, owing to the presence of chrome-bearing mica, or brown to yellow owing to limonite formed from oxidation of pyrite. On Morros do Vento, a mineralized zone 1,260 meters long has

an average content of 0.008 percent equivalent U_3O_8 and 10 grams of gold per metric ton of rock. This mineralized zone ranges from one-half to 10 meters in thickness but averages about 2 meters. The mineralized zone apparently parallels the strike of the enclosing sedimentary rocks and from place to place it consists of either conglomerate or quartzite. Numerous sections measured across the mineralized zone show that about 45 percent of the host rock is quartzite and the remaining 55 percent is conglomerate. The boundary of the mineralized rock at some places coincides with the edge of a conglomerate lens or a quartzite bed, but at other places the boundaries are within lenses or beds having otherwise uniform lithology. Some mineralized zones or shoots that have well-defined boundaries transect both quartzite and conglomerate beds.

It is apparent that the mineralization does not favor any lithologic unit in the quartzite-conglomerate sequence. Moreover there seemingly is no correlation between high values of gold and uranium and any particular rock type. It would appear, therefore, that this ore deposit is not a placer, which is the origin that has been suggested for the somewhat similar South African deposits, and for gold-bearing conglomerates of Blind River, Ontario (Davidson, 1957). Rather, the minerals probably were emplaced by hydrothermal solutions introduced along a possible north-south fracture or fracture zone, apparently parallel to the bedding. This conclusion is strengthened by the presence of quartz stringers and veins and the extensive sericitization and chloritization.

REFERENCES

Bateman, J. D., 1958, Uranium-bearing auriferous reefs at Jacobina, Brazil: Econ. Geology, v. 53, p. 417-425.

Branner, J. C., 1910, The geology and topography of the Serra de Jacobina, State of Bahia, Brazil: Am. Jour. Science, 4th ser., v. 30, p. 385-392.

Davidson, C. F., 1957, On the occurrence of uranium in ancient conglomerates: Econ. Geology v. 52, p. 668-693.

Oliveira, A. I., and Leonardos, O. H., 1943, Geologia do Brazil, 2nd ed.: Ministerio da Agricultura, Rio de Janeiro.

White, M. G., 1956, Uranium in the Serra de Jacobina, in Peaceful uses of atomic energy: Geneva, United Nations Internat. Conf. Proc., v. 6, p. 140-142.

White, M. G., 1957, Uranium in the auriferous conglomerates at the Canavieiras gold mine, State of Bahia, Brazil: Engenharia, Mineracao e Metalurgia, v. 26, no. 155, Nov., p. 279-282.

HYDROLOGIC STUDIES

5.   MAGNITUDE AND FREQUENCY OF FLOODS IN SUBURBAN AREAS

By R. W. CARTER, Washington, D. C.

The effect of suburban development on the magnitude of floods may be evaluated by examining the relations between floods of a given recurrence interval and the drainage area, lag time, and a length-slope parameter. Although these relations may not measure the effect as precisely as would be possible with "before and after" records of rainfall and streamflow, they do permit fairly accurate prediction, using existing records, of the effect of suburban development upon flood peaks.

Suburban development changes two of the basic elements that determine the magnitude and timing of the volume and peak of the flood hydrograph. The average infiltration rate is decreased because rooftops and city streets are impervious. The lag time between rainfall excess and the flood hydrograph is decreased because of storm sewers and improvements to the principal stream channels. The net effect of these changes on the magnitude and frequency of floods in the vicinity of Washington, D.C., has been evaluated.

The percentage of impervious surface area in basins in which suburban development is virtually complete is fairly low. For example, the percentages for Little Falls Branch near Bethesda, Md., and Four Mile Run near Alexandria, Va., based on aerial photographs taken in 1955, are 12.6 and 11.5, respectively. An approximation of the effect of impervious area on flood peaks is given by equation (1), which is based on the following assumptions:

1. The average rainfall-runoff coefficient of 0.3 as determined from rainfall-flood volume studies for storms in the Washington, D.C., area applies to flood peaks as well as to flood volumes.
2. The effect of the changes in impervious area is independent of the size of flood.
3. Seventy-five percent of the rainfall volume on impervious surfaces reaches the stream channel.
4. The impervious area consists of many fairly small areas randomly distributed throughout the basin.

$$K = \frac{0.30 + 0.0045\,I}{0.30} \qquad (1)$$

In this equation K is the factor by which all flood peaks are increased by the percent of impervious area, I. For example, if 10 percent of the area is impervious, the value of K is 1.15. The effect of imperviousness is small relative to other effects of suburban development on flood peaks.

The average time interval, T, between the centroids of rainfall excess and of the resulting flood hydrograph, was determined for each of 20 streams in the immediate vicinity of Washington, D. C. The time distribution of rainfall excess was determined from continuous records of rainfall and time-infiltration curves. The criteria for selection of storms were (a) a uniform areal distribution and (b) a short duration time relative to the lag time.

In figure 5.1, lag times are shown as a function of $L/\sqrt{S}$ where L is the total length from the gaging point to the rim of the basin measured along the principal channel, and S is the weighted slope of an order of 3 or greater of all stream channels in the basin. The weighted slopes were computed as follows:

$$S = \left[\frac{\Sigma\,L_i}{\Sigma\,(L_i/\sqrt{S_i})}\right]^2 \qquad (2)$$

Curve 1 on figure 5.1 is the relation for undeveloped areas in the Piedmont province near Washington, and may be expressed as

$$T = 3.10\left(\frac{L}{\sqrt{S}}\right)^{0.6} \qquad (3)$$

Snyder (1958) found that a similar equation with different coefficients, but the same exponent, applied to areas in California, Virginia, and other states.

The lower limit of the relation of lag time to $L/\sqrt{S}$ is probably defined by curve 3 on figure 5.1, which is based on data given by Snyder for basins that are completely sewered and have no natural channels.

Values of lag time for basins that are partly sewered, but with the principal stream channels maintained in their natural condition, should plot between curves 1 and 3. The points numbered 7, 10, 22, 23, and 24 on figure 5.1 are for such basins in the vicinity of Washington where suburban development is virtually complete. These points tend to define curve 2 which can be expressed

$$T = 1.20\left(\frac{L}{\sqrt{S}}\right)^{0.6} \qquad (4)$$

The slopes of curves 2 and 3, figure 5.1, have been made identical to the slope of curve 1, although the slopes of the curves 2 and 3 are not well defined by available data.

The effect of changes in lag time on the magnitude and frequency of floods may be determined by a multiple regression technique. The magnitude of floods of a given recurrence interval for undeveloped basins is considered to be a function of T and A, where A is the size of the drainage basin in square miles. Data for developed basins may also be used to determine this relation if the effect of imperviousness on flood peaks is first accounted for, and if it is assumed that the effect of T and K are independent. Data for developed and undeveloped basins have thus been used to define an equation of the form,

$$\frac{\overline{Q}}{K} = f(A,T) \qquad (5)$$

The magnitude of the flood discharge $\overline{Q}$ in cfs, which corresponds to a recurrence interval of 2.33 years, was determined for each of 18 streams from the record of maximum annual peak discharges. For each stream the annual peaks were plotted against the recurrence interval computed as $(n + 1)/m$ where m is the order number and n is the number of years of record. The period 1951 to 1959 was used. The value of $\overline{Q}$ for each stream was determined from the discharge-recurrence relation.

The constants in the functional expression of equation (5) were defined by multiple regression using values of $\overline{Q}$ and T computed from records for each stream and using the value of K from equation 1. The value of K from equation 1 was 1.00 for nine of the streams and ranged from 1.00 to 1.19. The equation of the regression is

$$\frac{\overline{Q}}{K} = 223\,A^{0.85}\,T^{-0.45} \qquad (6)$$

with a standard error of −22 and +29 percent. The value of the exponent of A is significant at the
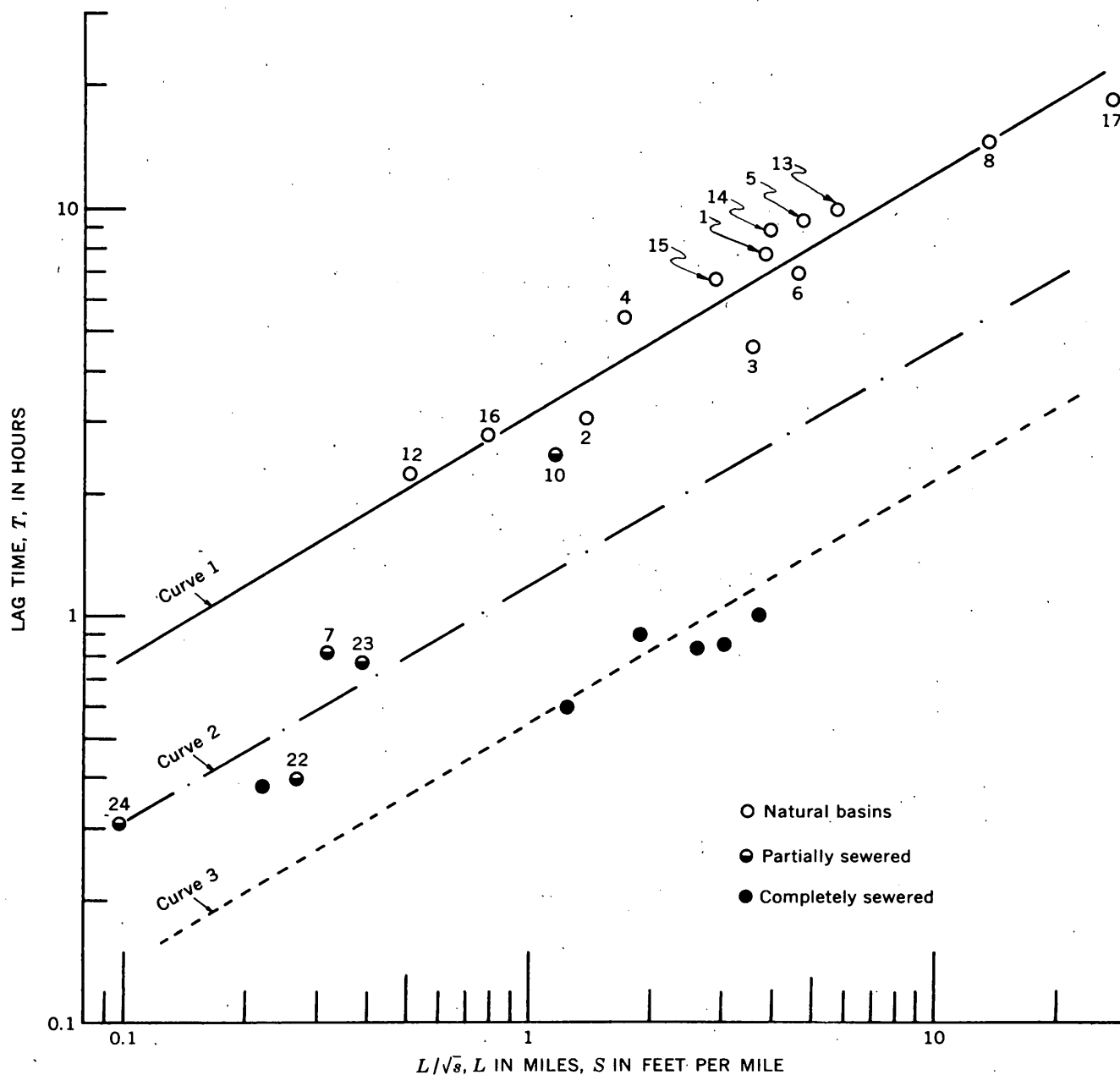
FIGURE 5.1.—Effect of suburban development on lag time.

99 percent confidence level; the value of the exponent of T at the 98 percent level. Data used to derive the equation include a range in A from 3.9 to 546 square miles, and a range in T from 1.2 to 18.6 hours.

The effect of suburban developments on floods with a recurrence interval of 2.33 years may be evaluated by use of figure 5.1, and equations (1) and (6). For example, assume that the relation between T and $L/\sqrt{S}$ changes the values given in curve 1 to the values given on curve 2 (fig. 5.1) because of suburban development, and that the percent im-

perviousness is increased from 0 to 12 percent. Then

$$\frac{\overline{Q}\ (\text{Suburban})}{\overline{Q}\ (\text{Undeveloped})} = \left(\frac{3.10}{1.20}\right)^{0.45} \left(\frac{.354}{.300}\right) = 1.8$$

The ratio 1.8 is believed to be the maximum effect of complete suburban development on flood peaks of any recurrence interval for drainage basins larger than 4 square miles in the Washington area.

REFERENCE

Snyder, Franklin F., 1958, Synthetic flood frequency: Am. Soc. Civil Engineers Proc. v. 84, no. HY5, 22 p.

6. EFFECT OF ARTIFICIAL STORAGE ON PEAK FLOW

By WILLIAM D. MITCHELL, Champaign, Ill.

As a supplement to the regular network of gaging stations, many districts now operate a network of high-water partial-record stations. Practical considerations have dictated that many of these be located at culverts, or other channel constrictions, at which the peak flows may be materially affected by artificial storage. To be of maximum value in regional flood studies, the recorded amounts of such peak flows should be increased to account for the effect of artificial storage. The problem is complicated by the lack of complete hydrographs for most sites; only the peak stage and outflow discharge are observed for any given flood, therefore the usual methods of flood routing cannot be applied. How, then, can an observed outflow peak be transformed to the corresponding inflow peak?

Various arbitrary solutions have yielded highly varying results, leading to the conclusion that a satisfactory solution could be obtained only by making a tabulation of I/O (inflow peak divided by outflow peak) resulting from routing all possible inflow hydrographs through all possible reservoirs. Then, given an appropriate description of a specific inflow hydrograph and specific reservoir, the tabulations would provide the appropriate correction factor. Obviously, it would be impractical to route an infinite number of hydrographs through an infinite number of reservoirs, but it appeared feasible to make detailed studies of a few combinations, and arrange the results in such manner that interpolations might be made for others. It is possible to make such interpolations if inflow hydrographs and storage-outflow relations are reduced to dimensionless bases.

Inflow hydrographs may be described in terms of Q, the instantaneous discharge, and H, the time from beginning of rainfall excess, and it is postulated that Q is determined by H; A, the size of the drainage area; P_e, the amount of rainfall excess; D, the duration of the rainfall excess; and T and k, characteristic times for a given drainage basin that indicate the time lag between rainfall and runoff. These factors are combined into the dimensionless ratios (QT/AP_e), (H/T), (k/T), and (D/T), leading to families of inflow hydrographs in which the first ratio is the ordinate, the second is the abscissa, and the third and fourth are distinguishing parameters.

Reservoir routing requires an expression of the form $S = KO^x$, in which S is the storage, K is a constant depending upon the relative capacities of the reservoir and the outlet, O is the outflow, and x depends on the relative slopes of the stage-discharge and stage-storage curves. The minimum value of x is 0.67 which would apply only to outflow at critical depth from a reservoir with vertical sides. The maximum x is indeterminate, but for many sites its value appears to be near 1; in fact, it is a common assumption in many reservoir problems that $S = KO$, and the storage is said to be linear. (Preliminary studies indicate that the methods here described may be expanded to include nonlinear storage, but the present analysis treats only linear storage.) In the expression $S = KO$, K has the dimension of time, and is reduced to a dimensionless base by dividing by T.

Sixteen dimensionless inflow hydrographs were routed through varying degrees of linear storage to obtain 128 outflow hydrographs. From these routings, pertinent tabulations were prepared as shown on table 1. On the first line, $K/T = 0$, so that the data are for the inflow hydrograph. Other lines are for outflow hydrographs, with K/T increasing to 2.0. The three central columns of the table represent, respectively, the time of occurrence of the peak, the magnitude of the peak, and the time of passage of the centroid of volume. The ratio for time of travel through the reservoir, t_v/T, may be obtained by subtracting value of t_v/T for $K/T = 0$ from other values of t_v/T.

TABLE 1.—*Results of routing inflow hydrographs through linear storage*

[$k/T = 1.0$; $D/T = 0.1$]

K/T	t_p/T	QT/AP_e	t_v/T	I/O
0.0	0.88	443.0	1.264	....
.1	.98	420.0	1.369	1.031
.3	1.16	359.6	1.588	1.204
.5	1.30	309.4	1.790	1.399
.7	1.44	272.4	1.977	1.590
1.0	1.60	232.4	2.237	1.863
1.5	1.80	188.5	2.636	2.297
2.0	1.96	159.6	3.012	2.713

The data may be arranged in several ways, but the most convenient arrangement appears to be that
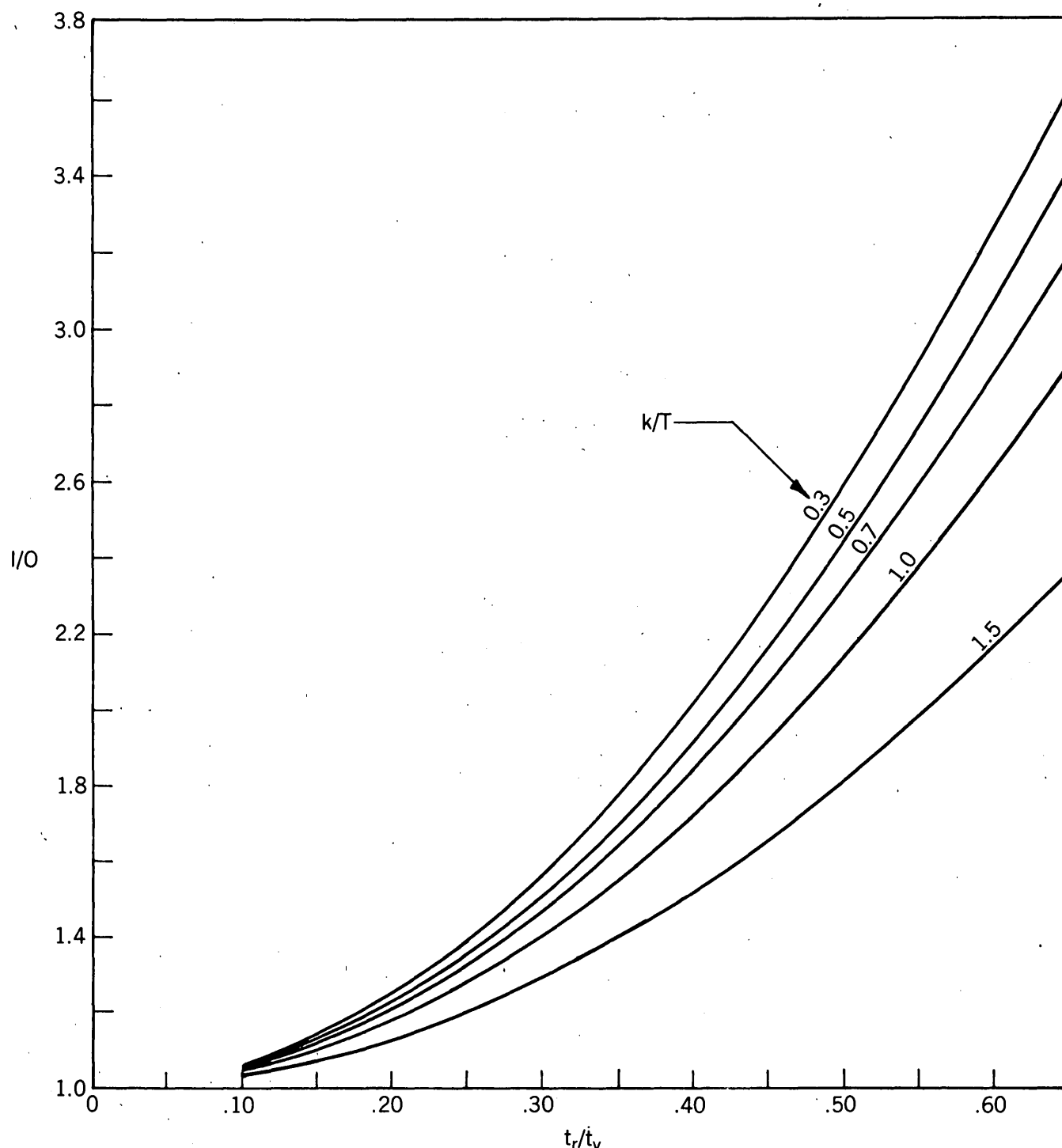
FIGURE 6.1.—I/O as a function of t_r, t_v, and k/T.

shown as figure 6.1, in which I/O is plotted as ordinate against t_r/t_v as abscissa for different values of k/T. Analysis of the tabulated data indicates that, for purposes of this plot, the ratio t_r/t_v should be computed by the formula:

$$t_r/t_v = 0.9 \, K/T/(1.00 + 0.7 \, D/T + 0.9 \, K/T)$$

Not all of the points plotted fit the curves perfectly, but only 2 of the 128 values are more than 10 percent from the curve, and these are for extreme conditions. (Both are for $k/T = 0.3$, $D/T = 1.5$; for $K/T = 1.5$, the error is 11.5 percent; for $K/T = 2.0$, 12.0 percent.) Two-thirds of the true values are within about 3 percent of the curve values.

To use figure 6.1, it is necessary to have values for D, K, T, and k. Values of D may be estimated from rainfall records, and K may be estimated from the storage-outflow curve. Work is continuing, as a part of another project, from which it is hoped to derive methods of estimating T and k from the physiographic characteristics of the drainage area.

Until these methods become available, it is suggested that T may be computed by one of the several formulas now available for computing time of concentration; values of k/T may be estimated from the steepness of the recession curve of surface runoff, using 0.3 for very rapid recession, 1.5 for very slow recession, and 0.7 for average recession.

⚒

7.   DISTINCTIVE CHARACTERISTICS OF GLACIER RUNOFF

By MARK F. MEIER and WENDELL V. TANGBORN, Tacoma, Wash.

Salient features of glacier runoff patterns may be brought out by comparing runoff data from two glacier-covered basins with data from three mountain basins that do not retain any significant snowfields throughout most years. These comparisons also show the influence of climatic factors, such as precipitation, on the runoff.

Most American glaciers behave as natural storage reservoirs that retain a predominant portion of the yearly total precipitation during a winter period of high precipitation, and release large quantities of water during a summer period of high temperatures and low precipitation. Thus, the annual variation of runoff from glacier-covered basins bears little or no relation to the annual variation of precipitation. This behavior is typical of all mountain drainage basins in areas of heavy snowfall, but the effect is most extreme for glacier-covered basins.

The distributions within a water year of runoff, precipitation, and degree-days for selected basins in Washington and Montana are shown in figure 7.1. The four basins in Washington are on the western slope of the Northern Cascade Mountains and include basins that are in both the non-glacier-covered foothills and on the largely glacier-covered crest of the range (table 1). Runoff and precipitation patterns from a different climatic environment are shown for a partly glacier-covered basin in the Northern Rocky Mountains of Montana. The data used in plotting the precipitation curves were not obtained from stations located within these basins but from selected Weather Bureau stations that are believed to have similar annual precipitation distributions.

These curves clearly demonstrate the long lag between precipitation and runoff that is characteristic of glacier-covered terrain. The curves from intermediate basins show that, as the mean elevation and amount of glacier-cover increases, appreciable runoff is delayed until later in the water year, and in a largely glacier-covered basin the highest monthly runoff occurs in July or August.

The role of the various solar and atmospheric energy sources in the production of meltwater runoff from either type basin is not developed in this article. However, there is an obvious qualitative relation between air temperature and runoff for a glacier-covered basin. This is shown by the cumulative degree-days above 32°F and runoff measured at the outlet of the Grinnell Creek basin (fig. 7.1).

Pronounced diurnal fluctuations in discharge are characteristic of the runoff from glacier-covered basins, reflecting diurnal fluctuations in the energy supplied for melting ice. Average daily curves of icemelt and runoff during clear weather are shown in figure 7.2 for the South Fork Cascade River basin. The asymmetric nature of the melting curve is due to a slow morning rise of incident solar radiation, caused by the basin's high eastern rim and a northwesterly slope of the ice surface. This condition occurs over about half of the basin area. The total daily runoff is less than the indicated daily icemelt because the icemelt recorder was located in a region of higher-than-average melt rates. At this time of the year the mean time of transit of meltwater from its point of generation to the gaging station at the outlet was of the order of magnitude of 4 hours.

In general, a thick, complete snowpack stores rainfall, releasing it gradually or retaining it as ice, whereas a bare ice or firm surface permits rapid
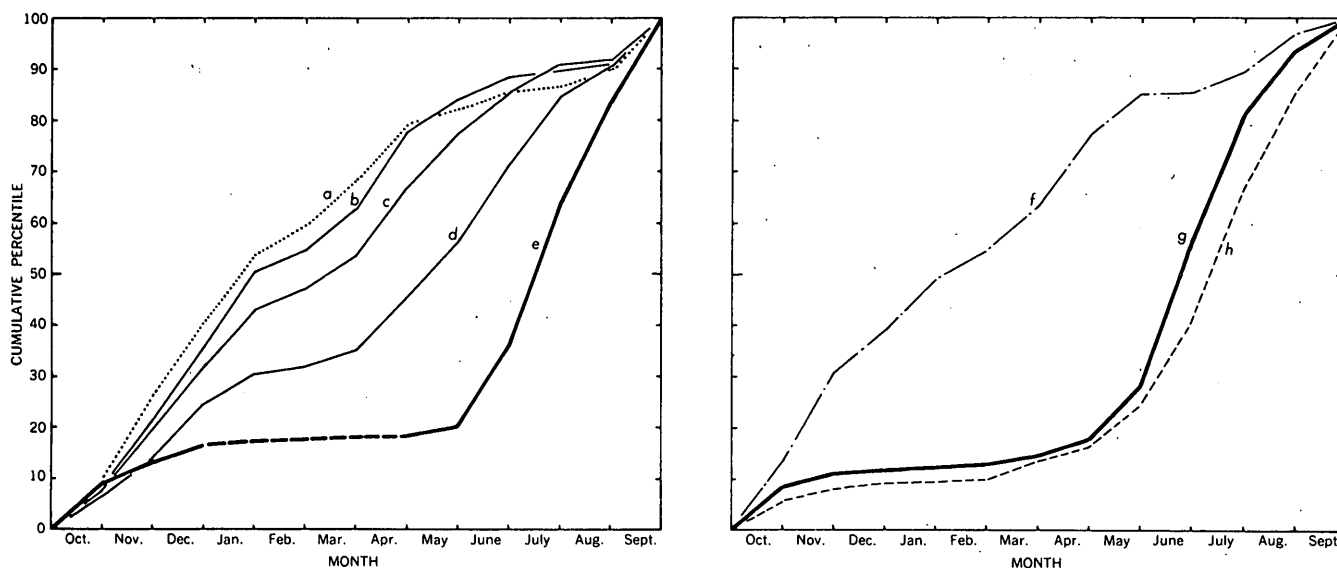
FIGURE 7.1.—Cumulative runoff and precipitation for selected drainage basins in the Northern Cascade Mountains, Wash., and the Northern Rocky Mountains, Mont.

a, Average precipitation at Darrington, Diablo Dam, and Sedro Woolley, Wash.

b, Runoff of Day Creek near Lyman, Wash.

c, Runoff of South Fork Nooksack River near Wickersham, Wash.

d, Runoff of Stetattle Creek near Newhalem, Wash.

e, Runoff of South Fork Cascade River at South Cascade Glacier, Wash.

f, Precipitation at Summit, Mont.

g, Runoff of Grinnell Creek near Many Glacier, Mont.

h, Degree-days above 32°F at Grinnell Creek near Many Glacier, Mont.

runoff of rainfall and produces a "flashy" hydrograph.

The effect of individual rain or snow storms on the runoff hydrograph is shown in figure 7.3. Inspection of these data shows that it is very difficult to forecast runoff from a given rainstorm. The rate of runoff following a rainstorm depends on (a) the amount of basin area covered with snow, (b) the thickness and density of the snowpack, (c) snow temperature, (d) whether the snow has been channeled by previous rain or periods of high melt rate, and (e) perhaps other factors. These factors show a normal seasonal variation, but may change rapidly and unpredictably in the fall.

Perhaps the most distinctive aspect of glacier hydrology is the natural change in ice storage from

TABLE 1.—Characteristics of drainage basins

Basin	Water year	Altitude		Drainage area (square miles)	Percent of area glacier-covered	Total yearly runoff (inches)	Physiographic description
		Mean (feet)	Maximum (feet)				
Day Creek near Lyman, Wash..........	1959	2,310	4,311	36.3	0	121	Low altitude forested foothills and low mountains.
South Fork Nooksack River near Wickersham, Wash.	1959	3,000	6,400	103	0	120	Forested foothills and few high peaks.
Stetattle Creek near Newhalem, Wash ..	1959	5,000	7,200	21.4	2	155	Forested valleys and high peaks near crest of range.
South Fork Cascade River at South Cascade Glacier, Wash.	1959	6,440	8,265	2.39	61	191	Bare slopes, jagged high peaks, little vegetation.
Grinnell Creek near Many Glacier, Mont.	1960	6,780	9,541	3.47	14	93	Bare slopes, jagged high peaks, some vegetation.
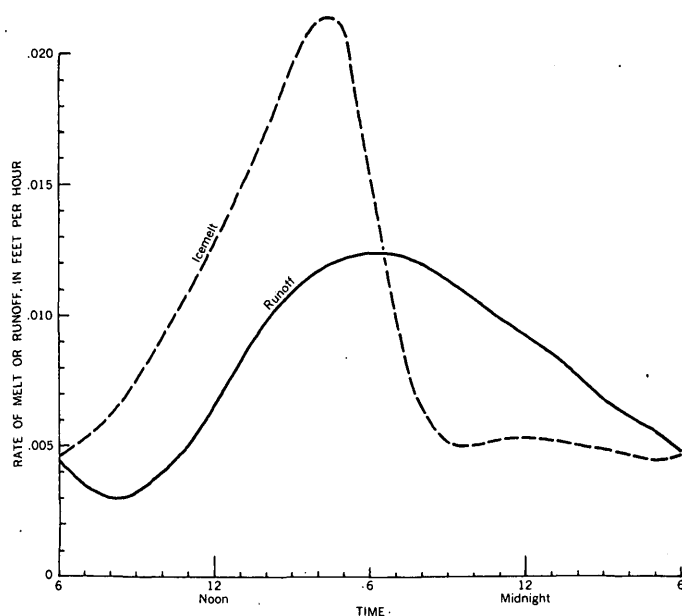
FIGURE 7.2.—Mean diurnal variation in rates of icemelt and runoff for 14 days of clear, warm weather occurring during period July 13–30, 1958. Icemelt was measured at station A, elevation 5,527 feet, on South Cascade Glacier. Runoff was measured at South Fork Cascade River at South Cascade Glacier, Wash., and was averaged over the total area of ice and snow in the drainage basin.

year to year. The storage changes tend to counteract the effects of cool wet, or warm dry years, as shown by table 2, which presents data from South Fork Cascade River during two contrasting years. Departures from long-term means of temperature and precipitation are reported for Newhalem, the nearest station for which these data are available. Loss of water through evaporation was found by our measurements to be negligible during the summer, and measurements on other glaciers have shown this to be generally true during the whole year. Thus, changes in the mass of a glacier represent true additions to, or withdrawals from, ice storage.

TABLE 2.—*Water budget for South Fork Cascade River at South Cascade Glacier, Wash., for two contrasting years*

Water year	South Fork Cascade River at South Cascade Glacier, Wash.			Newhalem, Wash.	
	Precipitation [1] (inches)	Runoff [2] (inches)	Change in storage [2] (inches)	Precipitation departure [3] (inches)	Temperature departure [3] (°F.)
1958....	[4] 130	[4] 200	−51	−14.2	+3.0
1959....	210	191	+17	+32.5	−0.8

[1] As measured at P1, 6,160 feet elevation, on South Cascade Glacier.
[2] Average values for whole drainage basin.
[3] Departures from 1931–55 means, by U.S. Weather Bureau.
[4] Part of the record estimated.
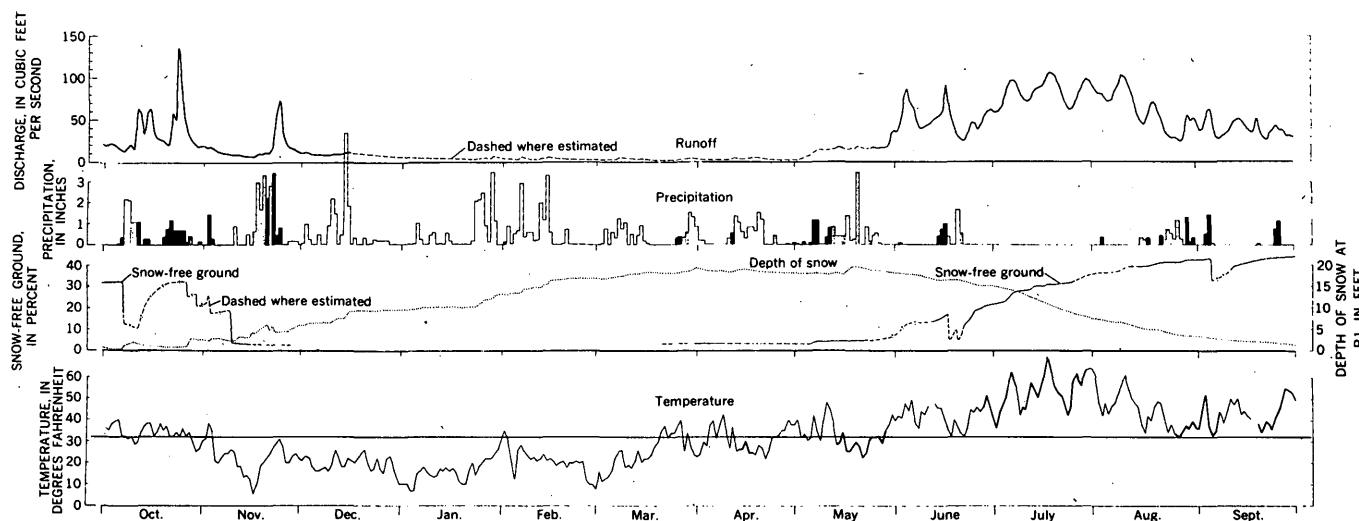
FIGURE 7.3.—Variation of runoff, precipitation, snow depth, percent of snow-free ground, and temperature for the drainage basin of South Fork Cascade River at South Cascade Glacier, Wash., during the 1960 water year. Dashed lines indicate periods of estimated record. Precipitation distribution during the period October 1, 1959, to April 3, 1960, and at several later short intervals was computed on basis of known total precipitation on South Cascade Glacier at P1 (6,160 feet) and known daily precipitation values at Darrington, Wash. Precipitation is differentiated into rain (solid black bars), mixed rain and snow (dotted bars), or snow (clear bars), on basis of free-air freezing levels over Seattle or actual observation. Snow depths were measured at P1 (6,160 feet). Temperature record is a composite of Darrington daily means minus 16°F (lapse-rate correction) shown by light lines, or actual measurement at research station at South Cascade Glacier (elevation 6,040 feet) shown by heavy lines.

8. RECENT HYDROLOGIC TRENDS IN THE PACIFIC NORTHWEST

By WILBUR D. SIMONS, Tacoma, Wash.

Annual runoff and annual precipitation in the Columbia River basin decreased, and annual mean temperature gradually increased between 1885 and 1945, according to an analysis by McDonald and Langbein (1948). To determine if these trends have continued, data for runoff, precipitation, and temperatures have been examined for the period 1885 to 1960—15 more years of record than was available to McDonald and Langbein. Annual deviations from the 1911–60 means were weighted for running 5-year periods according to the formula:

$$\frac{a + 2b + 3c + 2d + e}{9}$$

in which a, b, . . . are data for consecutive years, and the deviations were plotted against the middle year. The period 1911–60 was chosen as a reference because it was the longest period of concurrent records. In this preliminary analysis no adjustments of runoff were made for irrigation diversions or other modifications caused by the works of man.

Trend curves of annual streamflow for seven index stations are shown on figure 8.2. A distinct downward trend for the years prior to 1940 and an up-trend during succeeding years are evident. At 5 of the stations shown the 15-year average for the period 1946–60 was the maximum 15-year average of record, being surpassed only at those stations that had records during the 1890's. The flow of the Columbia River near The Dalles, Oreg., without considering the changes in flow regimen caused by the works of man, was only 7 percent less during the period 1946–60 than during the period 1891–1905.

Annual precipitation might be expected to show trends similar to those exhibited by streamflow data. Trend curves for five precipitation stations are shown on figure 8.3. An upward trend during the past 15 years is discernible in three of the five stations studied but at only one station is the precipitation greater during the past 15 years than during the late 1800's. The trends in annual precipitation
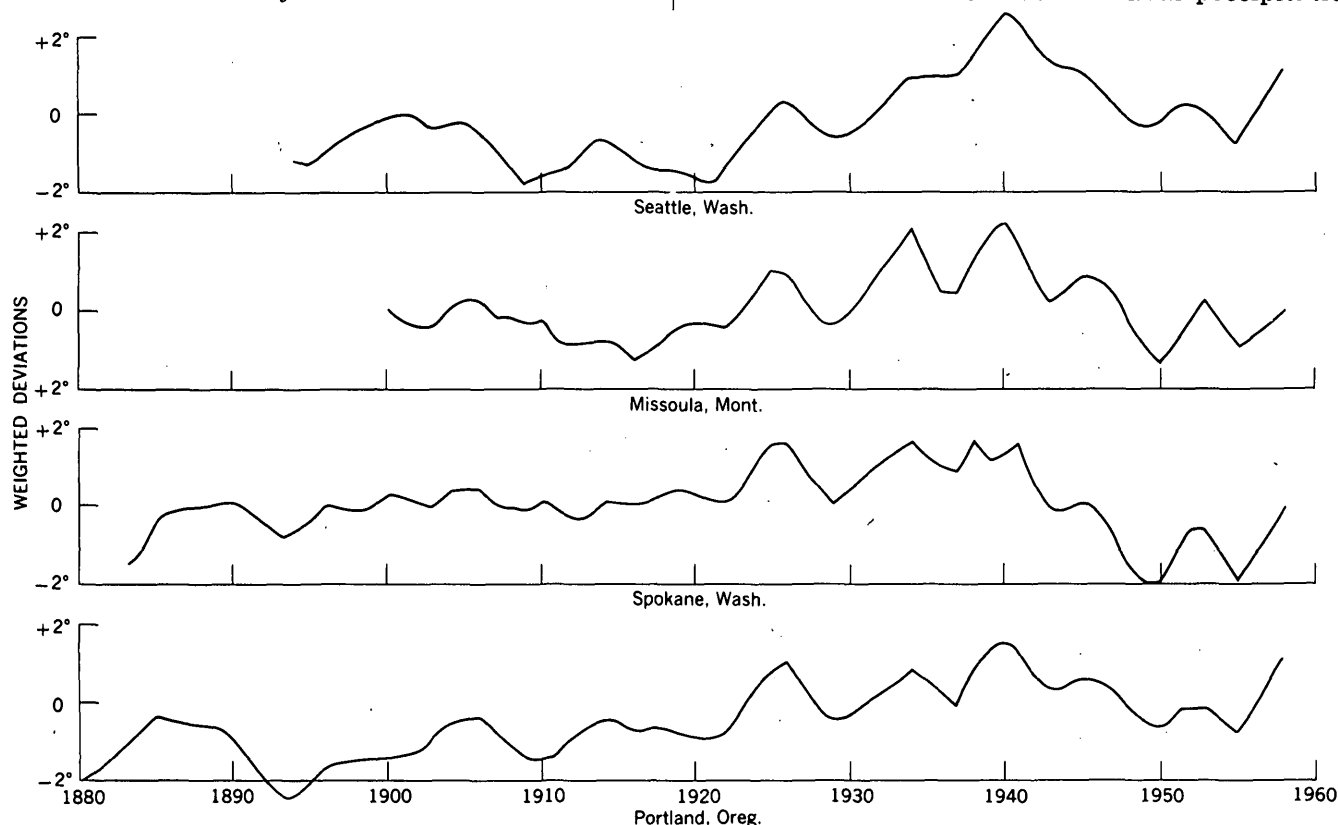
FIGURE 8.1.—Weighted deviations, in degrees Fahrenheit, from 1911–60 average annual temperatures at selected stations in the Pacific Northwest.
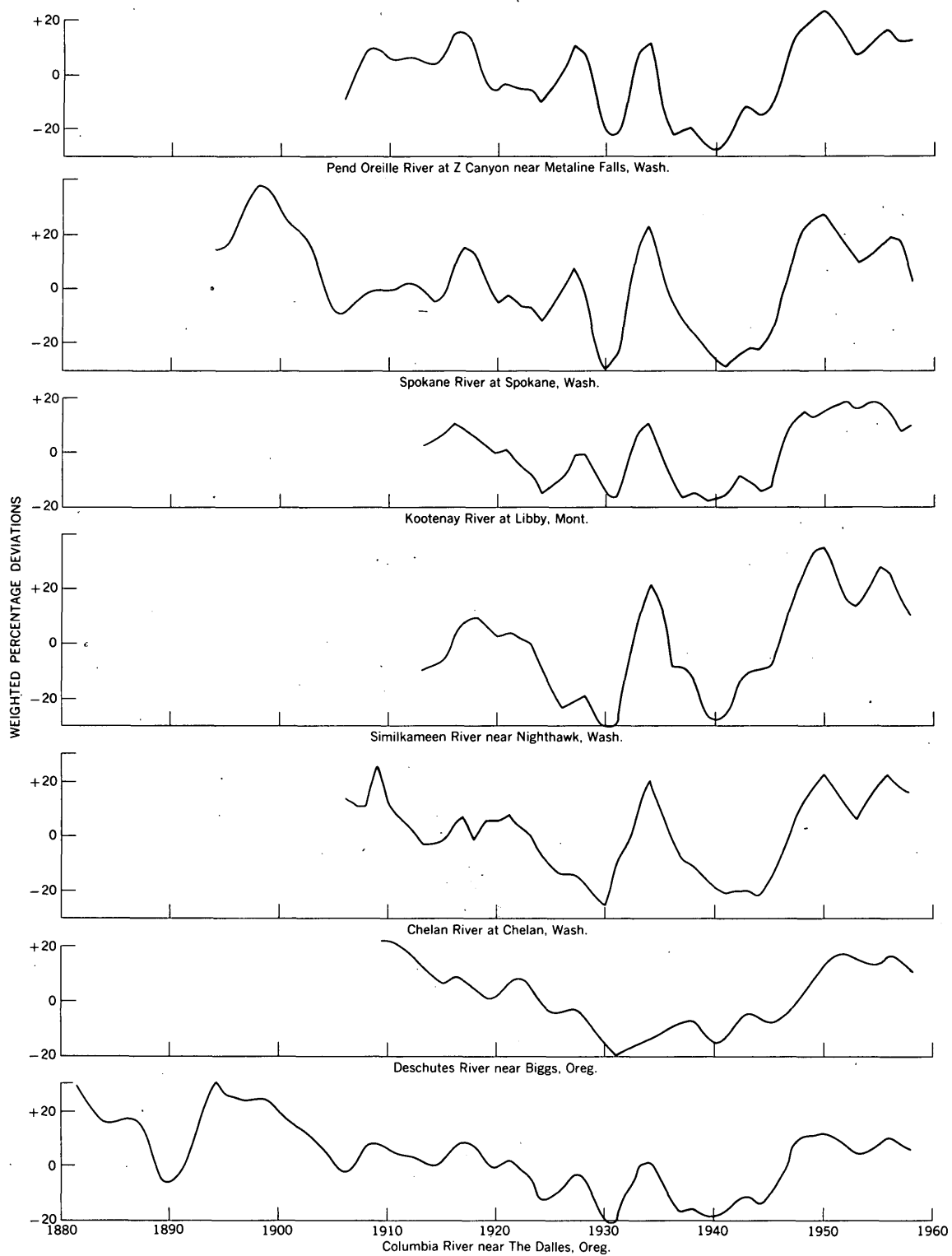
FIGURE 8.2.—Weighted percentage deviations from 1911–60 average annual precipitation at selected stations in the Pacific Northwest.
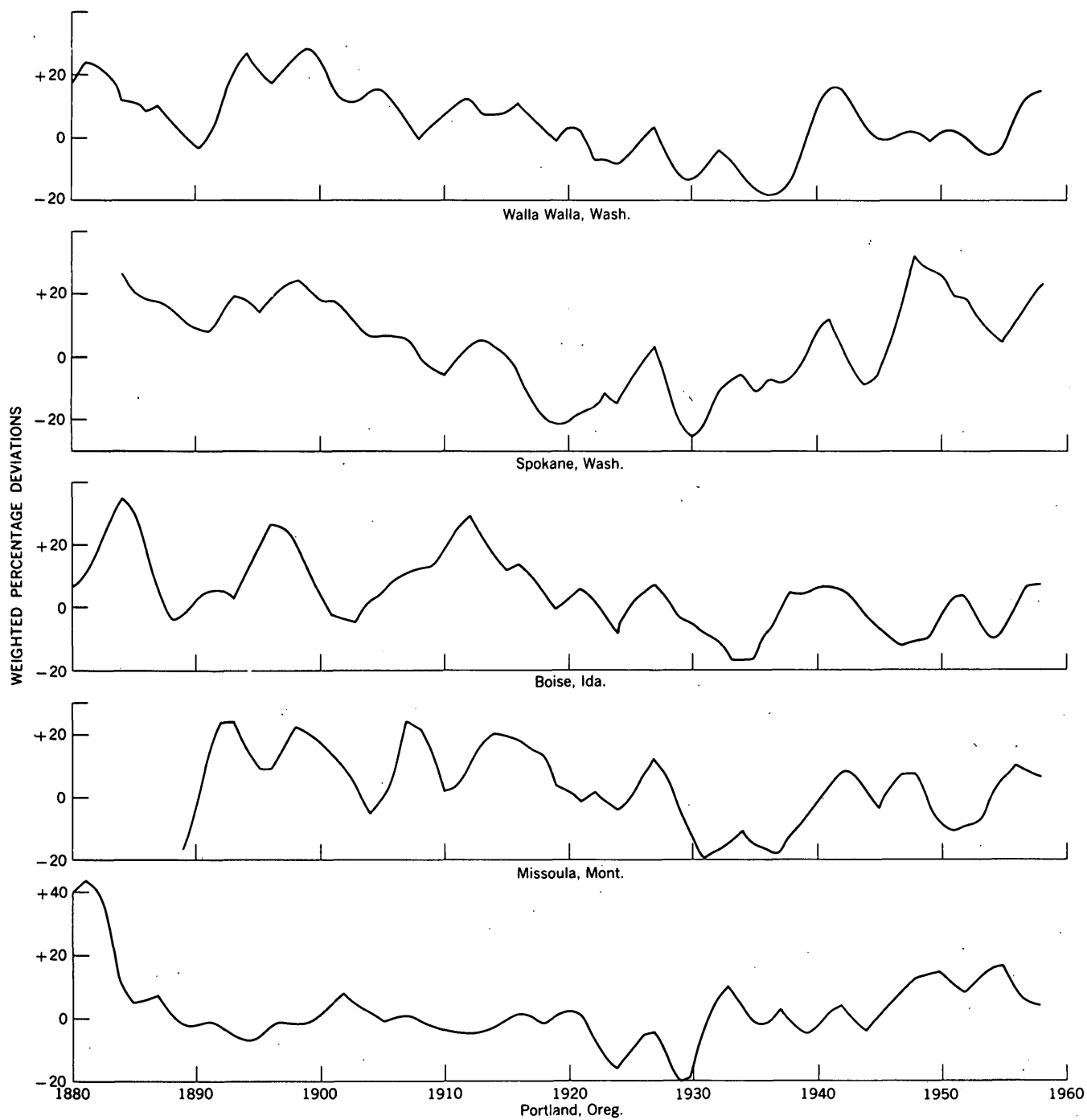
FIGURE 8.3.—Weighted percentage deviations from 1911–60 average discharges at selected gaging stations in the Columbia River basin.

are similar to the trends in annual runoff but are less clearly defined.

Trend curves for four temperature stations are shown on figure 8.1. Earlier records indicated a gradual rising temperature that reached a maximum about 1940. A downward trend since then is quite pronounced at each of the stations for which records were studied. However, at only one station do the recent temperatures reach the lower temperatures of the 1890's. The general tendency is for hot and dry years or wet and cool years to coincide.

Thus the analysis of data for the total 75-year period shows significant changes in trends and demonstates the necessity for continuing data collection and analysis in order to provide reliable information for development and evaluation of water-use projects.

REFERENCE

McDonald, C. C., and Langbein, Walter, 1948, Trends in runoff: Am. Geophys. Union Trans., v. 29, no. 3, p. 387–397.

9.   PRECIPITATION AS A VARIABLE IN THE CORRELATION OF RUNOFF DATA

By William J. Schneider, Washington, D. C.

Differences in runoff between basins are at least partly caused by differences in precipitation. Precipitation data, therefore, should be useful in improving the correlation between runoffs from different basins.

The effect of differences in precipitation on correlation of runoff can be expressed by either of two equations:

$$R_D = f(R_C, \Delta P) \tag{1}$$

$$R_D = f(R_C \text{ (adj)}) \tag{2}$$

in which R_D is the runoff of the dependent basin, R_C is the runoff of the control basin, ΔP is a measure of difference in precipitation between basins, and R_C(adj) is the runoff of the control basin adjusted for differences in precipitation between basins.

Investigations to date indicate that a logarithmic transformation of runoff data is necessary to obtain an essentially homoscedastic variance. The model equations using transformed runoff variables are:

$$\log R_D = a + b_1 \log R_C + b_2 \Delta P \tag{1a}$$

$$\log R_D = a + b_1 \log R_C \text{ (adj)} \tag{2a}$$

The term ΔP in equation (1a) may be obtained by using precipitation for either basin as the subtrahend in obtaining the difference in precipitation. Use of precipitation data for the dependent basin as the subtrahend will give a positive coefficient for b_2; use of precipitation data for the control basin as the subtrahend will give a negative coefficient.

In equation (2a) the adjusted runoff for the control basin is obtained as follows. The precipitation-runoff relation for the control basin is developed from the existing data. From this relation, two expected values of runoff (R_{PD} and R_{PC}) are determined. The first, (R_{PD}), is the expected value based on the precipitation for the dependent area, the second, (R_{PC}), is the expected value based on the precipitation for the control area. The difference ($R_{PD} - R_{PC}$) represents the expected difference in runoff from the control basin due to the difference in precipitation (ΔR_P), taking into account the magnitude of the precipitation. This difference in runoff is then added to the measured runoff to give

$$R_C \text{ (adj)} = R_C + \Delta R_P \tag{3}$$

which is then correlated directly with the runoff from the dependent basin.

A moderately extreme example of the effect of precipitation differences on the runoff relation between two basins is shown in the following results. Correlation of annual runoff of Albright Creek at East Homer, N. Y., (drainage area, 7.08 square miles) with runoff of SCS Watershed 97 at Coshocton, Ohio, (drainage area, 7.16 square miles) for the 15-year period 1941–55 gave a correlation coefficient of 0.47 and a standard error of estimate of +43 and −30 percent, based on the Coshocton area as the dependent variable. The inclusion of precipitation data in the form of ΔP as shown in equation

(1a) reduced the standard error of estimate to +15 and —13 percent, and resulted in a correlation coefficient of 0.93. Thus, the inclusion of ΔP accounted for an additional 64 percent of the variance in the data, reducing the residual variance from 78 to 14 percent. The use of adjusted runoff as indicated in equation (2a) reduced the standard error of estimate to +14 and —13 percent, and resulted in a correlation coefficient of 0.95. All regression coefficients were highly significant in both equations.

Improvement in determining runoff relations can also be demonstrated for basins that are close together. The areas drained by Sage Brook near South Berlin, N.Y., (drainage area, 0.70 square miles) and by Cold Spring Brook at China, N. Y., (drainage area, 1.51 square miles) are less than 25 miles apart. The correlation coefficient between annual runoffs for the 22-year period 1936–57 is 0.87 and the standard error of estimate for Sage Brook is +12 and —11 percent. Including precipitation data as described in equation (1a) reduced the standard error of estimate to +8 and —7 percent, and resulted in a correlation coefficient of 0.92. Model equation (2a) gave similar results.

Although the models used are considered satisfactory, it is not implied that they are the best ones for estimating runoff. The two examples are cited above merely to illustrate the feasibility of improving a determination of the relation between runoffs by considering differences in precipitation.

⚒

10.   REGIONAL LOW FLOW FREQUENCY ANALYSIS

By H. C. RIGGS, Washington, D. C.

The distribution of the population of annual minimum flows at a stream site would be useful in planning the optimum development of the flow. In hydrology the distribution of the population is never known; it can only be estimated from the data obtained at the site. The sample distribution so obtained may be considerably different from the population distribution; therefore some method is sought for obtaining a better estimate of the population distribution.

The shape and position of a frequency curve (which is the sample distribution) of annual minimum flows based on observational data at one site differ from those of a curve for another site because of differences in physical characteristics of the basins and because of differences in weather experienced. Examples are shown on figure 10.1. Both curves differ from their respective population curves because of the short periods of weather sampled. It is postulated that weather samples differ areally within a common time period. Therefore, some method of combining the experience at several stations while maintaining the characteristics of each individual station record should result in better estimates of the frequency distributions. Such a method is called a regional analysis.

Regional analysis is useful only when the correlation coefficient between minimum flows at two stations is less than 1, but greater than some minimum value. Remembering that the purpose of regional analysis is to reduce sampling error in the frequency curve, it can be seen that flows which are completely correlated must also have the same sampling error and, therefore, combining the experience cannot reduce this sampling error. Now consider the other extreme of poor correlation between flows. Poor correlation, might indicate that different weather samples were experienced at different basins, or that the reactions to a particular weather occurrence were different, or both. The last is the most likely. Here, the combined experience averages deviations that consist both of sampling errors and of effects of differences in basin characteristics. Averaging values of the latter component ordinarily will not improve the estimate of the frequency curve; it may even produce an estimate of reduced reliability.

Between total correlation and some minimum value of correlation is a range in which there is an opportunity for reducing individual sampling errors (some of which are assumed to be plus and some minus). This may be done by (a) relating the magnitude of the annual minimum flow at a certain
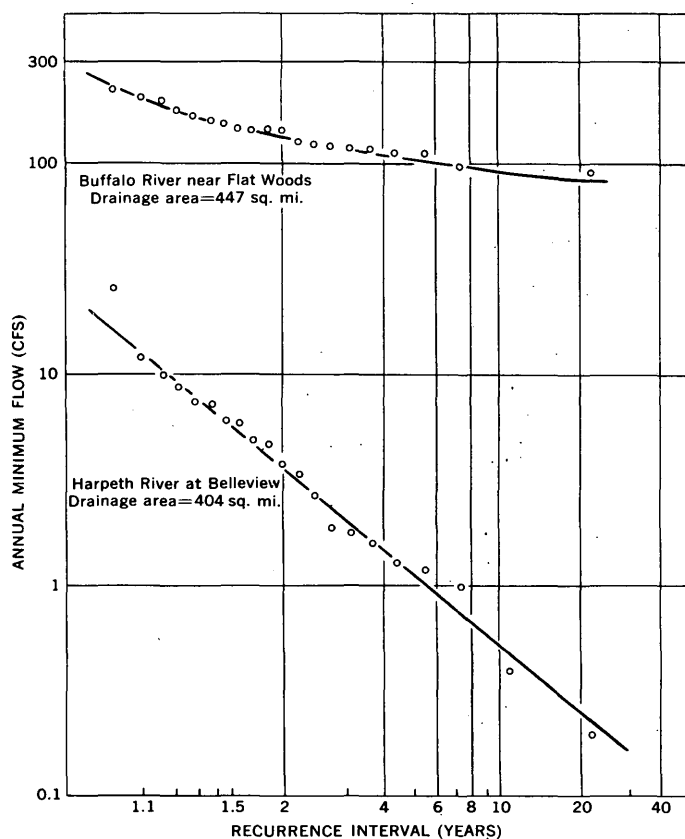
FIGURE 10.1.—Frequency curves of two Tennessee streams.

recurrence interval to the median annual minimum flow and to indexes which describe the differences in basin characteristics, and then (b) using the computed value rather than the value obtained from the frequency curve.

The method of regional analysis just described is applied to frequency curves of annual minimum 7-day average flows for 47 sites in the regions, roughly, of New England, Georgia, and Kansas. The dependent variable is Q_{20}, the discharge at 20-year recurrence interval from the frequency curve based on observations. The median annual minimum, Q_2, is also taken from the frequency curve. The effects of basin characteristics are described by drainage area (A) and by an index (S) of the slope of the base-flow recession curve, which is defined as the ratio (expressed as a percentage) of two discharges from the recession curve; the denominator of the ratio is Q_2 and the numerator is the discharge 10 days after the Q_2 discharge. The index S describes the integrated effect of geology, topography, vegetal cover, and to some extent climate, on the minimum flows.

The computed regression is—

$$\log Q_{20} = -2.58 + 1.13 \log Q_2 - 0.22 \log A + 1.35 \log S + 0.09 (\log Q_2) [\log (A/Q_2)]$$

The standard error of Q_{20} is −20 percent and +25 percent. The regression coefficient for the last term is statistically significant at the 5-percent level. All others are highly significant. Streams used in defining the equation have the following ranges of variables:

$$1.05 < Q_2 < 1,770 \text{ cfs}$$
$$4.12 < A < 11,220 \text{ sq mi}$$
$$6.7 < S < 94 \text{ percent}$$

The equation was solved for Q_{20} for each of the 47 sites and for 61 additional: 25 in Tennessee, 4 in California and Washington, 24 in North Carolina, and 8 in Turkey. The computed value of Q_{20} for each of the 108 sites is plotted against the corresponding value obtained from the individual frequency curve on figure 10.2. No geographical bias is apparent from study of the deviations. The wide range in magnitude of Q_{20} and the wide geographic range encompassed indicate that the relation should hold wherever (a) the rate of summer-and-fall base-flow recession is consistent from year to year and (b) the annual minimum flow occurs in the late summer or fall.
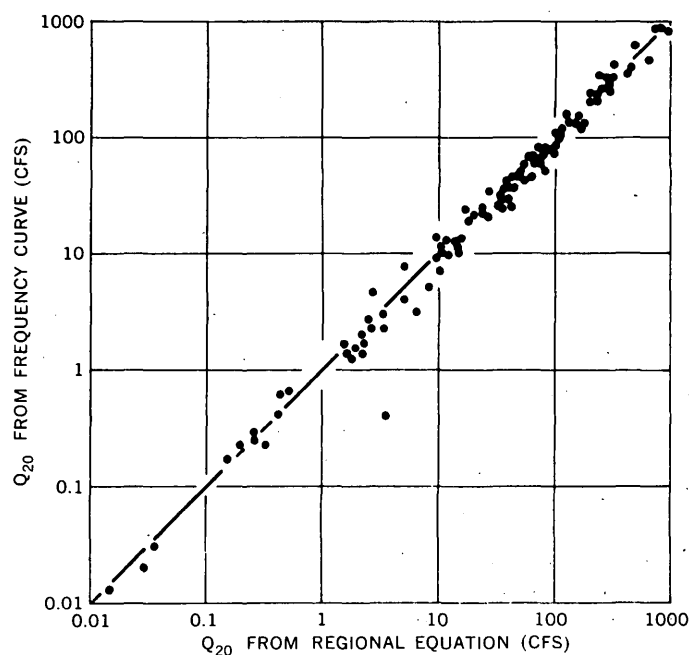
FIGURE 10.2.—Comparison of Q_{20} from the individual frequency curve with the corresponding Q_{20} from the regional equation.

The reliability of the regionalized values of Q_{20} is directly related to the proportion of the regression error that is sampling error, and to the reliability of Q_2. These two factors cannot be assessed at this time. However, the standard error of 25 percent does not seem excessive when one considers that there is some minimum sampling error below which no advantage would be gained by a regional analysis.

11. MODIFIED CONVEYANCE-SLOPE APPLIED TO DEVELOPMENT OF STAGE-FALL-DISCHARGE RATINGS

By William C. Griffin, Washington, D. C.

The common gaging-station rating is a relation between discharge and gage height. Ratings for gaging stations on streams with variable backwater effect must include an additional variable, fall (F), which is the difference in water-surface elevation at the ends of a reach of channel. Such ratings are called stage-fall-discharge ratings. All methods in general use for development of stage-fall-discharge ratings require trial and error solutions. This paper presents a direct approach.

In the Manning formula, $Q = \dfrac{1.486}{n} AR^{2/3}S^{1/2}$, Q is discharge in cubic feet per second; n is a roughness factor; A is cross-sectional area; R is hydraulic radius; and S is energy slope. The term $\dfrac{1.486}{n}AR^{2/3}$ is commonly called conveyance, K. Thus, the formula reduces simply to

$$Q = K\sqrt{S}. \qquad (1)$$

A curve of conveyance against stage could be developed from an instrument survey, and inasmuch as Q and K have the same units of cubic feet per second (slope is dimensionless), the stage-conveyance curve could be used as the base stage-discharge rating. The only additional requirement for a complete rating is a relation for determining $\sqrt{S}$. Intuitively, fall is the most logical factor to use in a relation curve to yield $\sqrt{S}$. If values of square root of slope as computed from the ratio of measured discharge to conveyance, when plotted against fall, define a satisfactory curve of relation, the rating process is complete.

An example is given below for the Ohio River at Cincinnati, Ohio. Data were not available for accurately defining a conveyance curve, but discharge measurements provided sufficient information, except for the roughness factor, n, for a fair approxi-

mation of conveyance at the measuring section. A value of 0.03 was selected for n; conveyance was computed for each of a sequence of discharge measurements; and the relation between conveyance and discharge was defined graphically (fig. 11.1). It was postulated that the shape of the conveyance curve would be more important than its position. Hence, an error in n would be critical only if instead of being constant as was assumed, n should have varied with stage.

The square root of energy slope was computed for each measurement, by dividing measured discharge by conveyance, and plotted against fall to define the right-hand curve of figure 11.1. This curve can be used in combination with the conveyance curve as the stage-fall-discharge rating for the station. To use the rating, if gage height and fall are given, conveyance and $\sqrt{S}$ can be obtained from the curves and the corresponding discharge is the product of these two.

The rating just described is virtually the same as the conventional constant-fall type of rating for variable backwater effect. This similarity would be more readily apparent if, for this particular station, equation 1 were modified as follows:

$$Q = 0.01\,K(100\,\sqrt{S}).$$

The advantage of the procedure described, then, is not that a new type of rating can be developed, but that a direct approach can be used to get a result that might never be apparent if an indirect method is attempted.

The fact that a workable relation was developed without the use of trial and error procedure probably means that there was no significant variation of n with stage. Any error that may have been made in the choice of 0.03 for n would have been compensated for in the computed values of $\sqrt{S}$.
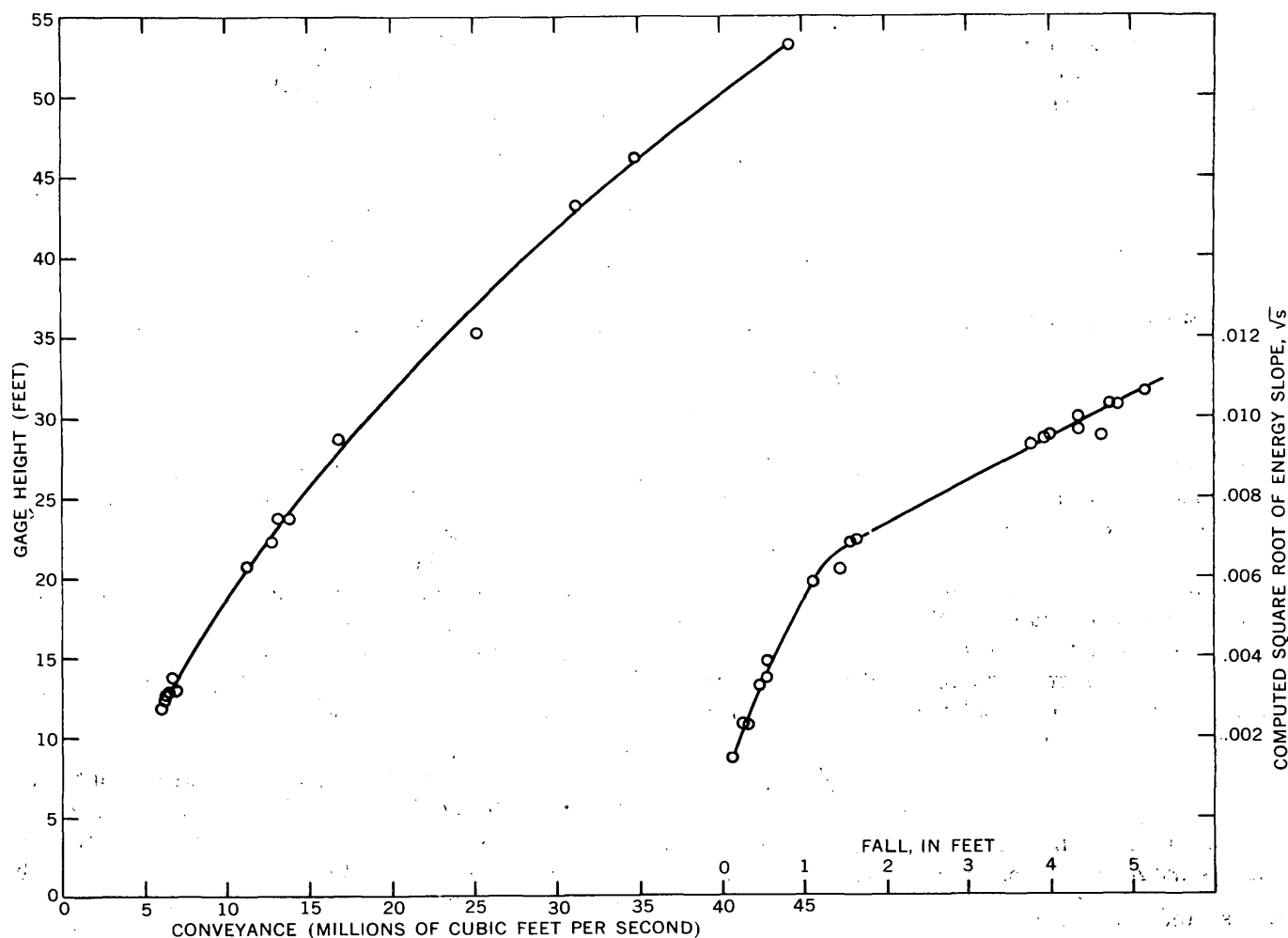
FIGURE 11.1.—Stage-fall-conveyance relation for the Ohio River at Cincinnati, Ohio.

One recognized limitation in the use of the modified conveyance-slope procedure for variable backwater ratings is at stations of the limiting-fall type, where backwater is not present all the time. A characteristic of stations of this type is that, for a given stage, discharge reaches a maximum rate at some amount of fall and does not increase with increasing fall. At such stations the modified conveyance-slope procedure would be applicable only for falls less than the limiting values, and it would be necessary to use the type of limiting-fall curve described by Mitchell (1954, p. 145) as the upper limit of discharge unaffected by variable backwater. Doubtless, other limitations will come to light as additional applications are made; their recognition will aid in delineating the conditions under which the method can be used to advantage.

REFERENCE

Mitchell, W. D., 1954, Stage-fall-discharge relations for steady flow in prismatic channels: U.S. Geol. Survey Water-Supply Paper 1164, 162 p.

12.   FLOW IN AN ARTIFICIALLY ROUGHENED CHANNEL

By H. J. KOLOSEUS and JACOB DAVIDIAN, Iowa City, Iowa

Work done in cooperation with the Iowa Institute of Hydraulic Research

A resistance coefficient, such as the Darcy-Weisbach f or the Manning n, is frequently used to evaluate the energy losses due to the retarding effect of channel surfaces on a moving fluid. The coefficient is assumed to be a function of the relative roughness, the shape of the channel, and the Reynolds and Froude numbers; however, the relationship has not been defined for most cases of open-channel flow. Hence, the resistance coefficient is estimated on the basis of judgment and experience.

As a first step toward a more rational determination of the resistance coefficient, a laboratory study of the effect of roughness concentration on open-channel flow was undertaken. The roughness elements, $\frac{3}{16}$-inch metal cubes, were arranged in diamond patterns commensurate in size with particular roughness concentrations. The upstream face of each cube was placed normal to the mean direction of fluid motion. Tests were conducted in two rectangular tiltable flumes, one 2 feet wide and 30 feet long, and the other 2.5 feet wide and 85 feet long.

The experimental program was designed to maximize the relative importance of the roughness influence. Koloseus (1958, Ph. D. Thesis Iowa State University) has previously shown for supercritical flow that the resistance coefficient for a rough channel of this type is independent of gravitational effects when the Froude number is less than 1.6, and is independent of viscous effects when $\sqrt{f} R k/4h$ exceeds 600. Within these limitations, it is assumed that f is a function of the relative height and the cube concentration; that is

$$f = G(k/4h, \lambda) \qquad (1)$$

where f is the resistance coefficient, $8ghS/V^2$; "G" means "function of"; g is the acceleration of gravity; h is depth of flow; S is the energy gradient; V is the average velocity; k is height of roughness ($k/4h$ is called the relative height of roughness); λ is roughness concentration, denoting the ratio of the total projected area of the roughness in the direction of mean fluid movement to the total floor area; R is Reynolds number, $4Vh/\nu$; and ν is kinematic viscosity.

Experimental data plotted on figure 12.1 define the relation,

$$\frac{1}{\sqrt{f}} = 2 \log \left[0.14 \lambda^{-0.9} (4h/k) \right] \qquad (2)$$

The scatter of values about the line for equation (2) (fig. 12.1) is remarkably small over 4-fold variation in $k/4h$ and the 64-fold variation in λ.

Equation (2) reduces to that of Nikuradse (1933) for flow in sand-roughened pipes when the roughness-concentration factor is ignored. Comparable changes in magnitude of either $k/4h$ or λ have approximately the same effect on the resistance coefficient. As with relative height, the roughness con-
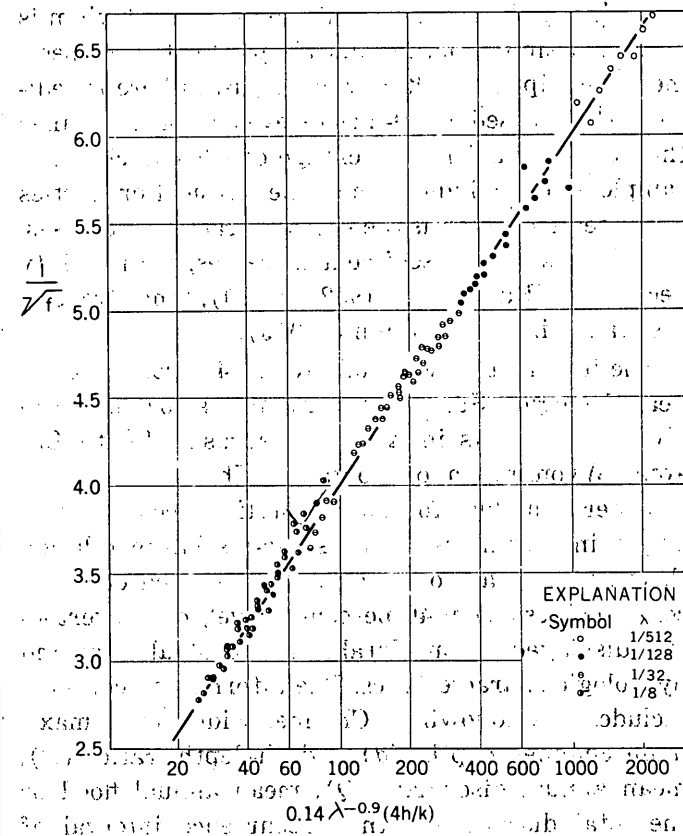
FIGURE 12.1.—Variation of the resistance coefficient with the relative height and the roughness concentration.

centration must be more than doubled in order to obtain a two-fold increase in the resistance coefficient.

REFERENCE

Nikuradse, J., 1933, Strömungsgesetze in rauhen Rohren: Verein Deutscher Ingenieure, Forschungsheft 361.

13.   DIMENSIONS OF SOME STABLE ALLUVIAL CHANNELS

By S. A. SCHUMM, Denver, Colo.

Several attempts have been made to develop a series of equations that can be used to calculate the dimensions of stable alluvial channels (Leliavsky, 1955). During recent investigations into the morphology of streams in a semiarid environment, information was collected that may have a practical application in the solution of such problems. This information indicates that the shape of alluvial channels and the stratification of channel deposits are significantly related to the type of sediment found within these channels (Schumm, 1960a, 1960b).

In this analysis the silt-clay content of alluvium is used as a simple but significant parameter for sediment description. Silt-clay as discussed here is sediment that passed a 200-mesh sieve or that is smaller than 0.074 mm. The percentage of silt and clay in a sample gives an indication of the physical properties of the sediment, for as the silt-clay fraction increases, cohesiveness of the sediment increases, permeability decreases (Burmister, 1952, p. 20), and tractive resistance increases (Dunn, 1959).

The information was collected at 41 cross sections near Geological Survey gaging stations, located on 29 rivers and creeks in Kansas, Nebraska, South Dakota, Wyoming, and Montana. The channels are considered stable, for gaging-station records show only minor changes in the stage-discharge relation through the years of record. The selected channels contained less than 40 percent gravel, but nevertheless displayed a considerable range of alluvial and hydrologic characteristics. The information collected includes the following: Channel width (w), maximum channel depth (d), width-depth ratio (F), mean annual discharge (Q), mean annual flood or the total discharge with a recurrence interval of 2.33 years (Q_b), median grain size of bed and bank sediment (D_{50}), percent silt-clay in bed (S_c) and banks (S_b), percent silt-clay in the perimeter of the channel (M) calculated as a weighted mean

$$M = \frac{S_c \times w + S_b \times 2d}{w + 2d}$$

As an indication of the range of variables occurring among the sampled sections, the extreme values for some alluvial, hydrologic, and morphologic characteristics of the channels are as follows:

Drainage area above gaging station	sq mi	212 to 56,700
Channel width	feet	25 to 800
Maximum channel depth	feet	2.3 to 18
Width depth ratio		2.5 to 138
Median grain size (bed)	mm	0.02 to 8.0
Median grain size (bank)	mm	0.01 to 0.33
Silt-clay in banks	percent	23 to 97
Silt-clay in bed	percent	0.2 to 87
Silt-lay in perimeter of channel	percent	1.4 to 89
Mean annual discharge	cfs	5.8 to 5,155
Mean annual flood	cfs	311 to 48,000

That a relationship exists between channel width and depth and discharge is well known and has been discussed most recently by Nixon (1959). The collected data afford an opportunity to relate channel width and depth not only to discharge but also to other variables.

Analyses of variance show that at the 0.05 level the following are significantly related to width: Percent silt-clay in banks, mean annual flood, mean annual discharge, weighted mean percent silt-clay. Percent silt-clay in the channel and median grain size in bed and banks are not significant at the 0.05 level. Mean annual flood and weighted mean percent silt-clay are most significantly related to width, for they are significant at the 0.001 level. These two variables were chosen for a multiple correlation analysis with channel width. The analysis yields the following equation for channel width:

$$w = 5.76 \, \frac{Q_b^{.45}}{M^{.36}} \tag{1}$$

The results of tests of the reliability of simple correlations and the multiple correlation between w, Q_b, and M are as follows:

	w and Q_b	w and M	w and (Q_b, M)
Coefficient of variation (r^2)	0.71	0.55	0.83
Coefficient of correlation (r)	.85	.74	.91
Standard error in log units (Se)	.21	.26	.16

The coefficient of variation indicates that 71 percent of the variation of width from the mean is explained by the use of Q_b alone. Fifty-five percent of the variation of width from the mean is explained by the use of M alone. When Q_b and M are combined by multiple correlation analysis, 83 percent of the variation of width from the mean is explained. The use of M explains 40 percent of the variation unexplained by the use of Q_b alone.

Analyses of variance indicate that of all variables tested, Q_b and M are most significantly related to channel depth, for they are significant at the 0.01 level. Multiple correlation analysis yields the following equation:

$$d = \frac{M^{.38} Q_b^{.29}}{5.37} \qquad (2)$$

The results of tests of the reliability of simple correlations and the multiple correlation between d, Q_b, and M are as follows:

	d and M	d and Q_b	d and (M, Q_b)
Coefficient of variation (r^2)	0.13	0.10	0.41
Coefficient of correlation (r)	.35	.32	.64
Standard error in log units (Se)	.21	.21	.16

Partial correlation analysis shows that only 13 percent of the variation of depth from the mean is explained by the use of M and only 10 percent through the use of Q_b alone. When Q_b and M are combined in the above equation, 41 percent of the variation is explained. This is a considerable improvement, but the unexplained variation is still great.

In both cases the use of M improved the accuracy of calculation of channel width and depth. Considerable variability remains in the correlations, but perhaps some of this may be explained by the innate variability of ephemeral streams. In any event, the introduction of a parameter for sediment type seems necessary before the accuracy of calculations of channel width and depth can be improved.

Although within the limits of the data used channel width can be calculated with some confidence, the calculation of maximum depth is considerably less accurate. However, maximum depth can be calculated in another way, by the use of an equation developed previously for width-depth ratio. Using data collected at 69 stations, which include the 41 with runoff data, it was found (Schumm, 1960b) that the channel shape expressed as a width-depth ratio (F) is related to M as follows:

$$F = 255\ M^{-1.08} \qquad (3)$$

In a practical application of the above to the prediction of stable channel dimensions, width-depth ratio can be calculated by equation 3 and channel width by equation 1. Maximum channel depth can be calculated by the use of equation 2 or by dividing the calculated width obtained by equation 1 by the calculated width-depth ratio.

It is recognized that equations 1 and 2 are empirical equations developed from a small amount of existing data; however, they demonstrate that equations for the calculation of channel width and depth can be significantly improved by the introduction of a parameter for sediment type.

REFERENCES

Burmister, D. M., 1952, Soil mechanics: New York, Columbia Univ. Press, 155 p.

Dunn, I. S., 1959, Tractive resistance of cohesive channels: Am. Soc. Civil Engineers Proc., Soil Mechanics and Foundations Div. Jour., Paper 2062, v. 85, no. SM 3.

Leliavsky, Serge, 1955, An introduction to fluvial hydraulics: London, Constable and Co. Ltd., 257 p.

Nixon, Marshall, 1959, A study of the bank-full discharges of rivers in England and Wales: Inst. of Civil Engineers Proc., v. 12, p. 157–174.

Schumm, S. A., 1960a, The effect of sediment type on the shape and stratification of some modern fluvial deposits: Am. Jour. Sci., v. 258, p. 177–184.

——, 1960b, The shape of alluvial channels in relation to sediment type: U.S. Geol. Survey Prof. Paper 352–B, p. 17–30.

14. SOME FACTORS INFLUENCING STREAMBANK ERODIBILITY

By I. S. McQueen, Denver, Colo.

A device designed to simulate the erosive action of a gently flowing stream was used to erode prepared samples of sediments to determine what physical properties control the erosion processes.

Circular pats of disturbed sediments were prepared and their moisture content and packing were controlled. Preliminary results (tables 1 and 2) indicate qualitatively which soil characteristics are important in controlling susceptibility to erosion.

TABLE 1.—*Average erosion rates, in milligrams per square centimeter of erosion surface per minute, and physical properties of sediment samples from sources in Colorado and Wyoming*

Soil properties	Soils				
	Dry pack			Undisturbed	
	A	B	C	D	E
Air dried soils:					
Erosion rates..........mg/cm²/min	213.7	319.6	579	14.1	21.3
Moisture content..........percent	2.0	2.0	1.2		
Bulk density..........g/cc	1.58	1.62	1.61	1.56	1.83
Moist samples:					
Erosion rates..........mg/cm²/min	144	238	491	7.7	4.9
Moisture content..........percent	20.0	18.0	13.2	15.7	26.4
Bulk density..........g/cc	1.37	1.62	1.59	1.36	1.35
Grain size distribution:					
Sand > .0625 mm..........percent	22	30	35		
Silt .004 to .0625 mm..........do....	42	52	46		
Clay < .004 mm..........do....	36	18	19		
Median diameter (d₅₀)..........mm	.012	.037	.060		
Sorting coefficient (√d₇₅/d₂₅).........	6.44	2.83	2.13		

TABLE 2.—*Effects of packing and moisture content on erodibility of pats of soil A*

Pretreatment	Moisture (percent)		Bulk density (g/cc)		Erosion (mg/cm²/min)	
	Dry pack	Puddled	Dry pack	Puddled	Dry pack	Puddled
Freshly prepared pat..........	20	16.6	1.33	1.71	237.4	3.9
Seasoned at ⅓ atmosphere........	20.1	17.2	1.41	1.80	50.0	.4
Seasoned at ½ atmosphere:						
Sample 1.................	14.8	18.3	1.56	1.79	125.2	.3
Sample 2.................	14.9	18.3	1.51	1.81	140.9	.5
Air dry:						
Sample 1.................	2.0	1.9	1.65	1.92	205.8	91.2
Sample 2.................	2.0	1.9	1.51	2.12	221.7	115.7
Average.................			1.48	1.86	163.3	35.3

APPARATUS AND METHODS

The erosion device was designed to apply a uniform eroding force to the vertical face of a cylindrical pat of soil 3 inches in diameter and up to 3 inches high. The force applied is equivalent to that of a stream flowing past a vertical streambank with a flow velocity of 1.2 fps measured at a point 0.1 foot from the bank.

Circular pats of disturbed sediments were prepared by two methods (dry packed and puddled) as follows:

Dry packed.—300 g of soil passing a No. 10 U. S. Standard sieve (2 mm) was placed in a paper-lined Buchner funnel with a funnel tremie. After saturation from the bottom with distilled water a vacuum was applied to the funnel to consolidate the sample pat and reduce the moisture content to approximately field capacity.

Puddled.—300 g of soil passing a No. 10 U. S. Standard sieve (2 mm) was saturated with distilled water and mixed thoroughly. This was then transferred to a paper-lined Buchner funnel and a vacuum was applied to reduce the moisture content to approximately field capacity.

Following preparation, the pats were removed from the funnels and some of each kind of pat were tested in the erosion device immediately, some were seasoned on a Richards pressure plate at specified moisture tensions, and some were air dried before testing.

In addition to the disturbed soil pats, four relatively undisturbed samples of two soils (D and E, table 1) were obtained with a Lutz sampler. Two of these were saturated and then drained to field moisture condition on a Richards pressure plate before testing. The other two were air dried before testing on the erosion device.

The results of the erosion tests and the physical properties of the samples are shown in tables 1 and 2. Grain size distribution was not obtained for the undisturbed samples.

SOIL FACTORS AND ERODIBILITY

Among the important soil properties that control erosion are antecedent moisture, grain size distribution, packing, and chemistry. The soils used were chosen and the sample pats were prepared to indicate which soil properties have the greatest influence on erosion.

Differences in antecedent moisture cause differences in the erodibility of a soil (table 2). Air dry pats erode rapidly because of forces developed by the hydration of clay particles and reduced cohesion

between particles. This is more evident in the puddled than in the dry-packed samples because the expansion of the clay particles is more disruptive in a consolidated tightly packed sample. This hydration or "slaking" action may explain why intermittent streams sometimes have higher rates of erosion than perennial streams. The erosion rate of moist soils increases as moisture content increases.

The erodibility of soils is influenced by the grain-size distribution (table 1). In general, a poorly sorted sediment with a small median-grain size will resist erosion better than a well-sorted sediment with a larger median-grain size. This may not, however, hold true for coarse sands in streams with low velocities.

Packing includes a group of related properties such as porosity, bulk density, structure, texture, cementing, and pore-size distribution that are associated with the way the sediments are deposited and the forces applied to them since deposition. The two methods of sample preparation were used to simulate extremes of packing. The erosion rates of the dry-packed samples were from 2 to over 400 times as high as the corresponding puddled samples (table 2), indicating that differences in packing can cause extreme differences in the erodibility of a sediment.

The effect of chemistry on erodibility was not defined by the data obtained because it was masked by the effects of packing and antecedent moisture content.

CONCLUSIONS

This study was undertaken to explore the feasibility of determining in the laboratory an erodibility index for soils. For such an index to be of value, the erodibility of a given soil would have to be constant or would have to have a direct relation to some measurable property of the soil. The data obtained indicate that erodibility of a given soil is extremely variable. It is influenced by packing and by antecedent moisture content. Erosion rates determined on disturbed samples have little relation to actual erosion because the change in packing resulting from the disturbance changes the erodibility. Changes in moisture content and the freezing and thawing of natural undisturbed sediments may change their packing and hence change their erodibility so much that any index obtained would have little meaning in terms of actual field erosion rates.

Comparisons can be made between different sediments to determine which are more susceptible to erosion but the rate of erosion to be expected under a given set of conditions cannot as yet be determined from laboratory analyses of sediments.

---

15. AN EXAMPLE OF CHANNEL AGGRADATION INDUCED BY FLOOD CONTROL

By NORMAN J. KING, Denver, Colo.

Studies by Leopold and Miller (1956) show that ephemeral streams, like perennial streams, maintain a quasi-equilibrium between erosion and deposition. A change in one or more of the hydraulic factors affecting the stream system results in adjustments in the other factors accordingly. Below a stream junction, for example, the increased discharge should be accompanied by a corresponding increase in channel dimensions since $Q = wdv$, in which Q is discharge, w is width, d is depth, and v is velocity. Leopold and Miller (1956) show that width, depth, and velocity change in the downstream direction as simple power functions of discharge. Significantly, the power function relating width to discharge approximates the sum of the power functions relating depth and velocity to discharge. It follows, therefore, that width—the channel dimension in ephemeral streams that can be measured most easily—is also the most responsive to changes in discharge.

Measurements above and below arroyo junctions made by Miller (1958, table 4) show that with few exceptions the width below the junction of all but very small arroyos is equal to or greater than the width of the larger tributary. Based on the expression $a = k (b+c)$, in which a is the channel width below the junction and b and c are the tributary widths, Miller's measurements show the coefficient k to average 0.68.

If increased discharge forms a wider channel below a junction, it might be reasoned that a decrease
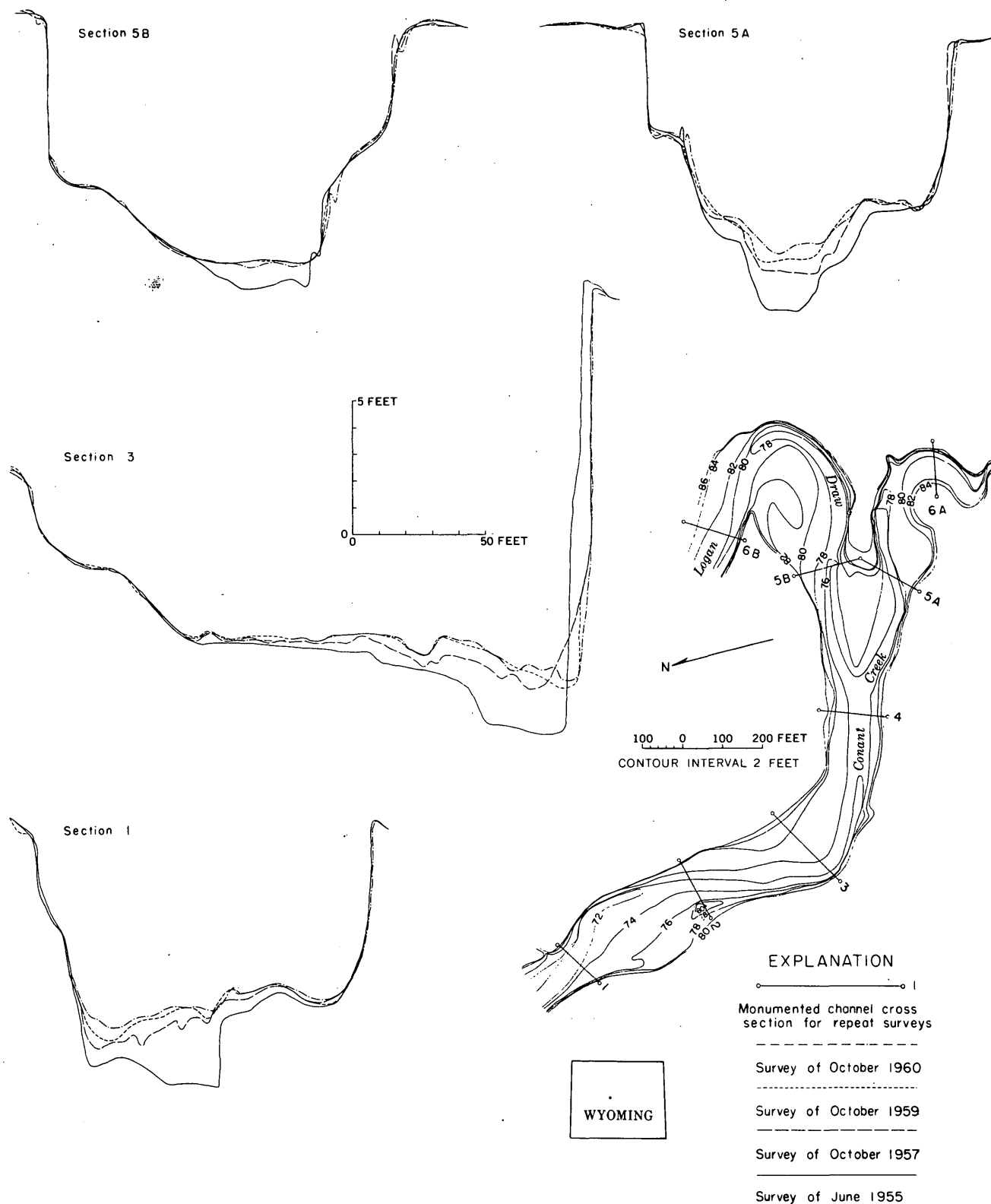
FIGURE 15.1.—Cross sections showing progressive aggradation in the channel of Conant Creek downstream from the mouth of Logan Draw, Fremont County, Wyo.

in discharge in one of the tributaries as a result of artificial controls would have the opposite effect. At first, aggradation would be expected because flow emerging from the uncontrolled tributary would spread across the wider reach thereby decreasing its depth and velocity of flow. According to Schumm and Hadley (1957) aggradation would continue until the bed of the channel becomes oversteepened; then the newly formed deposit would be trenched by headward erosion to form a channel that is once again in quasi-equilibrium with the discharge.

Completion by the Bureau of Land Management in 1953 of a flood-control and water-use project on Logan Draw in the southeastern part of the Wind River basin, Wyoming (King, 1959), is affording an opportunity to test the above reasoning, to measure the rates of aggradation, and to determine the time necessary to complete a cycle of channel adjustment. Logan Draw is an ephemeral stream that heads on Beaver Rim and trends generally northward to its junction with Conant Creek, which in turn drains through Muskrat Creek to the Wind River. Above the junction of Logan Draw and Conant Creek the drainage basins of the two streams are very much alike. Logan Draw has a channel length of 21.3 miles, a drainage area of 60.4 square miles, and a sandy bed that carries perennial underflow. Conant Creek above the junction has a channel length of 18.4 miles, a drainage area of 58.9 square miles, and a sandy bed that also carries perennial underflow. Both basins head at about the same altitude on Beaver Rim, experience the same general storm events, have similar topography, and are underlain by the same general rock types. It is probable, therefore, that both channels experience flow simultaneously, that their discharge is of about the same magnitude, and that the peak discharges reach the junction at about the same time. A comparison of channel cross sections above and below the junction (fig. 15.1) show an increase in width below the junction. Depending on the points of measurement the coefficient k of Miller (1958, p. 13) ranges from about 0.6 to 0.8.

Since completion of the water-control structures in Logan basin, no flows have reached the mouth of Logan Draw, whereas numerous runoff events have occurred in Conant Creek. The channel downstream from the junction has aggraded as expected (fig. 15.1). This in turn has induced aggradation in both tributary channels for a short distance above the junction (sections 5A and 5B, fig. 15.1). However, the newly formed deposit thins rapidly upstream so that no aggradation has occurred at section 6B (fig. 15.1) on Logan Draw and almost a foot of channel degradation has occurred at section 6A (fig. 15.1) on Conant Creek. In the aggraded reach the small inner channel that normally contained low flows has been largely filled and is now protected by vegetation that induces further aggradation (fig. 15.2). Repeat surveys (fig. 15.1) show that the greatest aggradation (2.7 acre-feet in the surveyed reach) occurred during the period 1955–57. Aggradation in the

FIGURE 15.2.—Conant Creek channel downstream from the mouth of Logan Draw (1960). Only vestiges remain of the inner channel that once carried low flows.

same reach during the periods 1957–59 and 1959–60 was 0.7 and 0.3 acre-foot respectively.

The number of runoff events, the amount of runoff, or the maximum discharge of Conant Creek during the period (1955–60) is not known. However, these data are available for Logan Draw and are believed to be representative of Conant Creek basin for reasons previously stated. These data show no unusual storm events or high discharges, but they do show a wide range in runoff during the periods between surveys. For example, runoff during the period 1955–57 was 28.3 acre-feet per square mile compared to 5.1 and 3.2 acre-feet per square mile during the periods 1957–59 and 1959–60, respectively. The data are admittedly meager, but they

suggest that runoff and the amount of sediment deposited in the reach shown on figure 15.1 are directly proportional.

REFERENCES

King, N. J., 1959, Hydrologic data, Wind River and Fifteen Mile Creek basins, Wyoming, 1947–54: U.S. Geol. Survey Water-Supply Paper 1475–A, p. 1–44.

Leopold, L. B., and Miller, J. P., 1956, Ephemeral streams—Hydraulic factors and their relation to the drainage net: U.S. Geol. Survey Prof. Paper 282–A, p. 1–37.

Miller, J. P., 1958, High mountain streams—Effects of geology on channel characteristics and bed material: New Mexico Bur. Mines and Mineral Resources Mem. 4, p. 1–52.

Schumm, S. A., and Hadley, R. F., 1957, Arroyos and the semiarid cycle of erosion: Am. Jour. Sci., v. 255, p. 161–174.

16.   SOME EFFECTS OF MICROCLIMATE ON SLOPE MORPHOLOGY AND DRAINAGE BASIN DEVELOPMENT

By RICHARD F. HADLEY, Denver, Colo.

Northerly facing slopes generally are steeper, less dissected, and support a more luxuriant growth of vegetation than southerly facing slopes, which often are deeply rilled and nearly barren. Because of these differences in erosion there is a tendency for the thalweg of the major stream channel in an east-west oriented basin to be shifted to the south side of the valley floor by the debris fans and alluvial aprons of eroded material derived from the south-facing slopes. This type of channel migration has caused an asymmetrical development of many drainage basins studied by the writer in the High Plains, by Bass (1929) in Kansas, Melton (1960) in southeastern Wyoming and southern Arizona, and Emery (1947) in southern California where geology and regional climatic conditions are distinctly different. An attempt is made here to state quantitatively the effects on basin morphology and drainage development due to direction of slope or the exposure, or more precisely, due to the microclimate.

A preliminary study was made in the Cheyenne River basin of east-central Wyoming in six small drainage basins underlain by the Fort Union formation of Paleocene age. The bedrock units are virtually flat-lying, thus minimizing the possibility of downdip migration of stream channels and asym-

metrical basin development that might be caused by folding.

Slope gradients are compared with exposure on figure 16.1 for an area of one-half square mile that includes part of the drainage areas of the six basins in which the other measurements were made. The slope of the land surface and direction of exposure were measured at 50 points equally spaced in a grid. The diagram shows that the steepest slopes face north, northeast, and northwest, whereas the gentlest slopes face south, southeast, and south-southwest.

Vegetation counts made on several slopes using line-intercept transects show that the plant cover on southerly-facing slopes is only 28 percent of that occurring on northerly-facing slopes. The sparse vegetation cover on southerly-facing slopes is probably caused by moisture deficiency due to rapid evaporation and melting of snow cover on the slopes that receive more direct solar radiation. Vegetation protects the slope from sheet erosion and rilling.

Drainage density, expressed as miles of channel per square mile of drainage area, was determined separately for both the north and south sides of the six drainage basins. The basins were divided into two sides by a line virtually parallel to the axial channel in each basin. Results of these computations,
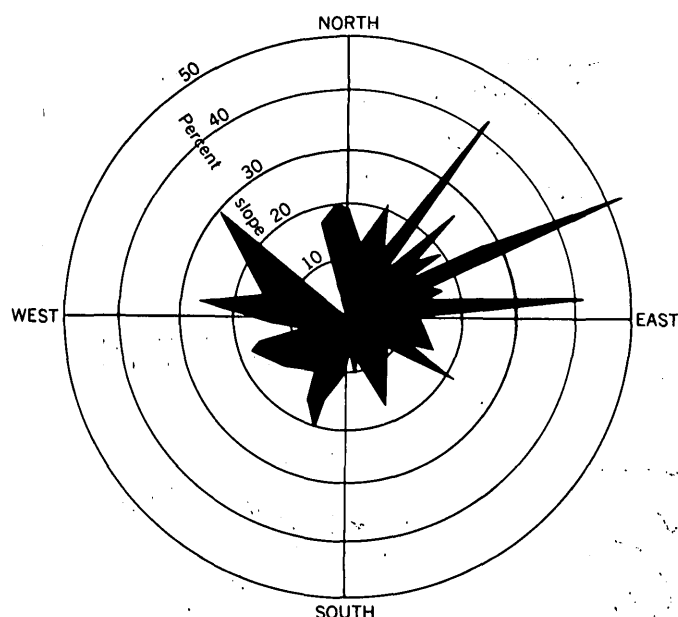
FIGURE 16.1.—Diagram showing relation between exposure and degree of slope at 50 localities.

tabulated below, show that the drainage density on the south-facing sides of the basins is more than twice that on the north-facing sides.

Drainage density, in miles per square mile, for six basins in east-central Wyoming

Drainage basin (fig. 16.2)	Area (sq miles)	Drainage density	
		North-facing side	South-facing side
1	0.16	5.0	15.1
2	.10	3.3	12.1
3	.09	6.2	17.0
4	.14	6.2	8.5
5	.76	5.0	8.5
6	.23	5.6	6.7
Average		5.2	11.3

Drainage basin asymmetry has been expressed as the difference in slope angles on the north- and south-facing slopes within a single basin (Emery, 1947; Melton, 1960). In the six drainage basins considered here, asymmetry is simply a measure of the deviation of the main channel from a position along the central axis of the basin. Several measurements were made of the distance from the main channel to both north and south drainage divides in each of the basins in figure 16.2 (p. B-34). The lines of measurement were perpendicular to the axis of the channel. The ratio of the mean value of all measurements from the channel to the northern

divide to the mean value of all measurements to the southern divide in each basin is termed the index of symmetry. An index of 1.0 denotes perfect symmetry. The indexes of symmetry range from 1.22 to 1.97 for the six basins indicating that the main channel in each of these basins has been displaced appreciably to the south by erosional debris derived from south-facing slopes.

A reconnaissance has been made of basins having a wider range of bedrock and climate to determine the relative importance of the several variables being considered. A group of drainage basins was selected along a traverse nearly parallel to the 15-inch rainfall line in the western part of the High Plains from central Texas to northwestern Nebraska. Thus, the variable parameter of mean annual rainfall, as it might affect slope erosion and plant life, was minimized and the differences caused by mean annual temperature, particularly the frequency of freezing and thawing, were accentuated. The basins in the southern part of the High Plains were underlain by the Ogallala formation of Pliocene age and the basins in northwestern Nebraska were underlain by the Brule and Chadron formations of Oligocene age. Measurements included degree and direction of slope and basin symmetry. These data are summarized as follows:

Number of basins	Location of basins	Average index of symmetry	Mean slope (percent)	
			North-facing	South-facing
4	Lat 32° N.; near Big Spring, Tex.	1.38	20	19
4	Lat 41° N.; near Cheyenne, Wyo.	0.92	24	23
2	Lat 43° N.; near Harrison, Nebr.	1.37	23	16

The indexes of symmetry for the basins near Cheyenne, Wyo. are contradictory to the indexes for the other basins studied, but this may be due to differences in the resistance to erosion of gravel in the Ogallala formation, which underlies the basins.

REFERENCES

Bass, N. W., 1929, Geology of Cowley County, Kansas: Kansas State Geol. Survey Bull. 12, p. 19.
Emery, K. O., 1947, Asymmetrical valleys of San Diego County, Calif.: Bull. So. Calif. Acad. Sci., v. 46, pt. 2, p. 61-70.
Melton, M. A., 1960, Intravalley variation in slope angles related to microclimate and erosional environment: Bull. Geol. Soc. America, v. 71, p. 133-144.
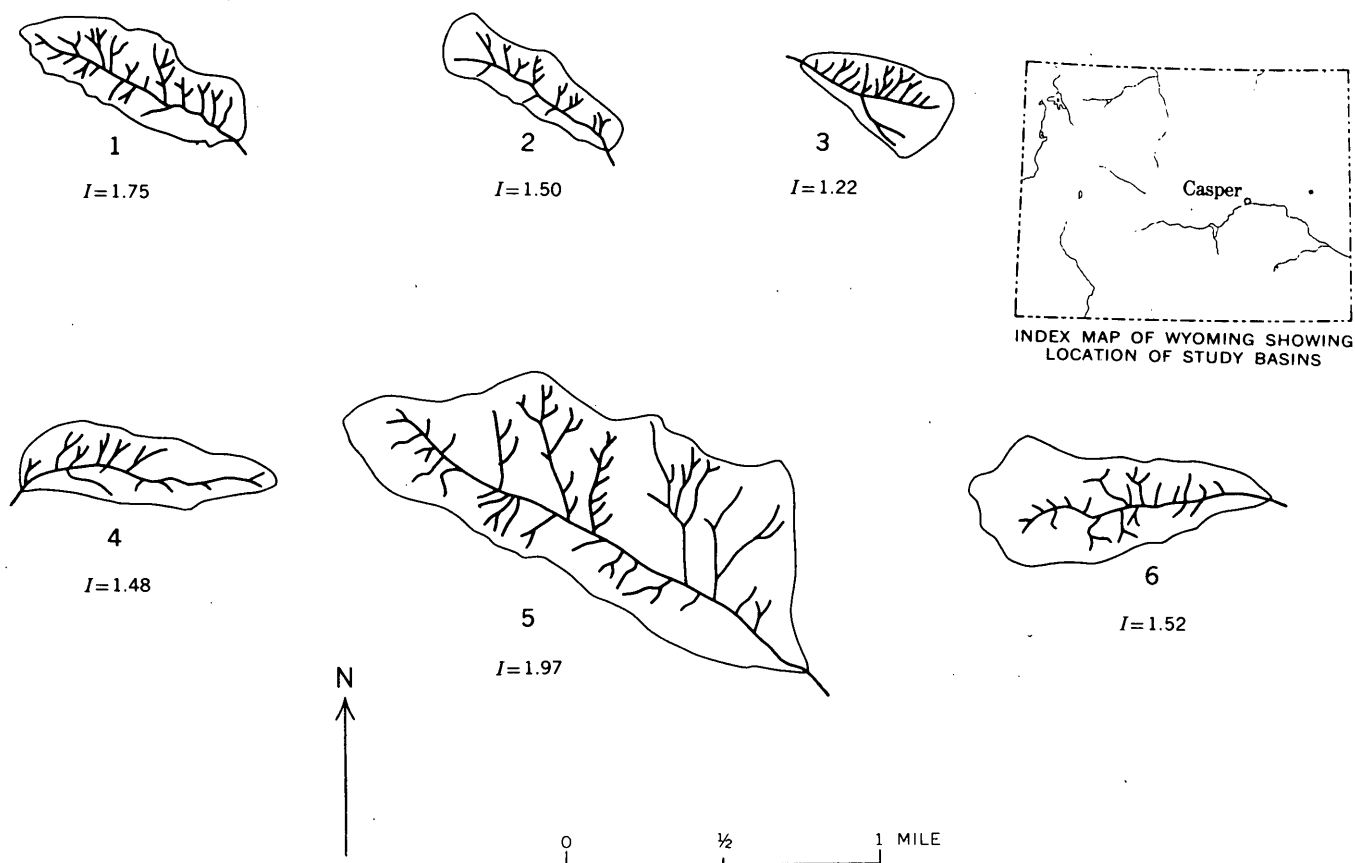
FIGURE 16.2.—Maps of drainage network in six basins. I is index of symmetry.

17.   HYDROLOGIC SIGNIFICANCE OF BURIED VALLEYS IN GLACIAL DRIFT

By STANLEY E. NORRIS and GEORGE W. WHITE, Columbus, Ohio

Work done in cooperation with the Ohio Department of Natural Resources, Division of Water

Bedrock valleys containing permeable outwash deposits are recognized as important sources of ground-water supply in glaciated regions. Commonly, in water-resources investigations of drift-covered areas, contour maps are made of the bedrock surface, and the buried valley systems are described and interpreted. These studies have provided data of considerable value, not only about ground-water resources, but also about the sequence and chronology of Pleistocene events. Similarly, buried valleys cut in till, rather than in bedrock, have been discovered in northeastern Ohio, in the course of current investigations on the hydrology of the glacial deposits. Such valleys have been observed in deep cuts for highways and strip mines, and recognized elsewhere by analysis of subsurface and hydrologic data. For example, near Ashland, Ohio, during construction of Interstate Route 71 in November 1958, a spring with a discharge of approximately 165 gallons per minute was opened by the power shovel when a deep cut was made in thick till. The water flowed from an interbedded deposit

of silt and sand containing a minor amount of coarse gravel which, at the orifice, occurs in a shallow valley in a gray unnamed till at what is now known to be a disconformity between this till and an overlying till recently named the Millbrook (White, written communication, 1961). The relatively large discharge of the spring strikingly demonstrates that large quantities of water can be transmitted through glacial materials of generally low permeability.

Permeable deposits in till-enclosed valleys constitute zones of relatively high permeability in the till, and are highly important in ground-water circulatory systems in areas of glacial terrane. They function much as do open joints and solution cavities in limestone in conducting water through an otherwise poorly permeable medium. The deposits they contain are typically referred to by well drillers as "gravel pockets" or "gravel stringers" in the till. Locally, the deposits are sources of water to farm and suburban wells; however, their significance as aquifers has been generally overlooked. These buried deposits are important as potential sources of water in many so-called "water-short" areas in northeastern Ohio, where thick till generally overlies relatively impermeable bedrock.

Some of the buried valleys in till appear to have been cut by streams in interglacial or interstadial times and filled during these times, as illustrated in figure 17.1. Others, as in the example in figure 17.2, appear to have been cut by meltwater streams from nearby ice and filled by ice readvance before any

FIGURE 17.2.—Sketch of cut made for superhighway, center of sec. 27, Perry Township, Richland County, Ohio, showing buried shallow valley in lowest of three tills. 1, Till, dark drab gray, calcareous; 2, till, olive-brown, calcareous; 3, silt, yellow; 4, gravel and coarse sand, calcareous, water-bearing; spring in each of 3 units; 5, till, bluish-gray, calcareous; 6, till, yellow-brown, calcareous; 7, till, dark-brown, calcareous below 4 feet; depth of leaching shown by dashed line.

weathering of the deposits could take place. The examples illustrated are typical of many that have been found. Some, as in figure 17.1, are completely preserved beneath a later till cover; others, as in figure 17.2, have had part of their fillings (and probably part of their upper valley walls as well) removed by erosion before or during later till deposition. These may be similar, in part, to buried meltwater channels in Minnesota described by Schneider and Rodis (1959), at least some of which may have been cut in glacial drift rather than bedrock.

These buried valleys are unconformities and occur at the contact between two tills. Individual tills in northeastern Ohio have been distinguished and mapped (White, 1960, and Art 176) on the basis of variations in their mineralogy, petrology, texture, color, and mechanical properties. Identification of till contacts in the subsurface provides clues to the location of buried valleys that may contain permeable sand and gravel deposits.

FIGURE 17.1.—Sketch of cut made for superhighway, NE¼-NW¼ sec. 33, Perry Township, Morrow County, Ohio, showing buried valley in till. 1, Till, very dark gray, calcareous; 2, till, yellow-brown or olive-brown, calcareous; 3, till, yellow-brown, noncalcareous; 4, sand, fine, calcareous, water-bearing; 5, silt, sandy, upper part noncalcareous; 6, clay, very dark gray; 7, silt and colluvium, highly weathered; 8, till, dark-brown, calcareous; 9, soil and weathered dark-brown till.

REFERENCES

Schneider, Robert, and Rodis, H. G., 1959, Aquifers in meltwater channels along the southwest flank of the Des Moines lobe, Lyon County, Southeastern Minnesota [abs.]: Geol. Soc. America Bull., v. 70, p. 1671.
White, G. W., 1960, Classification of Wisconsin glacial deposits in northeastern Ohio: U.S. Geol. Survey Bull. 1121-A. 12 p.

18.   PLAN TO SALVAGE EVAPOTRANSPIRATION LOSSES IN THE CENTRAL SEVIER VALLEY, UTAH

By RICHARD A. YOUNG and CARL H. CARPENTER, Richfield, Utah

Work done in cooperation with the Utah State Engineer

The Sevier River, as a source of irrigation water, is one of the most highly developed streams in the United States. At four points along its course in the central Sevier Valley the stream is completely diverted into irrigation systems, but return flow and ground-water discharge replenish the flow for downstream users. Severe drought conditions, extensive invasion by phreatophytes of low economic value, poor drainage practices, and outmoded irrigation systems have combined in the past decade to diminish the irrigation supply. A ground-water investigation, begun in 1956 and completed in 1960, has resulted in a greater knowledge of the hydrology of this highly complex river system.

The central Sevier Valley (fig. 18.1) occupies a syncline modified by a graben (fig. 18.2). The initial syncline was formed in late Jurassic time, and folding continued throughout Cretaceous and Tertiary times. The faulting that formed the graben may have started after Miocene time because it involves volcanic rocks of Oligocene or Miocene age. Renewed faulting took place in Pleistocene and Recent time and cut the Sevier River formation of late Pliocene or early Pleistocene age. The graben was subsequently filled with alluvium from the side slopes and with poorly sorted valley fill deposited by the ancestral Sevier River. Faulting, lava flows, and salt-dome intrusions have resulted in constrictions across the valley that form basins which contain large supplies of ground water. Largest of these basins are Circle Valley, the Sevier-Sigurd area, and the Gunnison-Sevier Bridge area.

The ground water in these basins is in approximate dynamic equilibrium; that is, ground-water inflow essentially equals ground-water outflow. The basins are filled to capacity and the ground water is under artesian pressure throughout much of the valley. The Sevier River acquires the overflow or natural ground-water discharge from each basin; this flow is diverted at some downstream point to satisfy irrigation demands.

It has long been considered impossible to utilize ground water to stabilize or increase the irrigation supply without interference with established water rights. Results of this investigation verify this premise but also suggest that some water now wasted by low-value vegetation may be salvaged. The confining materials that cover the artesian basins in the central Sevier Valley are permeable. Thus the artesian pressure from underneath, together with saturation by irrigation from above, raises the water table to a level within reach of phreatophytes. Dense growths of low-value phreatophytes cover much of the land surface overlying the artesian areas, and an estimated 60,000 to 70,000 acre-feet of ground water is lost by evapotranspiration annually from the three main basins. Much of the phreatophyte growth occurs along river banks, creek channels, drains, and irrigation canals. A coordinated program of phreatophyte eradication, improved irrigation management, and lowering of the high water table by improved drainage practices and by pumping of wells could salvage as much as 50 percent of the water annually lost to evapotranspiration by low-value plants.

It is difficult to estimate to what extent pumping may be utilized to salvage evapotranspiration losses without interference with established water rights, but careful development should minimize that interference. The following table gives a breakdown of estimated annual ground-water discharge from the three main basins:

Basin	Estimated loss by low-value phreatophytes (acre feet)	Other artificial and natural discharge from the ground-water basins. Includes springs, drains, flowing wells, and pumped wells (acre feet)
Circle Valley	10,000	5,000
Sevier-Sigurd	30,000	37,000
Gunnison-Sevier Bridge	30,000	18,000
Total	70,000	60,000

This table indicates that more water is lost by low-value phreatophytes than is used from all present ground-water sources. If half the water now lost to low-value phreatophytes could be salvaged by pumping without seriously affecting the present
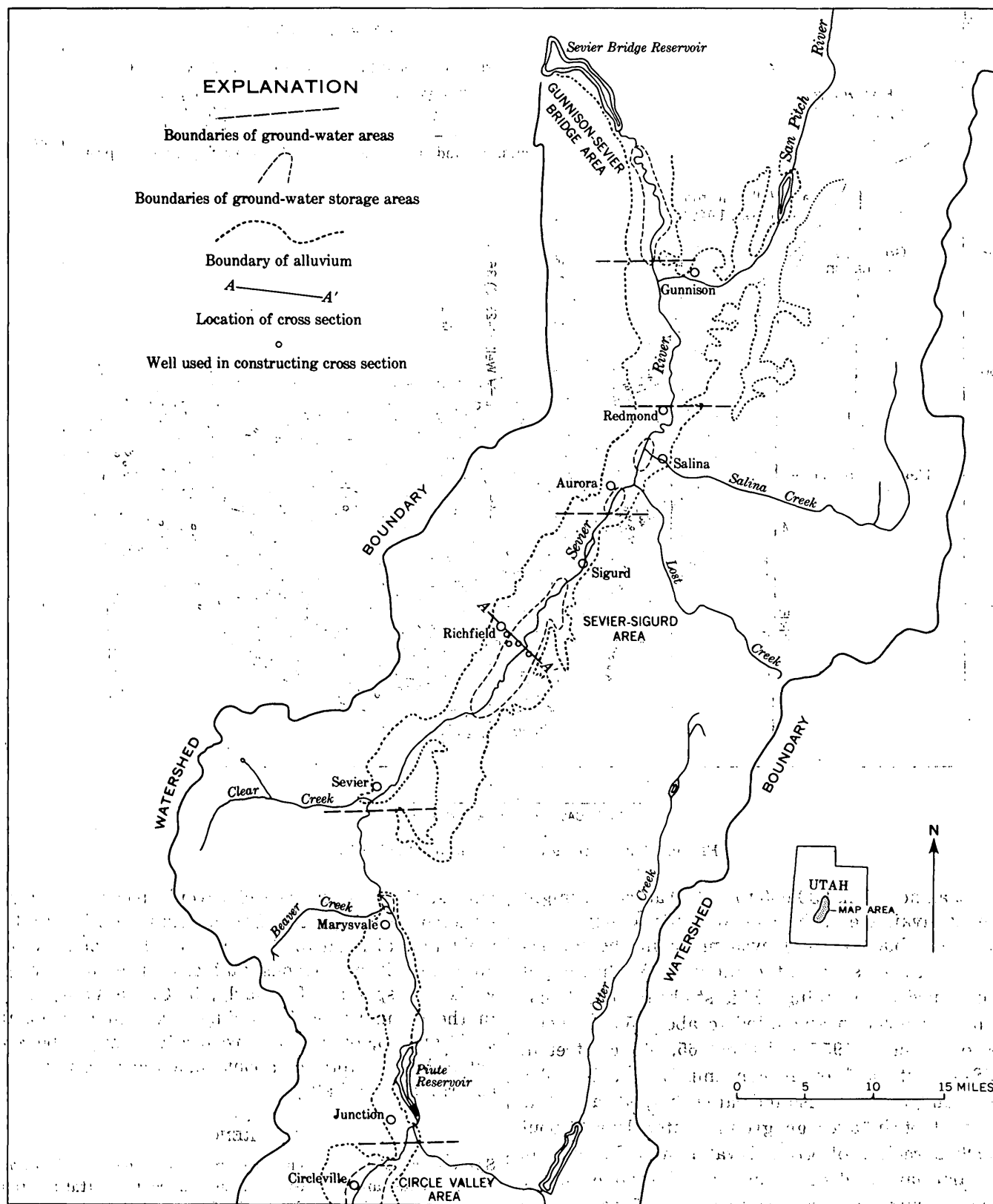
FIGURE 18.1.—Map of central Sevier Valley, Utah, showing areas of ground-water storage.
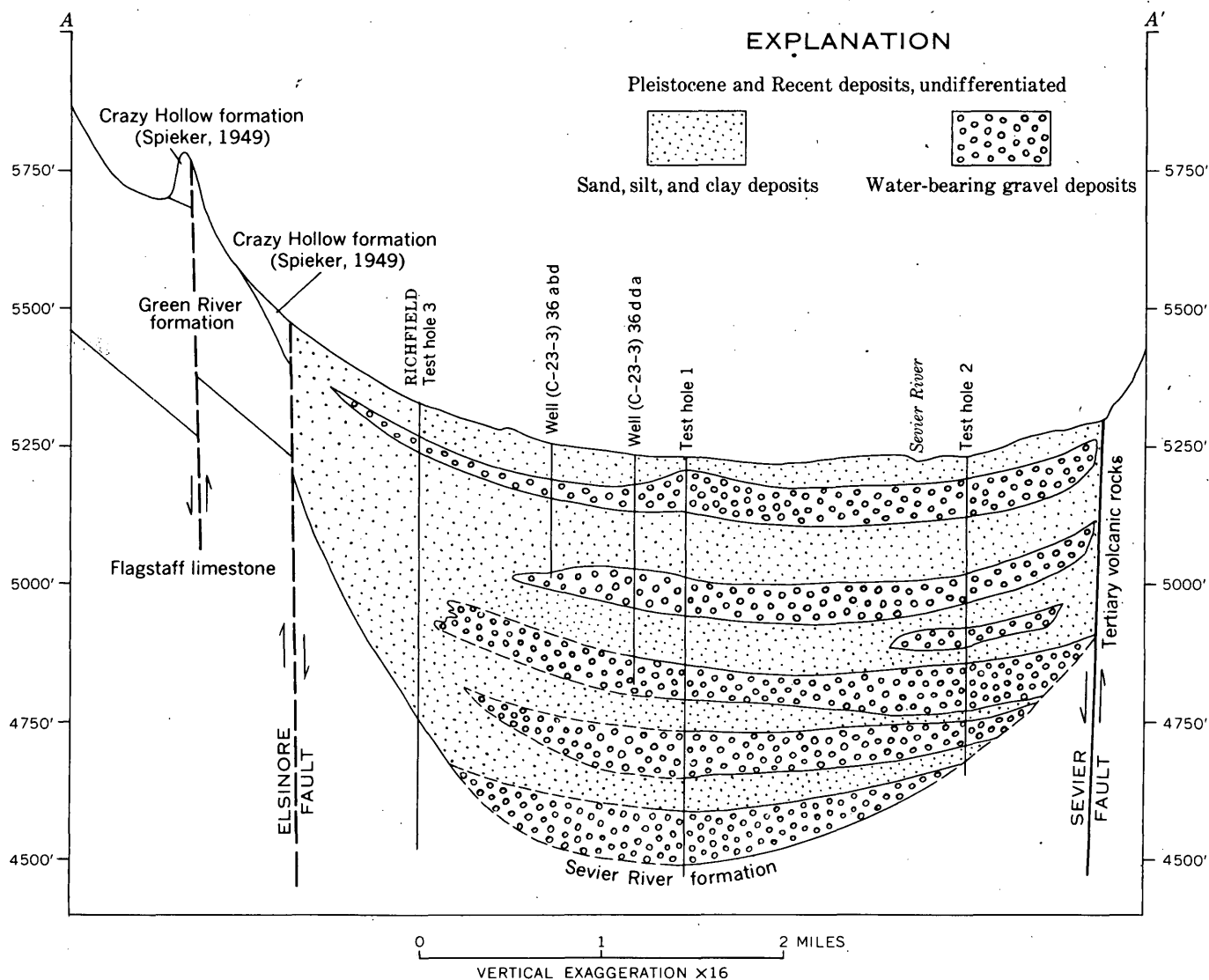
FIGURE 18.2.—Geologic section across Sevier Valley.

rights, an additional 30,000 to 35,000 acre-feet might be made available in the central Sevier Valley.

A water-budget study was made in the Sevier-Sigurd area to estimate the annual yield that might be obtained by pumping. This study indicated that evapotranspiration amounted to about 55,000 acre-feet of water in 1957 and about 65,000 acre-feet in 1958—about half of it consumptive waste. The water-budget study also indicated that, for a decline of one foot in average ground-water level, about 20,000 acre-feet of ground-water was discharged. The artesian head of the wells and springs in the Sevier-Sigurd area ranges from 1 to 7 feet above land surface. If large wells were spaced and constructed properly, the Sevier-Sigurd basin might yield an additional 15,000 acre-feet of water to wells annually without seriously affecting present flowing wells and springs. Similarly, in Circle Valley and in the Gunnison-Sevier Bridge area an additional 5,000 and 15,000 acre-feet respectively might be developed, for a total of about 35,000 acre-feet in the central Sevier Valley.

REFERENCE

Spieker, E. M., 1949, The transition between the Colorado Plateaus and the Great Basin in central Utah: Utah Geol. Soc. Guidebook no. 4, 106 p.

19.   RELATION BETWEEN STORAGE CHANGES AT THE WATER TABLE AND OBSERVED WATER-LEVEL CHANGES

By R. W. STALLMAN, Denver, Colo.

Meinzer (1923, p. 28) defined specific yield as the ratio of (a) the water removed by gravity drainage from a saturated rock to (b) the volume of the rock. Specific yield, both as a concept and as a characterization of the hydraulic properties of water-bearing materials, plays a useful role in hydrologic studies. However, in many situations the variables affecting the ground-water flow system are not interrelated adequately by the basic assumptions inherent in the specific yield concept. Specific yield may be defined algebraically as

$$q = S_y \frac{dh}{dt} \qquad (1)$$

where q is the rate of increase of water storage in the saturated zone (expressed as a length per unit time), S_y is the specific yield, and dh/dt is the slope of the curve water-table height (h) versus time (t). Equation (1) was adopted as the basis for the "transpiration-well method" by White (1932), was applied by Gatewood and others (1950) for measuring ground-water use by vegetation, and is still in use (Stallman, Art. 20).

If the position of the water table changes in response to changes in flow in the saturated zone, equation (1) may be considered an abbreviation of a differential equation which defines the relationship among head, storage, and aquifer-conductivity with respect to water movement. Two-dimensional flow through a homogeneous unconfined aquifer may be expressed approximately as

$$T \left[\frac{\partial^2 h}{\partial x^2} + \frac{\partial^2 h}{\partial y^2} \right] + W = S_y \frac{\partial h}{\partial t} \qquad (2)$$

in which T is the aquifer transmissibility, and W is the rate of recharge to the saturated zone expressed as a length per unit time.

Flow in the saturated zone as defined by equation (2) is illustrated in figure 19.1. The first term on the left side of equation (2) is an expression of the rate of change of storage due to variations in flow in the x-y plane. The accretion rate W also accounts for a part of the total rate of change of storage and is either added to or subtracted from the flow through the aquifer. Thus, the rate W, as defined, represents the rate of interchange of liquid between the saturated and unsaturated zones.
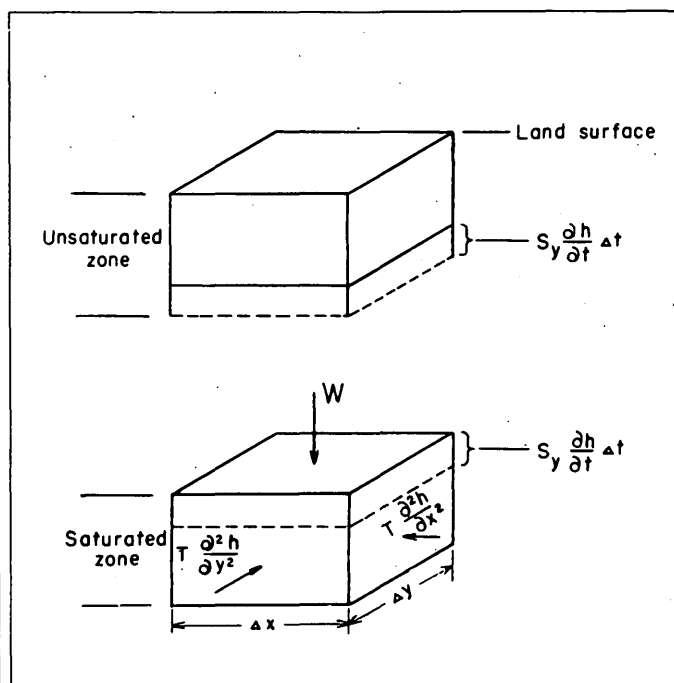
FIGURE 19.1.—Flow relations in the saturated zone.

In equation (1), q generally is assumed to be the rate at which water is removed from the saturated zone by evapotranspiration. This presumes that $q = W$, and that the first term in equation (2) is negligible compared with W. Though this might be considered a reasonable presumption, there has been little, if any, evidence developed to support it. From data for one small group of wells (Stallman, 1956, p. 454) it was determined that lateral flow changes, given by the first term in equation (2), accounted for more than one-third of the calculated W during a short period of observation. One set of water-level altitudes showed W to be a positive quantity while $\partial h / \partial t$ was negative according to analysis by equation (2). Thus, equation (1) would have indicated a water loss from the zone of saturation even though recharge occurred, as demonstrated by the analysis using equation (2). This one example suggesting analytical inadequacy in equation (1) cannot be considered conclusive evidence that equation (2) must always be used for calculating W; it emphasizes the need for a more cautious approach in assigning physical significance to q as calculated by means of equation (1).

In the derivation of equations (1) and (2) it was assumed that flow in the unsaturated zone does not affect the storage changes in the saturated zone. This assumption is inherent in the definition of specific yield. However, the saturated and unsaturated zones form one continuous hydraulic system. Thus, even though the hydraulic characteristics of both zones are different from one another, it should be evident from the fundamental concepts of hydraulics that any change of either head or velocity in the unsaturated zone will be reflected to some degree as a change of head everywhere in the saturated zone. Therefore, the water table will move in response to the distribution of flow in both contiguous zones, and it does not appear reasonable to relate the position of the water table solely to flow in the saturated zone as has been done in the derivation of equations (1) and (2).

The relation between discharge from the saturated zone and its effect on the position of the water table is shown schematically in figure 19.2. The column shown represents a flow tube which extends from some distant point where head is controlled by say, surface-water stages, through the aquifer, to a point on the land surface. Flow through the saturated zone discharges into the unsaturated zone, from which it is discharged into the atmosphere by evapotranspiration. At a particular discharge rate A, a given head distribution will be established in the system commensurate with all the hydraulic boundary conditions imposed on the aquifer. The resulting water-table position is at a. If the discharge through the surface is increased to rate B, the head at all points in the system will be decreased to accommodate the increase in velocity at all points in the system. Thus, with discharge at rate B the position of the water table is b. For a given value of A/B, the difference between the altitudes of a and b is chiefly dependent on the ratio of the hydraulic conductivities of the saturated and unsaturated zones to steady-state flow, and therefore is not necessarily directly related to a change of storage in the system.

Flow through the unsaturated zone is chiefly vertical. Thus, the extent to which the water-table position is dependent on flow in the unsaturated zone might be determined from study of vertical flow components in the vicinity of the water table. Field measurement of such vertical flow components is not practicable by the techniques now available, but recent work (Mosetti, 1960; Suzuki, 1960; and Stallman, 1960) has indicated the feasibility of measuring very small ground-water velocities by analysis of the underground temperature distribu-
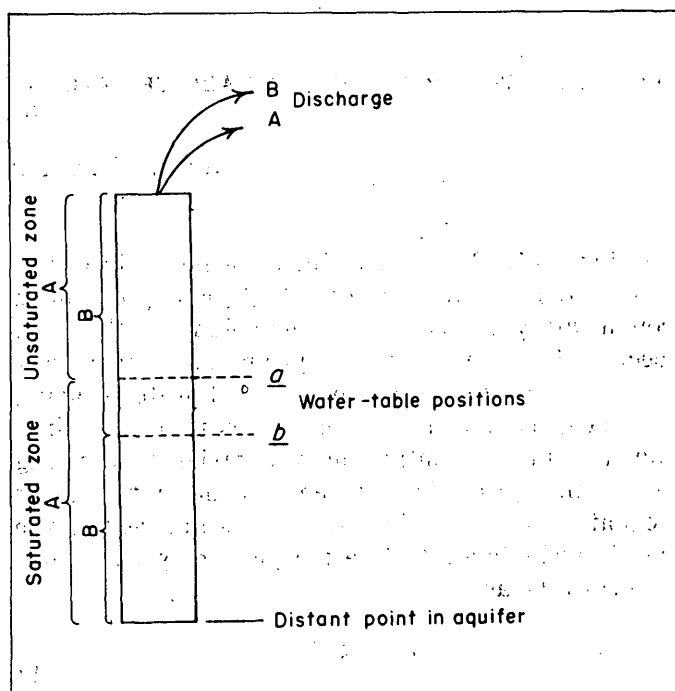
FIGURE 19.2.—Change of the water-table position due to changes in rate of discharge from the saturated zone.

tion. From such data, it should be possible to make a direct evaluation of the adequacy of equations (1) and (2), and to document the significance of the concept illustrated by figure 19.2.

REFERENCES

Gatewood, J. S., Robinson, T. W., Colby, B. R., Hem, J. D., and Halpenny, L. C., 1950, Use of water by bottom-land vegetation in lower Safford Valley, Arizona: U.S. Geol. Survey Water-Supply Paper 1103, 210 p.

Meinzer, O. E., 1923, Outline of ground-water hydrology: U.S. Geol. Survey Water-Supply Paper 494, 71 p.

Mosetti, Ferrucio, 1960, Thermometric study of the movement of ground water: (Presented orally by Prof. Mario Picotti), Internat. Union Geodesy and Geophysics Mtg., Helsinki.

Stallman, R. W., 1956, Numerical analysis of regional water levels to define aquifer hydrology: Am. Geophys. Union Trans., v. 37, p. 451–460.

——, 1960, Notes sur l'emploi de reseignements thermiques pour l'evaluation de la vitesse d'eau souterraine (Notes on the use of temperature data for computing ground-water velocity): Soc. Hydrotechnique de France, Jour. de L'hydraulique (Nancy, 1960), Quest. 1, Rapp. 3, p. 1–7.

Suzuki, Seitaro, 1960, Percolation measurements based on heat flow through soil with special reference to paddy fields: Jour. Geophys. Res., p. 2883–2885.

White, W. N., 1932, A method of estimating ground-water supplies based on discharge by plants and evaporation from soil—results of investigations in Escalante Valley, Utah: U.S. Geol. Survey Water-Supply Paper 659–A, 105 p.

20.   THE SIGNIFICANCE OF VERTICAL FLOW COMPONENTS IN THE VICINITY OF PUMPING WELLS IN UNCONFINED AQUIFERS

By R. W. Stallman, Denver, Colo.

Most algebraic equations used for analyzing pumping tests (see Theis, 1935; Wenzel, 1942; Ferris, 1949; Jacob, 1950; and Brown, 1953, for example) have been derived using the assumption that flow to wells occurs only in horizontal planes as shown schematically on figure 20.1A. However, where the upper surface of the ground-water body is unconfined and free to move as head in the aquifer changes, paths of flow originate at the unconfined or free surface and terminate at the well as shown schematically on figure 20.1B. Downward flow from the free surface is most pronounced during the initial period of pumping. The water table is lowered most rapidly near the pumped well, and in that region the effects of downward movement on flow become progressively less significant as pumping continues. Thus, it is generally recognized that flow conditions become essentially like those found in artesian aquifers only after long periods of pumping in unconfined aquifers. Nevertheless, it is common practice to utilize the equations defining artesian conditions to determine the characteristics of unconfined aquifers from pumping tests lasting only a few hours. Validity of such practice has been supported more by wishful thinking than by real evidence that the assumption of purely horizontal flow leads to a satisfactory analysis. Furthermore, there are as yet no quantitative data to indicate how long a period

of pumping is required before flow may be satisfactorily defined by the assumptions made in deriving analytical expressions like the Theis equation.

Boulton (1954) and Kirkham (1959) have developed methods for analyzing unconfined flow to wells, taking account of the vertical flow components at the water table. However, these methods are founded on other restrictive assumptions, and provide little or no direct evaluation of the effects of vertical flow components on radial flow relations. Without such an evaluation the need for more lengthy analytical methods is open to question.

The relative effects of vertical flow components on changes in head at the water table might be ascertained by a form of Boulton's (1954, p. 568) differential equation defining the free surface. For an anisotropic formation, Boulton's equation is

$$\frac{S_y}{P_r}\frac{\partial s}{\partial t} = \left(\frac{\partial s}{\partial r}\right)^2 + \left[\left(\frac{\partial s}{\partial z}\right)^2 - \frac{\partial s}{\partial z}\right]\frac{P_z}{P_r} \quad (1)$$

in which S_y is the specific yield, s is the decline of the water table, r is the distance from the center of the well to the point where the decline is observed, z is the distance upward from the confining bed to the point where the decline is observed, t is time, and P_r and P_z are the permeabilities for radial and vertical flow of water, respectively. If the value of the
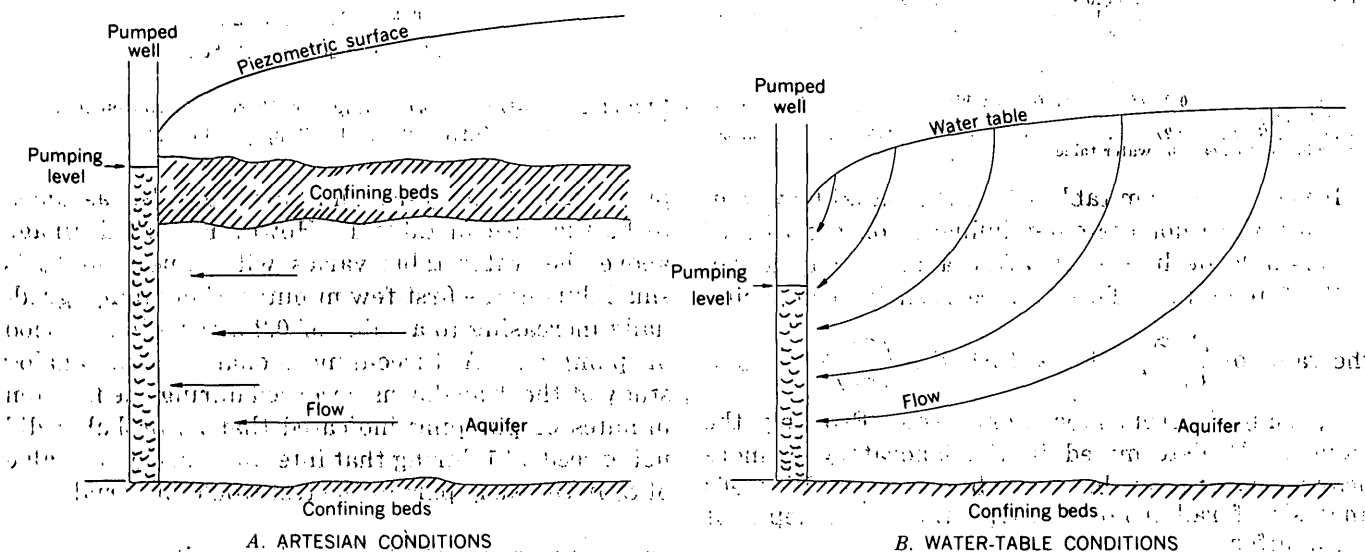
FIGURE 20.1.—Schematic diagrams of instantaneous flow paths.

left side of equation (1) is nearly equal to $(\partial s/\partial r)^2$, the effects of vertical flow components on the rate of water-table decline are negligible and the flow is essentially horizontal.

Pumping-test data collected near Grand Island, Nebr., by Wenzel (1942, p. 117–122) afford an opportunity for demonstrating, by means of equation (1), the effects of vertical flow components. The aquifer at the test site is composed of unsorted sands and gravels and is about 100 feet thick. The pumped well was 24 inches in diameter and was drilled to a depth of about 37 feet below the water table. Drawdowns were observed in 80 nearby observation wells. According to Wenzel's (1942, p. 125) analysis of the field data, $S_y = 0.2$ and $P_r = 140$ ft. per day, approximately. However, laboratory tests indicated (Wenzel, 1942, p. 118) that the value of P_r at the water table may be much less, say as low as 65 ft. per day.

Graphs of s versus r and s versus t are shown on figure 20.2 to illustrate the finite-difference method used for computing $\partial s/\partial t$ and $\partial s/\partial r$ from test observations. This procedure was applied also to drawdowns observed at other times after pumping began. Values of $\partial s/\partial t$ and $\partial s/\partial r$ computed for selected times are given in table 1.

TABLE 1.—*Drawdown rates and water-table gradients at $r = 50$ feet for Wenzel's (1942) Grand Island, Nebr., pumping test*

t (min)	$\dfrac{\partial s}{\partial t}$ (ft/day)	$\dfrac{\partial s}{\partial r}$	$\dfrac{S_y}{P_r}\dfrac{\partial s}{\partial t}$ [1]	$\dfrac{S_y}{P_r}\dfrac{\partial s}{\partial t}$ [2]	$\left(\dfrac{\partial s}{\partial r}\right)^2$
50	11.0	2.7×10^{-2}	1.6×10^{-2}	3.4×10^{-2}	7.3×10^{-4}
100	7.2	2.5×10^{-2}	1.0×10^{-2}	2.2×10^{-2}	6.2×10^{-4}
300	2.9	2.9×10^{-2}	4.1×10^{-3}	8.9×10^{-3}	8.4×10^{-4}
700	1.0	2.4×10^{-2}	1.4×10^{-3}	3.1×10^{-3}	5.8×10^{-4}
2,000	.45	2.4×10^{-2}	6.4×10^{-4}	1.4×10^{-3}	5.8×10^{-4}

[1] Letting $S_y/P_r = 0.2/140$ day per ft from Wenzel's (1942, p. 125) pumping-test analysis.
[2] Letting $S_y/P_r = 0.2/65$ day per ft from Wenzel's (1942, p. 118) laboratory value of P_r near the water table.

It is evident from table 1 that the radial flow components were not the chief influence on the rate of water-table decline, even after about a day and a half of pumping. This can be seen by comparing the value of $\dfrac{S_y}{P_r}\dfrac{\partial s}{\partial t} = 1.4 \times 10^{-3}$ with $\left(\dfrac{\partial s}{\partial r}\right)^2 = 5.8 \times 10^{-4}$, using P_r from laboratory tests. Probably the value of P_r determined in the laboratory is more nearly correct than the value obtained from Wenzel's analysis of radial flow through the entire depth of the aquifer.

The coefficient S_y, the specific yield, is generally considered a constant in the equations used for
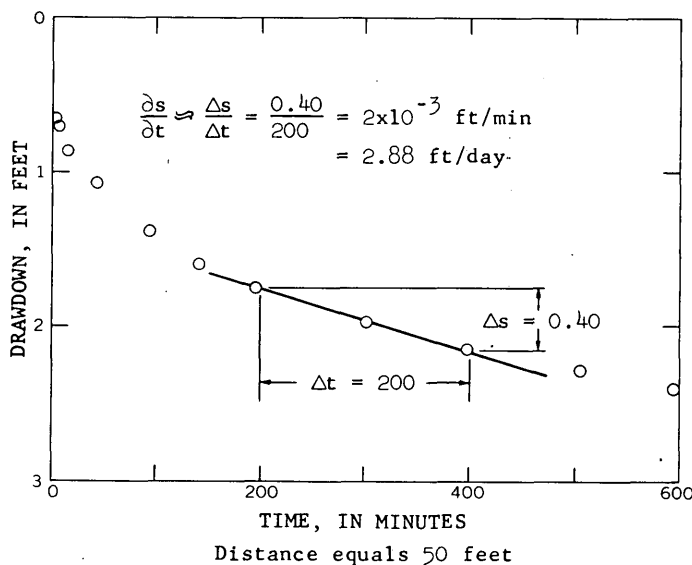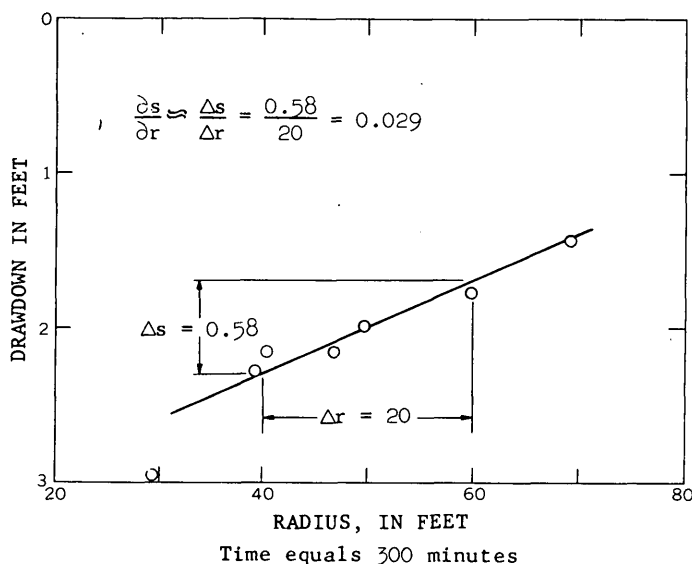
FIGURE 20.2.—Drawdown changes with respect to distance and time (after Wenzel, 1942, p. 117–122).

pumping-test analysis, and this was also assumed to be the case in table 1. However, pore drainage above the water table varies with time, and S_y is small during the first few minutes of pumping, gradually increasing to a value of 0.2 after a long period of pumping. A three-dimensional electric analog study of the drawdowns observed during the first ten minutes of pumping indicated that S_y probably did not exceed 0.01 during that interval. Such a low value of S_y in the early part of the test would materially decrease the value of $\dfrac{S_y}{P_r}\dfrac{\partial s}{\partial t}$, bringing it more nearly equal to $(\partial s/\partial r)^2$ than indicated in table 1.

It can be shown that, at any time

$$\frac{Q}{S_y} = 2\pi \sum_{r_w}^{\infty} \left(\frac{\Delta s}{\Delta t}\right)_r r \, \Delta r \qquad (2)$$

in which Q is the rate of pumping, and r_w is the radius of the pumped well. According to equation (2), $S_y = 0.11$ at $t = 50$ minutes in the Grand Island test. The error in the latter analysis is believed to be less than 20 percent. Thus, the conclusion drawn from table 1, that vertical flow components at this site are significant for at least 1½ days of pumping, is not affected appreciably by changes in S_y with respect to time.

The aquifer tested is not unique in thickness, specific yield, or permeability; therefore, vertical flow components may be important in most unconfined aquifers during the initial period of pumping. Equations based on the assumption that flow is essentially horizontal thus are likely to yield erroneous values of both P and S_y, and additional error due to assuming S_y constant may be expected if the duration of the test is only a few hours.

REFERENCES

Boulton, N. S., 1954, The drawdown of the water table under nonsteady conditions near a pumped well in an unconfined formation: Inst. Civil Engineers (British) Proc., p. 564–579.

Brown, R. H., 1953, Selected procedures for analyzing aquifer test data: Am. Water Works Assoc. Jour., v. 45, p. 844–866.

Ferris, J. G., 1949, Ground water, Chap. 7, in C. O. Wisler and E. F. Brater, Hydrology: New York, John Wiley and Sons, 408 p.

Jacob, C. E., 1950, Flow of ground water, Chap. 5, in Hunter Rouse, Engineering Hydraulics: New York, John Wiley and Sons, 1039 p.

Kirkham, Don, 1959, Exact theory of flow into a partially penetrating well: Geophys. Res. Jour., v. 64, p. 1317–1327.

Theis, C. V., 1935, The relation between the lowering of the piezometric surface and the rate and duration of discharge of a well using ground-water storage: Am. Geophys. Union Trans., p. 519–524.

Wenzel, L. K., 1942, Methods for determining permeability of waterbearing materials: U.S. Geol. Survey Water-Supply Paper 887, 192 p.

21. METHODS FOR STUDY OF EVAPOTRANSPIRATION

By O. E. LEPPANEN, Phoenix, Ariz.

The evaporation processes of nature are the largest item in the water balance of the United States. The 17 Western States receive 2,000 maf (million acre-feet) of precipitation of which MacKichan (1957) estimated that only 5 maf is used directly by man. C. H. Hardison (written communication Feb. 21, 1952) calculated the runoff from these states to be 440 maf—about 22 percent of the precipitation. J. S. Meyers (written communication, 1960) estimates that evaporation from free-water surfaces is 24 maf. Thus, most of the precipitation in the West returns to the atmosphere by evapotranspiration from vegetation and land surfaces.

Most quantitative estimates of evapotranspiration are made by considering long-term averages of rainfall and runoff in a basin, or by analysis of irrigation records. These methods are not suitable for estimating short-term water demands or for assigning relative water-use indices to various vegetation-covered surfaces. More sensitive methods are desirable not only for direct practical application—but also for development of a better understanding of the physical mechanism involved, so that wasteful evapotranspiration can be controlled.

The most direct method of measuring evapotranspiration is a water budget: first, the inflow (precipitation, irrigation) and outflow (seepage, runoff) are measured, then after accounting for changes in soil-moisture storage, the net loss is attributed to evapotranspiration. This method fails, except under very special circumstances, because of difficulties in measurement.

Another method is the energy budget. Directly analogous to the water budget, the energy budget accounts for inflow, outflow, and storage of heat. The singular advantage of this method lies in the fact that the term that describes evapotranspiration is large numerically, having been weighted by the energy necessary for change-of-phase. Measurement errors in water flow become less significant. The

energy budget has been applied successfully to the measurement of evaporation from lakes and there is no theoretical reason why it could not be applied also to measurement of evapotranspiration.

Experiments have been made in an area in eastern Nebraska to test the application of the energy budget. A site near Fairmont, Nebr., was carefully chosen in a loess plain with soil formed on Peorian loess. Below the Peorian, at a depth of about 5 meters, lies the Loveland loess. Nearby wells indicated ground water to be at depths exceeding 30 meters. The surface has a slope of about 1:750, and no runoff was anticipated or observed. The area had been seeded with alfalfa late in the previous season. The alfalfa grew slowly in April, rapidly in May, matured in June, and was mowed on June 30. A second crop then grew, but somewhat less vigorously.

A water budget was first computed using the records from a local raingage and soil moisture data that were obtained from six sets of soil samples taken during the study. Information from a neutron-scattering soil-moisture meter, which was used several times weekly, allowed interpolation between samplings. Deep seepage, or percolation, was considered to be zero because of the existence at a depth of 5.2 meters of a buried soil that apparently was very impervious to soil-moisture movement.

The results of the water budget are shown in table 1.

TABLE 1.—*Evapotranspiration computed from the water budget for the experimental site at Fairmont, Nebr., for selected periods, in centimeters of water*

Period, 1958		Change in soil-moisture storage	Precipitation	Evapo-transpiration
From	To			
April 14	May 13	+ 1.9	7.1	5.2
May 13	June 9	−23.0	4.0	27.0
June 9	July 15	+ 9.3	15.2	5.9
July 15	August 5	− 2.7	9.5	12.2
August 5	September 2	−13.2	5.6	18.8
September 2	September 29	+ 6.4	14.2	7.8
Total			55.6	76.9

Measurement of items in the energy budget required extensive instrumentation. A net-exchange radiometer measured thermal radiation, the major energy source. Changes in heat storage in the soil, although small, were measured. Heat brought in by rain was accounted for. Heat conducted from the surface of vegetation as sensible heat was computed using the ratio developed by Bowen (1926)[1]. The

[1] Because a practical field instrument to measure the conducted heat is not yet available, the Bowen ratio, which relates heat lost by conduction to heat lost by evaporation, has been widely used to compute conducted heat.

temperature and humidity gradients above the surface were determined by measurements in the vegetation and at levels of ½, 1, 2, and 8 meters above the vegetation. Anemometers were also installed at these levels. About 1.4 million observations of temperatures and humidities were analyzed using an electronic computer.

Evapotranspiration, calculated from the water budget during a 168-day season, was 0.46 cm per day. Evapotranspiration, calculated from the energy budget ranged from 0.57 cm to 0.92 cm per day, depending on the levels above the surface that were used in selecting the meteorological data needed to calculate the Bowen ratio. These results suggest that the Bowen ratio, as calculated in this experiment, is not applicable to evapotranspiration measurement.

To investigate the data for seasonal bias, and to observe the effect of changing the length of the observation period, evapotranspiration was calculated for six periods of about a month each. Results are listed in table 2. The levels above the vegetation used in calculating the Bowen ratio are ½ and 1 meter.

TABLE 2.—*Comparison of water-budget and energy-budget evapotranspiration rates for intervals throughout the season, in centimeters of water per day*

Period, 1958		Water-budget evapotranspiration	Energy-budget evapotranspiration
From	To		
April 14	May 13	0.18	0.41
May 13	June 9	1.00	.79
June 9	July 15	.16	.58
July 15	August 5	.58	.55
August 5	September 2	.67	.58
September 2	September 29	.29	.42

The results for the shorter periods show no better agreement with the water budget than do the seasonal figures.

Comparison with data from lakes indicates that the conducted-energy term is a large item in the evapotranspiration energy budget but is a small item in a lake-evaporation energy budget. The reason is that water absorbs and stores most of the radiant energy falling upon it, but vegetation converts radiant energy to a combination of conducted and latent heat. Thus, the theory and method of calculating the Bowen ratio becomes critical in the evapotranspiration energy budget. The energy-

budget method is, however, theoretically correct, and further analyses of the data from this and similar experiments in determining the conducted energy should resolve discrepancies in results from the water-budget and energy-budget methods.

REFERENCES

Bowen, I. S., 1926, The ratio of heat losses by conduction and by evaporation from any water surface: Phys. Rev., v. 27, p. 779-787.
MacKichan, K. A., 1957, Estimated use of water in the United States, 1955: U.S. Geol. Survey Circ. 398, 18 p.

22. WATER MOVEMENT AND ION DISTRIBUTION IN SOILS

By R. F. MILLER and K. W. RATZLAFF, Denver, Colo.

Divalent calcium and magnesium both have greater replacing ability than monovalent sodium in ion exchange reactions with soil colloids (Kelley, 1948, p. 57). Therefore, when calcium and magnesium exceed the sodium in water moving through the soil, the proportion of calcium and magnesium in solution should decrease in the direction of water movement as a result of adsorption to ion exchange surfaces, and the proportion of sodium should increase in the direction of water movement as a result of its displacement from ion exchange surfaces (Rible and Davis, 1955).

Because of this relation, the direction and pattern of moisture movement in soils can be interpreted from soil chemistry. The depths to which untilled soils in arid and semiarid climates are most frequently wetted also are reflected by the relative concentrations of soluble ions in the soil profiles.

The greater solubility of sodium salts also permits sodium to move farther through the soil in the direction of water movement than calcium or magnesium. This is especially true when the ions in solution are concentrated by the processes of evaporation and the use of water by plants—a condition that causes precipitation of the less soluble salts (Gardner and others, 1957).

The relations between water movement and ion distribution in two soils with different internal drainage characteristics have been studied by the writers. The relative proportions of soluble calcium plus magnesium and sodium in consecutive vertical portions of the two soil profiles are expressed as differences in soluble sodium percentage (SSP).

$$\text{SSP} = \frac{\text{Soluble Na}}{\text{Soluble Na} + (\text{Ca} + \text{Mg})} \times 100$$

A residual coarse-silt loam soil near Palo Alto, Calif., (table 1 and fig. 22.1) is characteristic of soils with unimpeded internal drainage. Winter rainfall frequently provides enough moisture to wet the base of the soil profile. The soluble sodium percentage increases with depth, as a result of progressive adsorption of calcium and magnesium from soil water onto the ion exchange surfaces, whereas sodium is displaced from ion exchange surfaces into the water moving down through the soil profile. A gradual decrease in total salts in the soil with depth reflects the loss of ions from solution to ion exchange surfaces and frequent flushing of the soil. A higher concentration of both calcium plus magnesium and sodium in the top five inches of soil, as compared with the next layer below, indicates that precipitation of salts occurs as they are concentrated by evaporation.

An alluvial medium-silt loam soil near Fort Apache, Ariz., (table 1 and fig. 22.1) is characteristic of deep permeable soils that commonly do not receive enough moisture to become wet throughout the profile. The A horizon is moistened by summer showers, but the B horizon is moistened to field capacity primarily by snowmelt. Moisture apparently moves down into the C horizon only in response to temperature and moisture tension gradients. Apparently the buried B horizon impedes capillary movement of water downward.

The increase in soluble sodium percentage from the 2A horizon into the 1A horizon reflects capillary rise of water as the surface soil dries. The decrease in calcium plus magnesium and the increase in sodium indicate that ion exchange is primarily responsible for the increase. The gradual increases in
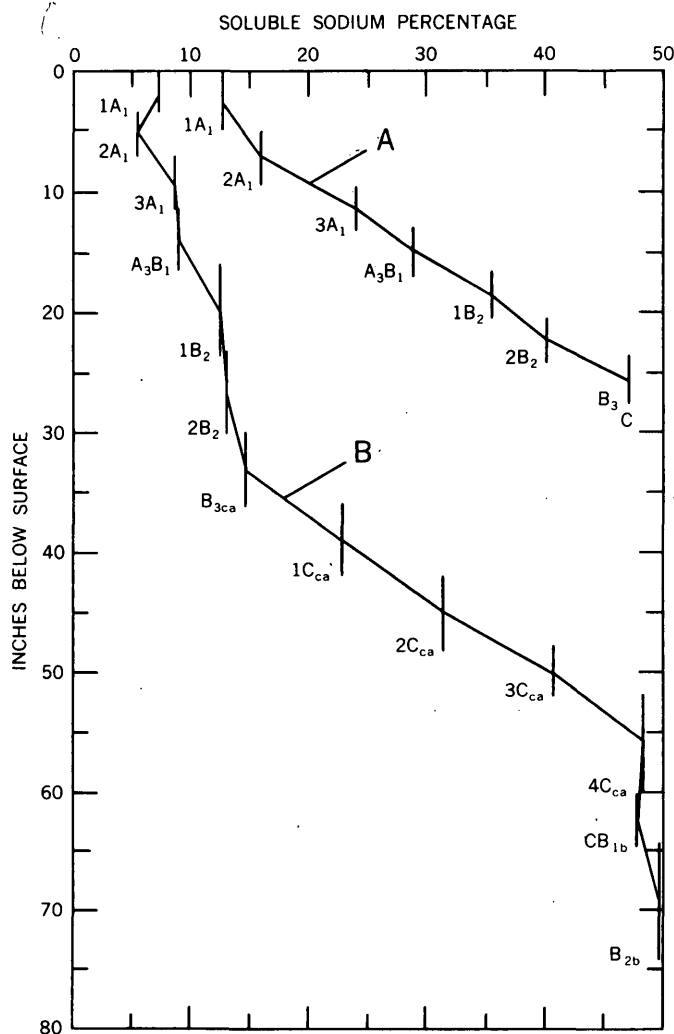
FIGURE 22.1.—Changes in soluble sodium percentage (SSP) with depth through a residual coarse-silt loam soil near Palo Alto, Calif. (curve A), and an alluvial medium-silt loam soil near Fort Apache, Ariz. (curve B). Numbers and letters to left of curves designate soil horizons.

TABLE 1.—*Distribution of ions with depth in soils*

Residual coarse-silt loam soil near Palo Alto, Calif.				Alluvial medium-silt loam soil near Fort Apache, Ariz.			
Depth below soil surface (Inches)	Extract from saturated soil paste (Milli-equivalents per liter)			Depth below soil surface (Inches)	Extract from saturated soil paste (Milli-equivalents per liter)		
	Ca+Mg	Na	Total		Ca+Mg	Na	Total
0-5.......	6.69	0.97	7.66	0-3........	4.00	0.31	4.31
5-9.......	3.90	.78	4.68	3-7........	4.88	.30	5.18
9-13......	3.16	.97	4.13	7-12.......	4.40	.30	4.70
13-17......	2.30	.97	3.27	12-17......	5.20	.38	5.58
17-20.5.....	2.17	1.19	3.36	17-24......	4.20	.46	4.66
20.5-24.....	1.83	1.23	3.06	24-30......	4.00	.46	4.46
24-27......	1.54	1.37	2.91	30-36......	4.88	.85	5.73
				36-42......	4.08	1.25	5.33
				42-48......	5.52	2.54	8.06
				48-54......	5.60	3.81	9.41
				54-60......	8.00	7.55	15.55
				60-65......	12.12	11.10	23.22
				65-74......	17.60	17.10	34.70

accumulation of moisture above the more porous calcareous C horizon; but there is no evidence of capillary rise from this zone of possible moisture accumulation. The top of the C horizon is apparently the depth to which water frequently penetrates and is retained at or near the field storage capacity.

Movement of some moisture down through the C horizon by capillarity is reflected by the sharper increase in soluble sodium percentage with depth. This sharper increase indicates precipitation of calcium from solution and is apparently the result of both ion exchange and salt solubility. The increase in soluble sodium percentage in both directions from the top of the B horizon reflects capillary rise from accumulated moisture above the impeding B_{2b} horizon and some movement of water down through the impeding B_{2b} horizon. The accumulation of salts but no increase in soluble sodium percentage reflect the entrapment and evaporation of accumulated water at the impeding zone.

soluble sodium percentage to the base of the B horizon and the little corresponding increase in total ion concentration reflect downward movement of water and frequent flushing. The increases in soluble sodium percentage are attributed primarily to ion exchange. The slight accumulation of calcium plus magnesium at the base of the B horizon reflects some

REFERENCES

Gardner, R., Whitney, R. S., and Kezer, A., 1957, Slick spots in Western Colorado soils: Colorado State College Exp. Sta. Tech. Bull. 26, p. 1-13.

Kelley, W. P., 1948, Cation exchange in soils: New York, Reinhold Pub. Corp., 144 p.

Rible, J. M., and Davis, L. E., 1955, Ion exchange in soil columns: Soil Science, v. 79, p. 41-47.

23.   COMPRESSION OF ELASTIC ARTESIAN AQUIFERS

By S. W. Lohman, Denver, Colo.

The concepts of the occurrence of water in artesian aquifers have changed considerably in the last 35 years. Artesian aquifers formerly were considered to have only the properties of conduits for conducting water from the recharge areas to the points of discharge (such as wells) and to have no property of storage, as now known. Confining beds were regarded as impermeable, whereas we now know that an artesian aquifer may be confined by a relatively impermeable stratum or simply by a stratum having permeability lower than that of the aquifer. Only wells that flowed at or above the land surface were considered artesian by many earlier workers. Now artesian wells are considered by most authorities to be those in which the water is confined under pressure beneath a relatively impermeable stratum or a stratum of lower permeability than the aquifer, and in which the water rises above the point at which it is first found in drilling.

Meinzer and Hard (1925, p. 90–93) were the first to recognize that an artesian aquifer does not perform like a rigid system, but as one having volume elasticity and hence variations in storage capacity with changes in the internal buoyant force due to changes in artesian head. The evidence that a large part of the water discharged from artesian wells came from storage by compression of the aquifers with loss of artesian head led to Meinzer's classic theory of the compressibility and elasticity of artesian aquifers (1928).

It has long been recognized that two types of compression are involved: elastic compression of elastic media, such as a clean sand or sandstone; and plastic deformation of bodies, lenses, or beds of clay in or adjacent to the aquifer. The amount of elastic compression, with which the remainder of this paper is chiefly concerned, is small but nevertheless significant. The amount of plastic deformation of clay bodies may be rather large, and has caused subsidence of the land surface of from a few feet to several tens of feet where artesian water or oil has been withdrawn in large quantities. (See Gilluly and Grant, 1949; Winslow and Doyel, 1954; Poland and Davis, 1956; and the report of the Inter-Agency Committee on Land Subsidence in the San Joaquin Valley (1958); see also papers in this volume by Poland, Art. 25; Lofgren, Art. 24; Miller, Art. 26).

The next important step in our understanding of the manner in which artesian aquifers release water from storage was the development by Theis (1935), through analogy with the mathematical theory of heat conduction, of an equation for the non-steady-state flow of ground water through permeable media to a discharging well, which is

$$s = \frac{Q}{4\pi T} \int_{\frac{r^2 S}{4Tt}}^{\infty} (e^{-u}/u)\, du \qquad (1)$$

in which s is the drawdown in water level at distance r from a well discharging at constant rate Q from an extensive homogeneous and isotropic aquifer having a coefficient of transmissibility T (permeability times thickness) and a coefficient of storage S after a period of discharge t. This important equation, which for the first time introduced the elements of time (t) and coefficient of storage (S), has become the foundation of quantitative ground-water hydrology. The coefficient of storage (S), which is a dimensionless constant, was defined by Theis (1938, p. 894) as " * * * the volume of water, measured in cubic feet, released from storage in each column of the aquifer having a base 1 foot square and a height equal to the thickness of the aquifer, when the water table or other piezometric surface is lowered 1 foot." Thus, if in an artesian aquifer having a coefficient of storage of 2×10^{-4} (0.0002) the head is lowered 400 feet in an area of one square mile (about 2.79×10^7 ft²), more than 2.23×10^6 ft³ of water is released from artesian storage.

Jacob (1940, p. 575, 576) pointed out that the release of water from artesian storage involves not only compression of the aquifer but also elastic expansion of the contained water, and that the components of the coefficient of storage may be defined by

$$S = \gamma \theta m \left[\frac{1}{E_w} + \frac{b}{\theta E_s} \right] \qquad (2)$$

in which S is the coefficient of storage; γ is the specific weight of water (62.4 lb ft⁻³/144 in² ft⁻² = 0.434 lb in⁻² ft⁻¹); θ is the porosity of the aquifer; m is the thickness of the aquifer, in feet; E_w is the bulk modulus of elasticity of water (3×10^5 lb in⁻²); b is the effective part of unit area of the aquifer that

responds elastically [1]; and E_s is the bulk modulus of elasticity of the aquifer. It is convenient to use the reciprocal β in place of $\frac{1}{E_w}$, the value of β being 3.3×10^{-6} in² lb⁻¹.

By combining Hooke's Law of elasticity with equation (2), I shall propose an equation for determining the amount of elastic subsidence or compression from other known factors. Hooke's Law states that, within the elastic limit, strain is proportional to stress. In notation convenient to the problem, Hooke's Law may be written

$$\Delta m = \frac{m}{E_s}\Delta p \qquad (3)$$

in which Δm is the change (reduction) in thickness of the aquifer (amount of elastic subsidence), in feet; m and E_s are as defined for equation (2); and Δp is the change (reduction) in artesian pressure, in lb ft⁻².

Dividing both sides of equation (2) by γ, assuming b to be unity, substituting the reciprocal β for $\frac{1}{E_w}$, and expanding, equation (2) becomes

$$\frac{S}{\gamma} = \theta m \beta + \frac{m}{E_s} \qquad (4)$$

Equation (3) may be written

$$\frac{m}{E_s} = \frac{\Delta m}{\Delta p} \qquad (5)$$

Combining equations (4) and (5) and solving for Δm gives the desired equation

$$\Delta m = \Delta p \,(S/\gamma - \theta m \beta) \qquad (6)$$

Thus, in an elastic or reasonably elastic artesian aquifer, for which S is known from a pumping (Theis, 1953) or flow (Jacob and Lohman, 1951) test, θ is known from core or sample tests, m is known from a driller's log or electric log, it is possible to compute from equation (6) the amount of elastic subsidence of the land surface (compression of aquifer) Δm, for a given regional decline in artesian pressure Δp. For example, although studies of the Denver artesian basin are not yet completed, preliminary information (George H. Chase, U.S. Geological Survey, written communication, Jan. 23, 1961) indicated that average values for wells in the basal sandstone and conglomerate of the Arapahoe formation (Upper Cretaceous) in the Denver metro-

politan area are about: $S = 5 \times 10^{-4}$, $\theta = 0.33$, $m = 200$ ft, and $\Delta p = 260$ lb in⁻² (600 ft decline in head). Using equation (6) [2]

$$\Delta m = 2.6 \times 10^2 \text{ lb in}^{-2} \left[(2.31 \text{ ft lb}^{-1}\text{ in}^2) \,(5 \times 10^{-4}) \right.$$
$$\left. - (0.33)\,(2 \times 10^2 \text{ ft})\,(3.3 \times 10^{-6} \text{ in}^2 \text{ lb}^{-1}) \right]$$
$$= 2.6 \times 10^2 \text{ lb in}^{-2}$$
$$\left[11.55 \times 10^{-4} \text{ ft lb}^{-1}\text{ in}^2 - 2 \times 10^{-4} \text{ ft lb}^{-1}\text{ in}^2 \right]$$
$$= 0.25 \text{ ft}$$

Using the above value of Δm, and other known factors, equations (3) or (5) may be solved for E_s, which is found to be about 2.1×10^5 lb in⁻²—a reasonable value for a sandstone or conglomerate.

The studies now in progress by Mr. Chase will include a comparison of the total computed elastic compression of this and overlying and underlying artesian aquifers with the total subsidence of the land as indicated by old and new leveling by the U. S. Coast and Geodetic Survey.

It should again be stressed that equation (6) gives only the *elastic* compression or subsidence, and that the greater subsidence that has occurred in many areas is due to *plastic* deformation of associated clay.

REFERENCES

Gilluly, James, and Grant, U. S., 1949, Subsidence in the Long Beach Harbor area, Calif.: Geol. Soc. America Bull., v. 60, p. 461–529, 28 fig.

Inter-Agency Committee on Land Subsidence in the San Joaquin Valley, 1958, Progress report on land-subsidence investigations in the San Joaquin Valley, Calif., through 1957: Sacramento, Calif., 160 p., 45 pls.

Jacob, C. E., 1940, On the flow of water in an elastic artesian aquifer: Am. Geophys. Union Trans., pt. 2, p. 574–586, 4 figs.

Jacob, C. E., and Lohman, S. W., 1952, Nonsteady flow to a well of constant drawdown in an extensive aquifer: Am. Geophys. Union Trans., v. 33, p. 559–569, 9 fig.

Meinzer, O. E., 1928, Compressibility and elasticity of artesian aquifers: Econ. Geology, v. 23, p. 263–291.

Meinzer, O. E., and Hard, H. H., 1925, The artesian water supply of the Dakota sandstone in North Dakota, with special reference to the Edgeley quadrangle: U.S. Geol. Survey Water-Supply Paper 520–E, p. 73–95, pl. 6, 7, fig. 7, 8.

Poland, J. F., and Davis, G. H., 1956, Subsidence of the land surface in the Tulare-Wasco (Delano) and Los Banos-Kettleman City area, San Joaquin Valley, Calif.: Am. Geophys. Union Trans., v. 37, no. 3, p. 287–296, 12 figs.

Theis, C. V., 1935, The relation between the lowering of the piezometric surface and the rate and duration of discharge of a well using ground-water storage: Am. Geophys. Union Trans. 16th Ann. Mtg., p. 519–524, 2 figs.

---

[1] In an aquifer composed of uncemented granular material the value of b is unity. In a solid aquifer, as a limestone having tubular channels, b is apparently equal to the porosity. The value of b for a sandstone doubtless ranges between these limits, but in the development that follows, a value of unity has been assumed.

---

[2] It is convenient to use the reciprocal of γ (0.434 lb in⁻² ft⁻¹), which is 2.31 ft lb⁻¹ in².

Theis, C. V., 1938, The significance and nature of the cone of depression in ground-water bodies: Econ. Geology, v. 33, p. 889-902, 2 figs.

Winslow, A. G., and Doyel, W. W., 1954, Land-surface subsidence and its relation to the withdrawal of ground water in the Houston-Galveston region, Texas: Econ. Geology, v. 49, p. 413-422.

24.   MEASUREMENT OF COMPACTION OF AQUIFER SYSTEMS IN AREAS OF LAND SUBSIDENCE

By BEN E. LOFGREN, Sacramento, Calif.

Work done in cooperation with the California Department of Water Resources

Land subsidence affects an area of more than 2,500 square miles in the San Joaquin Valley, Calif., and is the result of compaction of unconsolidated alluvial and lacustrine deposits as ground-water levels are lowered by heavy pumping. The subsidence occurs in areas where the aquifers are confined or semiconfined. Twenty specially designed compaction recorders have been installed in the areas of maximum subsidence. Two to 5 years of records show that compaction measured by recorders is directly related to changes in water level, and is approximately equal to the surveyed subsidence of the land surface.

In areas of maximum subsidence, ground-water levels show a general downward trend, and subsidence rates range from 0.4 to 1.5 feet per year. In these areas, 1 foot of subsidence has been observed for each 10 to 25 feet of water-level decline. Compaction of the unconsolidated deposits takes place as the artesian pressure decreases, thus transferring more of the overburden load to grain-to-grain contacts of the aquifer. The compaction is due chiefly to a nonelastic rearrangement of the grains of the deposit and results in a permanent decrease in volume. A small part of the compaction is elastic, and samples tested in the laboratory for consolidation show minor rebound when unloaded. However, rebound or expansion of the aquifer system has not been observed in the field measurements.

EQUIPMENT

A special type of recorder is being used to measure the rate and magnitude of compaction occurring at depth. As shown in figure 24.1, the assembly consists of a heavy weight emplaced in the formation below the bottom of a well casing, with an attached cable stretched upward in the casing and counter-
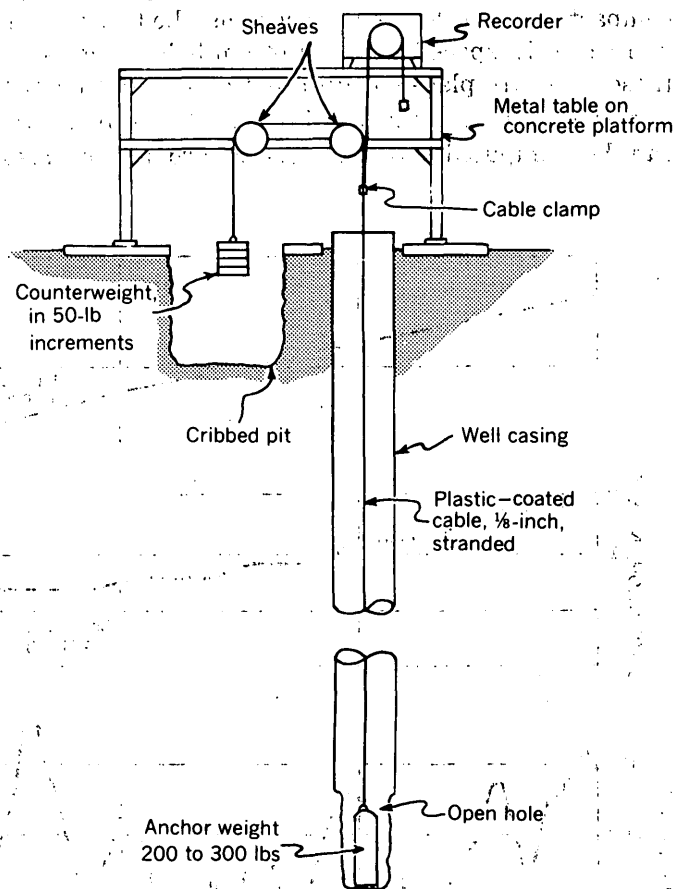
FIGURE 24.1.—Diagram of compaction-recorder installation.

weighted at the land surface to maintain constant tension. A monthly recorder mounted over the open casing is used to measure directly the amount of cable that appears above the casing as subsidence occurs. At the land surface it appears as if the bottom-hole weight is rising; actually, the land sur-

face is settling with respect to the bottom-hole weight.

The success of this method and equipment depends largely on the elastic characteristics of the cable under tension. After considerable experimentation, a specially manufactured ⅛-inch, stainless steel, 7 × 7 stranded, plastic-coated cable was selected, and seems to meet the rigorous requirements very well. Ball-bearing sheaves are used to reduce the frictional drag of the system.

Compaction recorders have been installed in unused irrigation wells and in specially drilled wells. At most sites, the bottom weight is placed in an open hole 15 to 25 feet below the bottom of the well casing so that measurements of vertical shortening are independent of the casing.

At several locations in the San Joaquin Valley, compaction recorders have been installed in two or more closely spaced wells. Bottom-hole weights in these wells are placed at different depths so that the compaction occurring at different depth intervals can be computed. Water-level recorders are also generally installed in or near the compaction-recorder well to record fluctuations and trends of ground-water levels as compaction continues.

RESULTS

A compaction recorder of the type shown in figure 24.1 installed in well 19/17–35N1 has been measuring the rate of compaction in the upper 2,000 feet of unconsolidated alluvial deposits near Huron, California. Subsidence of nearby bench mark B 889 has been determined by periodic leveling traverses of the U. S. Coast and Geodetic Survey. In addition, the changes in hydraulic support in the underlying artesian aquifer system have been determined by frequent water-level measurements in well 19/18–27M1.

The correlation between subsidence of the surface bench mark, vertical compaction, and water-level fluctuation is shown in figure 24.2. The water level in well 19/18–27M1 fluctuates 50 feet or more each year in response to heavy pumping in the area, and has declined about 40 feet during the 4.8-year period
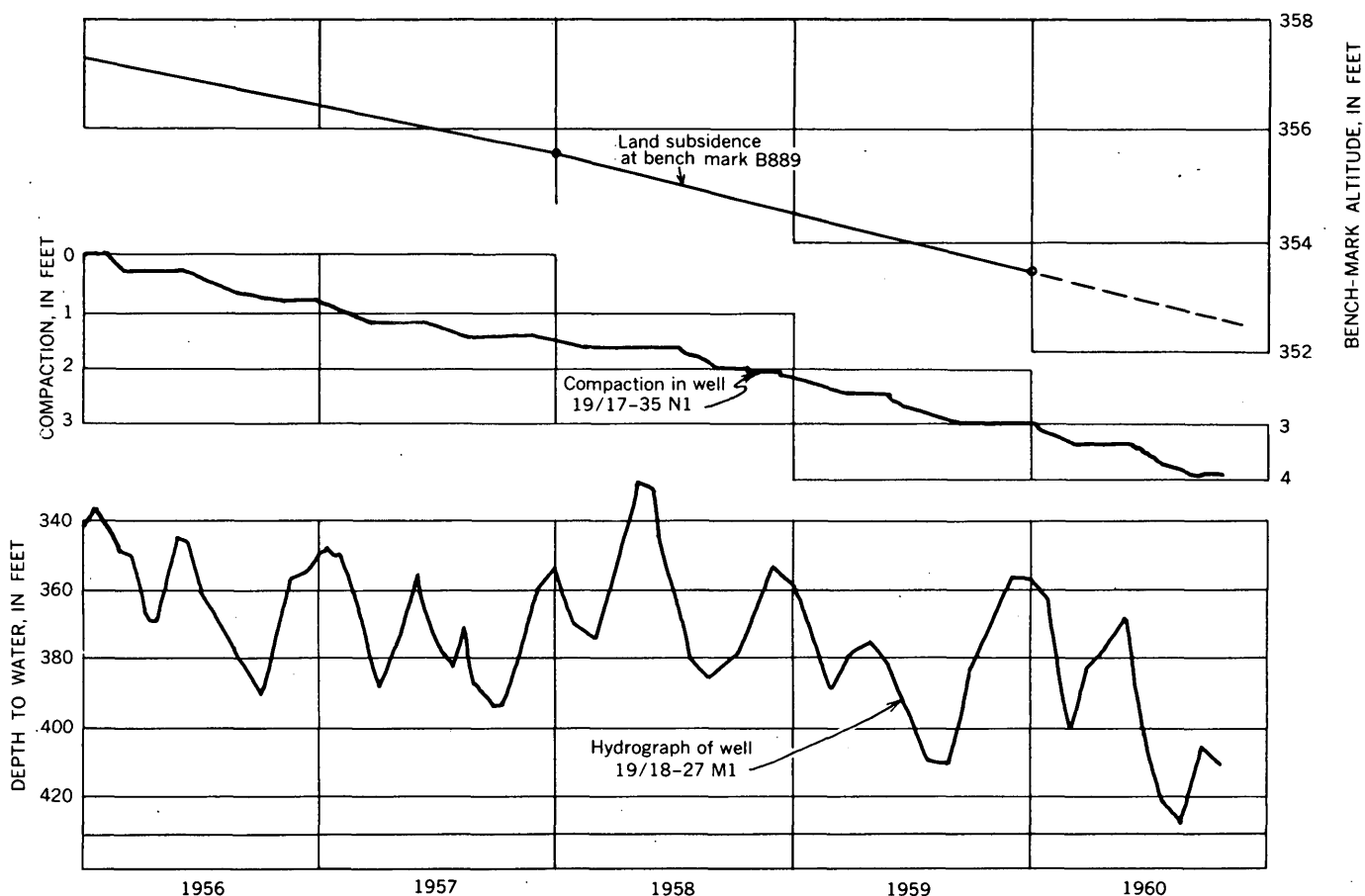
FIGURE 24.2.—Graph showing measured subsidence, compaction, and water-level change near Huron, Calif.

shown on the graph. This water-level decline has resulted in a measured compaction of 3.8 feet within the 2,000-foot depth interval of the compaction recorder, and a total subsidence of the land surface of 4.6 feet. Thus, subsidence near Huron is continuing at a rate of 0.96 foot per year, and 1 foot of subsidence has occurred for each 10 feet of water-level decline. The compaction that occurred in the upper 2,000 feet of deposits during the 4.8-year period represented 82 percent of the total subsidence, suggesting that 18 percent, or 0.84 foot of compaction, occurred in the deposits below 2,000 feet. This assumption is reasonable, because nearby wells withdraw water from below 2,000 feet.

Inspection of figure 24.2 shows that each major change in hydraulic support, as indicated by the hydrograph of well 19/18–27M1, is reflected in the compaction graph. During periods of rapid water-level decline, compaction occurs at a maximum rate. Conversely, during periods of rising water levels, the compaction rate declines. No expansion has been detected by the compaction recorder during periods of water-level rise.

Figure 24.3 A is a diagrammatic cross section through an area of active subsidence near Oro Loma, Calif. The relative positions of the depth anchors of the three compaction recorders operating at this site are shown in relation to the principal hydrologic
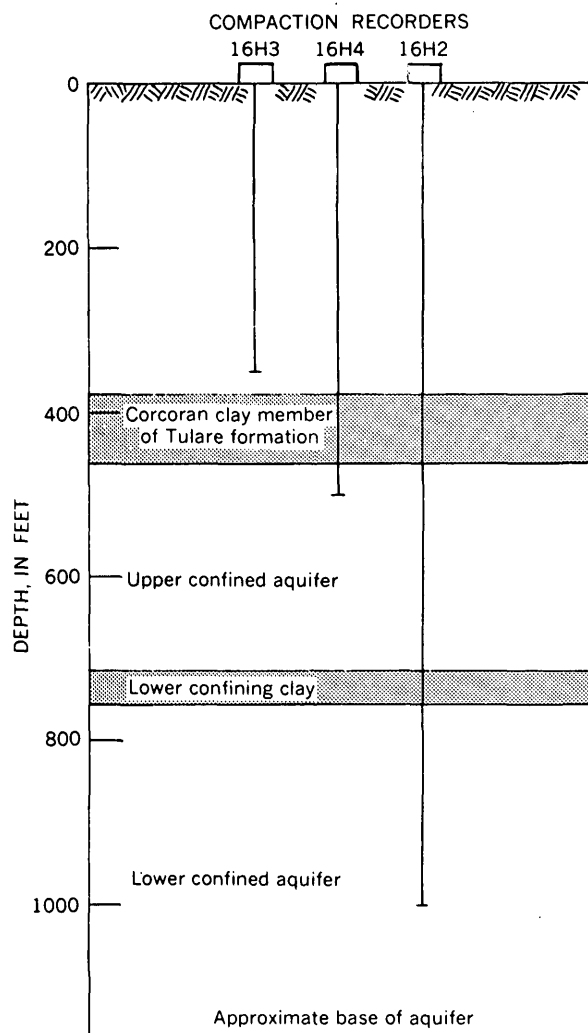
A. RELATION OF MULTIPLE RECORDERS TO
THE HYDROLOGIC UNITS
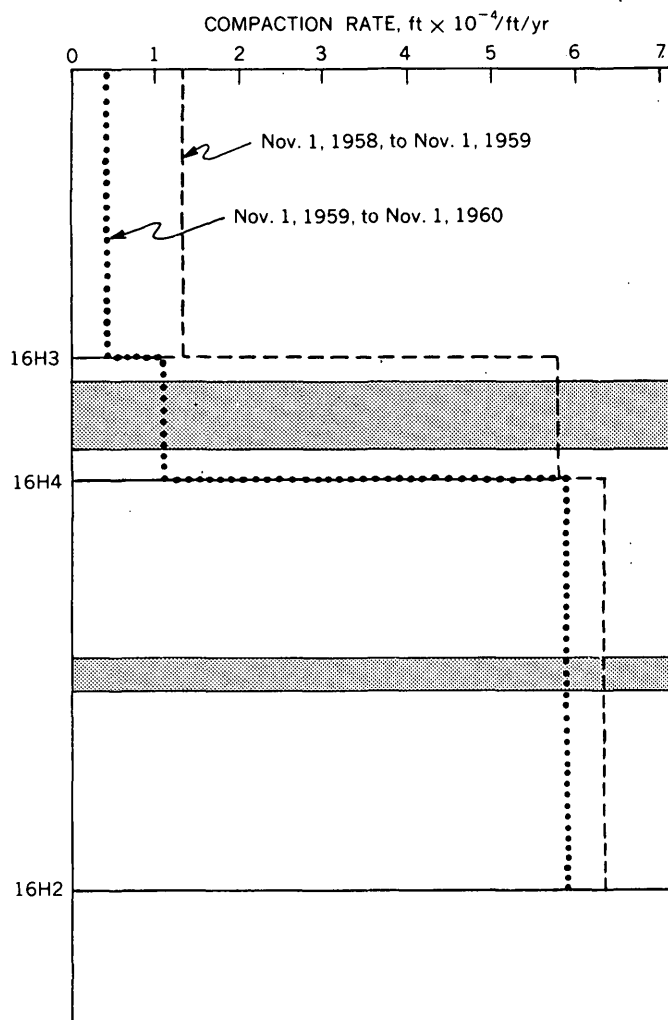
B. MEASURED COMPACTION RATE OF DEPOSITS
IN THREE DEPTH ZONES

FIGURE 24.3.—Compaction rates near Oro Loma, Calif., as measured by three compaction recorders. A, Relation of multiple recorders to hydrologic units; B, measured compaction rate of deposits in three depth zones.

units. Recorder 16H3 measures the total compaction occurring between the surface and the anchor at 350-foot depth. Similarly, recorders 16H4 and 16H2 measure the compaction occurring between the surface and their respective 500-foot and 1,000-foot anchor depths. By comparing the record of any two recorders, the magnitude and rate of compaction occurring in each depth zone are obtained.

Figure 24.3 B shows the rate of compaction that occurred in each of three depth zones for two periods of recording. For comparison, these rates have been converted to unit values and represent the average amount of vertical shortening that occurred in each foot of thickness each year. The compaction rate in the 350- to 500-foot depth zone decreased greatly during the second year of record.

From November 1, 1959, to November 1, 1960, 0.014 foot of compaction occurred in the 0- to 350-foot depth zone (0.40 ×10⁻⁴ ft/ft/yr), 0.016 foot of compaction occurred in the 350- to 500-foot depth zone (1.07 × 10⁻⁴ ft/ft/yr), and 0.292 foot of compaction occurred in the 500- to 1,000-foot depth zone (5.84 × 10⁻⁴ ft/ft/yr). The total 0.322 foot of compaction measured by the 1,000 foot recorder approximately equaled the amount of subsidence of a nearby Coast and Geodetic Survey bench mark. These measurements suggest that during this 1-year period, little or no compaction was occurring within the unconsolidated deposits below 1,000 feet.

25. THE COEFFICIENT OF STORAGE IN A REGION OF MAJOR SUBSIDENCE CAUSED BY COMPACTION OF AN AQUIFER SYSTEM

By J. F. POLAND, Sacramento, Calif.

Meinzer (Meinzer and Hard, 1925) was the first to conclude that the water discharged by wells tapping an artesian aquifer (the Dakota sandstone) had been derived largely from storage. He reasoned that water withdrawn from storage was released by compression of the aquifer. Subsequently Meinzer (1928) considered release from storage by expansion of the water, described evidence for the compressibility and elasticity of artesian aquifers, and stated (p. 289) that "* * * artesian aquifers are apparently all more or less compressible and elastic though they differ widely in the degree and relative importance of these properties."

Following development in 1935 of Theis' equation for non-steady-state flow of water to a discharging well, Theis (1938, p. 894) defined the coefficient of storage as " * * * the volume of water, measured in cubic feet, released from storage in each column of the aquifer having a base 1 foot square and a height equal to the thickness of the aquifer when the water table or other piezometric surface is lowered 1 foot."

Shortly thereafter Jacob (1940) postulated that when water is removed from and pressure is decreased in an elastic artesian aquifer, stored water is derived from three sources: (a) expansion of the confined water, (b) compression of the aquifer, and (c) compression of the adjacent and included clay beds. He concluded that the third source is probably the chief one in the usual case. He stated (p. 574) "* * * that because of the low permeability of the clays (or shales) there is a time-lag between the lowering of pressure within the aquifer and the appearance of that part of the water which is derived from storage in those clays (or shales)." To avoid mathematical complications, however, he assumed that release of stored water from the clay beds is instantaneous. He defined the coefficient of storage in terms of the three sources of water, as

$$S = \gamma\theta m \left[\frac{1}{E_w} + \frac{b}{\theta E_x} + \frac{c}{E_c} \right]. \tag{1}$$

In this equation S is the coefficient of storage; γ is the specific weight of water (0.434 lb/in²/ft); θ is the porosity of the aquifer; m is the thickness of the acquifer, in feet; E_w[1] is the bulk modulus of elasticity of the water (3 × 10⁵ lb/in²); b is the proportion of the plane of contact between the aquifer and the confining layer over which the hydrostatic pressure is effective (unity for an aquifer composed of uncemented granular material); E_x is the bulk modulus of elasticity of the aquifer matrix; E_c is the modulus of compression of clay beds; and c is a dimensionless

[1] β, the reciprocal of E_w, is 3.3 × 10⁻⁶ in² lb⁻¹.

quantity that depends largely on the thickness, configuration, and distribution of the intercalated clay beds.

Elsewhere in this volume Lohman (Art. 23) briefly reviews the development of the concepts of the occurrence of water in artesian aquifers beginning with Meinzer's classic work, and derives an equation for determining the amount of *elastic* compression of artesian aquifers from known declines in artesian pressure and known hydrologic properties of the aquifers. Lohman's equation (Art. 23, this volume) is expressed in the form

$$\Delta m = \Delta p \, (S/\gamma - \theta m \beta), \qquad (2)$$

in which Δm is the reduction in thickness of the aquifer (amount of elastic compression), in feet, and Δp is the reduction in artesian pressure in lbs/ft². The other terms are as defined for equation (1). Lohman's equation (2) affords a means of evaluating the second component of equation (1), $\gamma m b/E_s$, when E_s is not known.

In areas where intensive ground-water development has drawn down the artesian head substantially (a hundred to several hundred feet) in highly compressible confined aquifer systems containing many clay interbeds, major subsidence of the land surface has occurred. For example, land subsidence from this cause has reached 2 to more than 20 feet in parts of the San Joaquin Valley (see Art. 24 by Lofgren and Art. 26 by Miller) and 9 feet in the Santa Clara Valley, both in California, and several feet in the Houston-Galveston area in Texas (Winslow and Wood, 1959). The subsidence probably is caused almost wholly by compaction of the intercalated and confining beds of clay, silty clay, and clayey silt, both by plastic deformation and mechanical rearrangement of grains, and to that extent is inelastic and permanent. In such aquifer systems the water taken from storage as defined by the coefficient of storage derived from short-term pumping tests may represent a very small part of the water actually removed from storage.

APPLICATION TO THE LOS BANOS-KETTLEMAN CITY AREA

Subsidence in the Los Banos-Kettleman City area on the central west side of the San Joaquin Valley (for location see map in Art. 26 by Miller) extends over 1,100 square miles and ranges from 1 to 22 feet. In most of this area, about all the subsidence is known to be caused by compaction of the confined aquifer system (see Art. 24 by Lofgren).

We can compute approximate values for the components of the coefficient of storage in equation (1) for an example in the Los Banos-Kettleman City area. Average values used for the confined aquifer system are as follows: coefficient of storage from short-term pumping tests about 1×10^{-3}, $\theta = 0.4$, $m = 700$ feet (aquifer thickness, excluding for this example the clayey interbeds aggregating about 300 feet in thickness), and $\Delta p = 130$ lb in^{-2} (300 feet decline in head).

The first element of equation (1), the component of S due to elastic expansion of the water (identified here as S_1) is $\gamma \theta m \beta$.

$$S_1 = (0.434 \text{ lb in}^{-2} \text{ ft}^{-1}) \, (0.4) \, (700 \text{ ft}) \, (3.3 \times 10^{-6} \text{ in}^2 \text{ lb}^{-1}) = 4 \times 10^{-4}$$

The elastic compression of the aquifer (elastic subsidence of the land surface) can be computed from equation (2), using the S obtained from short-term pumping tests, as follows:

$$\Delta m = 130 \text{ lbs in}^{-2} \left[(1 \times 10^{-3})/(0.434 \text{ lb in}^{-2} \text{ ft}^{-1}) - (0.4) \, (700 \text{ ft}) \, (3.3 \times 10^{-6} \text{ in}^2 \text{ lb}^{-1}) \right] = 0.18 \text{ ft}$$

Thus, the second component of S in equation (1), identified here as S_2, is the elastic compression divided by the artesian-head decline or 0.18 ft/300 ft $= 6 \times 10^{-4}$.

The component of storage derived from compaction of the clayey interbeds and confining beds (S_3) can be estimated approximately from the gross subsidence of the land surface. In this area, the ratio of subsidence to head decline ranges about from 1/10 to 1/25. If we use a ratio of 1/20 (subsidence = 15 feet for 300 feet of head decline), then the component of storage derived from compaction (both elastic and inelastic) of the clayey sediments is

$$\frac{15 \text{ ft} - 0.18 \text{ ft}}{300 \text{ ft}} = 0.05 \text{ or } 5 \times 10^{-2}$$

Summing the three components, $S_1 + S_2 + S_3$, gives a long-term unit storage yield of 0.051. Thus, S_3, the stored water released by compression or compaction of the clayey beds, is about 50 times as great as the water released by elastic expansion of the water and elastic compression of the aquifer (components S_1 and S_2). In other words, in this example, the coefficient of storage derived from a short-term pumping test gives a volume only about one-fiftieth that of the long-term (15 to 25 years) yield from storage.

This is an extreme example because it is computed for one of the most compressible aquifer systems for which data are now available. However, it serves to emphasize that the storage derived from compaction of the clayey interbeds and confining beds may be many times as great as that derived from elastic expansion of the water and elastic compression of the aquifer.

Moreover, this component, S_3, is a variable. The stored water yielded by the clayey beds would be large only during the first decline of artesian pressure. If the pressure subsequently recovered to (or near to) the initial conditions, and then was drawn down again through the same interval, the compression of the clayey beds, if mostly preconsolidated during the first drawdown phase, would be only a small fraction of that in the first phase of pressure decline, probably less than 10 percent.

REFERENCES

Jacob, C. E., 1940, On the flow of water in an elastic artesian aquifer: Am. Geophys. Union Trans. 21st Ann. Mtg., pt. 2, p. 574–586, 4 figs.
Meinzer, O. E., 1928, Compressibility and elasticity of artesian aquifers: Econ. Geology, v. 23, p. 263–291.
Meinzer, O. E., and Hard, H. A., 1925, The artesian water supply of the Dakota sandstone in North Dakota, with special reference to the Edgeley quadrangle: U.S. Geol. Survey Water-Supply Paper 520–E, p. 73–95, pls. 6–7, figs. 7–8.
Theis, C. V., 1935, The relation between the lowering of the piezometric surface and the rate and duration of discharge of a well using ground-water storage: Am. Geophys. Union Trans. 16th Ann. Mtg., p. 519–524, 2 figs.
Theis, C. V., 1938, The significance and nature of the cone of depression in ground-water bodies: Econ. Geology, v. 33, p. 889–902, 2 figs.
Winslow, A. G., and Wood, L. A., 1959, Relation of land subsidence to ground-water withdrawals in the upper Gulf Coast region, Texas: Am. Inst. Mining Metall. Petroleum Engineers Trans., v. 214; Mining Engineering, p. 1030–1034.

26. COMPACTION OF AN AQUIFER SYSTEM COMPUTED FROM CONSOLIDATION TESTS AND DECLINE IN ARTESIAN HEAD

By R. E. MILLER, Sacramento, Calif.

In the parts of the San Joaquin Valley shown on figure 26.1, the land surface has been subsiding at rates up to 1.5 ft/yr owing to large withdrawals of artesian water from poorly consolidated late Cenozoic sediments. By refining a method outlined by Gibbs (1960), the compaction in the confined aquifers is being computed at selected core-hole sites in the San Joaquin Valley. The method of computation is based upon Terzaghi's theory of consolidation (1943, p. 266–267), using the results of one-dimensional consolidation tests made upon core samples of the aquifer system, and the decline in artesian head that has occurred. An extension of this technique can be used to predict future subsidence.

COMPUTATION OF AQUIFER COMPACTION

The computation of aquifer compaction at core hole 12/12–16H1 in the Los Banos-Kettleman City area in the western part of the San Joaquin Valley (fig. 26.1) is a typical example of the method being used in the present studies. In this area there has been no decline in the water table, but intensive pumping from the confined aquifer system has caused a substantial drawdown of artesian head. The procedure for making the computations was as follows:

1. The upper and lower limits of the confined aquifers were determined from the electric logs of nearby wells.
2. Then, as shown in figure 26.2, the aquifer and overburden is divided into sufficient segments so that each segment could be represented by a single consolidation test typical for that segment.
3. The artesian head of the confined aquifers was determined from the static levels in nearby wells and converted into pounds per square inch. The decline in aquifer pressures was estimated for the aquifer system for the period 1937–59 using the static-level records of the wells for previous years.
4. The overburden load on the aquifers in pounds per square inch was computed from the wet unit weight of the core samples. There has
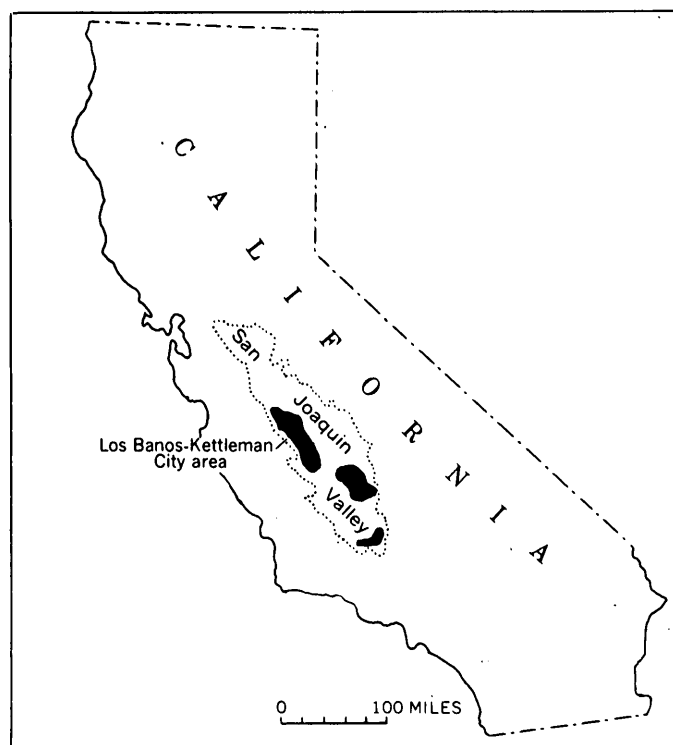
FIGURE 26.1.—Areas of land subsidence in the San Joaquin Valley, Calif.

been no decline in the water table in this area between 1937 and 1959. This means that no compaction occurred in segments 1, 2, and 3 during this period and that there was no decrease in overburden load on the confined aquifers owing to dewatering of the sediments above the water table.

5. The effective load on the top segments of the confined aquifers was computed for the periods for which the aquifer pressures had been determined by subtracting the aquifer pressure from the bulk weight of the aquifer overburden. The maximum load that could occur would be when the artesian pressure is zero and the full weight of the overburden bears on the aquifer.

6. One-dimensional consolidation tests were made on the core samples of the aquifer system for the maximum load range that could occur in the aquifers. These tests were made in the Earth Laboratory of the Bureau of Reclamation at Denver, Colo. An increase in loading results in a decrease in the void ratio of the sample tested. Clays tend to consolidate more under load than sands, but not as rapidly.

7. The compaction occurring in each segment of an aquifer system can be computed for any specified aquifer pressure decline if the effective load change on the segment can be determined. In determining the effective load on the segment, the buoyant weight of any overlying aquifer segments is added to the effective weight of the overburden load. The aquifer pressures at the core-hole site are shown in figure 26.2 and the effective loading on each aquifer segment is listed in table 1.

As illustrated in figure 26.2, two confined aquifers are present in this area. The principal aquifer is the lower one. Pumping from this aquifer was locally decreased shortly after 1953, owing to the availability of surface water from a nearby canal. Consequently the static levels of wells perforated in the lower aquifer were lowest in 1953 and have shown a slight amount of recovery since that time. The greatest effective load on the lower aquifer was in 1953, therefore, and the load at that time was used as a maximum for computing compaction in the lower aquifer. In the upper aquifer, which is tapped by only a few domestic wells, there has been a small but steady decline in static level between 1937 and 1959.

8. The compaction due to the load change on each segment of the aquifer system was computed from the void-ratio change which was determined graphically from the extension of the straight-line part of the one-dimensional consolidation curves. Compaction was computed by the equation

$$\Delta h = \frac{e_1 - e_2}{1 + e_1} h$$

in which Δh = compaction, in feet; e_1 = initial void ratio; e_2 = void ratio after loading, and h = thickness of aquifer segment, in feet.

The ultimate compaction determined for the confined aquifers as a result of the change in artesian pressure from 1937 to 1959, and the part of that compaction computed to have occurred by 1959 are shown in table 1.

9. A complicating factor that must be considered is the time lag of compaction. In segments of the aquifer that have very low permeability, years or even decades might be required before enough water is displaced so that all of the computed compaction can occur. The time required for the computed compaction to be

SELF POTENTIAL	RESISTIVITY	SEGMENTS	DESCRIPTION	VECTORS SHOWING PRESSURE-LOADING DISTRIBUTION
Millivolts	Ohm-meters			
← 25 +	0 15 30			

OVERBURDEN LOAD ON ARTESIAN AQUIFERS

1 — OVERBURDEN (Silt, clay, and some sand)

400 psi

644 psi

2
3

4 — UPPER CONFINING CLAY (Diatomaceous)

5
6
7
8 — UPPER ARTESIAN AQUIFER (Fine sand, silt, and clay)

1937   1959

169 psi   145 psi

9 — ARTESIAN PRESSURE

10
11 — LOWER CONFINING CLAY
12
13
14
15 — LOWER ARTESIAN AQUIFER (Fine to coarse sand, silt, and clay)

1937   1953

206 psi
260 psi

16
17 — ARTESIAN PRESSURE

DEPTH, IN FEET: 0, 100, 200, 300, 400, 500, 600, 700, 800, 900, 1000

FIGURE 26.2.—Logs and diagram of pressure-loading distribution for the aquifer system at core hole 12/12-16H1, San Joaquin Valley, Calif.

TABLE 1.—*Effective loading and compaction at core hole 12/12–16H1 computed for the period 1937–59*

Segment number (See fig. 26.2)	Thickness (feet)	Effective load 1937 (psi) [1]	Effective load		Ultimate compaction [2] (feet)	Compaction completed by 1959		Amount of residual compaction as of 1959 (feet)
			Lower aquifer, 1953 (psi) [1]	Upper aquifer, 1959 (psi) [1]		Percent	Feet	
5	48	231		255	1.13	89	1.00	0.13
6	45	247		271	.56	100	.56	.00
7	20	265		289	.52	100	.52	.00
8	25	272		296	.16	100	.16	.00
9	87	284		308	.76	26	.20	.56
10	24	323		347	.12	100	.12	.00
11	38	334		358	.35	63	.22	.13
12	24	384	438		.28	100	.28	.00
13	52	395	449		.34	100	.34	.00
14	32	419	473		.31	100	.31	.00
15	71	433	487		1.08	100	1.08	.00
16	69	465	519		.75	100	.75	.00
17	160	495	549		1.74	100	1.74	.00
Total					8.10		7.28	0.82

[1] Pounds per square inch.
[2] Compaction estimated to occur as result of artesian-head change, 1937–59.

completed can be estimated from the consolidation coefficient which is determined as part of the one-dimensional consolidation test. The equation given by Terzaghi and Peck (1948, p. 241) for computing the compaction time is

$$t = \frac{Th^2}{C_v}$$

in which t = compaction time, in years; T = time factor; h = thickness of aquifer segment, in feet; and C_v = consolidation coefficient, in ft²/year.

If drainage can take place from both top and bottom of the aquifer segment, $(h/2)^2$ is used in place of h^2. The time required for various percentages of compaction to be completed is not a linear relation, for the time depends upon T, which is a pure number nonlinearly related to the percent of compaction completed. Thus $T = 1.0$ for about 93 percent compaction, $T = 0.2$ for 50 percent compaction, and $T = 0.0076$ for 10 percent compaction.

Compaction of the upper confining clay occurs by drainage into the underlying aquifer as a result of the downward pressure differential. The time required for this compaction to be nearly completed (about 93 percent) can be estimated from the preceding equation, using the values $T = 1$, $h = 86$ feet, and $C_v = 0.92$ ft²/yr for the load range of 200 psi to 400 psi.

$$t = \frac{1 \times 86^2}{0.92} = \text{about 8,000 years}$$

Similarly, half of the compaction would be completed in about 1,600 years, but 10 percent of the compaction would be completed in only about 60 years. This would indicate that only a small amount of compaction has occurred in this confining clay segment during the relatively short period between 1937 and 1959.

By this method the percent of compaction completed in each segment of the aquifer at core hole 12/12–16H1 was computed and is shown in table 1. Secondary consolidation effects have not been considered in these approximate computations of compaction.

COMPARISON OF COMPUTED SUBSIDENCE TO MEASURED SUBSIDENCE

Releveling of bench marks by the U. S. Coast and Geodetic Survey indicated that 7.8 feet of land-surface subsidence occurred in the vicinity of core hole 12/12–16H1 between 1937 and 1959. The total ultimate computed compaction of the aquifers due to pressure decline between 1937 and 1959 is 8.1 feet. The part of this ultimate compaction computed to have occurred by 1959 for segments 5 through 17 (fig. 26.2) is 7.28 feet. In addition, the rate of compaction of the upper confining clay (segment 4) has been calculated as approximately 0.01 foot per year. Thus, the total compaction computed to have occurred in segments 4 through 17 from 1937 to 1959 is 7.5 feet, compared to a measured land-surface subsidence of 7.8 feet. The residual compaction

estimated to occur after 1959 as a result of the de-cline in artesian pressure from 1937 to 1959 is 0.8 foot in segments 5 through 17. Additional compaction in the upper confining clay (segment 4) is estimated to continue at a rate of roughly 0.01 foot a year unless the artesian pressure in the upper artesian aquifer recovers appreciably.

REFERENCES

Gibbs, H. J., 1960, A laboratory testing study of land subsidence: The First Pan American Conference on Soil Mechanics and Foundation Engineering Proc., 1959, Mexico City, v. 1, p. 13–36.

Terzaghi, Karl, 1943, Theoretical soil mechanics: New York, John Wiley & Sons, 510 p.

Terzaghi, Karl, and Peck, R. B., 1948, Soil mechanics in engineering practice: New York, John Wiley & Sons, 566 p.

27. DEVELOPMENT OF AN ULTRASONIC METHOD FOR MEASURING STREAM VELOCITIES

By H. O. WIRES, Columbus, Ohio

Work done in coperation with the U.S. Army Corps of Engineers and the California Department of Water Resources

Continuous records of streamflow in tidal or backwater reaches are difficult to obtain by conventional methods because the velocity of flow is not a simple function of water-surface elevation. The number of such reaches in which flow records are needed is increasing as more streams are controlled by reservoirs and as the flow in tidal reaches becomes increasingly important in the total development of water resources. Continuous records of velocity would allow computation of flow at any time, and efforts have been directed toward development of instrumentation for that purpose.

A system has been devised that utilizes the difference in velocity of propagation of sound in the upstream and downstream directions to measure the velocity of streamflow. In this system transducers are installed near each streambank at an angle θ with the direction of flow as shown on figure 27.1. Ultrasonic waves are generated and received at both installations. The difference in travel time of the wave in the upstream and downstream direction is related to the velocity of streamflow and this relation can be derived mathematically.

A continuous wave transmission system using received-wave displacement as a measure of the difference in travel time was first designed and constructed under contract by Raytheon Manufacturing Company. After testing the system at several locations and under many separate conditions it was concluded that phase stability requirements could

not be achieved. The extreme fluctuations of phase and amplitude encountered could be ascribed to multipath interference phenomena due to such causes as thermal and energy gradients and boundary reflections.

A second system has been devised, which eliminates the defects of the continuous wave transmission system. The basic characteristics of the new system, which is known as the pulse repetition frequency (PRF) method, are:

1. Upstream and downstream sound velocities are measured simultaneously over a single acoustic path.
2. A transmitted pulse with a sharp leading edge is used to eliminate multipath effects. The first
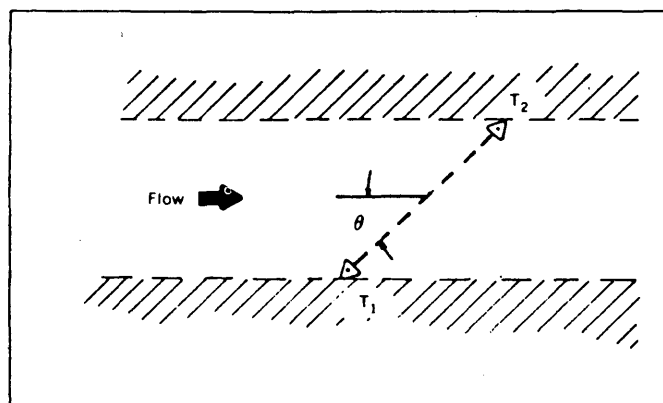
FIGURE 27.1.—Installation of transducers in a stream channel.

arrived signal is used and any immediately following signals are gated out.

3. Flow velocity is related to the mean of the differences between the downstream and upstream propagation velocities.

A system having these characteristics is shown diagrammatically on figure 27.2. A 135- acoustic pulse is transmitted from the upstream transducer and received at the downstream transducer. The energy from this pulse activates a keying circuit and another 135- pulse is transmitted from the upstream transducer. The 85- electro-acoustic circuit operates simultaneously with, and in the same manner as, but in the opposite direction from the 135-circuit. The two-pulse repetition frequencies (PRF) are fed into a computing circuit, the output of which is proportional to the difference frequency.

It is easily shown that the difference frequency is proportional to the velocity of streamflow.
Let: v = velocity of moving medium

c = velocity of sound with no flow
d = length of acoustic path
θ = angle between downstream acoustic path and downstream flow path

Then: Velocity of sound propagation downstream
$$c_{12} = c + v \cos \theta$$
Velocity of sound propagation upstream
$$c_{21} = c - v \cos \theta$$
The times of travel are

$$t_{12} = \frac{d}{c_{12}} = \frac{d}{c + v \cos \theta} \text{ and } t_{21} = \frac{d}{c_{21}} = \frac{d}{c - v \cos \theta}$$

The pulse repetition frequencies, f_{12} and f_{21}, are given by the reciprocals of these equations and the velocity of the streamflow is

$$v = \frac{d}{2 \cos \theta} (f_{12} - f_{21})$$

The computing circuits consist of two PRF multipliers, two motor-driven amplifiers, a synchro-differ-
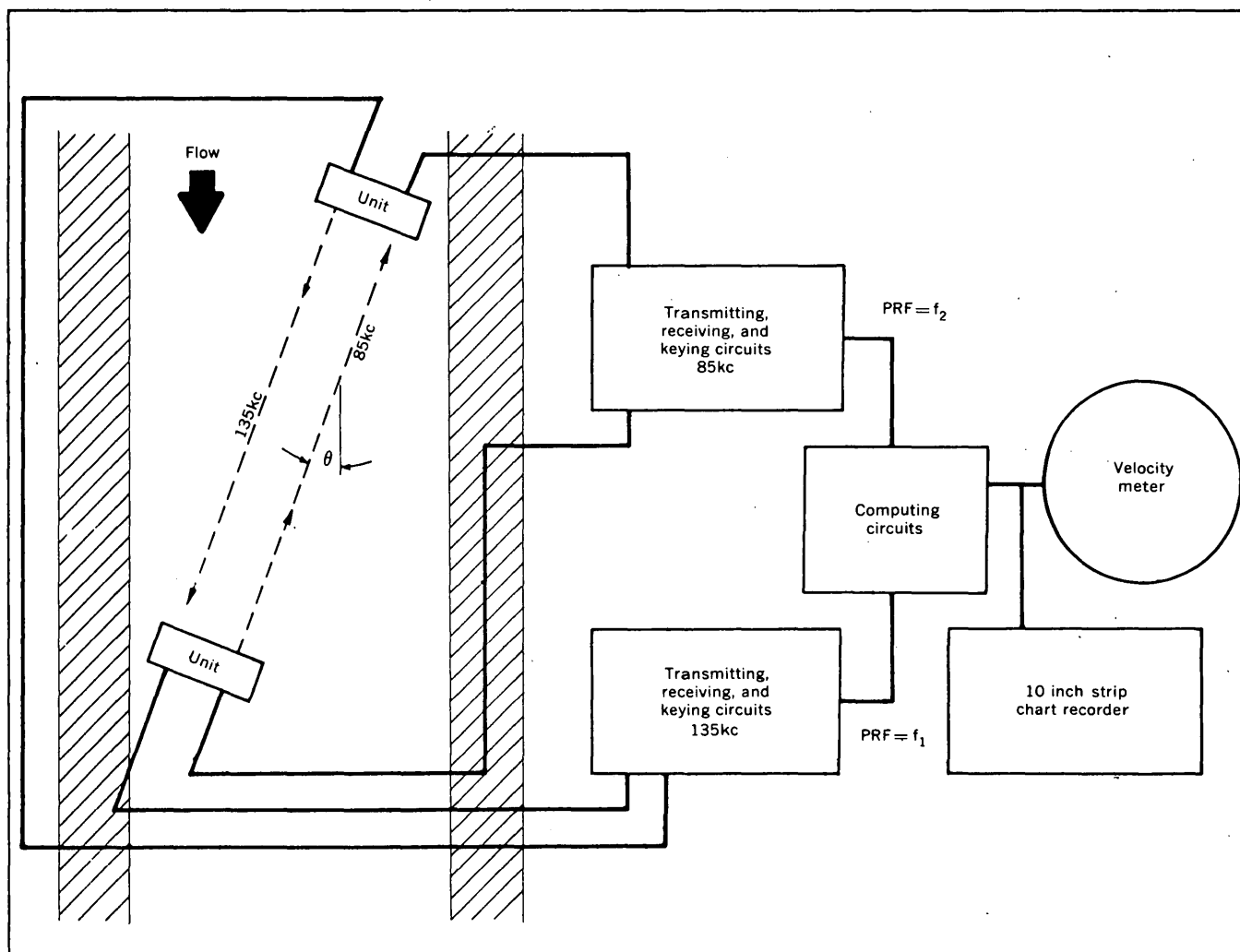
FIGURE 27.2.—Diagram of the PRF system.

ential, and a synchro-generator. The multipliers are used to bring the pulse repetition frequencies close to 60 per second. The synchro-differential subtracts the two frequencies, and the output of the synchro-generator is proportional to this difference frequency. The generator output is fed into a circuit which multiplies this signal by the constant $d/(2 \cos \theta)$. This product voltage appears on a meter and is recorded on a 10-inch strip chart.

The velocity of flow equation shows that, in addition to the two pulse-repetition frequencies, it is necessary only to determine d and θ to compute the river velocity. These two quantities are easily and accurately measured. As the upstream and downstream transmissions are sent simultaneously the effects of any fluctuations caused by changes in the acoustic properties of the water are eliminated.

The PRF system has been installed on the Sacramento River at Sacramento, Calif. Several problems in the original design and operation of the equipment, such as selection of proper cable for adequate transmission, determination of automatic gain control requirements, and prevention of extensive record blanking from occasional missed pulses, have been resolved, and a record is now being obtained to be used for analysis of the method.

※

28.　PRELIMINARY DESIGN OF AN ELECTRIC ANALOG OF LIQUID FLOW IN THE UNSATURATED ZONE

By R. W. Stallman, Denver, Colo.

The solution of hydrologic problems, in which the details of liquid flow through the unsaturated zone are significant, has been hampered by a lack of simple means for computing the relation between time, flow, moisture content, and space.

Normally flow in the unsaturated zone is one-dimensional, nonsteady, and occurs approximately vertically. The differential equation relating the variables of liquid flow for this condition may be stated as

$$ k_l \frac{\partial^2 h_l}{\partial z^2} + \frac{\partial k_l}{\partial z}\left[\frac{\partial h_l}{\partial z} + 1\right] = \Phi \frac{\partial \theta_l}{\partial t} \qquad (1) $$

in which k_l is the conductivity to liquid flow, h_l is the liquid head at point z above an arbitrarily established horizontal reference plane, Φ is the porosity, θ_l is the liquid content expressed as a fraction of the porosity, and t is time. The conductivity k_l is a nonlinear function of the liquid content of θ_l; consequently it is very difficult to find mathematical solutions satisfying both equation (1) and the highly variable field boundary conditions at the upper and lower limits of the unsaturated zone. Philip (1955) devised an efficient iteration process for finding a solution to a form of equation (1) for continuous infiltration from the land surface. Subsequently Youngs (1957), by laboratory studies, demonstrated that Philip's method gave accurate forecasts of flow ensuing from infiltration. Nelson (1960) recently determined nonsteady liquid drainage from initially saturated sediments by solving the differential equations of flow using digital computing equipment. Youngs (1960) applied the capillary-tube hypothesis of unsaturated flow to calculate drainage from saturated media as a function of time.

Use of Philip's iteration process is limited to a hydraulically homogeneous profile and increasing water content during infiltration from the land surface. Although digital computing equipment is capable of solving the problem regardless of complicating nonhomogeneities and variable boundary conditions, experience has indicated that the costs of such solutions are generally higher than can be afforded in ordinary hydrologic investigations. In an effort to obtain a versatile and low-cost computing system for the study of liquid flow through the unsaturated zone, electric analog techniques for solving equation (1) were considered. The following describes preliminary plans for an electric analog system believed capable of solving problems in one-dimensional vertical flow through nonhomogeneous profiles under a variety of boundary conditions.
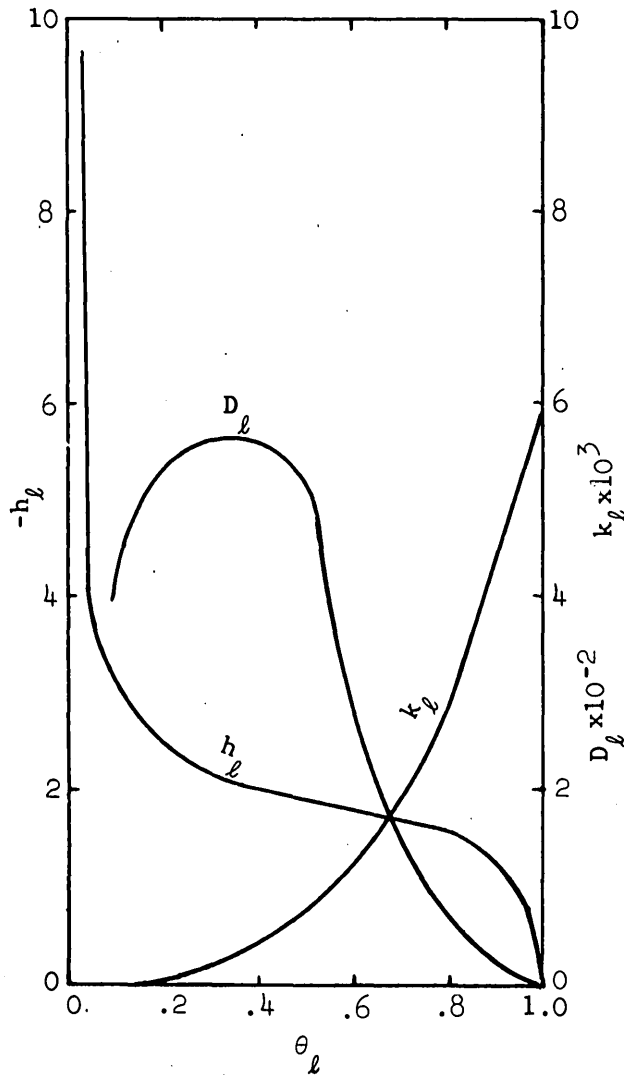
FIGURE 28.1.—Hydraulic characteristics of unsaturated porous media.

For electrical simulation, equation (1) may be more conveniently written in the following form:

$$\left[\frac{\partial^2 h_l}{\partial z^2}\right] + \frac{\partial \log k_l}{\partial z}\left[\frac{\partial h_l}{\partial z} + 1\right] - D_l\frac{\partial h_l}{\partial t} = 0 \quad (2)$$

in which $D_l = \frac{\Phi}{k_l}\frac{\partial \theta_l}{\partial h_l}$, the liquid diffusivity of the unsaturated porous media. Neglecting hysteresis, the curve of D_l versus θ_l may be obtained directly from curves of k_l versus θ_l and h_l versus θ_l characterizing the porous media. An example of a set of these curves is given in figure 28.1.

Consider equation (2) as comprising three separate terms, each defining a single component of flow accumulation at a point, z. The first gives the rate of change of storage for a hydraulically homo-

$$I_A \cong \frac{\partial^2 h_l}{\partial z^2} \cong \frac{\partial^2 e}{\partial z^2}\frac{1}{R}$$

$$I_B \cong \frac{\partial \log k_l}{\partial z}\left[\frac{\partial h_l}{\partial z} + 1\right]$$

$$I_C \cong D_l\frac{\partial h_l}{\partial t} \cong C_e\frac{\partial e}{\partial t}$$
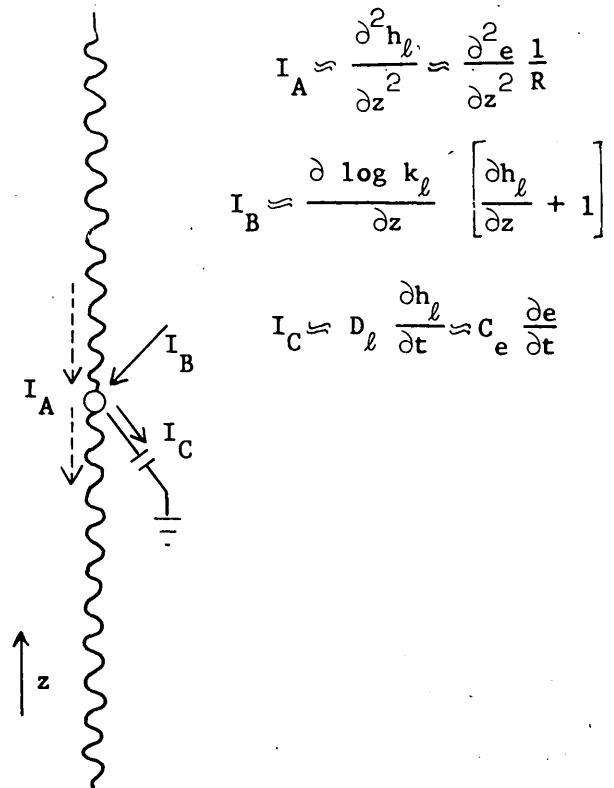
FIGURE 28.2.—Electrical currents analogous to terms in equation of flow.
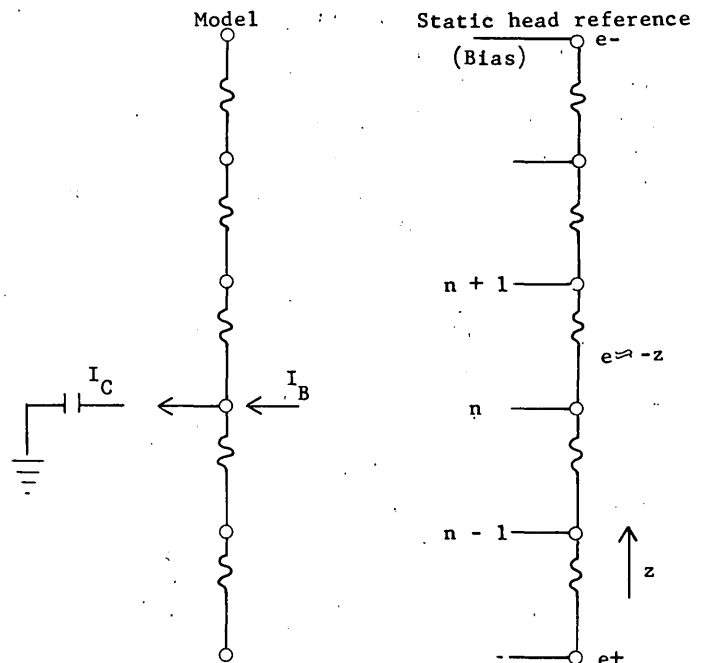
FIGURE 28.3.—Schematic diagram of analog and bias circuits.
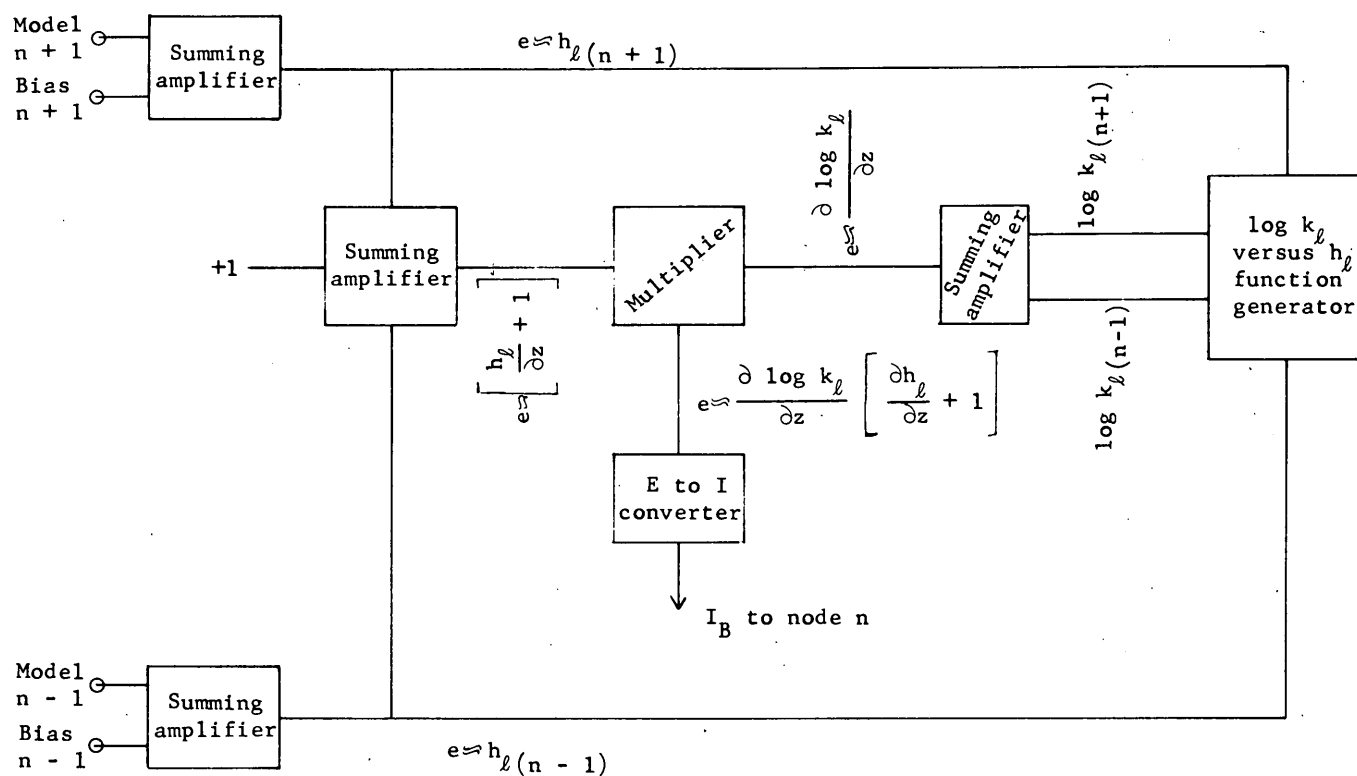
FIGURE 28.4.—Computer for determining I_B.

geneous element, the second identifies variations due to hydraulic heterogeneity and gravity, and the third accounts for changes as a function of time and storage capacity. The electrical counterparts of these terms are currents (I) added to a point in a resistive element, with a constant resistance (R) per unit length, as shown in figure 28.2. The continuous resistance element must be viewed as a series of finite elements because it does not appear practical to model I_B and I_C at each point along its length. Accordingly, a finite-difference approximation to equation (2) is represented by the electrical model shown in figure 28.3. A voltage divider at the right in figure 28.3 serves as a reference for static head conditions in the profile and for dynamic evaluation of k_l and D_l as the analysis proceeds.

As can be shown by finite-difference techniques, I_A to any node n in the model is simply the resultant of current flow from points $n + 1$ and $n - 1$. Simulation of I_B is much more difficult. A schematic of a proposed circuit for calculating I_B is given in figure 28.4. The output may be fed directly to node n. However, to effect a solution, only the e versus I_B converter (the last element in the circuit of figure 28.4) need be constructed at each node. By adding memory to this converter, it will be possible to switch the circuit of figure 28.4 continuously over the network of nodes, changing the value of I_B at each pass. Use of such a switching arrangement would permit solving problems of one-dimensional flow with only one set of the equipment shown in figure 28.4. The third term of equation (2) may be simulated at each node by an electronic element whose capacity changes as a function of voltage at the node. The latter element is to be designed so that the capacity versus node-voltage curve is congruent with an appropriate curve of D_l versus h_l, such as the one shown in figure 28.1. Varying boundary conditions, in terms of either liquid head or flow rates, may be applied to both or only one end of the resistor elements and bias control.

Analog construction is underway with the objective of solving for drainage from homogeneous pro-

files; computed results will be compared with laboratory data already available in the U. S. Geological Survey Hydrologic Laboratory, Denver, Colo. Once these initial phases are completed, studies will be made of drainage from nonhomogeneous profiles. It seems that the basic analog plan described here can more easily be modified to account for nonhomogeneities than other analytical techniques thus far considered. Nevertheless, the search for a more efficient analog system is being continued while development work on the above electric analog continues.

REFERENCES

Nelson, R. W., 1960, Ground water movement rates: Am. Geophys. Union Ground-Water Symposium, Pacific Northwest Hydrologic Research Committee, Nov. 16, Portland, Oregon, oral presentation.

Philip, J. R., 1955, Numerical solution of equations of the diffusion type with diffusivity concentration-dependent: Faraday Soc. Trans., v. 51, p. 885–892.

Youngs, E. G., 1957, Moisture profiles during vertical infiltration: Soil Sci., v. 84, p. 283–290.

——, 1960, The drainage of liquids from porous materials: Jour. Geophys. Res., v. 65, p. 4025–4030.

29. DIRECT-READING CONDUCTIVITY BRIDGE

By I. S. McQUEEN and C. R. DAUM, Denver, Colo.

One measurement that has been useful in selecting desirable water sources and in identifying the aquifer supplying a given well is specific conductance, which is an indicator of the total dissolved solids in water. Laboratory analyses of water samples usually include this measurement. A conductivity bridge that could be used in the field would permit more rapid selection and identification of water sources, and would guide in the choice of sources for which more complete chemical analyses should be made. Available conductivity measuring equipment did not appear to be suitable for field use because of inconvenient operation, lack of sensitivity, or instability.

Preliminary requirements for a suitable instrument include the following: (a) a range of 0 to 10 millimhos, (b) provision for temperature measurement and temperature compensation, (c) provision for use of a conductivity cell with a cell constant of 2 and for a limited range of adjustment for variations between cells, (d) portability, (e) low power consumption, and (f) simplicity of use.

The newly designed instrument described here fulfilled all these requirements and several that were subsequently proposed. The circuit diagram for the completed bridge is shown in figure 29.1.

A transistorized oscillator supplies a 1,000-cycles-per-second signal for excitation and a small high impedance earphone is used to detect the null or balance point. The bridge measures either the resistance of a thermistor directly in ohms or the specific conductance of a water sample in millimhos by using a precision 10-turn variable resistor for the measuring arm and selected resistors for the ratio arms.

The resistance of the measuring arm, using a 0- to 5,000-ohm variable resistor and a 10-turn micrometer dial, is $\frac{1,000\ D}{2}$ ohms, in which D is the dial reading (0.00 to 10.00). Then, with the operation selector switch S_1, in position 2 and the bridge in balance, the following relationship holds:

$$\frac{1,000\ D}{2\ R_{th}} = \frac{600}{1,200}$$

$$1,000\ D = R_{th} \qquad (1)$$

means that when measuring resistance the dial in which R_{th} is the resistance of the thermistor. This reads directly from 0 to 10,000 ohms to the nearest 10 ohms.

A thermistor with a nominal resistance of 2,000 ohms at 25°C is used to measure the temperature of
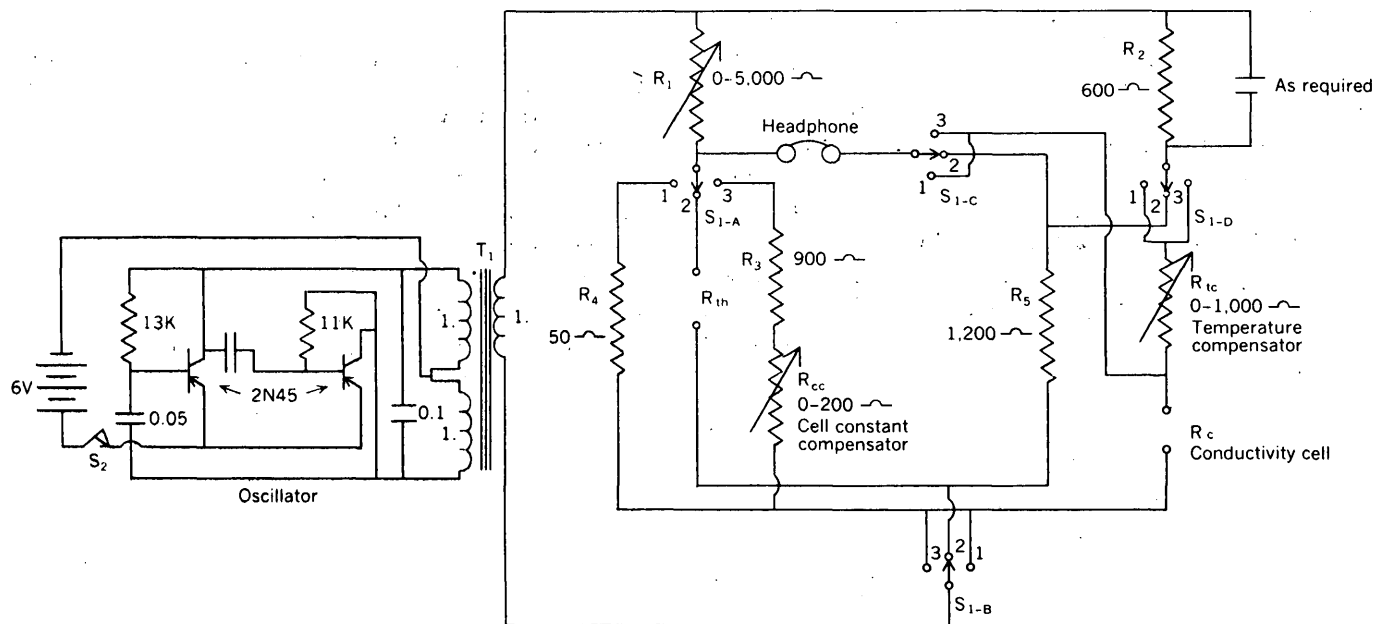
FIGURE 29.1.—Conductivity bridge circuit.

solutions. A calibration curve for this thermistor was obtained by laboratory measurements, so that the temperature of a solution can be obtained from this curve and the resistance readings. The temperature-compensation dial on the bridge is set for this temperature, and the bridge then measures the conductivity adjusted to a standard temperature of 25°C. Temperature compensation was calibrated according to data of U.S. Salinity Laboratory [1].

With the operation selector switch in position 3 and the bridge in balance, the following relation holds:

$$\frac{1,000\ D}{2(600 + R_{tc})} = \frac{900 + R_{cc}}{R_c}$$

in which R_{tc} is the resistance of the temperature correction resistor, R_{cc} is the resistance of the cell constant compensating resistor, and R_c is the resistance of the conductivity cell in an unknown solution. By definition $R_c = K/EC$, in which K is the cell constant and EC is the specific conductance of the solution. By substituting in the above formula we obtain:

$$1,000\ D\ K/2 = EC\ (600 + R_{tc})\ (900 + R_{cc}) \quad (2)$$

With a cell constant of 2 and a temperature of 25°C, $R_{tc} = 400$ ohms and $R_{cc} = 100$ ohms. Substituting

these values in equation 2 and simplifying we find that:

$$EC = D/1,000$$

Therefore, the dial reads directly in millimhos. The cell-constant compensation resistor was calibrated to keep the above equation in balance for cell constants of 1.8 to 2.2 [2].

Position 1 on the operations selector switch (S_1) was added to permit the use of a microdip cell with a cell constant of 0.1. The balance relation for this position is:

$$1,000\ D\ K/2 = EC\ (600 + R_{tc})\ 50$$

When the cell constant is 0.1 the bridge reads directly in millimhos.

A sensitive balance was difficult to obtain on samples with high conductivity when using a microdip cell; therefore, a small transistorized amplifier (not shown in fig. 29.1) was built as a separate unit to sharpen the null point. A capacitor placed in parallel with the 600-ohm ratio arm of the bridge also sharpens the null point. The use of the microdip cell had been limited to the laboratory in the past.

A series of 17 samples was measured in the field with this bridge. Repeat measurements were made

---

[1] $1,000\ f_t = 600 + R_{tc}$ where f_t = temperature factors from table 15, p. 90, Agricultural Handbook No. 60, U.S. Dept. of Agriculture, and R_{tc} is the resistance of the temperature-correction resistor.

[2] $\dfrac{1,000\ K}{2} = 900 + R_{cc}$. When $K = 1.8$, $R_{cc} = 0$, and when $K = 2.2$, $R_{cc} = 200$ ohms.

using a standard conductivity bridge. The measure-
ments agree within about 2 percent. The standard
deviation of the differences is 9.3 micromhos and

students "t" for the paired data is 0.438 which in-
dicates that there is no significant difference be-
tween the pairs of analyses.

⚒

GEOLOGY AND HYDROLOGY OF EASTERN UNITED STATES

30.   AGE OF THE "RIBBON ROCK" OF AROOSTOOK COUNTY, MAINE

By Louis Pavlides, Robert B. Neuman, and William B. N. Berry, Beltsville, Md., Washington, D. C.,
and Berkeley, Calif.

Discovery of Middle Ordovician graptolites estab-
lishes the age of at least part of the "ribbon rock"
in eastern Aroostook County, Maine. The "ribbon
rock" (originally the ribbon limestone) was as-
signed as a member of the Aroostook limestone in
and north of the Presque Isle area (fig. 30.1) and
classed as Middle Silurian in age (White, 1943, p.
129). Earlier, Twenhofel (1941, p. 169) suggested
that these rocks might be of Late Ordovician age
and possibly equivalent to similar rocks, such as the
Whitehead formation of the Gaspé Peninsula in
Quebec. Twenhofel's suggested Ordovician age as-
signment was followed by Boucot and others (1960)
in a recent compilation of the geology of northern
Maine. "Ribbon rock" in the Bridgewater area (fig.
30.1) is reassigned as a member of a new formation
in a forthcoming report (Pavlides, in press).

"Ribbon rock" underlies large parts of eastern
Aroostook County (fig. 30.1) corresponding closely
with the fertile potato-growing regions. The unit
consists of beds of medium-gray to bluish-gray lime-
stone several inches to several feet thick, separated
by somewhat thinner layers of gray calcareous to
greenish-gray noncalcareous slate. Limestone beds
range in composition from relatively pure carbonate
layers to argillaceous limestone and to calcareous
siltstone. Some layers that are complexly deformed
are found in sequence with beds having more regular
stratification. Interbeds of graywacke, and lenses of
graywacke and slate and of slate, are also included
in the unit. Stratigraphic boundaries of the "ribbon
rock" are poorly defined and little studied over broad
areas; in parts of the Bridgewater area, however,
the "ribbon rock" is underlain by graywacke and

slate, and overlain, at places gradationally, by more
argillaceous rock.

The "ribbon rock" is highly deformed. Tightly
compressed folds plunge steeply, some are nearly
vertical, and a few are inverted. Thus, most beds are
steeply inclined or vertical, and some are overturned.
Steep to vertical slaty cleavage is common, especially
south of Mars Hill, where a steep lineation results
from the intersection of bedding and cleavage.

Graptolites that for the first time permit reliable
age determination of the "ribbon rock" were found
in 1960 at a roadside exposure 2 miles east of Colby
(locality 3 of fig. 30.1) by W. H. Forbes, amateur
paleontologist of Washburn, Maine, who has made
several other valuable fossil discoveries in this area
(Berry, 1960a). The fossils occur through several
feet of calcareous siltstone. They are, on the whole,
poorly preserved, most having been stretched or
compressed. Many, however, are preserved in re-
lief, and some that are preserved as molds yielded
latex peels that afford good material for study.

W. B. N. Berry examined the collection and identi-
fied the following forms:

> *Amplexograptus* sp.
> *Amplexograptus* cf. *A. perexcavatus* (Lapworth)
> *Climacograptus* cf. *C. typicalis* mut. *posterus* Ruedemann
> *Diplograptus?* spp. (two distinct kinds of this form are
>   represented; one is long and slender, the other shorter
>   and wider)
> *Orthograptus* aff. *O. truncatus* (Lapworth)
> *Orthograptus truncatus* cf. var. *intermedius* (Elles and
>   Wood)
> Other orthograptids of the *O. truncatus* type

Some of the orthograptids of the *O. truncatus* type
are probably new. Their poor preservation, how-
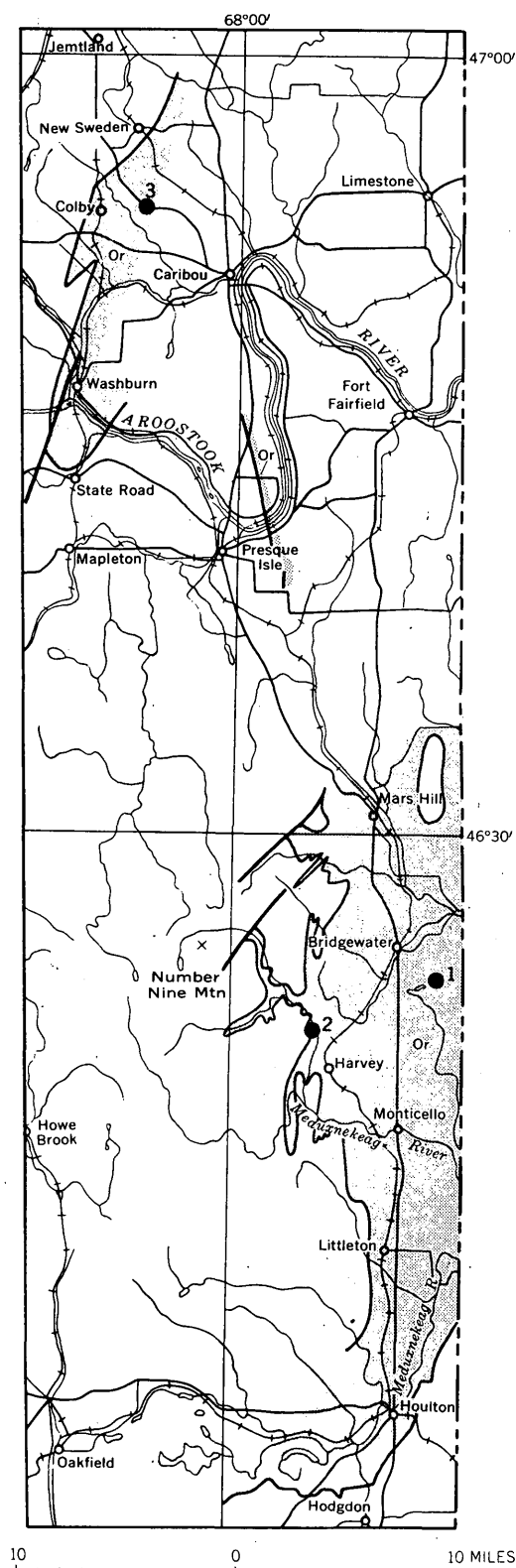
FIGURE 30.1.—Known distribution of "ribbon rock" (Or) in Aroostook County, Maine. Northern part modified from White, 1943, plate 24; southern half from geologic mapping by Louis Pavlides. Numbers refer to fossil localities. Igneous rocks within "ribbon rock" belt not shown.

ever, and that of the questionable *Diplograptus*, prohibits more certain identification.

The assemblage of many orthograptids of the *truncatus* group (especially the presence of *O. truncatus* cf. var. *intermedius*), other large diplograptids, and the *Climacograptus* of the *C. typicalis* group, is probably representative of the zone of *Orthograptus truncatus* var. *intermedius*. Closely similar assemblages have been recognized by Berry (1960b, p. 38) from the Snake Hill and Canajoharie shales in New York, and the Magog shale in Quebec. Berry (1960b, p. 38–39) discussed correlation of the zone with the standard New York Ordovician stages, and concluded that it was equivalent to the Trenton.

Other fossils that have been found in the "ribbon rock" include elongate aggregates of ovoid pellets that were found about 1¾ miles southeast of Bridgewater (locality 1 of fig. 30.1). These aggregates are about 5 cm long, and 1 cm in cross section. The individual pellets are closely packed and arranged parallel to the borders of the aggregates. They are 2 to 3 mm long and slightly more than ½ mm in diameter. Dr. Walter Häntzschel of the Geologisches Staatsinstitut, Hamburg, examined these pellets in 1958 and he suggested they were the work of mud-ingesting worms, perhaps worms that had been given the generic name *Tomaculum* by Groom (1902). Such pellets were originally found in Ordovician rocks in England, and they have also been found in Ordovician rocks of France, Germany, and Czechoslovakia (Pénau, 1941). It is noteworthy that Dr. Häntzschel's identification preceded Forbes' discovery of the graptolites, and came at a time when many still considered these rocks to be of Silurian age.

Minute fossils, none larger than 3 mm and mostly fragmentary, have been found in thin sandstone layers about 5 miles southwest of Bridgewater (locality 2 of fig. 30.1). The fossils include smooth ostracodes, fragments of bryozoan zoaria, and brachiopods, but the material is inadequate for specific identification. Brachiopods, represented by an orthoid, a rhynchonellid, and a leptellid, do not contradict the age assignment indicated by the graptolites.

Rocks like those of "ribbon rock" are present to the east in New Brunswick, and the northeast along highways between Grand Falls, N. B., and Matapedia, Quebec, at the southwestern end of the Gaspé Peninsula. They extend, also, from Matapedia (Crickmay, 1932; Béland, 1958, 1960) across the Gaspé Peninsula to Percé (McGerrigle, 1953), the type locality of the Upper Ordovician Whitehead for-

mation. Although the Whitehead has an unusual shelly fauna (Schuchert and Cooper, 1930; Cooper and Kindle, 1936), its lithologic similarity to the "ribbon rock" suggests that within this belt rocks of this kind span a considerable segment of Ordovician time.

REFERENCES

Béland, Jacques, 1958, Preliminary report on the Oak Bay area: Quebec Dept. Mines Prelim. Rept. 375, 12 p.

————, 1960, Preliminary report on Rimouski; Matapedia area: Quebec Dept. Mines Prelim. Rept. 430, 18 p.

Berry, W. B. N., 1960a, Early Ludlow graptolites from the Ashland area, Maine: Jour. Paleontology, v. 34, p. 1158–1163.

————, 1960b, Graptolite faunas of the Marathon region, West Texas: Texas Bur. Econ. Geology Pub. 6005, 179 p.

Boucot, A. J., Griscom, Andrew, Allingham, J. W., and Dempsey, W. J., 1960, Geologic and aeromagnetic map of northern Maine: U.S. Geol. Survey open-file report.

Cooper, G. A., and Kindle, C. H., 1936, New brachiopods and trilobites from the Upper Ordovician of Percé, Quebec: Jour. Paleontology, v. 10, p. 348–372.

Crickmay, G. W., 1932, Evidence of Taconic orogeny in Matapedia Valley, Quebec: Am. Jour, Sci., ser. 5, v. 24, p. 368–386.

Groom, Theodore, 1902, The sequence of the Cambrian and associated beds of the Malvern Hills: Geol. Soc. London Quart. Jour., v. 58, p. 89–135.

McGerrigle, H. W., 1953, Geological map of Gaspé Peninsula: Quebec Dept. of Mines.

Pavlides, Louis, in press, Geology and manganese deposits of the Maple and Hovey Mountains area, Aroostook County, Maine: U.S. Geol. Survey Prof. Paper 362.

Pénau, Joseph, 1941, Die Anwesenheit von *Tomaculum problematicum* im Ordovicium West-Frankreichs: Senckenbergiana, v. 23, p. 127–132.

Ruedemann, Rudolf, 1936, Ordovician graptolites from Quebec and Tennessee: Jour. Paleontology, v. 10, p. 385–387.

Schuchert, Charles, and Cooper, G. A., 1930, Upper Ordovician and Lower Devonian stratigraphy and paleontology of Percé, Quebec: Am. Jour. Sci., ser. 5, v. 20, p. 161–176, 265–392.

Twenhofel, W. H., 1941, The Silurian of Aroostook County, northern Maine: Jour. Paleontology, v. 15, p. 166–174.

White, W. S., 1943, Occurrence of manganese in eastern Aroostook County, Maine: U.S. Geol. Survey Bull. 940–E, p. 125–161.

31. RATIO OF THORIUM TO URANIUM IN SOME PLUTONIC ROCKS OF THE WHITE MOUNTAIN PLUTONIC-VOLCANIC SERIES, NEW HAMPSHIRE

By Arthur P. Butler, Jr., Denver, Colo.

Work done in cooperation with the U.S. Atomic Energy Commission

---

Plutonic rocks of the White Mountain plutonic-volcanic series, in New Hampshire, are slightly alkalic and somewhat more radioactive than calc-alkalic rocks of other igneous suites in New Hampshire (Billings and Keevil, 1946). Some additional study of the distribution of uranium and thorium in rocks of this series is being carried on as one aspect of the Geological Survey's investigation of uranium and thorium in selected suites of igneous rocks. Preliminary summary of analyses for uranium has shown that felsic rocks of this series are 2 to 3 times as rich in uranium as their counterparts among calc-alkalic rocks (Larsen and others, 1956, p. 70–72). Thorium analyses were not available when the summary of uranium analyses was reported. The amounts of thorium and uranium and the thorium-uranium ratios in 24 samples of these rocks are summarized here.[1]

Work toward the results reported here began in part under the leadership of the late E. S. Larsen, Jr., and has benefited materially from consulation with E. S. Larsen, 3d, and David Gottfried on many problems.

The plutonic rocks of the series range in composition from gabbro to granite. As shown by analyses (Chapman and Williams, 1935, table 1), most of the rocks (but particularly the felsic rocks) are slightly richer in sodium and potassium and poorer in calcium than corresponding types of calc-alkalic rocks. The bulk of the rocks cropping out

---

[1] Lyons (Art. 32) presents somewhat similar data for rocks of three older plutonic series in New Hampshire.

are granite, quartz syenite, and syenite (Billings and Keevil, 1946, table 1). Biotite granite occupies about 55 percent of the area of outcrop of the series.

The plutonic rocks are intruded in many separate masses, some simple and some composite. The main mass, also called the White Mountain batholith (Billings, 1956, p. 70), is a composite group of intrusions. It is about 33 miles long east-to-west and about 25 miles wide. Granites of this mass were sampled fairly systematically in order to obtain nearly representative data for the largest mass of rock. Consequently, the data reported here are probably more nearly representative of the bulk of the granite in the batholith than are the data for other types of rock and for granites from other locations.

Samples analyzed for thorium were chosen from a much larger number of samples analyzed for uranium (Larsen and others, 1956, p. 72; Butler, 1956). The samples so chosen represent the range of uranium contents and of the rock types sampled. They include samples of gabbro, biotite-quartz monzonite, biotite and pyroxene-amphibole syenites, fayalite-amphibole quartz syenite, amphibole granite, and biotite granite (Conway).

Analyses for uranium and thorium were made in the Washington laboratory of the Geological Survey by the methods described by Grimaldi and others (1952) and Levine and Grimaldi (1958), respectively. A summary of the results of those analyses and of the thorium-uranium ratios is given in table 1.

The average uranium and thorium contents in biotite granite and some amphibole granite of the White Mountain plutonic series are somewhat greater than the average contents of these elements in granites of the Oliverian and New Hampshire

plutonic series, two of the older calc-alkalic plutonic series in New Hampshire (tables 2 and 4, Art. 32, this volume). However, the average values of the thorium-uranium ratio in biotite granite and amphibole granite of the White Mountain series is 3.8 to 4.3, which falls within the range of the ratios 3.3 to 4.3 reported by Lyons (Art. 32, this volume) in the two nearby older granites, and within the range 3.7 to 4.7 reported by Larsen and Gottfried (1960) in granites and quartz monzonites from three western batholiths. In other rocks of the White Mountain plutonic-volcanic series, rather scattered data suggest somewhat larger values for the thorium-uranium ratio in amphibole granite of outlying masses and in some syenites than in biotite granite and amphibole granite of the main mass.

Among the granite masses of the White Mountain plutonic-volcanic series the rocks of the main batholithic mass are slightly richer in both uranium and thorium than their counterparts in the outlying masses. Also among the felsic rocks those with lesser uranium contents tend to have higher Th/U ratios than the rocks richer in uranium. This relation, decrease in Th/U ratio with increase of uranium, is even more distinct if the samples of felsic rocks are grouped by intervals of uranium content without regard to petrographic type or geographic position as shown on page B–69.

The biotite granite (Conway granite) is the only rock type for which there are enough samples to make a similar comparison among samples of one rock type. In 5 samples of this granite containing 10 ppm or more uranium the value of the Th/U ratio is 3.1 whereas in 5 samples containing less than 10 ppm uranium it is 5.6. No petrographic features of

TABLE 1.—*Thorium and uranium contents and Th/U ratios in some igneous rocks of the White Mountain plutonic-volcanic series, New Hampshire*

[Analysts, A. B. Caemmerer, E. Y. Campbell, L. B. Jenkins, and Roosevelt Moore]

Rock type and general location	Number of samples	Uranium (parts per million)		Thorium (parts per million)		Th/U	
		Range	Average	Range	Average	Range	Average [1]
Gabbro, Belknap Mountains	1	....	0.9	....	0.9	....	1.0
Biotite quartz monzonite, Merrymeeting stock	1	....	3.5	....	18.7	....	5.3
Pyroxene syenite, Pilot range	1	....	1.2	....	10.2	....	8.5
Pyroxene syenite, main mass	1	....	2.5	....	9.5	....	4.5
Amphibole-biotite syenite, Belknap Mountains	2	6.9 – 8.0	7.5	25.0 – 33.5	29.3	3.1 – 4.9	3.9
Quartz syenite, north side Pilot Range mass	1	....	4.1	....	27.0	....	6.6
Amphibole granite, Pilot range mass	2	2.4 – 3.5	2.9	14.0 – 21.0	17.5	5.8 – 6.0	5.9
Amphibole granite (Mount Osceola type), main mass	3	3.6 – 9.9	7.4	25.0 – 40.5	30.5	3.4 – 6.9	4.3
Biotite granite, smaller masses	3	4.3 – 14.2	9.7	30.0 – 44.0	35.3	2.3 – 7.0	3.8
Biotite granite, main mass	9	5.2 – 25.5	13.0	33.0 – 77.0	49.4	2.0 – 8.2	3.8

[1] The average Th/U ratio is the ratio of the means of the Th and U contents.

Uranium (range, in parts per million)	Number of samples	Uranium (average, in parts per million)	Thorium (average, in parts per million)	Th/U
10–25.5........	7	15.9	51.6	3.3
5–10..........	8	7.6	36.0	4.7
1.2–5.0.......	8	3.2	19.4	6.3

the samples have been observed which might explain the differences in uranium contents from sample to sample or the difference in Th/U ratios between the group of samples richer in uranium and that leaner in uranium. At present, an explanation for this difference is lacking.

REFERENCES

Billings, M. F., 1956, The geology of New Hampshire, Pt. II, Bedrock geology: New Hampshire State Planning and Devel. Comm., Concord.

Billings, M. P., and Keevil, N. B., 1946, Petrography and radioactivity of four Paleozoic magma series in New Hampshire: Geol. Soc. America Bull., v. 57, no. 9, p. 797–828.

Butler, A. P., Jr., 1956, White Mountain plutonic series, New Hampshire, in Geologic investigations of radioactive deposits—Semiannual progress report for June 1 to Nov. 30, 1956: U.S. Geol. Survey TEI–640, issued by U.S. Atomic Energy Comm. Tech. Inf. Serv. Ext. Oak Ridge, Tenn.

Chapman, R. W., and Williams, C. R., 1935, Evolution of the White Mountain magma series: Am. Mineralogist, v. 20, no. 7, p. 502–530.

Grimaldi, F. S., May, Irving, and Fletcher, M. H., 1952, U.S. Geological Survey fluorimetric methods of uranium analysis: U.S. Geol. Survey Circ. 199, 20 p.

Larsen, E. S., Jr., Phair, George, Gottfried, David, and Smith, W. L., 1956, Uranium in magmatic differentiation, in Contributions to the geology of uranium and thorium by the United States Geological Survey and Atomic Energy Commission of the United Nations International Conference on Peaceful Uses of Atomic Energy, Geneva, Switzerland, 1955: U.S. Geol. Survey Prof. Paper 300, p. 65–74.

Larsen, E. S., 3d, and Gottfried, David, 1960, Uranium and thorium in selected suites of igneous rocks: Am. Jour. Sci., Bradley volume, v. 258–A, p. 151–169.

Levine, Harry, and Grimaldi, F. S., 1958, Determination of thorium in the parts per million range in rocks: Geochim. et Cosmochim. Acta, v. 14, p. 93–97.

32.   URANIUM AND THORIUM IN THE OLDER PLUTONIC ROCKS OF NEW HAMPSHIRE

By JOHN B. LYONS, Hanover, N. H.

Work done in cooperation with the U.S. Atomic Energy Commission

Field studies in New Hampshire (Billings, 1937) have established the existence of four Paleozoic plutonic series, one of Taconic age (the Highlandcroft series), two of Acadian age (the Oliverian and New Hampshire series), and one of post-Devonian age (the White Mountain series). Chemical and spectrochemical data relating to the distribution of uranium and thorium in the three older series are summarized in this report [1]. The analytical work was done in the Geological Survey laboratories by Marian Schnepfe, Alice Caemmerer, Roosevelt Moore, E. Y. Campbell, and L. B. Jenkins.

[1] A paper by Butler (Art. 31, this volume) presents somewhat similar data for rocks of the younger White Mountain plutonic-volcanic series.

HIGHLANDCROFT PLUTONIC SERIES

All intrusives of this series have been metamorphosed to the greenschist facies. The rocks originally were quartz diorites, granodiorites, or quartz monzonites, and consist now of varying amounts of albite, microcline, epidote, quartz, chlorite, hornblende, sphene, zircon, apatite, and opaque minerals. Uranium and thorium analyses for some rocks of this series are listed on table 1.

Sphene (586 ppm), zircon (342 ppm), apatite (30 ppm), and epidote (5 ppm) are the most uraniferous minerals. The sphene and epidote account for approximately 42 percent of all the uranium in the rock.

TABLE 1.—*Chemical analyses for uranium and thorium in rocks of the Highlandcroft plutonic series*

Rock type	Number of samples analyzed	Uranium (ppm)		Number of samples analyzed	Thorium (ppm)		Mean Th: U ratio
		Mean	Range		Mean	Range	
Quartz monzonite...	6	3.7	2.7-5.0	3	12.6	10.6-14.8	3.4
Granodiorite......	1	3.0	....	1	11.8	....	3.9
Sodaclase-tonalite...	1	3.1	....	1	11.3	....	3.6

OLIVERIAN PLUTONIC SERIES

Domal plutons of the Oliverian series consist of the following petrographic types (Billings and Keevil, 1946, p. 816): quartz diorite, 10 percent; granodiorite, 30 percent; quartz monzonite, 30 percent; granite, 17 percent; and syenite, 13 percent. These rocks are at grade with the surrounding epidote amphibolite and amphibolite facies rocks, and consist of varying quantities of quartz, microcline, oligoclase-andesine, hornblende, biotite, epidote, muscovite, apatite, sphene, and opaque minerals.

Uranium and thorium analytical data for rocks in the Oliverian series are presented on table 2.

Uranium contents of minerals concentrated from 5 samples of the Oliverian series are shown on table 3. There is a consistent relation between the uranium content of each mineral and the kind of rock from which the mineral was extracted; the more felsic the rock, the higher the uranium content of each of its minerals.

Approximately 70 percent (59 percent to 78 percent) of the total uranium in any rock of the Oliverian series is tied up in sphene and epidote—both of which are of metamorphic origin.

NEW HAMPSHIRE PLUTONIC SERIES

Stocks and sheetlike plutons of this series consist of the following rock types (Billings and Keevil, 1946, p. 812): diorite, 1 percent; amphibolite, 1 percent; quartz diorite to granodiorite, 23 percent; Bethlehem gneiss (granodiorite to quartz monzonite), 14 percent; Kinsman quartz monzonite, 26

TABLE 2.—*Chemical analyses for uranium and thorium in rocks of the Oliverian plutonic series*

Rock type	Number of samples analyzed	Uranium (ppm)		Number of samples analyzed	Thorium (ppm)		Mean Th: U ratio
		Mean	Range		Mean	Range	
Granite..........	13	5.8	1.8-13.0	10	19.3	7.5-32	3.3
Quartz monzonite..	8	3.1	1.1-5.3	5	12.1	6.2-21	3.9
Granodiorite......	15	2.5	0.8-5.0	5	14.6	6.5-38	5.8
Quartz diorite.....	15	1.9	0.8-3.6	6	7.1	2.9-14.8	3.7
Pegmatite........	3	9.1	1.3-13.7	2	4.2	3.6-4.7	0.46
Aplite...........	3	9.3	2.1-15.9	3	39.2	5.5-57	4.2
Wallrocks and inclusions.......	6	1.3	0.6-1.8	....	....	....	....

TABLE 3.—*Uranium contents of minerals of the Oliverian plutonic series*

[In parts per million]

Mineral	Number of determinations	Range	Mean
Quartz..............	5	0.25– 1.45	0.77
Potassium feldspar....	5	.25– 1.45	.72
Plagioclase..........	5	.25– 2.3	.97
Hornblende..........	1	.84	.84
Biotite and chlorite...	4	1.11–24.6	9.9
Epidote.............	4	11.7 –204	85.
Sphene.............	5	220–411	308.
Apatite.............	4	11.1 –26.3	19.1
Zircon.............	5	466–2770	1317.

percent; and Concord (and other) granite, 29 percent. These rocks are surrounded by amphibolite- and granulite-facies metamorphic rocks, with which they are at grade. Minerals include quartz, microcline, oligoclase-andesine, biotite, muscovite, garnet, hornblende, monazite, xenotime, allanite, zircon, and opaque minerals.

Uranium and thorium contents of the major rock types of this series are listed on table 4.

Minerals have been separated from 4 samples of the New Hampshire series and analyzed for uranium (table 5). Abnormally high uranium concentrations recorded for some of the minerals in these samples are the result of the inclusion of a pegmatite sample; its minerals cause the abnormality.

Rocks of the New Hampshire series have between 50 percent and 90 percent of their total uranium distributed among the major rock-forming silicates.

CONCLUSIONS

At least three deductions or conclusions can be drawn from the analyses: (a) Uranium and thorium

TABLE 4.—*Chemical analyses for uranium and thorium in rocks of the New Hampshire plutonic series*

Rock type	Number of samples analyzed	Uranium (ppm)		Number of samples analyzed	Thorium (ppm)		Mean Th: U ratio
		Mean	Range		Mean	Range	
Granite..........	7	4.3	2.8-5.8	5	18.3	10.7-28.5	4.3
Quartz monzonite (chiefly Kinsman)	15	3.3	1.5-6.3	6	15.7	9.1-19.4	4.8
Quartz monzonite to granodiorite (Bethlehem gneiss)..........	28	3.6	2.2-5.2	10	14.9	11.7-18.6	4.1
Quartz diorite......	2	3.1	2.9-3.4	1	12.2	....	3.9
Pegmatite........	3	16.7	4.7-39	3	3.9	2.8-5.0	0.23
Aplite............	3	7.2	3.3-14.2	2	28.6	4.3-52	4.0
Wallrocks and inclusions........	5	3.3	0.8-5.0	1	16.0	....	4.9

TABLE 5.—*Uranium contents of minerals of the New Hampshire plutonic series*

[In parts per million]

Mineral	Number of determinations	Range	Mean
Quartz	4	0.10– 2.5	0.92
Potassium feldspar	4	.10– 1.8	.67
Plagioclase	4	.30– 6.6	2.34
Biotite	3	.53– 2.6	1.71
Muscovite	4	1.4 – 3.1	2.20
Garnet	2	0.88– 5.5	3.14
Magnetite	4	2.0 –39.5	23.2
Ilmenite	3	2.0 –32.7	17.0
Pyrite	2	16.7 –373	195.
Apatite	4	1.3 –16.4	13.8
Monazite	3	624–2570	1516
Xenotime	1	798	798
Zircon	3	500–20,000	6700

analyses confirm the earlier work of Billings and Keevil (1946), based on alpha counts, both as to the general level of radioactivity, and the increase in radioactivity in the more felsic rocks of these series; (b) the thorium:uranium ratios for these rocks lie within expectable ranges for calc-alkaline plutons. Much lower ratios for pegmatites compared to aplites (table 4) indicate that the two rock types belong to different fractions of the parent magma; (c) neocrystallization during metamorphism apparently causes a redistribution of uranium and thorium. Sphene and epidote formed during recrystallization serve as traps for radioactive elements.

REFERENCES

Billings, M. P., 1937, Regional metamorphism of the Littleton-Moosilauke area, New Hampshire: Geol. Soc. America Bull., v. 48, p. 463–566.

Billings, M. P., and Keevil, N. B., 1946, Radioactivity of four Paleozoic magma series in New Hampshire: Geol. Soc. America Bull., v. 57, p. 797–828.

33.   DISTANCE BETWEEN BASINS VERSUS CORRELATION COEFFICIENT FOR ANNUAL PEAK DISCHARGE OF STREAMS IN NEW ENGLAND

By JACOB DAVIDIAN and M. A. BENSON, Iowa City, Iowa, and Washington, D. C.

One interesting sidelight of a recent investigation of flood-frequency relations in New England was a study of the coefficient of correlation between annual peak discharges for different pairs of streams in that area. Floods at many of the gaging stations in the area result from a few major storms that are widespread and affect many streams at the same time, rather than from scattered storms of small areal extent. It was of interest to determine a median coefficient of correlation of annual peak discharges between gaging stations in New England in order to determine the interdependence of the peak-flood data.

To avoid the prohibitive amount of work of computing the 13,366 possible individual correlations between the 164 gaging stations used in the investigation, an estimate was made by correlating data for pairs of stations selected at random. The 164 stations were numbered consecutively from 1 to 164. Then, a table of random numbers was used from which groups of three digits were selected. The first 400 numbers of magnitude less than 165 were listed; adjacent numbers were paired. Thus, 200 pairs of numbers of magnitudes 1 to 164, representing the stations with those numbers, were available and their selection was shown by a statistical test (chi-square) to be truly random.

The airline distance between the geographic centers of the drainage basins of each pair of stations was then measured. The distribution of these distances for the 200 pairs of stations indicated that the median distance was about 94 miles, with a range from 8 to 403 miles.

The range of distances from 8 to 403 miles was subdivided into increments of about 20 miles, and a random sampling of the pairs of stations in each increment was made to cut down further the amount of work of computing correlations between stations. Within the group of stations 75 to 110 miles apart, all of the available pairs in the list of 200 were tested to obtain a better value of the correlation coefficient for the median distance of 94 miles. A total of 54
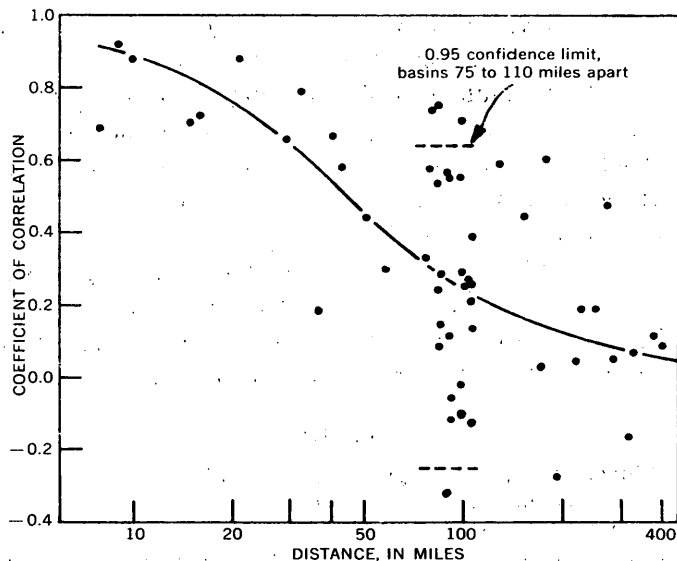
FIGURE 33.1.—Relation between correlation coefficient of annual peak discharges and distances between basins.

pairs was used. The annual peak discharges for the selected pairs were listed for concurrent periods and were ranked in order of magnitude. For each pair, the Spearman rank coefficient of correlation was determined. Of the 54 pairs, 8 had negative correlation coefficients.

In figure 33.1 the coefficient of correlation between stations (arithmetic scale) is plotted against distance between stations (logarithmic scale). A coefficient of correlation of about 0.26 corresponds to the median distance of 94 miles, and is taken to be the median correlation coefficient for the 164 New England stations that were considered in the original study. The curve has been drawn so that the extremes would be asymptotic to 1.0 and 0.0. The curve shows an increasingly good correlation with decreasing distance separating the basins.

The 27 pairs of stations between 75 and 110 miles apart were studied more thoroughly to test the significance of the scatter within the band. These 27 pairs have an average of 17.3 years of concurrent records. The 95-percent confidence belt for the sample correlation coefficient of 0.26 and the sample size of 17.3 ranges between −0.25 and +0.64. This means that although a median value of 0.26 is indicated on the illustration, pure chance alone leads to a scatter between −0.25 and +0.64 for 95 percent of the observations. These limits are somewhat approximate because the periods of record have been averaged. For these 95-percent confidence limits, 1.35 points would be expected outside the limits; actually there are 4 points, which is a significant difference statistically and which suggests the possibility of unknown factors causing more scatter than could be expected by chance alone. Negative coefficients of correlation are to be expected by chance for stations having relatively short concurrent records. Had the average length of concurrent record between pairs of stations been about 45 years instead of 17.3 years, the 95-percent confidence limits for a median correlation coefficient of 0.30 would have been 0.0 to +0.55.

It is generally considered that stations with like characteristics will have a higher degree of correlation than stations with unlike characteristics. Therefore, an attempt was made to relate the departures of correlation coefficient from the median curve of the graph shown with (a) difference in drainage area size, (b) ratios of drainage area size, (c) number of years of concurrent record, (d) difference in an "orographic factor" evaluated in the New England flood-frequency study, and (e) difference in average winter temperatures (a measure of the difference in the types of flood peaks). None of these seemed to relate to the departures in the degree of correlation.

It might be expected that a correlation between two small drainage areas, for example 100 miles apart, would be less than the correlation between two large areas the same distance apart. Any such differences cannot be detected in this set of data, possibly because the differences are much smaller than the variations due to chance. Apart from distance between stations, present hydrologic knowledge cannot aid us in predicting which pairs of stations would correlate well or which would correlate poorly. Even though two drainage basins were separated by a high mountain barrier transverse to the storm winds, the annual peak discharges for each, though far different in magnitude, might be proportional.

This study indicates that a high coefficient of correlation between the annual peak discharges of two streams picked at random may be due to chance. In estimating peak discharge for years of no record, a station that appears to correlate best may not give better results than one of the other stations. Additional research on the use of correlative estimates of flood peaks is needed.

34. PLEISTOCENE STRATIGRAPHY OF BOSTON, MASSACHUSETTS

By C. A. KAYE, Boston, Mass.

An excavation in 1960 for a large underground garage in the lower slopes of Beacon Hill, at the western edge of the Boston Common, proved to be a key exposure for the unraveling of the Pleistocene stratigraphy of the area. Evidence for 4—and probably 5—ice advances and 3 marine transgressions occur in, or under, the garage and the surrounding lowland. Study of many hundreds of deep borings in the Boston basin, and soil-mechanics test data on compaction of materials, support these conclusions.

Preglacial surface.—Bedrock beneath the garage (fig. 34.1) consists of argillite of the Cambridge slate. The argillite is altered to a soft white kaolinitic saprolite under the southeastern part of the site, where it is buried by about 85 feet of Pleistocene deposits. Similar saprolite has been found in deep borings in at least six other places in the Boston basin. In one of the garage borings, weathered argillite was found to be overlain by 10 feet of fairly coarse quartz sand in a white clay matrix. This resembles kaolinitic quartz sands of Late Cretaceous age (Raritan(?) formation) on Martha's Vineyard, Block Island, Long Island, and New Jersey. Patchy remnants of Coastal Plain sediments may therefore occur in the Boston basin.

Drift I.—In 9 borings at the garage site, as much as 30 feet of very compact till was found at the base of the Pleistocene section (fig. 34.1). It is prevailingly a pebble till, poor in cobbles and boulders, and somewhat variegated in color. The high degree of compaction of the till is shown by standard penetration tests (Terzaghi and Peck, 1948, p. 265) which average more than 100 blows per foot. This thin dense till has been found in many deep borings in the Boston basin but has not been recognized on the surface.

Clay I.—As much as 25 feet of fairly soft to compact olive-gray unoxidized clay, sandy clay, and very fine sand was found between Drifts I and II in five garage borings. The clay is identical in appearance to certain clays along the New England seaboard that are recognized from sparse fossils to be of marine origin. Standard penetration tests ranged from 5 to 40 blows per foot. Clay I has not been recognized in surface exposures, and borings in the Boston area indicate that it has been preserved in only a few places.

Drift II.—This consists mostly of thick outwash, but some underlying till is associated with it in several of the garage borings (fig. 34.1). Outwash

Borings on, or referred to, this cross section
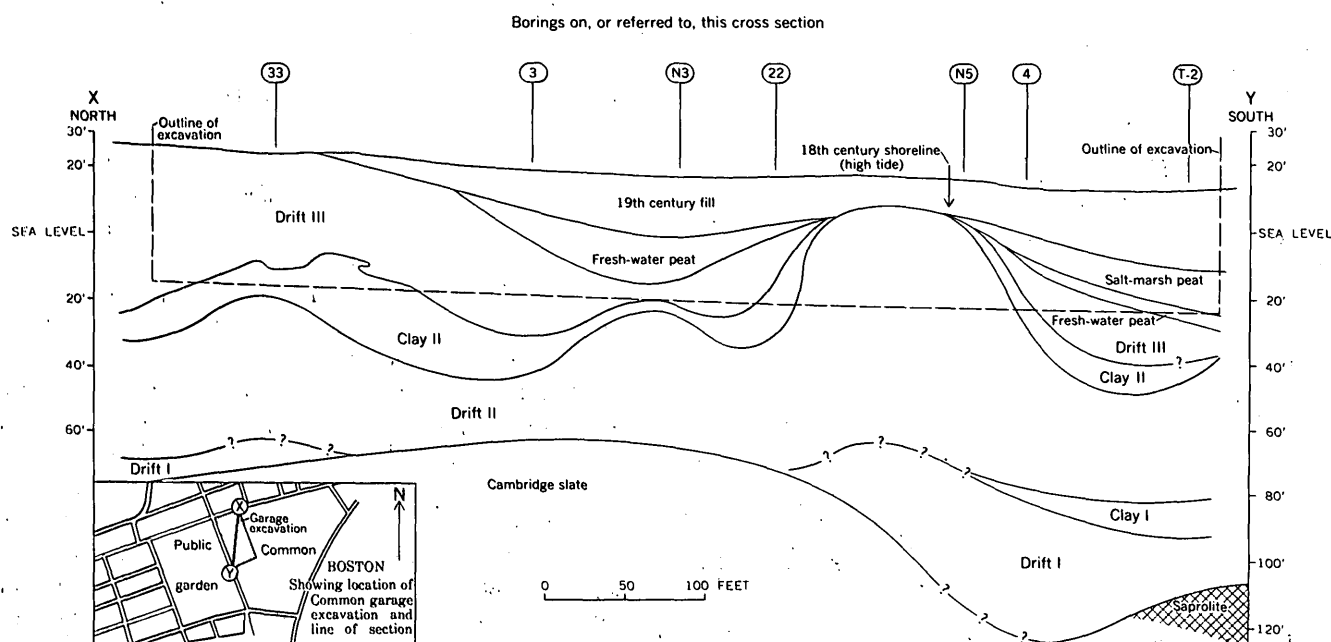
FIGURE 34.1.—North-south geologic cross section, lower Boston Common, at site of underground garage.

of Drift II was well exposed in the garage excavation and crops out at the surface quite widely in the Boston area. It is characteristically a brown, well-oxidized coarse gravel interbedded with somewhat lesser amounts of fine gravel and sand and relatively sparse layers of compact yellow silt. Outwash under the garage is about 65 feet in maximum thickness and it is oxidized throughout. Sparse samples and drillers' logs are inconclusive as to whether the underlying associated till is oxidized. Pebbles of schist and argillite in the outwash show varying degrees of decomposition, but, in general, most granitic rocks and feldspars appear fresh. At the garage the gravel has been folded into a series of three anticlines (fig. 34.1), presumably by the action of the ice that deposited Drift III.

Clay II.—Another clay having the physical characteristics of marine clays overlies Drift II at the garage excavation (fig. 34.1). It is unoxidized (blue gray to slightly greenish gray) except where close to the present surface. Clay II was deformed with Drift II. This is evident from numerous small faults in the gravel, formed during the folding, which extend up into the clay. Stratification of the clay—

FIGURE 34.2.—Contact of Drift III (above) and Clay II (below), showing scant signs of disturbance. East wall of excavation, underground garage, Boston Common.

marked by alternating lighter and darker laminae—is well marked in some zones. The contact of the clay and the overlying till is generally quite sharp; in places the bedding of the clay shows no disturbance whatever at the contact (fig. 34.2), in others gross bedding disturbances in the clay are evident to a depth of 3 or 4 feet below the contact. In several places in the excavation the contact is deformed into fairly large waves (fig. 34.1).

Drift III.—At the garage excavation more than 30 feet of till overlies Clay II. It appears to be the major component of Beacon Hill drumlin and probably the other drumlins of the Boston area. It is very well graded but has sparse boulders up to 10 feet in diameter. Cobbles and stones are predominantly of Cambridge slate and are generally conspicuously striated. A fabric study of the pebbles shows a preferred orientation of axial planes parallel to the long axis of Beacon Hill and adjacent drumlins (approximately S. 70° E.). The maximum depth of oxidation seen in the till at the garage excavation was 25 feet, although deep borings in Beacon Hill show the till there to be oxidized to a maximum depth of 65 feet. Differences in depth of oxidation are probably due mainly to differential erosion of the oxidized zone by the ice responsible for Drift IV. Fragments of shells—mostly very thick shelled *Mercenaria mercenaria*—occur in the till of Beacon Hill and other drumlins. These are possibly derived from Clay II.

Clay III.—This clay forms the bulk of the marine clay in the Boston basin and attains a thickness of 180 feet in a few places. In physical appearance it resembles the two older clays. It crops out as a patch over Drift III in the northeast corner of the garage excavation at about 15 to 25 feet altitude. Many borings in the Boston area show that it overlies drumlin till (Drift III); therefore, there can be no doubt that it is separate from, and younger than, Clay II. Borings indicate that where overlain by Drift IV, Clay III is oxidized to a depth of about 3 feet. Where exposed at the surface it is oxidized to a maximum depth of 10 feet. Marine mollusks were found in Clay III by the writer at West Lynn, at the north edge of the Boston basin, and Foraminifera were reported by Stetson and Parker (1942, p. 42) from the clay in Boston Back Bay. Sparse embedded cobbles and small stones suggest ice-rafting and therefore deposition at a time when an ice front *may* have been close to Boston. Spruce pollen is very abundant in the upper 10 feet at West Lynn (Estella B. Leopold, written communication), thus supporting a cold climate—or periglacial—depositional environ-
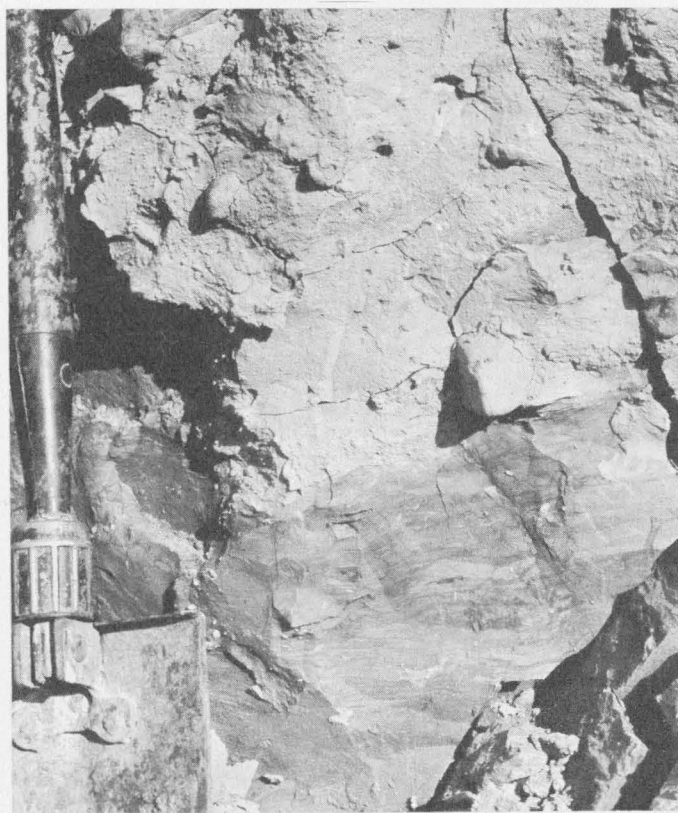
TABLE 1.—*Pleistocene deposits of Boston, Mass.*

Deposit	Description	Remarks	Depth of oxidation [1]	Direction of ice flow	Relative sea level [2]	Suggested age in years	Standard Pleistocene sequence
Drift IV	Boston basin: mostly outwash. Uplands: till and outwash.		In outwash generally less than 4 ft, in till 1½ ft.	S. 10°–30° E.	Lower than −30 ft.	13,000	Late Wisconsin (Cary substage; Lexington substage of Judson)
Oxidation of Clay III					Lower than −35 ft.	15,000	
Clay III	Marine clay. More than 180 ft thick under lowlands. Precompressed to depths of 70 ft.	Possibly deposited when ice front was not far from Boston.	3 ft under Drift IV, 10 ft elsewhere.		Found to altitude +25 ft in Boston. Contains fairly deep water fauna suggesting sea level above +50 ft.	26,000	Middle Wisconsin (Tazewell substage)
Oxidation of Drift III					Lower than − 20 ft.	28,000	
Drift III	The drumlin till.	Very compact in drumlins; less compact as ground moraine.	Maximum 65 ft in drumlins; where less, oxidized zone probably eroded by Late Wisconsin ice.	S. 60°–80° E.	Possibly above +50 ft.	65,000	Early Wisconsin (Iowan substage)
Clay II	Probably marine.	Probably source of shells in Drift III. May have been deposited during advance of Iowan ice.	None where recognized. May have been eroded.		Possibly about +50 ft.	75,000	Early Iowan (?) Sangamon interglacial
Oxidation of Drift II					−45 ft (?)	77,000 (?)	Sangamon interglacial
Drift II	Mostly gravelly outwash; some associated till.	Folded in places.	65 ft or more in sand and gravel. Some pebbles decomposed.	Unknown.	Below −75 ft.	100,000	Illinoian
Clay I	Probably marine.	Recognized only in borings.	None noted; possibly eroded.		−45 ft or above.	(?)	Early Illinoian (?) Yarmouth (?)
Drift I	Very compact till.	Recognized with certainty only in deep borings.	None noted.	Unknown.	(?)	(?) (?)	Kansan or Nebraskan

[1] Oxidized zone of all units but Drift IV was subject to erosion by later ice.
[2] Altitudes refer to present mean sea level.

ment. Although much of the clay is very soft (standard penetration test, 2 to 3 blows per foot), soil mechanics studies (A. Casagrande, written communication) show that it is precompressed (Terzaghi and Peck, 1948, p. 67) to a depth of as much as 70 feet below its surface. It is thought that this precompression resulted from the ensuing glaciation responsible for Drift IV.

Drift IV.—Overlying Clay III in many places in Cambridge and the Back Bay are outwash gravels that are only slightly oxidized and rarely exceed 20 feet in thickness. They are correlated with the poorly compacted and barely oxidized tills (oxidation generally less than 2 feet) that are found with patchy distribution on the uplands surrounding the Boston basin. This drift belongs to what Judson (1949) termed the Lexington substage of the Wisconsin. It is now fairly certain that the late Wisconsin ice responsible for it flowed approximately S. 20° E. and covered the entire Boston basin, probably reaching the outermost moraines off the southeastern New England shore. The direction of ice movement is in marked contrast to that of the drumlin-forming Iowan ice (table 1), which flowed approximately S. 70° E.

Table 1 summarizes the more salient facts about the Pleistocene section. Relative ages were assigned to the later drifts primarily on the basis of their depths of oxidation.

REFERENCES

Judson, S. S., Jr., 1949, The Pleistocene stratigraphy of Boston, Massachusetts, and its relation to the Bolyston Street Fishweir, in Johnson, F., ed., The Boylston Street Fishweir II: Phillips Acad., Robt. S. Peabody Foundation for Archaeology Papers, v. 4, no. 1, p. 7–48.
Stetson, H. C., and Parker, F. L., 1942, Mechanical analysis of the sediments and the identification of the Foraminifera from the building excavation, in Johnson, F. and others, The Boylston Street Fishweir: Phillips Acad., Robt. S. Peabody Foundation for Archaeology Papers, v. 2, p. 41–44.
Terzaghi, Karl, and Peck, R. B., 1948, Soil mechanics and engineering practice: New York, John Wiley & Sons, 566 p.

35.   IRON ORES OF ST. LAWRENCE COUNTY, NORTHWEST ADIRONDACKS, NEW YORK

By B. F. LEONARD and A. F. BUDDINGTON, Denver, Colo., and Princeton, N. J.

St. Lawrence County is a major producer of magnetite and crystalline hematite concentrates from low-grade ores of Precambrian age. The rocks of the district are mainly granitic. They are separated into an older quartz syenite gneiss series and a younger granite and granite gneiss series. Metasedimentary rocks, migmatites, and other rocks are subordinate. All the rocks except some granites and basaltic dikes have in some measure been dynamothermally metamorphosed.

The iron ore bodies are restricted to a structural knot of metasedimentary rocks and younger granitic rock, the latter representing members of the granite and granite gneiss series. Within this knot, developed at the intersection of two dominant regional structural trends, the metasedimentary rocks and sheets of younger granitic rock have been pressed into variously oriented isoclinal folds against buttresses of older granitic rock (fig. 35.1). Other major structural controls for iron-oxide mineralization have been recognized. All the major deposits are (a) on or within a mile of the borders of great areas of subperpendicular lineations, or (b) well within the central zone of subparallel lineations at places where lineations culminate, diverge, or change markedly in trend[1]. All the deposits are within a mile of the axes of major synclinal folds. Moreover, all the deposits are within 500 feet of at least one facies of the younger granite and granite gneiss.

The iron ores are of two types: magnetite deposits in skarn or marble (skarn ores), and mag-

[1] Subparallel lineations are mineral lineations whose rake is within 30° of the strike of the foliation, and subperpendicular lineations are those whose rake is within 30° of the direction of dip of the foliation (Buddington, 1956).
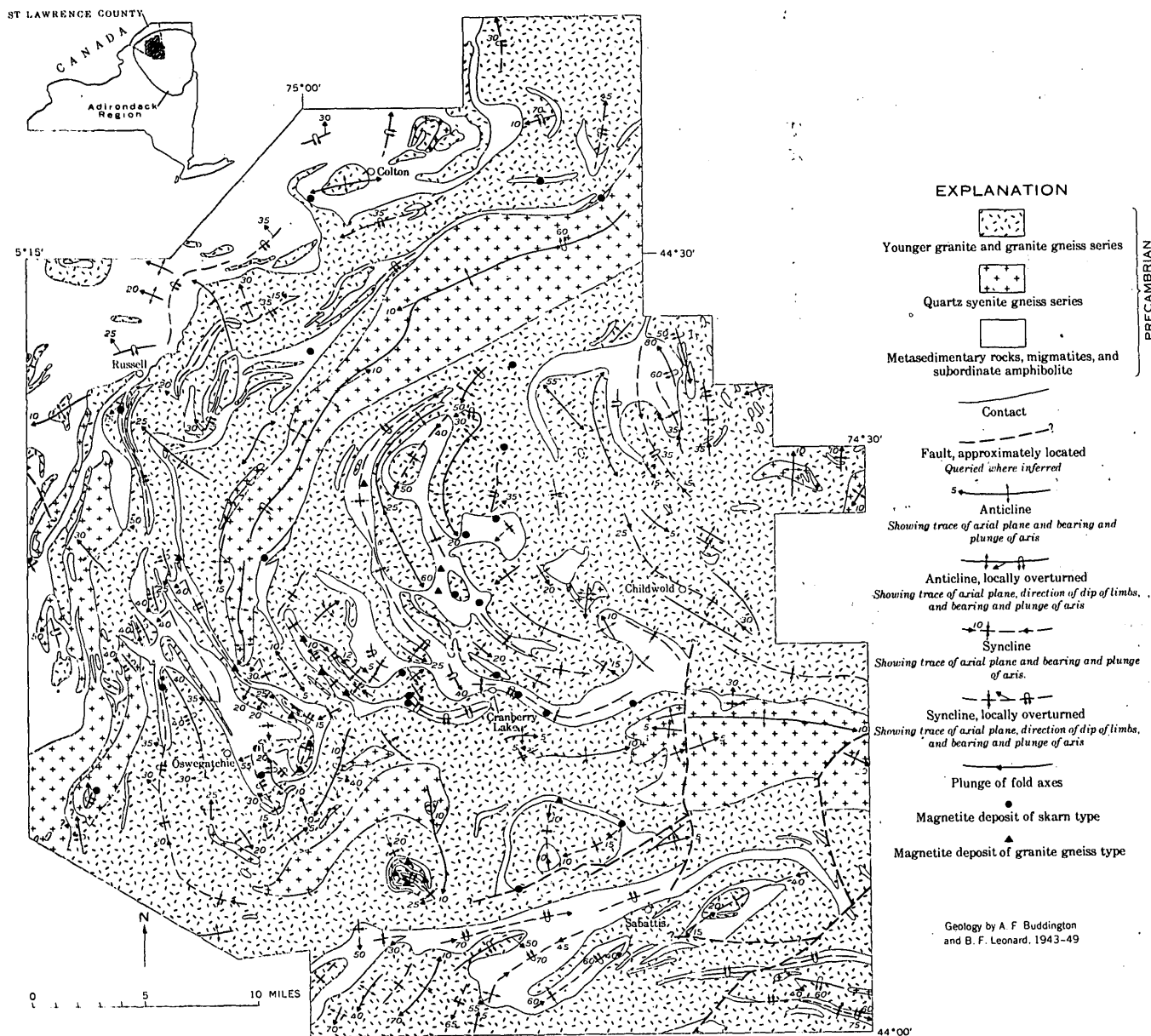
FIGURE 35.1.—Relation of magnetite deposits to major rock units and fold axes, St. Lawrence County magnetite district, New York.

netite deposits—with or without hematite—in microcline granite gneiss (granite gneiss ores).

Magnetite, virtually nontitaniferous, is the only significant iron oxide in skarn ores. The principal gangue mineral is green clinopyroxene, though biotite or dark amphibole is conspicuous locally. The skarn ores are variable in grade (generally 30-44 percent magnetic Fe), complex in structure, and small to moderate in size, tending to yield massive ore bodies. One major deposit and parts of several others are in skarn that was partly replaced by quartz, untwinned barium-bearing potassium feld-spar, fluorite, barite, and scapolite before introduction of the magnetite.

The granite gneiss ores contain magnetite, accompanied in some places by slightly titaniferous primary crystalline hematite. This hematite, with or without martite, forms sizable ore bodies locally. The principal nonmetallic minerals are quartz, untwinned barium-bearing potassium feldspar, biotite, manganiferous almandite, and sillimanite. The granite gneiss ores form disseminated deposits of uniformly low grade (generally about 25 percent recoverable Fe), remarkable continuity, and moder-

ate to very large size. One ore deposit is in gneiss that was partly replaced by quartz, barium-bearing potassium feldspar, fluorite, barite, and spessartite before introduction of iron oxide.

The iron ore deposits are mainly concordant with the complex structure of the country rock which they replace. At very large and very small scales, the deposits are nevertheless discordant. In shape, the deposits are tabular, fishhook, linear, mimetic after multiple drag folds, and "complex." Deposits of complex shape are controlled by sets of intersecting fold axes of two or more distinct generations. Most deposits of the district, though imperfectly known, seem to have two long dimensions and one short one; that is, they are sheetlike rather than lath- or rod-shaped. Many deposits have a fishhook shape, the ore having replaced the nose and part of one limb of a syncline.

Though magnetite and hematite are the only ore minerals in the deposits, other metallic minerals are associated with them. Arranged roughly according to decreasing frequency and quantity, these minor associates are pyrite, pyrrhotite, chalcopyrite, sphalerite, molybdenite, bornite, ilmenite, marcasite(?), chalcocite, covellite, vonsenite, loellingite, graphite, unidentified minerals, and valleriite(?). Vonsenite (ferrous ferric borate) is an important mineral in one deposit. A little maghemite, very likely supergene, has been found in a single deposit. The rarer metallic minerals are detectable only under the microscope. There seems to be no systematic distribution of sulfides according to type of magnetite deposit, though concentrations of pyrrhotite are usually associated with skarn ores and concentrations of pyrite with granite gneiss ores. Most of the metallic minerals associated with magnetite and hematite are related to the main mineralizing episode that yielded the iron oxides. However, some metallic minerals belong to a later stage, and a few are referred to a stage of late hydrothermal mineralization that yielded minerals of the epidote group, zeolites, fluorite, quartz, calcite, clay minerals, and others.

The magnetite deposits and the hematite bodies locally associated with them are closely related in space, time, and origin. They are thought to be high-temperature replacement deposits effected by emanations from younger granite magma, though the ultimate source of the iron is still conjectural. The deposits represent one aspect of a process that, under slightly different and definitely cooler conditions, yielded pyritic sphalerite deposits, pyrite and pyrrhotite deposits, and perhaps also tremolite-talc

deposits in the Grenville lowlands northwest of the massif. (Cf. Engel and Engel, 1958.)

The first major deformation of the Adirondack rocks took place after the consolidation of the quartz syenitic rocks and before their intrusion by scattered dikes of hypersthene metadiabase. Subsequently, younger granite magma was intruded into the metasedimentary rocks and partly metamorphosed older igneous rocks. This magma, which consolidated chiefly as hornblende-microperthite granite, differentiated to give a volatile-enriched phase that worked upward and outward, crystallizing as alaskite, in part as "roof rock," in part as satellitic sheets and phacolithic bodies in the metasedimentary rocks. Probably the same fundamental magma also yielded a high-potassium, volatile-enriched phase that intruded the metasedimentary rocks as thin sheets, reacted with the country rock, and in places metasomatized it extensively, yielding heterogeneous microcline granite gneiss. Locally, the younger granitic rocks were deformed. An advance wave of metasomatism by volatile emanations rich in F, OH, and Si, locally accompanied by B, Cl, and P, preceded the intrusion of some of the granite and formed skarn. Once the skarns had been developed and partly enriched in iron, and the heterogeneous microcline granite gneiss had formed, both rocks were locally modified by introduction of quartz, untwinned potassium feldspar, fluorite, barite, and scapolite or spessartite. Such modification, appreciable only where skarn was enclosed in microcline granite gneiss, represents a continuation or renewal of the same process that developed all the microcline granite gneisses of the district.

At sites favorable because of their structure and their proximity to the supply of metasomatizing solutions, the skarns were subjected to the progressive introduction of more iron. Initially, iron was substituted within the silicate lattice of diopside, producing salites and ferrosalites. Where the appropriate concentrations of volatiles existed, pyroxenes were locally replaced by amphiboles or by micas. Local access of Fe^{+3}, or perhaps merely local oxidation of Fe^{+2}, permitted the development of andradite skarn. At some appropriate but unknown pressure, temperature, and degree of concentration, the silicates could no longer accommodate all the Fe within their lattices; at that stage, magnetite was precipitated, closely followed by a series of simple sulfides, minor in quantity. Very similar processes, locally affecting biotite- or sillimanite-microcline granite gneiss, resulted in the formation of magnetite deposits in those rocks. Perhaps the local de-

velopment of hematite in the granite gneiss ores (representing an increased oxidation state of the Fe) is analogous to the local development of andradite in the skarns, where primary hematite is lacking. Progressive decrease in the concentration of Fe, decreasing temperature, and a change in the character of the metasomatizing solutions toward a dilute water-rich fluid led to local alteration and partial leaching of ore and wall rocks, followed by deposition of hydrous silicates, calcite, and sporadic base-metal sulfides. At some later date—possibly in late Precambrian time, possibly in Silurian or younger time—a few of the deposits were faulted. Still later, faults, joints, and permeable rock units conveyed surface waters downward, yielding local masses of earthy hematite and chlorite.

The evidence of supergene alteration of the deposits is generally slight, for the bedrock of the region was thoroughly scraped by Pleistocene glaciers. "Rotting," leaching, limonitization, and clay-mineral alteration are apparent at the suboutcrop of some deposits deeply mantled by glacial debris. Earthy hematite and chlorite form streaks and small masses along joints, faults, mica-rich zones, and marble layers in a few deposits. This type of alteration is comparable to that which affected the sulfide-bearing schists of the nearby Grenville lowlands and resulted in the development of scattered bodies of supergene hematite in marble.

The regional geology and ore deposits of the district are treated by Buddington and Leonard in reports now in preparation. Critical structural features are discussed by Buddington (1956), whose paper lists the major references on regional geology of the northwest Adirondacks. Representative magnetite deposits are described by Buddington and Leonard (1945) and by Leonard (1952, 1953). Mineralogic features of a borate-bearing skarn deposit are presented by Leonard and Vlisidis (in press). Preliminary exploration of several deposits is summarized by Balsley, Hawkes, and others (1946), Hawkes and Balsley (1946), Millar (1947), and Reed and Cohen (1947). Regional aeromagnetic and geologic data are shown on maps by Balsley, Hawkes, and others (1946), and by Balsley, Buddington, and others (1954a, 1954b, 1959a, 1959b). Magnetic effects due to Fe-Ti oxide minerals in the country rock are interpreted by Balsley and Buddington (1958), and the usefulness of these minerals as geothermometers is demonstrated by Buddington, Fahey, and Vlisidis (1955).

REFERENCES

Balsley, J. R., and Buddington, A. F., 1958, Iron-titanium oxide minerals, rocks, and aeromagnetic anomalies of the Adirondack area, New York: Econ. Geology, v. 53, p. 777–805.

Balsley, J. R., Buddington, A. F., and others, 1954a, Aeromagnetic survey and geologic map of the Cranberry Lake quadrangle, New York: U.S. Geol. Survey Geophys. Inv. Map GP–118.

———, 1954b, Total aeromagnetic intensity and geologic map of Stark, Childwold, and part of Russell quadrangles, New York: U.S. Geol. Survey Geophys. Inv. Map GP–117.

———, 1959a, Aeromagnetic and geologic map of the Oswegatchie quadrangle, St. Lawrence, Herkimer, and Lewis Counties, New York: U.S. Geol. Survey Geophys. Inv. Map GP–192.

———, 1959b, Aeromagnetic and geologic map of the Tupper Lake quadrangle, St. Lawrence, Hamilton, and Franklin Counties, New York: U.S. Geol. Survey Geophys. Inv. Map GP–193.

Balsley, J. R., Hawkes, H. E., and others, 1946, Aeromagnetic map showing total intensity 1,000 feet above the surface of part of the Oswegatchie quadrangle, St. Lawrence County, New York: U.S. Geol. Survey Geophys. Inv. Prelim. Map 1.

Buddington, A. F., 1956, Correlation of rigid units, types of folds, and lineation in a Grenville belt, p. 99–119 in Thomson, J. E., ed., The Grenville problem: Royal Soc. Canada Spec. Pubs. 1, 119 p.

Buddington, A. F., Fahey, Joseph, and Vlisidis, Angelina, 1955, Thermometric and petrogenetic significance of titaniferous magnetite: Am. Jour. Sci., v. 253, p. 497–532.

Buddington, A. F., and Leonard, B. F., 1945, Geology and magnetite deposits of the Dead Creek area, Cranberry Lake quadrangle, New York: U.S. Geol. Survey Prelim. Rept. 106053 [mimeographed].

Engel, A. E. J., and Engel, C. G., 1958, Progressive metamorphism and granitization of the major paragneiss, northwest Adirondack Mountains, New York. Part I. Total rock: Geol. Soc. America Bull., v. 69, p. 1369–1413.

Hawkes, H. E., and Balsley, J. R., 1946., Magnetic exploration for iron ore in northern New York: U.S. Geol. Survey Strategic Minerals Inv. Prelim. Rept. 3–194 [mimeographed].

Hawkes, H. E., Balsley, J. R., and others, 1946, Aeromagnetic survey at three levels over Benson Mines, St. Lawrence County, New York: U.S. Geol. Survey Geophys. Inv. Prelim Map 2.

Leonard, B. F., 1952, Magnetite deposits and magnetic anomalies of the Brandy Brook and Silver Pond belts, St. Lawrence County, New York: U.S. Geol. Survey Mineral Inv. Field Studies Map MF–6.

———, 1953, Magnetite deposits and magnetic anomalies of the Spruce Mountain tract, St. Lawrence County, New York: U.S. Geol. Survey Mineral Inv. Field Studies Map MF–10.

Leonard, B. F., and Vlisidis, A. C. (in press), Vonsenite at the Jayville magnetite deposit, St. Lawrence County, New York: Am. Mineralogist.

Millar, W. T., 1947, Investigation of magnetite deposits at Star Lake, St. Lawrence County, N. Y. (to November 1945): U.S. Bur. Mines Rept. Inv. 4127.

Reed, D. F., and Cohen, C. J., 1947, Star Lake magnetite deposits, St. Lawrence County, N. Y. (November 1945 to November 1946): U.S. Bur. Mines Rept. Inv. 4131.

☿

36.   CHARACTERISTICS OF SEICHES ON ONEIDA LAKE, NEW YORK

By John Shen, Washington, D. C.

Seiches are series of oscillating standing waves caused by strong winds or sudden changes in barometric pressure. Depending on the nature of such disturbing sources, seiches may be uninodal, binodal or multinodal; any number may coexist. Good examples of seiches have been observed frequently at a Geological Survey recording gage at Brewerton, Oneida Lake, N. Y. A recording of the water-surface fluctuations during typical seiches is shown in figure 36.1.

In general, seiche waves possess the characteristics of shallow-water waves and may thus be closely approximated by sine functions. For a simple rectangular basin, the period of oscillation may be computed by

$$T = \frac{2 L}{k\sqrt{g\, D}}, \qquad (1)$$

in which L is the length of the basin; D is the depth of the basin; g is the gravity acceleration; and, k is the number of nodes.

Equation 1 is applicable only to a closed basin of constant depth. For irregular basins, Du Boys (1891) proposed the equation:

$$T = \frac{2}{k}\int_0^L \frac{d\,x}{\sqrt{g\, d}}, \qquad (2)$$

in which d is the depth corresponding to a length increment, dx, along the line of greatest depth through the basin. Du Boys' equation is considered applicable to parabolic and quartic basins which approximate many natural lakes (Chrystal, 1906).

After the disturbing source of a seiche ceases to exist, the oscillations continue with diminishing amplitudes. The effect of such damping may be described by a decay-type function (Keulegan, 1959, p. 34):

$$A = A_o e^{-\alpha m}, \qquad (3)$$

where, A_o is the amplitude of oscillation at the initial set-up; A is the amplitude at any one subsequent interval; m is the order number of the oscillations and is equal to the time elapsed from A_o divided by the wave period; and, α is a constant, known as the modulus of decay, depending on the physical characteristics of the basin.

The period of oscillation of Oneida Lake was computed by Du Boys' equation. A longitudinal profile of the lake was obtained by plotting the mean depth along its navigation line, and this profile, shown on figure 36.2, was used to represent the section of greatest depth. Details of the computation for summation of $dx/\sqrt{d}$ are shown on table 1. Assuming the seiches on Oneida Lake are uninodal, the period of oscillation would be:

$$T = \frac{2 \times 20{,}630}{\sqrt{32.2} \times 60 \times 60}$$
$$= 2 \text{ hours, 1 minute.}$$

Comparing with the actual observed period of 1 hour and 57 minutes, the computed value is a close approximation.
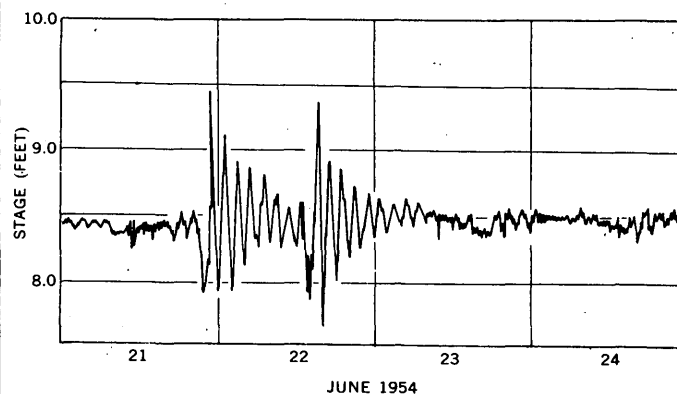
FIGURE 36.1.—Water-surface oscillations on Oneida Lake, during seiches of June 21 to 22, 1954.
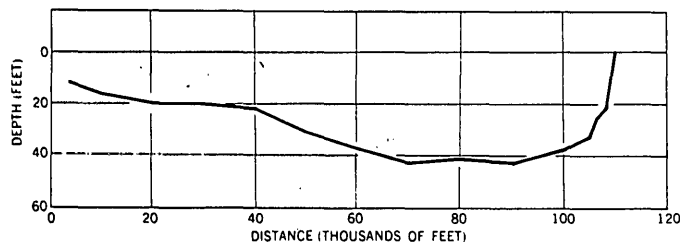
FIGURE 36.2.—Longitudinal profile of Oneida Lake.

The damping characteristics of Oneida Lake were also investigated. By rearranging equation 3, we have

$$\log \left(\frac{A}{A_{_{\it o}}}\right) = -\,0.434\alpha m. \qquad (4)$$

The value of α may be readily determined by plotting values of $(A/A_{_o})$ against values of $0.434m$ on semi-log graph paper. Figure 36.3 shows such a plot for the seiches which occurred on Oneida Lake during June 21 to 22, 1954. From this plot, the value of α was found to be 0.476.

The foregoing example illustrates the exponential damping characteristics of a natural basin. Other natural basins having greater moduli of decay are known. For example, Lake Erie possesses a value of $\alpha = 0.86$ (Hunt and Bajorunas, 1959).

The nodes would not be symmetrically located for an irregular basin; however, the position of the
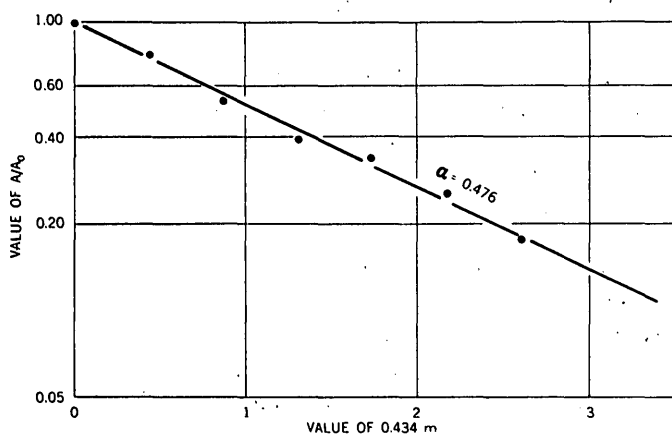
FIGURE 36.3.—Determination of α, the modulus of decay, of Oneida Lake.

TABLE 1.—*Computation of seiche period of Oneida Lake.*

Station, x	Δx (in feet)	d (in feet)	$\sqrt{d}$	$\Delta x / \sqrt{d}$	$1/\sqrt{gd}$
110,000					
	10,000	26	5.10	1,960	0.0345
100,000					
	10,000	39	6.25	1,600	.0282
90,000					
	10,000	41	6.40	1,560	.0275
80,000					
	10,000	42	6.48	1,540	.0271
70,000					
	10,000	39	6.25	1,600	.0282
60,000					
	10,000	34	5.82	1,720	.0303
50,000					
	10,000	27	5.19	1,930	.0340
40,000					
	10,000	21	4.58	2,180	.0384
30,000					
	10,000	20	4.47	2,240	.0395
20,000					
	10,000	18	4.24	2,360	.0416
10,000					
	6,700	12	3.46	1,940	.0509
3,300					
Σ	106,700			20,630	

node or nodes may be approximately determined by plotting the value of $1/\sqrt{gd}$ against the distance, x, and measuring the area under the resulting curve. A uninode will occur at a value of x that divides the area into 2 equal parts; binodes will occur at the values of x that divide the area into 4 equal parts. On this basis the position of the uninode on Oneida Lake was found to be at 48,300 feet (fig. 36.2).

REFERENCES

Chrystal, G., 1906, On the hydrodynamical theory of seiches: Trans. Roy. Soc. Edinburgh, v. 41, p. 599–649.

Du Boys, P., June 1891, Essai théorique sur les seiches: Archives des Sciences Physiques et Naturelles, Genève, p. 628.

Hunt, I. A., and Bajorunas, L., June 1959, The effect of seiches at Conneaut Harbor: Am. Soc. Civil Engineers, Proc. v. 85, WW 2, p. 31–41.

Keulegan, G. H., July 1959, Energy dissipation in standing waves in rectangular basins: Jour. Fluid Mechanics, Cambridge, v. 6, p. 33–50.

37.   VARIATIONS OF pH WITH DEPTH IN ANTHRACITE MINE-WATER POOLS IN PENNSYLVANIA

By WILBUR T. STUART and THOMAS A. SIMPSON, Arlington, Va.

When mining of anthracite coal was a flourishing industry during the 1920's and during the years of World War II, the water pumped from the mines was strongly acid and created pollution problems in the streams. When the coal was exhausted and the mines abandoned, pools of water accumulated in the underground workings. In some mines the pools drained naturally, and in others water was pumped to prevent overflow into adjacent active mine workings. These waters had considerable range in acid content (Felegy, Johnson, and Westfield, 1948) and their action on the pumping machinery required acid-resisting components. Knowledge of the areas or zoning of the acid waters might make control of pollution easier and reduce the cost of handling the water.

During the investigation, under Public Law 162, 84th Congress, of pump projects relating to anthracite mine drainage, it was noted that the pH of the water in certain flooded mines varied with the depth below the surface of the pool. In some pools less acidic or fresh-water zones occurred near the surface above more acid waters at depth.

Vertical shafts penetrating flooded mines were randomly selected in each of the four anthracite fields of Pennsylvania for determining the presence of layering of the acid water. Isolated unpumped pools, pools pumped periodically, and pools having continuous circulation by overflowing were included in the sampling. At each shaft the pool was sampled 25 feet below the pool surface and 75 to 100 feet above the bottom of the shaft. One or two samples were taken at points uniformly spaced between the upper and lower sampling levels.

The sampling was done by lowering a stoppered thick-walled bottle on a measured line to the desired depth. A long and a short open capillary tube through the stopper permitted the water to enter the bottle and the air to be released. The time that the bottle was in position at the sampling site was long compared to the time required to lower and raise it to the pool surface. Large bottles were used at depths of more than 400 feet, medium sizes be-

tween 100 and 400 feet, and small sizes for near-surface samples.

The pH of the samples was determined immediately at the shaft collars by a Beckman Model N pH meter. The pH was determined to the nearest 0.01 unit, but in reporting the results in table 1, the determination is rounded to the nearest 0.05 unit.

Table 1 shows the range in pH in eleven mine-water pools in the four anthracite fields. The pools at the South Wilkes-Barre and Henry mines are relatively new pools isolated from other mines and have not been pumped. The pH in these pools indicate more acid water at depth. The Greenwood mine contains an isolated new pool and the level of the pool is rising at present. The pH in this pool indicates more acid water in the lower sections. The pool in the Clearspring mine is about 15 years old and has not been pumped. It reportedly receives recharge from and discharges to the buried valley of the Susquehanna River. The range in pH in this pool does not indicate any significant layering of acid water.

The mine-water pools in the Exeter, Schooley, No. 7, Reliance, and Packer mines are not appreciably layered. The pools have been pumped at intervals either to prevent overflow or to obtain water for processing of prepared coal. Water enters pools at each of these mines at several levels corresponding to the points where the mine shafts intersect water-bearing coal beds. This tends to keep the pool water mixed and helps prevent acid layering.

The mine-water pools in the Hazelton and Locust Gap mines overflow to drainage tunnels. The amount of vertical flow in the shaft is unknown, but is probably significant. Slight differences in pH at depths within the pools of these mines were observed, but they are insufficient to indicate layering of the acid water.

REFERENCE

Felegy, E. W., Johnson, L. H., and Westfield, J., 1948, Acid mine-water in the anthracite region of Pennsylvania: U.S. Bur. Mines Tech. Paper 710.

TABLE 1.—*pH of water at different levels below surface of mine-water pools in anthracite fields of Pennsylvania*

Sampling point		Altitude of collar of shaft (feet above sea level)	Altitude of surface of mine-water pool (feet above sea level)	Date of sampling	Sample number	Altitude of sampling point (feet above or below sea level)	pH	Remarks
Mine	Shaft							
Northern anthracite field								
Exeter.............	Red Ash....	580	485	Jan. 9, 1961...	1	460	6.80	Pool formed after 1949 and was pumped to prevent over-flow until about July 1959.
					2	330	6.85	
					3	200	6.85	
					4	60	6.65	
Clear-spring........	Clear-spring.	578	528	Jan. 4, 1961..	1	503	6.85	When mine was in operation, the pH of pumped discharge was 6.5 on May 27, 1941. Pool formed before 1944; not pumped since.
					2	473	6.75	
Schooley...........	No. 1........	558	423	Jan. 9, 1961..	1	398	6.40	When mine was in operation, the pH of pumped discharge was 6.7 on May 23, 1941. Pool formed after Jan. 1951. Pumping ceased July 1959.
					2	278	6.20	
					3	158	6.40	
					4	33	6.75	
South Wilkes-Barre.	No. 5.......	589	89	...do.........	1	64	7.10	When mine was in operation, the pH of pumped discharge was 5.1 on May 19, 1941. Pool formed after June 1958.
					2	−61	3.65	
					3	−236	4.00	
					4	−411	4.10	
No. 7.............	No. 2.......	545	508	Jan. 10, 1961..	1	473	6.90	When mine was in operation, the pH of pumped discharge was 3.2 on June 10, 1941. Pool formed after May 1954.
					2	335	6.25	
					3	185	6.50	
					4	72	6.35	
Henry.............	Red Ash....	561	448	April 20, 1960.	1	438	7.35	When mine was in operation, the pH of pumped discharge was 3.9 on May 15, 1958. Pool formed after Jan. 1959. Shaft destroyed June 1960.
					2	348	6.00	
					3	148	5.10	
					4	−162	5.30	
Eastern middle anthracite field								
Hazelton..........	Hazelton....	1,580	1,091	Nov. 13, 1957.	1	1,070	3.20	Water rises in shaft and over-flows through drainage tunnel at altitude 1,091 feet.
					2	900	3.40	
					3	750	3.20	
				Jan. 10, 1961..	1	1,066	3.60	
					2	955	3.80	
					3	848	3.60	
Western middle anthracite field								
Locust Gap........	Locust Gap..	1,284	797	Jan. 11, 1961..	1	772	4.55	Mine-water pool overflows through drainage tunnel at altitude 747 feet.
					2	647	4.50	
					3	522	5.85	
					4	284	5.50	
Reliance...........	Reliance.....	1,058	979	Jan. 12, 1961..	1	954	6.10	When mine was in operation, pH of pumped discharge was 2.7 on Sept. 18, 1941, and 4.0 on Sept. 23, 1946. Water pumped sporadically from shaft.
					2	756	5.85	
					3	556	5.65	
					4	356	5.95	
Packer No. 5......	No. 5.......	1,108	963	Jan. 13, 1961..	1	938	6.70	When mine was in operation, pH of pumped discharge was 4.9 on Sept. 16, 1941. Pool formed after Sept. 1957.
					2	678	6.55	
					3	318	6.70	
					4	58	6.55	

TABLE 1.—pH of water at different levels below surface of mine-water pools in anthracite fields of Pennsylvania—Continued

Sampling point		Altitude of collar of shaft (feet above sea level)	Altitude of surface of mine-water pool (feet above sea level)	Date of sampling	Sample number	Altitude of sampling point (feet above or below sea level)	pH	Remarks
Mine	Shaft							
Southern anthracite field								
Greenwood........	No. 10......	1,002	452	Jan. 12, 1961..	1	427	4.20	When mine was in operation, pH of pumped discharge was 3.6 on July 2, 1941, and 3.1 on Oct. 15, 1946. Pool formed after May 1960. Pumping at shaft ceased Nov. 1960.
					2	372	4.00	
					3	172	3.75	
					4	42	2.80	

38. ANGULAR UNCONFORMITY SEPARATES CATSKILL AND POCONO FORMATIONS IN WESTERN PART OF ANTHRACITE REGION, PENNSYLVANIA

By J. Peter Trexler, Gordon H. Wood, Jr., and Harold H. Arndt, Washington, D. C.

Geologists working in Pennsylvania generally have thought that the Pocono formation rests conformably on the Catskill formation, although Willard (1939, p. 19–21) believed a disconformity intervenes in northern Pennsylvania. The present authors, mapping in the western part of the Anthracite region in eastern Pennsylvania, found that the contact is a regional, low- to high-angle unconformity in an area of more than 600 square miles.

At most localities in the western part of the Anthracite region (fig. 38.1) the predominantly red, main body of the Catskill formation is overlain by an upper gray member that consists chiefly of gray and green sandstone, shale, and conglomerate, with local interbeds of red sandstone and shale. This gray member, which ranges in thickness from 0 to 2,400 feet, is absent at some localities north and northeast of Pine Grove (fig. 38).

The overlying gray Pocono formation is composed mainly of sandstone and conglomerate, and ranges in thickness from 700 to 1,200 feet. The basal unit is a widespread pebble conglomerate, perhaps the Griswold Gap conglomerate of White (1883, p. 47–52), which ranges in thickness from 2 to 100 feet.

Because of the similarity between the gray beds in the upper part of the Catskill formation and beds of the Pocono formation, White (1883, p. 49–52) recognized a "Pocono-Catskill transition group." This "transition group" is designated as the gray member of the Catskill formation in this report. White further stated that a geologist would assign the gray beds to the Pocono at one locality and to the Catskill at another, depending on the presence or absence of red beds. Although other geologists generally placed the contact between the Catskill and Pocono formations at the top of the uppermost red bed, the present investigation confirmed that the red beds in the gray member are of local extent and that the contact, where placed at the top of the uppermost red bed, was at different stratigraphic positions at different localities. Therefore, the writers followed White (1883, p. 46–49) in placing the contact between the Catskill and Pocono formations at the base of the widespread pebble conglomerate, which locally rests on red beds or gray sandstone in the gray member or on the red, main body of the Catskill formation.

EVIDENCE FOR THE UNCONFORMITY

Three miles southeast of Lykens, near the nose of the Joliet anticline, the gray member of the Catskill formation attains its maximum thickness of about 2,400 feet (fig. 38.2). To the west, on both limbs of the anticline, the upper 2,000 to 2,300 feet of the

EXPLANATION

PMr

Post-Pocono rocks

Mp

Pocono formation

MDcg

Gray member of the Catskill formation

Lower Mississippian

MISSISSIPPIAN AND PENNSYLVANIAN

MISSISSIPPIAN

Dc

Main body of the Catskill formation and older rocks

Upper Devonian

DEVONIAN

Conformable contact

Unconformable contact, no angularity observed

xxxxxxx
Unconformable contact, angularity observed between the basal conglomerate of the Pocono formation and the gray member of the Catskill formation

....
Unconformable contact, basal conglomerate of the Pocono formation rests on the red main body of the Catskill formation

Fault, showing relative horizontal movement

PENNSYLVANIA

MAP AREA

FIGURE 38.1.—Map showing angular unconformity between the Catskill and Pocono formations in the western part of the Anthracite region, Pennsylvania.
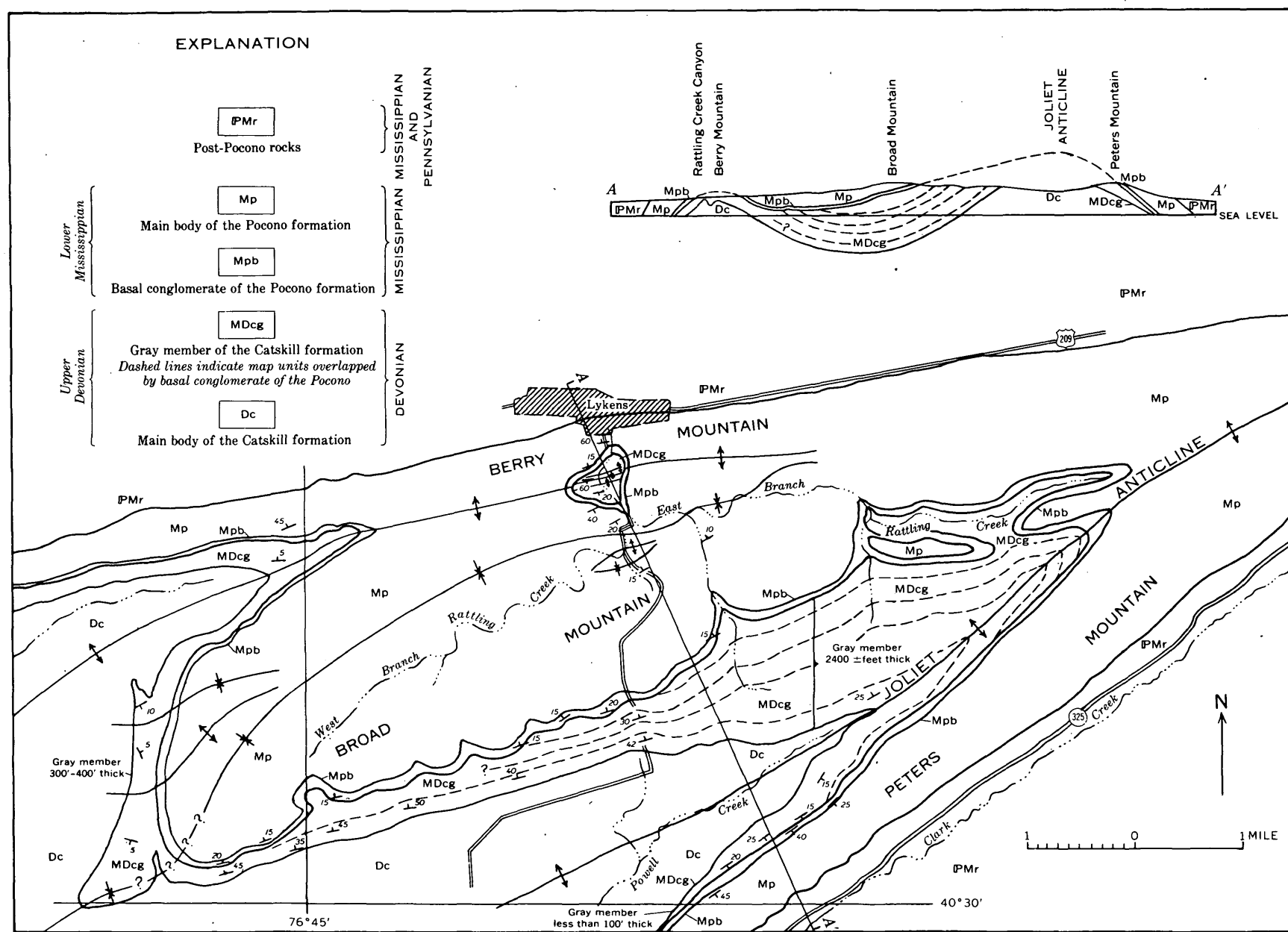
FIGURE 38.2.—Geologic map and structure section showing angular relations between the gray member of the Catskill formation and the basal conglomerate of the Pocono formation south of Lykens, Pa.

member are gradually overlapped by the basal conglomerate of the Pocono formation. Along the southern flank of Broad Mountain, on the north limb of the anticline, the gray member dips 10° to 30° more steeply northward than the overlying Pocono beds. On Peters Mountain, on the south limb of the anticline, the Pocono dips as much as 25° more steeply southeastward than the gray member. These stratigraphic and structural relations indicate that an angular unconformity separates the gray member of the Catskill and the basal conglomerate of the Pocono, and that locally the gray member dipped about 25° to the north when the Pocono formation accumulated.

About 1 mile south of Lykens in the canyon cut through Berry Mountain by Rattling Creek, two sharp anticlines and a syncline in the gray member underlie a simple asymmetric anticline in the Pocono formation (fig. 38.2). The discordance is as great as 75°. Thus, the angular unconformity noticed on Broad and Peters Mountains is also present here.

Although the evidence is not obvious at other localities, the regional unconformity between the Catskill and Pocono formations throughout the western part of the Anthracite region (fig. 38.1) is indicated by local differences in dip and strike across the contact. The unconformity is also indicated by the truncation of red and gray beds in the gray member of the Catskill formation, which explains the variations in the thickness of the gray member and the local absence of the member north and northeast of Pine Grove.

AGE OF THE UNCONFORMITY

The Catskill formation is generally considered to be Late Devonian and the Pocono formation Early Mississippian in age. However, a pinnule of a fossil plant collected by the authors from a bed in the gray member of the Catskill formation about 500 feet above the base of the member has been tentatively identified as *Adiantites* sp. (S. H. Mamay, oral communication, 1960), indicating a probable Early Mississippian age for at least the upper part of this member. Read (1955, p. 8) included the beds here designated as the gray member in the lower part of the Pocono formation and in his Early Mississippian *Adiantites* zone. This fossil evidence indicates that deposition of gray, green, and red beds of the Catskill formation continued into Early Mississippian time. The age of the Catskill formation in the Anthracite region, consequently, is now designated as Late Devonian and Early Mississippian. Because the unconformity is underlain and overlain by rocks of Early Mississippian age, it also is of Early Mississippian age.

SIGNIFICANCE OF THE UNCONFORMITY

The angular unconformity between the Catskill and Pocono formations is the result of folding, uplift, and erosion that occurred after deposition of the gray member of the Catskill formation and before deposition of the basal conglomerate of the Pocono formation. The authors believe that this deformation was a late phase of the Acadian orogeny and that the Acadian disturbance, which heretofore was generally believed to be of Middle and Late Devonian age, continued into Early Mississippian time in eastern Pennsylvania. Woodward (1957a, 1957b) postulated that the Acadian orogeny affected the Valley and Ridge province of eastern Pennsylvania, but did not describe specific localities where Acadian folds could be distinguished from later Appalachian folds. The angular unconformity between the Catskill and Pocono formations provides definite structural evidence of the Acadian orogeny in the Valley and Ridge province of eastern Pennsylvania. The Acadian folds underlying the unconformity are obscured by folds resulting from the Appalachian orogeny, mainly because the trend of the folds formed during this later orogeny generally parallel those formed during the Acadian. Compression was from the southeast during both orogenies. This probably explains why definite Acadian folds have not been previously distinguished, and substantiates Woodward's (1957b, p. 2320) hypothesis on the occurrence of Acadian folds and the parallelism of these folds to Appalachian folds in eastern Pennsylvania.

The unconformity provides the only widespread recognizable contact between the gray member of the Catskill formation and the Pocono formation in the western part of the Anthracite region, and may be the same as the disconformity postulated by Willard (1939, p. 19–21) for northern Pennsylvania. Recognition of this unconformity, which is the upper contact of the Catskill formation, should eliminate some of the difficulties encountered in the past in mapping and correlating units in the upper part of the Catskill formation and in the lower part of the Pocono formation.

REFERENCES

Read, C. B., 1955, Floras of the Pocono formation and Price sandstone in parts of Pennsylvania, Maryland, West Virginia and Virginia: U.S. Geol. Survey Prof. Paper 263, 32 p., 20 pls.

White, I. C., 1883, The geology of the Susquehanna River region in the six counties of Wyoming, Lackawanna, Luzerne, Columbia, Montour, and Northumberland: Pennsylvania Geol. Survey, 2d ser., Bull. G–7, 464 p.

Willard, Bradford, 1939, The Devonian of Pennsylvania, Middle and Upper Devonian: Pennsylvania Geol. Survey, 4th ser., Bull G–19, 481 p.

Woodward, H. P., 1957a, Structural elements of northeastern Appalachians: Am. Assoc. Petroleum Geologists Bull., v. 41, no. 7, p. 1429–1440.

———, 1957b, Chronology of Appalachian folding: Am. Assoc. Petroleum Geologists Bull., v. 41, no. 10, p. 2312–2327.

39. REEFS IN THE FORT PAYNE FORMATION OF MISSISSIPPIAN AGE, SOUTH-CENTRAL KENTUCKY

By ROBERT E. THADEN, RICHARD Q. LEWIS, J. MARK CATTERMOLE, and ALFRED R. TAYLOR, Columbia, Ky.

Work done in cooperation with the Kentucky Geological Survey

Geologic mapping and studies in the Amandaville, Breeding, Burkesville, Creelsboro, Cumberland City, Jamestown, and Wolf Creek Dam quadrangles in south-central Kentucky, being done in cooperation with the Kentucky Geological Survey, have partly delineated several limestone reefs in the Fort Payne formation of Early Mississippian age. They are well exposed in the valleys of the Cumberland River and its larger tributaries between Burkesville and Jamestown, Ky., and are less well exposed in shallower valleys to the west and north. The area includes parts of Adair, Russell, Clinton, and Cumberland Counties. Butts (1922, p. 78–83), Klepser (1937), and Stockdale (1939, p. 138) noted the presence of limestone in the Fort Payne formation, and Klepser (1937) pointed out that limestone masses in this area are like bioherms.

The Fort Payne formation overlies the Chattanooga shale of Devonian and Early Mississippian age and underlies the Warsaw limestone of Late Mississippian age (Stockdale, 1939, p. 52–54). The Fort Payne is about 250 to 270 feet thick and, where reefs are not present, is composed almost entirely of siltstone and shale. Within the Fort Payne interval reefs may occupy any position, but possibly are more numerous near the base. Some inconclusive evidence suggests that the northernmost reefs tend to occur stratigraphically higher than those to the south. The large reefs (fig. 39.1) trend generally N. 65° to 80° W. This observation, together with information from oil wells in surrounding counties, indicates that the reefs occur in a belt of unknown width that may trend in the same general direction as the individual reefs.

The reefs range in size from thin isolated lenticular bodies a few tens of feet in lateral extent to blocky and thick-bedded bodies more than 100 feet thick, more than 1 mile wide, and 15 or more miles long. Indeed, many of the large reefs locally make up most of the Fort Payne formation.

Small reefs are found throughout the Fort Payne, vertically and laterally, but apparently are most numerous in the vicinity of the large reefs. The small reefs generally are thicker and are convex upward. At their margins the reefs consist largely of overlapping sheets of reef-derived detritus which grade into the main reef body, are steeply crossbedded away from the main reef, and tongue into the adjacent shale and siltstone.

Some reefs are made up of limestone from top to bottom; others are multiple, superposed limestone bodies separated by shale and siltstone beds; still others are discontinuous short segments of limestone separated laterally by shale and siltstone. The margins of the large reefs are not unlike the margins of the small ones. Tongues and fingers of limestone a few feet to several tens of feet in thickness may extend thousands of feet into the surrounding shale and siltstone. These tongues may be either compact limestone or recemented reef-derived detritus. Bedding is absent in some parts of the main body of individual reefs; elsewhere there may be undulating bedding or gentle crossbedding. Bedding in the tongues, although at some places like that in the
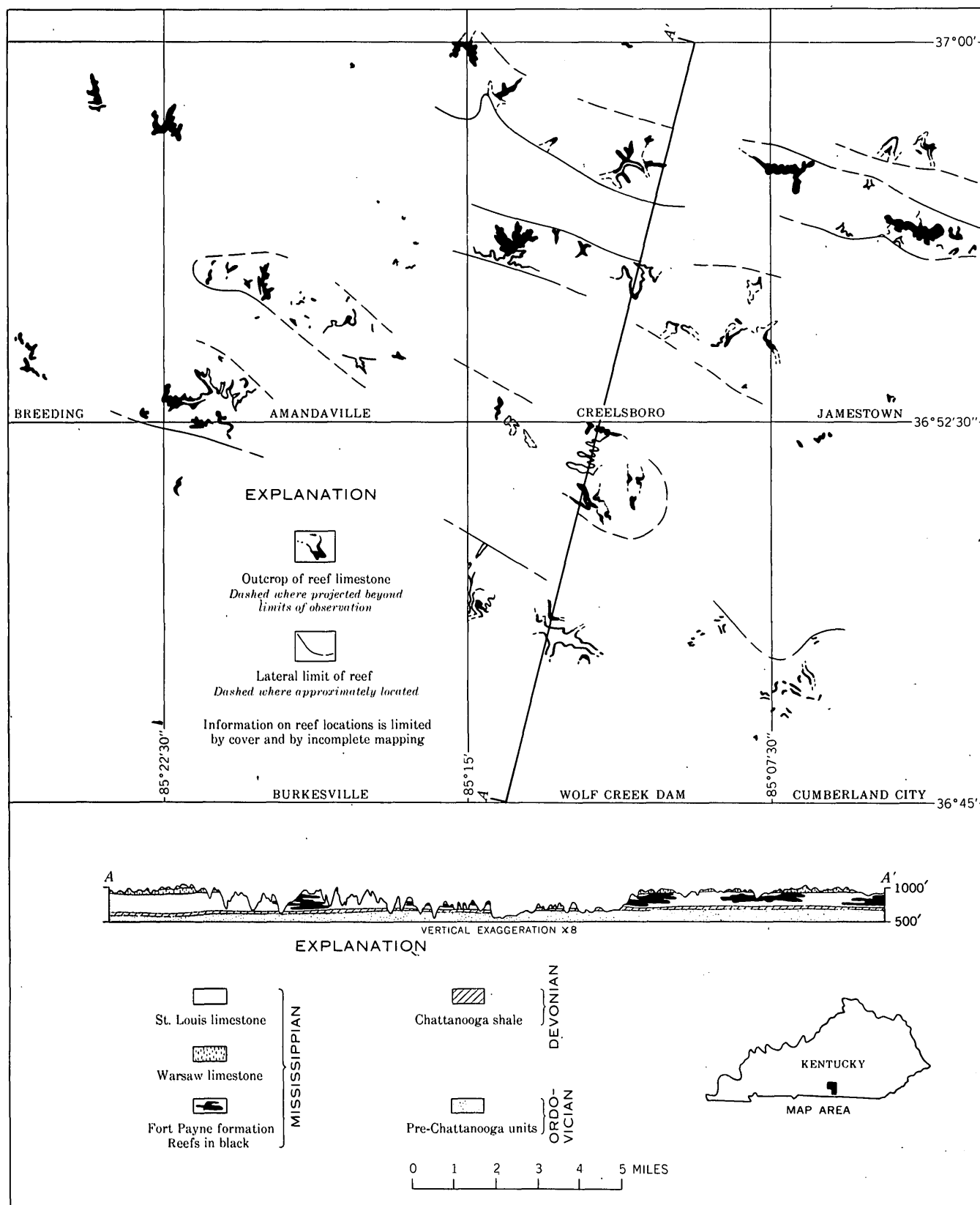
FIGURE 39.1.—Outcrop pattern and stratigraphic position of reefs in the Fort Payne formation in part of south-central Kentucky.

main body of the reefs, characteristically is cross-bedded at steep angles. Dips of crossbeds may exceed 20°, though dips of 8° to 10° are more common. The inclination of crossbedding nearly everywhere is to the south.

Limestone in the reefs commonly is coarse grained, arenaceous and argillaceous, and gray to bluish gray. Fossils are common in coarse-grained limestone, less abundant in fine-grained limestone. Large crinoid stem segments are particularly abundant; in places the reefs are essentially a "crinoid hash." Brachiopods and bryozoans, though not as abundant as crinoids, are common. Chert lenses and pods, quartz geodes, and small irregular masses of pale-blue chalcedony less than an inch in diameter are abundant in parts of the limestone as well as in the nearby siltstone and shale. Near the reefs, especially in laterally equivalent beds, the siltstone and shale are much more calcareous and darker than elsewhere in the formation.

Petroleum and natural gas have been produced from limestone reefs in the Fort Payne formation in Wayne County southeast of the area of the present study and in parts of Hart, Barren, and Metcalf Counties to the northwest of the area. Local names have been given to the producing horizon in nearly every oil pool in these counties, but the producing horizons are also widely known as the "Beaver sand" or "Beaver Creek sand." The present production of petroleum and natural gas from reef limestone in the Fort Payne formation in Kentucky has been small in comparison with production from rocks of Ordovician age. It is likely that additional knowledge of the size, trend, and physical properties of the reefs will assist in future exploration.

REFERENCES

Butts, Charles, 1922, The Mississippian series of eastern Kentucky; Kentucky Geol. Survey, Series 7, vol. 7, 188. p.

Klepser, Harry J., 1937, The Lower Mississippian rocks of the Eastern Highland Rim; Ohio State Univ. Abstracts, Doc. 24, p. 181-187.

Stockdale, Paris B., 1939, Lower Mississippian rocks of the East-Central Interior; Geol. Soc. America Spec. Paper 22.

40. THE TUSCALOOSA GRAVEL IN TENNESSEE AND ITS RELATION TO THE STRUCTURAL DEVELOPMENT OF THE MISSISSIPPI EMBAYMENT SYNCLINE

By MELVIN V. MARCHER, Nashville, Tenn.

Work done in cooperation with the Tennessee Division of Geology

The Tuscaloosa gravel of Late Cretaceous age occurs as outliers capping many of the hills and ridges on the Western Highland Rim of Tennessee. In the southwestern part of the Rim a maximum thickness of 150 feet has been preserved; elsewhere the thickness is 30 feet or less.

On the basis of its lithologic characteristics the Tuscaloosa can be subdivided into a western and eastern facies. Of the two, the western facies is more widespread and is typical of the formation over most of the area. The eastern facies is restricted to a narrow northward-trending belt along the eastern margin of the Western Highland Rim.

LITHOLOGIC CHARACTERISTICS

Size analyses indicate that the western facies of the Tuscaloosa gravel is a mixture of three distinct sedimentary components. Frequency curves show separate peaks for gravel, medium sand, and fine sand.

The gravel component (larger than 13 mm in diameter) consists mainly of chert plus a small amount of sandstone. Much of the chert gravel was derived from formations of Devonian (Camden chert) and Mississippian (Fort Payne, Warsaw, and St. Louis formations) ages.

Sandstone pebbles, although rare in the Tuscaloosa gravel, are relatively widespread. These peb-

bles are not indigenous to the area and did not come from formations now exposed in western Tennessee.

Most of the sand in the western facies consist of angular chert and quartz grains. These grains, particularly the chert, resemble partly weathered Camden and Fort Payne chert that has been mechanically crushed.

All samples studied contain very minor amounts of rounded and frosted quartz sand which, like the sandstone and quartz pebbles, did not come from rocks now exposed in the area.

Kaolinite, montmorillonite, and mica are present in all samples analyzed. Kaolinite is dominant (20 to 40 percent of total sample) in all samples except one, which contains 20 to 30 percent montmorillonite. In all other samples montmorillonite makes up 10 percent or less of the total sample.

The eastern facies of the Tuscaloosa gravel contains all the components of the western facies and in addition contains beds of well-sorted sand and gravel, siliceous siltstone containing fragmentary plant fossils, heavy minerals, and an abundance of quartz sand and quartz pebbles. The contrast in sorting, lithologic diversity, and mineral content indicates a marked difference both in source and depositional environment.

SOURCE

The pebbles of Mississippian chert are clearly of local origin. The Camden chert is present only in the Western Valley of the Tennessee River and in the subsurface farther west. Thus pebbles of the Camden chert in the Tuscaloosa have been transported 10 to 50 miles from the west.

Because pebbles of the Camden chert were transported from the west, the sandstone pebbles, which are thoroughly intermixed in the main mass of the Tuscaloosa gravel, must have been transported from that direction also. The most probable source beds for the sandstone pebbles include the Lamotte and Roubidoux formations, which were exposed in western Tennessee during Tuscaloosa time (Grohskopf, 1955, p. 14–16 and pl. 3).

Angular chert and quartz grains seem to have been developed by attrition of Camden and Fort Payne chert during transport. The rounded and frosted quartz-sand grains in the main mass of the gravel probably were derived from the St. Peter or Dutch Creek formations, which formerly cropped out in western Tennessee and western Kentucky.

Kaolinite and montmorillonite are both developed by weathering of the Camden and Fort Payne chert. Thus these components are of both local and distant origin. Some of the montmorillonite could have developed by alteration of volcanic glass which also occurs in the fine fraction of the Tuscaloosa.

Because the quartz pebbles so abundant in the eastern facies of the Tuscaloosa are not mixed throughout the main mass of the gravel as they should be if they had come from the west, it is inferred that they were derived from some other direction. The most probable source was Pennsylvanian bedrock in northwestern Mississippi and western Kentucky. The beds of well-sorted sand and heavy minerals associated with the quartz gravel may also have come from the same areas.

PALEOGEOLOGY AND PALEOGEOGRAPHY DURING TUSCALOOSA DEPOSITION

The western facies of the Tuscaloosa gravel is probably a series of coalesced stream deposits because the deposits lie at the base of a transgressive marine sequence; because of the apparent lack of significant chemical difference between the source areas and the deposits; and because of the textural similarity between the deposits and typical valley-fill deposits.

The eastern facies of the Tuscaloosa may represent shoreline deposits where waves and currents winnowed the stream-transported sediments from the west and brought in additional components from the north and south (fig. 40.1).

As demonstrated by the source of some of the Tuscaloosa gravel components, the area west of the Western Highland Rim was a highland during Late Cretaceous time. Paleogeologic maps of the northern Mississippi Embayment (Freeman, 1953, pl. 3, Caplan, 1954, pl. 4, and Grohskopf, 1955, pl. 3) show that this topographic highland was also a structural high and that beds as old as Cambrian were exposed on its crest. This structural feature, first postulated by Wilson (1939), has been named the Pascola arch by Grohskopf (1955, p. 25).

Reconstruction of the Pascola arch based on stream gradients estimated from the maximum size pebbles in the Tuscaloosa gravel and eastward thickening of post-Tuscaloosa sediments indicates that the arch stood nearly 1,000 feet above sea level during Tuscaloosa deposition. More than 8,000 feet of strata had been eroded from the crest of the arch by the beginning of Tuscaloosa deposition.
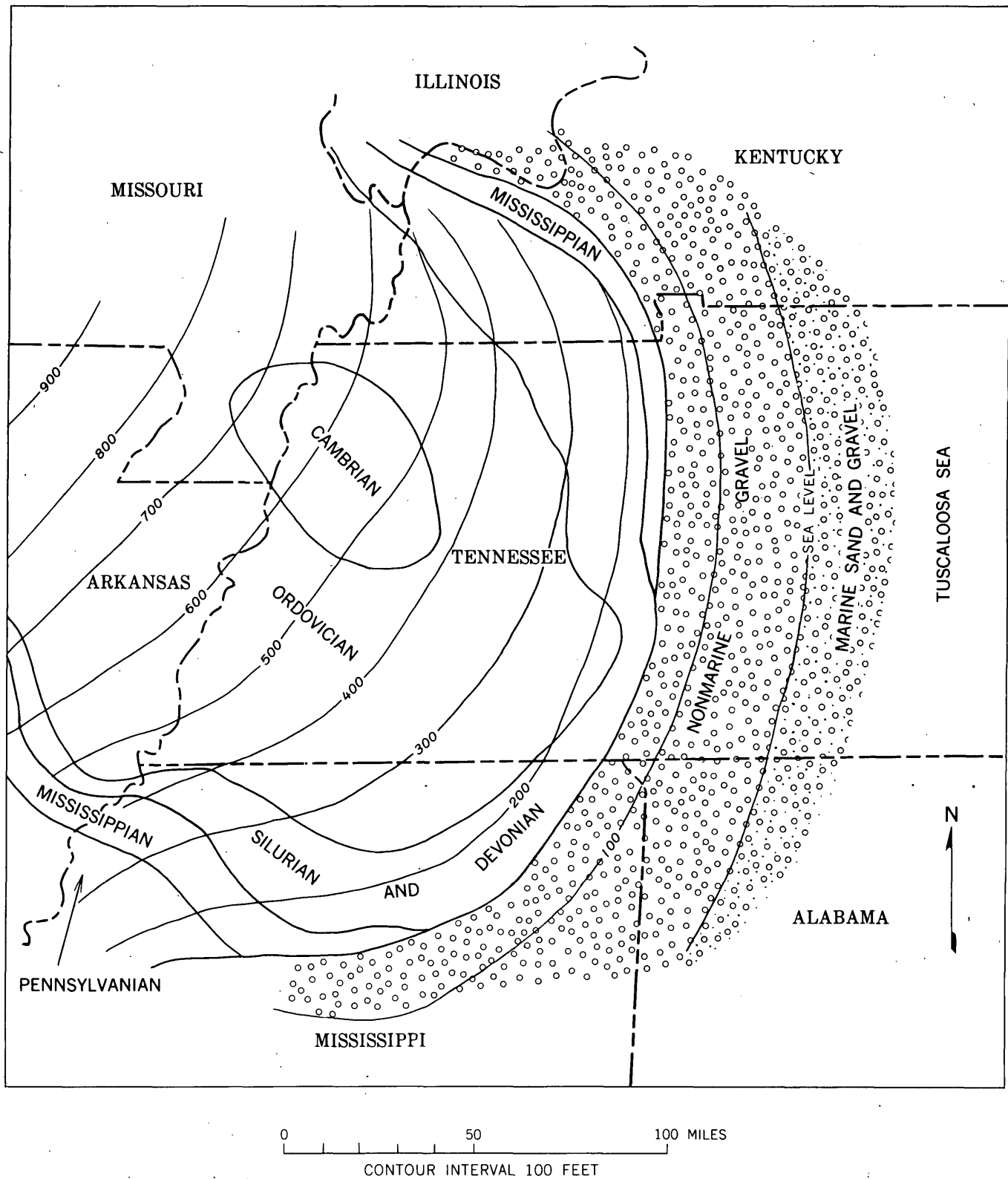
FIGURE 40.1.—Paleogeology and paleogeography of western Tennessee and adjoining areas during Tuscaloosa deposition. Contours show topography of Pascola arch.

DEVELOPMENT OF THE MISSISSIPPI EMBAYMENT SYNCLINE

During and shortly after deposition of the Tuscaloosa gravel the Pascola arch began to subside. Most of the subsidence occurred near the synclinal axis that generally follows the present course of the Mississippi. Superposition of the synclinal bend across the now-buried high resulted in faults that cut Paleozoic rocks and, in some areas, that extended upward into the overlying younger strata.

REFERENCES

Caplan, W. M., 1954, Subsurface geology and related oil and gas possibilities of northeastern Arkansas: Arkansas Div. Geology Bull. 20, 124 p.

Freeman, L. B., 1953, Regional subsurface stratigraphy of the Cambrian and Ordovician in Kentucky and vicinity: Kentucky Geol. Survey Bull. 12, 352 p.

Grohskopf, J. G., 1955, Subsurface geology of the Mississippi Embayment of southeast Missouri: Missouri Geol. Survey and Water Res., 2d ser., v. 37, 133 p.

Wilson, C. W., Jr., 1939, Probable connection of the Nashville and Ozark domes by a complimentary arch: Jour. Geology, v. 47, no. 6, p. 583–597.

---

41.   SYSTEMATIC PATTERN OF TRIASSIC DIKES IN THE APPALACHIAN REGION

By PHILIP B. KING, Menlo Park, Calif.

Nearly 30 years ago Bucher (1933, p. 351-353) observed that a promising field for tectonic research would be the Triassic dikes that traverse the rocks of the Appalachian region in the eastern United States. The present note reaffirms this observation, and indicates new data that have become available since the time of Bucher's writing.

During preparation of a revised tectonic map of the United States (Cohee and others, 1961 in press) it was decided that these dikes were an item of sufficient tectonic interest to be plotted on this edition of the map. Their map pattern was therefore compiled from all published sources; in addition, unpublished data for North and South Carolina were contributed by W. R. Griffitts and W. C. Overstreet, and for New England by John Rodgers.

NEWARK GROUP AND ASSOCIATED FEATURES

Sedimentary rocks of the Newark group of Late Triassic age form elongate strips of outcrop from Nova Scotia southwestward along the strike to South Carolina. Probable subsurface extensions of the Newark group farther east and south are also known from drilling and from geophysical surveys. The nature and occurrence of the Newark group has been summarized recently (Reeside and others, 1957, p. 1459–1461; McKee and others, 1959, p. 12, 13, 18, 24, pls. 4, 5, 7, 9).

The extent and pattern of the present outcrop areas of the Newark group are determined largely by normal faults, along which the Newark has been dropped against older rocks on one or both sides. Present outcrop areas may have nearly the original extent of the deposits, as the nature of deposits adjacent to the major bordering faults indicates that these were in process of displacement during sedimentation. However, the major faults and the numerous minor faults continued to be displaced after the close of the depositional epoch. Trends of faults and outcrop areas conform grossly to the northeastward strike of the older rocks, which had been produced by deformation of the Appalachian region prior to Late Triassic time. Also, the larger strips of outcrop of the Newark group are paired on each side of the central axis of the Appalachian deformed belt, with the faults which border them dropped antithetically toward the axis (McKee and others, 1959, p. 24, pl. 9).

Newark sedimentation was accompanied by much igneous activity. Interbedded with the sedimentary rocks in the northern outcrop areas are flows of mafic lava. Both here and in outcrop areas farther south the sedimentary rocks are intruded by extensive stocks and sills of igneous rock, mostly classed as diabase, but including other mafic varieties. Even more abundant are the dikes, discussed below, which extend far away from the Newark areas. At least some of the intrusives are related to the lava flows and faults, but the age of others can be determined only within wide limits. Possibly these intrusives

formed during a long time span, but they appear to be so closely related, not only among themselves but to the other features associated with the Newark group, that they all must be broadly of Late Triassic age.

DIKES

Narrow steeply dipping mafic dikes intrude the Newark group in all its outcrop areas and in places branch from the larger intrusives. They also extend into the surrounding older rocks and are common even far distant from the Newark outcrops. Most of the outlying dikes intrude the metamorphic and

plutonic rocks of the Piedmont province, although a few extend northward into the Paleozoic rocks of the Valley and Ridge province near Harrisburg, Pa. Southeastward, many dikes extend to the edge of the Atlantic Coastal Plain, where they pass unconformably beneath Cretaceous and younger strata.

The dikes have been observed and located mostly as an incident to other geological investigations, and have seldom been a specific field of study, so that many more data regarding them could still be obtained. The accompanying map (fig. 41.1) reflects this present state of information. The abundant dikes shown in Pennsylvania and Maryland were
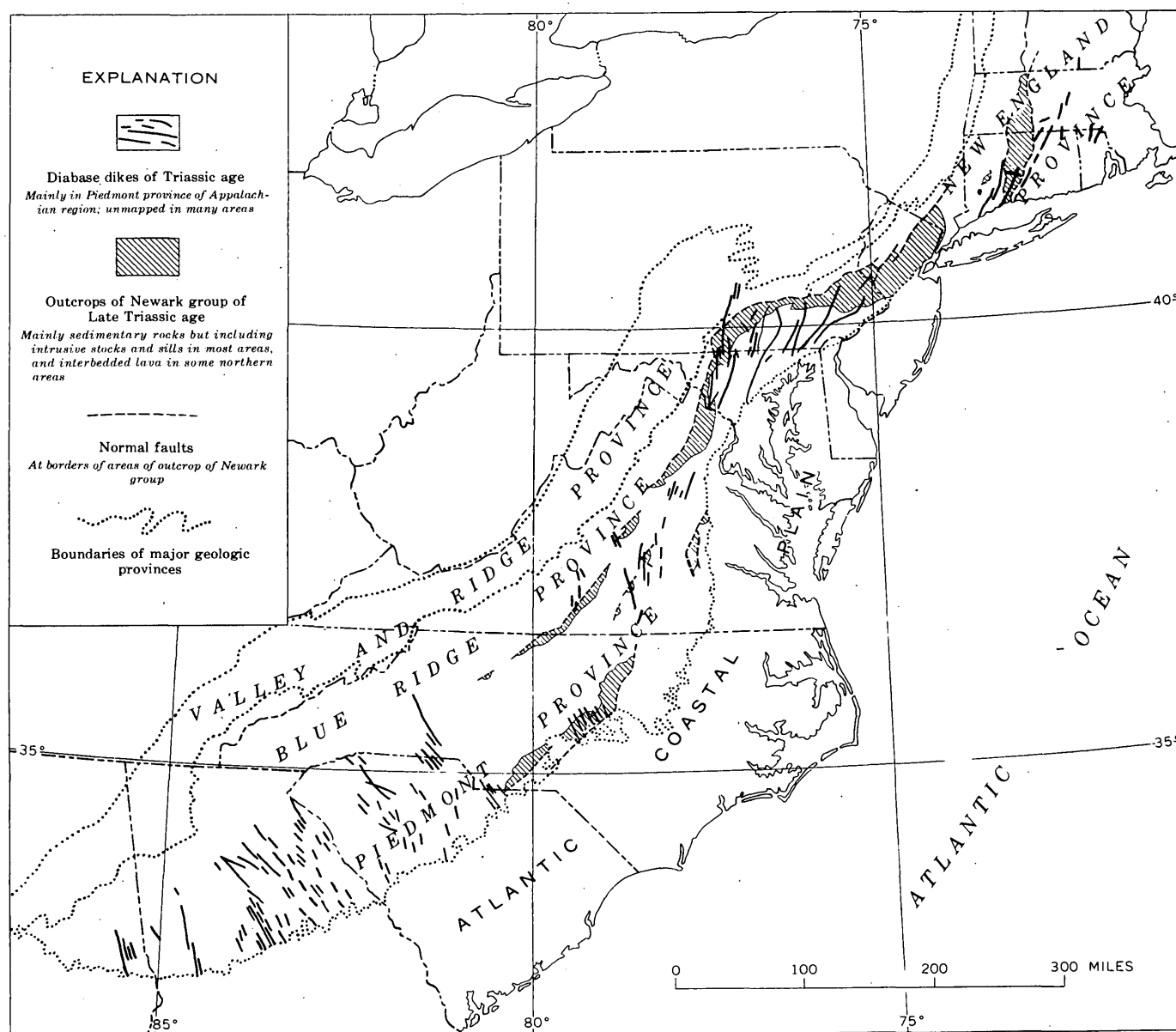
FIGURE 41.1.—Sketch map of the Appalachian region of the eastern United States, showing known occurrences of dikes of Triassic age, and areas of outcrop of the Newark group.

mapped in detail many years ago, and those in Georgia more recently by Lester and Allen (1950). Very few dikes, by contrast, are shown in North Carolina. Here, in a 30-mile segment of the Deep River basin, Reinemund (1955, p. 54–61, pls. 1, 4) mapped hundreds of transverse dikes, yet the geologic map of North Carolina (Stuckey, 1958) shows no dikes in the segments of the basin on either side. Probably some dikes, perhaps many, occur in these other segments, but are so far unmapped.

The dikes are sufficiently known, however, to permit significant generalizations regarding their pattern. Although dikes of different trends cross or intersect, most dikes locally have a common trend. However, these local common trends vary systematically from one part of the Appalachian region to another. In the southwestern 400-mile segment of the Appalachians, from Alabama to North Carolina, the dikes trend consistently northwestward (fig. 41.1). In southern Virginia the trend changes to north-northwestward and in northern Virginia to northward. Across Maryland and Pennsylvania the northward trend changes to northeastward, and this same trend continues into New England.

The trends of the dikes are everywhere discordant to the trends of the structures of the enclosing rocks, and they are everywhere straighter than these structures. In the southwestern 400-mile segment of the Appalachian region the dikes extend nearly at right angles to the trends of the outcrop areas of the Newark group and the associated faults, as well as to the strike of the older rocks. Farther northeastward they cross the structures in the Triassic and older rocks diagonally. Moreover, in Pennsylvania and adjacent States, the dikes are not deflected by the marked sinuosities in the trend of the Newark rocks and their associated faults.

INTERPRETATION

Dikes, stocks and sills, normal faults, and sedimentary basins all formed in the Appalachian region during Late Triassic or closely related times, and are manifestations of a stress pattern, or succession of stress patterns, which existed in the region during those times.

Dikes are products of regional tension directed horizontally in the crust (Anderson, 1951, p. 30). Those in the Appalachian region, which cut cleanly through all other structures, probably reflect the deep-seated tensile stresses that existed during Late Triassic time. In the southwestern segment they indicate that the trend of the axis of greatest tension,

or of least compressive stress, was to the northeast, but in the northeastern segment this axis curves in an arc to the east, and finally to the southeast.

A different pattern is shown by the normal faults and sedimentary basins of the Newark group. These follow closely the strike of the older rocks amidst which they lie, and may have been conditioned by fracture and displacement along existing lines of weakness. Pairing of the major basins and associated faults on opposite sides of the central axis of the Appalachians suggests that this axis was again raised into a broad arch during Triassic time.

Differences between the stress pattern suggested by the dikes and that by the faults and sedimentary basins are seemingly incompatible. Possibly the two patterns existed at slightly different times, but more likely the faults and basins are an expression of superficial stresses which were contemporaneous with the deep-seated stresses that produced the dikes.

Be that as it may, the stress patterns of Late Triassic time in the Appalachian region appear to have been more systematic, and the tectonic history more complex than has generally been assumed. An eventful tectonic history of the region during Triassic time has also been suggested recently by Woodward (1957, p. 1437–1439), on the basis of other evidence and with a different interpretation. It would appear that further study of the Triassic phase of the tectonic evolution of the Appalachian region is warranted. The nature, history, and pattern of the Late Triassic dikes will be a useful tool in such studies.

REFERENCES

Anderson, E. M., 1951, The dynamics of faulting and dyke formation, with applications to Britain, 2d ed.: Edinburgh, Oliver & Boyd, 206 p.
Bucher, W. H., 1933, The deformation of the earth's crust: Princeton, N. J., Princeton Univ. Press, 518 p.
Cohee, G. V., and others, 1961, Tectonic map of United States: U.S. Geol. Survey (in press).
Lester, J. G., and Allen, A. T., 1950, Diabase of the Georgia Piedmont: Geol. Soc. America Bull., v. 61, p. 1217–1224.
McKee, E. D., and others, 1959, Paleotectonic map of the Triassic system: U.S. Geol. Survey Misc. Geol. Inv. Map I–300, 33 p., 9 pls.
Reeside, J. B., Jr., and others, 1957, Correlation of the Triassic formations of North America, exclusive of Canada: Geol. Soc. America Bull., v. 68, no. 11, p. 1451–1513.
Reinemund, J. A., 1955, Geology of the Deep River coal field, North Carolina: U.S. Geol. Survey Prof. Paper 246, 159 p.
Stuckey, J. L., 1958, Geologic map of North Carolina: North Carolina Dept. Conserv. Dev., Div. Mineral Resources.
Woodward, H. P., 1957, Structural elements of northeastern Appalachians: Am. Assoc. Petroleum Geologists Bull., v. 41, p. 1429–1440.

42.   RAINFALL AND MINIMUM FLOWS ALONG THE TALLAPOOSA RIVER, ALABAMA

By H. C. RIGGS, Washington, D. C.

A major problem in hydrology is the estimation of the frequency distribution of an event such as a flood or drought. Ordinarily this is obtained by some analysis of the recorded events. Frequently one or more of the recorded events appear unusual with respect to the others and the proper interpretation is not apparent. This is the problem posed by the annual minimum flows for the Tallapoosa River at Wadley, Ala., for 1924-1955 as shown on figure 42.1.

The three lowest points (fig. 42.1) appear "out of line" with the others, particularly if a typical frequency curve that flattens at the low end is postulated. Several explanations are possible: the actual recurrence intervals of these three minimum flows are much greater than indicated by the period of record; the three lowest minimum flows are lower than natural flows because of emergency withdrawals upstream; or the frequency curve should be concave downward instead of concave upward.

To choose the correct explanation, additional information is needed. The minimums occurred in 1925, 1931, and 1954. It is unlikely that the first two were affected by emergency withdrawals of water because water requirements were not great in the earlier years. Much additional information would be required to define the shape of the frequency curve. This leaves only the possibility of making
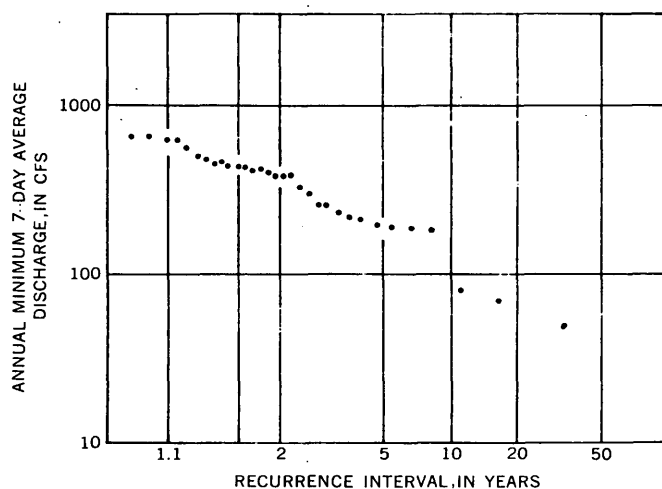
FIGURE 42.1.—Drought frequency plot, Tallapoosa River at Wadley, Ala.
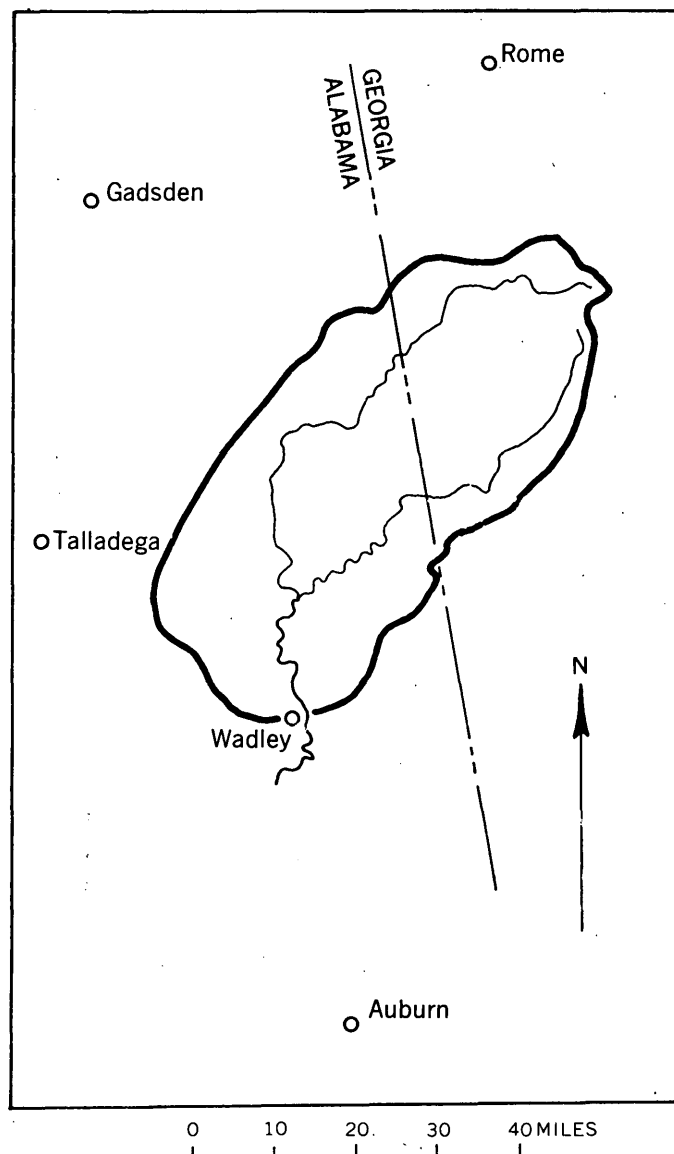
FIGURE 42.2.—Map of Tallapoosa River basin above Wadley, Ala., showing location of long-record rainfall stations.

better estimates of the recurrence intervals of the three lowest discharges.

If it could be shown that extremely low annual minimum flows coincide with extremely low precipitation, then the rainfall record could be used to indicate whether lower minimum flows had occurred in the longer period covered by the rainfall record. Four rainfall records near the Tallapoosa River basin are
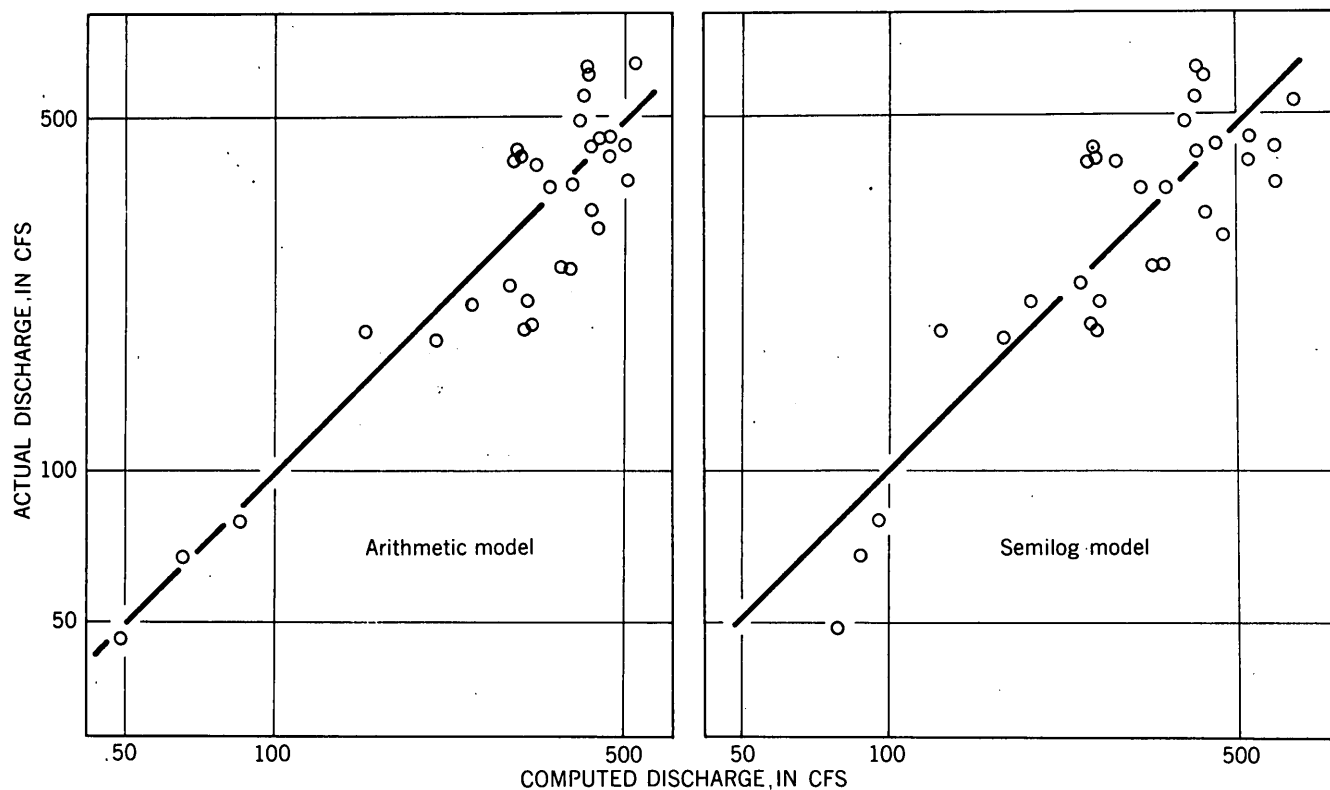
FIGURE 42.3.—Comparison of discharges computed by two equations with actual discharge.

available for the period 1888–1955. These records are used in the following analysis.

The principal factors affecting the magnitude of an annual minimum flow are the amount and distribution of precipitation during the year or part of the year. For this study the winter, spring, and early summer precipitation is considered an index of the relative amount of ground water available to the stream on July 31, and the August-September precipitation an index of the opportunity for depletion of this ground-water supply.

Locations of long-rainfall-record stations in the vicinity of the Tallapoosa basin are shown on figure 42.2. Comparison of these rainfall records showed that no two agreed very well in the summer months because of the irregularity of thunderstorm activity. Therefore, all four records were used. The two indexes selected are January-through-July precipitation in percent of normal and August-September precipitation in percent of normal. These percentages were computed for each rainfall record and then averaged over the four records to obtain the index values.

Annual minimum flows were related to the two precipitation indexes by standard regression methods using two models, one arithmetic and one semilog.

The regression equations are

$$Q = 356 + 12(JJ) + 43\ (AS)$$

and

$$\log Q = 2.49 + 0.023\,(JJ) + 0.079(AS)$$

where Q is the annual minimum 7-day average discharge, (JJ) is the January-through-July precipitation index, and (AS) is the August-September precipitation index.

Plots of computed values of Q against actual values for both equations are shown on figure 42.3. The results appear similar except that the arithmetic model fits the three low points better.

Both equations were solved for Q using rainfall indexes from 1888 to 1955, and the results are plotted on figure 42.4. These plots indicate that the three lowest minimum flows in the period of streamflow record 1924–1955 probably were also the lowest in the period 1888–1955. Therefore, the recurrence intervals assigned to these flows are recomputed on the basis of a 68-year period (1888–1955) rather than a 32-year period (1924–1955). The points as originally plotted and the three adjusted points are shown on figure 42.5. A straight line is a reasonable interpretation of the frequency relation if the adjusted points are used.
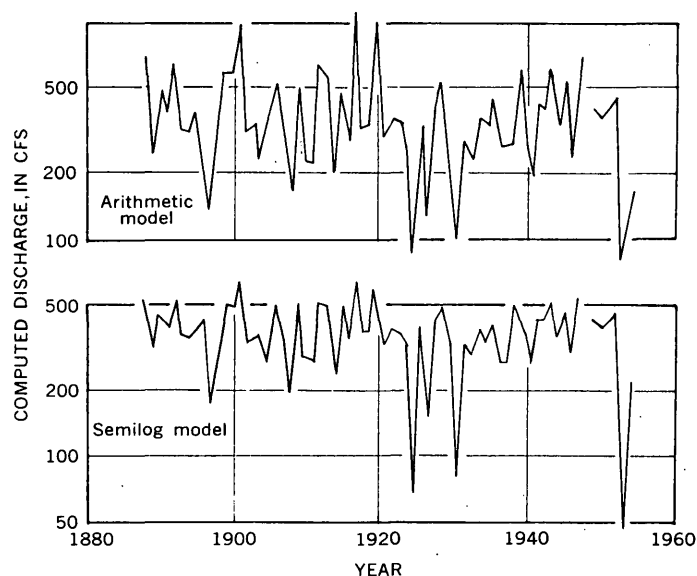
FIGURE 42.4.—Annual minimum 7-day average discharges for Tallapoosa River at Wadley computed by two equations.

The equations indicate that greater than normal January-through-July precipitation virtually precludes a very low annual minimum. Both precipitation indexes must be low in order to obtain an extremely low annual minimum flow.

The method outlined here is restricted to streams having their minimums in the late summer. The indexes used are rather rough and undoubtedly the regression could be improved by use of more appropriate ones. A model is needed to account for the July, August, and September precipitation in a year in which the minimum occurred in September, and that would ignore the August and September precipitation for the year in which the minimum occurred in July. However, the results are sufficiently reliable to demonstrate the usefulness of precipitation records for improving estimates of the recurrence intervals of very low annual minimum discharges. The method should be applicable to other streams having suitable basin characteristics, and having precipitation records for much longer periods than streamflow records.
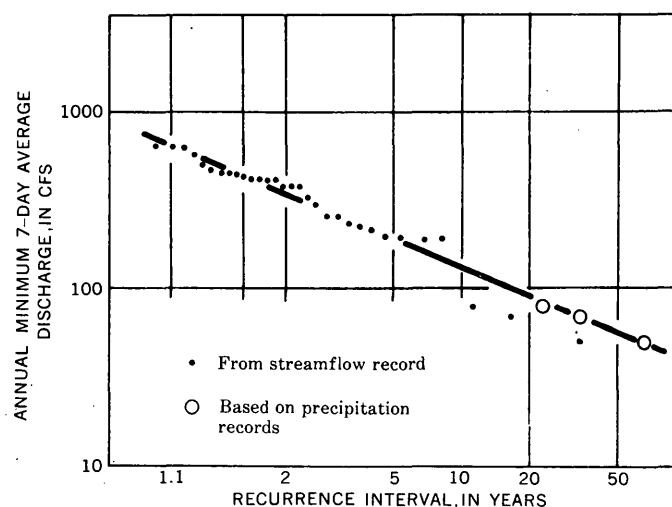
FIGURE 42.5.—Drought frequency curve based on both streamflow and precipitation records, Tallapoosa River at Wadley, Ala.

⚒

43.   STRESS MODEL FOR THE BIRMINGHAM RED IRON-ORE DISTRICT, ALABAMA

By THOMAS A. SIMPSON, Arlington, Va.

Open fracture systems associated with tight folds and major faults were observed to be the controlling factors that influenced the direction of ground-water movement in the red iron-ore mines of the Birmingham district. The parallelism of the northeasterly trending folds and faults in the Birmingham red iron-ore district suggests a common origin as the result of compression from the southeast. The orientation of the joints in relation to the folds and faults suggests a second stress field that acted as compression from the south.

The area is underlain by sedimentary rocks about 15,000 feet thick ranging in age from Cambrian to Pennsylvanian. These rocks have been folded into parallel and subparallel northeasterly trending anticlines and synclines. The composite structure, the Birmingham anticline, is overturned to the northwest and cut by a low-angle thrust along its north-

North

F_2

F_1

2°

20°

42°

F_2

68°

F_1

West

18°

F_2

40°

60°

F_1

90°   East

F_1

Strike of major folds and faults
Arrows indicate direction of
strike-slip movement

EXPLANATION

F_1
Initial stress system

Strike of joints resulting
from initial stress system

F_2
Second stress system

Strike of joints resulting
from second stress system

F_2

South
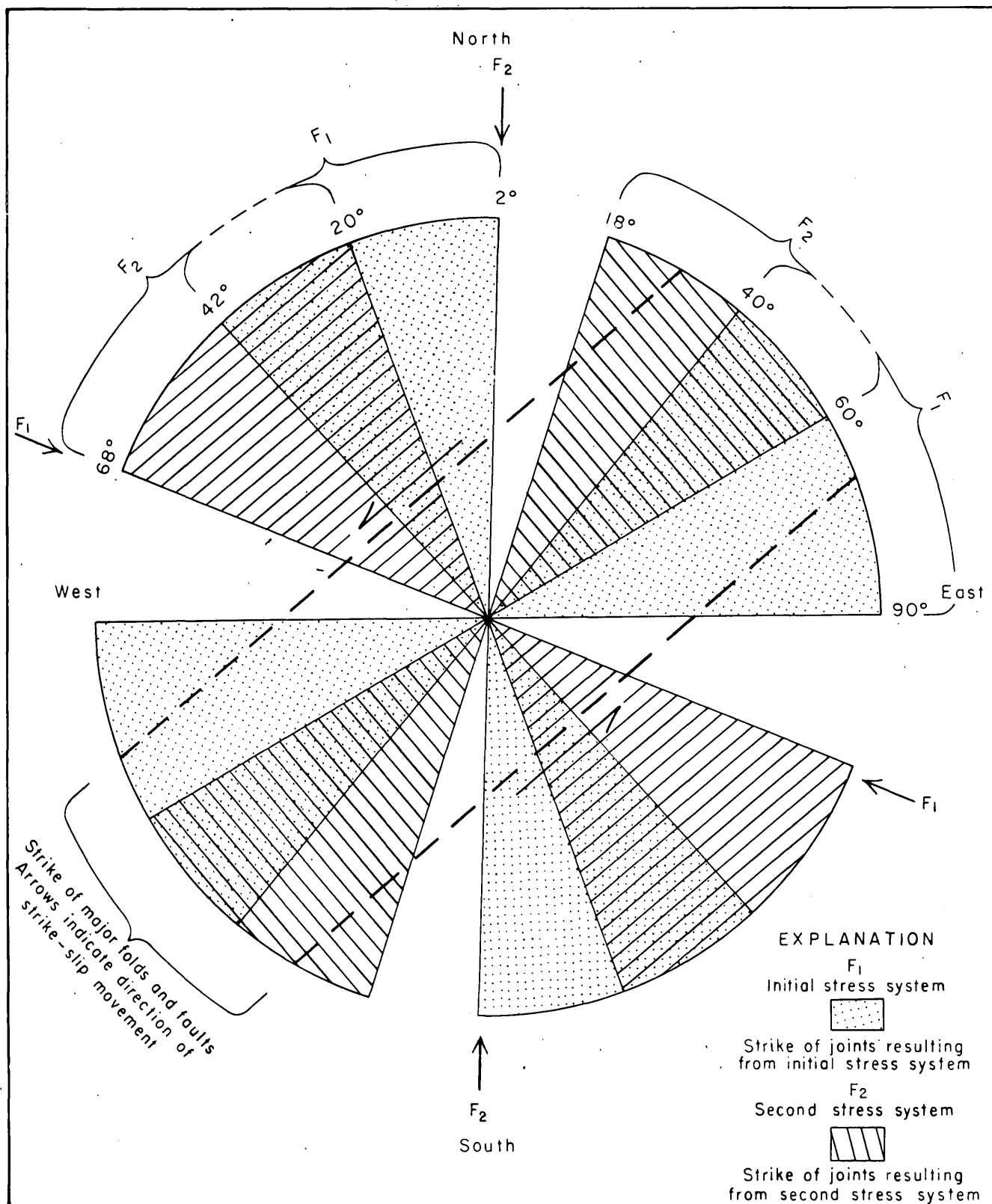
FIGURE 43.1.—Diagram showing strike of joints, folds, and faults in the Birmingham red iron-ore district.

west margin. The Ishkooda-Potter fault system in the northern part of the district strikes N. 40°–50° E. and consists of high-angle reverse and normal faults. The Shannon fault system in the central part of the district strikes generally N. 50° E. and consists of a large normal fault and several subsidiary faults. The Dickey Springs-Patton fault system strikes N. 44°–53° E. and consists of several high-angle normal faults and a major high-angle reverse fault. Some of the faults in the district show evidence of strike-slip movement at underground and surface exposures.

The strikes of the joints and major structural features commonly observed in the district are shown on figure 43.1. Most of the joints trend from N. 2° E. to N. 68° W. or from N. 18°–90° E. The greatest concentration of joint sets lie within relatively narrow limits from N. 20°–40° W. and from N. 30°–70° E., which is parallel and subparallel to the strikes of the major folds and faults.

The orientations of the folds, faults, and joints can be explained as the result of two separate stress fields acting in the area. The initial stress field (F_1) originated as compression from the southeast. This stress field produced the northeasterly trending folds and thrusts, and the conjugate joint systems indicated on figure 43.1.

The second stress field (F_2) originated as compression from the south and produced strike-slip movement along preexisting northeasterly trending fractures. Joint systems formed in this field are rotated counterclockwise relative to the first joint systems. The concentration of joints shown on figure 43.1 can be explained as the overlapping of the joint systems formed in the two stress fields.

The stress model just described accounts for the major structural features and for the jointing observed in the Birmingham district.

⚒

44.   WATER-TEMPERATURE DISTRIBUTION IN A TIDAL STREAM

By FREDERICK W. WAGENER, Columbia, S. C.

Work done in cooperation with South Carolina Public Service Authority

Water-temperature and velocity observations were made in a tidal reach of Waccamaw River at Conway, S. C. to determine and explain variations in water temperature during a tidal cycle. These observations provided data for studying the vertical distribution of temperature, and for comparing the results with similar studies on nontidal streams.

Other studies of temperature distribution in nontidal South Carolina streams having velocities exceeding 1.5 fps (feet per second) indicate little vertical variation in temperature. Temperature observations were made at both 0.2 and 0.8 of the total depths at more than 300 vertical-profile stations and at each foot of depth at several dozen others, but at only a few of the stations was the temperature variation more than 0.1° F. The depth of the streams at these stations was as much as 19 feet and water temperature ranged from 54° to 92° F.

The temperature, velocity, and depth observations discussed in this paper were made during a tidal cycle from 7 a.m. to 7:18 p.m. on September 23, 1958. The temperature observations were made by lowering the small probe of an electric thermometer into the water to the desired depth. The stage, discharge, air temperature, and water temperature during the tidal cycle are shown on figure 44.1.

Water temperatures were obtained periodically at the 0.2 and 0.8 depths at 16 stations across the stream, which provided a total of 113 pairs of observations. For 72 of these pairs, temperatures were the same at 0.2 and 0.8 depths; for 21 pairs the temperature difference was 0.1° F; for 9 pairs the difference was 0.2° F; and for the remaining 11 pairs the difference was greater than 0.2° F. Sixteen additional sets of water temperatures were obtained periodically at selected stations, observations being
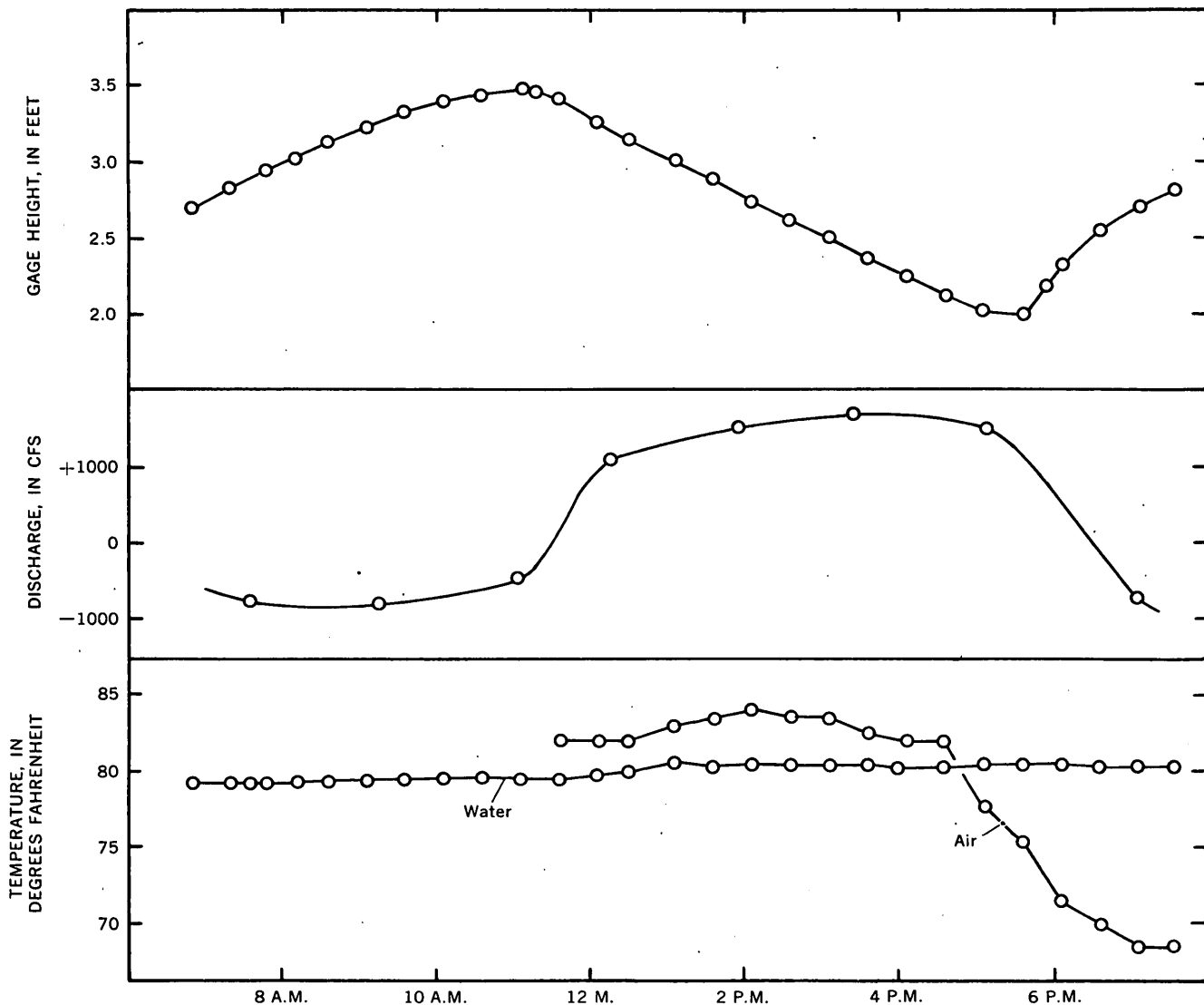
FIGURE 44.1.—Physical conditions during tidal cycle.

made at each foot of depth. For 13 of these sets, the maximum variation in the vertical was 0.1° F; for the three remaining sets the variation was 0.2° F or more. Temperature differences that exceeded 0.2° F can be arranged in two groups. The first group comprises temperature differences observed at times of velocity less than about 0.25 fps., high solar radiation, and little or no wind. At these times, a minimum amount of turbulent mixing occurs and heating of the water near the surface by solar radiation is at a maximum. Such conditions favor a temperature differential. The greatest observed temperature difference resulting from the combination of these conditions is shown by the temperature profile for station 150 at 11:18 a.m. (fig. 44.2).

A second period during which relatively high temperature differentials occurred was 45 to 60 minutes after high tide. Velocities at that time increased to 0.5 fps or more, which is usually sufficient to cause turbulent mixing. During this period, however, it seems that a slug of warmer water released from storage passed by the measuring section. This warmer water probably originated either in an extensive shallow borrow pit connected with the river 0.3 mile upstream or in Kingston Lake which is connected with the river 0.6 mile upstream. The temperature and velocity hydrographs, figure 44.3, show the effects of this warmer water. The difference in temperature between the 0.2 and 0.8 depths at 12:10

p.m. was 0.8° F shortly after the direction of flow had changed from upstream to downstream, but within two hours the difference was again negligible.

The results of the investigation indicate that when velocities exceed about 0.25 fps, turbulent mixing is sufficient to preclude temperature differences of more than 0.2° F from top to bottom except when water at a higher temperature enters the stream a short distance above the measuring section; when velocities are less than about 0.25 fps, however, temperature differences up to 1.3° F can be caused by solar radiation.
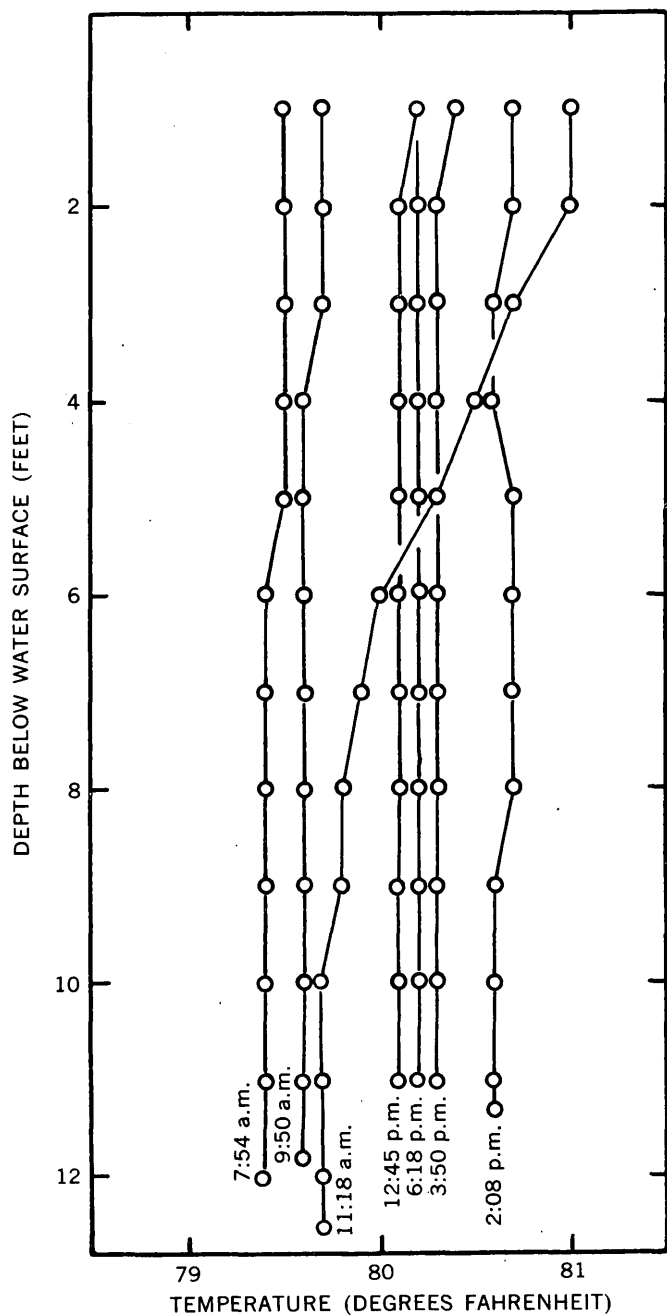
FIGURE 44.2.—Temperature profiles at station 150.
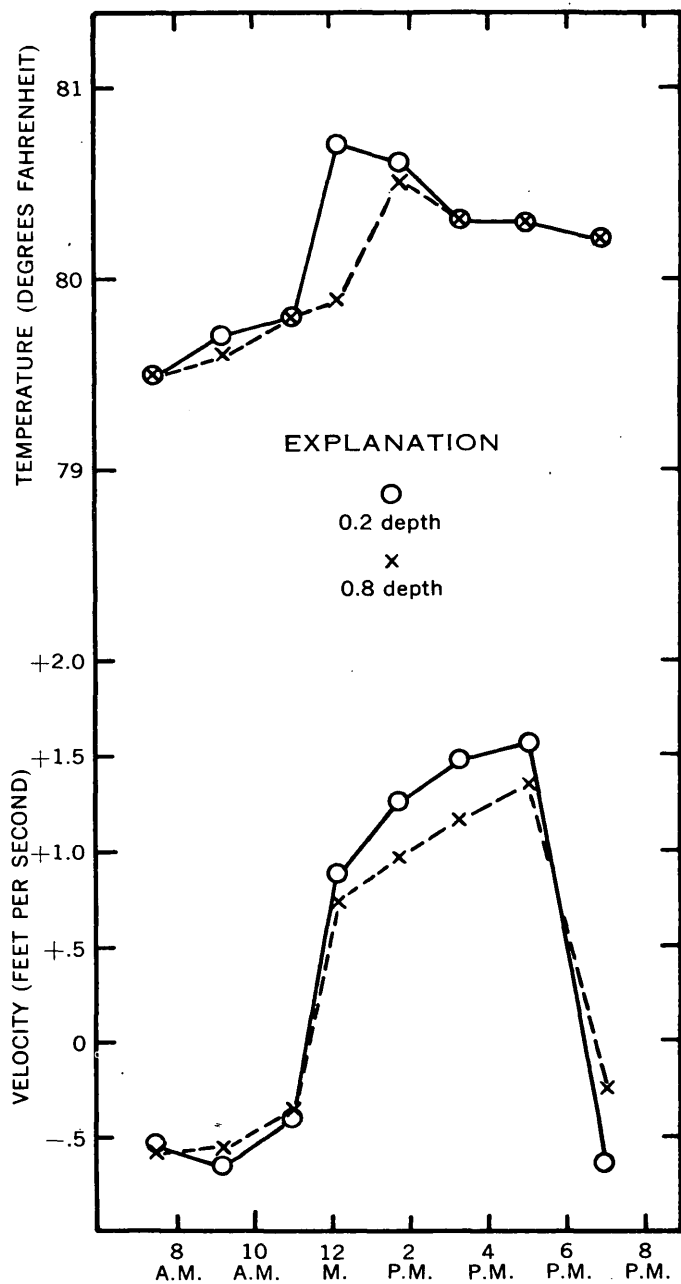
FIGURE 44.3.—Temperature and velocity observations at station 100.

45.   RECENT LEAD-ALPHA AGE DETERMINATIONS ON ZIRCON FROM THE CAROLINA PIEDMONT

By WILLIAM C. OVERSTREET, HENRY BELL, III, HARRY J. ROSE, JR., and THOMAS W. STERN, Beltsville, Md., and Washington, D. C.

Lead-alpha ages have recently been determined for 21 zircon concentrates separated from granite, granodiorite, and syenite exposed in the Piedmont of North and South Carolina. The location of the samples is shown on figure 45.1, and descriptions of the sources of the zircon are listed in table 1. Results of the analyses and the calculated ages of the zircon crystals are given in table 2.

Radioactivity determinations on igneous or pyroclastic rocks in the Piedmont offer the only means of determining the ages of these rocks, as the intruded sedimentary rocks contain no fossils. The

TABLE 1.—*Sources of the zircon*

No. on
fig. 45.1   *Source and sample no.*

1. U.S. National Museum collection. Large zircon crystals stated to have come from a locality 4 miles east of Tigerville, Greenville County, S. C. Zircon-rich vermiculite deposits thought to be source of the specimen. Sample USNM 105674.

2. U.S. National Museum collection. Large zircon crystals from the Jones Mine, Henderson County, N. C. Vermiculite-bearing syenite pegmatite. Sample USNM 80114.

3. Zircon panned from 200 pounds of saprolite of fine-grained massive granite exposed in deep road cuts 0.9 mile southwest of Blackjack, Fairfield County, S. C. Rock is marginal phase of pluton represented by sample 59–OT–102. Sample was free of inclusions, but exposure shows blocky inclusions of amphibolite, biotite-hornblende schist, and feldspathic kyanite-muscovite schist. Sample 59–OT–107.

4. Zircon panned from 290 pounds of saprolite of massive biotite-granite exposed at the intersection of S. C. Rte. 20–19 and the Rockton-Rion Railroad 5.5 miles S. 20° W. of Winnsboro, Fairfield County, S. C. Sample 59–OT–102.

5. Zircon panned from 260 pounds of saprolite of coarse-grained massive porphyritic biotite granite having phenocrysts of pink microcline up to ¾ inch in length, exposed on S. C. Rte. 97 at a point 1.1 miles north of White Oak Creek, Kershaw County, S. C. Sample 59–OT–110.

6. Zircon panned from 180 pounds of saprolite of very coarse grained massive porphyritic biotite granite exposed on the east side of Lowrys-Baton Rouge road at a point 0.5 mile west of the junction with U.S. Rte. 321 near Lowrys, Chester County, S. C. Sample 59–OT–101.

7. Zircon panned from 220 pounds of saprolite of fine-grained massive biotite granite exposed in deep road cuts on both sides of the Leeds-Wilksburg road at a point opposite the Leeds Lookout Tower, Chester County, S. C. Sample 59–OT–100.

8. Samples from Isenhour Quarry on N. C. Rte. 73 about 0.5 mile east of Concord, Cabarrus County, N. C. Samples are composites of 20-pound samples taken from different parts of the body of rock.

TABLE 1.—*Sources of the zircon*—Continued

No. on
fig. 45.1   *Source and sample no.*

Zircon panned from 60 pounds of saprolite of medium-grained biotite granite in the southern dike in quarry. Sample IPE.

Zircon panned from 60 pounds of saprolite of biotite granite forming the northern dike in the quarry. Sample IPF.

Zircon panned from 100 pounds of saprolite at the main body of biotite granite. Sample IPG.

Zircon panned from 100 pounds of saprolite at the main body of biotite granite. Sample IPH.

Zircon panned from 260 pounds of syenite in a dike cutting granite and gneissic granodiorite. Sample HB–39–59.

Zircon panned from 60 pounds of saprolite of gneissic granodiorite; both the granite and the syenite intrude the gneissic granodiorite. Sample IPA.

Zircon panned from 40 pounds of saprolite of gneissic grandiorite. Sample IPB.

Zircon panned from 40 pounds of saprolite of gneissic granodiorite. Sample IPC.

Zircon panned from 40 pounds of saprolite of gneissic granodiorite. Sample IPD.

9. Zircon panned from 340 pounds of saprolite of coarse-grained, massive augite syenite exposed in a quarry on the north side of N. C. Rte. 49 just west of the intersection with U.S. Rte. 601 about 2.5 miles south of Concord, Cabarrus County, N. C. Sample 56–OT–11 and 56–OT–11a.

10. Zircon panned from 200 pounds of saprolite of porphyritic granite exposed on county road between Watts and S. C. Rte 71 at a point 2 miles south of route 71 in Abbeville County, S. C. Nonmagnetic fraction at 1.5 amperes in Frantz Separator; sample 59–OT–111 (N.M. 1.5). Magnetic fraction at 1.5 amperes; sample 59–OT–111 (M 1.5).

11. U.S. National Museum collection. Large zircon crystals from gneiss exposed 4.5 miles east of Iva on the line between Anderson and Abbeville Counties or in Abbeville County, S. C. Sample USNM 97589.
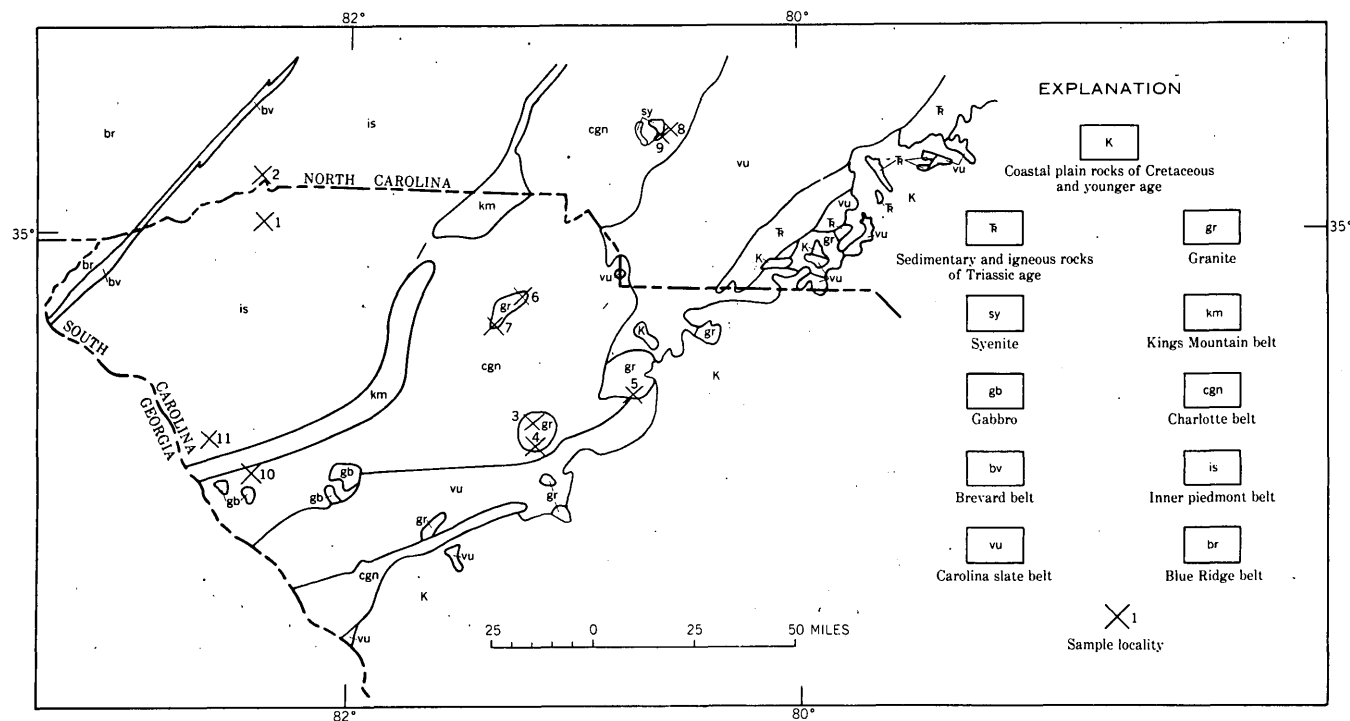
FIGURE 45.1.—Major rock units and location of zircon samples in the Piedmont of North and South Carolina.

rocks studied are now saprolite, so that only resistant minerals can be used for age determinations. Despite a lack of positive knowledge concerning the absolute ages of these rocks, many tentative ideas have been presented regarding their relative ages. Major syntheses of the regional geology of the Southeastern States evolved by Arthur Keith (1923, p. 309–380) and Anna I. Jonas (Mrs. G. W. Stose) (1932, p. 228–243), though profoundly different in tectonic and stratigraphic interpretation, generally attributed a Precambrian age to the bulk of the metasedimentary rocks and to some of the plutonic igneous rocks. The massive igneous rocks were considered to be late Paleozoic in age. Both Keith and Jonas recognized the polymetamorphic character of some of the schist and gneiss, and, despite differences in opinion as to the mechanics of the metamorphism, they attributed it to processes operating in Precambrian and in late Paleozoic time. Recently another major synthesis of Appalachian geology has been presented by P. B. King (1951, p. 119–144; 1955, p. 332–373) who proposes that the metamorphosed sedimentary and volcanic rocks of the Carolina Piedmont and the igneous rocks, intruded during several orogenic episodes, are Paleozoic in age.

Recent geologic observations in the Carolina Piedmont support King's view (Kesler, 1944, p. 755–782; Griffitts and Overstreet, 1952, p. 777–789; Kesler, 1955, p. 374–387; Overstreet and Griffitts, 1955, p. 549–577; Stuckey and Conrad, 1958, p. 3–51; Stromquist and Conley, 1959, p. 1–36; Bell and Overstreet, 1959, p. 1–5; Long, Kulp, and Eckelmann, 1959, p. 585–603; Bell, 1960, p. B189–B191; and Overstreet and Bell, 1960, p. B197–B199). They show 3 sequences or episodes of sedimentation, volcanism, igneous intrusion, folding, and metamorphism. Erosional unconformities bracket the 3 episodes. The Paleozoic geologic events shown schematically in table 3 were deduced by Overstreet and Bell as a result of reconnaissance mapping during which it was recognized that the metasedimentary rocks of the South Carolina Piedmont consist of slate-belt rocks of various ages raised to different grades of regional metamorphism, and that unconformities in the slate belt correlate with unconformities in the Kings Mountain belt.

The unconformities correlated between the slate and the Kings Mountain belts are those below episodes B and C, table 3. A postulated unconformity beneath episode A has not been observed in the

TABLE 2.—*Lead-alpha ages of zircon from rocks in the Piedmont of North and South Carolina*

[Alpha activity measurements by T. W. Stern; spectrographic analyses of lead by H. J. Rose, Jr., T. W. Stern, and H. W. Worthing.]

No. on fig. 45.1	Sample No.	Alpha counts per milligram per hour	Average lead content from duplicate determinations (parts per million)	Calculated age [1] (millions of years)
1	USNM 105674	269	28	255±30
2	USNM 80114	439	51	280±30
3	59-OT-107	346	37	260±30
4	59-OT-102	477	53	270±30
5	59-OT-110	170	17	245±30
6	59-OT-101	306	32	255±30
7	59-OT-100	145	28	460±50
8	IPE	377	68	445±50
	IPF	458	68	360±40
	IPG	433	78	430±50
	IPH	398	49	300±35
	HB-39-59	262	49	450±50
	IPA	132	28	505±55
	IPB	123	25.5	495±55
	IPC	117	19	380±100
	IPD	132	26	470±55
9	56-OT-11	24	3.0	305 ⎫ 425±110
	56-OT-11a	22	5.0	540 ⎭
10	59-OT-111 (NM 1.5)	344	82	565±65
	59-OT-111 (M 1.5)	481	102	505±55
11	USNM 97589	172	40	550±60

[1] Lead-alpha ages (rounded to nearest 5 million years) were calculated from the equations:

(1) $t = \dfrac{C\ Pb}{\alpha}$ where t is the calculated age in millions of years, C is a constant based upon the U/Th ratio and has the value 2485, Pb is the lead content in parts per million and α is the alpha counts per milligram per hour; and

(2) $T = t - 1/2\ kt^2$ where T is the age in millions of years corrected for decay of uranium and thorium, and k is a decay constant based upon the U/Th ratio and has a value of 1.56×10^{-4}.

U/Th ratio from X-ray fluorescence analyses by F. J. Flanagan is 1.0 for samples 59-OT-100, 59-OT-101, 59-OT-102, 59-OT-110, and 59-OT-111 (M 1.5); assumed 1.0 for other samples.

Piedmont of southern North Carolina or in South Carolina. Some measure of the probable age of the unconformities and of the sedimentary and pyroclastic rocks they bracket have been sought by the authors through the lead-alpha ages of zircons from plutonic igneous rocks emplaced during one or another of the three episodes listed in table 3. Many pounds of saprolite were panned to obtain each zircon concentrate. In addition, three samples of coarse-grained zircon were kindly given to the writers by G. S. Switzer of the U.S. National Museum.

Direct measurements of the ages of the sediments in the three episodes is being attempted by A. A. Stromquist, A. M. White, and T. W. Stern by analyzing zircon from felsic lavas interbedded with the sediments. This work, however, is not yet completed.

The results of lead-alpha age determinations on 17 of the 21 samples fall into three groups (table 4)

which correspond to the position of their host rocks in the three geologic episodes shown on table 3. The analyses are most consistent and seem to show the best agreement with presently available field data in the youngest group of samples, and increasingly less consistent in the older groups.

The results from four samples do not fit with the recognized field relations. One sample of zircon (59-OT-100) with an age of 460 ± 50 m.y. (million years) was collected from fine-grained granite thought to be a marginal phase of the oval pluton represented by sample 59-OT-101 having an age of 255 ± 30 m. y. The older sample may be contaminated by nonradiogenic lead or by an older generation of zircon. The samples of zircon from Cabarrus County, N. C., 56-OT-11 and 56-OT-11a (425 ± 110 m.y.), HB-39-59 (450 ± 50 m. y.), are thought to come from rocks occupying structural positions similar to the episode-C syenite. Low lead and alpha activity of the zircon from samples 56-OT-11 and 56-OT-11a make satisfactory analysis very difficult, but sample HB-39-59 was satisfactory for analysis, and it also gave an unexpectedly old age. Possibly some syenite was emplaced during episode B, but the field evidence presently restricts syenite to episode C.

The probable ages of the unconformities between the three episodes can be interpreted from the three groups of ages shown on table 4. The unconformity between episodes C and B apparently formed between 400 and 260 m.y. ago. In order to allow for the deposition of the sediments in which episode-C syenite and granite is emplaced, the unconformity is probably closer to 400 than to 260 m.y. old. It apparently was formed between Ordovician and Devonian time.

The ages of the zircon crystals from rocks in episode A doubtless are modified by loss of lead during the profound metamorphism of episode B. We do not yet know when these rocks were emplaced, but it is likely that they were intruded into sediments of late Precambrian and Cambrian age. The unconformity between episodes B and A may have been formed between Cambrian and Ordovician time.

REFERENCES

Bell, Henry, III, 1960, A synthesis of geologic work in the Concord area, North Carolina, *in* Short papers in the geological sciences: U.S. Geol. Survey Prof. Paper 400-B, p. B189-B191.

Bell, Henry, III, and Overstreet, W. C., 1959, Relations among some dikes in Cabarrus County, North Carolina: South Carolina Div. Geology, Geol. Notes, v. 3, no. 2, p. 1-5.

TABLE 3.—*Summary of Paleozoic geologic events in the Carolina Piedmont*

Era	Episode of folding, meta-morphism, and igneous activity	Rock		Metamorphism	
		Sedimentary	Igneous	Regional	Contact
		Unconformity			
	C		Syenite, gabbro, py-roxenite, norite; granitic rocks, typi-cally form circular plutons and elongate cross-cutting bodies; felsic and mafic flows and dikes associated with the pyroclastic and sedimentary rocks.	Syenite, gabbro, pyroxe-nite, norite and granites unaffected by progres-sive regional metamor-phism, but show some retrogressive features chiefly resulting from cataclasis; felsic and mafic dikes and flows show effects of low-grade regional meta-morphism.	None attributable to syenite; feeble local contact effect from gabbro, pyroxenite, and norite; feeble in-crease in metamor-phism at granite con-tacts; no metamor-phism attributable to felsic and mafic feeder dikes.
		Argillite, graywacke, pyroclastic rocks.		Progressive, seldom ex-ceeding greenschist facies; slight retro-gressive.	
Paleozoic		Unconformity			
	B		Granitic rocks, typically concordant plutons; gabbro, pyroxenite, andesite dikes; mafic flows, and felsic dikes and flows associated with pyroclastic and sedimentary rocks.	Widespread migmatiza-tion; retrogressive effects such as recrystallization of biotite attributable to episode C.	Granites of episode B react retrogressively on inclusions of gab-bro and pyroxenite of episode B; may have large contact aureoles in green-schist and albite-epidote amphibolite zones; little or no aureoles in higher grade zones; no evi-dence of metamor-phism induced by feeder dikes for mafic and felsic flows; retrogressive effects associated with the granites of episode C.
		Argillite, graywacke, pyroclastic rocks, local sandstone and limestone; now seen as schists, gneisses, migmatites, quart-zites and marble.		Progressive, ranging from greenschist facies to sillimanite-garnet sub-facies; retrogressive features attributable to episode C locally com-mon; highest-grade rocks show some re-crystallization of biotite and retrogression of sillimanite to sericite.	
		Unconformity			
	A		Granitic rocks.	Apparently strongly meta-morphosed in episode B.	Relations essentially unknown.
——?—— Late Precambrian		Graywacke, pyro-clastic rocks, local limestone; now seen as schists, gneisses, calc-silicate rocks; migmatites common.		Progressive, ranging from greenschist facies to sillimanite-garnet sub-facies; locally retro-gressive.	
		Unconformity, widespread erosion			
Precambrian		Basement unobserved in the Carolina Piedmont			

TABLE 4.—*Correlation of selected lead-alpha ages of zircon crystals*

Episode of folding, metamorphism, and igneous activity (table 3)	Rock	Sample No.	Lead-alpha age (millions of years)
Unconformity below sedimentary rocks of Late Triassic age		
C	Syenite	U.S.N.M. 105674	255 ±30
	Syenite	U.S.N.M. 80114	280 ±30
	Granite	59-OT-107	260 ±30
	Granite	59-OT-102	270 ±30
	Granite	59-OT-110	245 ±30
	Granite	59-OT-101	255 ±30
	Unconformity		
B	Granite	IPE	445 ±50
	Granite	IPF	360 ±40
	Granite	IPG	430 ±50
	Granite	IPH	300 ±35
	Unconformity		
A	Gneissic granodiorite	IPA	505 ±55
	Gneissic granodiorite	IPB	495 ±55
	Gneissic granodiorite	IPC	380 ±100
	Gneissic granodiorite	IPD	470 ±55
	Granite	59-OT-111 (N.M. 1.5)	565 ±65
	Granite	59-OT-111 (M 1.5)	505 ±55
	Gneiss	USNM 97589	550 ±60

Griffitts, W. R., and Overstreet, W. C., 1952, Granite rocks of the western Carolina Piedmont: Am. Jour. Sci., v. 250, p. 777–789.

Jonas, A. I., 1932, Structure of the metamorphic belt of the southern Appalachians: Am. Jour. Sci., 5th ser., v. 24, p. 228–243.

Keith, Arthur, 1923, Outlines of Appalachian structure: Geol. Soc. America Bull., v. 34, no. 2, p. 309–380.

Kesler, T. L., 1944, Correlation of some metamorphic rocks in the central Carolina Piedmont: Geol. Soc. America Bull., v. 55, p. 755–782.

———, 1955, The Kings Mountain area, *in* Russell, R. J., ed., 1955, Guides to southeastern geology: Geol. Soc. America Guidebook, 1955 Ann. Mtg., p. 374–387.

King, P. B., 1951, The tectonics of middle North America: Princeton, N. J., Princeton Univ. Press, p. 3–203.

———, 1955, A geologic section across the southern Appalachians: an outline of the geology in the segment in Tennessee, North Carolina, and South Carolina, *in* Russell, R. J., ed., 1955, Guides to southeastern geology: Geol. Soc. America Guidebook, 1955 Ann. Mtg., p. 332–373.

Long, L. E., Kulp, J. L., and Eckelmann, F. D., 1959, Chronology of major metamorphic events in the southeastern United States: Am. Jour. Sci., v. 257, no. 8, p. 585–603.

Overstreet, W. C., and Bell, Henry, III, 1960, Geologic relations inferred from the provisional geologic map of the crystalline rocks of South Carolina, *in* Short papers in the geological sciences: U.S. Geol. Survey Prof. Paper 400–B, p. B197–B199.

Overstreet, W. C., and Griffitts, W. R., 1955, Inner Piedmont belt, *in* Russell, R. J., ed., 1955, Guides to southeastern geology: Geol. Soc. America Guidebook, 1955 Ann. Mtg., p. 549–577.

Stromquist, A. A., and Conley, J. F., 1959, Geology of the Albemarle and Denton quadrangles, North Carolina: Carolina Geol. Soc., Field Trip Guidebook, p. 1–36.

Stuckey, J. L., and Conrad, S. G., 1958, Explanatory text for geologic map of North Carolina: North Carolina Dept. Conserv. Devel., Div. Mineral Resources, Bull. 71, p. 3–51.

· ⚒

46. TIDAL FLUCTUATIONS OF WATER LEVELS IN WELLS IN CRYSTALLINE ROCKS IN NORTH GEORGIA

By J. W. STEWART, Atlanta, Ga.

The semidiurnal water-level fluctuations of a tidal period were observed in wells in metamorphic crystalline rocks during a geologic and hydrologic study at the Georgia Nuclear Laboratory in Dawson County, Ga. The laboratory is about 45 miles north-northeast of Atlanta, at lat 34°25'N. and long 84°8'W., about 240 miles west of the Atlantic Ocean and 300 miles north of the Gulf of Mexico. This is believed to be the first reported occurrence of tidal fluctuations in wells drilled in metamorphic rocks.

The Georgia Nuclear Laboratory site is underlain by metamorphic crystalline rocks and by a mantle of
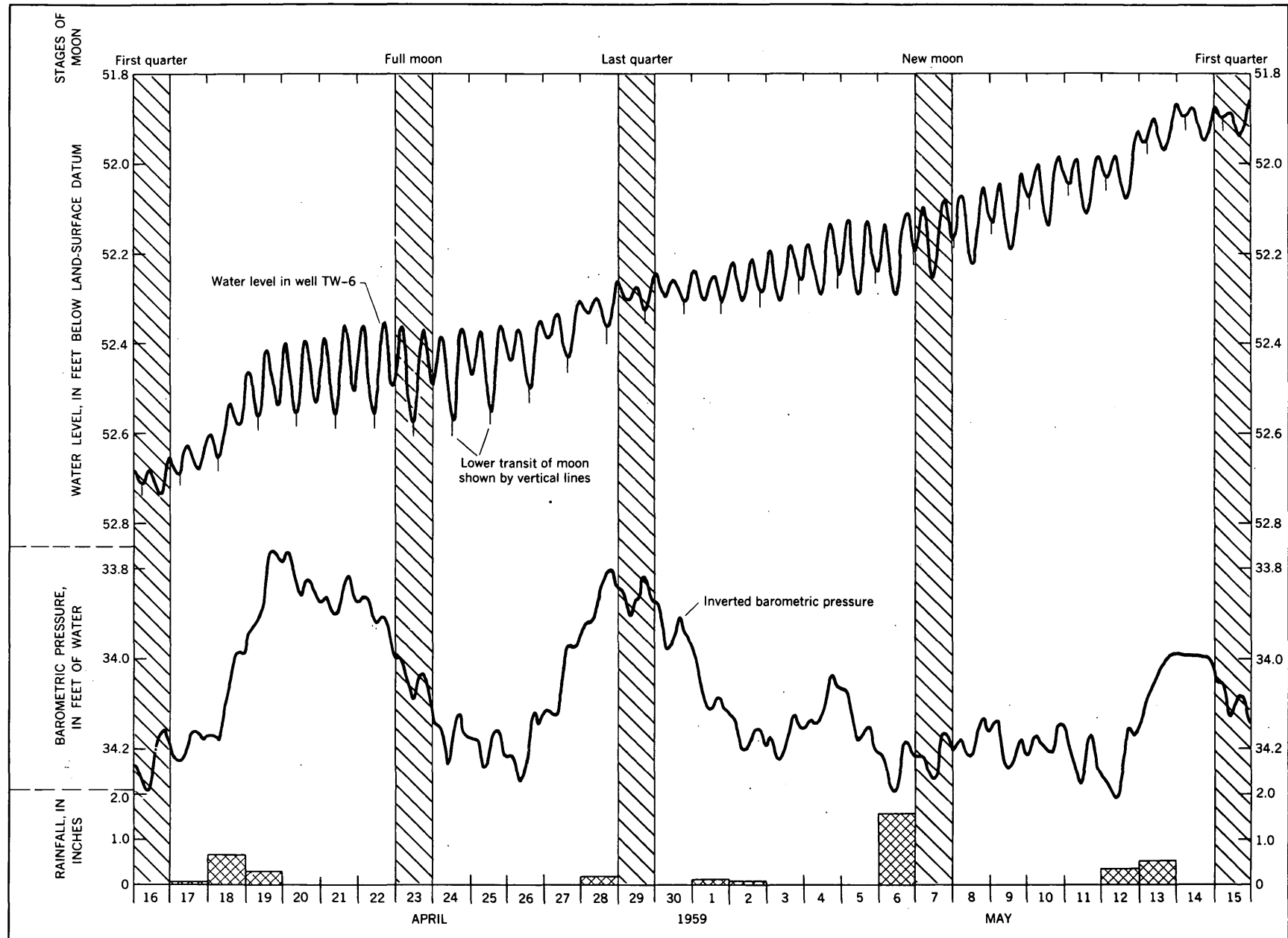
FIGURE 46.1.—Water-level fluctuations in well TW-6, inverted barometric pressure, and rainfall.

saprolite derived from weathering of these rocks. The saprolite consists of a soil cover, a zone of highly weathered saprolite, and a zone of slightly to moderately weathered saprolite. Bedding and foliation at the site dip about 50° to 70° SE. Ground water is found both in the saprolite and in the unweathered rock, but on high hills and ridges ground water generally occurs only in hard rock.

Of twenty-six 6-inch wells in the area, four bottom at a depth of 400 feet and 22 at depths ranging from 50 to 137 feet. Water levels in the wells ranged from about 4 feet below land surface in valleys to as much as 60 feet below land surface on hills and ridges. Tidal fluctuations were observed in 3 of the 4 wells 400 feet deep. None of the other wells showed tidal fluctuations, but the water levels in most of the wells were affected by changes in barometric pressure.

Figure 46.1 shows the water-level fluctuations observed in well TW–6 during a lunar cycle and the corresponding barometric pressure changes and rainfall during the cycle. The water level in the well did not appear to be affected to any great extent by changes in barometric pressure.

In general, ground water at the laboratory site occurs under confined and unconfined conditions in the saprolite and under confined conditions in the hard unweathered rock. Ground water occurs in the pore spaces and in fractured quartz veins in the saprolite, and the degree of confinement of the water depends upon the composition, thickness, and extent of the saprolite, and differences in the permeability of the beds. The porosity of the saprolite averages about 46 percent. On the other hand, the unweathered rocks are dense and massive, and ground water occurs chiefly in joints and other openings in the rock. The porosity of the unweathered rock averages about 4 percent. Where the rock is close to the surface many of the joints and cracks are filled with clay and silt to depths slightly above or below the water table. Thus, the overlying clay and silt zones, the dense nonpermeable rock, and the sealed joints and cracks above the zone of saturation probably cause local confinement of the water in the hard rock.

A well drilled in quartz-mica schist and another in biotite schist showed very distinct tidal fluctuations; another well drilled in the quartz-mica schist showed less pronounced fluctuations; and one well drilled in quartz-mica-amphibole schist showed no fluctuations.

The transmissibility of the quartz-mica schist was 210 gpd/ft (gallons per day per foot), whereas the transmissibility of the biotite schist was 60 gpd/ft, and that of the quartz-mica-amphibole schist was 7 gpd/ft.

For two wells the average daily retardation of the moon's transit for the periods of records computed was 49.1 and 48.8 minutes (U. S. Naval Observatory, 1957), and the average daily retardation of the peaks and troughs in the wells for the same periods was 48.1 and 49.8 minutes, respectively. The tidal fluctuations in a third well were partly masked by recharge from precipitation, and the average daily retardation of the peaks and trough could not be determined with acceptable accuracy.

The water-level fluctuations were more regular and the amplitude of the fluctuations was greater during periods of new and full moon, when the tide-producing forces were greatest, than they were during periods of the first and last quarters when the tide-producing forces were smallest. The amplitude of the maximum fluctuations was about 0.25 foot and the amplitude of the minimum fluctuations was about 0.01 foot. The lowest water levels in the wells generally coincided with the time of the moon's transit at upper and lower culmination, as shown by the short vertical lines in figure 46.1.

The following evidence indicates that the semidiurnal fluctuations of water levels are the result of earth tides produced by the attraction of the moon and sun: (a) two daily cycles of water-level fluctuations occur in the wells, about 50 minutes later each day; (b) the close agreement of the average daily retardation of the peaks and troughs in the wells with that of the average daily retardation of the moon's transit; (c) the occurrence of regular fluctuations of maximum amplitudes during periods of new and full moon and irregular fluctuations of minimum amplitudes during periods of the first and last quarters of the moon; and (d) the coincidence of the lowest water levels in wells with that of the moon's transit at upper and lower culmination.

REFERENCE

U.S. Naval Observatory, 1957, The American Ephemeris and Nautical Almanac for the year 1959: Nautical Almanac Office.

GEOLOGY AND HYDROLOGY OF WESTERN CONTERMINOUS UNITED STATES

47.   A NEW MAP OF WESTERN CONTERMINOUS UNITED STATES SHOWING THE MAXIMUM KNOWN OR
INFERRED EXTENT OF PLEISTOCENE LAKES

By J. H. FETH, Menlo Park, Calif.

Maps showing Pleistocene lakes of the Basin and Range Province were published by Meinzer (1922) and Hubbs and Miller (1948). The one compiled by Hubbs and Miller is accompanied by a lengthy bibliography and provides essentially complete coverage of the Great Basin. A new map, figure 47.1, includes new information gathered as a result of the large amount of geologic mapping done during the last 15 years. This recent mapping has refined some of the earlier data, and has also disclosed many additional areas, some of large size, that were occupied by Pleistocene lakes both within and outside the areas covered by the earlier maps. The large number of lakes outside the Basin and Range Province have not been shown previously on a single compilation.

Names are not shown for the Pleistocene lakes on figure 47.1 because many of them are either unnamed or are named only informally and because many others have been given more than one name. A list of references, table 1, is keyed by number to individual lake basins or to groups of basins shown on the map (fig. 47.1). The list merely supports the map and does not constitute a complete bibliography on the subject. In general, the reference given for each lake basin is the earliest one found that is accompanied by a map showing the outline of the Pleistocene lake.

TABLE 1.—*References for map showing extent of Pleistocene lakes*

Map no., (fig. 47.1)	Reference
1........	Hobbs, W. H., 1945, Geol. Soc. America Bull., v. 56, no. 12, p. 1167.
	Bretz, J. H., Smith, H. T. U., and Neff, G. E., 1956, Geol. Soc. America Bull., v. 67, no. 8, p. 957–1049.
2........	Alden, W. C., 1932, Physiography and glacial geology of eastern Montana and adjacent areas: U. S. Geol. Survey Prof. Paper 174, 133 p.
	Bretz, J. H., Smith, H. T. U., and Neff, G. E., 1956, Geol. Soc. America Bull., v. 67, no. 8, p. 957–1049.
3........	Alden, W. C., 1932, Physiography and glacial geology of eastern Montana and adjacent areas: U. S. Geol. Survey Prof. Paper 174, 133 p.

TABLE 1.—*References for map showing extent of Pleistocene lakes*—(Continued)

Map no., (fig. 47.1)	Reference
4........	Moulder, E. A., and Kohout, F. A., 1958, U. S. Geol. Survey Water–Supply Paper 1424, 198 p.
5........	Schwennesen, A. T., and Meinzer, O. E., 1918, U. S. Geol. Survey Water–Supply Paper 425–E, p. 131–158.
	Newcomb, R. C., 1958, Am. Jour. Sci., v. 256, no. 5, p. 328–340.
6........	Pardee, J. T., 1910, Jour. Geology, v. 18, no. 4, p. 376–386.
	Langton, C. M., 1935, Jour. Geology, v. 43, no. 1, p. 27–60.
	Fox, P. P., 1955, Geol. Soc. America Bull., v. 66, no. 12, p. 1713.
7........	Allison, I. S., 1953, Oregon Dept. Geol. and Min. Industries Bull. 37, 18 p.
8........	Wheeler, H. E., and Cook, E. F., 1954, Jour. Geology, v. 62, p. 525–536.
9........	Orr, P. C., 1959, oral communication.
10........	Howard, A. D., 1937, Geol. Soc. America Spec. Paper 6, xii, 159 p.
11........	Trauger, F. D., 1950, U. S. Geol. Survey open-file rept., 287 p.
12........	Piper, A. M., and others, 1939, U. S. Geol. Survey Water–Supply Paper 841, 189 p.
	Wallace, R. E., and Calkins, J. A., 1956, U. S. Geol. Survey Min. Inv. Field Studies Map MF-82.
13........	Meinzer, O. E., 1922, Geol. Soc. America Bull., v. 33, no. 3, p. 541–552.
14........	Jenkins, O. P., 1951, California Div. Mines Econ. Minerals Map 2 (revised 1951).
15........	Hubbs, C. L., and Miller, R. R., 1948, Utah Univ. Bull., v. 38, no. 20, p. 18–166.
16........	Russell, I. C., 1885, U. S. Geol. Survey Mon. 11, 288 p.
17........	Gilbert, G. K., 1890, U. S. Geol. Survey Mon. 1, 438 p. [1]
18........	Love, J. D., Weitz, J. L., and Hose, R. K., 1955, Geologic map of Wyoming: U. S. Geol. Survey.
19........	W. P. Irwin, 1959, oral communication.
20........	Frink, J. W., and Kues, H. A., 1954, Am. Assoc. Petroleum Geologists Bull., v. 38, no. 11, p. 2357–2371.
	Davis, G. H., and Poland, J. F., 1957, U. S. Geol. Survey Water-Supply Paper 1360–G, p. 409–588.
21........	Matthes, F. E., 1930, U. S. Geol. Survey Prof. Paper 160, 137 p.
22........	Russell, I. C., 1889, U. S. Geol. Survey 8th Ann. Rept., p. 261–394.
23........	Mayo, E. B., 1934, Science n. s., v. 80, no. 2065, p. 95–96.
24........	Miller, W. J., 1928, Jour. Geology, v. 36, no. 6, p. 510–525.

[1] In light of recent studies (M. D. Crittenden, oral communication, 1961), the Escalante arm of Lake Bonneville has been deleted.
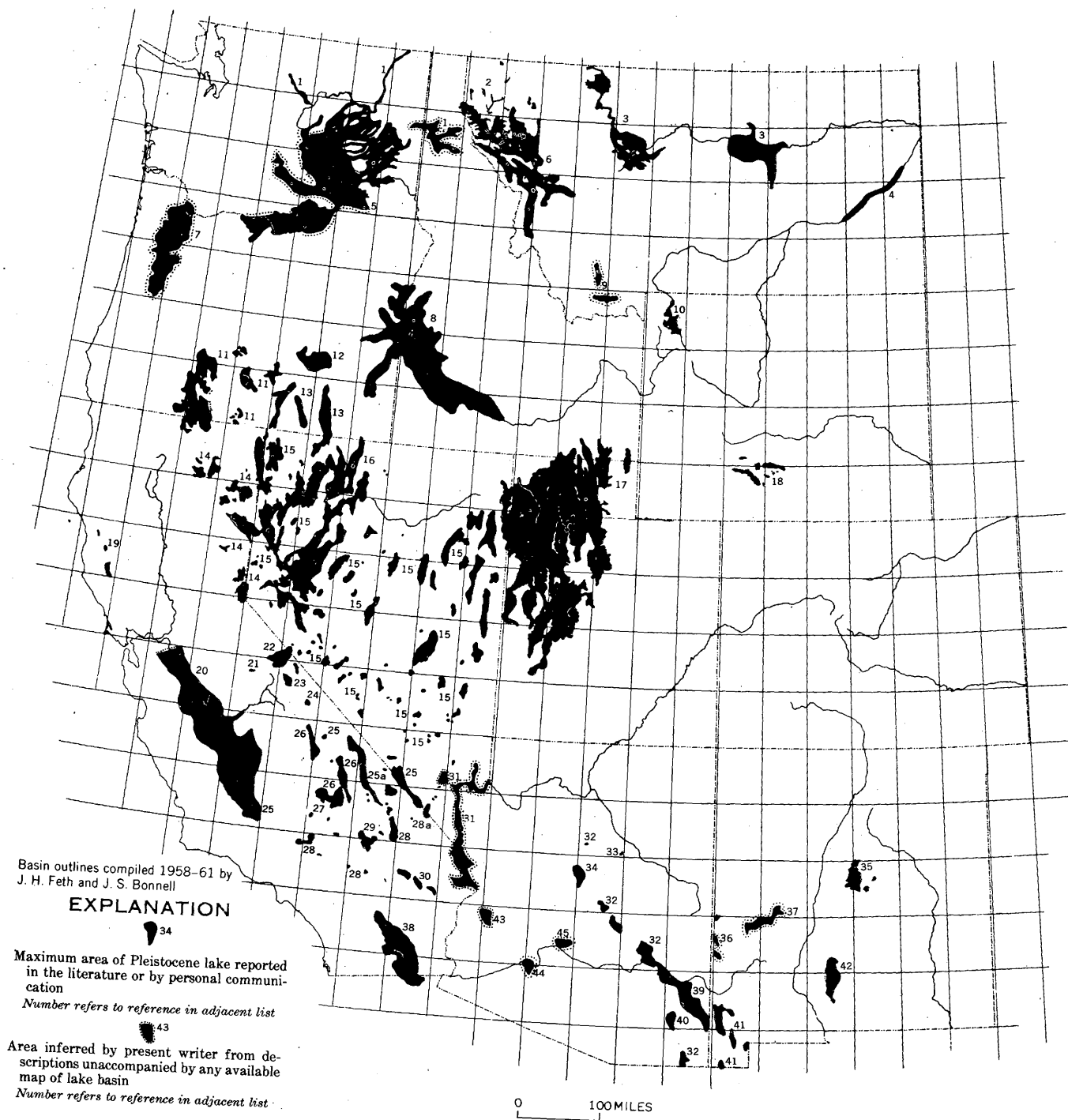
FIGURE 47.1.—Map of western conterminous United States showing maximum known or inferred extent of Pleistocene lakes reported in the literature.

TABLE 1.—*References for map showing extent of Pleistocene lakes*—(Continued)

Map no., (fig. 47.1)	Reference
25.........	Miller, R. R., 1946, Jour, Geology, v. 54, no. 1, p. 43–53.
	Blackwelder, Eliot, 1933, Geog. Review, v. 23, no. 3, p. 464–471.
26.........	Gale, H. S., 1914, U. S. Geol. Survey Bull. 580–L, p. 251–323.
27.........	Dibblee, T. W., Jr., 1952, California Div. Mines Bull. 160, p. 7–43.
28.........	Thompson, D. G., 1929, U. S. Geol. Survey Water-Supply Paper 578, 759 p.
	Hewett, D. F., 1956, U. S. Geol. Survey Prof. Paper 275, 172 p.
	Jenkins, O. P., 1951, California Div. Mines Econ. Minerals Map 2 (revised 1951).
29.........	Buwalda, J. P., 1914, California Univ., Dept. Geol. Sci. Bull., v. 7, p. 443–464.
30.........	Bassett, A. M., Kupfer, D. H., and Barstow, F. C., 1959, U. S. Geol. Survey Bull 1045–D, p. 97–138.
31.........	Longwell, C. R., 1936, Geol. Soc. America Bull., v. 47, no. 9, p. 1393–1476
	C. R. Longwell, 1959, oral communication.
32.........	Feth, J. H., previous work.
33.........	Merrill, G. P., 1908, Smithsonian Inst. Washington Misc. Collections No. 50, p. 461–498.
34.........	Jenkins, O. P., 1923, Am. Jour. Sci., 5th ser., v. 5, no. 25, p. 65–81.
35.........	Meinzer, O. E., 1911, U. S. Geol. Survey Water-Supply Paper 275, 89 p.
36.........	R. H. Weber, 1959, written communication.
37.........	Powers, W. E., 1933, Science n. s., v. 77, p. 51–52.
38.........	Brown, J. S., 1923, U. S. Geol. Survey Water-Supply Paper 497, 292 p.

TABLE 1.—*References for map showing extent of Pleistocene lakes*—(Continued)

Map no., (fig. 47.1)	Reference
39.........	Schwennesen, A. T., 1917, U. S. Geol. Survey Water-Supply Paper 425–A, p. 1–36.
40.........	Meinzer, O. E., and Kelton, F. C., 1913, U. S. Geol. Survey Water-Supply Paper 320, 231 p.
41.........	Schwennesen, A. T., 1918, U. S. Geol. Survey Water-Supply Paper 422, 152 p.
42.........	Kottlowski, F. E., 1958, Geol. Soc. America Bull., v. 69, no. 12, p. 1733–1734.
43.........	Metzger, D. G., 1952, *in* Halpenny, L. C., and others, U. S. Geol. Survey open-file rept., p. 171–176.
44.........	Coates, D. R., 1952, *in* Halpenny, L. C., and others, U. S. Geol. Survey open-file rept., p. 159–164.
45.........	Wolcott, H. N., 1952, *in* Halpenny, L. C., and others, U. S. Geol. Survey open-file rept., p. 171–176.

REFERENCES

Hubbs, C. L., and Miller, R. R., 1948, The zoological evidence; Correlation between fish distribution and hydrographic history in the desert basins of western United States, *in* The Great Basin: Utah Univ. Bull., v. 38, no. 20, p. 18–166.

Meinzer, O. E., 1922, Map of the Pleistocene lakes of the Basin-and-Range Province and its significance: Geol. Soc. America Bull., v. 33, no. 3, p. 541–552.

48.   RECENT FLOOD-PLAIN FORMATION ALONG THE CIMARRON RIVER IN KANSAS

By S. A. SCHUMM and R. W. LICHTY, Denver, Colo.

Areas of particular interest to the geomorphologist are ones in which processes of erosion or deposition are occurring at a rapid rate. A striking example is the valley of Cimarron River in southwestern Kansas, where within the past 46 years substantial changes have occurred in the widths of the channel and of the flood-plain.

The river in Kansas was described by Haworth (1897) in the latter part of the 19th century as follows: "The Cimarron seems to have reached base-level and to have begun meandering across its flood plain. Beautiful oxbow curves are frequent, and a sluggish nature is everywhere manifest during times of low water." Figure 48.1 illustrates the general appearance of the channel prior to 1914. Although the river bed both to the southeast and to the southwest in Oklahoma has always been relatively wide and sandy during historic times, the Cimarron Valley in Kansas prior to a destructive flood in 1914 was quite different, as shown by comparison of figures 48.1 and 48.2.

McLaughlin (1947) described the channel widening and flood plain destruction which followed the flood of 1914. He reported that in 1874 the channel

FIGURE 48.1.—Valley of Cimarron River in southeastern Meade County, Kans., prior to the flood of 1914. Photograph taken by Willard Drake Johnson, U.S. Geological Survey, during the 1890's.

of Cimarron River had an average width of 51 feet in 6 counties of southwestern Kansas as measured along section lines. Channel width increased to an average of 1,160 feet measured at the same sections in 1939. Discharge records at Liberal, Kans., and dates of highway bridge destruction indicate that channel width may have been at a maximum in 1942.

FIGURE 48.2.—Present channel of Cimarron River near Waynoka, Okla. The channel in Kansas had much the same appearance during the period of channel widening, 1914 to 1942.

TABLE 1.—*Average width of Cimarron River channel in Kansas by counties*

County	Number of cross sections measured	Years measured and average channel width (feet)			
		1874 [1]	1939 [1]	1954	1960
Morton..................	31	56	2,050	800	910
Stevens.................	11	43	1,500	630	....
Grant...................	19	54	630	190	190
Haskell.................	5	32	480	250	260
Seward..................	40	28	900	440	535
Meade...................	14	92	1,050	850	800
Weighted average........	....	48	1,200	560	....

[1] From McLaughlin, 1947; measurements at 34 localities not used in the tabulation.

During a period of 29 years (1914 to 1942), the Cimarron River in Kansas was altered from a narrow meandering stream (fig. 48.1) to one which had destroyed most of its former flood plain (fig. 48.2).

A major flood in 1942 was followed by a period of above-average rainfall; however, floods were of low to moderate intensity until 1950. Examination of aerial photographs reveals that during the 15-year period between 1939 and 1954 the channel of Cimarron River narrowed an average of 640 feet, from 1,200 feet to 560 feet (table 1). The narrowing apparently occurred because the above-average precipitation in the first half of this period promoted a vigorous growth of vegetation which anchored the sediments in parts of the channel and prevented erosion during flooding.

Average channel widths for five counties were measured on aerial photographs in 1960 and are listed on table 1. A slight widening is suggested by the measurements. This may be the result of a moderately large flood in 1958 preceded by a period of low rainfall. It is doubtful, however, that the channel will become as wide as it was in 1939. In that earlier period, vegetation on the flood plain was mostly grass, whereas cottonwood, willow, and saltcedar trees are growing abundantly on the present flood plain. The deeper tree roots will undoubtedly tend to stabilize the new flood plain. They will tend to resist bank erosion by binding together the alluvium and, where exposed, by increasing channel roughness, which has the effect of decreasing the velocity of flow at the banks.

To summarize, the destruction of the flood plain in 1914 occurred during a period of large floods

and deficient precipitation. Flood-plain construction occurred during a 9-year period when no large floods occurred and precipitation was above normal. Apparently flood-plain growth depended on the establishment and survival of vegetation in the stream channel.

REFERENCES

Haworth, Erasmus, 1897, Underground waters of southwestern Kansas: U.S. Geol. Survey Water-Supply Paper 6, 65 p.

McLaughlin, T. G., 1947, Accelerated channel erosion in the Cimarron valley in southwestern Kansas: Jour. Geology, v. 55, p. 76–93.

49.   ABNORMAL BEDDING IN THE SAVANNA SANDSTONE AND BOGGY SHALE IN SOUTHEASTERN OKLAHOMA

By Thomas A. Hendricks, Denver, Colo.

Some sandstone units within the Savanna sandstone and Boggy shale of Pennsylvanian age in the McAlester district of southeastern Oklahoma have an unusual type of bedding in areas as large as a half mile across. Where abnormally bedded the individual sandstone units are coarser grained and thicker than elsewhere. Consequently, they are more resistant to erosion, so that the areas are topographically high and the outcrops of the sandstone beds form promontories extending updip from the normal trace of the cuesta front. A good example of the abnormally dipping sandstone beds about 6 miles east of McAlester was mapped partly by planetable and partly by sketching and is shown on figure 49.1.

Subaqueous land-slip deposits have been observed in the Savanna sandstone and Boggy shale by Dane, Rothrock, and Williams (1938), Hendricks (1939), and others. They differ from the abnormally bedded deposits here discussed in several ways, particularly in that the bedding and lithologic types are disordered.

In the area of abnormal bedding (fig. 49.1) the sandstone beds are as much as 10 feet thick, are laminated but have no shale partings or beds, and consist of medium- to coarse-grained sands. The cementation varies by beds so that some are markedly more resistant to erosion than others and crop out prominently. The angle between the abnormal bedding and the regional dip of true bedding is commonly about 30°, or close to the angle of repose of sand. Local increases of dip of abnormal bedding to higher angles are believed to be due to movement after initial deposition. In many places, such as along section A-A' (figs. 49.1 and 49.2), the strike

of the abnormally dipping beds is relatively straight and the bedding planes are subparallel. The sharp bend at the west end of each bed is due to topography. Beds of this type have been described by Dane, Rothrock, and Williams (1938, p. 163–164). Where they have been observed they dip to the south, and may be traced for as much as half a mile. Other steeply dipping beds have a roughly concentric outcrop pattern. Remnants of a sandstone unit with steeply and concentrically dipping beds are shown in the lower part of figure 49.1, but the abnormally bedded sandstone has been removed by erosion in most of the west half of original area of occurrence. At other places and on relatively level surfaces, the outcrop of such beds is continuous in a crude circle.

The beds with abnormal dips terminate sharply and without curvature against the underlying shale beds at most places, but locally the dip of some beds decreases at the lower contact (fig. 49.2).

The shale underlying the sandstone unit in the area of figure 49.1 contains thin beds of fine-grained sandstone having on their bottom surfaces miniature flute casts, groove casts, prod marks, and other features considered characteristic of turbidity-current deposition. The orientation of these features indicates a current direction from west to east, which is nearly parallel to the axis of the basin of deposition of the Savanna sandstone (Hendricks, 1939, p. 273).

Invertebrate marine fossils are common in this shale unit 50 feet or more below the sandstone unit shown in figure 49.1, and 25 to 45 species have been identified from each of several collections from this shale from other places in the McAlester district

EXPLANATION

Resistant sandstone bed

Less resistant sandstone bed

Outline of dip slope

Contact of sandstone and shale

Shale containing thin sandstone beds

Dip of abnormal beds

Regional dip

A ————— A'

Line of section

0   100   200   300   400 FEET
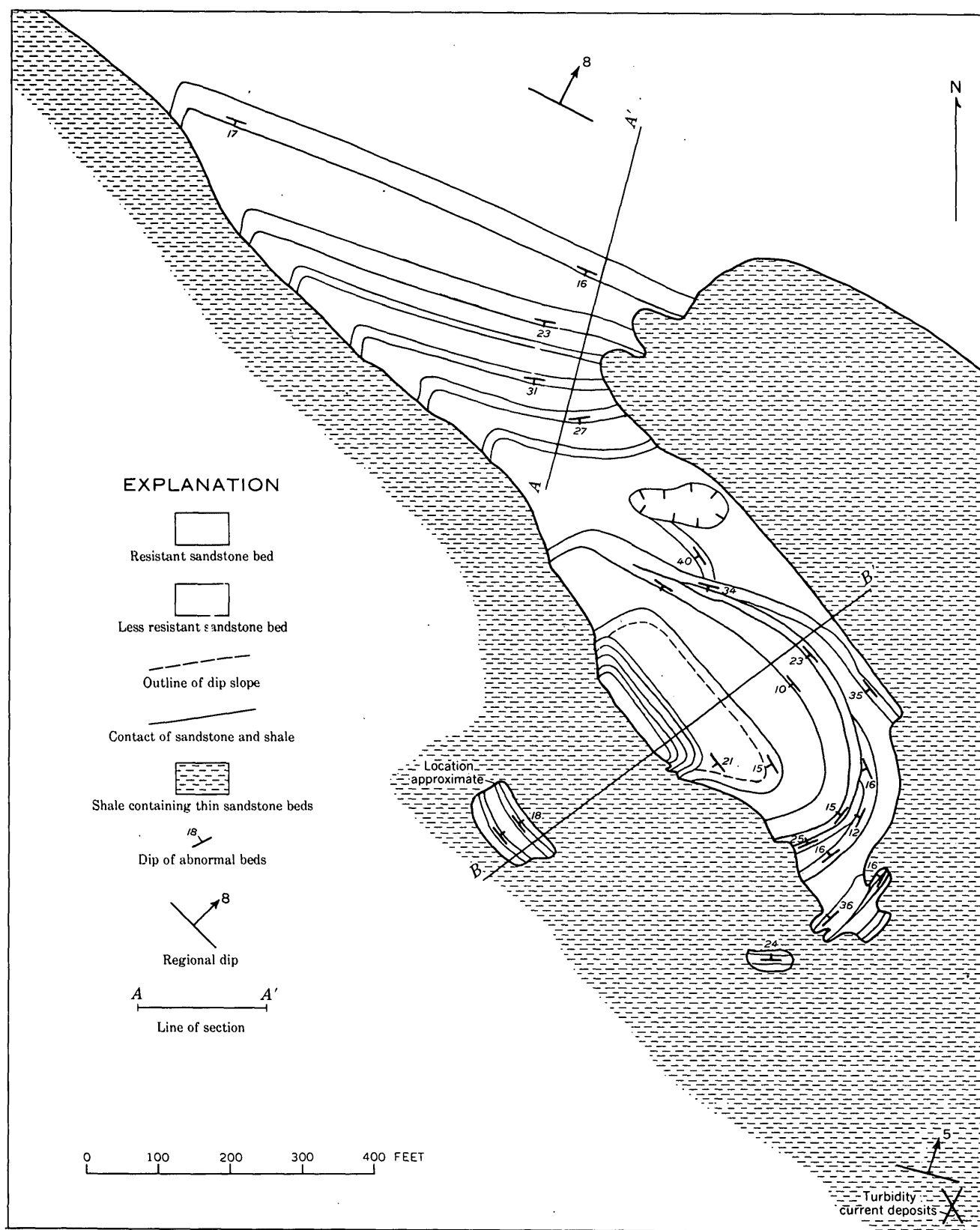
FIGURE 49.1.—Sketch map of an area of Savanna sandstone with abnormal bedding, E1/2 sec. 32, T. 6 N., R. 16 E., Pittsburg County, Okla. See sections, figure 49.2.
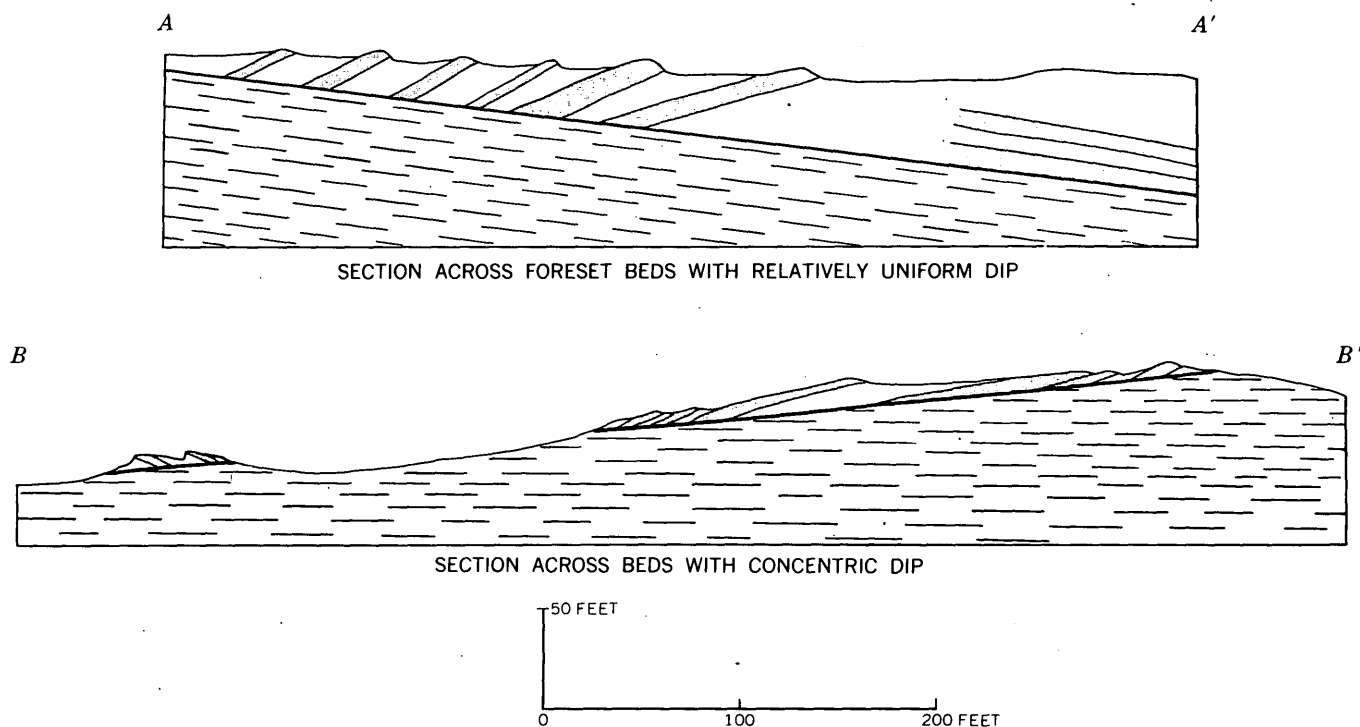
FIGURE 49.2.—Cross sections in area (fig. 49.1) of Savanna sandstone with abnormal bedding. Resistant beds in the sandstone unit are shaded.

(Hendricks, 1937). The brachiopods and pelecypods characteristically still have the two valves joined.

Some of the sandstone units with abnormal bedding, such as the one in the area of figure 49.1, are overlain within a few feet by a coal zone; others are overlain by shale that contains a few marine fossils.

These features suggest the following interpretation of the conditions of deposition for a sequence of beds containing in its middle part a sandstone with abnormal bedding:

1. Clay and silt were deposited in water shallow enough to be hospitable for a varied fauna but so deep that waves and currents did not uncover and disjoin fragile bivalves. Such deposition could occur a short distance below wave base. A heavy rain of clay and silt probably buried the organisms very quickly and was periodically interrupted by weak turbidity currents that moved generally parallel to the axis of the basin of deposition and deposited thin beds of sand.

This type of deposition continued until the basin was filled nearly to sea level, and produced a mud flat which at times may have been exposed at low tide, as is suggested by discontinuous red beds in this zone.

2. Sheetlike currents from the north carried sand across the submerged mud flats. The subparallel straight beds with abnormal dip (section A-A', fig. 49.2) are believed to have been formed nearshore as foreset beds by deposition from these strong currents flowing over a broad area.

The centripetally or concentrically dipping beds (section B-B', fig. 49.2) are believed to have formed by scour and fill by somewhat stronger currents. The current is believed to have developed locally strong eddies that scoured, in the unconsolidated sediments, deep elliptical holes similar to those formed when a river breaks through a levee (Hendricks and Parks, 1950, p. 91–92). Subsequent currents passing above the scour hole carried sediment of mixed grain size with the coarser sizes at the bottom. These coarser sizes dropped into the still water of the scour hole from all sides and formed foreset beds with crudely concentric attitudes. Successive flood currents produced other concentric foreset beds inside those previously deposited.

3. At times, mud and sand were subsequently deposited to form broad coastal swamps in which

coal-forming materials were deposited. At other times, subsidence deepened the water and initiated another major cycle of deposition.

Conditions that resulted in the deposition of the abnormally dipping beds were repeated locally during the accumulation of many sandstone units throughout about 3,000 feet of beds in the Savanna and Boggy formations.

REFERENCES

Dane, C. H., Rothrock, H. E., and Williams, J. S., 1938, Geology and fuel resources of the southern part of the Oklahoma coal field, pt. 3. The Quinton-Scipio district, Pittsburg, Haskell, and Latimer Counties: U.S. Geol. Survey Bull. 874-C, p. 151-253.

Hendricks, T. A., 1937, Geology and fuel resources of the southern part of the Oklahoma coal field, pt. 1, McAlester district, Pittsburg, Atoka, and Latimer Counties: U.S. Geol. Survey Bull. 874-A, p. 1-90.

———, 1939, Geology and fuel resources of the southern part of the Oklahoma coal field, pt. 4, The Howe-Wilburton district, Latimer and LeFlore Counties: U.S. Geol. Survey Bull. 874-D, p. 255-300.

Hendricks, T. A., and Parks, Bryan, 1950, Geology of the Fort Smith district, Arkansas: U.S. Geol. Survey Prof. Paper 221-E, p. 67-93.

50.   RESERVOIR EVAPORATION AND SEEPAGE, HONEY CREEK, TEXAS

By F. W. KENNON, Oklahoma City, Okla.

This report describes an investigation of evaporation and seepage losses from 12 flood-retarding reservoirs in the upper 36 square miles of Honey Creek basin (fig. 50.1), a tributary of the Trinity River. Records are available for the period October 1952 through September 1959. Honey Creek watershed is in north-central Texas about 35 miles north of Dallas. It lies in the Black Prairie physiographic province and is underlain by the Austin chalk of Late Cretaceous age, which is composed primarily of chalk, marl, and claystone.

The surface areas of the reservoirs range from 12 to 44 acres and capacities range from 81 to 421 acre-feet at the elevations of the outlets. Water-stage recorders were installed at reservoirs 11 and 12 (fig. 50.1) and staff gages were installed at the other 10 reservoirs. Precipitation was measured at 14 places in the basin during the investigation. Evaporation from reservoirs 11, 12, and 13 was measured by the mass-transfer method for the period October 1957 through September 1959. Evaporation from the remaining reservoirs during this period was assumed to be the average of evaporation amounts measured at reservoirs 11, 12, and 13.

As a check, evaporation was estimated by two other methods at reservoir 12 for the previous 5-year period, October 1952 to September 1957. First, for periods of no inflow or outflow, previously estimated seepage was subtracted from reservoir water-stage recession adjusted for precipitation. Thirty-three months of evaporation records were so computed. Monthly evaporation figures obtained by this method agree well with those obtained by the mass-transfer method.

Secondly, estimates of evaporation were made from observations at a 24-inch screened sunken pan located about 30 miles directly west of Honey Creek. A correlation between the pan and reservoir 12 was obtained by comparing evaporation from the pan with evaporation from the reservoirs as determined by mass transfer and the method described above. Estimate of evaporation during periods of inflow or outflow could then be made by measuring evaporation from the pan.

The annual (water-year) evaporation, in feet, determined for reservoir 12 by the mass-transfer and other methods is given below:

1953	1954	1955	1956	1957	1958	1959
5.01	5.16	5.04	6.31	4.76	4.25	5.41

The average of the annual evaporation rates is 5.13 feet. The average annual precipitation on reservoir 12 for 1953-1959 was 2.93 feet. Hence, the average net annual evaporation loss was 2.20 feet.

During periods of no surface inflow or outflow, reservoir seepage equals stage recession plus precipitation on the pool minus evaporation. There was little monthly variation in the reservoir depths so
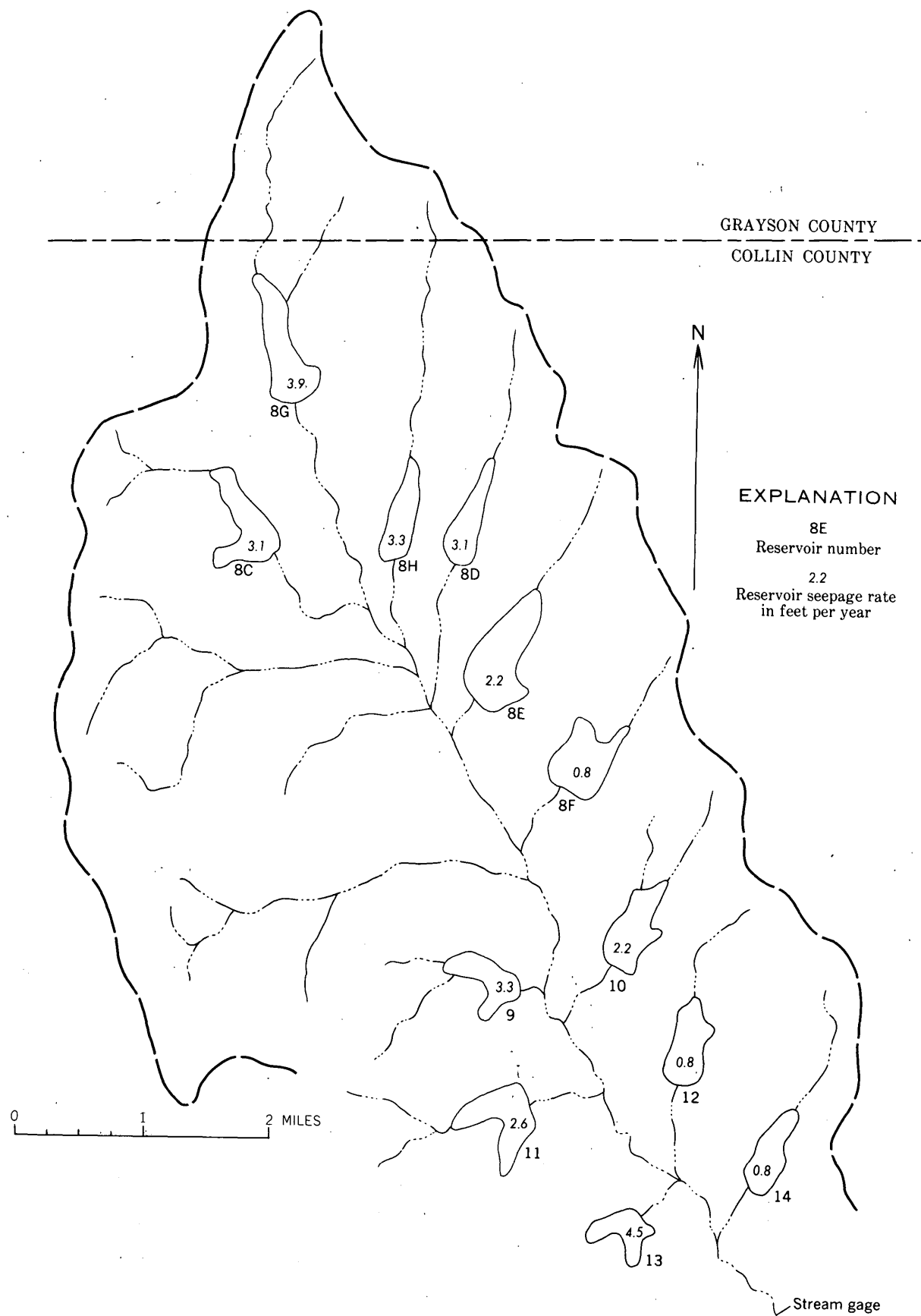
FIGURE 50.1.—Honey Creek basin, Texas, showing location of reservoirs and average annual seepage rates.
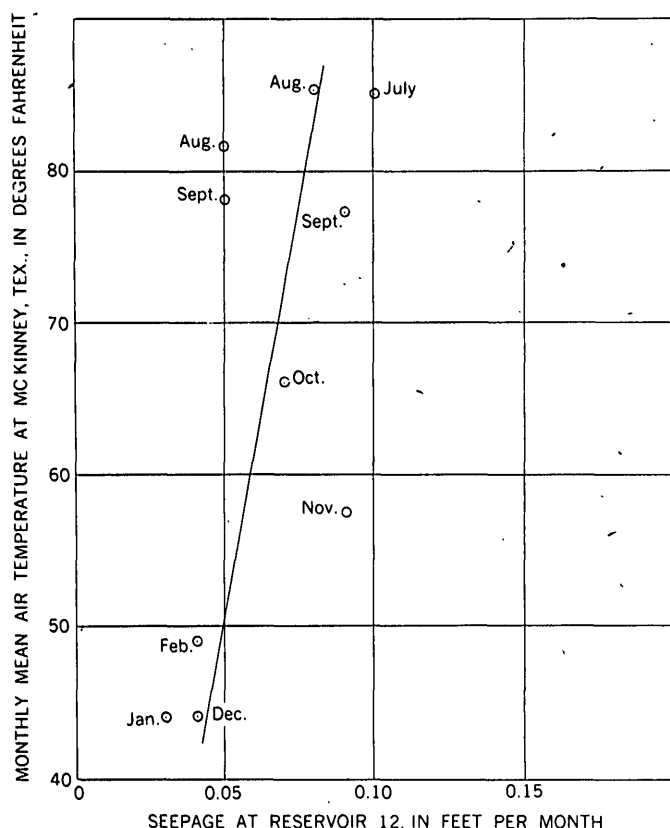
FIGURE 50.2.—Relation of seepage at reservoir 12 to monthly mean air temperature at McKinney, Tex.

the effect of head on seepage was essentially constant. No water spilled over during the two periods July 1958 to February 1959 and August to September 1959, and inflow was reported on only 9 days during this time. Thus an observational period of almost a year is available for determining monthly seepage at all reservoirs. The variation in seepage rates for the 12 reservoirs is shown in figure 50. The rates ranged from 0.8 foot to 4.5 feet and averaged 2.6 feet per year.

The seepage rate varied with temperature as shown in figure 50.2. If the seepage flow is laminar, the rate of flow should vary inversely with the viscosity of the water, which in turn is dependent upon the temperature.

Undoubtedly some water passes under or around each of the earth dams. The flow in the channels immediately below the dams was not measured when water in the reservoirs was not spilling over, but during rainless periods, the flow frequently is reported to be zero at the stream gage about one mile below reservoir 14. This suggests that no significant amount of seepage water is passing from the reservoirs into the drainage systems below them. Furthermore, during the month of December 1955, the estimated seepage from the lower six reservoirs, Nos. 9 to 14, was 12.1 acre-feet. The area of the stream channels below this group of reservoirs is about 11 acres. Evaporation from the reservoirs for the month was estimated to be 0.21 foot. Evaporation from a wetted channel bottom probably would be considerably less than that from a reservoir, because the channels are deeply incised and bordered by a dense protecting fringe of trees. In addition, transpiration by riparian vegetation is negligible during December. However, if the lake evaporation figure of 0.21 foot is used, channel evaporation would be only 2.3 acre-feet, and 9.8 acre-feet of seepage water is unaccounted for. As no surface flow passed the stream gage that month, it seems that the major portion of the reservoir seepage must leave the basin by underflow through cracks and fissures in the underlying Austin chalk and enter the regional body of ground water.

51. PRE-PENNSYLVANIAN PALEOZOIC STRATIGRAPHY, MOCKINGBIRD GAP QUADRANGLE, NEW MEXICO

By GEORGE O. BACHMAN, Denver, Colo.

Wedge-edges of Paleozoic rocks of pre-Pennsylvanian age are exposed in two general areas in south-central New Mexico. One area is the Caballo and Fra Cristobal Mountains and has been discussed by Kelley and Silver (1952). The other area is in and near the Mockingbird Gap quadrangle, and includes parts of the San Andres and Oscura Mountains. Darton (1928, p. 194) described briefly the
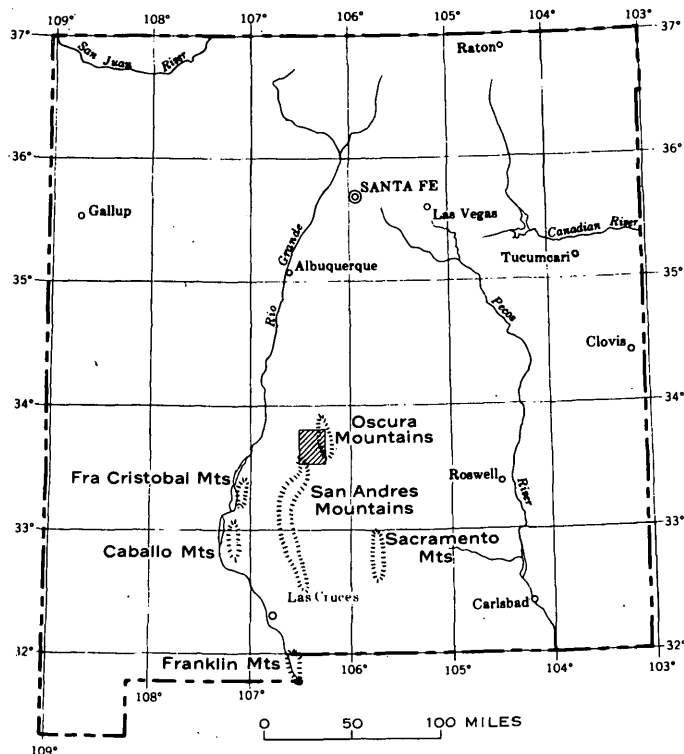
FIGURE 51.1.—Index map of New Mexico showing location of Mockingbird Gap quadrangle and some nearby mountain ranges.

stratigraphic relations in the second area; they have received renewed attention during recent geologic mapping.

The Mockingbird Gap quadrangle (fig. 51.1) and nearby areas are in the White Sands Missile Range to which access is prohibited to the general public. I express my appreciation to the Commanding General, White Sands Missile Range, and his staff, whose cooperation made this study possible.

STRATIGRAPHY

Bedrock exposed in and near the Mockingbird Gap quadrangle ranges in age from Precambrian to Permian. The Fusselman dolomite of Middle Silurian age wedges out about 28 miles south of the quadrangle (Kottlowski and others, 1956, p. 27) and is not discussed here.

Bliss sandstone.—The Bliss sandstone of Late Cambrian and Early Ordovician age forms a prominent ledge and rests on an undulatory surface on Precambrian crystalline rocks in the Mockingbird Gap Hills and in the southern part of the Oscura Mountains. The Bliss consists chiefly of medium-gray to dark-brown sandstone and quartzite. The dominant constituents are medium-grained, subangu-

lar to subrounded quartz grains. It also includes some medium-grained carbonate pellets; and locally a quartz granule conglomerate is at the base of the formation.

The Bliss sandstone is about 250 feet thick (Cloud and Barnes, 1948, p. 369) in the type area, which is in the Franklin Mountains near El Paso, Tex. The thickness of the Bliss in the Mockingbird Gap quadrangle ranges from 19 feet to a wedge-edge (fig. 51.2). Local irregularities in thickness are due to relief of the underlying Precambrian surface. The El Paso formation overlies the Bliss gradationally except in the northern part of the Mockingbird Gap Hills (fig. 51.2, section C) where Lower Pennsylvanian strata overlie the Bliss unconformably.

El Paso formation.—The El Paso consists chiefly of light- to medium-gray finely crystalline dolomite and calcareous dolomite that weathers light olive to yellowish gray. Individual beds are 2 inches to 2 feet thick. Microscopically the rocks consist of a fine mosaic of anhedral to subhedral carbonate crystals, scattered grains of quartz, and a few grains of glauconite. Fine- to medium-grained quartz sand locally constitutes 15 to 20 percent by weight of the basal part of the formation in the quadrangle; this proportion decreases upward.

The El Paso is 125 feet thick in the southern part of the Oscura Mountains (fig. 51.2, section D). It thins rather uniformly northward and wedges out about the middle of the Oscura Mountains (fig. 51.2, section G). Locally near its northern termination, the thickness is variable because of channeling by overlying Pennsylvanian strata. The El Paso is 17 feet thick in the southern part of the Mockingbird Gap Hills, and is absent in the northern part of the Hills (fig. 51.2, sections B and C).

The part of the El Paso formation present in the Mockingbird Gap quadrangle is believed to be equivalent to the basal part of the El Paso at its type locality in the Franklin Mountains where the total formation is 1,590 feet thick (Cloud and Barnes, 1948, p. 74). The El Paso in the quadrangle is very similar lithologically to the Sierrite limestone at the base of the El Paso group as defined by Kelley and Silver (1952, p. 42–45).

Montoya dolomite.—In the Oscura Mountains the Montoya dolomite of Middle and Late Ordovician age (Kottlowski and others, 1956, p. 24–25) rests with a sharply defined irregular contact on the El Paso formation. In parts of southern New Mexico the Cable Canyon sandstone of Kelley and Silver (1952, p. 58–59) is present at the base of the Mon-
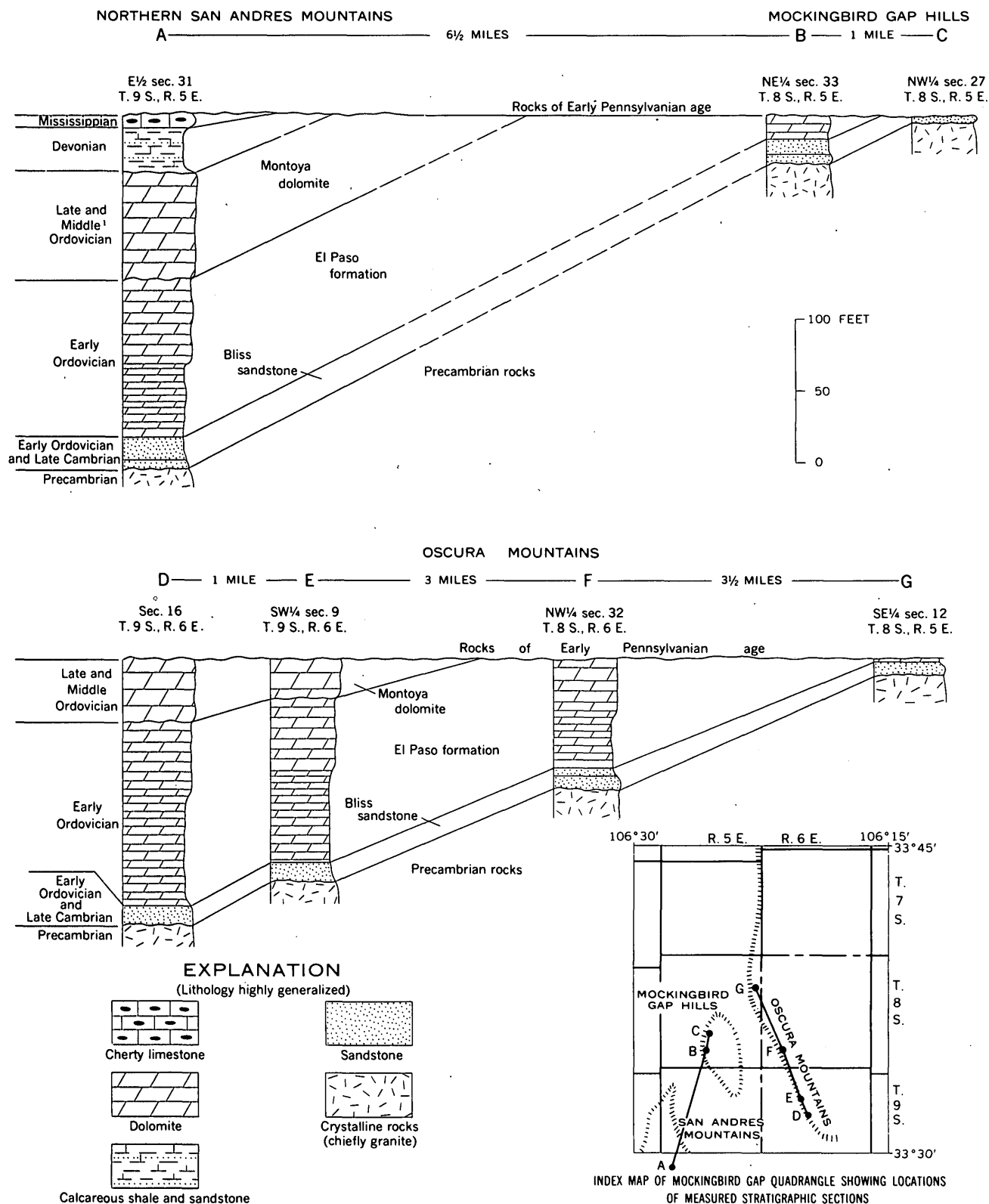
FIGURE 51.2.—Columnar sections showing wedge-edges of pre-Pennsylvanian Paleozoic strata in the Mockingbird Gap area, New Mexico.

toya dolomite, but this sandstone is absent in the Mockingbird Gap quadrangle.

The Montoya in the Oscura Mountains consists of medium dark-gray to olive-gray evenly bedded dolomite that weathers with a deeply pitted surface. The beds range in thickness from 1 to 6 feet. Insoluble residues consisting mainly of clay constitute 3 to 5 percent by weight of the rock.

The Montoya is 429 feet thick in the Franklin Mountains (Pray, 1958, p. 35). It thins northward to 43 feet thick in the southern part of the Oscura Mountains (fig. 51.2, section D), and it wedges out within 2 miles farther north in sec. 9, T. 9 S., R. 6 E. It is absent in the Mockingbird Gap Hills. The Montoya thins northward at a fairly uniform rate in the Oscura Mountains, except for local channels filled with deposits of Pennsylvanian age.

Lithologic comparisons with other areas indicate that only the basal part of the Montoya—the Upham dolomite of Kelley and Silver (1952, p. 59–60) —is represented in the Oscura Mountains.

Devonian and Mississippian rocks.—Rocks of Devonian or Mississippian age were not observed in the Mockingbird Gap quadrangle; however, they are well exposed in the San Andres Mountains to the south and they were traced to a wedge-edge about a mile south of the quadrangle. The Devonian rocks consist of fine-grained calcareous sandstone and calcareous shale, and they are 30 feet thick about 200 yards south of the wedge-edge (fig. 51.2, section A). At the same locality Mississippian rocks are represented by cherty medium-gray limestone 10 feet thick. This limestone is believed to be equivalent to the Alamogordo member of the Lake Valley limestone of Laudon and Bowsher (1949, p. 57) in the Sacramento and San Andres Mountains.

Pennsylvanian rocks.—Strata of Pennsylvanian age truncate older strata in a general northward direction, and in the northern part of the quadrangle the Pennsylvanian rocks rest directly on the Precambrian rocks. At the base of the Pennsylvanian rocks are sandstone and granule conglomerate in lenses that locally are more than 40 feet thick. One of these beds was traced in the Oscura Mountains for more than a mile across the wedge-edge of the Montoya. Fragments of underlying Paleozoic formations were not definitely recognized as constituents of the beds, but some local lenses of chert frag-

ments at the base of the Pennsylvanian probably were derived from preexisting formations. These lenticular sandstone beds are believed to represent channel deposits, although locally they may be lag deposits or a regolith on the pre-Pennsylvanian erosional surface.

INTERPRETATION

Kelley and Silver (1952, p. 132–134) postulated an east-west hinge-line north of the Caballo Mountains along which the region to the south was tilted downward periodically during Paleozoic time. Observations in the Oscura and northern San Andres Mountains strongly support this hypothesis, but it is suggested that the hinge line may have had a slight northeastward trend and that it extended at least as far as the Oscura Mountains. Data from the Mockingbird Gap quadrangle, along with observations by Kelley and Silver (1952) and Kottlowski and others (1956), suggest that the pre-Pennsylvanian tilting and beveling occurred during Early or Middle Ordovician, Early Silurian, and Late Silurian or Early Devonian time.

The Bliss in the Mockingbird Gap area is probably a basal deposit of a transgressing Late Cambrian and Early Ordovician sea. The overlying pre-Pennsylvanian Paleozoic limestones and dolomites are marine deposits where they wedge out, and the rock facies do not indicate that the shorelines of the ancient seas were very near the present Oscura Mountains during deposition of these rocks.

REFERENCES

Cloud, P. E., Jr., and Barnes, V. E., 1948, The Ellenburger group of central Texas: Texas Univ. Bur. Econ. Geology Pub. 4621.

Darton, N. H., 1928, "Red Beds" and associated formations in New Mexico: U.S. Geol. Surv. Bull. 794.

Kelley, V. C., and Silver, Caswell, 1952, Geology of the Caballo Mountains: New Mexico Univ. Pub. in Geology 4.

Kottlowski, F. E., Flower, R. H., Thompson, M. L., and Foster, R. W., 1956, Stratigraphic studies of the San Andres Mountains, New Mexico: New Mexico Inst. Mining and Tech., Bur. Mines and Mineral Resources, Mem. 1.

Laudon, L. R., and Bowsher, A. L., 1949, Mississippian formations of southwestern New Mexico: Geol. Soc. Amer. Bull., vol. 60, p. 1–88.

Pray, L. C., 1958, Stratigraphic section, Montoya group and Fusselman formation, Franklin Mountains, Texas: West Texas Geol. Soc., Guidebook, Franklin and Hueco Mountains, p. 30–42.

52.   PRELIMINARY RESULTS OF TEST DRILLING IN DEPRESSIONS ON THE HIGH PLAINS, LEA COUNTY, NEW MEXICO

By JOHN S. HAVENS, Lovington, N. Mex.

Work done in cooperation with the New Mexico State Engineer

The Ogallala formation of Tertiary age, which covers the High Plains in Lea County, N. Mex., consists mostly of very fine grained sandstone 0 to 250 feet thick overlain by as much as 20 feet of caliche caprock. The caprock surface is dotted with numerous closed depressions ranging in diameter from a few yards to more than half a mile and ranging in depth from a few inches to more than 30 feet. Previous investigators have suggested that the depressions may have been caused by deep-seated collapse of soluble underlying formations (Judson, 1950, p. 254, 272).

The depressions seem to be alined in swales that are remnants of an old drainage system. Groups of depressions show a general alinement down the slope of the land surface, which is 10 to 15 feet per mile to the southeast or south-southeast.

The main drainage into the depressions generally is on the northwestern side. With some exceptions there are no connections between depressions.

Test drilling has been done in and near several of the depressions, using both core and auger drills. Two typical depressions that were drilled are designated depressions 8 and 9, and are approximately 1 mile from the western edge of the High Plains, and about 3 miles north of the town of Maljamar, N. Mex. (see figure 52.1).

Information from drilling indicates that the depressions are surficial features not related to solution of deeply buried gypsum or salt. The Ogallala formation shows no signs of collapse beneath the depressions. A sequence of events leading to the stratigraphic relations shown on the cross sections of depressions 8 and 9 (figs. 52.2 and 52.3 on p. B–124 and B–125) might be described as follows:
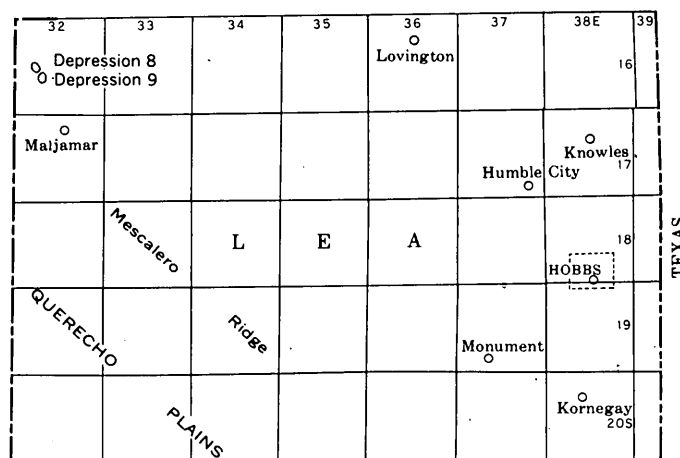
FIGURE 52.1.—Central part of Lea County, N. Mex., showing locations of depressions 8 and 9.

1. The caliche caprock was dissolved away in local areas along old stream channels.
2. Poorly consolidated sandstone of the Ogallala formation was exposed to the wind and the initial shallow depressions in the caliche were deepened by deflation.
3. The depressions were partly filled by sandy silty clay and silty clay carried into the depressions by inflowing streams following heavy rains. Traces of caliche in depression 8 (fig. 52.2) may be caliche rubble washed into the depressions from the sides.

REFERENCE

Judson, S. S., Jr., 1950, Depressions of the northern portion of the southern High Plains of eastern New Mexico: Geol. Soc. America Bull., v. 61, no. 3, p. 254, 274.

EXPLANATION

Residual soil   Alluvium   Alluvium
                   Silty clay   *Sandy silty clay*

Caliche cap rock   Ogallala formation
                        Sandstone

                   Traces of caliche

N

0   400   800 FEET

CROSS SECTION A-A' THROUGH DRILL HOLES

60 FEET

30

0
0   400   800 FEET

CROSS SECTION B-B' THROUGH DRILL HOLES
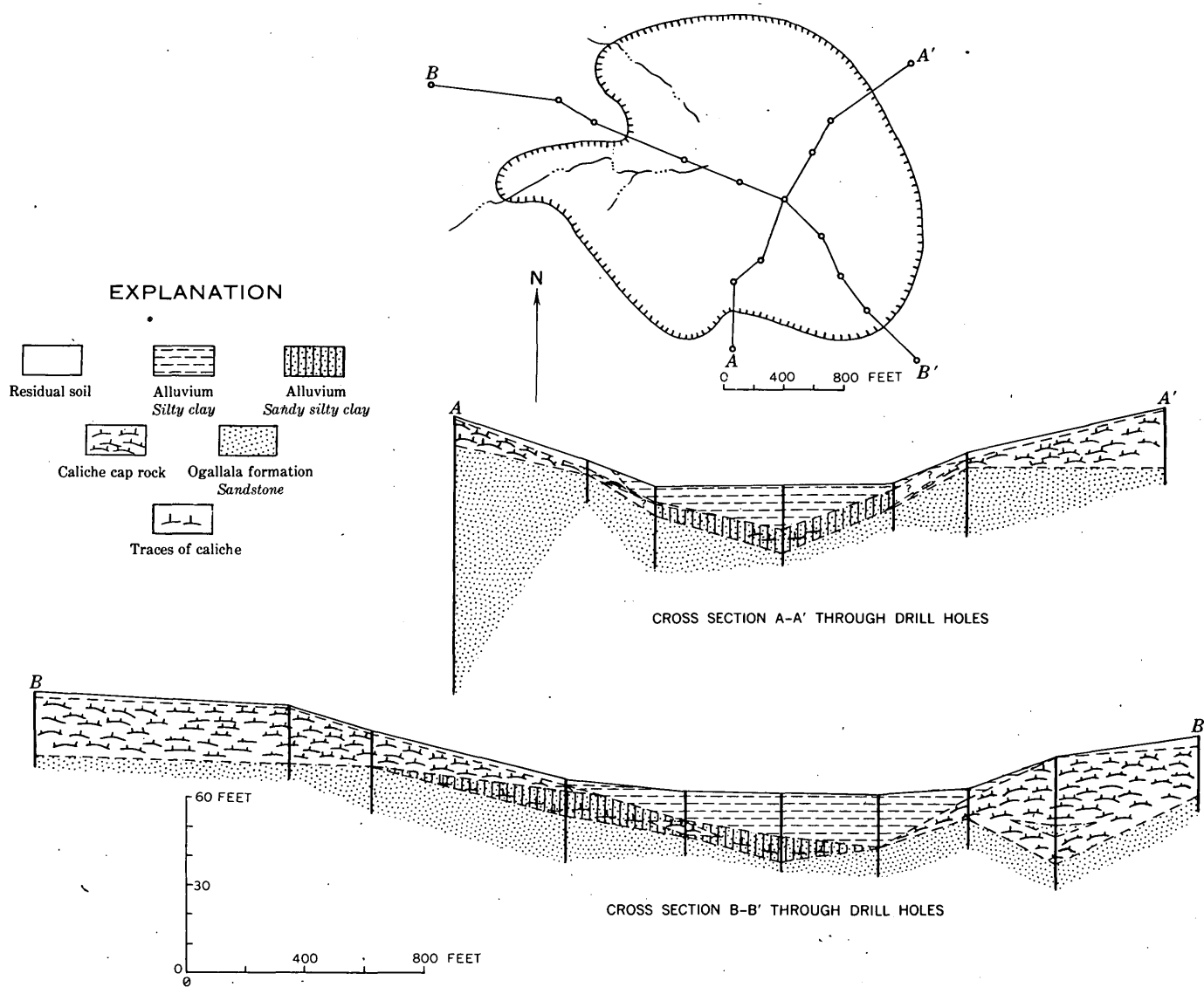
FIGURE 52.2.—Sections and map of depression 8, SW¼ sec. 20, T. 16 S., R. 32 E., Leo County, N. Mex.
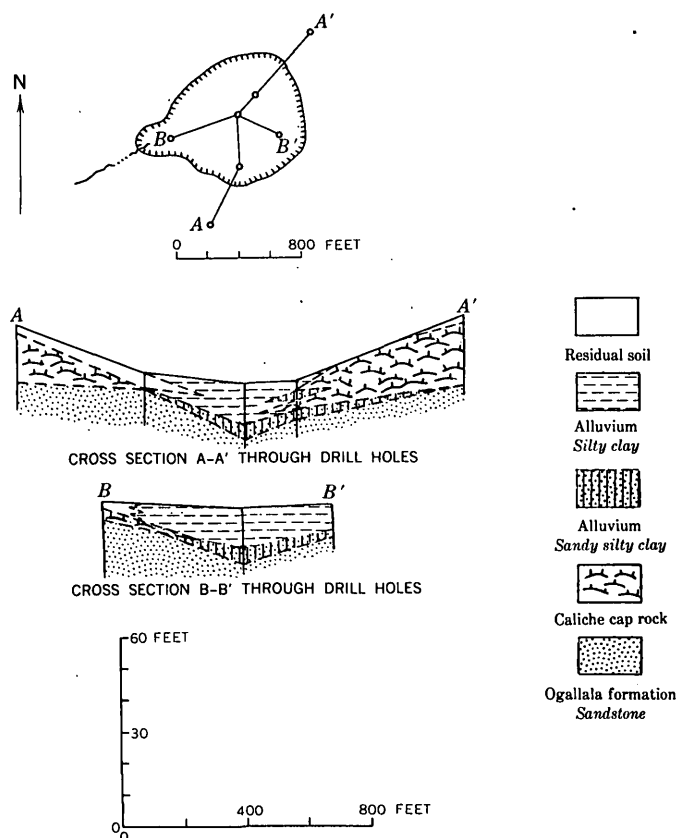
FIGURE 52.3.—Sections and map of depression 9, N½ sec. 29,
T. 16 S., R. 32 E., Lea County, N. Mex.

53.   LOWER MEMBER OF MURAL LIMESTONE OF EARLY CRETACEOUS AGE, BISBEE QUADRANGLE, ARIZONA

By PHILIP T. HAYES and EDWIN R. LANDIS, Denver, Colo.

The Mural limestone and the underlying Morita formation, both of Early Cretaceous age, were established by Ransome (1904, p. 56) on the basis of their exposures on and below the south-facing cliffs of Mural Hill in the Bisbee quadrangle (fig. 53.1). Although he mapped the Mural as a single unit, he recognized two distinct members, a lower member about 300 feet thick containing thin-bedded impure limestone, and an upper member about 250 feet thick of thick-bedded pure limestone. Ransome noted that widely separated thin beds of impure limestone

are present in the upper part of the underlying Morita formation but chose his contact at the top of a prominent bed of hard buff sandstone. The contact is arbitrary but is a readily recognizable mapping horizon over a wide area.

As a result of detailed paleontologic work in the Ninety One Hills area, 8 miles south of Mural Hill, Stoyanow (1949, p. 6) restricted the name Mural to the upper member of Ransome's original unit, and named the Lowell formation (Stoyanow, 1949, p. 8) to include the lower member of Ransome's Mural
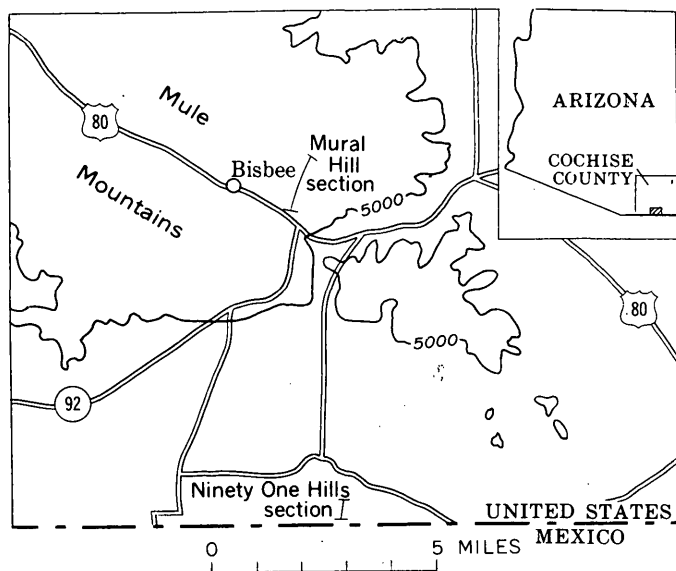
FIGURE 53.1.—Index maps showing location of Bisbee quadrangle, Cochise County, Ariz., and location of measured sections shown on figure 53.2.

and the upper beds of the Morita formation down to the base of the lowest fossiliferous limestone bed.

In the course of current mapping in the Bisbee quadrangle, we investigated the feasibility of mapping and the stratigraphic value of both the base of Ransome's Mural limestone and the base of Stoyanow's Lowell formation. We found that the base of the lower member of the Mural limestone as defined by Ransome can be mapped readily within narrow stratigraphic limits in the quadrangle, whereas the base of the Lowell formation is not a readily traceable horizon. Mapping during the present investigation has shown that, in addition to the lower member of the Mural limestone, Stoyanow included 580 feet of the upper part of the original Morita formation in his Lowell formation. Furthermore, in remapping the area in the vicinity of the type section of the Lowell formation (Stoyanow, 1949, p. 8–12), we discovered that about 160 feet of rock in the upper part of the Lowell formation evidently is duplicated across a normal fault.[1] Fortunately, this duplication does not alter Stoyanow's faunal zonation.

Because Stoyanow (1949, p. 8) did not specifically state that he was including hundreds of feet of the Morita formation in his Lowell formation, several writers (Gilluly, 1956, p. 74; Gillerman, 1958, p.

---
[1] As nearly as we can determine, units 2c and 3b of the type Lowell formation (Stoyanow, 1949, p. 9) are the same and the fault lies near the middle of unit 2d.

43; Fergusson, 1959, p. 43) have assumed that the term "Lowell" was just a new name for the lower member of the Mural limestone. This led Gilluly (1956, p. 74) to conclude that the lower member of the Mural thickens from about 400 feet near Mural Hill to 1,104 feet in the Ninety One Hills. Actually, the lower member of the Mural is only about 360 feet thick in the Ninety One Hills. The general
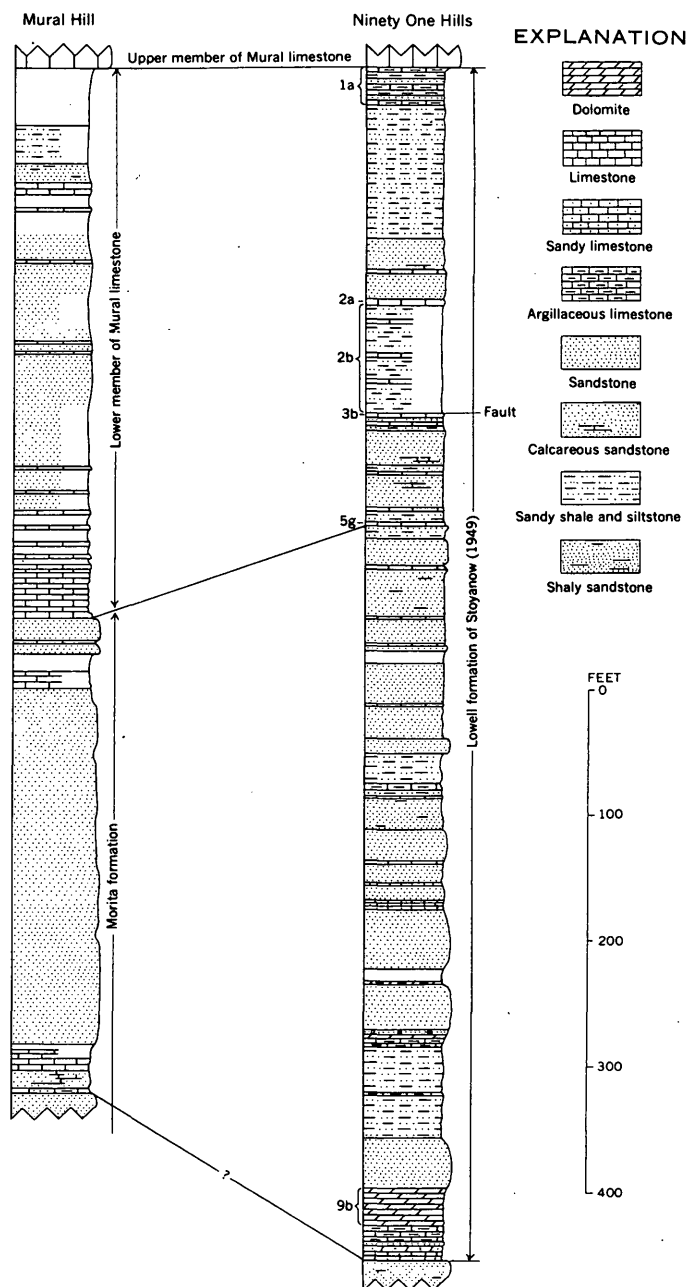
FIGURE 53.2.—Stratigraphic sections showing relations between lower member of Mural limestone and Lowell formation of Stoyanow (1949). Ninety One Hills section modified from Stoyanow (1949, p. 6–10); unit numbers beside column are his.

similarity in thickness and lithology of the sequence at the two localities is shown in figure 53.2.

These findings, along with other observations made during recent fieldwork, indicate that facies changes within and variations in thickness of Lower Cretaceous rock units in southeastern Arizona are not as extreme as heretofore commonly believed.

REFERENCES

Fergusson, W. B., 1959, The Cretaceous system of southeastern Arizona, *in* Arizona Geol. Soc., Southern Arizona Guidebook II, April, 1959: p. 43–47.

Gillerman, Elliot, 1958, Geology of the central Peloncillo Mountains, Hidalgo County, New Mexico, and Cochise County, Arizona: New Mexico Bur. Mines and Mineral Resources Bull. 57, 152 p.

Gilluly, James, 1956, General geology of central Cochise County, Arizona: U.S. Geol. Survey Prof. Paper 281, 169 p.

Ransome, F. L., 1904, The geology and ore deposits of the bisbee quadrangle, Arizona: U.S. Geol. Survey Prof. Paper 21, 168 p.

Stoyanow, Alexander, 1949, Lower Cretaceous stratigraphy in southeastern Arizona: Geol. Soc. America Mem. 38, 169 p.

54.   ORIGIN OF CROSS-STRATA IN FLUVIAL SANDSTONE LAYERS IN THE CHINLE FORMATION (UPPER TRIASSIC) ON THE COLORADO PLATEAU

By JOHN H. STEWART, Menlo Park, Calif.

Cross-strata are a distinctive feature of the sandstone layers of the Chinle formation (Upper Triassic) on the Colorado Plateau. Channel-filling sediments, conglomerate lenses, carbonized and silicified plant material, and locally remains of dryland and fresh-water animals are associated with the cross-stratified layers (Stewart and others, 1959); the combination of these features clearly indicates that the cross-stratified layers are of fluvial origin. The descriptions given apply mainly to the cross-strata in the Shinarump and Moss Back members of the Chinle formation.

Tabular planar sets of cross-strata (fig. 54.1)—units of cross-strata with flat surfaces of erosion as upper and lower boundaries (McKee and Weir, 1953)—are common in the Chinle formation, and locally, at least, are the dominant type of cross-strata in the Shinarump and Moss Back members. The sets generally range in thickness from one-half foot to 2 feet. Some sets can be traced laterally along exposures for at least 200 feet. In plan view, the cross-strata appear as laminae dipping and striking uniformly. In cross section, the cross-laminae are concave upward and become tangential downwards with the bounding surface of the set. The maximum dip of cross-strata is generally about 25°.

Tabular planar cross-strata probably formed in transverse bars (fig. 54.1) similar to those described by Sundborg (1956, p. 207, 270–272) in the river Klarälven in Sweden. These bars are 0.05 to 0.5 meter high and 2 to 20 meters apart. The upstream side of the bars is flat and dips upstream at an angle of about 1°. The downward side is steep and roughly at the angle of repose. Sediment is carried up the backside of the bar and deposited on the frontside, in the manner of the foreset beds of a delta building out into a body of water. As the front of the bar is built forward by continued deposition, a tabular layer of cross-strata is left. McDowell (1960) has described the formation of cross-strata by "sand waves"—the same features that Sundborg calls transverse bars—in recent deposits of the Mississippi River.

Trough sets of cross-strata are also common in the Chinle formation, although in the Shinarump and Moss Back members they may be less abundant than tabular planar sets. These cross-strata occur in sets that have curved surfaces of erosion as upper and lower boundaries (fig. 54.1). In plan view, the sets are narrow elongate features commonly 5 to 20 feet long and 2 to 5 feet wide, with blunt terminations upstream. The cross-strata, in plan view, are curved and convex upstream. In a cross section cut along the length of the trough, the sets are lens shaped and average about 2 feet thick. In a section cut across the trough, the lower boundary of the set

TABULAR PLANAR CROSS-STRATA

TROUGH CROSS-STRATA

TRANSVERSE BARS AND TABULAR PLANAR CROSS-STRATA

ARCUATE BARS AND TROUGH CROSS-STRATA
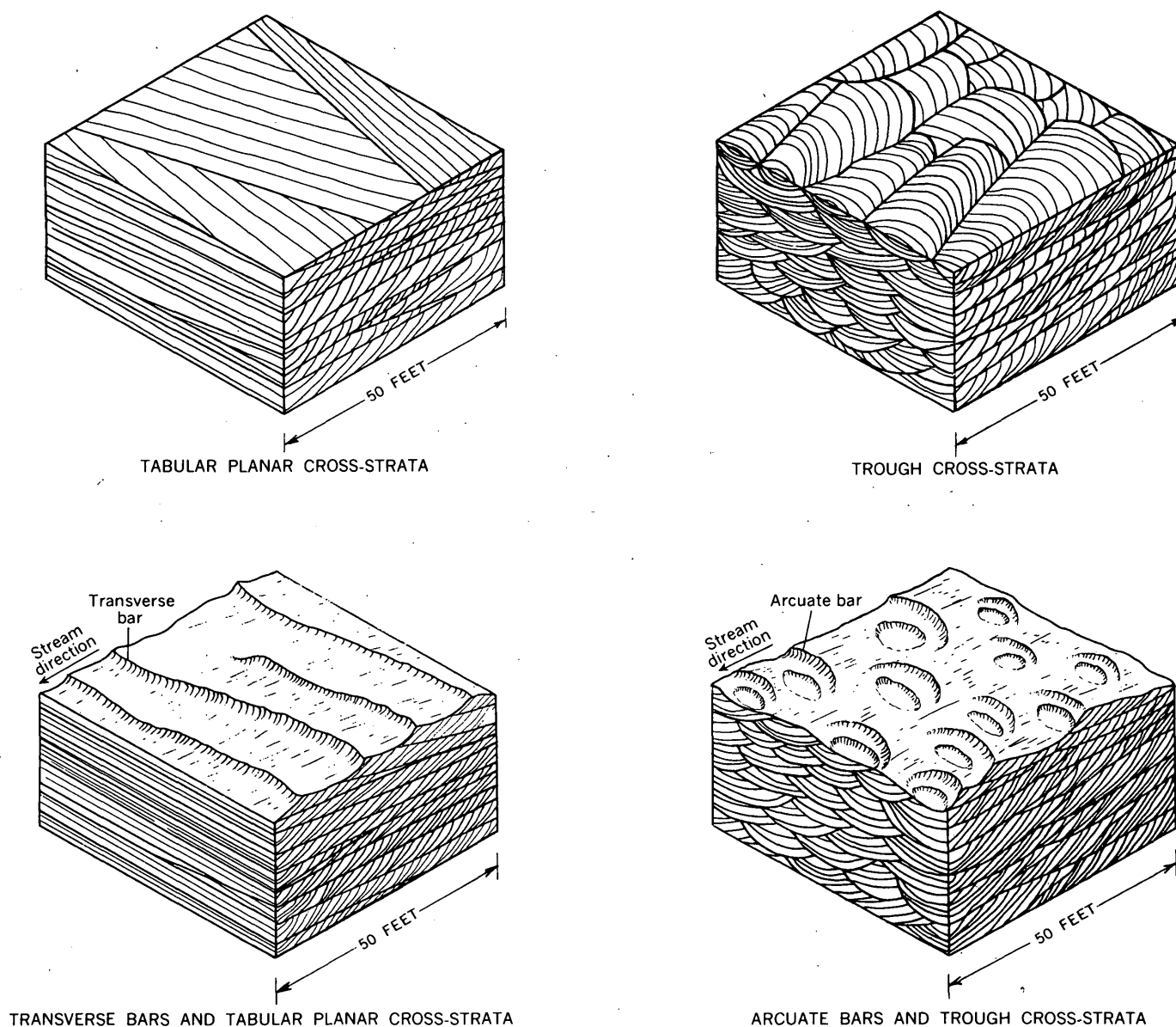
FIGURE 54.1.—Tabular planar and trough cross-strata and bar types.

is gently U-shaped. The maximum dip of the cross-strata is generally about 25°.

Trough cross-strata are generally thought to form by scouring of a trough and later filling of the trough (McKee and others, 1953; McKee, 1957; Stokes, 1953). Stokes (1953) ascribes the formation of troughs to water vortices that scour the stream bottom in much the same way that a tornado picks up debris on land. Such turbulent vortices, according to Matthes (1947, p. 259), are the most powerful agents of stream scour and produce troughs on stream bottoms.

Some trough sets of cross-strata may have formed by filling of troughs produced by such vortices, but another process, or a modification of the above process, is suggested here to explain the formation of many, perhaps most, of the trough cross-strata in the Chinle formation. They may have formed by the downstream migration of arcuate bars that are similar to barchan dunes in shape (fig. 54.1). Erosion would take place, perhaps in part by vortex action, in the area between the two arms of the crescent. In such a manner, the trough is extended downstream as the arcuate bar migrates downstream. Formation of trough cross-strata in this way is similar to the formation of tabular planar cross-strata in transverse bars, except for the dif-

FIGURE 54.2.—Overturned cross-strata in Moss Back member of Chinle formation in southeastern Utah.

ferent shape of the bars and the formation of troughs ahead of the bars by erosion.

The suggested mode of formation adequately explains the shape of the trough sets and the curvature, in plan view, of the cross-strata. In addition, tabular planar and trough cross-strata commonly are associated with one another and with intermediate types, suggesting that both may be formed by constructional deposition in bars. Finally, observations in modern streams indicate that transverse bars ("sand waves") have a tendency to break up along strike into crescentic-shaped parts (Bucher, 1919, p. 172). Trough cross-strata, following the hypothesis, would form in these crescentic, or arcuate bars.

Many of the cross-strata in the Chinle formation are peculiarly deformed so that the upper part of the cross-strata are drawn downstream; thus the individual laminae in cross section have the shape of a U laid on its side (fig. 54.2).

This type of cross-strata is termed "overturned" cross-strata by Potter and Glass (1958). This deformation probably is caused by a flowage of sand shortly after deposition of the cross-strata. Observations in modern streams show that the top few feet of the sand bed often have the consistency of "quicksand" and that they commonly move downstream as a "fluid" mass. This motion of the top few feet of the sand bed has been observed by

a civil engineer who descended in a diving bell to the bottom of the Mississippi at a point where the depth was 65 feet and the bottom of sand. Stepping to the bed, he sank into it about 3 feet, and then thrusting his arm into the yielding mass, could feel its flowing motion to a depth of 2 feet, the velocity diminishing downward

(Gilbert, 1914, p. 156). A similar motion down to 3 meters was observed on the gravel beds of the upper part of the Rhine and one of its small tributary streams (Bucher, 1919, p. 169–170). This motion presumably would cause the laminae to deform. The diminishing downward velocity could account for the observed diminishing "bending" of the strata downward.

REFERENCES

Bucher, W. H., 1919, On ripples and related sedimentary surface forms and their paleogeographic interpretations: Am. Jour. Sci., 4th ser., v. 47, p. 149–210, 241–269.

Gilbert, G. K., 1914, The transportation of debris by running water: U.S. Geol. Survey Prof. Paper 86, 263 p.

Matthes, G. H., 1947, Macroturbulence in natural stream flow: Am. Geophys. Union Trans., v. 28, p. 255–262.

McDowell, J. P., 1960, Cross-bedding formed by sand waves in Mississippi River point-bar deposits [abs.]: Geol. Soc. America Bull., v. 71, no. 12, pt. 2, p. 1925.

McKee, E. D., 1957, Flume experiments on the production of stratification and cross-stratification: Jour. Sed. Petrology, v. 27, p. 129–134.

McKee, E. D., Evensen, C. G., and Grundy, W. D., 1953, Studies in sedimentology of the Shinarump conglomerate of northeastern Arizona: U.S. Atomic Energy Comm. Tech. Rept. RME–3089, 48 p., issued by U.S. Atomic Energy Comm. Tech. Inf. Serv., Oak Ridge, Tenn.

McKee, E. D., and Weir, G. W., 1953, Terminology for stratification and cross-stratification in sedimentary rocks: Geol. Soc. America Bull., v. 64, p. 381–390.

Potter, E. P., and Glass, H. D., 1958, Petrology and sedimentation of the Pennsylvanian sediments in southern Illinois—A vertical profile: Illinois State Geol. Survey Rept. Inv. 204, 60 p.

Stewart, J. H., Williams, G. A., Albee, H. F., and Raup, O. B., 1959, Stratigraphy of Triassic and associated formations in part of the Colorado Plateau region, *with a section on* Sedimentary petrology by R. A. Cadigan: U.S. Geol. Survey Bull. 1046–Q, p. 487–576.

Stokes, W. L., 1953, Primary sedimentary trend indicators as applied to ore finding in the Carrizo Mountains, Arizona and New Mexico, Part 1: Tech. Rept. for April 1, 1952 to March 31, 1953: U.S. Atomic Energy Comm. Tech. Rept. RME–3043 (pt. 1), 48 p., issued by U.S. Atomic Energy Comm. Tech. Inf. Serv., Oak Ridge, Tenn.

Sundborg, Ake, 1956, The river Klarälven—a study of fluvial processes: Geografiska Annalar, v. 38, no. 2–3, p. 127–316.

55.   FOSSIL WOODS ASSOCIATED WITH URANIUM ON THE COLORADO PLATEAU

By RICHARD A. SCOTT, Denver, Colo.

Work done in cooperation with the U.S. Atomic Energy Commission

Fossil woods and other organic debris commonly occur with uranium in deposits of Triassic and Jurassic age on the Colorado Plateau. The possibility that woods of differing systematic affinities might have different capacities for localizing uranium has been suggested as an explanation for the highly variable uranium content of organic matter from a single mineralized zone. Woods associated with uraniferous minerals from various deposits on the Colorado Plateau were collected and studied to evaluate this possibility.

AFFINITIES OF THE WOODS

All structurally preserved woods collected from the Colorado Plateau belong to *Araucarioxylon* Kraus, a form genus for fossil woods like those of the modern coniferous family Araucariaceae. All Upper Triassic woods examined belong to one species, *A. arizonicum* Knowlton (fig. 55.1 *A* to *C*). Two undescribed species of *Araucarioxylon* are present in Jurassic strata (Morrison formation).

Lack of diversity among Plateau woods is puzzling, for floras of the times are known to have been varied. The Chinle flora contained members of all major groups of vascular plants except dicotyledons (Daugherty, 1941); cycadeoids and other vascular plants except dicotyledons were common in Morrison time. Spore and pollen assemblages bear out the diversity (Scott, 1960). A possible explanation for this anomaly is that uranium deposits commonly are found in channel fills and floodplain deposits, depositional environments favoring degradation. Remains of small plants became too degraded to identify. Some entire logs were affected to an extent that eliminated cell-wall details necessary for identification. Coalified exteriors are present on many logs with silicified cores, indicating that degradation proceeded centripetally. Relatively intact wood could persist in the interiors of large logs even when smaller remains were degraded; consequently, large size of the araucarians—logs 5 feet in diameter are known—may have been a selective factor favoring their structural preservation. Organic trash zones commonly associated with ore bodies on the

Colorado Plateau probably were derived from various plants.

LACK OF RELATION BETWEEN WOOD TYPE AND URANIUM

Absence of marked systematic diversity among Plateau woods collected impedes direct evaluation of the possible effect of wood type upon uranium fixation. Nevertheless, several observations indicate that systematic differences were not important factors affecting uranium content of fossil woods.

Nature of the plant remains.—Variations in effectiveness in uranium fixation for woods of different species would derive from chemical differences among them. The organic components of wood comprise two major groups: cell-wall components consisting of holocellulose and lignin make up 80 to 90 percent of the wood substance; and so-called extraneous components consisting of resins, oils, tannins, and pigments make up the rest. Degradation of wood in nature results first in the loss of cellulosic and at least part of the extraneous components (Varossieau and Breger, 1951; Barghoorn, 1952). Later, the lignin may be altered and ultimately transformed to humic compounds. Uranium mineralization in the sandstone-type deposits of the Plateau followed deposition of the sediments by a geologically significant time interval (Stieff, Stern, and Milkey, 1953), and unsilicified plant remains present during mineralization were composed chiefly

FIGURE 55.1—Triassic wood associated with uranium. A, *Araucarioxylon arizonicum* Knowlton; transverse section; ×60. B, *Araucarioxylon arizonicum* Knowlton; tangential section; ×45. C, *Araucarioxylon arizonicum* Knowlton; radial section; ×90. D, Wood structure in asphaltite derived from *Araucarioxylon arizonicum* Knowlton; note crushing and distortion at upper margin; the parallel lines are rays; transverse section; ×45. E, Wood structure in asphaltite derived from *Araucarioxylon arizonicum* Knowlton; note intrusion into silicified wood; the larger cells at lower right and scattered; ×45. F, Uraninite in *Araucarioxylon arizonicum* Knowlton; the white material is the uraninite seen by reflected light; it is associated with the cell wall components, probably uniting with but not replacing them; ×90.
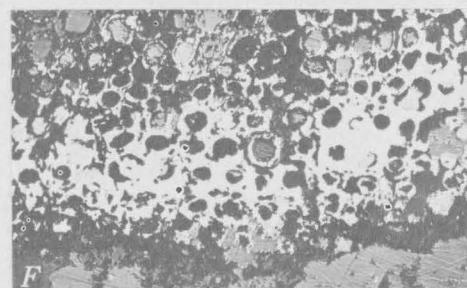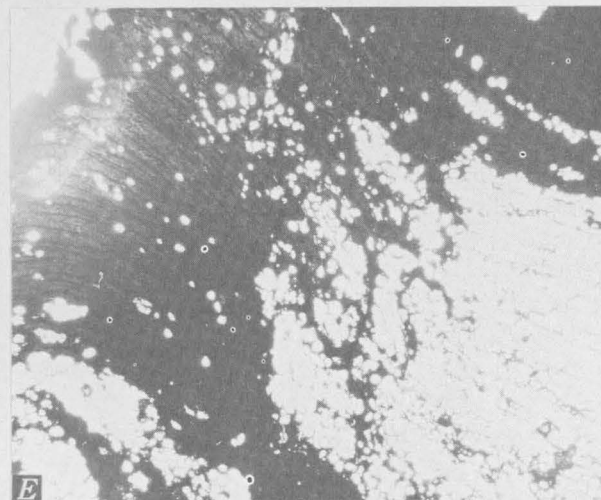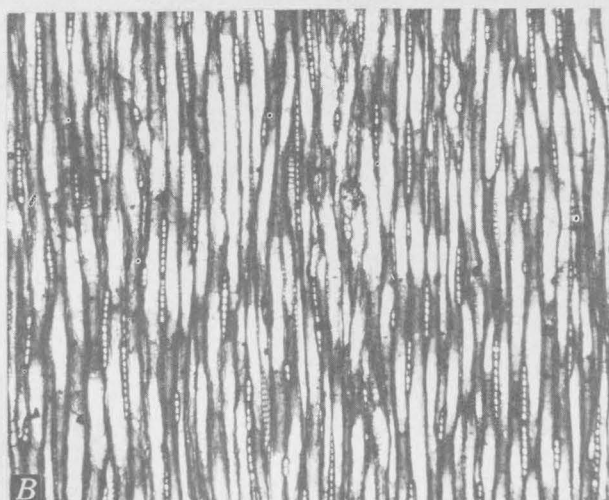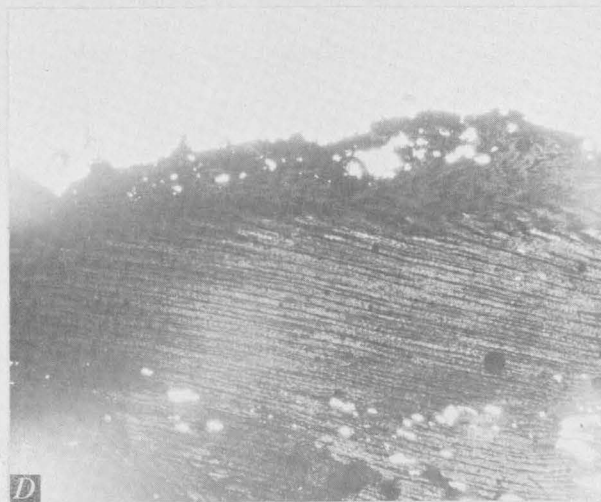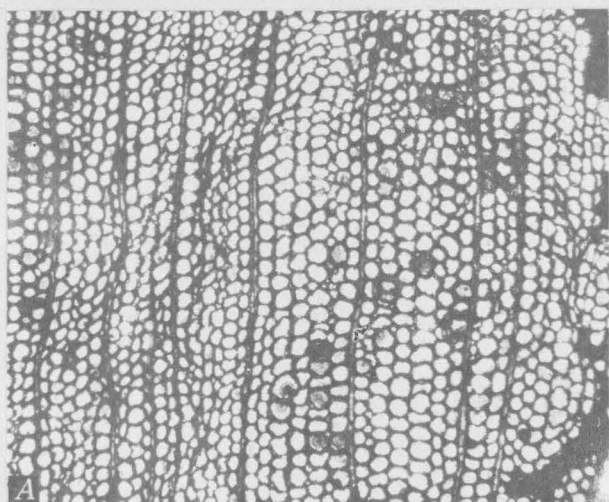
of lignin residues and their derivatives. Any original compositional differences would have been minimized by degradational and diagenetic changes prior to mineralization.

Variation in uranium content among samples of a single species.—Eight samples of coalified wood from Temple Mountain, Utah, all determined as *Araucarioxylon arizonicum*, contained the following percentages of uranium (Roosevelt Moore, analyst): 0.0005, 0.007, 0.007, 0.16, 0.33, 0.69, 1.3, and 5.8. Ash from each of two samples of the same species from the Adams mine on the west side of the San Rafael Swell, Utah, have uranium contents of 0.09 percent and 8.5 percent. This large range within the single species demonstrates that factors in the depositional environment at the time of mineralization, other than the affinities of the plant material, effected marked variation in uranium concentration.

Association of uranium with organic matter from diverse plant sources.—Uranium has been found associated with organic material from a variety of plants. For example, a sample of ash from wood of *Callixylon*, which has pteridophytic relationships (Beck, 1960), has been found to contain 2.58 percent uranium (Breger and Schopf, 1955), and ash from a lignite of Tertiary age contained 0.3 percent uranium, chiefly associated with the organic matter (Breger, Deul, and Rubenstein, 1955). Araucarian conifers are not yet known from North American Tertiary rocks; presumably the Tertiary lignite is of nonaraucarian origin. Garrels and Pommer (1959) reported that fresh spruce wood and Tertiary lignite were equally effective in reducing uranium to uraninite, a mineral commonly found (along with coffinite) in ores associated with coalified wood and other carbonaceous material (Weeks, Coleman, and Thompson, 1959). Concentration of uranyl ions by silicified dicotyledonous woods has been described by Barghoorn (written communication, 1956).

Thus, various organic materials have the ability to effect fixation, and the available evidence does not suggest that systematic differences among plants that contributed organic remains were significant factors in producing ore.

TEMPLE MOUNTAIN ASPHALTITE WITH WOOD STRUCTURE

There is disagreement as to whether the so-called uraniferous "asphaltite" at Temple Mountain, Utah, was derived from petroliferous (Kelley and Kerr, 1958) or plant (Breger and Deul, 1959) sources. Some sections of silicified wood include regions of black, apparently amorphous, asphaltite. When ground sufficiently thin, remnants of original wood structure are visible in these asphaltites (fig. 55.1, *D* and *E*). Cellular structure is present even in some asphaltite that had been forced by pressure in a plastic state into fractures in silicified wood (fig. 55.1, *E*). This evidence indicates that at least some of the Temple Mountain asphaltites were derived from wood.

REFERENCES

Barghoorn, E. S., 1952, Degradation of plant tissues in organic sediments: Jour. Sed. Petrology, v. 22, p. 34–41.

Beck, C. B., 1960, The identity of *Archeopteris* and *Callixylon*: Brittonia, v. 12, p. 351–368.

Breger, I. A., and Deul, Maurice, 1959, Association of uranium with carbonaceous materials, with special reference to the Temple Mountain region *in* Garrels, R. M. and Larsen, E. S. 3d, Geochemistry and mineralogy of the Colorado Plateau uranium ores: U.S. Geol. Survey Prof. Paper 320, p. 139–149.

Breger, I. A., Deul, Maurice, and Rubenstein, Samuel, 1955, Geochemistry and mineralogy of a uraniferous lignite: Econ. Geology, v. 50, p. 206–226.

Breger, I. A., and Schopf, J. M., 1955, Germanium and uranium in coalified wood from Upper Devonian black shale: Geochim. et Cosmochim. Acta, v. 7, p. 287–293.

Daugherty, L. H., 1941, The Upper Triassic flora of Arizona: Carnegie Inst. Washington Pub. 526, 108 p.

Garrells, R. M., and Pommer, A. M., 1959, Some quantitative aspects of the oxidation and reduction of the ores *in* Garrels, R. M. and Larsen, E. S., 3d, Geochemistry and mineralogy of the Colorado Plateau uranium ores: U.S. Geol. Survey Prof. Paper 320, p. 157–164.

Kelley, D. R., and Kerr, P. F., 1958, Urano-organic ore at Temple Mountain, Utah: Geol. Soc. America Bull., v. 69, p. 701–756.

Scott, R. A. 1960, Pollen of *Ephedra* from the Chinle formation (Upper Triassic) and the genus *Equisetosporites*: Micropaleontology, v. 6, p. 271–276.

Stieff, L. R., Stern, T. W., and Milkey, R. G., 1953, A preliminary determination of the age of some uranium ores of the Colorado Plateaus by the lead-uranium method: U.S. Geol. Survey Circ. 271.

Varossieau, W. W., and Breger, I. A., 1952, Chemical studies on ancient buried wood and the origin of humus: Estrait du Compte Rendu: 3ieme Cong. Stratig. et de Geol. du Carbonifere-Heerlen.

Weeks, A. D., Coleman, R. G., and Thompson, M. E., 1959, Summary of the ore mineralogy *in* Garrels, R. M. and Larsen, E. S., 3d, Geochemistry and mineralogy of the Colorado Plateau uranium ores: U.S. Geol. Survey Prof. Paper 320, p. 65–79.

56.   LATE CENOZOIC EVENTS OF THE LEADVILLE DISTRICT AND UPPER ARKANSAS VALLEY, COLORADO

By Ogden Tweto, Denver, Colo.

In the upper Arkansas Valley, Colo., unconsolidated deposits of Pliocene and younger age form a thick cover over the bedrock (fig. 56.1). In the Leadville mining district, the nature and extent of these deposits and, especially, the topography of the buried bedrock surface, are of direct concern to the mining industry. Studies there have shown that the bedrock surface is very irregular, as it is furrowed by deep canyons and displaced by faults younger than some of the covering materials. This rough bedrock topography markedly affects the distribution of geologic formations and ore deposits, and also affected the pattern of oxidation of the ores. Erosional, depositional, and tectonic events that led to formation of this rough surface and its cover are illustrated in figure 56.2, and the two principal unconsolidated deposits are described briefly below.

Subsurface data indicate that the bedrock floor of the Arkansas Valley has a relief of more than 1,000 feet. Although older materials may fill the deeper depressions, insofar as known the floor is overlain by massive brown sandy silt and interbedded gravel, sand, and minor volcanic ash of Pliocene age. These deposits, the "lake beds" of earlier reports (Emmons, 1886, p. 72; Emmons, Irving, and Loughlin, 1927, p. 17), are here given the name Dry Union formation, for Dry Union Gulch, 5 miles south of Leadville. A landslide scarp near the mouth of this gulch (sec. 23, T. 10 S., R. 80 W.) exposes about 260 feet of strata in the upper part of the formation. Thickness of the formation in the Arkansas Valley ranges widely, as the top is irregularly eroded and the surface beneath the base has high relief. Maximum thickness of about 800 feet is known from surface distribution and exploratory openings in the Leadville area, but geophysical data suggest that locally the formation may be as much as 2,000 feet thick. The formation probably underlies most of the Arkansas Valley from Leadville to Salida and also occurs farther downstream near Howard (fig. 56.1), as noted by Powers (1935, p. 189). The formation is covered by younger deposits in many places but is widespread at the surface in the Salida area, where about 500 feet of it is exposed (Van Alstine and Lewis, 1960).

The detrital sediments that compose the Dry Union formation in the Leadville area are chiefly silt, sand, and gravel deposited in alluvial fans.
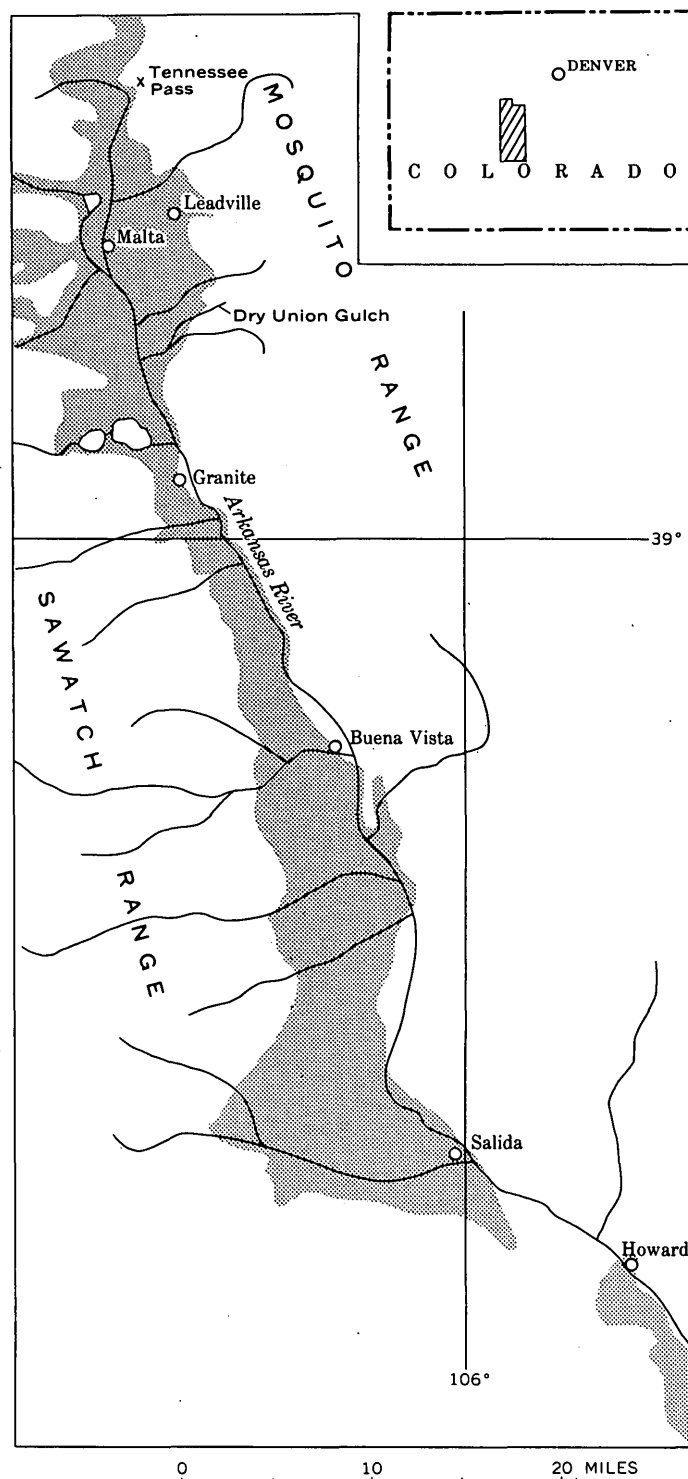
FIGURE 56.1.—Distribution of unconsolidated deposits, upper Arkansas Valley. Major deposits indicated by pattern.

Valley axis

Pediment

A

EXPLANATION

Pleistocene

Malta gravel

Deposits of glacial episode 1

QUATERNARY

Pliocene

Dry Union formation

TERTIARY

Bedrock surface

Fault

EXPLANATION

Deposits of glacial episode 4

Deposits of glacial episode 3

Deposits of glacial episode 2

———III———

Valley floor during episode 3

———II———

Valley floor during episode 2

Surface of prepediment materials

II

III

Pediment

B

Cirque

9

8

7

6

5

4

Stream

C

FIGURE 56.2.—Sketches showing effects of Late Cenozoic events. Not drawn to scale. *A*, diagrammatic cross section showing relations at pediment stage. *B*, diagrammatic cross section showing relations of deposits and valley floors of glacial episodes 2, 3, and 4. *C*, map showing distribution of terminal moraines of glacial episodes 4 through 9 in a typical valley.

They are characteristically ill-sorted and occur either in lenses or in thick beds (5 to 30 feet thick) that show little or no internal stratification. Channel structures are numerous. Pebbles and cobbles—some of them wind polished and many of them angular—are scattered throughout the formation but are most abundant near the mountain slopes. The sediments consist chiefly of angular grains of relatively fresh rock derived from adjoining mountain slopes. Leached zones and caliche-cemented zones probably formed during episodes of subaerial weathering while the sediments accumulated.

The Dry Union formation appears to have been derived from mountains somewhat lower than those of today, in an arid and possibly cold climate. No plant or animal fossils have been found in the formation in the Leadville area, except for a few poorly dated vertebrate remains in one mine (Emmons, Irving, and Loughlin, 1927, p. 19). Vertebrate remains found in the Salida area indicate an early Pliocene age (Van Alstine and Lewis, 1960).

During the later Pliocene, the Dry Union formation was stripped from some areas and dissected to depths of at least a few hundred feet in others. Icecap glaciation, the first of nine glacial episodes recognized in the region, then occurred, probably in the early Pleistocene. Following this glaciation the glacial deposits were deeply weathered, and tributary valleys of the Arkansas were enlarged and deepened in the glacial drift, Dry Union formation, and bedrock. These valleys had reached depths of a few hundred feet and widths of as much as a mile when a climatic change or tectonic movement caused the streams to deposit coarse gravel, which eventually filled the valleys completely.

This gravel, the "high terrace gravel" of earlier reports (Emmons, Irving, and Loughlin, 1927, p. 15) is here named the Malta gravel for the railroad station of Malta, 3 miles southwest of Leadville. As seen in a cut 60 feet high at this station and also in many other places along the upper Arkansas Valley, the Malta gravel is buff, massive, coarse, and dirty. It shows little stratification except that imparted by the shingled arrangement of cobbles and by a few small lenses of sand or silt. The gravel is a mixture of materials of all sizes from silt to small boulders, but rounded cobbles 4 to 10 inches in diameter predominate. Near the mountain slopes, the gravel is composed entirely of rock of local origin, but near the valley axis it is a blend of rock from various sources. No fossils have been found

in it, but traces of humus occur locally. The gravel fills old valleys so its thickness varies widely; shafts and drill holes have revealed as much as 300 feet of gravel.

Deposition of Malta gravel transformed dissected, hilly areas to rolling surfaces of much lower relief. During the waning stages of gravel deposition, streams planed off the "highs" on these surfaces, producing pediments. These pediments, the "high terraces" of earlier reports (Capps, 1909; Behre, 1933; Powers, 1935), were once widespread along the upper Arkansas Valley but now exist as erosional remnants partly covered by glacial deposits.

Since the pediments were formed, glaciation, stream erosion, and faulting have further modified the Arkansas Valley. Glacial episodes 2 and 3 occurred after dissection of the pediments had begun, but before the Arkansas River and its tributaries had reached their present levels (fig. 56.2 B). By the time of glacial episode 4, these valleys were at essentially their present levels. Episodes 4, 5, 6, and 7, which probably constitute the Wisconsin glacial stage, occurred in relatively rapid succession, and their glaciers were successively less extensive (fig. 56.2 C). They were followed by two minor glacial episodes, numbers 8 and 9.

Faults that displace the unconsolidated deposits trend about parallel to the Arkansas Valley and are downthrown on the side nearer the valley axis. They are believed to be reactivated Laramide faults. As shown by the unconsolidated deposits and related land forms, movement occurred on the faults: (a) after deposition of the Dry Union formation; (b) after glacial episode 1; (c) late in the stage of pedimentation; and, possibly (d) after the Arkansas River had reached approximately its present level.

REFERENCES

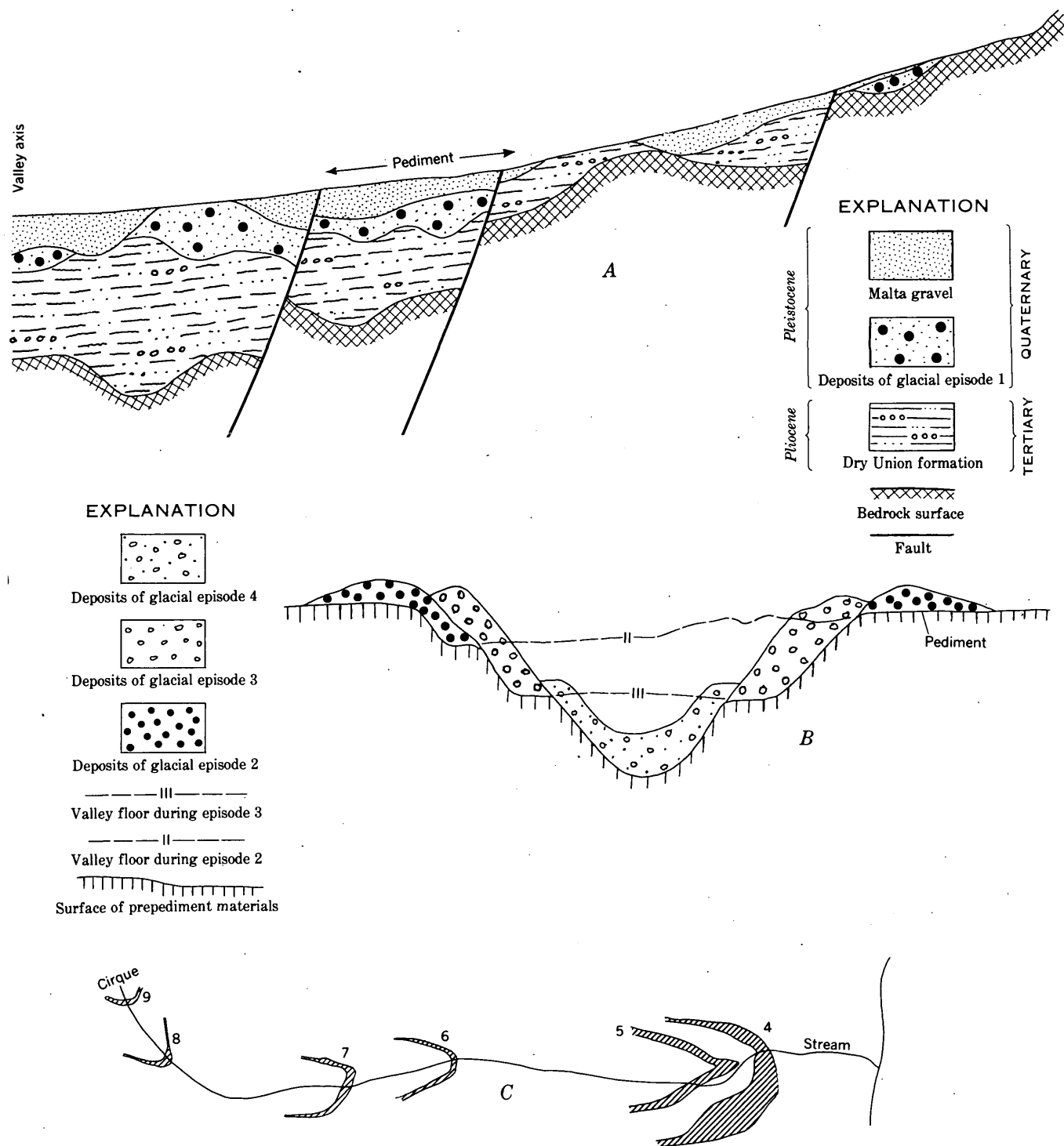Behre, C. H., Jr., 1933, Physiographic history of the upper Arkansas and Eagle Rivers, Colorado: Jour. Geology, v. 41, p. 785–814.

Capps, S. R., 1909, Pleistocene geology of the Leadville quadrangle, Colorado: U.S. Geol. Survey Bull. 386.

Emmons, S. F., 1886, Geology and mining industry of Leadville, Colorado: U.S. Geol. Survey Mon. 12.

Emmons, S. F., Irving, J. D., and Loughlin, G. F., 1927, Geology and ore deposits of the Leadville mining district, Colorado: U.S. Geol. Survey Prof. Paper 148.

Powers, W. E., 1935, Physiographic history of the upper Arkansas Valley and the Royal Gorge, Colorado: Jour. Geology, v. 43, p. 184–199.

Van Alstine, R. E., and Lewis, G. E., 1960, Pliocene sediments near Salida, Chaffee County, Colorado, in Short papers in the geological sciences: U.S. Geol. Survey Prof. Paper 400-B, p. B245.

57. MOVEMENT OF THE SLUMGULLION EARTHFLOW NEAR LAKE CITY, COLORADO

By Dwight R. Crandell and D. J. Varnes, Denver, Colo.

General relations of the Slumgullion earthflow, about 2 miles south of Lake City, Colo., have long been known (Endlich, 1876; Cross, 1909; Howe, 1909, p. 40–41; Atwood and Mather, 1932, p. 163–164). A brief examination of the earthflow in June 1958 revealed a stable flow about 700 years old that is being overridden by a younger flow (Crandell and Varnes, 1960). This paper presents some data on the amount and rate of movement of the younger flow during the past 20 years, and discusses the type of deformation that is occurring.

Both parts of the Slumgullion earthflow head in a large cirquelike basin (fig. 57.1) about 4,500 feet in diameter, on the northeastern margin of the Lake City caldera (Burbank, 1947). The source rocks consist of hydrothermally altered latite flows and breccias of Tertiary age; abundant montmorillonite in the earthflows is derived from these altered rocks.

The older flow is about 4 miles long and extends from the source area to a position across the valley of Lake Fork of the Gunnison River. It descends from an altitude of about 11,400 feet to 8,800 feet at an average gradient of 650 feet per mile.

The active earthflow is about 2.4 miles long and from 500 to 1,000 feet wide. It descends from an altitude of 11,400 feet to 9,700 feet at an overall gradient of about 700 feet per mile. The toe of the earthflow is steep and unstable, and both it and the body of the flow are dotted with leaning trees. The active earthflow is separated from the older earthflow by lateral cracks, along which movement occurs. The active flow also is broken by open transverse cracks in many areas, into which some of the surface drainage disappears.

Velocity of the active earthflow has been studied in three ways: the displacements of trees were determined from air photographs made in 1939 and in succeeding years, and from measurements made on the ground; control stakes installed in 1958 were checked periodically; and an automatic time-lapse motion picture camera (Miller, Parshall, and Crandell, Art. 135) was installed at the flow margin to record movement between June and October 1960.

Comparison of aerial photographs shows that certain recognizable trees near locality C (fig. 57.1)

moved 194 feet in the 13-year period 1939–52, an average velocity of 15 feet per year. Trees at a point about 3,000 feet from the head moved at an average rate of 5.8 feet per year in this same period.

Near locality D, the displacement of trees that could be located on aerial photographs taken in 1951 was measured directly on the ground in 1959; these measurements indicate an average velocity of 16 feet per year. Control stakes installed in 1958 moved at a rate of about 20.0 feet per year at locality D, about 15.5 feet per year at locality C, 8.5 feet per year at locality B, and 2.5 feet per year at locality A. During the period 1940–52 the toe advanced an estimated distance of 30 feet, also an average rate of 2.5 feet per year.

The time-lapse motion picture camera study of the active earthflow at locality D during the summer of 1960 recorded a constant velocity of 0.04 feet per day.

We think that the virtually constant velocity from year to year and from season to season at a given point indicates that neither long-term nor seasonal fluctuations of temperature and precipitation have much effect on movement. Maximum lubrication and pore-water pressure probably exist in the flow at all times, and the entire flow probably would be accelerated only by the addition of a large amount of material at the head by a landslide, or an earthquake.

Control stakes were installed across the entire width of the active earthflow at locality D (fig. 57.2). Stakes in the center move at a slightly greater velocity than those along the sides. This, and the evidence of decreased velocity downslope, suggest viscous flowage, contrary to an earlier opinion (Crandell and Varnes, 1960) that the earthflow is moving without internal deformation. The velocity decrease below locality D suggests thickening between locality C and the toe, but this possibility has not yet been verified by field observation.

The overall rather slow rate of movement poses the question of how the toe of the active flow got to its present position of some 12,000 feet beyond its source. The oldest tree found near the toe is a leaning dead spruce with 330 growth rings; no ap-

FIGURE 57.1.—Aerial view of Slumgullion earthflow. Note that the younger, active earthflow occupies only a small part of the source area of the older earth-flow. Deepest part of Lake San Cristobal determined by sounding is 90 feet at point ×, near bottom of photograph. (Enlargement of Department of Agriculture photograph DOM–1A–8, taken September 9, 1951.)
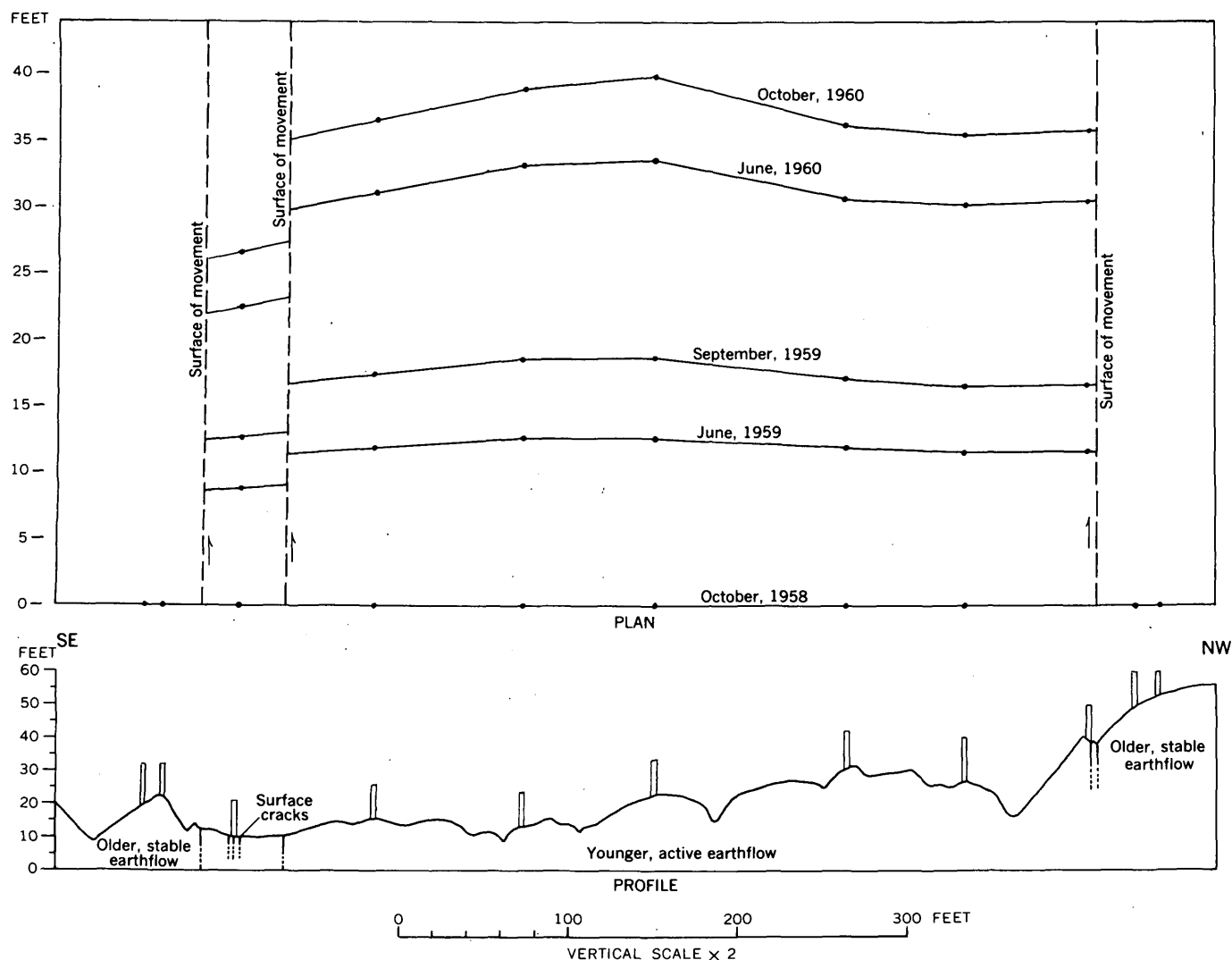
FIGURE 57.2.—Plan and profile of younger, active earthflow at locality *D*, showing differential movement of control stakes between October 1958 and October 1960.

preciably larger trees were seen, either alive or dead, although trees as old as 700 years grow on the older earthflow. Probably, therefore, the younger flow originated not much more than 350 years ago. But at its present velocity, the toe would have progressed only 875 feet from the source area in that length of time.

Several possible reasons may account for this apparent anomaly. The flow may have come nearly to its present position in a relatively short time by rapid flowage, and then may have continued to creep slowly. The earthflow also may periodically lengthen rapidly by a wave that progresses from the head to the toe, possibly propagated by sliding of new material onto the head. Slower velocity near the head of the earthflow than at the middle between 1939

and 1952 suggests such a wavelike motion. Finally, the toe may possibly advance in quick surges following a long period of very slow movement. A surge would be encouraged by a gradually accumulated bulge in the lower part of the flow. Although the active part of the Slumgullion earthflow might be a reactivated part of the older, stable flow, age of vegetation growing on the two parts suggests otherwise. Much of the older flow, however, probably has been incorporated in the active flow, especially near the source area.

REFERENCES

Atwood, W. W., and Mather, K. F., 1932, Physiography and Quaternary geology of the San Juan Mountains, Colorado: U.S. Geol. Survey Prof. Paper 166, 176 p.

Burbank, W. S., 1947, Lake City area, Hinsdale County, *in* Mineral Resources of Colorado: Colorado Min. Res. Board, p. 439–443.

Crandell, D. R., and Varnes, D. J., 1960, Slumgullion earth-flow and earthslide near Lake City, Colorado [abs.]: Geol. Soc. America Bull., v. 71, no. 12, pt. 2, p. 1846.

Cross, C. W., 1909, The Slumgullion mudflow [abs.]: Science, new ser., v. 30, p. 126–127.

Endlich, F. M., 1876, Report of F. M. Endlich, *in* U.S. Geol. Geog. Survey of the Territories Ann. Rept. 1874.

Howe, Ernest, 1909, Landslides in the San Juan Mountains, Colorado: U.S. Geol. Survey Prof. Paper 67, 58 p.

58.   RELATIONS OF METALS IN LITHOSOLS TO ALTERATION AND SHEARING AT RED MOUNTAIN, CLEAR CREEK COUNTY, COLORADO

By P. K. THEOBALD, JR., and C. E. THOMPSON, Denver, Colo.

Tungsten, molybdenum, lead, arsenic, zinc, and copper have been determined by geochemical field methods in 268 samples of lithosol (poorly developed soil) from the Red Mountain area, Clear Creek County, Colo. (fig. 58.1). These data establish distinct anomalies for each of the elements and suggest two stages of mineralization.

The crest of Red Mountain is underlain by a plug of argillized quartz monzonite porphyry of Tertiary age (fig. 58.2 *A*). Surrounding the plug is silicified, argillized, or chloritized quartz monzonite of Precambrian age. Two principal sets of shear zones trend N. 5° E. and N. 70° E. and dip 85° SE. and 75° NW., respectively. Both are characterized by a large number of small discontinuous gouge zones; only a few faults are continuous enough to be shown on the map.

The Urad mine, on the southeast slope of Red Mountain, has produced molybdenum (Vanderwilt, 1947, p. 225), and previous work (Theobald and Thompson, 1959) demonstrated the presence of tungsten in the same area. To establish the distribution of these metals and to search for other potential ore metals in this intensely altered area, the lithosols on the slopes of Red Mountain and the opposing slope to the north were systematically sampled and analyzed. Landslide and morainal debris are abundant on the steep (30° or more) slopes, but most of these materials are easily identified and were avoided in sampling. There is no evidence for distortion of the geochemical patterns by down-slope creep.

Areas of anomalously high values for tungsten and molybdenum roughly coincide and trend northeasterly (fig. 58.2 *B*). The tungsten background is less than 20 parts per million (ppm) and anomalous values range from 40 to 3,000 ppm. The molybdenum

background is less than 4 ppm, and anomalous values range from 6 to 7,000 ppm. Maximum values for both elements are in the zone of silicification. A northeast-trending fault marks one edge of the area containing anomalous amounts of molybdenum and of the area containing more than 30 ppm of tungsten.

Anomalously high concentrations of lead and arsenic occur in nearly coextensive generally north-trending areas. The lead background is probably 25 ppm or less, but this value has been obtained in only 6 samples from the northern edge of the area sampled. Anomalous values range from 50 to 6,000 ppm. The lead anomaly (fig. 58.2 *C*) is exceptionally large; in nearly a square mile the lead content exceeds 200 ppm and in nearly a quarter of a square
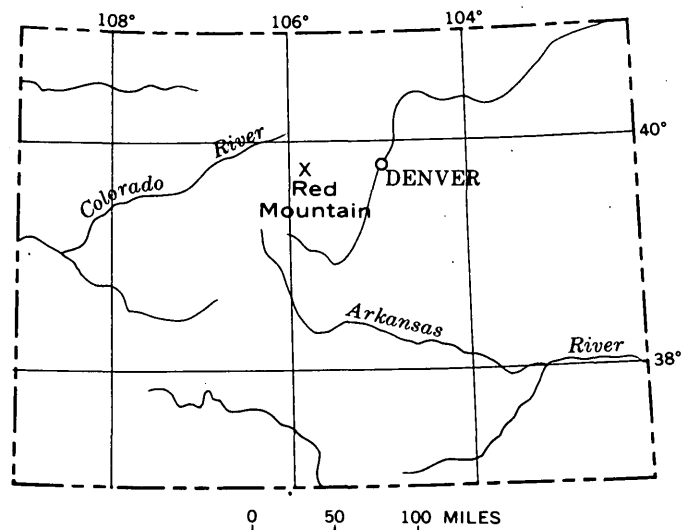
FIGURE 58.1.—Index map of Colorado showing location of this study.
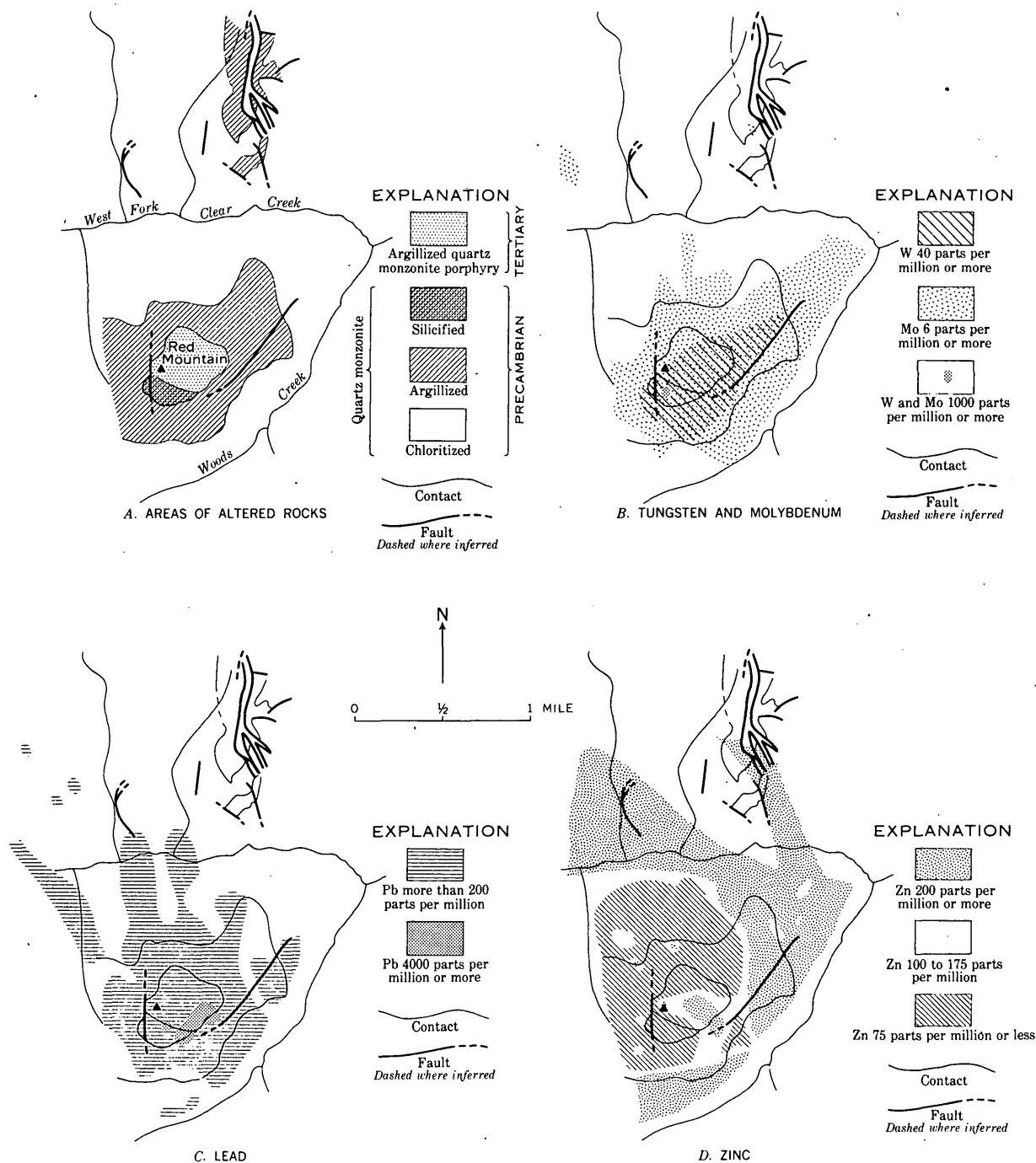
FIGURE 58.2—Maps showing the distribution of major rock types and faults, areas of altered rocks, and the distribution of tungsten, molybdenum, lead, and zinc in lithosols at Red Mountain, Clear Creek County, Colo.

mile it exceeds 1,000 ppm. The arsenic background (not illustrated) is 10 ppm, and anomalous values range from 20 to 120 ppm. Lead and arsenic are most abundant on the south margin of the porphyry plug and generally east of both the zone of silicification and the area containing maximum tungsten and molybdenum values.

The zinc background is 100 to 150 ppm; anomalies in the area sampled (fig. 58.2 D) are both positive (200 to 2,000 ppm) and negative (75 to less than 25 ppm). The negative anomaly approximately coincides with areas of argillized or silicified rock and with the area of maximum values for tungsten and molybdenum. The positive anomaly forms an arc

immediately outside of the negative anomaly, generally in the area of chloritization. High values are found in some samples from the south margin of the porphyry plug at approximately the same places as the maximum values for lead and arsenic. The pattern is unrelated to structural features. It could have been produced in large part by hypogene redistribution of metals inherent to the rocks, although some zinc may have been introduced with lead and arsenic.

The copper pattern (not illustrated) is complex. Background is 20 to 30 ppm. A negative anomaly, 10 ppm or less, has the general configuration of the negative zinc anomaly. The negative anomaly is bisected by a north-trending group of positive anomalies, 40 to 150 ppm, that coincides with the area of highest lead values.

All these anomalies have maxima lying along the south boundary of the porphyry plug. The maxima for tungsten and molybdenum, coincide with the zone of silicification, in the area of zinc and copper lows. The maxima for lead and arsenic, and the minor zinc and copper high, lie along the edge of the porphyry east of the zone of silicification. Areas of high tungsten and molybdenum are elongate parallel to the northeast-trending shears and

areas of high molybdenum are locally elongate parallel to north-trending shears. Areas of highest lead and arsenic values are parallel to north-trending shears, but they apparently have no relation to either the northeast-trending shears or the zones of alteration. These patterns suggest that tungsten was introduced and copper and zinc were redistributed during or shortly following alteration and that the northeast-trending shears were open at this time. The three elements were dispersed from conduits in the area of silicification. Introduction of molybdenum probably occurred at this time but continued into a later stage of mineralization when the principal open fractures were the north-trending shears. The northeast-trending shears and the conduit for metals introduced in the early period of mineralization were effectively closed before lead, arsenic, and some zinc and copper were distributed along the north-trending shears from conduits on the southeast margin of the porphyry plug.

REFERENCES

Theobald, P. K., Jr., and Thompson, C. E., 1959, Geochemical prospecting with heavy mineral concentrates used to locate a tungsten deposit: U.S. Geol. Survey Circ. 411.

Vanderwilt, J. W., 1947, Mineral resources of Colorado: State of Colorado Mineral Resources Board.

59. HYDROLOGY OF SMALL GRAZED AND UNGRAZED DRAINAGE BASINS, BADGER WASH AREA, WESTERN COLORADO

By GREGG C. LUSBY, Denver, Colo.

Work done in cooperation with Forest Service, Fish and Wildlife Service, Bureau of Land Management, and Bureau of Reclamation.

Erosion and runoff on much rangeland in the Western States have greatly damaged manmade structures, and also caused the loss of great quantities of soil and hence decreased the productivity of the land.

A need for quantitative data on the effectiveness of treatment-practices on rangelands has long been recognized, particularly for the Colorado Plateau in western Colorado and eastern Utah where the soils on thousands of square miles of land are held

in place by only a sparse vegetation cover. In 1953 a project was begun at Badger Wash to compare and evaluate changes in runoff and sediment yield from paired grazed and ungrazed drainage basins and to determine sources of sediment in the drainage basins.

The Badger Wash basin is in western Colorado in an area of intricately dissected terrain along the base of the Book Cliffs a few miles east of the Utah-Colorado boundary and about 25 miles west of

TABLE 1.—*Precipitation and runoff at Badger Wash, 1954-1959*

[A, grazed basin; B, ungrazed basin]

Drainage basin	Drainage area (square miles)	Precipitation and runoff (inches)											
		1954		1955		1956		1957		1958		1959	
		Precipitation	Runoff	Precipitation	Runoff	Precipitation	Runoff	Precipitation	Runoff	Precipitation	Runoff	Precipitation	Runoff
1A.......	0.066	4.97	1.08	3.24	1.06	2.12	0	8.03	1.15	2.95	0	4.31	0.44
1B.......	.084	4.68	.95	3.10	.82	1.94	0	7.58	1.29	2.95	0	4.46	.20
2A.......	.167	5.04	1.11	3.82	1.21	1.90	.02	8.17	1.35	2.74	.01	4.31	.57
2B.......	.158	4.80	1.07	3.64	.96	2.09	0	7.81	.68	2.69	0	4.38	.39
3A.......	.059	4.76	.90	3.71	1.06	1.90	.02	7.02	2.34	2.69	0	4.31	.72
3B.......	.048	4.79	.84	3.48	1.06	1.82	.02	7.18	1.81	2.71	0	4.43	.30
4A.......	.022	4.61	.91	3.49	1.29	2.28	.03	7.48	1.29	2.41	.03	3.90	.60
4B.......	.019	4.60	.79	3.50	.91	2.29	0	7.88	.98	2.54	0	3.94	.29

Grand Junction. Badger Wash is a tributary of West Salt Wash, which in turn is a tributary of the Colorado River. The Badger Wash basin is underlain entirely by the Mancos shale of Late Cretaceous age, but the lithology of the bedrock differs somewhat in various parts of the basin. Shale in the west and north parts of the basin contains several thin flat-lying sandstone layers. The sandstone resists erosion and locally forms areas of low relief with sandy soils. On the southeast side of the basin sandstone is absent. Throughout the basin relatively steep slopes merge at their bases with gentle colluvial slopes. Stream channels are everywhere incised into the bedrock.

Eight small drainage basins, ranging in size from 12 to 107 acres, were studied. The basins were matched in four pairs so that the basins in each pair were nearly similar in drainage area, topographic characteristic, soil type, and vegetation. One basin of each pair was fenced to prevent grazing, and the other received normal grazing for the area. Runoff and sediment yield from each drainage basin was measured in a reservoir at the lower end of the basin. Nine recording rain gages were installed so that at least two gages were located in each pair of basins. Point rainfall, measured at the gages, was adjusted to areal rainfall on the watersheds by the Thiessen polygon method.

Precipitation and runoff at each of the eight drainage basins for the period 1954-59 are shown in table 1. The precipitation and runoff were measured from about April 1 to October 31 each year. Precipitation during the winter months occurs mostly as snow and does not produce appreciable runoff. Table 1 shows a decrease in runoff from ungrazed areas as compared to grazed areas. The average runoff was 6 percent less for the ungrazed areas than for the grazed areas in 1954, and it was 51 percent less for ungrazed areas than for the grazed areas in 1959.

Table 2 shows sediment yield at the four pairs of watersheds during the period 1954-59. A reduction in sediment yield from ungrazed areas is indicated by these data. Channel cross-sections were measured at 49 places and line transects were measured at 8 places to determine the main areas of erosion. No change in ground level could be detected along the 8 transects, but channels at 75 percent of the cross-sections measured had increased in cross-sectional area during the period 1954-58, including channels in both grazed and ungrazed basins. The increase in size of channel consisted in most cases of an increase in both width and depth. Cross sections at two places are shown in figure 59.1.

Weather Bureau precipitation records for Fruita, Colo., about 16 miles southeast of Badger Wash, show that rainfall in the area was below normal in 5 of the 6 years between 1954 and 1959. The largest storm during the period occurred in July 1955. About 1.25 inches of rain fell in 30 minutes and produced runoffs of 0.74 to 1.02 inches at rates approaching 1,900 cubic feet per second per square mile. Storms of about this intensity occur at about 10-year intervals.

TABLE 2.—*Sediment yield at Badger Wash, 1954-1959*

[A, grazed basin; B, ungrazed basin]

Drainage basin	Sediment yield (acre-feet per square mile)				
	April 1954– July 1955	July 1955– Nov. 1956	Nov. 1956– Oct. 1957	Oct. 1957– Nov. 1958	Nov. 1958– Oct. 1959
1A............	10.8	0	3.80	0	4.48
1B............	7.41	0	0	0	.06
2A............	14.1	0	2.46	0	1.98
2B............	15.3	0	.70	0	2.13
3A............	12.5	0	1.70	0	3.71
3B............	8.37	0	.82	0	2.88
4A............	20.4	0	9.55	0	2.82
4B............	14.7	0	4.21	0	2.68
(1)	13.5	0	3.09	0	2.89
(2)	12.0	0	.74	0	1.72

[1] Average, all grazed areas.
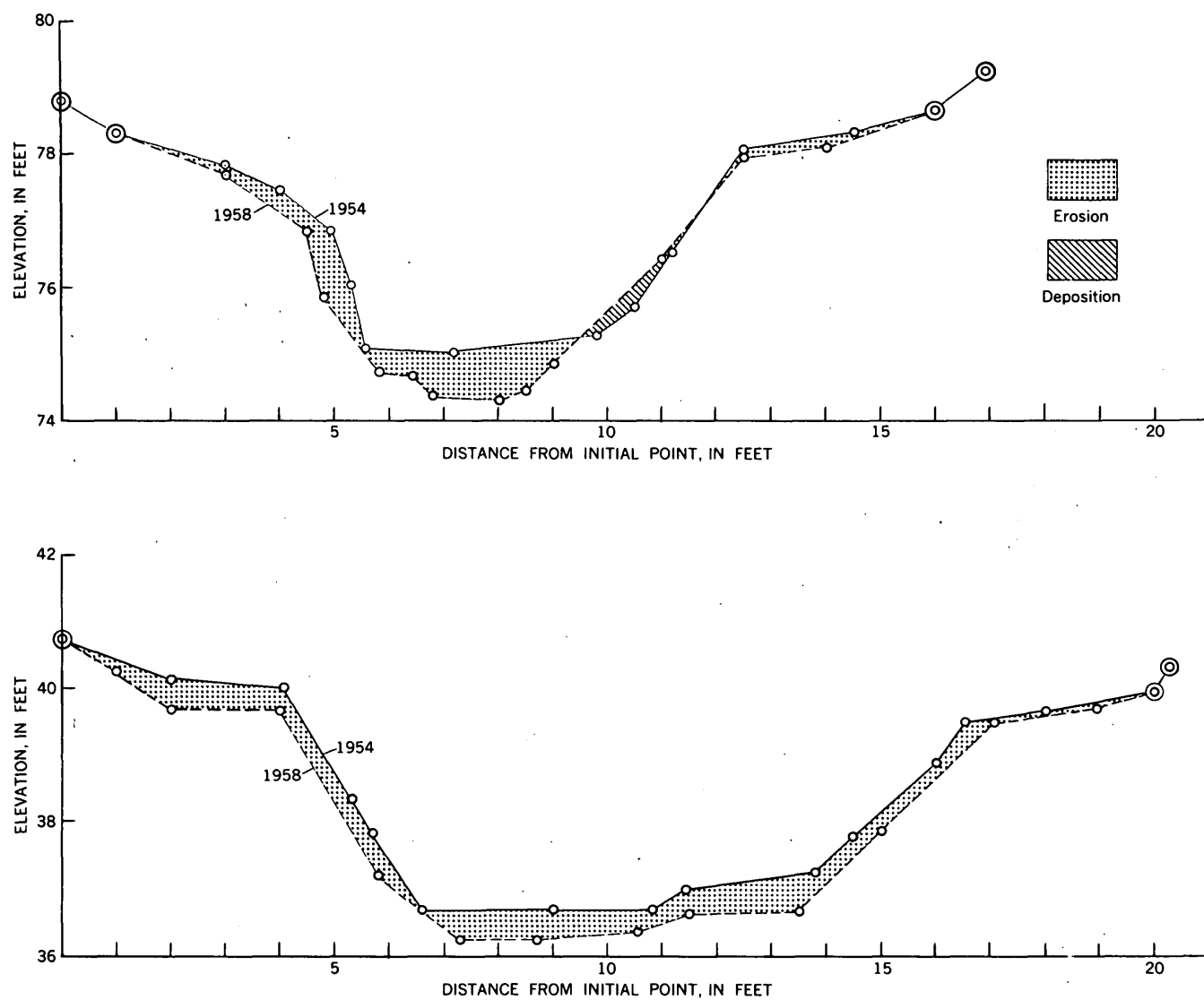[2] Average, all ungrazed areas.

FIGURE 59.1.—Cross sections of gullies showing changes in channels between 1954 and 1958 at Badger Wash, Mesa County, Colo.

60. ABANDONMENT OF UNAWEEP CANYON, MESA COUNTY, COLORADO, BY CAPTURE OF THE COLORADO AND GUNNISON RIVERS

By S. W. LOHMAN, Denver, Colo.

Work done in cooperation with the Colorado Water Conservation Board

Unaweep Canyon is a spectacular gorge cut to a depth of 1,500 to 3,300 feet across the Uncompahgre Plateau between the towns of Whitewater and Gateway, Colo. (fig. 60.1 *D*). The nearly vertical-walled inner gorge, 500 to 1,200 feet deep, was cut in hard Precambrian crystalline rocks. The more gently sloping upper walls of the canyon were cut in softer Mesozoic sedimentary rocks. The canyon is occupied by two small streams, one of which flows northeastward (East Creek) and the other southwestward (West Creek) from a gentle divide in the bottom of the gorge about 11 miles east of the crest of the plateau (fig. 60.1 *D*). The divide now stands about 2,500 feet above Grand Junction and Gateway.

That such an immense canyon could not have been cut by such small streams flowing in opposite directions was recognized as early as 1875 by members of the Hayden Survey, who attributed the cutting to the Gunnison River (Peale, 1877, p. 58, 59) or the Grand [Colorado] River (Gannett, 1882, p. 785). They believed that the canyon was abandoned solely because of renewed uplift of the Uncompahgre Plateau [arch], however, and did not recognize the more obvious possibility—stream capture. Stokes (1948, p. 39) correctly attributed the abandonment to stream capture, but did not tell the complete story which, I believe, involved two successive major stream captures, later renewed uplift of the Uncompahgre arch, and one later minor stream capture. Only the highlights of these events can be given in this brief account—the details are given in a report now in preparation.

The courses of the ancestral Colorado and Gunnison Rivers probably were established by superposition on widespread lava flows of post-Green River age (Hunt, 1956, p. 67 and 68) remnants of which still cap several high plateaus, including Grand Mesa. During subsequent epeirogenic uplifts and some renewed differential uplift of the Uncompahgre arch probably as late as Pliocene time, the streams cut downward without regard to underlying structures such as the Uncompahgre arch—a northwestward plunging faulted anticline that had been formed in part by gentle warping at about the close of the Cretaceous but mainly by more vigorous deformation in post-Green River time. Figure 60.1 *A* shows my concept of what the major drainage and topographic features may have been in Pliocene time just prior to capture of the ancestral Colorado River. The soft Mancos shale (Upper Cretaceous) had been partly stripped from the hard core of the Uncompahgre arch into which the ancestral Colorado River had cut, and the ancestral Book Cliffs capped by the resistant Mesaverde group (Upper Cretaceous) were much closer to the arch than they are now. The ancestral Colorado and Gunnison Rivers were baseleveled on the hard Precambrian rocks in Unaweep Canyon, which retarded downcutting in and upstream from the canyon for a long period of time. The subsequent tributary shown at the left (fig. 60.1 *A*), however, though carrying much less water than the master stream, had only the soft Mancos shale to cut, so was able to erode headward rapidly around the plunging arch. Hunt (1956, p. 68) suggested that this tributary was established by superposition on deposits at least as old as the Browns Park formation. If such deposits once were present, however, they have since been removed by erosion. Normal headward erosion in soft rock while the master stream was baseleveled on hard rock seems a more likely mode of origin of the tributary.

CAPTURE OF ANCESTRAL COLORADO RIVER

The subsequent tributary continued to cut headward until only a low divide of shale separated it from the ancestral Colorado River (fig. 60.1 *A*). Then, probably during some large flood in Pliocene time, the ancestral Colorado breached its banks and spilled over into the headwaters of the tributary. With the aid of this greatly increased supply of water, the tributary cut down rapidly into the soft Mancos shale, captured the ancestral Colorado, and isolated the ancestral Gunnison River (fig. 60.1 *B*). Soon after this capture, another tributary was cutting southward in the soft shale and was about to capture the ancestral Gunnison.
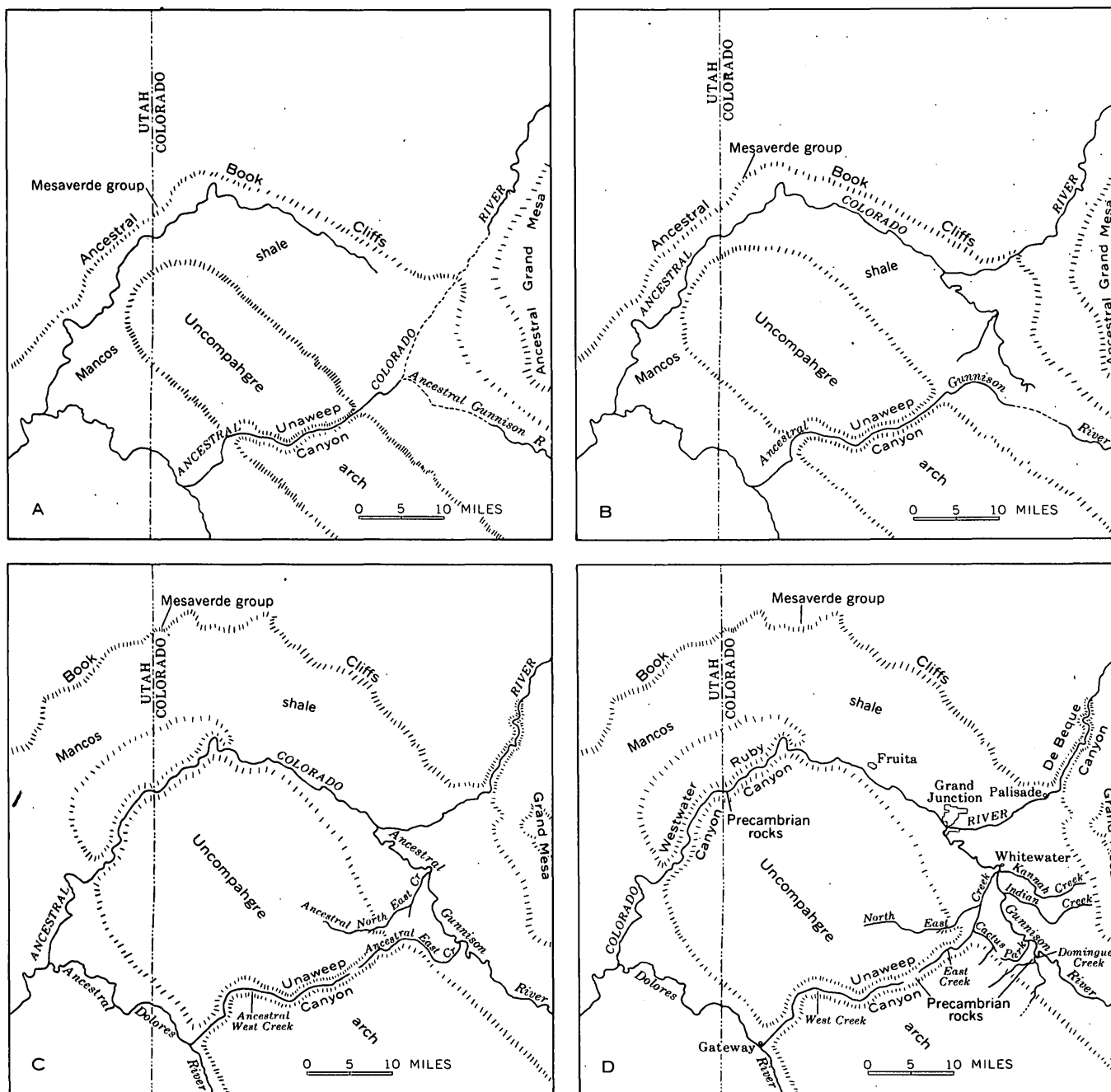
FIGURE 60.1.—Sketch maps of a part of western Colorado and eastern Utah, showing probable drainage pattern and topographic features at four successive stages of development. Solid drainage lines taken from Moab and Grand Junction, Utah-Colorado topographic maps by the Army Map Service; dashed drainage lines are hypothetical. A, just prior to capture of ancestral Colorado River; B, after capture of ancestral Colorado River and just prior to capture of ancestral Gunnison River; C, after capture of ancestral Gunnison River; and D, present drainage pattern, after renewed uplift of the Uncompahgre arch and capture of East Creek.

CAPTURE OF ANCESTRAL GUNNISON RIVER

Figure 60.1 *C* depicts my concept of what the drainage pattern and topographic features may have been sometime after capture of the ancestral Gunnison River. The divide between ancestral East and West Creeks had migrated from a point near the ancestral Gunnison River to the northeastern end of Unaweep Canyon, and was still migrating slowly southwestward. Meanwhile, a short tributary of ancestral North East Creek was cutting southward toward ancestral East Creek.

Evidence that Unaweep Canyon was occupied by the ancestral rivers was provided when basalt pebbles were found in high terrace gravels along West Creek about 4½ miles above Gateway (F. W. Cater, U.S. Geological Survey, written communication, Dec. 1960). Basalt pebbles have not been found in gravels of the Dolores River (fig. 60.1 *D*), but are abundant along both the Colorado and Gunnison Rivers east of the arch. Cater believed it likely that the basalt pebbles found near Gateway were reworked by ancestral West Creek from deposits laid down earlier in Unaweep Canyon by the ancestral Colorado River.

RENEWED UPLIFT OF THE UNCOMPAHGRE ARCH

There is evidence that the renewed uplift of the Uncompahgre arch that may have begun in Pliocene time before abandonment of Unaweep Canyon probably continued in latest Pliocene or earliest Pleistocene time after abandonment, when uplift and crustal warping were renewed in the nearby San Juan Mountains (Atwood and Mather, 1932, p. 25–27). This renewed uplift, which is discussed in more detail in a report now in preparation, had a profound effect upon the subsequent erosional development in and above the Grand Junction area (fig. 60.1 *D*), but seemingly was not the cause of any of the stream captures.

CAPTURE OF EAST CREEK

There is evidence that ancestral East Creek formerly joined the ancestral Gunnison River along the course shown in figure 60.1 *C*, through what is now known as Cactus Park (fig. 60.1 *D*), but that later, in the Pleistocene, East Creek was captured by a tributary of North East Creek to form the present drainage pattern. A gentle divide in Cactus Park now separates small tributaries of East Creek and

the Gunnison River. Near the northwest end of Cactus Park about 200 feet above the new channel of East Creek just 0.6 mile to the west, is a small patch of terrace deposits containing cobbles and pebbles of basalt, quartzite, and crystalline rocks. These deposits are about 800 feet below the divide in Unaweep Canyon, so probably were not deposited by the ancestral Colorado or Gunnison Rivers. At least the basalt and probably also some of the other rock types were brought into Unaweep Canyon by these rivers, and then probably were carried back to the northeast by ancestral East Creek.

POSSIBLE FUTURE STREAM CAPTURES

The Colorado River has cut about 15 feet into hard Precambrian rocks at two places in Ruby Canyon just east of the Utah State line, and the Gunnison River has reached Precambrian rocks at the mouth of Dominguez Creek (fig. 60.1 *D*). Thus once again downcutting by the two rivers is being retarded by hard rock. When Ruby and Westwater Canyons have developed deep inner gorges in hard crystalline rocks, and the Book Cliffs and adjacent belt of Mancos shale have retreated farther to the north, these canyons may be abandoned through capture of the Colorado River by a subsequent tributary cutting in the Mancos shale around the Uncompahgre arch. Similarly, when a deep gorge in Precambrian rocks has been cut by the Gunnison, tributaries of Indian Creek or Kannah Creek could cut headward around the gorge and capture this reach of the Gunnison River. However, other possible future events, such as renewed uplift or pronounced climatic changes, could alter or prevent such changes.

REFERENCES

Atwood, W. W., and Mather, K. F., 1932, Physiography and Quaternary geology of the San Juan Mountains, Colorado: U.S. Geol. Survey Prof. Paper 166, 34 pl., 25 figs., 176 p.

Gannett, Henry, 1882, The Unaweep Canyon [Colo.]: Pop. Sci. Monthly, v. 20, p. 781–786.

Hunt, C. B., 1956, Cenozoic geology of the Colorado Plateau: U.S. Geol. Survey Prof. Paper 279, 86 figs., 99 p.

Peale, A. C., 1877, Geological report on the Grand River district: U.S. Geol. Geog. Survey Terr. (Hayden), Ann. Rept. 9, p. 31–102, maps.

Stokes, W. L., 1948, Geology of the Utah-Colorado salt dome region, with emphasis on Gypsum Valley, Colorado, *in* Utah Geol. Soc. Guidebook to the geology of Utah, no. 3: 11 figs., 50 p.

61.   TRIPARTITION OF THE WASATCH FORMATION NEAR DE BEQUE IN NORTHWESTERN COLORADO

By JOHN R. DONNELL, Denver, Colo.

The Wasatch formation thins from 5,500 feet near the eastern margin of the Piceance Creek basin in northwestern Colorado to a featheredge along the western margin of the basin. Through most of the Piceance Creek basin the Wasatch is a monotonous sequence of brightly colored claystone beds, a few massive lenticular arkosic sandstone beds, and a few thin limestone beds; and no attempt has been made heretofore to map separate units.

Within an area of several hundred square miles in Garfield and Mesa Counties the Wasatch formation can be subdivided into three mappable members (fig. 61.1). The upper and lower members are mainly claystone similar to the undifferentiated Wasatch elsewhere. The middle member is mainly sandstone that forms steep ledges, in marked contrast to badlands topography formed by the upper and lower members.

The upper member of the Wasatch in a measured section north of Plateau Creek, shown on figure 61.2, is 930 feet thick. It thins to the northwest, west, and southwest, as does the entire Wasatch formation, and thickens to the northeast, east, and southeast. The southeastward thickening is accompanied by a partly compensating thinning of the overlying Douglas Creek member of the Green River formation.

The upper member weathers to many colors, but red predominates in the upper part. The top of the highest persistent thick band of red claystone is used to identify the contact between the Wasatch and overlying Green River formations. A single such band, greater than 10 feet thick, was traced 20 miles along the Colorado River. South and east of De Beque, red claystones appear in progressively younger beds, and along Plateau Creek just east of the area shown on figure 1, red claystones intertongue with and overlie rocks about 400 feet thick belonging to the Douglas Creek member of the Green River formation.

The middle member of the Wasatch attains its maximum thickness of 530 feet along Plateau Creek in T. 10 S., R. 96 W. It thins to the northeast, north, northwest, and southwest and disappears in T. 8 S., R. 99 W., and Tps. 10 and 11 S., R. 97 W. East and south of the exposures on Plateau Creek the middle member of the Wasatch is known only from bore holes. Sandstone beds of the middle member are easy to discern on electrical logs of wells along Plateau Creek for a distance of 8 miles east of the area shown on figure 61.1. Farther east some sandstone beds are indicated on electrical logs at about the interval of the middle member, but these beds are thin and widely separated by thick claystone beds.

The source of detritus in the middle member of the Wasatch probably was southeast of the area mapped. The sandstone beds thicken and become more numerous and coarse grained to the southeast. In T. 9 S., R. 96 W. (fig. 61.2), the middle member includes several conglomerate beds that contain pebbles as much as 3 inches in diameter of quartz, quartzite, and black, red, and brown chert. The sandstone in the middle member is mostly poorly sorted and feldspathic; locally the sandstone is an arkose, which suggests a nearby source.

The upper contact of the middle member rises in section to the northwest; the lower contact is the base of the lowest persistent sandstone, and (unlike the upper contact) it is at about the same stratigraphic horizon everywhere in the area.

The lower member of the Wasatch formation is about 650 feet thick in the measured section, figure
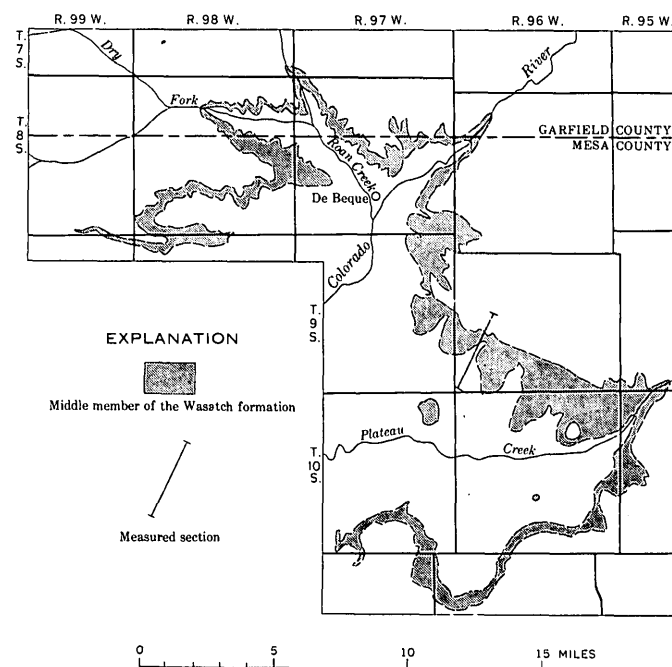
FIGURE 61.1.—Areal distribution of the middle member of the Wasatch formation. See figure 61.2 for measured section.
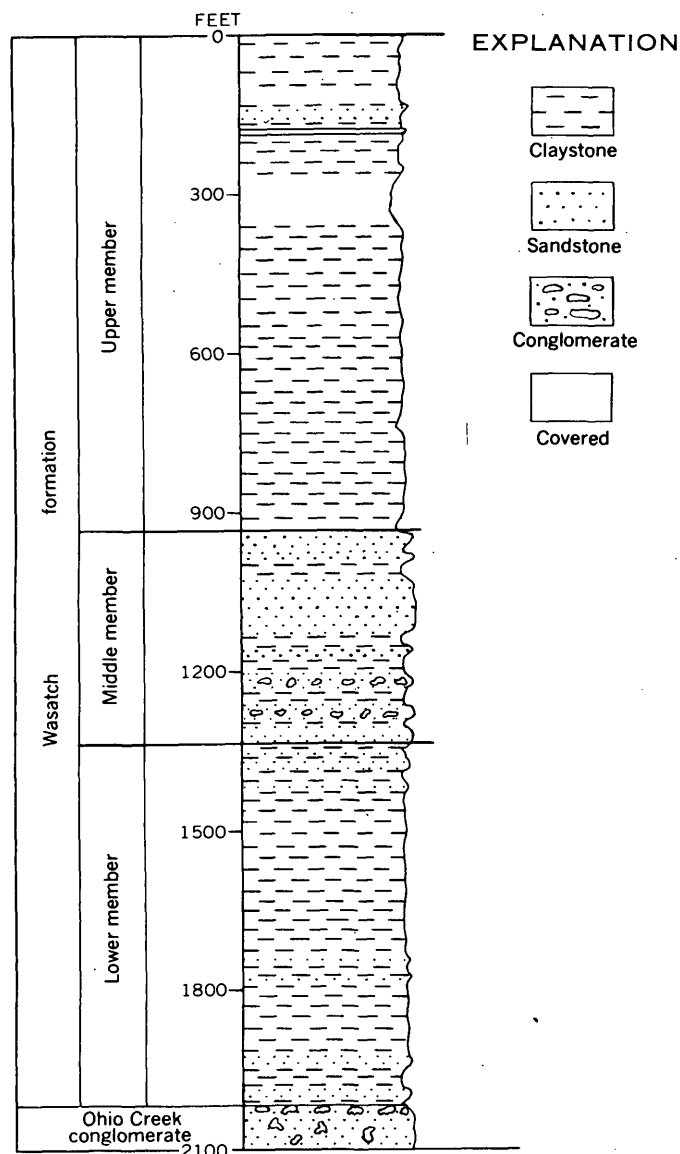
FIGURE 61.2.—Generalized stratigraphic section of the Wasatch formation.

61.2. This member has a fairly constant thickness in the western part of the area, but increases in thickness eastward. The lower member is lithologically similar to the upper member except that the lower member contains more and thicker carbonaceous claystone beds. One thick carbonaceous unit is near the top of the member just east of De Beque; and another is 75 feet above the base of the member at the east end of De Beque Canyon, about 4 miles southwest of De Beque. The lower unit contains a low-grade coal bed.

Several lenticular sandstone units are interbedded with brightly colored claystone in the lower 100 feet of the member, and this sandy sequence probably correlates with drab shale and sandstone beds that contain late Paleocene plants in the lower part of the Wasatch formation north and east of Rifle. Beds of undescribed thickness in the lower part of the Wasatch formation near De Beque were called the Plateau Valley beds by Patterson (1939), who reports that they contain Paleocene vertebrate fossils. The fossils were found in or just above the lenticular sandstone beds in the lower part of the lower member at two places; one is south of De Beque in T. 9 S., R. 97 W., and the other west of De Beque in T. 8 S., R. 97 W. The vertebrate-bearing Plateau Valley beds of Patterson are not sufficiently distinctive to be distinguished easily from the main body of the lower member of the Wasatch formation, and they are not differentiated on the map.

In the De Beque area the Wasatch formation is everywhere underlain by conglomeratic sandstone, the Ohio Creek conglomerate, which is the oldest Tertiary unit.

REFERENCE

Patterson, Bryan, 1939, New *Pantodonta* and *Dinocerata* from the upper Paleocene of Western Colorado: Field Mus. Nat. History Pub. 1441, Geol. ser., v. 6, no. 24, p. 351–384.

62. DIAMICTITE FACIES OF THE WASATCH FORMATION IN THE FOSSIL BASIN, SOUTHWESTERN WYOMING

By J. I. TRACEY, JR., S. S. ORIEL, and W. W. RUBEY, Washington, D .C., Denver, Colo., and Los Angeles, Calif.

Unsorted mudstone breccia forms an extensive facies of the Wasatch formation around the northern periphery of the Fossil basin ("Fossil syncline") north and west of Kemmerer, Wyo. The breccia consists of mixed angular fragments of rock of Mesozoic and Paleozoic age, some of them more than 20 feet across, in a pebbly red mudstone matrix.

The mudstone breccia fits the definition of the term diamictite recently proposed by Flint, Sanders, and Rodgers (1960a, b) for "terriginous sedimentary rocks that contain a wide range of particle sizes." Similar or related deposits of about the same age have been noted in other parts of Wyoming by Knight (1937), Love (1939, p. 60–62), Tourtelot (1957, p. 5, 21), Keefer (1958), and Soister (1960). The rocks resemble fanglomerate described by Sharp (1948) from the Bighorn Mountains, the Ridgway and Gunnison "tillites" from Colorado (Van Houten, 1957), and many mudflows and "lahar" (volcanic mudflow) deposits, although little or no volcanic material is present.

Upper Paleozoic and Mesozoic rocks of the southern part of the Wyoming overthrust belt form the structural framework of the Fossil basin, which contains variegated mudstone, sandstone, and conglomerate of the Wasatch formation, and laminated limestone, marlstone, claystone, and oil shale of the Green River formation, both of Eocene age. As in other regions (Sears and Bradley, 1924; Bradley, 1926), sequences of the laminated beds of the Green River are separated by tongues of the Wasatch formation, showing periodic encroachment of fluvial sediments into lakes in which the Green River formation was deposited. The diamictite facies of the Wasatch apparently formed during most of this period of deposition, for it grades in some places into normal variegated beds of the main body of the Wasatch formation, below basal Green River strata, and in other places it spreads out over uppermost Green River strata.

Diamictite overlies older rocks of the thrust belt on Dempsey Ridge [1] in the Tunp Range, along the Great Basin–Colorado River Divide, and it forms large fanlike masses projecting into the Dempsey Basin along the east side of Dempsey Ridge, as in the NW¼ sec. 15, T. 24 N., R. 118 W. These fan-like masses are large aprons of material, in part deltas, dumped into the borders of the Green River lake, as shown in several places where as many as three tongues of limestone of the Green River formation pinch out westward within the diamictite; an example is in the S½ sec. 3, T. 23 N., R. 118 W.

Thicknesses of the diamictite facies cannot be measured accurately at most localities. Maximum thicknesses probably do not exceed 500 feet. Despite moderate ranges in thickness, the facies is remarkably continuous along strike, but thins basinward to an edge within one to several miles.

Rock of the diamictite facies, more than 100 feet thick, fills remnants of channels cut in older rock across the crest of Rock Creek Ridge, 2 miles west of Dempsey Ridge. It is also found in Rock Creek valley, between exposures on Rock Creek Ridge and on Dempsey Ridge; rocks on the west are 500 to 1,000 feet lower than on Dempsey Ridge, whose western flank coincides with a normal fault.

Most common boulders and blocks are from the Mesozoic Ankareh formation, Nugget sandstone, Twin Creek limestone, Preuss sandstone, and Ephraim conglomerate, and from the upper Paleozoic Wells and Amsden formations. Blocks of quartzitic conglomerate from the Ephraim are especially common locally and are the coarsest; some are up to 20 feet in length.

The extraordinary range in particle sizes of the deposits is striking. A complete gradation of shapes and angularity, as well as concentrations, of coarse fragments is also evident. Orientation of blocks is not evident; the deposits seem chaotic or jumbled.

Gravitational sliding and solifluction seem to us the most probable explanations of origin. Deposits filling channels cut into older rocks likely originated as mudflows. Slopes forming the margins of the basin in Eocene time were steep and deeply weathered, and the hillsides and drainageways in times of abnormal rainfall were probably choked with debris that was being moved basinward.

Normal faulting since Wasatch time has greatly altered topographic relations. The nearest present outcrop of Ephraim conglomerate that might have

---

[1] Localities cited here are shown on U.S. Geological Survey topographic sheets for the Sage, Kemmerer, and Cokeville quadrangles, unless otherwise noted.

served as a source for the material along Dempsey Ridge is 6 miles west and more than 2,000 feet lower.

Other exposures of the diamictite facies are found along the northeast periphery of the Fossil basin, on the western slopes of Commissary Ridge. Large blocks of upper Paleozoic to Upper Cretaceous rocks were derived from formations that underlie the Ridge. In places they are in a pebbly red mudstone matrix, in others they lie free on a gently sloping surface and probably are relict blocks of the diamictite facies.

Large accumulations of rubble on Boulder Ridge, north and south of Sage station in the Sage quadrangle, may be part of the diamictite facies. The boulders and blocks come mostly from Paleozoic limestones exposed now in the Crawford Range some miles to the southwest. One very large block of Ordovician dolomite 2 miles north of Sage is more than 600 feet long. Others are 40 to 60 feet long.

About 4 miles south-southwest of Sage, in parts of secs. 25, 35, and 26, T. 21 N., R. 120 W., a large mass of steeply dipping Cambrian, Ordovician, and Devonian limestone and dolomite, 3,800 feet long, 1,400 feet wide, and 200 feet high, seems to be surrounded and underlain by Lower Cretaceous mudstone and sandstone. Rocks composing this mass strike nearly normal to similar Paleozoic strata exposed ½ to 3 miles northwest and southwest in the northern part of the Crawford Mountains. The mass may be a klippe of the nearby Crawford thrust plate; possibly it is merely a slid block similar in origin to, though differing greatly in scale from, the rubble that makes up the bulk of the diamictite facies.

A diamictite facies of the Wasatch formation has also been recognized along the western margin of the Green River basin south of LaBarge Creek in the Fort Hill quadrangle, where it was previously mapped by Schultz (1914, pl. 1) as the conglomeratic Almy formation of the Wasatch group. The facies intertongues here, also, with the Green River formation and is not, at least in this area, older than the main body of the Wasatch formation, as generally supposed.

Farther north along the western margin of the Green River Basin, a lower member of the Wasatch formation, consisting of pebbly red mudstone and some large blocks, extends almost continuously for 40 miles or more northward along the east sides of Deadline and Meridian Ridges, to Horse Creek in the Big Piney quadrangle and beyond. Throughout the region the diamictite facies may have accumulated soon after the major overthrust plates had moved into their present positions. In a few places, however, as in the northern part of Deadline Ridge, in the S½ sec. 32, T. 29 N., R. 114 W., the diamictite is involved in the thrusting. Distribution of the facies was evidently controlled by proximity to steep slopes and mountainous relief, the growth of which need not have coincided more than generally in time and place with final movements of the thrust plates.

REFERENCES

Bradley, W. H., 1926, Shore phases of the Green River formation in northern Sweetwater County, Wyoming: U.S. Geol. Survey Prof. Paper 140–D, p. 121–131.

Flint, R. F., Sanders, J. E., and Rodgers, John, 1960a, Symmictite: a name for nonsorted terrigenous sedimentary rocks that contain a wide range of particle sizes: Geol. Soc. America Bull., v. 71, p. 507–510.

———— 1960b, Diamictite, a substitute term for symmictite: Geol. Soc. America Bull., v. 71, p. 1809.

Keefer, W. R., 1958, Cenozoic landslides versus klippen [abs.]: Geol. Soc. America Bull., v. 69, no. 12, pt. 2, p. 1732.

Knight, S. H., 1937, Origin of the giant conglomerates of Green Mountain and Crook's Mountain, central Wyoming [abs.]: Geol. Soc. America Proc. 1936, p. 84.

Love, J. D., 1939, Geology along the southern margin of the Absaroka Range, Wyoming: Geol. Soc. America Spec. Paper 20, 134 p.

Schultz, A. R., 1914, Geology and geography of a portion of Lincoln County, Wyo.: U.S. Geol. Survey Bull. 543, 141 p.

Sears, J. D., and Bradley, W. H., 1924, Relations of the Wasatch and Green River formations in northwestern Colorado and southern Wyoming: U.S. Geol. Survey Prof. Paper 132–F, p. 93–107.

Sharp, R. P., 1948, Early Tertiary fanglomerate, Big Horn Mountains, Wyoming: Jour. Geology, v. 56, no. 1, p. 1–15.

Soister, P. E., 1960, Landslide debris from Cretaceous rocks in the Wind River formation of early Eocene age, Wind River basin, Wyoming [abs.]: Geol. Soc. America Bull., v. 71, no. 12, pt. 2, p. 1982–1983.

Tourtelot, H. A., 1957, The geology and vertebrate paleontology of upper Eocene strata in the northeastern part of the Wind River basin, Wyoming, pt. 1, Geology: Smithsonian Misc. Coll., v. 134, no. 4, 27 p.

Van Houten, F. B., 1957, Appraisal of Ridgway and Gunnison "tillites," southeastern Colorado: Geol. Soc. America Bull., v. 68, p. 383–388.

63.   TONGUES OF THE WASATCH AND GREEN RIVER FORMATIONS, FORT HILL AREA, WYOMING

By S. S. ORIEL, Denver, Colo.

———————

Three tongues of the Green River formation and two tongues (as well as the main body) of the Wasatch formation, all of early Eocene age, have been recognized during mapping of the Fort Hill quadrangle.

The Fort Hill 15-minute quadrangle lies on the western margin of the Green River basin in western Wyoming, about 15 miles north of the town of Kemmerer. The Green River and Wasatch formations crop out in eastward-dipping cuestas that extend northward through the quadrangle. These cuestas have been cut by eastward-flowing tributaries of Green River. The facies relations (fig. 63.1) between the two formations are well exposed in steep bluffs along these tributaries.

The lower tongues were recognized and described by Donavan [1] (1950).

The main body of the Wasatch formation consists chiefly of variegated red, yellow, buff, purple, green, and gray mudstone with interbedded marlstone, sandstone, and lentils of conglomerate. The unit becomes increasingly conglomeratic westward.

The Fontenelle tongue of the Green River formation (Donavan, 1950, p. 63–64; Bradley, 1959, p. 1072) conformably overlies the main body of the Wasatch formation. Only the basal 50 to 60 feet of strata assigned to the Fontenelle by Donavan at his type section [2] and in adjoining areas is here included in the unit. As thus restricted, the tongue consists of very thinly laminated light-gray to white muddy limestone, marlstone, calcareous very fine grained sandstone, and calcareous mudstone.

A wedge of detrital rocks, about 250 feet thick in the Fort Hill quadrangle, overlies the Fontenelle tongue and is here assigned to the New Fork tongue of the Wasatch formation. The New Fork tongue consists dominantly of green and gray mudstone with numerous lenses of yellow, buff, and brown, very fine- to medium-grained sandstone. The basal 20 to 45 feet is locally thinly laminated; most of the sequence is like the Wasatch formation in coarseness of the mudstone bands but lacks the characteristic shades of red and purple. These beds grade laterally westward into mudstone and sandstone beds in which red is the dominant color, as in the SW1/4SW1/4 sec. 15 and NW1/4 sec. 26, T. 26 N., R. 114 W.

The New Fork tongue of the Wasatch formation is overlain by an unnamed middle tongue of the Green River formation. The middle tongue is divisible into two readily distinguishable and mappable units; a lower white unit composed mainly of white-weathering low-grade oil shale and white to gray limestone, and an upper buff to brown, locally pink, gray, or white limestone, marlstone, mudstone, siltstone, and sandstone unit. Both units are very thinly laminated and both grade westward into thicker bedded organic limestone of nearshore facies (Bradley, 1926) as do the other tongues of the formation.

Another wedge of detrital rocks composed mainly of green and gray mudstone and yellow to brown sandstone overlies the middle tongue of the Green River formation. This wedge, here informally designated the upper tongue of the Wasatch formation, is 200 feet thick in the central part of the Fort Hill quadrangle but only 100 feet thick along its eastern margin. This eastward thinning is due to eastward tonguing with algal and ostracodal limestone and laminated marlstone assigned to the Green River formation.

The uppermost unit of the sequence, directly beneath the Bridger formation, is here termed the upper tongue of the Green River formation. Rocks included are thinly and evenly bedded to laminated, tan, yellow to brown, and gray limestone, marlstone, mudstone, siltstone, and sandstone, particularly ostracodal, gastropodal, and algal limestone.

Recognition of the relations between the Green River and Wasatch formations in the Fort Hill area has been hampered by the presence of the two wedges of detrital rocks that do not fit original descriptions and definitions of either of the formations.

The name Wasatch was originally applied by Hayden (1869, p. 91) to variegated sandstone and claystone in which some shade of red predominated; the emphasis on red hues was again stressed in a later description (1870, p. 106, 113–114). The name Green River, on the other hand, was applied by

[1] Donavan, Jack H., 1950, Intertonguing of Green River and Wasatch formations in part of Sublette and Lincoln Counties, Wyoming: M.S. Thesis, Univ. Utah.

[2] Donavan, Jack H., 1950, Intertonguing of Green River and Wasatch formations in part of Sublette and Lincoln Counties, Wyoming: M.S. thesis, Univ. Utah. Donavan's type section, no. 7 (p. 40–41), is located erroneously in his description but is shown properly on his geologic map in the NW¼ sec. 13, T. 24 N., R. 115 W.
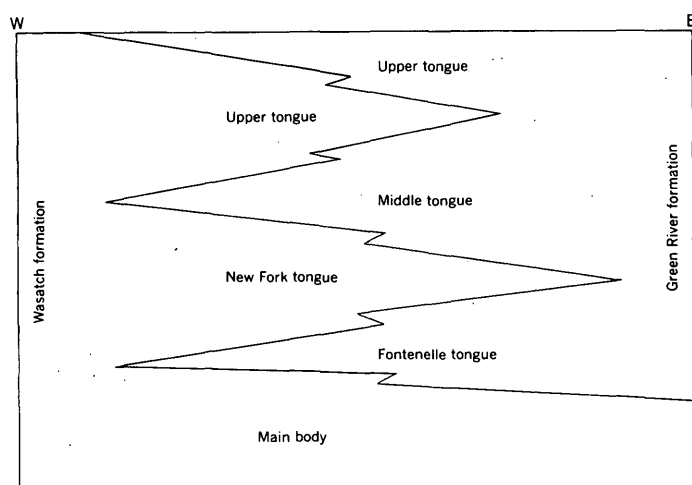
FIGURE 63.1.—Idealized section of Wasatch and Green River units in the Fort Hill area, Wyoming.

Hayden (1869, p. 90–91) to "thinly laminated chalky shales" which locally include "combustible or petroleum shales"; the peculiarly banded appearance of the rocks was stressed, although the abundance of limestone in the great range of compositions of the laminae was recognized. Emphasis in original descriptions, therefore, was on color for one unit and on primary structure for the other.

Some subsequent usage of the terms, however, has stressed genesis. Rocks considered to be of fluvial origin were assigned to the Wasatch formation; those of lacustrine origin to the Green River formation. Lack of assurance regarding the origin of the green mudstone—brown sandstone facies, however, makes adoption of this criterion impractical.

Rocks assigned here to the New Fork tongue of the Wasatch formation were included by Donavan (1950) in the Fontenelle tongue of the Green River formation in the Fort Hill area where they consist of green, not red, mudstone and brown sandstone. Beds similar to these, on the other hand, make up the bulk of the sequence assigned to the New Fork tongue (Donavan, 1950) farther north in its type area where, however, basal strata include red, brown, and purple mudstone. Color seems to have influenced the stratigraphic assignment.

Rocks in the two wedges of green mudstone and brown sandstone lack the dominant reds typical of the Wasatch formation yet do not contain the laminae diagnostic of the Green River formation. The absence of red is not unusual because green mudstone and yellow to brown sandstone form narrow, intermediate facies between more typical exposures of the two formations at many places elsewhere in the Green River and Fossil basins. Moreover, an absence of red may be expected close to the ancient lake in which the Green River formation was deposited, because of poor drainage and reducing conditions in contrast to the well-drained alluvial soils of higher elevations.

The two wedges of detrital rock are assigned here to the New Fork and unnamed upper tongues respectively of the Wasatch formation because:

1. Although dissimilar in color, the rocks are similar in every other respect (including composition, primary structures, and faunal content) to those commonly and originally assigned to the Wasatch.

2. The rocks are similar in every respect, including color, to some that are included in the formation at many other localities.

3. Assignment to the Wasatch formation facilitates recognition, through stratigraphic nomenclature, of two significant geologic events along the western margin of the Eocene Gosiute Lake, both marked by extensive deposition of detrital material advancing from the west and possibly by eastward regressions of the lake.

REFERENCES

Bradley, W. H., 1926, Shore phases of the Green River formation in northern Sweetwater County, Wyoming: U.S. Geol. Survey Prof. Paper 140–D, p. 121–131.

——— 1959, Revision of stratigraphic nomenclature of Green River formation of Wyoming: Am. Assoc. Petroleum Geologists Bull., v. 43, no. 5, p. 1072–1075.

Donavan, J. H., 1950, Intertonguing of Green River and Wasatch formations in part of Sublette and Lincoln Counties, Wyoming, in Guidebook to southwest Wyoming: Wyoming Geol. Assoc. 5th Ann. Field Conf., p. 59–67.

Hayden, F. V., 1869, Preliminary field report (3d ann.) of the U.S. Geol. Survey of Colorado and New Mexico, 155 p.

——— 1870, Sun pictures of Rocky Mountain scenery, with a description of the geographical and geological features and some account of the resources of the Great West: New York, 150 p.

64.   AGE OF THE EVANSTON FORMATION, WESTERN WYOMING

By W. W. Rubey, S. S. Oriel, and J. I. Tracey, Jr., Los Angeles, Calif., Denver, Colo., and Washington, D. C.

Renewed interest has arisen concerning the age of the Evanston formation because it provides a means for dating precisely some tectonic events in the thrust belt of western Wyoming. The formation was long of interest because of its bearing on the Laramie problem and therefore on the boundary between the Cretaceous and Tertiary systems (Veatch, 1907, p. 86-87; Schultz, 1914, p. 70-71).

The Evanston formation was formally named by Veatch (1906, p. 332) and defined (1907, p. 76) to include strata that were earlier referred to informally as the "Evanston beds" and "Evanston coal series." No type section was designated. Veatch's criteria (1907, p. 77) for distinguishing the formation from the underlying Adaville formation and from overlying strata, which he assigned to the Wasatch group, are still valid. Veatch failed to recognize the Evanston over much of its extent, however, and distinguished it (see his pl. 3) in only a few small areas near the town of Evanston.

Disagreements among paleontologists regarding the age of fossils found within the Evanston formation led Veatch (1907, p. 84-87) to discuss the problem at length. The age, he concluded tentatively, was early Tertiary, but he used the symbol KTe to designate the unit on maps and cross sections.

Geologists other than Schultz (1914, p. 68) have not made use of the Evanston formation as a mappable lithologic unit. Beds north of the type area formerly assigned to the Evanston by Schultz were defined as the Hoback formation by Eardley and others (1944).

Extensive exposures of the Evanston formation have been mapped by us in the Cokeville, Kemmerer, and Sage quadrangles, Lincoln County, and Big Piney quadrangle, Sublette County, Wyo. The belt of the rocks assigned by Veatch (1907, pl. 3) to his Almy formation in the eastern part of the Fossil basin belongs in the Evanston formation as well as scattered exposures well within the basin which he assigned to his Knight formation. Our assignment of these rocks to the Evanston is supported both by Veatch's published description and by comparison of certain distinctive rock types in the quadrangles mentioned with those in exposures at the type area. Exposures of the unit in both areas are similar in gross aspect and in some details, although not identical because of facies differences typical of continental strata.

Fossils in the Evanston formation in the Kemmerer, Sage, and Cokeville quadrangles include vertebrates, fresh-water invertebrates, leaves, and pollen. Ages inferred from these varied fossil forms are in agreement.

Vertebrates from near the base of the formation include the jaw of *Triceratops* cf. *T. flabellatus* Marsh, indicating probable Lance (=Hell Creek), latest Cretaceous age (G. E. Lewis, written communication, 1958), and numerous unidentifiable dinosaurian bone fragments indicative only of Mesozoic age. Mollusca from strata near but above the vertebrate horizon are different from those of Paleocene age and are regarded of probable Cretaceous or early Paleocene age (D. W. Taylor, written communication, 1960).

Leaves found about 50 feet above the base of the Evanston formation, about 20 miles north of the vertebrate localities, were identified by J. A. Wolfe (written communication, 1959) as *Dryophyllum subfalcatium* Lesquereux, *Cinnamomum linifolium* Knowlton, and *Dombeyopsis obtusa* Lesquereux and assigned a Lance (latest Cretaceous) age. A collection from a nearby locality yielded *Protophyllocladus subintegrifolius* (Lesquereux) Berry, *Ficus planicostata* Lesquereux, and *Cinnamomum affine* Lesquereux, also of Late Cretaceous age (R. W. Brown, written communication, 1958).

Fourteen species of pollen were identified from mudstone samples collected at one of the leaf localities. The presence of *Proteacidites annularis* Cookson, as well as other forms, indicates the samples are no younger than Late Cretaceous (E. B. Leopold, written communication, 1959).

Pollen species identified in samples from mudstone close to the *Triceratops* locality are even more varied; 32 species were recognized. The species *Schizaeoisporites pseudodorogensis* Potonié, *Osmundacidites wellmannii* Couper, *Proteacidites annularis* Cookson, and associated forms confirm the Late Cretaceous age of these rocks (E. B. Leopold, written communication, 1959).

Fossils found near the middle of the Evanston formation include Paleocene, possibly middle Paleo-

cene, leaves (R. W. Brown, written communication, 1958) and pollen (E. B. Leopold, written communication, 1959).

A varied vertebrate fauna has been reported 250 to 300 feet below the top of the unit by Gazin (1956, p. 708) who interprets the presence of *Plesiadapis* cf *P. fodinatus* Jepsen, *Pheocodus* sp., and other genera to indicate an early late Paleocene (Tiffany) age. No fossils have been found in uppermost strata assigned to the formation.

Additional collections of leaves and pollen from exposures in other parts of the Sage, Kemmerer, and Cokeville quadrangles confirm the Cretaceous and Paleocene age of the Evanston formation in this area.

Cretaceous age assignments for parts of the Evanston formation in the quadrangles under study are not in accord with the Paleocene age inferred for the unit in its type area some 30 miles to the south in earlier reports (for example, Brown, 1949; Eaton, 1955, p. 116).

The apparent discrepancy in age led us to re-examine exposures of the formation in its type area. The thickest section reported by Veatch (1907, p. 80) lies along the boundary between the western parts of secs. 18 and 19, T. 16 N., R. 120 W., north of the old settlement at Almy and is regarded by us as the informal reference section.

Fossils were collected by us directly below and above a main coal bed north of the old No. 7 mine (Veatch, 1907, pl. 3). Leaves were examined by R. W. Brown (1958), mollusks by D. W. Taylor (1960), and pollen by E. B. Leopold (1959, 1960), who conclude they indicate a Paleocene age.

No megascopic fossils were found considerably below the main coal bed. Samples of mudstone col-

lected directly above and below the horizon of the lowest conglomerate layer mentioned by Veatch (1907, p. 80), however, contain an assemblage of pollen of latest Cretaceous age (E. B. Leopold, written communication, 1961). Among the more critical species are *Aquilapollenites quadrilobus* Rouse, *Appendicisporites tricornitatus* Weyland and Greifeld, and *Proteacidities annularis* Cookson. The possibility that these forms are reworked from older rocks is considered unlikely.

Collections from the type area, therefore, seem to confirm the Cretaceous and Paleocene age of the Evanston formation, to verify the age assignments made by Knowlton and Stanton some 60 years ago (Veatch, 1907, p. 86–87), and to support Veatch's use of the map symbol KTe.

REFERENCES

Brown, R. W., 1949, Paleocene deposits of the Rocky Mountains and Plains: U.S. Geol. Survey prelim. map, scale 1:1,000,000, with descriptive notes.

Eardley, A. J., and others, 1944, Hoback-Gros Ventre-Teton [Range, Wyo.], field conference: Michigan Univ. geol. map, tectonic map, with sections, 2 sheets.

Eaton, E. C., 1955, Catalog of formations for Green River Basin and Adjacent areas, *in* Guidebook to the Green River Basin: Wyoming Geol. Assoc. 10th Ann. Field Conf., p. 114–121.

Gazin, C. L., 1956, The occurrence of Paleocene mammalian remains in the Fossil basin of southwestern Wyoming: Jour. Paleontology, v. 30, no. 3, p. 707–711.

Schultz, A. R., 1914, Geology and geography of a portion of Lincoln County, Wyoming: U.S. Geol. Survey Bull. 543, 141 p.

Veatch, A. C., 1906, Coal and oil in southern Uinta County, Wyoming: U.S. Geol. Survey Bull. 285–F, p. 331–353.

—— 1907, Geography and geology of a portion of southwestern Wyoming: U.S. Geol. Survey Prof. Paper 56, 178 p., 26 pl.

⚒

65. PERMAFROST AND THAW DEPRESSIONS IN A PEAT DEPOSIT IN THE BEARTOOTH MOUNTAINS, NORTHWESTERN WYOMING

By WILLIAM G. PIERCE, Menlo Park, Calif.

The discovery of permanently frozen ground in a peat deposit in the southeastern part of the Beartooth Mountains, northwestern Wyoming, is of interest because permafrost is of infrequent occur-

rence this far south in the Rocky Mountains. Associated with it are numerous thaw ponds, which indicate the presence of permafrost.

The Sawtooth peat deposit, named from Sawtooth

Mountain half a mile to the north, is in the western part of the Deep Lake quadrangle, at latitude 44°53'N. It is at an altitude of 9,700 feet, a few hundred feet below timberline in this area. The peat extends over an area 1,500 feet wide and 2,000 feet long and has an estimated thickness of 10 to 15 feet. Peat is not forming here now, but rather is being removed by erosion. The deposit lies in a broad northwest-trending valley that appears to be downfaulted on its southwest side. The shape and appearance of the valley suggest that it may be a pre-Wisconsin ice-scoured valley. The broad valley in which the peat was deposited is part of the Beartooth Mountains subsummit surface (peneplain of Bevan, 1925), a deeply weathered pre-Wisconsin surface developed on Precambrian granitic and gneissic rocks. During the most recent glaciation, presumably Wisconsin, deep valleys on three sides of the deposit were filled with ice that came up to about the level of the subsummit surface, but the peat deposit was not glaciated.

Two shallow holes were dug in the peat on August 24, 1956. At a depth of 15 inches a sharp contact between moist peat above and a solid frozen mass of ice and peat below was found in both holes. Although excavation into the solidly frozen peat was continued for only a few inches, it seems probable that the ice extends downward some distance in the peat. The deposit was visited again on July 30, 1957, and several additional holes were dug. Near the previous holes, solidly frozen peat occurred at a depth of 18 inches. A hole in the previously untested southern part of the deposit, which is marshy and grass-covered, also reached ice at a depth of 18 inches.

Patterned ground, in the form of polygons 5 to 10 feet across, is conspicuous in places (fig. 65.1). The polygons are in the peat and consist of shallow trenches separating slightly convex areas. They may have been formed by ice-wedges in the peat. Even more striking, however, are circular undrained depressions in the central part of the peat deposit. Superficially they resemble sink holes, about 6 feet deep and from a few feet to 40 feet in diameter. Their nearly flat bottoms are covered by 2 to 3 feet of water. The peat at the margins of the depressions is slowly caving downward, as shown by marginal cracks (fig. 65.2), and by circular cracks beyond the margin. The depressions are not due to solution, for neither the peat nor the underlying Precambrian rocks are readily soluble. There is no evidence to indicate that they resulted from water or wind erosion.

FIGURE 65.1.—Patterned ground in the Sawtooth peat deposit. Hammer in center for scale.

The origin of the depression was discussed with D. M. Hopkins, who suggested that they are thaw depressions, formed by melting of the ice beneath. The irregular land surface produced by this process has been called thermokarst by Russian scientists and cave-in lakes are one of its surface features (Muller, 1945). Hopkins (1949) proposed the name "thaw lakes" as synonymous with cave-in lakes, and defined thaw depressions as depressions that result from subsidence following the thawing of perennially frozen ground. The depressions in the Sawtooth peat seem to be clearly thaw depressions, formed by melting of ice within the peat. The depressions probably started forming where slight irregularities in the ground surface permitted a

FIGURE 65.2.—Two thaw depressions in the Sawtooth peat deposit. The cracks in the walls of the depressions indicate lateral growth by downward caving of the peat. These two depressions have grown until they now coalesce. Hammer on bank in foreground for scale.

little water to accumulate. The water in the depressions kept the underlying peat wet and permitted downward thawing to continue in the depressions during the summer months, while beyond the depressions the dry peat insulated the ice beneath it. As the ice thawed the volume of the peat and ice lessened and the depression deepened.

The peat is not older than Pleistocene. A sample of the peat, obtained from about a foot below the eroded top of the deposit was submitted for examination for pollen and diatoms and for a carbon 14 age determination. K. E. Lohman found an assemblage of diatoms (USGS diatom loc. 4209) that is no older than late Pleistocene, and he reports that the same diatom assemblage is living today in cool to cold ponds. The radiocarbon age of the sample (laboratory number W–459) is reported by Meyer Rubin as 7,570 years, ± 400 years. The C_{14} age thus indicates that the upper part of the peat bed is post-Wisconsin in age, but the lower part of the bed may be of late Wisconsin age.

The presence of perennial ice indicates that the present climate is cold enough at the altitude and latitude of the Sawtooth peat to maintain perma-

frost provided there is a few feet of exceptionally good insulating cover. The permafrost in the Sawtooth peat has an antiquity greater than just the last few years, for the thaw depressions have been in the process of developing for some time. If the rate of retreat measured by Wallace (1948) on the margins of some cave-in lakes in eastern Alaska is applicable, then the time required to form the larger depressions may have been less than a hundred to a few hundred years. However, their growth may have been intermittent, and, if so, a longer time may be represented.

REFERENCES

Bevan, Arthur, 1925, Rocky Mountain peneplains northeast of Yellowstone Park: Jour. Geology, v. 33, p. 563–587.

Hopkins, D. M., 1949, Thaw lakes and thaw sinks in the Imuruk Lake area, Seward Peninsula, Alaska: Jour. Geology, v. 57, p. 119–131.

Muller, S. W., 1945, Permafrost or perennially frozen ground and related engineering problems: Office, Chief of Engineers, U.S. Army Spec. Rept. Strategic Eng. Study 62, p. 83–84.

Wallace, R. E., 1948, Cave-in lakes in the Nebesna, Chisana, and Tanana River valleys, eastern Alaska: Jour. Geology, v. 56, p. 171–181.

66.   EVIDENCE FOR EARLY CRETACEOUS FOLDING IN THE BLACK HILLS, WYOMING

By GLEN A. IZETT, CHARLES L. PILLMORE, and WILLIAM J. MAPEL,
Denver, Colo.

The Lakota formation of Early Cretaceous age and its lithogenetic equivalents the Kootenai formation in central Montana and the lower part of the Cloverly formation in Montana and Wyoming are fluviatile and lacustrine deposits that extend in a relatively thin sheet over several hundred thousand square miles in the Western Interior region. Regional stratigraphic relations indicate that over broad areas the surface on which these rocks were deposited was essentially undisturbed by folding or faulting. However, mapping of the Lakota and adjacent formations along the west side of the Black Hills has shown that in two areas, folds having amplitudes of more than 100 feet in horizontal distances of 2 to 3 miles were formed in Early Cretaceous time. Similar folds that might be concealed

by unconformably overlying rocks in the adjacent Powder River basin would have interest for their oil and gas possibilities.

Early Cretaceous folding is indicated by local angular unconformities within and bounding the Lakota formation at a small dome in Barlow Canyon in T. 54 N., Rs. 65 and 66 W., Crook County, Wyo., about 5 miles north of Devils Tower, and at a small dome bisected by Oil Creek in T. 47 N., R. 62 W., Weston County, Wyo., about 8 miles north of Newcastle (fig. 66.1). The sequence of beds and the stratigraphic relations at the two localities are shown by figure 66.2.

At Barlow Canyon, the Morrison formation and part of the Redwater shale member of the underlying Sundance formation of Late Jurassic age are trun-
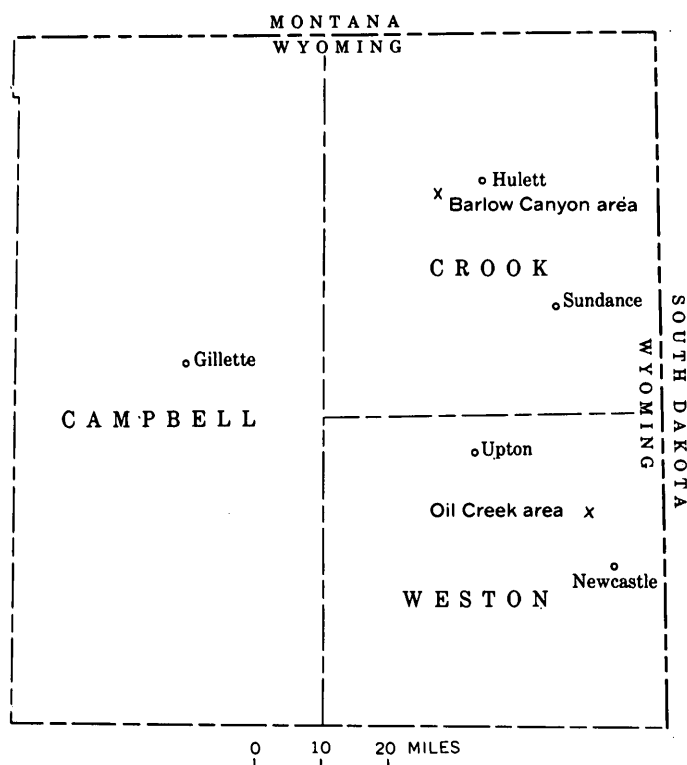
FIGURE 66.1.—Map showing location of Barlow Canyon and Oil Creek areas, northeastern Wyoming.

cated beneath an angular unconformity that dies out laterally in the basal part of the Lakota formation (fig. 66.2 *A*). Polished pebbles and cobbles of quartzite and chert in the basal part of the Lakota formation mark the position of the unconformity. At locality 3 (fig. 66.2 *A*), a basal conglomerate in the Lakota contains belemnite fragments derived from the underlying Redwater shale member of the Sundance. The Lakota thickens abruptly northward between localities 2 and 3 (fig. 66.2 *A*) in a manner that suggests the Lakota occupies a channel where the formation is thickest; however, folding and subsequent truncation of the upraised rocks probably accounts for the absence of most of the missing rocks in the Morrison and Sundance formations on the crest of the fold. The amplitude of the Early

Cretaceous fold at this locality is estimated to be about 125 feet, and the areal extent of the fold is about 4 square miles.

Two periods of folding can be recognized along Oil Creek (fig. 66.2 *B*). The lower part of the Lakota formation is truncated beneath an angular unconformity within the formation (locality 2), and the upper part is truncated beneath an angular unconformity at the base of the overlying Fall River formation (locality 3). At locality 2, the basal part of the Fall River formation contains granules and pebbles of quartzite and chert probably derived from erosion of the Lakota at the crest of the fold. The amplitude of the Early Cretaceous fold at Oil Creek is estimated to be about 200 feet, and the areal extent of the fold is about 2 square miles.

The limited extent of the folds in both areas suggests that folding was caused by local rather than regional forces. Redistribution of evaporites in the Spearfish (Triassic and Permian) or Minnelusa (Permian and Pennsylvanian) formations, which underlie the Lakota formation at shallow depths, seems a possible explanation for the folding. Repeated episodes of folding such as occurred at Oil Creek might indicate repeated episodes of flowage.

In both the Barlow Canyon and Oil Creek areas, the normally clayey Morrison formation grades laterally to massive fine-grained well-sorted grayish-white sandstone that in lithology and stratigraphic position resembles the Unkpapa sandstone—a thick sandstone that replaces the Morrison in the southern and eastern parts of the Black Hills (Darton and Paige, 1925, p. 11). Thick sandstone lenses are unusual in the Morrison on the west side of the Black Hills, and their occurrence at both folds suggests that the sandstone and the folds are related. No evidence was found of appreciable folding during deposition of the Morrison, however, and the relation, if any, is unknown.

REFERENCE

Darton, N. H., and Paige, Sidney, 1925, Description of the central Black Hills [with contributions by J. D. Irving]: U.S. Geol. Survey Geol. Atlas, Folio 219, 34 p.

A. BARLOW CANYON AREA

B. OIL CREEK AREA

FIGURE 66.2.—Sections showing truncated sedimentary rocks, Sundance, Morrison, and Lakota formations, west side of Black Hills, Wyo.

67.   STRUCTURE OF THE CLARK FORK AREA, IDAHO-MONTANA

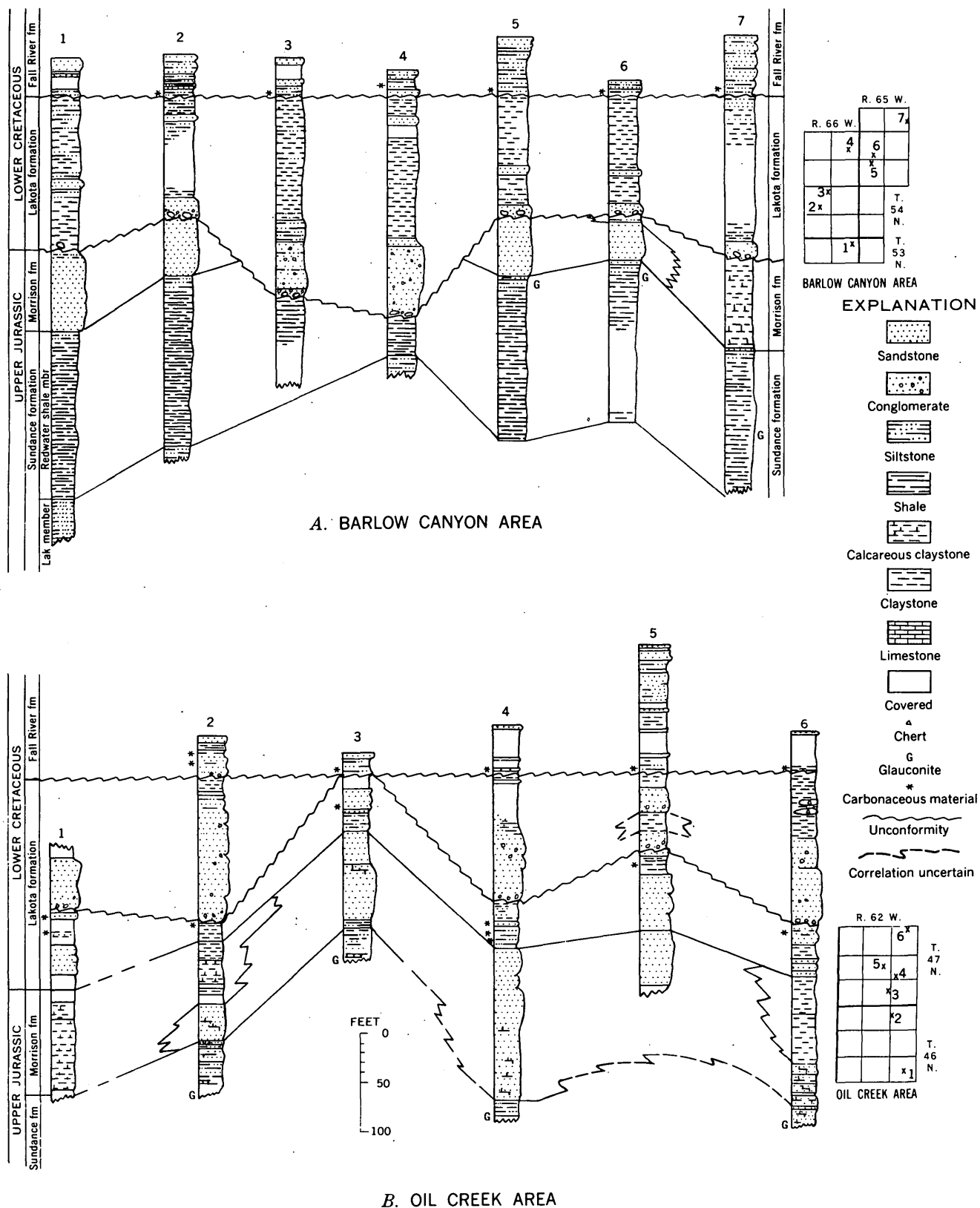By J. E. HARRISON, D. A. JOBIN, and ELIZABETH KING, Denver, Colo., and Washington, D. C.

Rocks of the Belt series of Precambrian age have been intruded north of the Hope fault by quartz diorite of Precambrian age (the Purcell sills), and both north and south of the fault by granodiorite of probable Cretaceous age (fig. 67.1). The Belt series here consists of about 40,000 feet of argillites, siltites, very fine grained quartzites, limestone, and dolomite. The granodiorite, which occurs as small plutons and sills scattered throughout most of the mapped area, is virtually identical chemically and petrographically with granodiorite in stocks exposed in the southwestern part of the Packsaddle Mountain quadrangle and with granodiorite in the Selkirk batholith (Gillson, 1927) which borders the Packsaddle Mountain quadrangle on the north.

The regional structural setting is relatively simple. The Hope fault, trending north-northwest across the area, separates a homocline in the Belt rocks to the north from a syncline to the south. The Hope fault also separates an intricate mosaic of steep-sided fault blocks to the south from a simpler mosaic to the north.

South of the Hope fault most of the blocks in the eastern part of the area are only slightly tilted and show folds only as drags near each fault. The dip of the beds increases westward in the west limb of the major syncline, and this regional dip has been increased further by tilting of some blocks in the western part of the area. In addition, many of the western blocks show internal folding throughout the block, though blocks that show extensive folding commonly are adjacent to blocks that show only drag folding near the faults. The bounding faults are steep to vertical, as is shown by the nearly straight traces of the faults across a topographic relief of about 4,000 feet. Some of the faults that are subparallel in strike appear to converge downward, and a few converge upward. Axes of drag folds are nearly horizontal and thus indicate dip-slip movement on the faults.

North of the Hope fault the blocks are at most slightly tilted. The principal interruption of the regional homocline is a zone, about 1,500 feet wide, of small folds that wrap around the exposed pluton of granodiorite.

Metamorphic grade of pelitic rocks is shown by numbers on figure 67.2. Samples indicated by 1's contain sericite and/or chlorite, but no secondary biotite. Samples indicated by 2's contain a little secondary biotite but still retain most of their original clastic texture. Samples indicated by 3's contain abundant secondary biotite and retain little or no original clastic texture.

Correlation between magnetic intensities, exposures of intrusive rocks, and metamorphic grade is excellent (fig. 67.2). Each area of exposed intrusive rocks shows up as a positive magnetic anomaly, and the Belt rocks of higher metamorphic grade are adjacent to intrusive masses or to positive anomalies. Study of Belt rocks near exposures of intrusive rocks suggests that only Belt rocks within about 2,000 feet of an intrusive body reached grade 3, so the positive magnetic anomalies where no intrusive rocks are exposed most likely represent buried but shallow plutons. The positive anomaly southeast of Clark Fork is the only one that does not have grade 3 rocks around it, and perhaps represents a slightly deeper intrusive body. Because Precambrian quartz diorite is known here only in sills in the Prichard formation and only north of the Hope fault (Anderson, 1930, pl. 14), all positive anomalies except the two at the north-central edge of the area probably represent bodies of Cretaceous(?) granodiorite.

Four of five joint sets common in the Belt rocks of the area are subparallel to four principal sets of block faults. It seems unlikely that the joints, which are products of tension, were formed at the time of the faults, which are products of shear.

An interpretation of the data available to date is shown in figure 67.3. The position of these sections is shown on figures 67.1 and 67.2. The structural rise from right to left in the sections is accompanied by a general stepping down of the blocks in the same direction. Some of the structural rise is toward an anticlinal crest, but part of it may also be due to upward pressure from a rising magma. If all the pressure had been upward, then sets of shear planes dipping about 45° should have formed, as they commonly do over salt domes. Because the faults are steep, they probably reflect a fracture pattern, perhaps originally expressed only by joints, established during regional folding. Local folding within certain of the keystone blocks, however, must have been in response to an upward punch, for some of the keystones are upside down (bounding faults known to converge upward); only an upward push
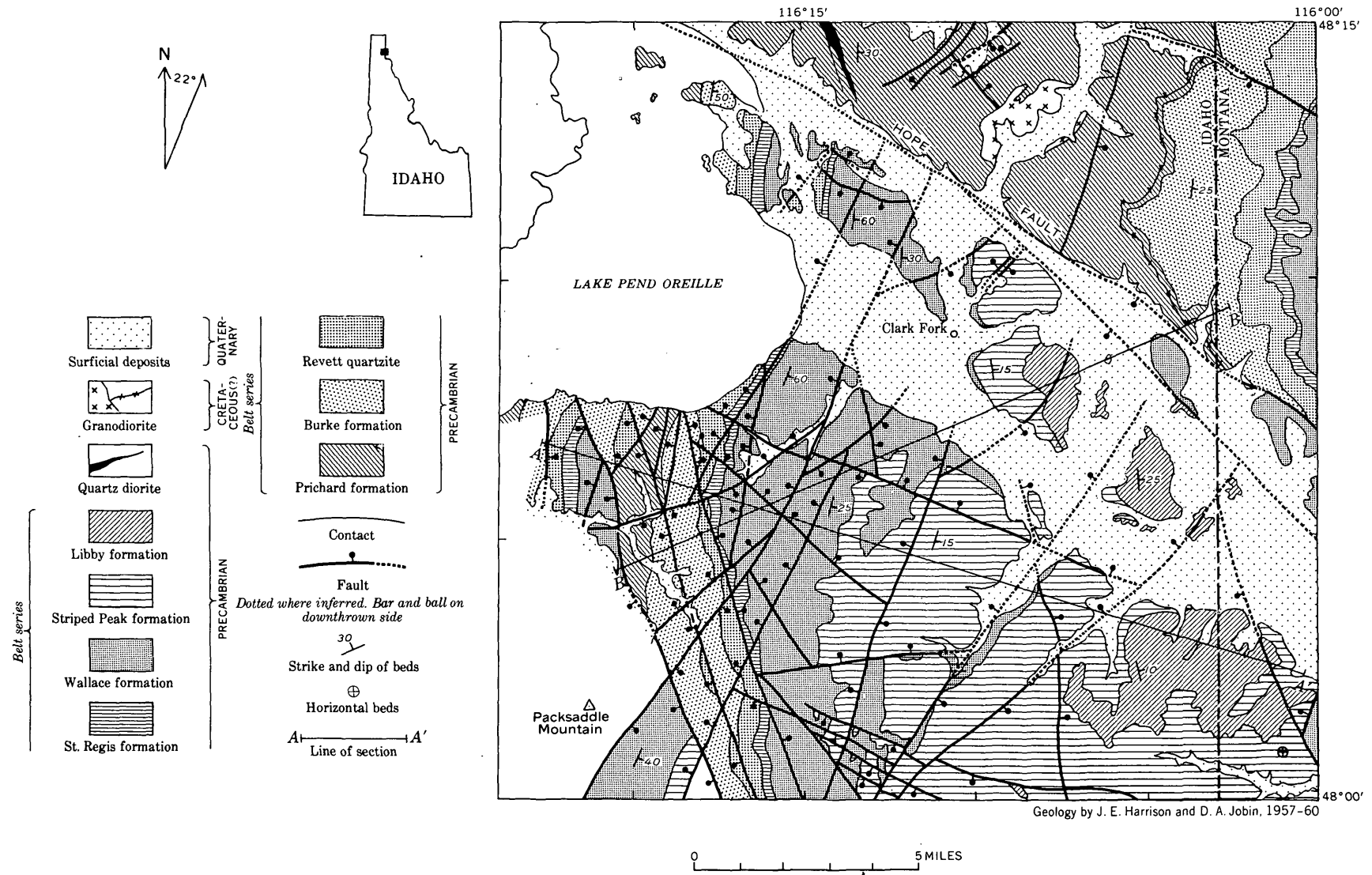
FIGURE 67.1.—Generalized geologic map of the Clark Fork quadrangle and part of the Packsaddle Mountain quadrangle, Idaho-Montana.

EXPLANATION

Cretaceous(?) granodiorite

Precambrian quartz diorite

Fault
*Bar and ball on
downthrown side*

1, 2, 3
Metamorphic grade of Belt
rocks
See text for explanation

—200—
Total intensity aeromagnetic
contour
*Dashed where inferred. In-
terval 50 gammas; contours
between 50-gamma interval
shown only where needed
to identify anomalies. Con-
tours based on 32 aerial
traverses south of the Hope
fault and 3 tie lines north
of it*

Geology in southwestern part of
map after Sampson, 1928, pl. 2

Aeromagnetic survey by J. L. Meuschke
and Elizabeth King, 1959

0   5 MILES

FIGURE 67.2.—Total intensity aeromagnetic map of the Clark Fork and Packsaddle Mountain quadrangles, showing intrusive rocks, faults, and metamorphic grade of Belt rocks.
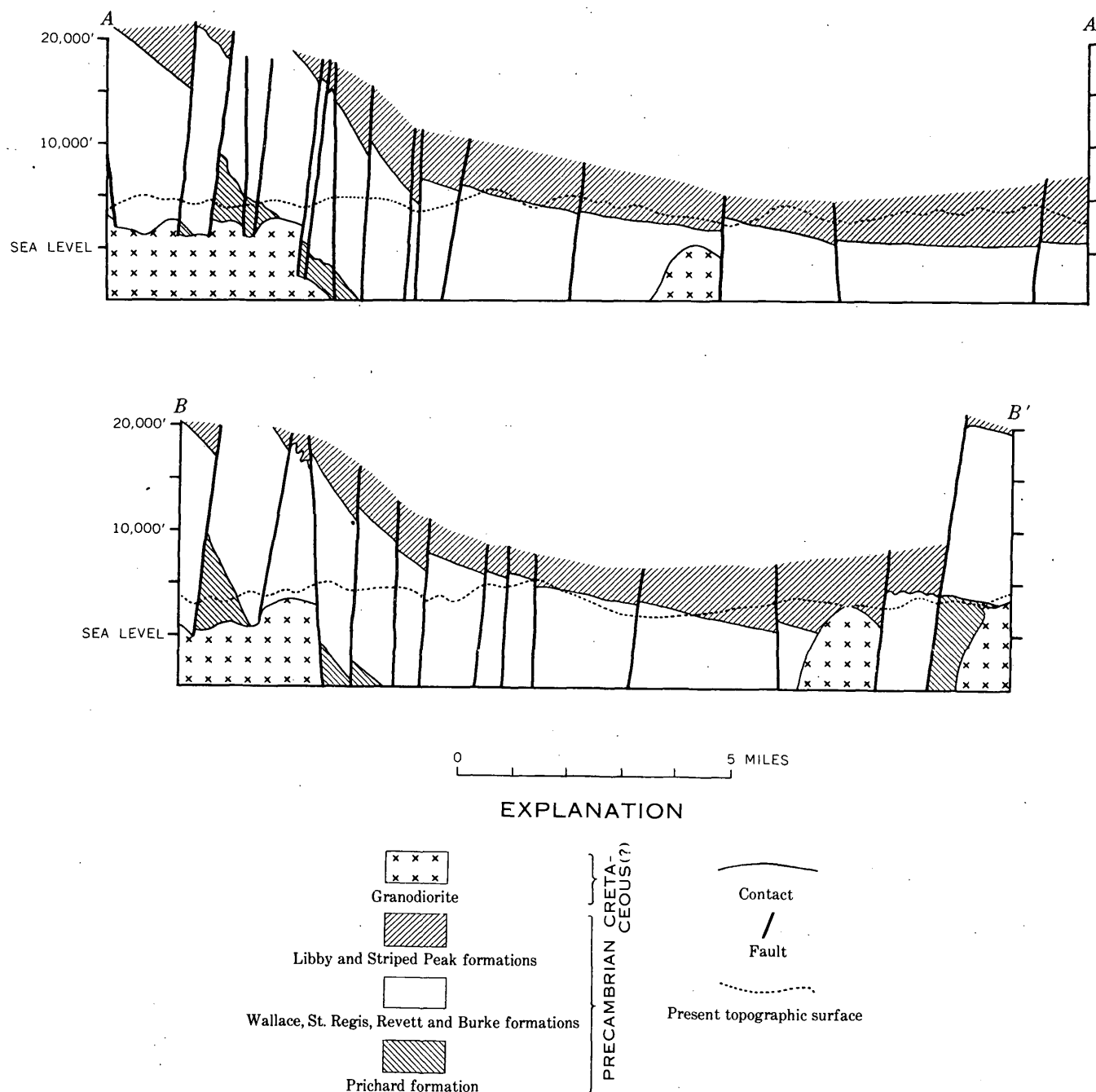
FIGURE 67.3.—Diagrammatic sections showing relation of blocks to intrusive rocks.

of these inverted keystones could cause the local lateral pressure required for the folding. The pattern of stepping down towards the main intrusive mass suggests collapse.

We infer the following sequence of events: Regional folding and fracturing; an upward push from a magma, particularly in the crest of the regional anticline; and block mosaic faulting and adjustment of the blocks over the magma. The adjustment con-

sisted of collapse in the flanks and crestal part of the syncline and of a combination of upraising and collapse in the anticlinal crest. Sampson (1928) has suggested a somewhat similar origin for a series of "intrusion faults" in the nearby Pend Oreille mining district. We suggest that the large intrusive mass in the Packsaddle Mountain quadrangle and the smaller masses northeast of it are cupolas on a batholith that extends under the whole area and

perhaps connects with the Selkirk batholith. The lack of block tilting, relatively small displacement of blocks, and the obvious shouldering aside of rocks adjacent to one of these cupolas lead us to infer that collapse over this large underlying mass was accompanied by intrusion of magma into the blocks by a process that included some shouldering aside.

REFERENCES

Anderson, A. L., 1930, Geology and ore deposits of the Clark Fork district, Idaho: Idaho Bur. Mines and Geology Bull. 12, 132 p.

Gillson, J. L., 1927, Granodiorites in the Pend Oreille district of northern Idaho: Jour. Geology, v. 35, p. 1–31.

Sampson, Edward, 1928, Geology and ore deposits of the Pend Oreille district, Idaho: Idaho Bur. Mines and Geology Pamph. 31, 25 p.

68.   PLEISTOCENE GEOLOGY OF THE CENTRAL PART OF THE LEMHI RANGE, IDAHO

By EDWARD T. RUPPEL and MORTIMER H. HAIT, JR., Denver, Colo., and Pennsylvania State University, University Park, Pa.

Pleistocene deposits in the central part of the Lemhi Range, in east-central Idaho, reflect the repeated occurrence of glacial or near-glacial climatic conditions during Pleistocene time (Dort, 1960). The earliest glaciation, probably in early Pleistocene time, left deposits that are now preserved at altitudes as low as 6,400 feet, well out in front of the moraines of later glaciations, west of the village of Leadore, and on a few interstream divides in the mountains. These deposits consist of unsorted pebbles, cobbles, and boulders of quartzite, and, rarely, small fragments of dense volcanic rock, which retain no distinctive glacial form; they have been so extensively eroded that they remain only as gravel veneers. The remains of a preglacial surface beneath the gravel veneers, and the probably related relatively broad, gently sloping interstream divides characteristic of the lower parts of the central Lemhi Range suggest that much of this surface was a pediment above which the higher part of the range seems to have been subdued and rounded.

Glacial deposits considered to be early Pleistocene in age have been recognized at only a few places in central Idaho; conspicuous among these places are the Whitecloud Peaks (Ross, 1929, p. 123–128; 1937, p. 93–95) and Stanley Basin [1] in south-central Idaho, and the Salmon River and Beaverhead Mountains near Salmon, Idaho (Anderson, 1956, p. 31–32).

The early glaciation was followed by a period of erosion during which much of the glacial debris was removed, and canyons were carved to depths of several hundred feet below the earlier surface. When this erosional period was interrupted by a second period of glaciation (probably in early Wisconsin time) the topography appears to have been much like today's except that it lacked the extreme features of alpine erosion, because the relations of the deposits of this stage to present topography suggest little deepening of valleys since the beginning of the second stage. The deposits of the second stage lie inside the deposits of the early stage in the Swan Basin, and are made up of quartzite, a small percentage of volcanic rock—appreciably more than in the early till—and rare fragments of dolomite, in a sand and silt matrix. The moraines of this stage are smoothed and rounded, drainage is well integrated in and across the moraine, and areas underlain by the moraine are characterized by irregularly distributed low rounded hills and shallow intervening basins. Trains of outwash extend out from the moraine in a few places.

The third, probably late Wisconsin, glacial stage is represented by deposits still more restricted than those of the second stage. The deposits contain abundant quartzite and abundant unweathered dolomite and volcanic rocks in a sand and silt matrix. Related outwash fans and small valley trains containing the same types of rock extend beyond the moraine in some places, and conceal older moraine and bedrock. The deposits are characterized also by slight modification of their original form, and by unintegrated drainage; soil development has been

[1] Williams, Paul L., 1957, Glacial geology of the Stanley Basin, Idaho: Washington Univ., Master of Science thesis.

slight to moderate on the deposits, and vegetation covers them in many places.

. A fourth glacial stage is represented by moraines deposited when ice reoccupied small sheltered cirques above an altitude of 9,000 feet. The topographic setting of these cirques seems to have offered maximum protection against ablation and to have favored snow accumulation, perhaps especially through retention of snow blown over the cirque walls into the cirque. The larger cirques do not contain moraines; their openness makes them more accessible than the sheltered cirques to the winds that almost constantly blow at the higher altitudes in the Lemhi Range, and probably snow could not accumulate as readily under such conditions. The larger cirques contain deposits of waste rock in talus, protalus ramparts, and small rock streams, that are probably contemporaneous with the moraines in the small cirques, for both have thin soils and very sparse vegetation.

The stage of cirque glaciation and related mass wasting was followed by a later stage of mass wasting in which waste rock accumulated in talus, protalus ramparts, and rock streams in many cirques and canyons; these deposits conceal older glacial and mass-wasting deposits and clearly are the youngest surficial deposits, other than stream deposits, in the central Lemhi Range. They are characterized by an absence of any soil or of drainage development, and by frontal slopes as steep as 40°; the growth of lichens on the rock fragments suggests that the deposits are not now receiving much rock waste or moving—but their fresh appearance strongly suggests that they represent a very recent period of more rigorous climate than that prevailing today.

Other mass-wasting deposits not clearly related to any one period of glacial or near-glacial climate are widespread below the lower limit of glacial deposits on Leadore Hill, south of Leadore. These deposits lie in canyons below remnants of the preglacial surface and several are near remnants of the early glacial·till but at altitudes well below the till and in canyons that clearly have been deepened many hundreds of feet since the early glacial stage. The deposits on the west flank of Leadore Hill are principally talus, most of which is now apparently stable or nearly so, as it is covered by a thin soil and by vegetation. The deposits on the east flank of Leadore Hill are diverse in form and origin, and include deposits on creep slopes, and deposits in mudflows, landslides, talus, protalus ramparts, and nivation moraine. The deposits on creep slopes are most widespread, and although many of them are now covered with vegetation, tilted trees and tears in the sod cover suggest that soil creep is still active. The deposits are clearly younger than the early glacial deposits, and probably began to form under the rigorous climatic conditions that prevailed at these lower altitudes during the later alpine and cirque glaciations in the higher parts of the Lemhi Range.

REFERENCES

Anderson, A. L., 1956, Geology and mineral resources of the Salmon quadrangle, Lemhi County, Idaho: Idaho Bur. Mines and Geology, Pamph. 106, 102 p.

Dort, Wakefield, Jr., 1960, Multiple glaciation, east side of Lemhi Range, Idaho [abs.]: Geol. Soc. America Bull., v. 71, no. 12, p. 1852.

Ross, C. P., 1929, Early Pleistocene glaciation in Idaho: U.S. Geol. Survey Prof. Paper 158–G, p. 123–128.

———— 1937, Geology and ore deposits of the Bayhorse region, Custer County, Idaho: U.S. Geol. Survey Bull. 877, 161 p.

⚒

69.   THE MICHAUD DELTA AND BONNEVILLE RIVER NEAR POCATELLO, IDAHO

By DONALD E. TRIMBLE and WILFRED J. CARR, Denver, Colo.

Late Pleistocene gravel at and near Pocatello, Idaho has been named the Michaud gravel (Trimble and Carr, in press). The Michaud gravel was deposited as a delta in the Pleistocene American Falls lake by an ancient stream, the Bonneville river of Gilbert (1890, p. 176), which drained glacial Lake Bonneville.

The Michaud gravel extends from the mouth of the Portneuf River canyon at Pocatello southwestward for about 18 miles almost to American Falls
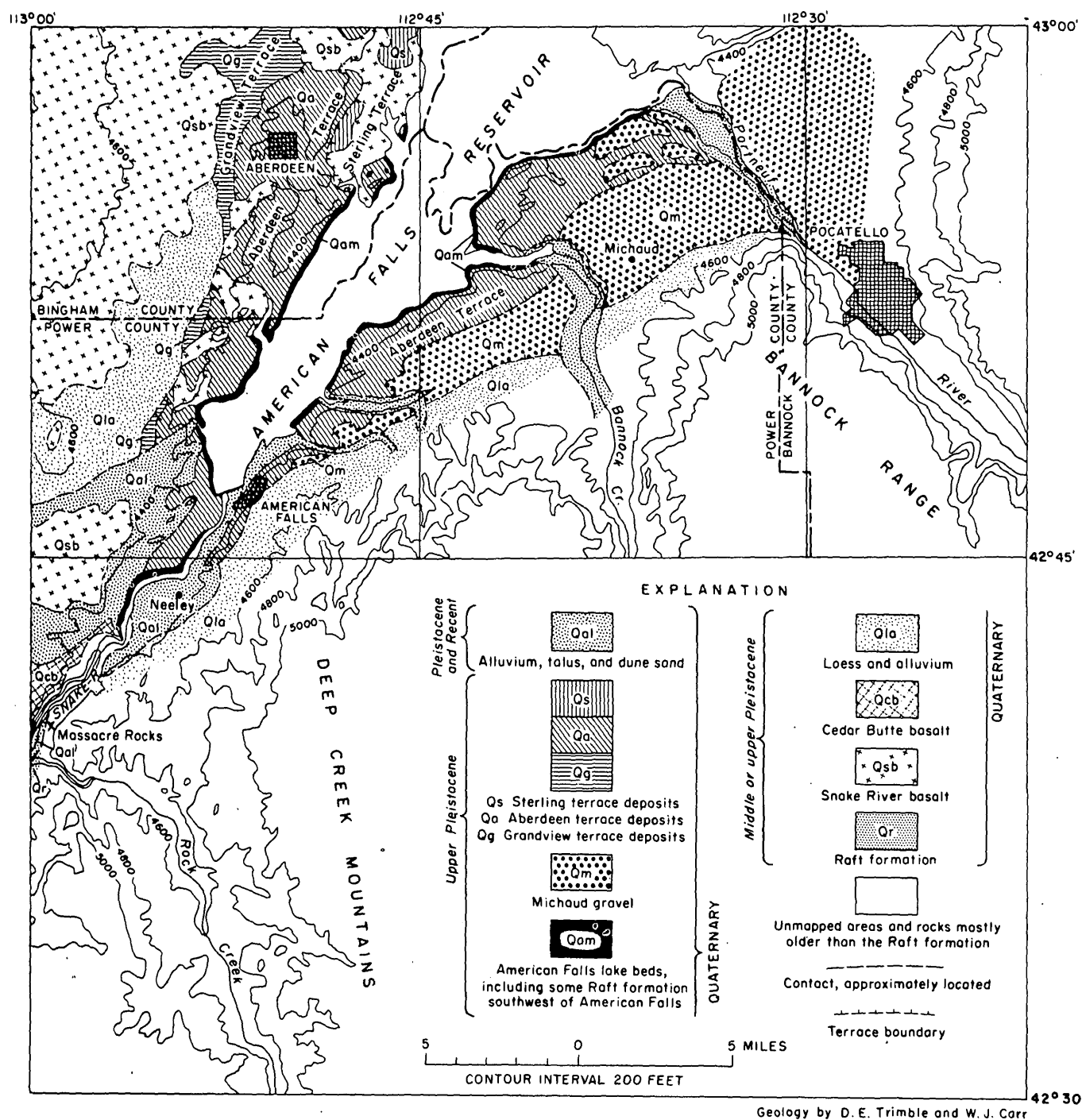
FIGURE 69.1.—Sketch map of the American Falls-Pocatello area showing generalized distribution of upper Quaternary rocks.

(fig. 69.1). It rests conformably on the unweathered surface of the American Falls lake beds, and it is limited areally at most places by two scarps, an upper one against which the gravel was deposited, and a lower one which is a lake-cut scarp at the back of the younger Aberdeen terrace (fig. 69.1).

The surface of the Michaud gravel was terraced, scoured, and channeled, and the prominent Aberdeen terrace, which is partly lacustrine and partly fluviatile, was cut on the gravel on the east side of the American Falls reservoir. The scours and channels are higher and older than the Aberdeen terrace, or are graded to it.
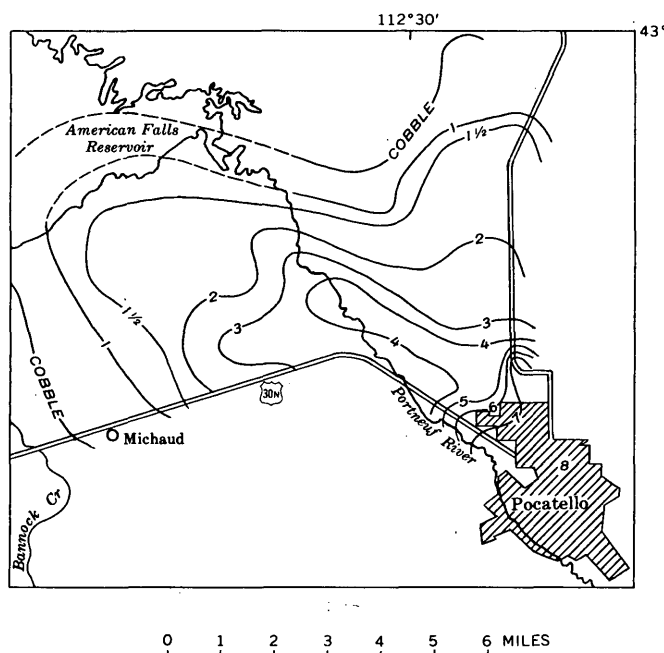
FIGURE 69.2.—Distribution of maximum boulder size in the Michaud gravel. Contours (in feet) of size larger than cobble. Dashed where no control available.

The Michaud gravel is 50 to 80 feet thick. The basal contact of the Michaud gravel with the American Falls lake beds is uniformly about 4,400 feet in altitude, and its upper surface ranges from about 4,450 to 4,480 feet in altitude.

The distribution of maximum boulder size in the Michaud gravel was mapped during the summer of 1960 (fig. 69.2). The contours show the rapid decrease in size away from the mouth of the Portneuf River canyon. At Pocatello, the gravel consists mainly of large boulders derived almost entirely from the Portneuf valley. East of Bannock Creek, near Michaud, the deposit is a cobbly gravel, but west of Bannock Creek it is a pebbly sand. Correlative deposits consisting mainly of fine sand and silt cover the Grandview terrace west of the American Falls reservoir (fig. 69.1).

The maximum diameter of boulders (about 8 feet) in the Michaud gravel at Pocatello suggests that the transporting stream had an unusually high velocity. Observations of Barrell, cited by Rubey (1952, p. 71), imply that stream velocities of between 4 and 12 miles per hour are necessary to move a cobble about 6 inches in diameter. Inasmuch as the radius of the largest object moved by a stream varies with the

square of the velocity, an 8-foot boulder probably indicates a current velocity of between 16 and 48 miles per hour. These are very broad and approximate limits, but when this general order of magnitude is compared with a median velocity of 3.54 miles per hour for the Mississippi River during one of its greatest floods (Rubey, 1938, p. 137), and with a maximum recorded velocity of about 16 miles per hour for any natural stream (Howard F. Matthai, oral communication, 1960), it is evident that the stream responsible for the Michaud gravel attained abnormal size and velocity, at least temporarily. Such a great stream in the Pocatello area could only have been the river flowing from Lake Bonneville. Other evidence of flooding along the Bonneville river has been discussed by Malde (1960, p. B295–B297).

The Michaud gravel has been dated late Pleistocene on the basis of mollusks (D. W. Taylor, written communication, 1960) and vertebrates, including Bison alleni (Hopkins, 1951, p. 195), found in the gravel. Now, however, the age of the Michaud gravel (and the time of overflow of Lake Bonneville) can be more nearly fixed. A radiocarbon date (W–929) for a peat layer 13 feet below the top of the American Falls lake beds is > 42,000 years B.P. (before present) according to Meyer Rubin (written communication, 1961), and shells (W–731) from the Aberdeen terrace deposit are dated at 29,700 ± 1,000 years B.P. (Trimble and Carr, in press). The Michaud gravel probably was deposited, therefore, about 30,000 to 40,000 years ago.

REFERENCES

Gilbert, G. K., 1890, Lake Bonneville: U.S. Geol. Survey Mon. 1, 438 p.
Hopkins, M. L., 1951, Bison (Gigantobison) latifrons and Bison (Simobison) alleni in southeastern Idaho: Jour. Mammalogy, v. 32, p. 192–197.
Malde, H. E., 1960, Evidence in the Snake River Plain, Idaho of a catastrophic flood from Pleistocene Lake Bonneville, in Short papers in the geological sciences: U.S. Geol. Survey Prof. Paper 400–B, p. B295–B297.
Rubey, W. W., 1938, The force required to move particles on a stream bed: U.S. Geol. Survey Prof. Paper 189–E, p. 121–141.
—— 1952, Geology and mineral resources of the Harden and Brussels quadrangles (in Illinois): U.S. Geol. Survey Prof. Paper 218, 179 p.
Trimble, D. E., and Carr, W. J., (in press), Late Quaternary history of the Snake River in the American Falls region, Idaho: Geol. Soc. America Bull.

70. VOLCANIC ASH BEDS AS STRATIGRAPHIC MARKERS IN BASIN DEPOSITS NEAR HAGERMAN AND GLENNS FERRY, IDAHO

By HOWARD A. POWERS and HAROLD E. MALDE, Denver, Colo.

The upper Cenozoic detrital deposits exposed along the Snake River downstream from Hagerman, Idaho, contain numerous thin beds of siliceous volcanic ash that are indistinguishable in the field but that differ significantly in physical and chemical properties. By study of these properties several distinctive ash beds have been identified in discontinuous, widely separated outcrops. These ash beds can be used to demonstrate the stratigraphic relations of deposits otherwise devoid of marker beds, and they are indispensable, therefore, for recognizing facies changes and basin deformation. This paper describes two such beds of volcanic ash in a formation of late Pliocene and early Pleistocene age near Hagerman and Glenns Ferry.

Significant chemical comparisons of volcanic ash beds require laboratory separation of clean unaltered glass. The analyses given here are of glass shards scrubbed by ultrasonic agitation, separated from phenocrysts and other contaminants by flotation in diluted bromoform, and further cleaned by feeding through a Frantz magnetic separator. The cleaned shards in such samples are colorless and completely isotropic.

PETERS GULCH ASH LAYER

The Peters Gulch ash layer is named informally for Peters Gulch, 4 miles southwest of Hagerman, where sample E1810 was collected (fig. 70.1). The distinctive physical and chemical properties that identify this bed were determined from nine samples. Physically, the ash consists of about equal parts of extremely vesicular pumice grains and of complexly shaped glass shards, both of which are very weakly magnetic in the strong field of a Frantz separator. The particular combination of phenocrysts embedded in the glass shards (chevkinite, zircon, ilmenite, and magnetite) is different from the phenocryst assemblage in 60 samples from all other ash beds exposed in this region. (For descriptions of chevkinite in other ash beds, see Young and Powers, 1960.) Chemical analyses of glass shards separated from the ash are listed in table 1. Seven of the samples collected at various places along 3 miles of continuous outcrop from Peters Gulch northward indicate the variation found in amounts of constituents. Comparison with the 60 samples of other analyzed ash beds in this region shows that the Peters Gulch ash layer is highest in Cl, La, and Sn, and lowest in Ba and Sr. In brief, no other ash samples have the same combination of physical properties and chemical constituents.

Confident correlation of the Peters Gulch ash layer between localities as widely spaced as 24 miles (fig. 70.1) helps to reconstruct the terrain on which it was deposited. Where the ash is recognizable, it occurs as a bed a few inches thick, either in carbonaceous shale or in thin-bedded silt and clay. These fine-grained materials probably accumulated on a flood plain, as is suggested by paleoecological evidence and by sedimentary features (Malde and Powers, 1958). At the time of the ash fall this area may have been the floor of a broad, flat valley dotted with sloughs, shallow lakes, and a few channels along which the water moved sluggishly. Where the ash fell in slack water or on boggy ground, it had some chance for preservation as a recognizable bed, but where the ash fell in a channel, it was carried by currents and mixed with other debris.

The sedimentary equilibrium of a broad, flat valley implied by the fine-grained materials associated with the Peters Gulch ash layer is seemingly contradicted by the lithologic dissimilarities of the sediments that occur considerably above and below the beds in which the ash is found. At Peters Gulch the section consists dominantly of thin-bedded silt and clay with some fine sand and carbonaceous shale. In contrast, the section at King Hill consists of a massive sequence of coarse sand and fine gravel. At Clover Creek units of these different lithologies alternate. Such contrasting facies can be accounted for by the local geography. The deposits at Peters Gulch accumulated several miles from the margins of the basin, whereas those at King Hill were brought to the northern margin of the basin by steeply graded streams that drained granitic outcrops a few miles farther north. The mixed deposits at Clover Creek are in an intermediate position. The presence of the ash shows that sedimentation at these places was concurrent.

Differences in altitude of the Peters Gulch ash layer, as shown in figure 70.1, are mostly accounted for by displacements on high-angle faults that sep-

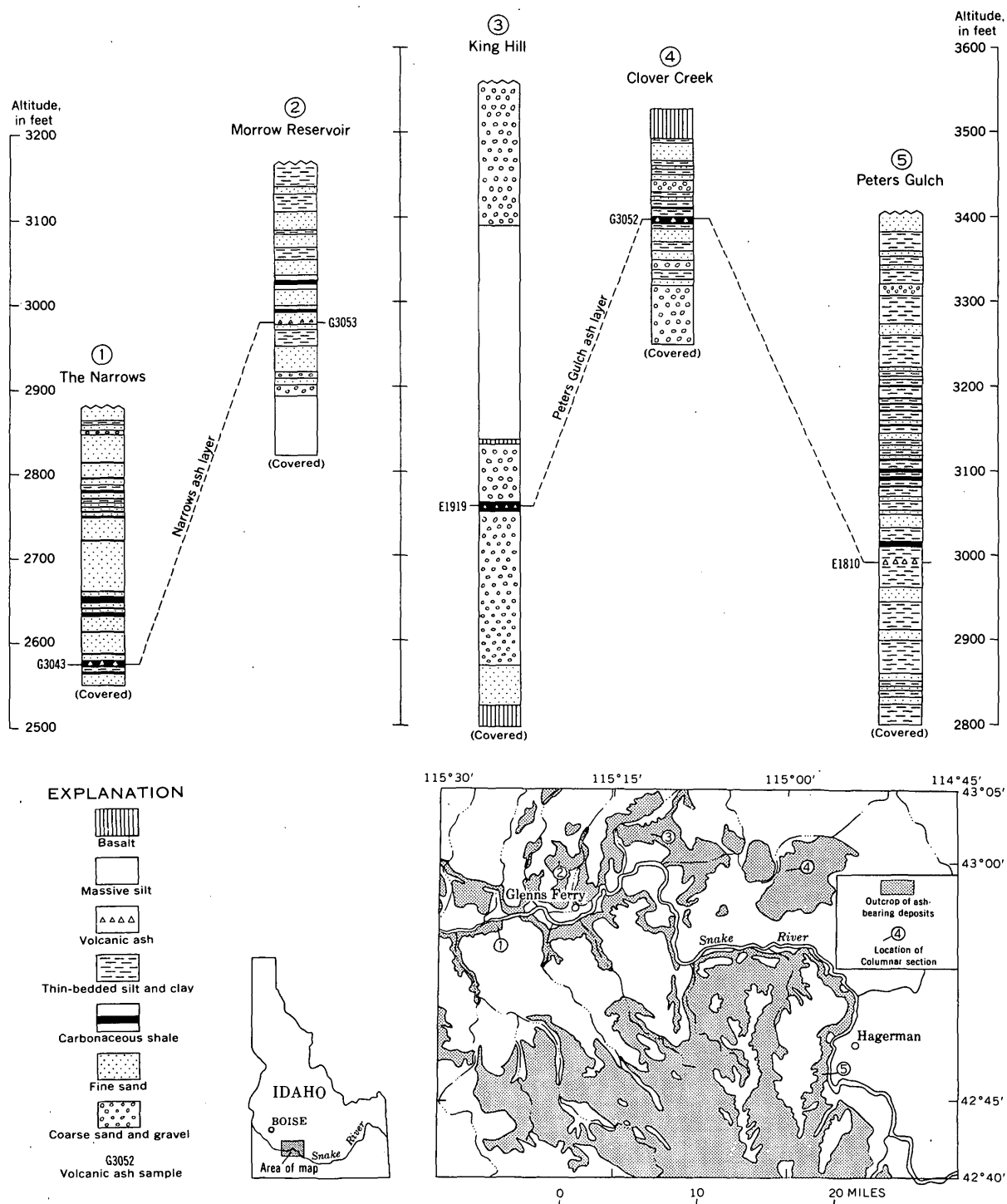FIGURE 70.1.—Generalized columnar sections and outline geologic map of ash-bearing deposits of late Pliocene and early Pleistocene age near Hagerman and Glenns Ferry, Idaho. Sections 1, 2, and 3 are each overlain by about 30 feet of basalt of middle Pleistocene age. Section 5 is overlain by 55 feet of alluvium of early Pleistocene age. The beds lie nearly horizontal at places where the sections were measured.

TABLE 1.—*Analyses of prepared samples of glass shards from the Peters Gulch ash layer*

[Chlorine analyses by V. C. Smith. Other chemical analyses as follows: sample E1810 by P. M. Montalta; samples E2308, B441, B443, E2309, B442, and B414 by L. N. Tarrant; sample E1919 by M. R. Kittrell; and sample G3052 by V. C. Smith. Quantitative spectrographic analyses by P. R. Barnett. ... indicates not determined.]

Sample No.	Location of sample	Chemical analyses														
		SiO_2	Al_2O_3	TiO_2	Fe_2O_3	FeO	MnO	MgO	CaO	Na_2O	K_2O	Cl	F	P_2O_5	CO_2	H_2O
E1810	Sec. 5 at Peters Gulch.....	69.82	12.49	0.12	0.77	1.10	0.05	0.13	0.59	2.32	6.72	.....	0.104	0.01	.....	5.19
E2308	1.9 mi. N. of Peters Gulch.	.....	.....							2.46	6.63	0.243	.103	.....	.....	5.10
B441	2.2 Do.................	.....	.....							2.48	6.34	.252	.098	.....	.....	5.29
B443	2.3 Do.................	.....	.....							2.42	6.57	.....	.098	.....	.....	5.07
E2309	2.6 Do.................	.....	.....							2.64	6.57	.252	.103	.....	.....	.....
B442	2.8 Do.................	.....	.....							2.43	6.33	.....	.098	.....	.....	5.05
B414	2.9 Do.................	69.56	12.35	.12	.77	1.10	.03	.08	.52	2.49	6.48	.....	.106	.00	.....	6.11
E1919	Sec. 3 near King Hill......	70.03	12.62	.13	.67	1.21	.04	.02	.56	2.26	6.16	.243	.103	.02	0.00	5.70
G3052	Sec. 4 at Clover Creek....	.....	.....	.....	.....	.....	.....	.....	.....	.....	.....	.....	.246	.106	.....	.....	.....

Sample No.	Location of sample	Quantitative spectrographic analyses														
		B	Ba	Be	Cu	Ga	La	Mo	Nb	Pb	Sn	Sr	V	Y	Yb	Zr
E1810	Sec. 5 at Peters Gulch.....	0.006	0.005	0.0011	0.0008	0.0033	0.014	0.0006	0.007	0.002	0.0011	0.0010	<0.0002	0.009	0.0008	0.043
E2308	1.9 mi. N. of Peters Gulch.	.007	.004	.0011	.0008	.0039	.008	.0004	.006	.002	.0009	.0008	<.0002	.006	.0007	.043
B441	2.2 Do.................	.006	.006	.0008	.0010	.0040	.014	.0006	.008	.002	.0012	.0009	<.0002	.009	.0008	.048
B443	2.3 Do.................	.005	.006	.0013	.0009	.0036	.016	.0005	.009	.002	.0012	.0008	<.0002	.011	.0008	.056
E2309	2.6 Do.................	.008	.005	.0010	.0009	.0038	.008	.0004	.006	.002	.0008	.0020	<.0002	.006	.0006	.040
B442	2.8 Do.................	.006	.007	.0011	.0010	.0038	.013	.0005	.007	.002	.0012	.0012	<.0002	.009	.0008	.046
B414	2.9 Do.................	.007	.003	.0012	.0009	.0036	.013	.0006	.007	.002	.0011	.0005	<.0002	.009	.0008	.039
E1919	Sec. 3 near King Hill......	.008	.008	.0010	.0008	.0034	.012	.0004	.008	.001	.0012	.0007	.0002	.008	.0007	.048
G3052	Sec. 4 at Clover Creek....	.007	.005	.0009	.0008	.0040	.009	.0004	.006	.002	.0009	.0005	.0002	.007	.0006	.030

arate the section at Clover Creek from King Hill and Peters Gulch.

THE NARROWS ASH LAYER

The Narrows ash layer is named informally for the Narrows, 5 miles west of Glenns Ferry, where sample G3123 was collected (fig. 70.1). The dis-tinctive combination of physical and chemical prop-erties that identify this bed were determined from three samples. Physically, the ash is made up of complexly shaped shards, some shards that are simply curved, and a few grains of pumice, all of which are nonmagnetic. The phenocrysts are brown hornblende, orthopyroxene, clinopyroxene, and mag-

TABLE 2.—*Analyses of prepared samples of glass shards from the Narrows ash layer*

[Chlorine and fluorine analyses by V. C. Smith. Chemical analysis of sample G3123 by D. F. Powers. Semiquantitative spectrographic analyses by R. G. Havens. ... indicates not determined.]

Sample No.	Location of sample	Chemical analyses														
		SiO_2	Al_2O_3	TiO_2	Fe_2O_3	FeO	MnO	MgO	CaO	Na_2O	K_2O	Cl	F	P_2O_5	CO_2	H_2O
G3123	Sec. 1 at the Narrows.....	72.18	12.40	0.22	0.47	0.64	0.04	0.26	1.14	2.92	4.34	0.115	0.020	0.04	0.01	4.70
G3053	Sec. 2 at Morrow Reservoir	.....	.....	.....	.....	.....	.....	.....	.....	.....	.....	.109	.016	.....	.....	.....
G3046	1 mi. S. of Morrow Res....	.....	.....	.....	.....	.....	.....	.....	.....	.....	.....	.115	.018	.....	.....	.....

Sample No.	Location of sample	Semiquantitative spectrographic analyses														
		B	Ba	Be	Cu	Ga	La	Mo	Nb	Pb	Sn	Sr	V	Y	Yb	Zr
G3123	Sec. 1 at the Narrows.....	0.002	0.07	<0.0001	0.0007	0.0007	<0.003	<0.0005	<0.001	<0.001	<0.005	0.007	0.001	0.001	0.0001	0.00
G3053	Sec. 2 at Morrow Reservoir	.003	.07	<.0001	.0007	.0007	<.003	<.0005	<.001	<.001	<.005	.007	.001	.001	.0001	.00
G3046	1 mi. S. of Morrow Res....	.003	.07	<.0001	.0007	.0007	<.003	<.0005	<.001	<.001	<.005	.007	.001	.001	.0001	.00

netite. Chemical comparison with the 60 samples of other ash beds in this region shows that the ash is very low in F, Ga, Y, Yb, and Zr (table 2).

The isolated outcrops where the Narrows ash layer is identified are not much alike and could not be correlated otherwise. The section at the Narrows is sandy with many beds of carbonaceous shale, whereas the section at Morrow Reservoir has fewer beds of carbonaceous shale and more layers of thin-bedded silt and clay. Apparently the ash fell on boggy ground or on a mud flat at the Narrows and in a body of slowly moving water at Morrow Reservoir.

The ash bed is now 400 feet lower in altitude at the Narrows than at Morrow Reservoir, but like the Peters Gulch ash layer it was probably de-posited on the floor of a broad, flat valley. If so, the present difference in altitude demonstrates moderate basin deformation. Because no faults were found during mapping, this difference in altitude is attributed to an average southwestward tilt of about 50 feet per mile.

The stratigraphic relation of the Peters Gulch ash layer to the Narrows ash layer has not been determined, but as more ash beds are identified a complete local sequence probably will be established.

REFERENCES

Malde, H. E., and Powers, H. A., 1958, Flood-plain origin of the Hagerman lake beds, Snake River Plain, Idaho [abs.]: Geol. Soc. America Bull., v. 69, no. 12, pt. 2, p. 1608.

Young, E. J., and Powers, H. A., 1960, Chevkinite in volcanic ash: Am. Mineralogist, v. 45, nos. 7–8, p. 875–881.

71. PATTERNED GROUND OF POSSIBLE SOLIFLUCTION ORIGIN AT LOW ALTITUDE IN THE WESTERN SNAKE RIVER PLAIN, IDAHO

By HAROLD E. MALDE, Denver, Colo.

A distinctive geometric pattern formed by soil mounds and stone pavements, which resembles the patterned ground of polar regions (Washburn, 1956), occurs on the dissected plateaus and marginal colluvial deposits north of the Snake River near Glenns Ferry, Idaho (figs. 71.1 and 71.2). The mounds and stone pavements are typically developed on gravel fans and on basaltic lava flows, but they are found also on such diverse materials as lake beds and welded tuff—all of middle Pleistocene or older age. Because the patterned ground is not developed on lithologically similar younger deposits in the same region, it is regarded as a relict landform. This paper concerns only the patterned ground in areas of basalt and gravel.

The soil mounds are monotonously uniform, particularly in relatively flat areas. A typical mound is circular, from 50 to 60 feet in diameter, and 3 feet high at the center. Generally the mounds are regularly spaced from 60 to 85 feet apart, measured from their centers. They are surrounded by a pavement of stones. Lithologically, the mounds consist mostly of friable light-colored silt that contains some angular fragments from the underlying rocks. These fragments usually are the size of pebbles, but a few are as large as cobbles and boulders. Below a depth of 18 inches the mound material is compact, loamy, and darker—seemingly a consequence of soil development—and rock fragments are more numerous. At a depth of 3 to 4 feet below the center of a mound, the mixture of silt and rock fragments grades downward rather abruptly into tightly packed gravel (or broken basalt), which emerges at the periphery of a mound to join the surrounding stone pavement.

The stone pavements that surround the mounds ordinarily consist of well sorted angular stones, which range from cobbles to boulders. A few of the stones are fractured. Depending on the spacing of the mounds, the pavement areas pinch and swell, in places being as much as 20 feet wide. At a few localities, where the mounds are far apart, the pavement areas form rubbly fields more than 100 feet across. The stones of the pavement that are tabular shaped commonly are oriented on edge and are turned parallel to the margins of the pavement so as to occupy the least space side-to-side (fig. 71.3).

FIGURE 71.1.—Vertical aerial photograph of patterned ground on part of a basalt plateau and on marginal blocky colluvium 9 miles northeast of Glenns Ferry, Idaho. The light colored spots on the plateau are mounds of silt covered with grass and sagebrush. The barren darker ground, which forms a network surrounding the mounds, consists of blocks dislodged from the underlying basalt. The light colored bands that trend downslope on the colluvium are also grass-covered silt. These strips of soil separate darker bands of sorted basalt fragments. The plateau slopes 1° southwestward, and the colluvium slopes 15° southeastward. The area shown is about 3,600 feet above sea level. [Enlarged from U.S. Department of Agriculture aerial photograph DLG–7G–98 taken Oct. 22, 1950.]

These upturned stones are so tightly wedged that several must be dislodged in order to remove one. They make the pavement comparatively rough, and large surface areas of the stones that comprise the pavement consequently are exposed to weathering. These stone surfaces are encrusted with lichens. Below the pavement layer the stones are smaller, less well sorted, and randomly arranged. In some basalt areas, stone fragments that are recognizably articulated with the underlying lava occur at a depth of 1 or 2 feet, and it is possible to walk at other places from a stone pavement onto a bare lava surface. In gravel areas, also, apparently undisturbed gravel occurs at a shallow depth.

The regular pattern expressed in flat areas by the soil mounds and stone pavements changes progressively to parallel bands of soil and stones as the angle of slope increases. Where the angle of slope is less than 1°, the mounds are fairly equally spaced and the stone pavements form rectangular or polygonal networks (area A of fig. 71.1). In areas of somewhat greater slope, where drainage channels are defined, the mounds are arranged in parallel rows separated by continuous gutterlike shallow troughs paved with stones (area B of fig. 71.1). On slopes of about 6°, the mounds are elliptical and the downhill sides of some encircling nets of stone pavement are broken so that adjacent mounds are connected down-
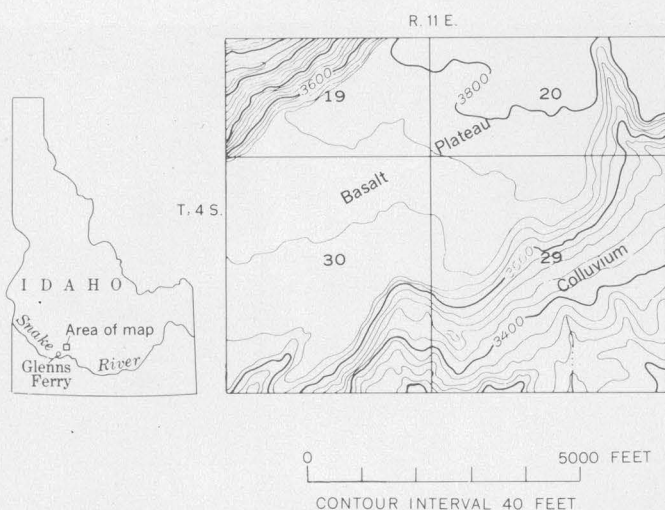
FIGURE 71.2.—Topographic map of the area 9 miles northeast of Glenns Ferry, Idaho, shown in the vertical aerial photograph reproduced as figure 71.1.

slope by a strip of soil (not well illustrated in fig. 71.1). At slope angles between 6° and 15°, most of the mounds are connected by such narrow strips of soil, much like beads on a string, and the pavement areas form continuous rocky bands. These alternate parallel bands of soil and stones trend directly downslope (area *C* of fig. 71.1). On slopes of 15° to 30°, the mounds along the bands of soil are indistinct, whereas lines of stone pavement are prominent (area *D* of fig. 71.1). On slopes steeper than 30°, a sorted pattern of soil and stones generally cannot be recognized.

Even though the patterned ground in flat areas differs from that on the slopes, the gradational change in pattern from one place to the other suggests that a similar process accounts for both. These gradational changes in pattern resemble the progressive modification of polygonal ground by solifluction on increasingly steeper slopes, as observed by Holmes and Colton (1960) near Thule, Greenland.

The soil mounds and stone pavements near Glenns Ferry apparently are now stable, as indicated by soil development and lichen growth, so the mechanism by which they formed can only be inferred. However, their great similarity to the patterned ground of polar regions implies development by frost sorting and by solifluction. If so, the patterned ground near Glenns Ferry may have developed during a former period of cooler and wetter climate.

Patterned ground that resembles the soil mounds and stone pavements near Glenns Ferry is reported elsewhere in the northwestern States. For example,

FIGURE 71.3.—A narrow stone pavement between soil mounds in an area of gravel at 3,900 feet altitude 12 miles north of Glenns Ferry, Idaho. Tabular stones are steeply or vertically oriented and are alined parallel to the margins of the pavement. The ruler is 7 inches long.

analogous patterned ground occurs on plateau basalt in eastern Washington and Oregon (Freeman, 1926; 1932; Waters and Flagler, 1929; and Kaatz, 1959) and on gravel fans and lava flows near Mount Shasta, California (Masson, 1949). A study of the distribution of such patterned ground, and a better understanding of its origins, could determine the former southward extent of cold and wet climatic conditions in this region and would help to establish ages for the land surfaces on which the pattern is found.

REFERENCES

Freeman, O. W., 1926, Scabland mounds of eastern Washington: Science new ser., v. 64, no. 1662, p. 450–451.

Freeman, O. W., 1932, Origin and economic value of the scabland mounds of eastern Washington: Northwest Sci., v. 6, no. 2, p. 37–40.

Holmes, C. D., and Colton, R. B., 1960, Patterned ground near Dundas (Thule Air Force Base), Greenland: Medd. om Grønland, v. 158. no. 6, 15 p.

Kaatz, M. R., 1959, Patterned ground in central Washington; a preliminary report: Northwest Sci., v. 33, no. 4, p. 145–156.

Masson, P. H., 1949, Circular soil structures in northeastern California: California Div. Mines Bull. 151, p. 61–71.

Washburn, A. L., 1956, Classification of patterned ground and review of suggested origins: Geol. Soc. America Bull., v. 67, p. 825–866.

Waters, A. C., and Flagler, C. W., 1929, Origin of the small mounds on the Columbia River Plateau: Am. Jour. Sci., 5th ser., v. 18, p. 209–224.

72. COLLAPSE STRUCTURES OF SOUTHERN SPANISH VALLEY, SOUTHEASTERN UTAH

By G. W. WEIR, W. P. PUFFETT, and C. L. DODSON, Menlo Park, Calif., Corbin, Ky., and Decatur, Ala.

Southern Spanish Valley, a few miles southeast of Moab, Utah, lies in a syncline of Mesozoic rocks that is superimposed on the subsurface salt-cored Moab anticline in late Paleozoic rocks (Baker, 1933; Shoemaker and others, 1958). On the east flank of the syncline are many small collapse structures (figs. 72.1 and 72.2). Most of the collapse structures are roughly oval in plan, a few hundred feet in diameter, and contain a mass of broken rock that has been dropped several hundreds of feet. They are found in all exposed formations from the Navajo sandstone (Triassic? and Jurassic) of the Glen Canyon group through a sandstone member of the Mancos shale (Upper Cretaceous)—a stratigraphic range of more than 3,000 feet. Although the vertical exposure of any of these collapse structures is only about 200 feet, they are inferred to be breccia pipes that extend several thousand feet below the surface.

Forty-five collapse structures were identified in and near southern Spanish Valley (fig. 72.1); an additional 33 collapse structures were noted in a reconnaissance north of this area to Moab. Most of the collapse structures lie on the east side of Spanish Valley within a northwest-trending belt that is about three-quarters of a mile wide and 10 miles long. The three collapse structures south of Pack Creek may be in another more westerly trending belt.

Most of the collapse structures are partly obscured by surficial deposits and form inconspicuous mounds or swales. The sharp boundaries of these structures are fault contacts that, in plan, consist of many short straight segments enclosing the core of broken rock (fig. 72.3). The bounding faults commonly dip steeply inward, but several outcrops of wavy fault planes suggest that they average about vertical. Displacements along these faults range from a few hundred feet to about 1,500 feet and may differ greatly in adjacent collapse structures.

The breccia within the bounding faults is made up of the country rock and younger sedimentary formations. In several collapse structures the breccia is roughly segregated into small mappable units (fig. 72.3), but more commonly the breccia is a jumbled mixture of fragments from many formations. The fragments within the breccia, which range from grains to huge blocks 50 feet across, are not slickensided, and the sand grains are not crushed and sheared. In general, the breccia is little altered except for the effects of removal of carbonate cement from sandstone units. For example, the breccia fragments are generally more friable than their parent rocks, and sandstone dikes and veinlets are common both in the breccia core and in the surrounding country rock. The edge of the core of the collapse structure south of the M4 Ranch locally shows a well-developed foliation that parallels the boundary fault; this foliation apparently resulted from flowage of the decemented sand and stretching
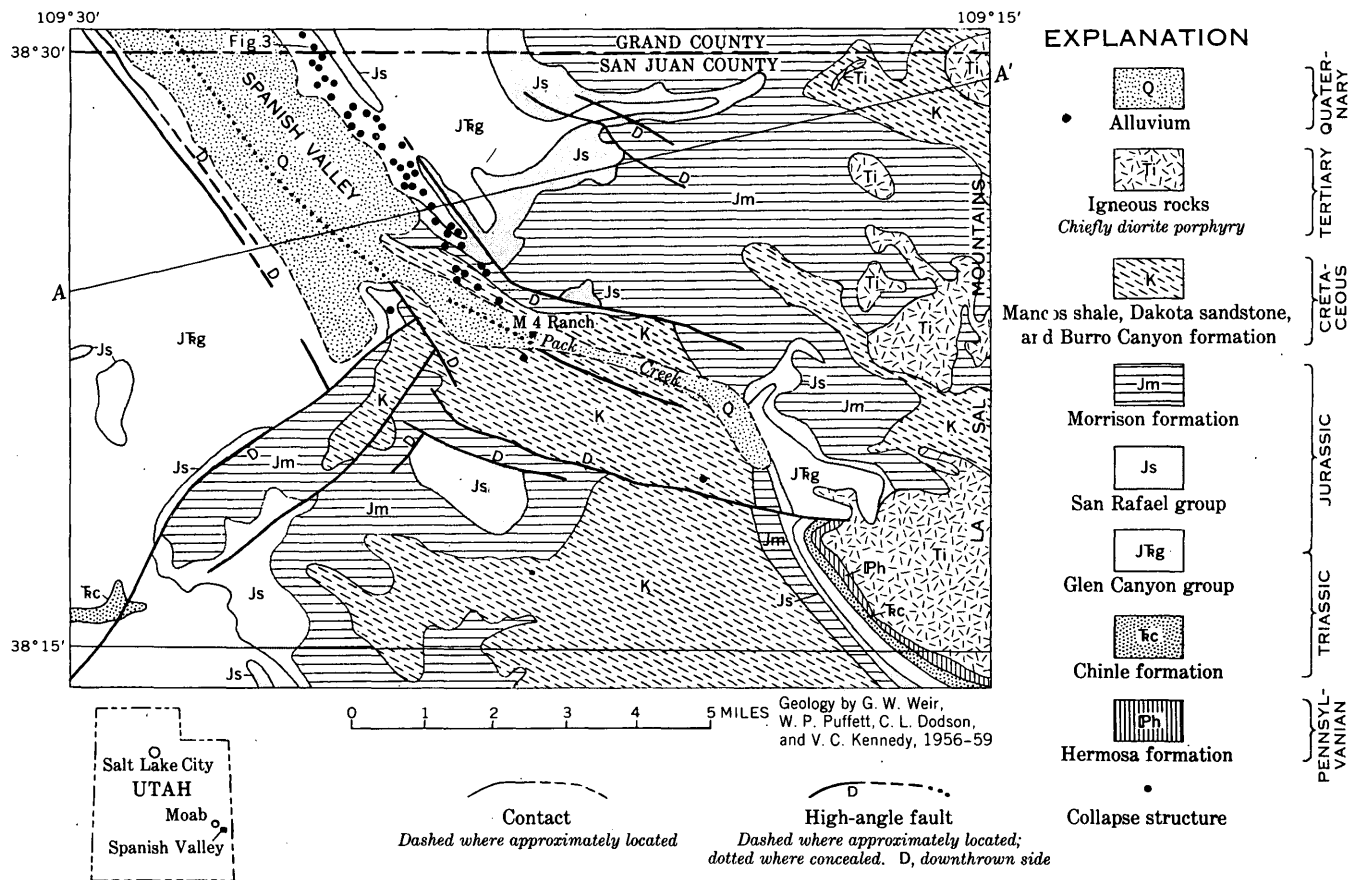
FIGURE 72.1.—Generalized geologic map of southern Spanish Valley and environs, Utah, showing location of section A–A' (fig. 72.2) and location of geologic map of collapse structure (fig. 72.3).

of clay particles in the sandstone. Some breccias are locally stained by iron and manganese oxides, but they do not resemble the hydrothermally altered breccias in the somewhat similar collapse structures of the San Rafael Swell (Kerr and others, 1957).

The collapse structures are Tertiary in age, for they are overlain by early Pleistocene deposits and they cut rocks as young as Late Cretaceous. Most likely all the collapse structures bottom in inclined Paleozoic limestone beds that flank the salt core of the Moab anticline beneath Spanish Valley, because displacements of many of the breccia cores exceed the thickness of the underlying Mesozoic rocks.

The origin of these collapse structures is uncertain but may be hypothesized as follows: Connate water, perhaps admixed with hydrothermal solutions,

Ti, Tertiary intrusive rocks, chiefly in laccoliths and stocks; Mᵏc, Mesozoic clastic rocks; Pᵏc, Paleozoic clastic rocks; Pᵏl, Paleozoic limestone; Pᵏe, Paleozoic evaporites, chiefly salt (Quaternary deposits not shown)
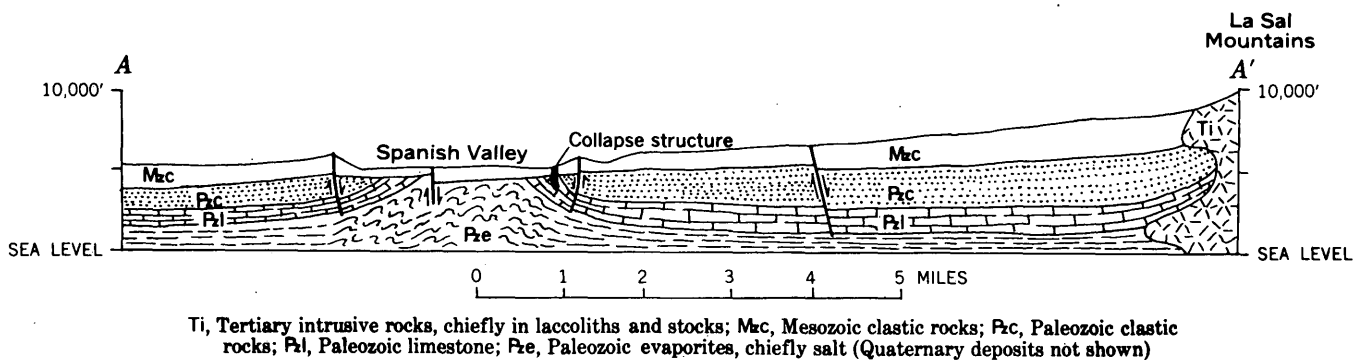
FIGURE 72.2.—Generalized section A–A' across southern Spanish Valley and environs, Utah.

0   100   200   300 FEET

CONTOUR INTERVAL 40 FEET
DATUM IS APPROXIMATE MEAN SEA LEVEL

Geology and topography by G. W. Weir
and W. P. Puffett, 1956

EXPLANATION

BRECCIA UNITS

Kd

Dakota sandstone (Upper Cretaceous)

Kbc

Burro Canyon formation (Lower Cretaceous)

Jmb
Jms

Morrison formation (Upper Jurassic)
Jmb, *Brushy Basin member.*
Jms, *Salt Wash member*

JŦu

Entrada sandstone (Upper Jurassic), Carmel
formation (Upper and Middle Jurassic),
and Navajo sandstone (Jurassic and
Triassic(?) undivided

COUNTRY ROCK

JŦn

Navajo sandstone (Jurassic and Triassic?)

Approximate contact

90 80
Fault, showing dip
Dashed where approximately located

70
Strike and dip of beds
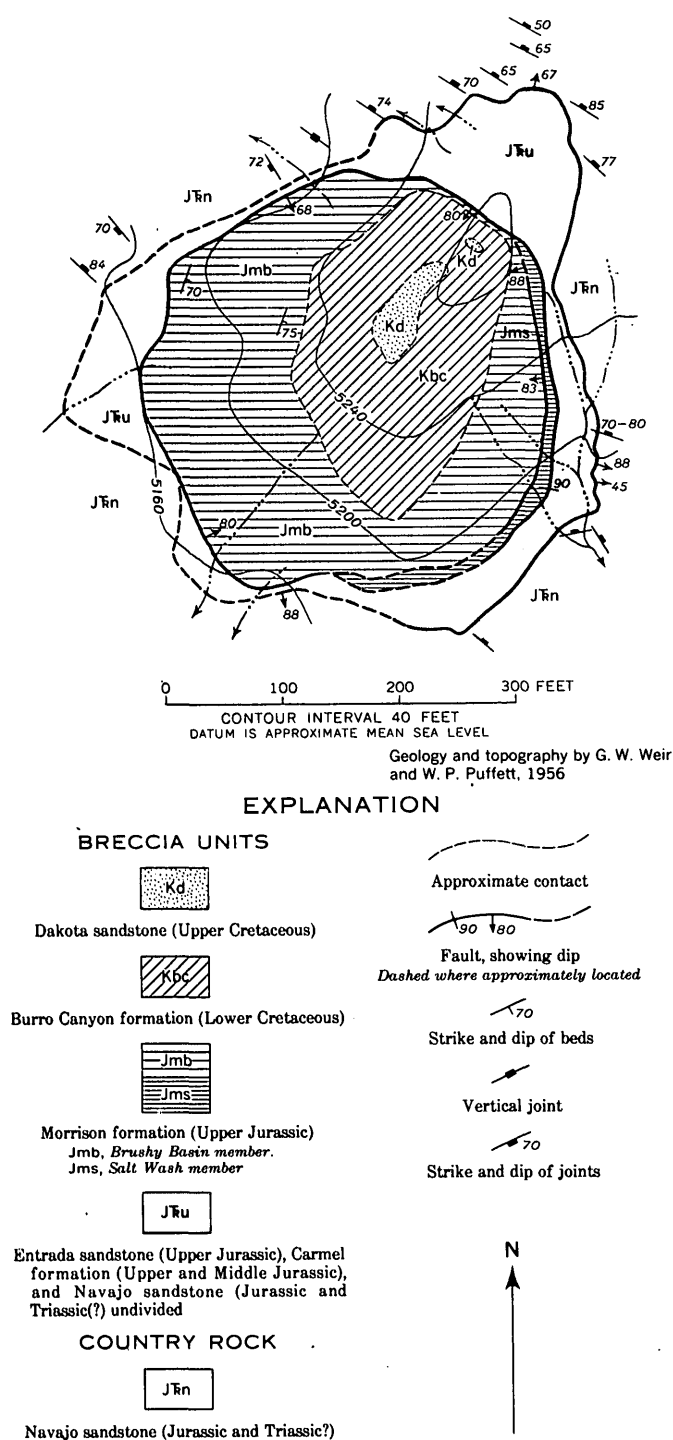
Vertical joint

70
Strike and dip of joints

N

FIGURE 72.3.—Simplified geologic map of collapse structure,
northeast rim of Spanish Valley, Utah.

moved downslope from igneous domes of the La Sal Mountains during the Tertiary and dissolved limestone in the upturned Paleozoic beds in the subsurface near Spanish Valley and thus created space for collapse breccia from the overlying formations. Moving upward along fracture channelways in the younger formations, the solutions removed carbonate cement so that these younger rocks caved into the open spaces. If these inferences and hypothesis are approximately correct, the collapse structures are the outcrops of breccia pipes that are as much as 5,000 feet high.

The collapse structures of Spanish Valley are not known to be mineralized, but they resemble in part other pipelike bodies of brecciated sedimentary rock that contain uranium ore such as the Temple Mountain collapse structure, Utah (Kerr and others, 1957; Keys and White, 1956), the Woodrow pipe, New Mexico (Hilpert and Moench, 1960), and the Orphan pipe, Arizona (Gabelman and Boyer, 1958).

REFERENCES

Baker, A. A., 1933, Geology and oil possibilities of the Moab district, Grand and San Juan Counties, Utah: U.S. Geol. Survey Bull. 841, 95 p.

Gabelman, J. W., and Boyer, W. H., 1958, Relation of uranium deposits to feeder structures, associated alteration, and mineral zones: Proc. Second United Nations Internat. Conf. on the Peaceful Uses of Atomic Energy, Geneva, Switzerland, v. 2, p. 338–350, 7 figs.

Hilpert, L. S., and Moench, R. H., 1960, Uranium deposits of the southern part of the San Juan Basin, New Mexico: Econ. Geology, v. 55, p. 429–464.

Kerr, P. F., Bodine, M. W., Jr., Kelley, D. R., and Keys, W. W., 1957, Collapse features, Temple Mountain Uranium area, Utah: Geol. Soc. America Bull., v. 68, p. 933–982.

Keys, W. W., and White, R. L., 1956, Investigations of the Temple Mountain collapse and associated features, San Rafael Swell, Emery County, Utah *in* Page, L. R., Stocking, H. E., and Smith, H. B., Contributions to the geology of uranium and thorium by the United States Geological Survey and Atomic Energy Commission for the United Nations International Conference on Peaceful Uses of Atomic Energy, Geneva, Switzerland, 1955: U.S. Geol. Survey Prof. Paper 300, p. 285–298.

Shoemaker, E. M., Case, J. E., and Elston, D. P., 1958, Salt anticlines of the Paradox basin, *in* Geology of the Paradox Basin: Intermountain Assoc. Petroleum Geologists Guidebook, 9th Ann. Field Conf., 1958, p. 39–59.

73.   AGE RELATIONS OF THE CLIMAX COMPOSITE STOCK, NEVADA TEST SITE, NYE COUNTY, NEVADA

By F. N. Houser and F. G. Poole, Denver, Colo.

The Climax composite stock consists of two separate, contiguous intrusive masses, a granodiorite and a quartz monzonite that do not necessarily differ greatly in age (Houser and Poole, 1960a). On the basis of crosscutting relations and of chemical and mineralogic characteristics observed in hundreds of feet of drill core and an 800-level tunnel, as well as in surface outcrops, it is concluded that the quartz monzonite is the younger. Numerous aplite and pegmatite dikes cut both masses. Field relations and a lead-alpha age determination (T. W. Stern, written communication, 1960) suggest an age for the Climax composite stock of Permian(?) to early Mesozoic.

The Climax stock intruded complexly folded and faulted carbonate rocks of the Pogonip group of Ordovician age. In fault contact with the Pogonip group are sedimentary rocks of Cambrian to possible Pennsylvanian age. The carbonate rocks have been thermally and metasomatically altered to marble and tactite for as much as 1,500 feet from the contact with the stock, although minor discontinuous metasomatic effects are noted in all rocks out to 3,000 feet. Pyroclastic rocks of the Oak Spring formation (Miocene(?) or younger) unconformably overlie parts of the stock and Paleozoic formations (Houser and Poole, 1960a, 1960b).

The granodiorite intrusive is light gray to greenish medium gray, equigranular, and predominantly medium grained (Houser and Poole, 1959). Its average composition, based on 19 modal analyses, is 28 percent quartz, 16 percent potassium feldspar, 45 percent plagioclase, and 9 percent biotite. The average grain size is about 2 mm, but the common range is ½ to 4 mm. The texture is granitic and very slightly porphyritic. No distinct inclusions of country rock are known.

The contact between granodiorite and adjoining quartz monzonite masses is generally vertical or very steep. In detail it is highly irregular and shows mutually penetrating fingers of each rock. These fingers are measurable in inches or feet in width and length. No glassy chilled zone has been noted in either rock. No systematic variation like that described for the quartz monzonite has been noted in the texture or composition of the granodiorite in relation to this contact.

The quartz monzonite intrusive is concluded to be younger than the granodiorite because of a transitional variation in texture and composition of the quartz monzonite inward from its contact with the granodiorite, and because similar transitions are found in the quartz monzonite where it intrudes the Pogonip group.

The quartz monzonite intrusive can be divided on the basis of grain size into a fine-grained variety, in which the average subhedral grains are from ¼ to 1 mm across, and a medium-grained variety in which they are from 1 to 1½ mm across. Fine-grained quartz monzonite occurs in a zone that parallels the border of the intrusive; the medium-grained variety makes up the remainder of the intrusive. The peripheral zone of fine-grained rock is from 50 to 800 feet wide; it averages 500 feet wide where the intrusive adjoins the granodiorite, and less than 100 feet wide where it adjoins the marble. In most places the fine-grained rock grades to the medium-grained variety within distances ranging from a few feet to 100 feet. In some places the two varieties are intimately intermixed; this is thought to be the result of autointrusion of older fine-grained material by younger medium-grained material.

Where in contact with the granodiorite intrusive, the quartz monzonite intrusive varies in composition from quartz diorite in the first 15 feet to granodiorite throughout the next 45 feet, and to quartz monzonite in the remainder of the mass. However, the zones vary considerably in width from place to place, and the boundaries are indefinite. Table 1 shows the mineralogic variations.

The fine-grained border zone of the quartz monzonite next to the marble is texturally similar to corresponding zones in the quartz monzonite next to the granodiorite although it is more highly variable mineralogically and chemically. Autointrusion similar to that observed in the vicinity of the contact with the granodiorite is also common near the contact with the marble.

TABLE 1.—*Changes in the essential mineral compositions, in volume percent, of the quartz monzonite intrusive at selected intervals from the contact with the granodiorite intrusives*

[tr, trace]

| Interval | Distance from granodiorite intrusive (feet) | Estimated volume percent of quartz monzonite intrusive [1] | Number of modal analyses | Volume percent | | | | | | | | Rock type |
				Quartz	Potassium feldspar [2]	Plagioclase	Biotite	Hornblende	Total	Total feldspar	Potassium feldspar of total feldspar	
1........	15 and less..	0.8	9	22	8	54	15	tr	99	62	13	Quartz diorite
2........	15–60......	2.2	5	27	17	46	8	tr	98	63	27	Granodiorite
3........	60–200.....	7	4	26	25	42	7	0	100	67	37.4	Quartz monzonite
4........	>200......	90	7	28	25	40	6	tr	99	65	38.5	Do.
	Weighted average composition[3]		....	28	25	40	6	tr	......	65	38.5	

[1] Based on the total exposed quartz monzonite stock.
[2] Includes proportioned amounts of potassium feldspar phenocrysts.
[3] Weighted for the various proportions of the intrusive represented in intervals 1 through 4.

The relative ages of the quartz monzonite and granodiorite are important in interpreting the lead-alpha age determination for the Climax stock. It has been concluded that the quartz monzonite is the younger intrusion, and because the lead-alpha age was determined for this intrusive, it applies as the youngest age limit for the intrusion of the preceding granodiorite.

Field relations indicate that the Climax stock was intruded no earlier than Permian(?) time. Strata of the Tippipah limestone of Permian(?) and Pennsylvanian age 10 miles to the southwest are without noticeable breaks in sedimentation and are without coarse clastics that would suggest nearby contemporaneous or previous structural deformation (P. P. Orkild, oral communication, 1960) such as the tight folding and high-angle faulting which next to the Climax stock (Houser and Poole, 1960a) preceded intrusion. Many of the metamorphic effects equivalent to those observed next to the stock are found throughout the formations of Ordovician through Mississippian age that had been involved in this deformation.

The field relations also indicate that the stock was intruded, exposed, and dissected before deposition of the Oak Spring formation, which is of Tertiary age, possibly Miocene or Pliocene (Johnson and Hibbard, 1957, p. 369).

Two lead-alpha age determinations made by T. W. Stern (written communication, 1960) for zircon from the medium-grained quartz monzonite give estimates of 330 ± 35 and 230 ± 25 million years. The younger of these two estimates is thought to be more nearly correct because it was substantiated by replicate determinations and it falls within the age limits established by field relations. Therefore, both intrusions of the Climax stock are dated tentatively as Permian(?) to early Mesozoic.

REFERENCES

Houser, F. N., and Poole, F. G., 1959, "Granite" exploration hole, Area 15, Nevada Test Site, Nye County, Nev.—interim report, Pt. A, Structural, petrographic, and chemical data: U.S. Geol. Survey TEM–836, open-file report.

———— 1960a, Preliminary geologic map of the Climax stock and vicinity, Nye County, Nev.: U.S. Geol. Survey Misc. Geol. Inv. Map I–328.

———— 1960b, Structural features of pyroclastic rocks of the Oak Spring formation at the Nevada Test Site, Nye County, Nev., as related to the topography of the underlying surface, *in* Short papers in the geological sciences: U.S. Geol. Survey Prof. Paper 400–B, p. B266–B268.

Johnson, M. S., and Hibbard, D. E., 1957, Geology of the Atomic Energy Commission Nevada Proving Grounds area, Nev.: U.S. Geol. Survey Bull. 1021–K, p. 333–384.

74.   RHYOLITES IN THE EGAN RANGE SOUTH OF ELY, NEVADA

By Daniel R. Shawe, Denver, Colo.

Rhyolite of Tertiary age in the Egan range south of Ely, White Pine County, Nev., occurs as (a) intrusive bodies, including a volcanic neck a mile across and a small sill; and (b) extensive dissected layers of welded tuff (fig. 74.1). Whether the intrusive rhyolite bodies are comagmatic with and mark the vents for the welded tuff ash flows is the subject of this paper. This possibility is in part suggested by the crude tendency for the welded tuff layers to dip outward from the neck (fig. 74.1), and in part by the superficial similarity of the rhyolites.

PETROLOGIC CHARACTER OF THE RHYOLITES

The intrusive rhyolite is generally a light- to dark-gray porphyritic rock composed of phenocrysts mostly about 1 to 2 mm across set in an aphanitic or glassy matrix that makes up about 75 to 80 percent of the rock. Glassy rhyolite forms a chilled border 100 to 200 feet wide around the volcanic neck. Flow structure is locally evident, generally as vertical banding in the volcanic neck and lineation in the sill. Much of the rhyolite in the neck is brecciated, and, as seen in thin section, flow lines are marked by strings of crushed crystals embedded in groundmass (fig. 74.2). Apparently deuteric or hydrothermal alteration affected large parts of the volcanic neck, as these parts are bleached light yellowish gray to almost white, and the rhyolite has become "porcelaneous." Another result of deuteric or hydrothermal action in the volcanic neck was the development of numerous small and imperfect "thunder-eggs"—cavities within dense, siliceous ellipsoidal shells lined with chalcedony and minor amounts of fluorite and manganese oxide. Oxidation occurred locally in the neck, as parts of the rhyolite are pinkish from "dusty" hematite. Small inclusions of chert or silicified limestone 1 mm to 1 cm in diameter are abundant.

Phenocrysts in intrusive rhyolite comprise subequal amounts of quartz, sanidine, and plagioclase (albite to oligoclase?), and about 1 percent of biotite; the size range is about 0.1 to 4 mm. Quartz occurs as euhedral to strongly corroded and embayed crystals; some is smoky. Sanidine forms subhedral to euhedral crystals; a few crystals contain intergrown quartz in graphic and myrmeckitic forms (fig. 74.3). Plagioclase forms subhedral to euhedral crystals, with slight oscillatory zoning and few albite and pericline twins. Biotite is dark brown to light yellowish brown and in places is charged with tiny specks of an iron oxide. Except for sparse iron ores, no accessory minerals were recognized.

The welded rhyolite tuff is similar in gross appearance to the intrusive rhyolite, except that almost everywhere it shows layering due to flattened pumice lapilli, and there is no obvious flow structure. Phenocrysts are mostly 1 to 2 mm across and are embedded in a glassy matrix constituting about 50 to 65 percent of the rock. In hand specimen, the tuffs appear no darker than the intrusive rhyolites, although crystals, especially mafic species, are more abundant in the welded tuffs. Inclusions of chert or silicified limestone in the welded rhyolite tuff appear to be more abundant than in the intrusive rhyolite, and they are not concentrated locally—as they are in the intrusive rock.

Phenocrysts in welded tuff comprise plagioclase (albite to andesine?), making up about 15 percent of the rock, lesser and subequal amounts of quartz, sanidine, and biotite, about 1 percent of pyroxene, iron ores, and pale hornblende, and traces of sphene, apatite, and zircon. The size range of all phenocrysts is about 0.1 to 4 mm. Plagioclase occurs as subhedral to euhedral crystals with slight to rather strong progressive zoning; a few crystals show ragged cores that are probably albite, rimmed with andesine(?) which is zoned outward progressively to albite. Albite and pericline twins are sharper and more abundant than in plagioclase of the intrusive rhyolite. Quartz is euhedral to strongly corroded and embayed (fig. 74.4); hand specimens show some smoky quartz like those of the intrusive rhyolite. Sanidine forms subhedral to euhedral crystals; a few of these have glass inclusions, in part zoned, but none contain graphic and myrmeckitic intergrowths of quartz. Biotite is strongly pleochroic, almost black to yellowish brown with a greenish cast, and commonly includes minute apatite crystals, and opaque iron minerals along cleavage traces. Accessory minerals aggregate less than 1 percent of the rock; they comprise iron ores, sphene (some diamond-shaped grains as much as 0.5 mm long), apatite, and zircon.
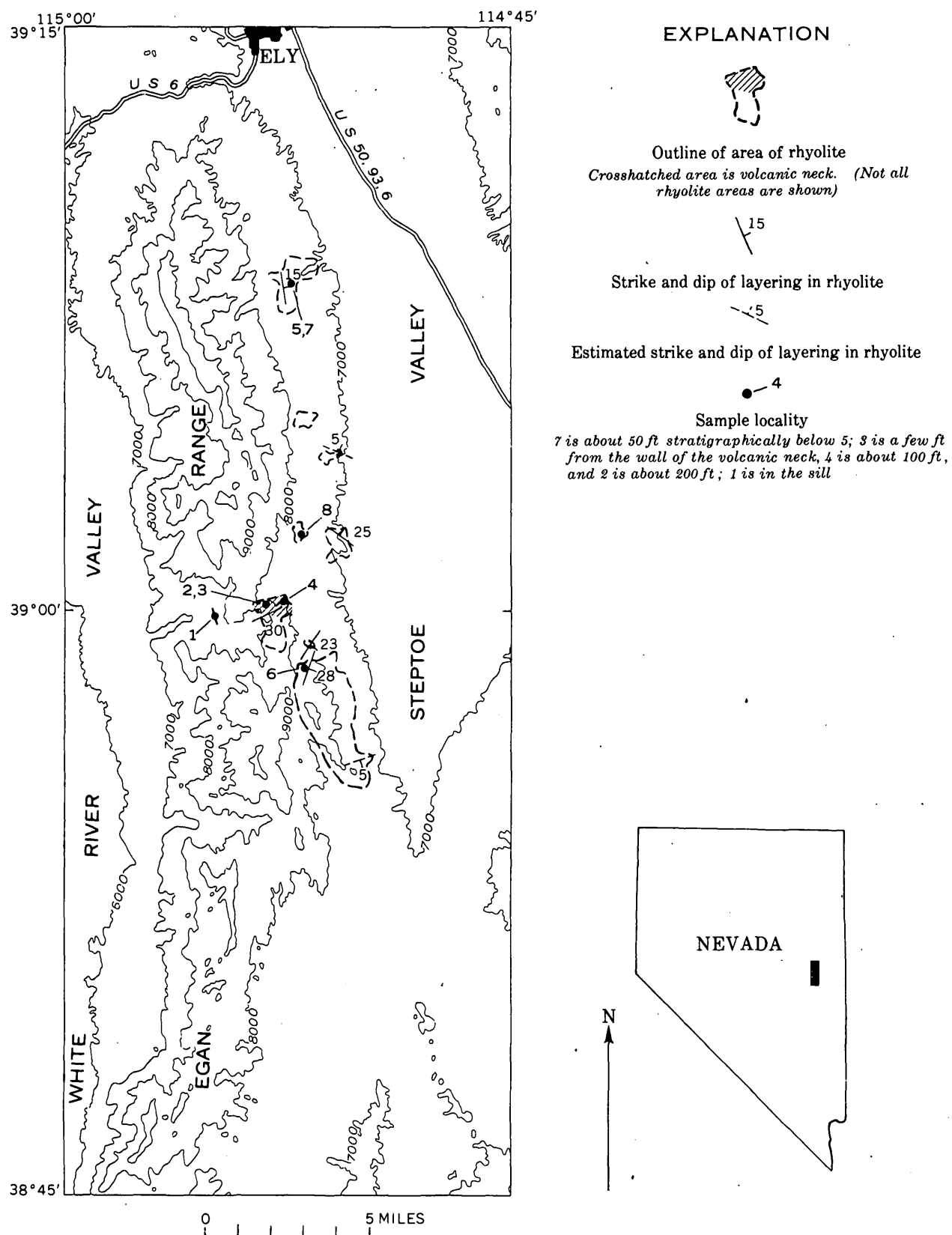
FIGURE 74.1.—Map showing areas of rhyolite and sample localities in the Egan range south of Ely, Nev.

TABLE 1.—*Chemical analyses and semiquantitative spectrographic analyses of eight rhyolites from the Egan range south of Ely, Nevada*

[Chemical analyses by Margaret Lemon; semiquantitative spectrographic analyses by Paul R. Barnett; d, detected; 0, looked for but not found (below limit of detectability)]

	Intrusive rhyolite				Arithmetic average of four intrusive rhyolites	"Comparison factor"	Arithmetic average of four extrusive rhyolites	Extrusive rhyolite			
	Sill	Volcanic neck						Welded tuff			
	Sample							Sample			
	1 (DRS-45-58)	2 (DRS-22-58)	3 (DRS-21-58)	4 (DRS-52-58)				5 (AB-23-5?)	6 (DRS-5-59)	7 (AB-22-58)	8 (DRS-28-58)
Chemical analyses											
SiO_2	75.36	73.09	72.92	72.49	73.47	>	69.71	70.50	70.28	69.46	68.58
Al_2O_3	13.55	13.59	13.63	13.45	13.56	<	14.11	14.31	13.97	14.62	13.55
Fe_2O_3	.31	.44	.51	.55	.45	<2X	1.12	1.07	1.09	1.11	1.21
FeO	.43	.34	.27	.25	.32	<4X	1.41	1.41	1.63	1.44	1.16
MgO	.07	.07	.14	.08	.09	<9X	.81	.74	.76	.84	.88
CaO	.84	.90	.97	.88	.90	<3X	2.85	2.89	3.21	2.98	2.30
Na_2O	3.80	3.42	3.48	3.30	3.50	>	2.51	3.02	2.48	2.97	1.56
K_2O	4.61	5.11	4.83	5.00	4.89	>	3.84	3.48	3.70	3.54	4.64
H_2O+	.35	2.46	2.66	3.33	2.20	>	1.81	1.43	1.38	1.53	2.88
H_2O-	.19	.12	.29	.23	.21	<5X	1.00	.36	.50	.61	2.52
TiO_2	.05	.05	.05	.05	.05	<9X	.45	.46	.45	.47	.43
P_2O_5	.09	.01	.01	.00	.03	<3X	.10	.10	.09	.10	.09
MnO	.07	.08	.07	.08	.08	>	.05	.05	.04	.05	.04
CO_2	.01	.01	.01	.01	.01	<2X	.02	.01	.03	.03	.00
Cl	.01	.03	.03	.02	.02	=	.02	.04	.01	.04	.00
F	.11	.14	.11	.13	.12	>2X	.07	.08	.03	.09	.07
Sub-total	99.85	99.86	99.98	99.85	....	....	....	99.95	99.65	99.88	99.91
Less O	.05	.07	.06	.05	....	....	....	.04	.01	.05	.03
Total	99.80	99.79	99.92	99.80	....	....	....	99.91	99.64	99.83	99.88
Semiquantitative spectrographic analyses [1]											
B	0	.0015	.0015	.0015	.0011	>	0	0	0	0	0
Ba	.003	.003	.003	.003	.003	<60X	.19	.15	.3	.15	.15
Be	.0003	.0003	.0003	.0003	.0003	>2X	.00015	.00015	.00015	.00015	.00015
Ce	0	0	0	0	0	<	.023	.015	.03	.03	.015
Co	0	0	0	0	0	<	.0003	.0003	.0003	.0003	.0003
Cr	d	d	.0003	d	<.0003	<	.0003	.00015	.0007	.0003	.00015
Cu	.0003	d	d	d	<.0003	<	.0003	.0003	.0003	.0003	.0003
Ga	.003	.003	.0015	.0015	.0023	>3X	.0009	.0007	.0007	.0015	.0007
La	0	0	0	0	0	<	.011	.007	.015	.015	.007
Nb	.003	.003	.003	.003	.003	>	.0019	.003	.0015	.0015	.0015
Nd	0	0	0	0	0	<	.009	.007	.015	.007	.007
Ni	0	0	0	0	0	<	<.0003	.0003	.0003	0	0
Pb	.003	.003	.003	.003	.003	>3X	.0009	.0007	.0007	.0015	.0007
Sc	.0003	.0003	.0003	.0003	.0003	<2X	.0007	.0007	.0007	.0007	.0007
Sn	.0007	.0007	.0007	.0007	.0007	>	0	0	0	0	0
Sr	.003	.003	.003	.003	.003	<20X	.06	.07	.07	.07	.03
V	0	0	0	0	0	<	.004	.003	.003	.007	.003
Y	.003	.003	.003	.003	.003	>	.0023	.003	.0015	.003	.0015
Yb	.0003	.0003	.0003	.0003	.0003	>	.00023	.0003	.00015	.0003	.00015
Zr	.007	.007	.003	.003	.005	<4X	.019	.015	.03	.015	.015

[1] Figures are reported to the nearest number in the series 7, 3, 1.5, 0.7, 0.3, 0.15, etc., in percent. These numbers represent midpoints of group data on a geometric scale. Comparisons of this type of semiquantitative results with data obtained by quantitative methods, either chemical or spectrographic, show that the assigned group includes the quantitative value about 60 percent of the time.

CHEMICAL CHARACTER OF THE RHYOLITES

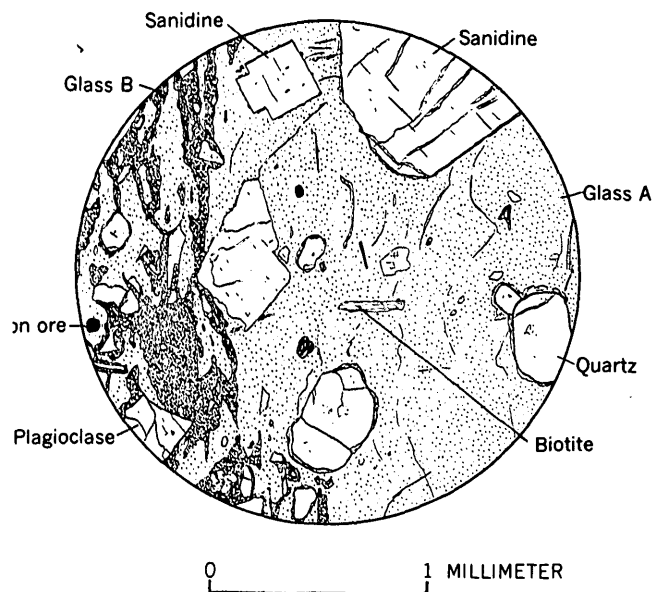The chemical character of four samples of intrusive rhyolite and four samples of welded rhyolite

FIGURE 74.2.—Pen-and-ink drawing of rhyolite from volcanic neck. Glass A is clear; glass B is comminuted containing numerous small fragments of broken crystals (sample 3).
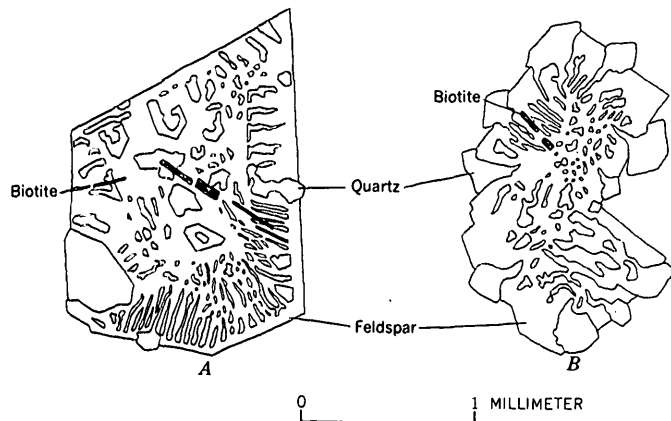

FIGURE 74.3.—Feldspar crystals with myrmeckitic and graphic intergrowths of quartz. Feldspar crystal A is sanidine from sill (sample 1). Feldspar crystal B is sanidine rimmed with plagioclase from volcanic neck (sample 4).

tuff is summarized in table 1. As shown in table 1, the four intrusive rhyolites form a group closely similar in composition, as do the four welded tuffs; the two groups are, however, chemically quite distinct. (See "Comparison factor" of the group averages, table 1.) For more valid comparison of the groups the analyses should probably be recalculated without H_2O, although this could not alter the basic differences between the two.

CONCLUSIONS

Both the petrologic and chemical data suggest that the intrusive and extrusive rhyolites were not closely related genetically. For example, the distinct differences between both plagioclase and sanidine phenocrysts in the two groups indicate that they probably were not derived from the same magma chamber, even at widely separated times. Further, the obvious chemical disparity between the intrusive rhyolite and the welded rhyolite tuff suggests that one is not related to the other through crystal fractionation.
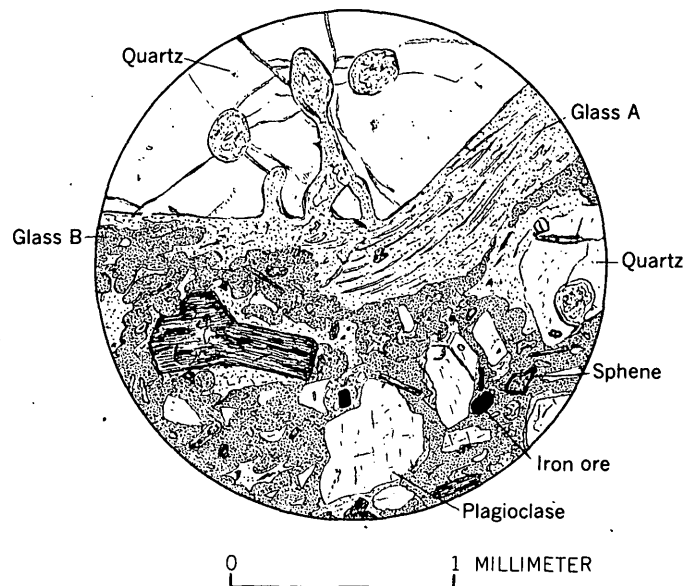

FIGURE 74.4.—Pen-and-ink drawing of welded rhyolite tuff. Glass A generally rims crystals, is vesiculated and fragmented; glass B forms matrix enclosing whole and broken crystals and particles of glass A (sample 8).

75. TECTONIC SIGNIFICANCE OF RADIAL PROFILES OF ALLUVIAL FANS IN WESTERN FRESNO COUNTY, CALIFORNIA

By WILLIAM B. BULL, Sacramento, California

Work done in cooperation with the California Department of Water Resources

---

The shape of an alluvial fan reflects part of its depositional history, which is controlled primarily by erosional and tectonic changes in the drainage basin upstream. The radial profiles of fans along the western border of the San Joaquin Valley in western Fresno County, Calif., are interesting features because they are segmented, and because they can be used to help decipher part of the tectonic history of the area.

The drainage basins of the fans head in two distinct mountainous areas. The small fans have drainage basins with ephemeral streams which head in the foothill belt of the Diablo Range. The large fans have drainage basins with intermittent streams which head in the main Diablo Range.

The overall radial profiles of the alluvial fans are concave upward, but the slope does not decrease at a uniform rate away from the mountain front. Instead the radial profiles are segmented. Profiles of fans whose streams head in the foothill belt have three straight-line segments; profiles of fans whose streams head in the main Diablo Range have four segments: three are straight lines but the uppermost segment may be concave upward. An example of each type of radial profile is shown in figure 75.1. The dots represent altitudes from topographic maps that have a 5-foot contour interval. The lengths of the segments and the angular relationships between them vary for different fans, but the profiles of adjacent fans generally are similar.

Near their apexes the fans accumulate deposits that have the same general slope as the valley upstream from the fan. Slope measurements from topographic maps of 10 streams show that the uppermost fan segments and the valleys upstream from the fans for a distance of ½ to 1 mile have the same general slope, although there have been periods of arroyo cutting during the last century. Five of these valleys have slightly lower gradients than their uppermost fan segments, and five have slightly higher gradients. For one stream, the slope of a terrace for three-fourths of a mile upstream from the fan is the same as the upper fan segment. The continuous slope implies that the terrace deposits were laid down at the same time as the upper deposits of the fan segment.

Valleys also tend to be cut down to the same gradient as the adjacent lower fan surface. This tendency is illustrated by the stream of Tumey Gulch where it is entrenched into the upper fan segment. More than a mile of the stream has been cut down to the same gradient as the adjacent lower fan segment.

Channel trenching helps preserve fan segmentation by restricting deposition to certain fan segments. At the present time deposition is not occurring on the upper fan segment of the fans whose streams head in the foothill belt, or on the upper two segments of the fans whose streams head in the main Diablo Range.

Climatic fluctuations, uplift of the mountains, and changes in base level should be considered as possible causes of fan segmentation. Neither the fans nor drainage basins show any evidence of marked base-level changes. Moisture studies of deep cores from the dry alluvial-fan deposits do not indicate major changes in rainfall or stream runoff. However, Pliocene and Pleistocene deposits on the summits of the foothill belt show that parts of the mountains were uplifted more than 2,000 feet during Pleistocene time. The uplift occurred mainly as monoclinal and anticlinal folding.

The drainage basins of western Fresno County have paired terraces that are commonly 100 to 300 feet above the present-day stream channels. These terraces represent periods of lateral planation and little downcutting followed by periods of accelerated downcutting, which made narrower valleys within the former wider valleys. The accelerated downcutting accompanies uplift in the mountain area, which steepens the stream gradient; as a result, the fan deposits also should have a steeper gradient. Thus, the result of uplift would be a "new fan" built out onto the older more gently sloping fan.
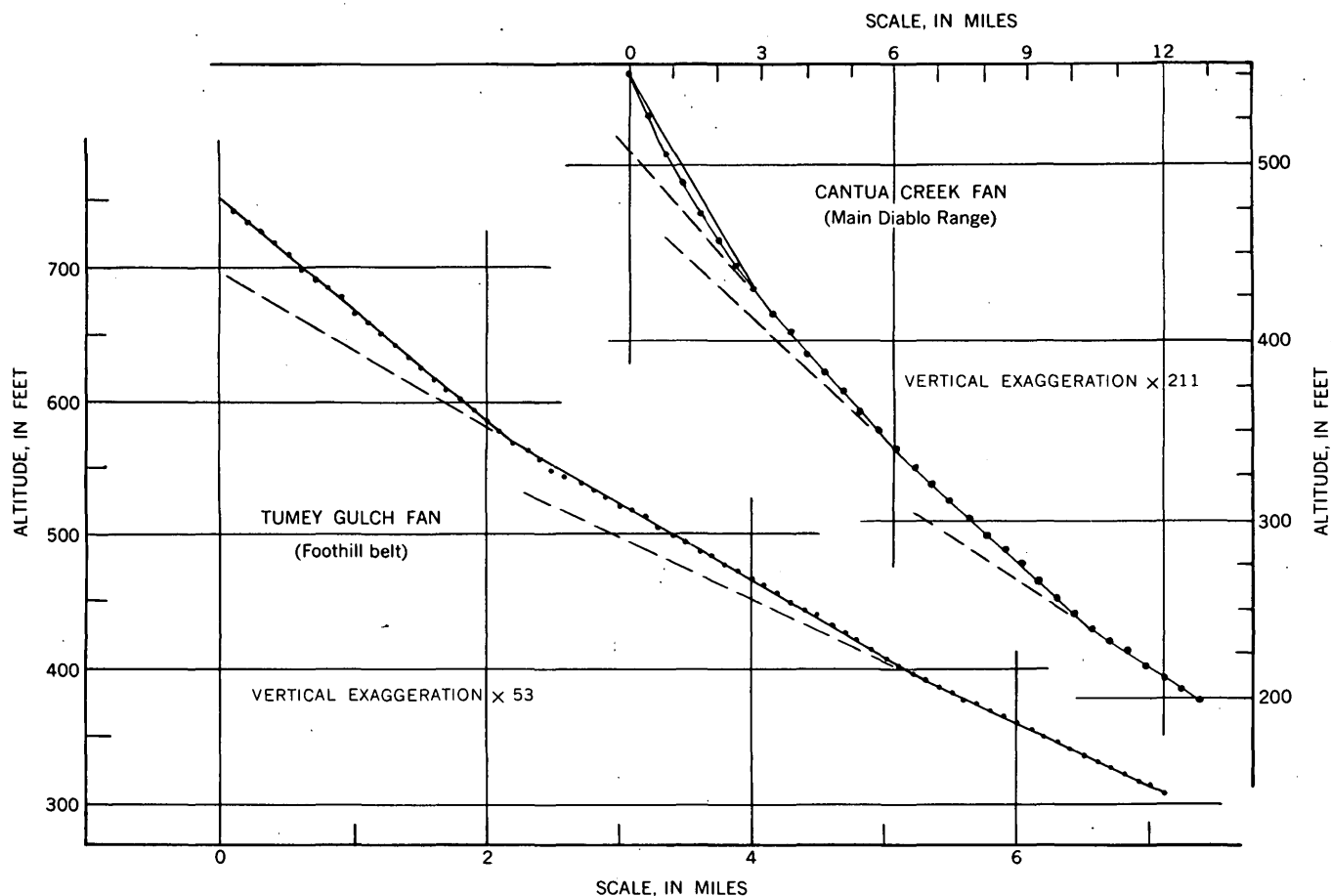
FIGURE 75.1.—Radial profiles of two alluvial fans in western Fresno County, Calif.

Some stages of alluvial-fan development are outlined by diagrams in figure 75.2. In figure 75.2a a fan and stream channel have developed a common gradient. Uplift steepens the stream gradient and the new fan deposits also have a steeper gradient (fig. 75.2b). The stream-channel gradient may have been steeper after the uplift, but the slopes in figure 75.2b represent equilibrium conditions near the end of the stage. Another period of uplift makes the youngest segment (fig. 75.2c), completing a fan similar to the Tumey Gulch fan (fig. 75.1). Deposition continues on the fan and the stream channel maintains the same slope as the fan by aggrading slightly (fig. 75.2d). An increase in the amount and intensity of rainfall causes temporary channel trenching (fig. 75.2e). The low terrace and the upper fan segment have the same slope, and the downstream end of the entrenched channel has the same gradient as the adjacent lower segment. The surficial deposits of respective fan segments generally are not of distinctly different ages. For example, deposition may have been occurring mainly on the upper segment a century ago, but channel trenching then caused deposition to occur mainly on the middle segment as the end of the channel moved downslope (fig. 75.2e). Thus, in the situation illustrated in figure 75.2e, deposition is restricted to the area downslope from the upper two fan segments, as it is for the streams that head in the main Diablo Range.

The segmented fans of western Fresno County indicate three or four episodes of uplift of the Coast Ranges rather than continuous uplift. Part of the uplift may have occurred in the last 3,000 years. Charcoal that was 10.5 feet below the surface of the upper (youngest) fan segment of the Arroyo Hondo fan is 1,040 ± 200 years old according to a radiocarbon age determination.[1] The total thickness of deposits of the fan segment at this locality is

---

[1] Radiocarbon age determination made by Meyer Rubin of the U.S. Geological Survey; sample W-793.

estimated to be 24 feet, which suggests that the segment is 2,000 to 3,000 years old, if a similar rate of deposition existed throughout its history.

Segmented fans apparently occur where the slope of the valley upstream from the apex has been made steeper than the slope of the fan. Large changes in fan slope probably indicate greater uplift and steepening of the valley upstream from the apex than do small changes in fan slope. The different radial profiles of fans whose streams head in the foothill belt for 50 miles along the western border of the San Joaquin Valley indicate different amounts or times of uplift and rates of erosion in their drainage basins.

The fans of streams that head in the foothill belt and main Diablo Range have a distinctive segmentation which reveals part of the tectonic history of their respective mountain areas. Fan segmentation should be helpful in deciphering part of the tectonic history of the drainage basins of other mountain ranges.
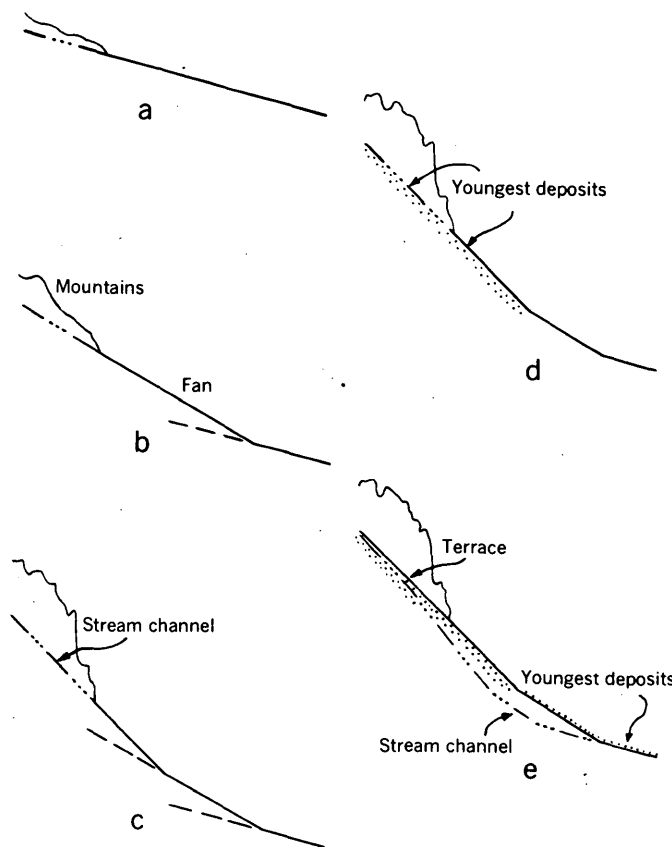
FIGURE 75.2.—Diagrammatic sketches showing segmented alluvial fan development in western Fresno County, Calif.

76. SOIL-MOISTURE STORAGE CHARACTERISTICS AND INFILTRATION RATES AS INDICATED BY ANNUAL GRASSLANDS NEAR PALO ALTO, CALIFORNIA

By F. A. BRANSON, R. F. MILLER, and I. S. MCQUEEN, Denver, Colo.

One of the chief determinants of the kinds and amounts of vegetation found on unplowed land surfaces is quantity of water stored in the soil and available for plant growth during the growing season. The annual-grasslands floral assemblage of California, although composed largely of introduced species, shows some striking contrasts on soils having different water-storage capacities. Certain indicator plants have been identified that may help in mapping soils of different textures, and in estimating quickly the hydrologic characteristics of soils in some local areas.

The vegetation and soils of three small basins (310, 245, and 170 acres) near Palo Alto were mapped and sampled in 1959. A metal frame of the type shown in figure 76.1 was used to measure the amounts and kinds of vegetation. Sampling locations were chosen at intervals along transects across
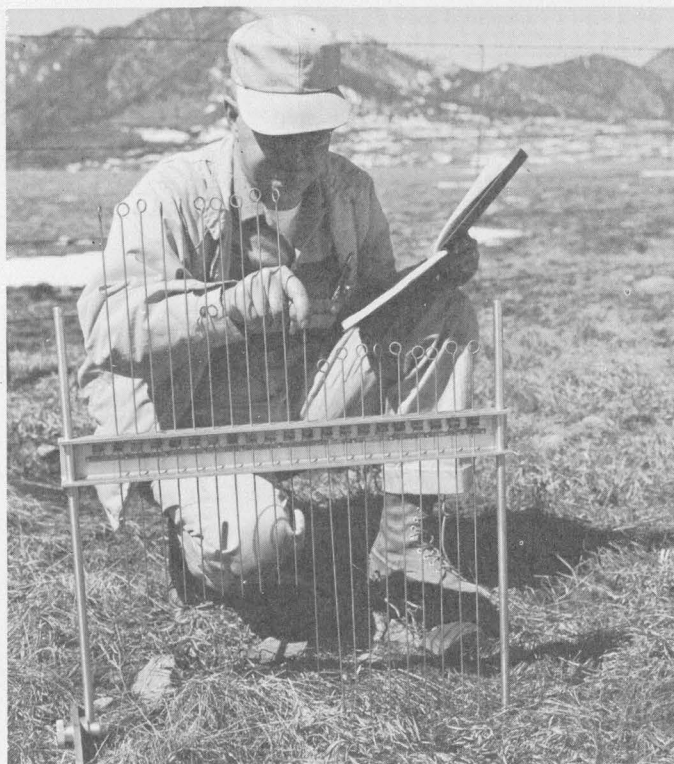
FIGURE 76.1.—Metal frame and pins used to measure amounts and kinds of herbaceous vegetation.

each basin. The annual precipitation on the basins is about 22 inches, most of it falling at moderate intensities from November to March.

The abundance, and commonly the kinds, of plants differed on the sandy and clayey soils in all three basins as shown on table 1. Most of the soils of the three basins were either sandy or clayey, generally with sharp boundaries between soil types, leaving only small areas of medium-textured soils. Because the medium-textured soils were so limited, only the vegetation and soil analyses of the sandy and clayey soils were studied in detail. Most of the soils developed in place on bedrock consisting of alternate shale and sandstone strata that Branner and others (1909) mapped as the Purisima formation of Tertiary age. Residual soils developed from these strata can be seen in figure 76.2.

Species that were more abundant on clayey than on sandy soils included wild oat, Italian ryegrass, bellardia, tarweed, and bur clover. Purple star thistle was found only on clayey soils. Soil cracks were present only in the clayey soils. Four or more hits (contacts) in soil cracks per 100 pins were recorded for clay soils of the three basins.

Greater amounts of vegetation and a greater variety of plant species grow on the sandy soils. Species present in most samples but more abundant on sandy soils included shoft chess and red-stem filaree. Species found only on the sandy soils were ripgut brome, California oatgrass, foxtail fescue, mouse barley, needlegrass, agoseris, bindweed, Spanish clover, two species of lupine, California poppy, and fiddle dock. Sandy soils were characterized by a greater number of vegetation contacts per 100 pins, more mulch, and less bare soil surface.

Trees and shrubs were widely but uniformly spaced in the three basins except for the few dense groves on north-facing slopes. The three important tree species in order of their abundance were valley oak (*Quercus lobata*), blue oak (*Q. douglasii*), and coast live oak (*Q. agrifolia*). The trees and shrubs did not appear to be affected by the different soil textures.

Some of the physical characteristics of the sandy and clayey soils of the basins studied are shown in table 2. The percent moisture at saturation and at field capacity were considerably greater in the clayey than in the sandy soil. The estimated field capacity in the clay soil was approximately double that of the sandy soil in the upper 2 feet of the two soils. Lineal shrinkage was nearly four times greater for the clayey than for the sandy soils.

FIGURE 76.2.—Residual soils developed on alternating strata of the Purisma formation. Sandstone is on the right and shale is on the left.

TABLE 1.—*Herbaceous vegetation on basins A, B, and C near Palo Alto, Calif.*

[Numbers are average hits per 100 pins, using device shown on figure 76.]

| | Basin and type of soil | | | | | |
| | A | | B | | C | |
	Sandy	Clayey	Sandy	Clayey	Sandy	Clayey
Grasses						
Avena fatua L. Wild oat	4.7	10.2	4.2	4.5	31.5	38.7
Bromus mollis L. Soft chess	53.0	16.2	49.4	8.5	47.2	26.0
Bromus rigidus Roth. Ripgut brome	1.3	......	1.2	......	9.2	......
Danthonia californica Boland California oatgrass	1.0	......	......	......	......	......
Festuca megalura Nutt. Foxtail fescue	......	......	17.9	......	3.8	......
Hordeum gussonianum Parl. Mediterranian barley	......	......	26.9	11.0	3.8	25.3
Hordeum murinum L. Mouse barley	......	......	.4	......	.5	......
Lolium multiflorum Lam. Italian ryegrass	17.7	30.0	17.2	75.0	43.8	74.7
Stipa cernua Stibbins and Love Needlegrass	1.0	......	......	......	......	......
Forbs						
Agoseris grandiflora (Nutt.) Greene Agoseris	......	......	1.0	......	......	......
Bellardia trixago (L.) All. Bellardia	0.7	2.2	......	......	......	......
Centaurea calcitrapa L. Purple star thistle	......	11.5	......	......	......	......
Convolvulus arvensis L. Bindweed	......	......	.4	......	......	......
Erodium cicutarium L 'Her. Red-stem filaree	44.7	35.5	53.6	24.5	3.8	1.3
Eschscholtzia californica Cham. California poppy	......	......	......	......	1.5	......
Lotus americanus (Nutt.) Bisch. Spanish clover	......	......	.3	......	......	......
Lupinus bicolor Lindl. Lupine	......	......	7.1	......	.5	......
Lupinus formosus Greene Lupine	......	......	......	......	.5	......
Madia sp. Mol. Tarweed	3.7	12.0	6.9	8.5	1.2	13.3
Medicago hispida Gaertn. Bur clover	5.3	3.5	9.0	11.5	2.2	6.0
Rumex pulcher L. Fiddle dock	......	......	.2	......	......	......
Unidentified forbs	......	.7	1.1	......	.5	.7
Vegetation contacts per 100 pins[1]	133.1	121.8	196.8	143.5	150.0	186.0
Other						
Mulch	98.7	93.3	103.8	107.0	121.8	110.0
Bare	3.0	13.2	.5	5.5	......	4.7
Soil cracks	......	4.4	......	4.0	......	4.7

[1] Total of grasses and forbs.

Although the soil moisture retention capabilities of the clayey soils exceeded those of the sandy soils, more herbaceous vegetation grew on the sandy soils, probably because of higher rates of infiltration of water, and because soil water is more readily available for plant use in the sandy soils. Infiltration rates of 1.35 to 13.85 inches per hour with a mean of 6.40 inches for 6 1-hour runs were measured for the sandy soils. The infiltration rate on an uncracked clay-loam soil was 0.18 inch per hour; however, the degree of soil cracking (shrinkage, table 2) and an almost complete absence of soil erosion, even on slopes exceeding 40 percent, indicated that moisture entered the clayey soils fairly readily. The cracks provide large areas for water entry until they are closed by swelling of the moistened clays.

TABLE 2.—*Some characteristics of a sandy soil and a clayey soil in the basins studied*

Depth from soil surface (inches)	Moisture at saturation [1] (percent)	Estimated field capacity [2] (percent)	Sand [3] (percent)	Silt [3] (percent)	Clay [3] (percent)	Lineal shrinkage [4] (percent)
Sandy soil						
0 – 4	24.0	12.0	54	30	16	4.7
4 – 9	25.2	12.6	55	31	14	5.6
9 – 14	23.6	11.8	55	30	15	5.0
14 – 19	24.8	12.4	56	26	18	4.8
19 – 24	31.0	15.5	49	32	19	8.0
24 – 27	26.8	13.4	44	43	13	4.3
Clayey soil						
0 – 4	50.8	25.4	19	33	48	19.2
4 – 7	49.7	24.8	17	23	60	19.8
7 – 10	48.4	24.2	17	31	52	19.6
10 – 13	48.6	24.3	16	34	50	19.0
13 – 16	48.8	24.4	20	31	49	19.0
16 – 19	48.6	24.3	18	32	50	18.6
19 – 23	49.1	24.6	20	32	48	18.7
23 – 26	46.6	23.3	21	31	48	18.4
26 – 30	46.6	23.3	26	27	47	21.1
30 – 34	42.1	21.1	28	35	37	19.5
34 – 38	32.8	16.4	40	29	31	11.3
38 – 42	23.4	11.7	56	27	17	8.0
42 – 46	21.2	10.6	61	32	7	4.7
46 – 51	21.2	10.6	65	30	5	5.2

[1] Method 27a (U.S. Salinity Laboratory Staff, 1954).

[2] One-half of percent moisture at saturation is shown as estimated field capacity.

[3] The sand fraction (greater than 74 microns) was determined by sieving, the silt (2 to 74 microns) and clay (less than 2 microns) fractions by hydrometer analyses.

[4] Lineal shrinkage $= 100\left(1 - \sqrt[3]{\dfrac{100}{\text{Volume change} + 100}}\right)$

REFERENCES

Branner, J. C., Newson, J. F., and Arnold, Ralph, 1909, Description of the Santa Cruz quadrangle [California]: U.S. Geol. Survey Geol. Atlas, Folio 163.

U.S. Salinity Laboratory Staff, 1954, Diagnosis and improvement of saline and alkali soils: U.S. Dept. Agriculture, Agr. Handb. no. 60, 160 p.

77.   CAUSES AND MECHANICS OF NEAR-SURFACE SUBSIDENCE IN WESTERN FRESNO COUNTY, CALIFORNIA

By WILLIAM B. BULL, Sacramento, Calif.

Work done in cooperation with the California Department of Water Resources

Near-surface subsidence on certain alluvial fans in western Fresno County, Calif., has destroyed or damaged ditches, canals, roads, pipelines, electric transmission towers, and buildings, and has made the irrigation of crops difficult. About 72 square miles have subsided and about 37 additional square miles probably would subside if irrigated. Three to 5 feet of subsidence is common, and more than 10 feet has occurred within small areas.

The subsidence results chiefly from the compaction of deposits by an overburden load as the clay bond supporting the voids is weakened by water percolating through the deposits for the first time. The amount of subsidence that occurs when water is applied is dependent mainly on the overburden load, natural moisture conditions, and the amount and type of clay.

The materials are deposited during the winters as mud-flows, water-laid sediments, and deposits intermediate between these two types. Some of the voids commonly found in these alluvial-fan deposits are openings between grains held in place by a dry clay bond, bubble cavities formed by air entrapped at the time of deposition, interlaminar openings in thinly laminated sediments, buried (but unfilled) polygonal cracks, and voids left by entrapped vegetation. An unusually large number of bubble cavities is shown in the clay in figure 77.1.

The average annual rainfall on the fans is only 6 to 8 inches. Plants and air remove much of the soil moisture during the hot, dry summers, reducing the moisture condition of the deposits to the wilting coefficient. Water from succeeding winter rains and floods does not percolate below the root zone; therefore the deposits continue to be moisture deficient after burial below the root zone.

Near-surface subsidence illustrates the significance of water in the natural compaction of sediments. Most alluvial sediments are compacted in the presence of excess water as the overburden load increases. However, on the fans susceptible to near-surface subsidence, the deposits are moisture deficient and only part of the compaction occurs as the overburden load is gradually increased. Later application of irrigation water allows the compaction to increase suddenly to the normal amount of compaction for a given overburden load, causing surface subsidence.

EFFECT OF OVERBURDEN LOAD

The amount of compaction due to wetting increases with an increase in overburden load, but most subsidence has been caused by compaction in the upper 200 feet of deposits. The surface of three irrigated test plots rose slightly immediately after the water was applied because the surface deposits swelled. When the water reached a depth of a few feet, the increased overburden load caused a net reduction in the volume of the deposits as the clay became wetter and lost part of its strength.

The effect of the overburden load on subsidence during the first 42 months of operation of Inter-Agency test plot B (Inter-Agency Committee, 1958, p. 61–67) is shown in figure 77.2. Bench marks were set within cased holes drilled beneath this test plot at depths of 25, 50, 75, 100, 150, and 300 feet. The amount of compaction within each depth interval above 150 feet was determined from periodic level-
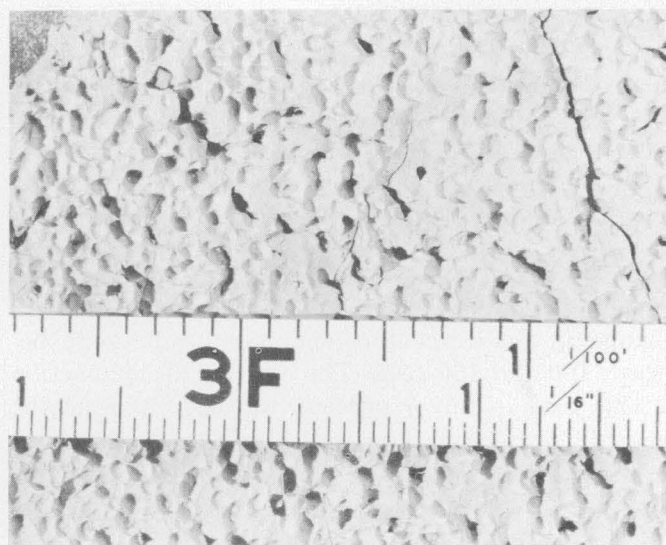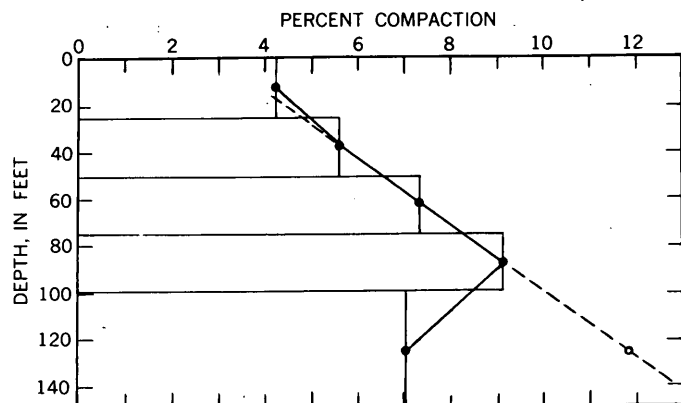

FIGURE 77.1.—Bubble cavities in clay.

FIGURE 77.2.—Effect of overburden load on compaction due to wetting, Inter-Agency test plot *B* after 42 months of operation.

ing of these bench marks. Each point in figure 77.2 represents the percent compaction within a 25-foot depth interval except the point at 125 feet which represents the 50-foot interval between 100 and 150 feet. To a depth of 100 feet, there is a nearly linear increase in the percent compaction with increasing depth. The reason for the decrease in the percent compaction of the 100- to 150-foot depth interval is discussed below.

STRENGTH OF CLAY

The strength due to clay in a deposit is dependent on the moisture content and on the type and amount of clay. These variables control the amount of compaction due to wetting under a given overburden load.

The strength of clay varies considerably for all moisture gradations between wet and dry. The natural moisture condition of the deposits susceptible to subsidence is about equivalent to the wilting coefficient, and subsidence is chiefly the result of compaction caused by increasing the moisture content of these deposits to a condition of field capacity.

A good example of the importance of moisture conditions is provided by the compaction record shown in figure 77.2. Although the lithology does not appear to change with depth there is a marked change in the percent compaction in the zone between 100 and 150 feet. The amount of compaction in this zone is only 7 percent, but the circle on the dashed (projected) line indicates that the amount of compaction for that overburden load should have been about 12 percent. Tests of cores showed a sharp increase in natural moisture content below about 125 feet. The higher moisture content would indicate an increase in the natural compaction of

the deposits below 125 feet, and therefore less compaction due to artificial wetting.

The effect of the amount of clay on compaction due to wetting is shown in figure 77.3. The consolidation tests were made on surface samples, therefore a 50-foot overburden load was simulated. The variable of post-depositional environment was eliminated, because the air-dry samples were collected a few months after they were deposited. The variable of textural features of the samples remains, but these features are controlled partly by clay content. Montmorillonite is the predominant clay mineral (R. H. Meade, written communication).

This leaves the amount of clay as the most important variable. The curve in figure 77.3 shows the amount of compaction that occurs when air-dry samples are wetted under load. The sample containing no clay did not compact when wetted. Samples containing more than about 30 percent clay not only had enough strength to resist compaction when wetted but they showed a net swell under the simulated overburden load. The maximum compaction
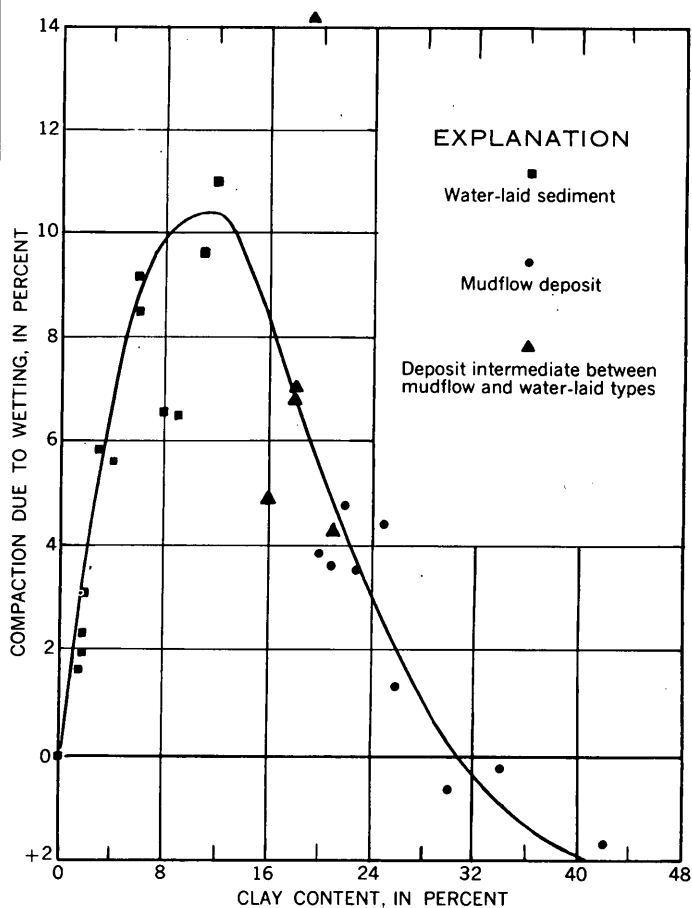

FIGURE 77.3.—Effect of clay content on compaction due to wetting under a simulated load of 50 feet of overburden.

for the samples tested occurred when the clay content was about 12 percent. If less than this amount is present, the dry overburden load already will have accomplished much of the compaction because there is not enough clay to preserve the larger voids.

As the amount of clay increases above about 12 percent, the resistance of the sample to compaction when wetted increases progressively with clay content. In addition, the montmorillonite clay minerals swell. Both factors reduce the compaction progressively, and for the samples tested, the net compaction decreased to zero at about 30 percent clay.

REFERENCE

Inter-Agency Committee on Land Subsidence in the San Joaquin Valley, 1958, Progress report on land-subsidence investigations in the San Joaquin Valley, Calif., through 1957: Multilithed, 160 p., 45 pls.

---

78. SPECIFIC GRAVITY OF SANDSTONES IN THE FRANCISCAN AND RELATED UPPER MESOZOIC FORMATIONS OF CALIFORNIA

By WILLIAM P. IRWIN, Menlo Park, Calif.

Work done in cooperation with the California Division of Mines

---

The specific gravity of sandstone was investigated as an adjunct in distinguishing between the Franciscan and related upper Mesozoic formations in the Coast Ranges and Sacramento Valley of California (fig. 78.1). In the Sacramento Valley the formations are of the shelf and slope facies, and constitute an essentially conformable sequence of strata that range in age from Late Jurassic to Late Cretaceous. For the purpose of this discussion the rocks of the Sacramento Valley sequence will be divided according to age into three units: the Knoxville formation of Late Jurassic age, the Lower Cretaceous, and the Upper Cretaceous. In the Coast Ranges most of the rocks of upper Mesozoic age are assigned to the Franciscan formation, a eugeosynclinal assemblage composed mostly of sandstone, but which includes approximately 10 percent greenstone and chert. The Franciscan also ranges in age from Late Jurassic to Late Cretaceous, and is more highly folded and faulted than the strata of the Sacramento Valley. The thickest section of the Sacramento Valley sequence is about 35,000 feet, whereas the Franciscan formation probably is considerably thicker.

Although the Franciscan is the dominant upper Mesozoic formation in the Coast Ranges, rocks of the Sacramento Valley sequence also are present, many as relatively small blocks folded and faulted into the Franciscan. Recognition of small structural blocks of strata of the Sacramento Valley sequence within areas underlain chiefly by the Franciscan formation is difficult in many places because completely satisfactory criteria for distinguishing between sandstones of the Sacramento Valley sequence and of the Franciscan formation have not been determined.

The specific gravity of 1,030 specimens of sandstone of both the Franciscan formation and the Sacramento Valley sequence was measured, including most of the specimens used by Bailey and Irwin (1959) for determination of K-feldspar content, and others collected throughout the Sacramento Valley and the northern and southern Coast Ranges. Specific gravity was measured on a direct-reading balance, with the specimen immersed in water. The average weight of the specimens is approximately 300 grams. Most of the specimens are essentially unweathered and impermeable, and for these the measurements represent bulk specific gravity. However, many of the sandstone units of the Upper Cretaceous of the Sacramento Valley sequence are permeable, and as the surfaces of the specimens were not treated to prevent penetration by water, values somewhat higher than bulk specific gravity were obtained.

Cumulative frequency distribution curves based on the specific gravity measurements are shown in
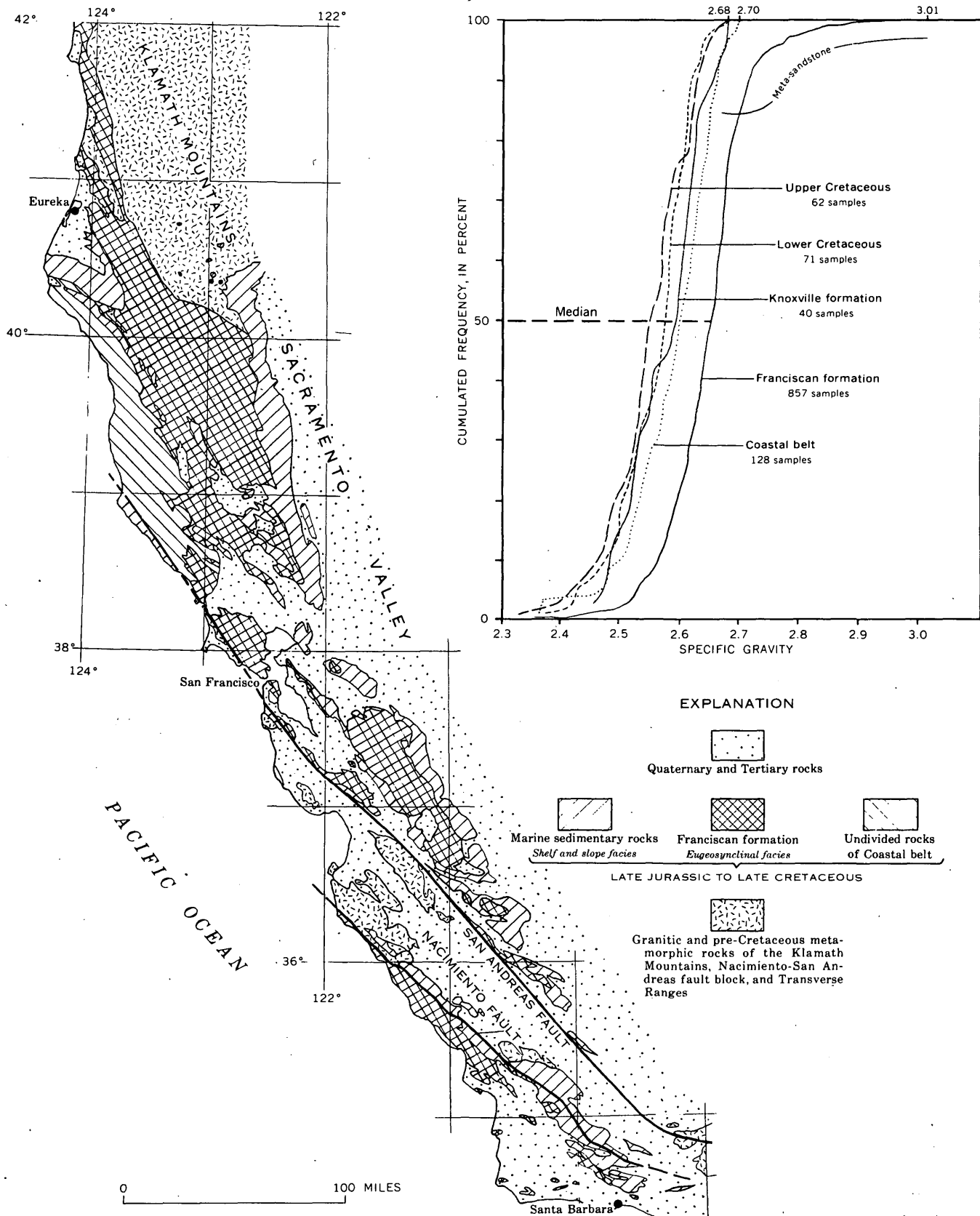
FIGURE 78.1.—Map showing distribution of the Franciscan and related upper Mesozoic formations, with graph showing cumulative frequency distribution curves of specific gravity of sandstones.

figure 78.1. The curve for sandstone in the Franciscan formation is well separated from and on the high specific gravity side of the curves for the three units of the Sacramento Valley sequence. The median specific gravity of the sandstone in the Franciscan is 2.65. The marked increase in specific gravity at the upper end of the Franciscan curve reflects metamorphism of the sandstone that generally is not recognized in hand specimen. E. H. Bailey of the Geological Survey studied the specimens that plot along this part of the curve and states (oral communication, January 1961) that most of the Franciscan sandstone with a specific gravity of 2.70, and all with a specific gravity of 2.71 or higher are metamorphosed; the metamorphism is chiefly of the plagioclase feldspar to form jadeite and lawsonite. About 22 percent of the specimens of sandstone in the Franciscan have a specific gravity higher than 2.68, the highest observed in rocks of the Sacramento Valley sequence.

The curves representing sandstone of the three units of the Sacramento Valley sequence are conspicuously lower than the curve for the Franciscan formation and are displaced progressively toward the low specific gravity side of the graph with decreasing age, although at some places the curves intermingle. As previously stated, many values for sandstone units of the Upper Cretaceous do not truly represent bulk specific gravity, and thus the curve for the Upper Cretaceous should be further to the left side of the graph than shown. Median values for the curves are 2.59 for the Knoxville formation, 2.57 for the Lower Cretaceous, and 2.55 for the Upper Cretaceous.

Reasons for the general differences in specific gravity of the sandstone of the several units are not surely known. However, one might speculate that the generally higher specific gravity of the sandstone in the Franciscan relative to the sandstone of the Sacramento Valley sequence results from a greater abundance of mafic volcanic fragments (high specific gravity), a general lack of K-feldspar (low specific gravity), and a high degree of compaction. The progressive decrease in specific gravity with decrease in age of the units of the Sacramento Valley sequence probably is related to the marked increase in K-feldspar content with decreasing age, and to a progressively smaller amount of compaction resulting from shallower depth of burial.

Specific gravities of 128 specimens of sandstone from the coastal belt of undivided sandstone, shale, and conglomerate are shown by a separate curve. A general lack of volcanic rocks, sparse paleontologic data, and results of study of K-feldspar content (Bailey and Irwin, 1959), suggest an affinity with the Sacramento Valley sequence. The cumulative frequency distribution curve for sandstone of the coastal belt also suggests this affinity, as it is close and generally parallel to the curves for the units of the Sacramento Valley sequence. Although generally somewhat to the right of the curves for the units of the Sacramento Valley sequence, it is far to the left of the curve for the sandstone of the Franciscan. The generally higher specific gravity indicated by the curve for the coastal belt, compared to the curves for units of the Sacramento Valley sequence, may reflect the presence of areas of unrecognized sandstone of the Franciscan formation within the coastal belt. This interpretation is supported by the presence of a few specimens with specific gravities above 2.68, which is higher than the specific gravity of any specimen collected from the Sacramento Valley sequence.

REFERENCE

Bailey, E. H., and Irwin, W. P., 1959, K-feldspar content of Jurassic and Cretaceous graywackes of northern Coast Ranges and Sacramento Valley, California: Am. Assoc. Petroleum Geologists Bull., v. 43, no. 12, p. 2797–2809.

79.   SOME EXTREMES OF CLIMATE IN DEATH VALLEY, CALIFORNIA

By T. W. ROBINSON and CHARLES B. HUNT, Menlo Park, Calif., and Denver, Colo.

The hydrologic basin of Death Valley, Calif., includes about 8,700 square miles, of which about 500 square miles is below sea level. The bottom of the basin, the salt pan, covers about 200 square miles and is more than 200 feet below sea level. Elevations in Death Valley range from 282 feet below sea level near Badwater, the lowest point in the United States, to 11,045 feet at Telescope Peak some 15 miles to the west.

The climatic measurements made at the National Park Service Headquarters, 3 miles north of Furnace Creek Ranch, for the period May 1958 to May 1959, are shown in figure 79.1. The conditions of low humidity, high summer temperatures, high evaporation, and low rainfall, shown graphically in the figure, typify the climate of Death Valley.

In the 48-year period, 1912 to 1960, the U.S. Weather Bureau at Furnace Creek Ranch, formerly Greenland Ranch, recorded the lowest average rainfall, 1.66 inches, of any official weather station in the United States. The average monthly rainfall ranges from a high of 0.29 inch in February to a low of 0.02 inch in June. There have been periods of more than a year in which less than 1 inch of rain has fallen and, during 1929, no measurable rainfall was recorded at this station. The station, 168 feet below sea level, is located on the edge of the salt pan. A frequency analysis of the precipitation records shows an annual precipitation of less than 1 inch during 40 percent of the time, and 3 inches or less for 96 percent of the time. Rainfall has exceeded 4 inches only twice in 48 years.

Temperatures greater than 120°F are common during the summer months. The highest air temperature ever measured in the shade at an official Weather Bureau station in the United States, 134°F, was recorded on July 10, 1913, at Greenland Ranch, now Furnace Creek Ranch. This recording is believed to have been exceeded only by 136°F reading that was observed at Azizia, Tripolitania in northern Africa on September 13, 1922, and which is generally accepted as the highest air temperature recorded under standard conditions (Hansen, 1960, p. 442). July is the hottest month with a long-time average maximum of 116°F. However, Furnace Creek Ranch does not appear to be the hottest place in the valley. Temperature records indicate that Badwater, about 15 miles south of the ranch on the salt pan, 280 feet below sea level, has maximum temperatures as much as 3°F higher; the average maximum for July was 122.5°F in 1959 and 120.4° in 1960, while at the ranch the average maximum was 119.3°F and 118.1°F. In July 1959, the highest temperature recorded at the ranch was 124°F, but at Badwater this temperature was exceeded on 11 days. Similarly in July 1960, 124°F was exceeded on only 1 day at the ranch but on 5 days at Badwater. Ground surface temperatures in excess of 160°F have been recorded in several parts of the valley. The maximum recorded was 190°F in August 1958, and was measured on the surface of massive gypsum at Tule Spring some 5 miles west of Badwater.

The average relative humidity for 2 years of record at the National Park Service Headquarters, May 1, 1958 to May 1, 1960 was 17.2 percent. The average maximum was 23.3 percent and the average minimum 11.7 percent. The highest recorded during this 2-year period was 74 percent and the lowest was 3 percent. The driest day was April 8, 1959 (see fig. 79.1), when the minimum was 4 percent and the maximum was 6 percent.

Pan evaporation in the hydrologic basin of Death Valley is the highest in the nation, exceeding 120 inches a year in most of the basin. It is greatest in Death Valley proper. In the two 12-month periods of record, May 1, 1958 to May 1, 1960, for the standard Weather Bureau pan at the National Park Service Headquarters, the evaporation was 155.05 and 144.66 inches. So far as can be ascertained, this is the highest evaporation from a standard pan ever recorded in the United States. Monthly pan evaporation ranged from a high of 22.71 inches in July 1960 to a low of 2.72 inches in January 1960. During 1958 and 1959 daily evaporation exceeded 1 inch once each summer, and in 1960 three times during the summer. The daily evaporation in June and July for the 3 years averages about 0.70 inch. The ratio of annual pan evaporation to rainfall—90 to 1—is a measure of the aridity of Death Valley. At no other locality in the United States is the ratio known to be this great.

Rainfall during late Pleistocene time was undoubtedly many times greater and evaporation much less than that of the past 50 years. Remnants of bars and shorelines indicate that during this time the precipitation in the basin was sufficient to maintain
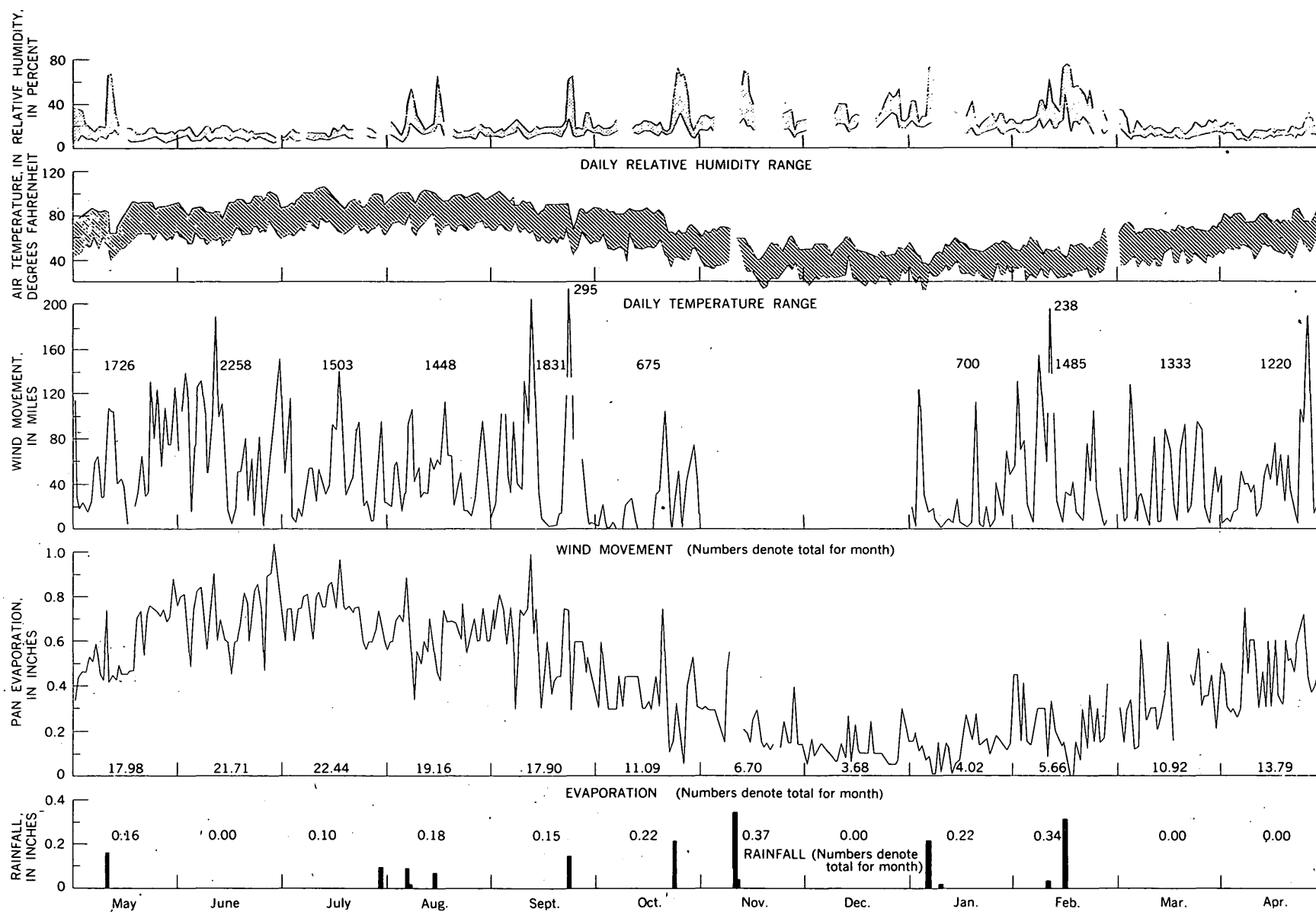
AIR TEMPERATURE, IN RELATIVE HUMIDITY, DEGREES FAHRENHEIT IN PERCENT

80
40
0

DAILY RELATIVE HUMIDITY RANGE

120
80
40

295
DAILY TEMPERATURE RANGE
238

WIND MOVEMENT, IN MILES

200
160
120
80
40
0

1726   2258   1503   1448   1831   675   700   1485   1333   1220

WIND MOVEMENT   (Numbers denote total for month)

PAN EVAPORATION, IN INCHES

1.0
0.8
0.6
0.4
0.2
0

17.98   21.71   22.44   19.16   17.90   11.09   6.70   3.68   4.02   5.66   10.92   13.79

EVAPORATION   (Numbers denote total for month)

RAINFALL, IN INCHES

0.4
0.2
0

0.16   0.00   0.10   0.18   0.15   0.22   0.37   0.00   0.22   0.34   0.00   0.00

RAINFALL (Numbers denote total for month)

May   June   July   Aug.   Sept.   Oct.   Nov.   Dec.   Jan.   Feb.   Mar.   Apr.

FIGURE 79.1.—Climatic observations during the period of May 1958 to May 1959 as recorded by the weather station at National Park Service Headquarters on Cow Creek in Death Valley, Calif.

a lake in Death Valley some 600 feet deep in places, more than 100 miles long and from 5 to 10 miles wide.

In spite of the extremes just described, the climate of Death Valley is delightful from about mid-September to about mid-May. This is attested to by the thousands of visitors who annually visit the valley during these months.

REFERENCE

Hansen, Harry, editor, 1960, The World Almanac: New York, New York World-Telegram and The Sun, 896 p.

⚒

80. STRATIGRAPHY OF DESERT VARNISH

By CHARLES B. HUNT, Denver, Colo.

Desert varnish, a natural dark stain of iron and manganese oxides on rock surfaces, is useful in the study of the stratigraphy of Recent deposits in the semiarid and arid west, for, in general, it permits separating deposits and surfaces that are no older than about 2,000 years from earlier ones.

As the name implies, desert varnish is best developed, or at least is most conspicuous, in desert regions, but the stain is by no means restricted to such areas. Similar stain, also consisting chiefly of iron and manganese oxides, covers rock surfaces in humid regions too.

The stain occurs on every type of rock, although it is least common on carbonate rocks. The surfaces stained may be the top or sides of stones lying about the surface; they may be vertical or overhanging cliffs or surfaces splashed by rivers or wetted by seeps. The stained surfaces may be exposed to direct sunlight or surfaces never reached by the sun, such as joint planes.

Engle and Sharp (1958), in an important contribution to the chemistry of desert varnish, studied trace elements occurring with the iron and manganese stain and concluded that (a) varnish on stones seated in soil or colluvium is derived largely from that material, (b) varnish on large bedrock surfaces comes from weathered parts of the rock, and (c) airborne materials are probably a minor contributor.

There is abundant archeological evidence throughout the Western States indicating that very little varnish has been deposited during the last 2,000 years. Only locally are stone artifacts and structures of the pottery and bow-and-arrow occupations—the occupations characteristic of the last 2,000 years— stained with desert varnish. In general they are not stained, whereas stone artifacts of the earlier, pre-pottery occupations commonly are stained, and the earliest ones darkly so. These generalizations are based on observations at many hundreds of archeological sites; the numerous and well-known prehistoric structures at Mesa Verde National Park are examples of pottery-age structures that are younger than the desert varnish staining the cliffs there (fig. 80.1). Also, in the Rocky Mountains, desert varnish characteristically is lacking on the most recent, historic and protohistoric glacial deposits in cirques, but is present on older ones (Moss, 1951, p. 877). Finally, on the gravel fans throughout the southwest, the elevated and older surfaces are stained with varnish, whereas the lowest surfaces, the youngest ones, are not. The archeological record and the supporting physical record are compelling that little varnish has been deposited in the Western States during the last 2,000 years.

The same appears to be true in arid regions in other parts of the world. Blackwelder (1948) cites evidence from Egypt indicating practically no deposition of desert varnish in 2,000 years, slight deposition in 5,000 years, and dark stain on older stonework.

There are exceptional localities. Iron and manganese oxides are being deposited at many seeps at the present time, but these clearly are isolated localities where conditions, still not understood, have been unusual and optimum for its deposition. Engle and Sharp (1958, p. 515–516) overemphasize such a locality—one where they infer varnish has been deposited in 25 years. But the total record indicates clearly that such deposition is highly localized and
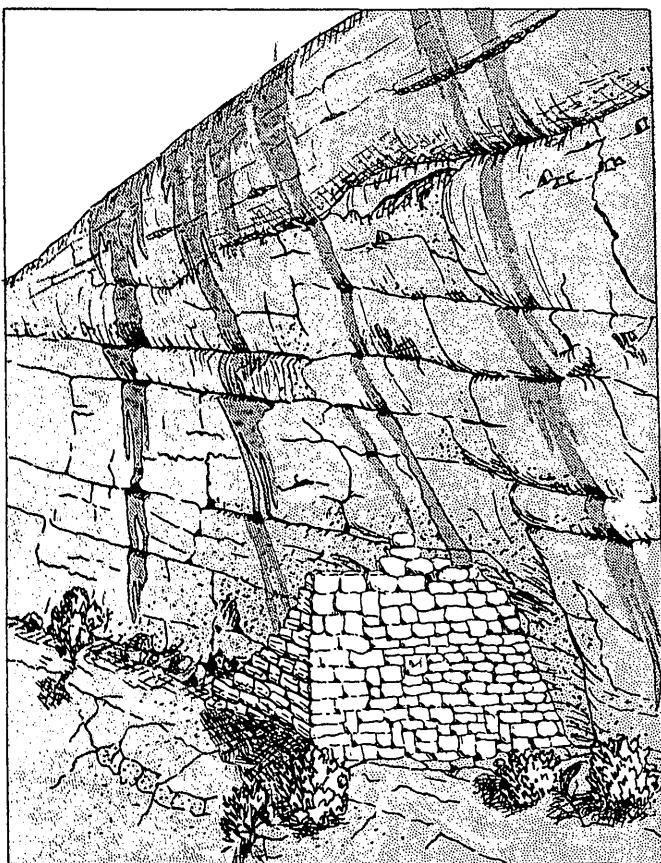
The origin of desert varnish still is uncertain. Water obviously is needed to transport the metals to the surfaces where they are deposited, and iron and manganese are being deposited at the present time at many wet places in the West and in the more humid parts of the country. Very little or no varnish is being deposited on surfaces that are not frequently wet. This restricted occurrence of newly deposited iron and manganese oxides suggests that the moisture requirements may be considerable. Deposition may be chiefly by physical-chemical processes, but I suspect that micro-organisms play a major role, as they are known to do in hastening the oxidation of iron compounds in mine waters. (See bibliography in Temple and Koehler, 1954).

Whatever the process of origin, the evidence about the age of desert varnish and the evident need for moisture to produce the deposits leads to the conclusion that the principal deposits are the product of pluvial periods. The last such pluvial time in the Western States was just prior to the Christian era. The archeological evidence indicates substantial deposition of desert varnish at that time and very little since then.

FIGURE 80.1.—Pottery-age cliff house dwellings and other structures (ca. 500 to 1300 A.D.) at Mesa Verde and elsewhere in the Southwest rarely are stained with desert varnish but generally are built against cliffs that are stained, and the masonry overlaps the stained surfaces.

exceptional. Were it otherwise, buildings and other surfaces, artificial and natural, that are as old as 25 years should generally be darkly stained.

REFERENCES

Blackwelder, Eliot, 1948, Historical significance of desert lacquer [abs.]: Geol. Soc. America Bull., v. 59, p. 1367.

Engle, C. G., and Sharp, R. P., 1958, Chemical data on desert varnish: Geol. Soc. America Bull., v. 69, p. 487–518.

Moss, J. H., 1951, Late glacial advances in the southern Wind River Mountains, Wyoming: Am. Jour. Sci., v. 249, p. 865–883.

Temple, K. L., and Koehler, W. A., 1954, Drainage from bituminous coal mines: West Virginia Univ. Bull. Eng. Exp. Sta., Research Bull. 25, 35 p.

81.   USE OF ARCHEOLOGY IN RECENT STRATIGRAPHY

By CHARLES B. HUNT and ALICE P. HUNT, Denver, Colo.

The changes in the tools of the prehistoric occupants of the United States provide a stratigraphic record that helps distinguish between older and younger Recent deposits. The earliest known occupations in the United States were in late Pleistocene time, but these are not sufficiently numerous nor well enough known to be helpful geologically. In this country late Pleistocene deposits are best iden-

tified by their content of Pleistocene species of elephants, camels, horses, and other mammals (Hunt, 1953).

Prehistoric occupations accompanied by a modern vertebrate fauna, the basis for Lyell's original definition of the Recent (Lyell, 1873; Forbes, 1846), can be divided into two major stages. The late stage roughly coincides with the Christian era, that is, the past 2,000 years, and it is characterized over much of the United States by pottery and the bow and arrow. Earlier peoples depended on basketry and the atlatl or spear.

The changes in tools did not occur simultaneously over the whole of the United States. In parts of central United States, for example, pottery was used before 1 A.D., whereas along much of the Pacific Coast pottery never was made. Similarly, the Indians of Florida continued to use the throwing stick (atlatl) almost to historic time. Nevertheless, the early stages of the Recent are prepottery and prebow-and-arrow, and are characterized by the heavy projectile points suitable for spears or the atlatl.

Archeologists distinguish many stages within the arrowpoint and atlatl stages, the two major ones, but for geological purposes a two-fold division of each is sufficient. Figure 81.1 illustrates a stratigraphic sequence of projectile points from the Basin and Range province, Colorado Plateau, and High Plains. The diagram, of necessity oversimplified, is adapted from other published chronologies, especially one by Krieger (1950). Some projectile-point types continued to be made from one stage into another, although in reduced numbers. Further, one must consider the associated traits and not depend on a single one. In paleontology it is the faunal assemblage rather than the individual fossil that is important; in archeology it is the collection of associated traits rather than the individual artifact that is important. For example, there is no difficulty in distinguishing a modern kitchen from a colonial one despite the fact that the modern kitchen may contain some colonial antiques.

In the western States the pottery and bow-and-arrow occupations commonly are on top of alluvial flood plains, and they may occur in dunes that have formed on top of the alluvium. Such dunes clearly are the product of the past 2,000 years, and the alluvium is earlier.

Where the underlying alluvium contains a modern fauna and is therefore Recent, the projectile points in the alluvium are likely to be those shown in the
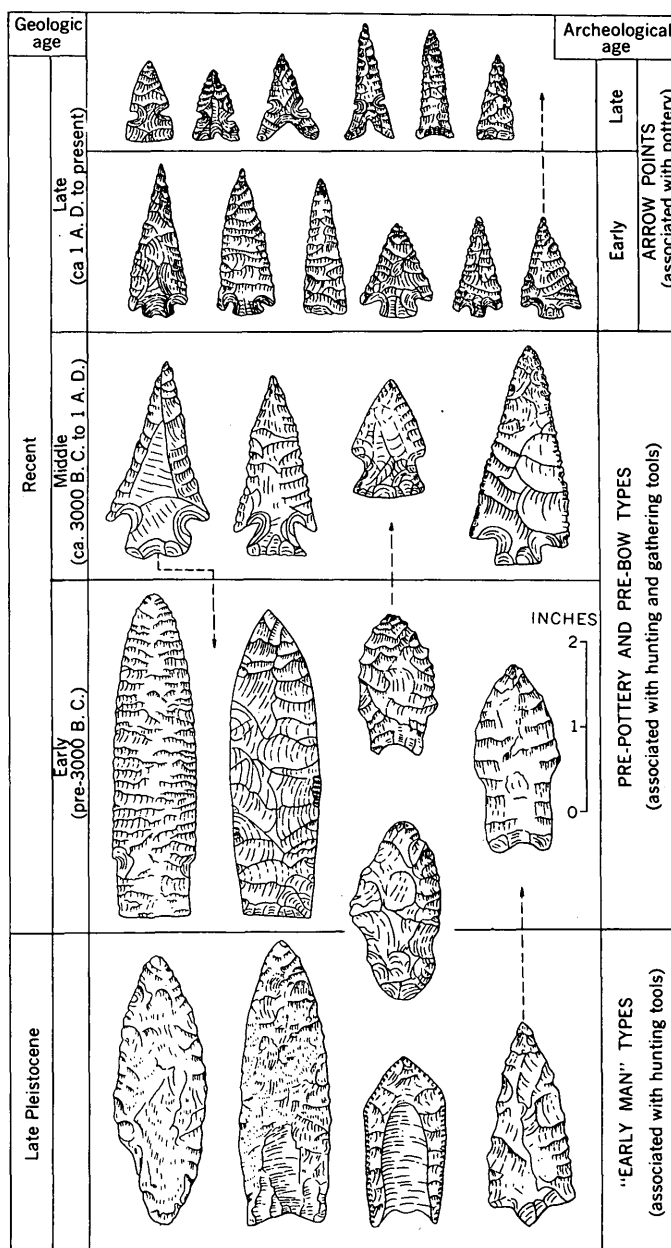
FIGURE 81.1.—Stratigraphy of some projectile point types of the Basin and Range province, Colorado Plateau, and High Plains.

middle row of figure 81.1. These are larger and heavier than the arrow points, which are later.

This Recent alluvium may overlap old sand dunes that are weathered reddish and stabilized. The projectile points most common in these dunes are like some indicated in figure 81.1 as early Recent. The alluvial, colluvial, or other deposits overlapped by the stabilized dunes generally are of Pleistocene age and can be so identified by their paleontological remains.

One of the limitations of the archeological record is that sites with sufficient tools to be useful for geologic stratigraphy and geologic mapping are mostly at the surface, and these provide only a limital date for the underlying deposit. Only rarely are diagnostic artifacts contained within a deposit over sufficient extent or in sufficient numbers to be exposed in a cross-section cut and thus useful in geologic mapping. Nevertheless, the sites, especially the younger ones, are sufficiently numerous to be of great assistance in many areas for distinguishing the different stages of Recent deposits.

REFERENCES

Hunt, C. B., 1953, Pleistocene-Recent boundary in the Rocky Mountain region: U.S. Geol. Survey Bull. 996–A, p. 1–25.
Lyell, Charles, 1873, Geologic evidences of the antiquity of man: 4th ed. London, p. 3–4.
Forbes, Edward, 1846, On the connexion between the distribution of the existing fauna and flora of the British Isles and the geologic changes which have affected their area, especially during the epoch of the northern drift: Geol. Survey of England and Wales, Mem., v. 1, pt. III, p. 402–403.
Krieger, A. D., 1950, A suggested general sequence in North American projectile points: Utah Univ. Anthropological Papers, no. 11, p. 117–124.

82. EVIDENCE OF STRIKE-SLIP MOVEMENT ON NORTHWEST-TRENDING FAULTS IN MOJAVE DESERT, CALIFORNIA

By T. W. DIBBLEE, JR., Menlo Park, Calif.

The western Mojave Desert region is transected by many prominent northwest-trending high-angle faults, as shown on figure 82.1. These are nearly parallel to the San Andreas fault and terminate south of the Garlock fault, and they cut Quaternary sediments and basalt; many have inconsistent or even alternating vertical displacements. Movements on these faults have been interpreted to be mainly dip-slip (Hewett, 1954, p. 17). However, geologic mapping of this region during the past few years reveals that structural and physiographic features adjacent to some of these faults indicate or suggest movements that are predominantly right lateral, as on the San Andreas fault, but on a smaller scale.

In the western part of this region, southwest of Mojave, two northwest-trending faults (fig. 82.1 A) show conclusive evidence of right-lateral displacement but no discernible vertical displacement. Vertical east-trending pre-Tertiary rock units transected by these two faults are offset as much as 1,500 feet, and several southward-draining stream-channels that dissect the overlying Quaternary fan gravel are deflected westward as they cross the faults.

Farther east, in the central part of the region, a northwest-trending fault (fig. 82.1 B) transecting an extensive exposure of Mesozoic granitic rock south of Boron offsets several hundred feet right laterally a network of vertical dikes of pegmatite and aplite (Dibblee, 1961).

Still farther east, metavolcanic rocks that are exposed on the southwestern side of the Helendale fault (fig. 82.1 C), notheast of Victorville, are ap-

parently displaced several miles northwestward. Vertical displacements on this fault are reversed at several places on its course and are small.

On the Lockhart fault (fig. 82.1 D) northeast of Boron, vertical displacements are small and alternating. On the northeast block undrained depressions formed in Quaternary alluvium along several north-trending branch faults (Dibblee, 1959) suggest that these branch faults may be in part tension fractures resulting from internal stresses set up by right-lateral drag movement of the block.
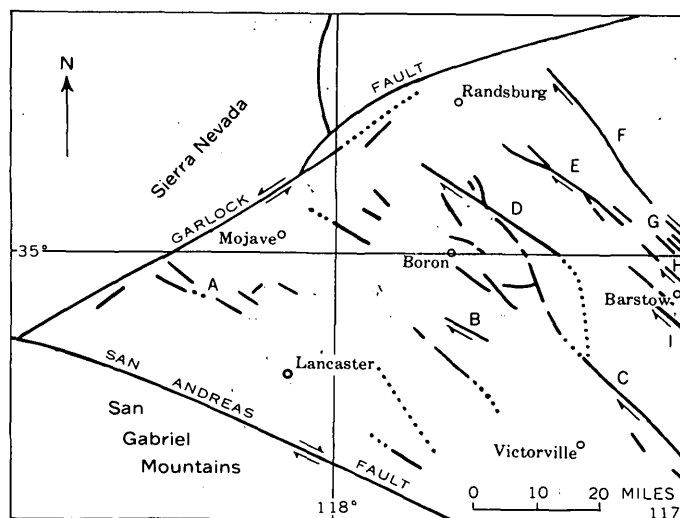

FIGURE 82.1.—Faults in the western Mojave Desert region (between San Andreas and Garlock faults). Position of faults referred to in text is indicated by letters.
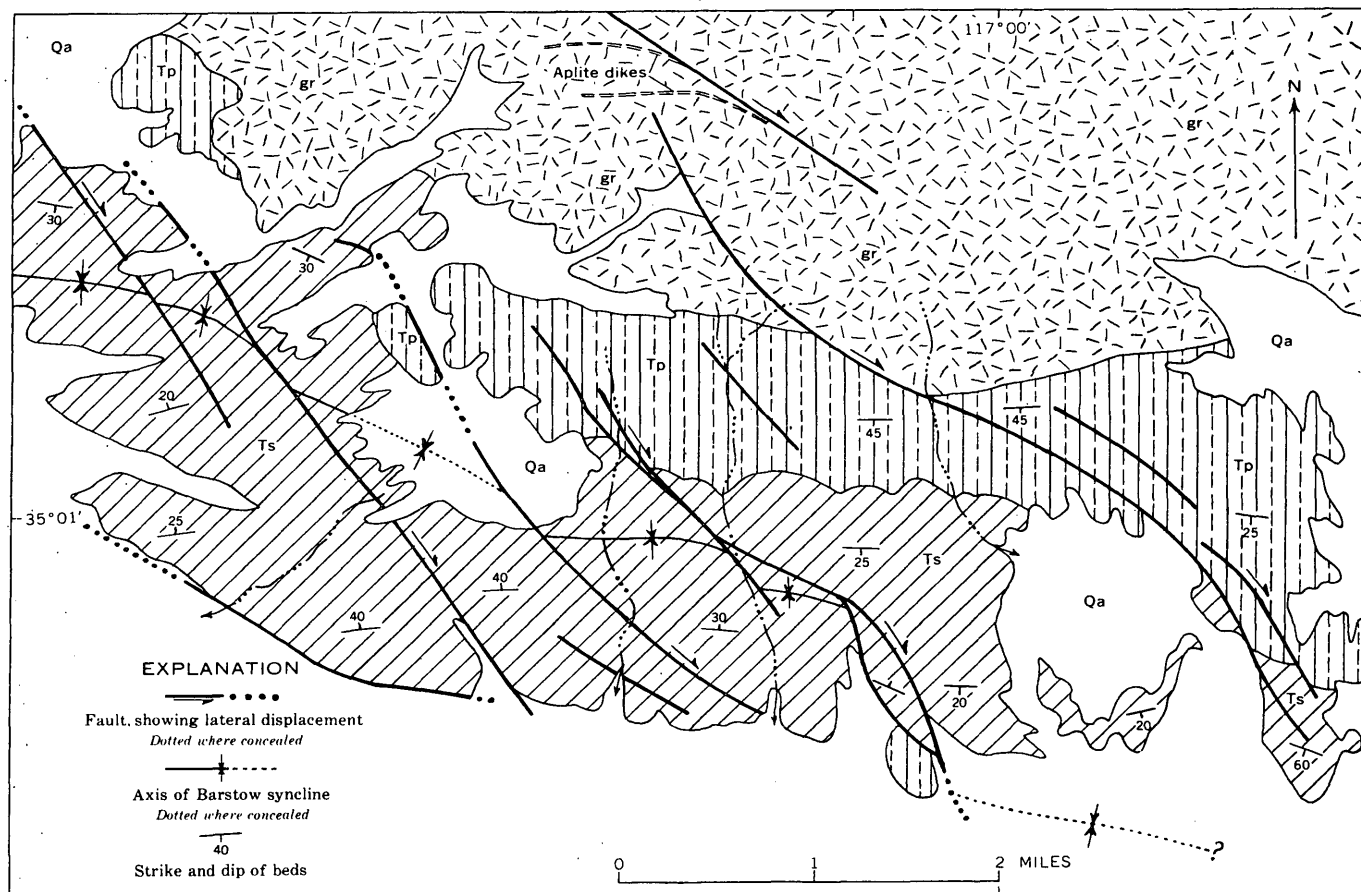
FIGURE 82.2.—Map of the Mud Hills near Barstow. Qa, alluvial sediments, Quaternary; Ts, sedimentary rocks, Miocene; Tp, mainly pyroclastic rocks, Miocene(?); gr, granitic rocks, Mesozoic.

Southeast and east of Randsburg, structural features in the Tertiary and Quaternary sedimentary and volcanic rocks strongly suggest right-lateral drag movement and displacement along the Harper and Blackwater faults (Hewett, 1954, pl. 1). The Harper fault (fig. 82.1 E) is a zone of several minor parallel faults along which Tertiary rocks are compressed into folds with axes trending east as compared to the northwesterly trend of the faults, and the axes of several folds are offset right laterally along several of the faults of this zone. The Blackwater fault (fig. 82.1 F), a few miles northeast, also offsets contacts of several rock units right laterally. Southeastward, both these faults pass into and apparently die out under a thin but extensive cover of Quarternary basalt; along the extensions of the fault traces this otherwise undeformed flow is buckled into several arches whose axes trend south of east, indicating right-lateral drag movement. Vertical displacements on these faults are small and inconsistent.

In the Mud Hills, 8 to 12 miles north of Barstow and a few miles southeast of the Quaternary basalt flow under which the Blackwater fault disappears, granitic rocks are overlain by some 6,000 feet of stratified rocks of Miocene age that are compressed into a symmetrical syncline with an axis trending nearly east. This axis and some contacts between rock units are offset right laterally by several northwest-trending faults (fig. 82.1 G) that diagonally transect the folded sequence as shown on figure 82.2. Nearly horizontal grooves can be seen on several of the fault planes where well exposed. On the southwest block of a fault north of the Mud Hills, aplite dikes are bent parallel to the fault where they approach it (fig. 82.2).

A northeast-dipping fault (fig. 82.1 H) near Barstow (Dibblee, 1960) has generally been regarded as a thrust fault (Waterman thrust of Bowen, 1954, p. 104–105, pl. 1) with vertical uplift on the northeastern block. Recent mapping reveals that it displaces a small granitic intrusion right laterally a

few hundred feet. The northeast-trending foliation of the gneiss of this area bends northwesterly, parallel to the fault along part of its course.

Another northwest-trending fault (fig. 82.1 *I*) southwest of Barstow (Dibblee, 1960), displaces right laterally the axis of at least one large east-trending fold in Quaternary alluvial sediments and terminates several drag folds east of the fault.

Evidence of right-lateral displacement on several other northwest-trending faults in the western Mojave Desert region is lacking, but their straight traces suggest all are high-angle or vertical faults. None shows evidence of left-lateral movement.

At a few places where some of the northwest-trending faults are exposed, the fault planes are generally vertical or dip steeply. Steep dips are suggested, also, by the generally straight traces of all the faults. They generally transect hilly terrain or alluviated valleys. Gravity data (Mabey, 1960) indicate that, with a few local exceptions, the faults do not bound the deep alluvial basins. Some form only low scarps, and none lies at the foot of high steep mountain fronts. Strike-slip displacements probably exceed vertical displacements along some of the faults; some show little or no geologic or physiographic evidence of vertical displacement, yet make conspicuous lineations on aerial photographs.

In marked contrast, most of the great normal faults of the region north of the Garlock fault trend north, sharply bound alluviated valleys and mountain ranges, have imposing fault-line scarps, commonly curve abruptly or jog, and dip toward the sunken valley blocks.

Presumably, the strike-slip movement of the northwest-trending faults are related to movement along the San Andreas fault, but the movements are of much smaller magnitude.

REFERENCES

Bowen, O. E., Jr., 1954, Geology and mineral deposits of the Barstow quadrangle, San Bernardino County, Calif.: California Div. Mines Bull. 164, p. 1–185.
Dibblee, T. W., Jr., 1959, Geologic map of the Boron quadrangle, California: U.S. Geol. Survey Mineral Inv. Field Studies Map MF–204.
——— 1960, Geologic map of the Barstow quadrangle, San Bernardino County, California: U.S. Geol. Survey Mineral Inv. Field Studies Map MF–233.
——— 1961, Geology of the Rogers Lake and Kramer quadrangles, California: U.S. Geol. Survey Bull. 1089–B.
Hewett, D. F., 1954, A fault map of the Mojave Desert region, [Pt.] 2, Chap. 4 of Jahns, R. H., ed., Geology of southern Cailfornia: California Div. Mines Bull. 170, p. 15–18.
Mabey, D. R., 1960, Gravity survey of the western Mojave Desert, California: U.S. Geol. Survey Prof. Paper 316–D, p. 51–72.

83.   ZONING OF SALINE MINERALS AT DEEP SPRING LAKE, CALIFORNIA

By Blair F. Jones, Washington, D. C.

The Deep Spring Valley is a relatively small intermontane basin in northern Inyo County, Calif. Drainage is wholly internal and the area possesses many features in common with the larger lacustrine closed basins of the region. At the southern end of the valley is a small playa known as Deep Spring Lake (fig. 83.1). The playa is nearly equidimensional and covers an area of approximately 5 square miles. The northeastern third of this area has a porous multilayered saline crust up to 16 inches thick and is underlain for the most part by fluid organic black mud. This area is outlined by a low levee built up in connection with a commercial attempt to obtain

potash salts. The playa south and immediately west of the levee is covered by a thinner saline crust, which overlies dense moist gray-green or brown mud. The western one-third of the area consists of clay, grading to silt and sand toward the playa margins; much of this area is marked by very shallow alluvial channels and is covered by efflorescent salt crust.

The distribution of saline minerals in the Deep Spring Lake deposits is largely dependent on the hydrography of the area. About two-thirds of the area enclosed by the levee contains a perennial body of dense highly colored brine, which is exposed in a
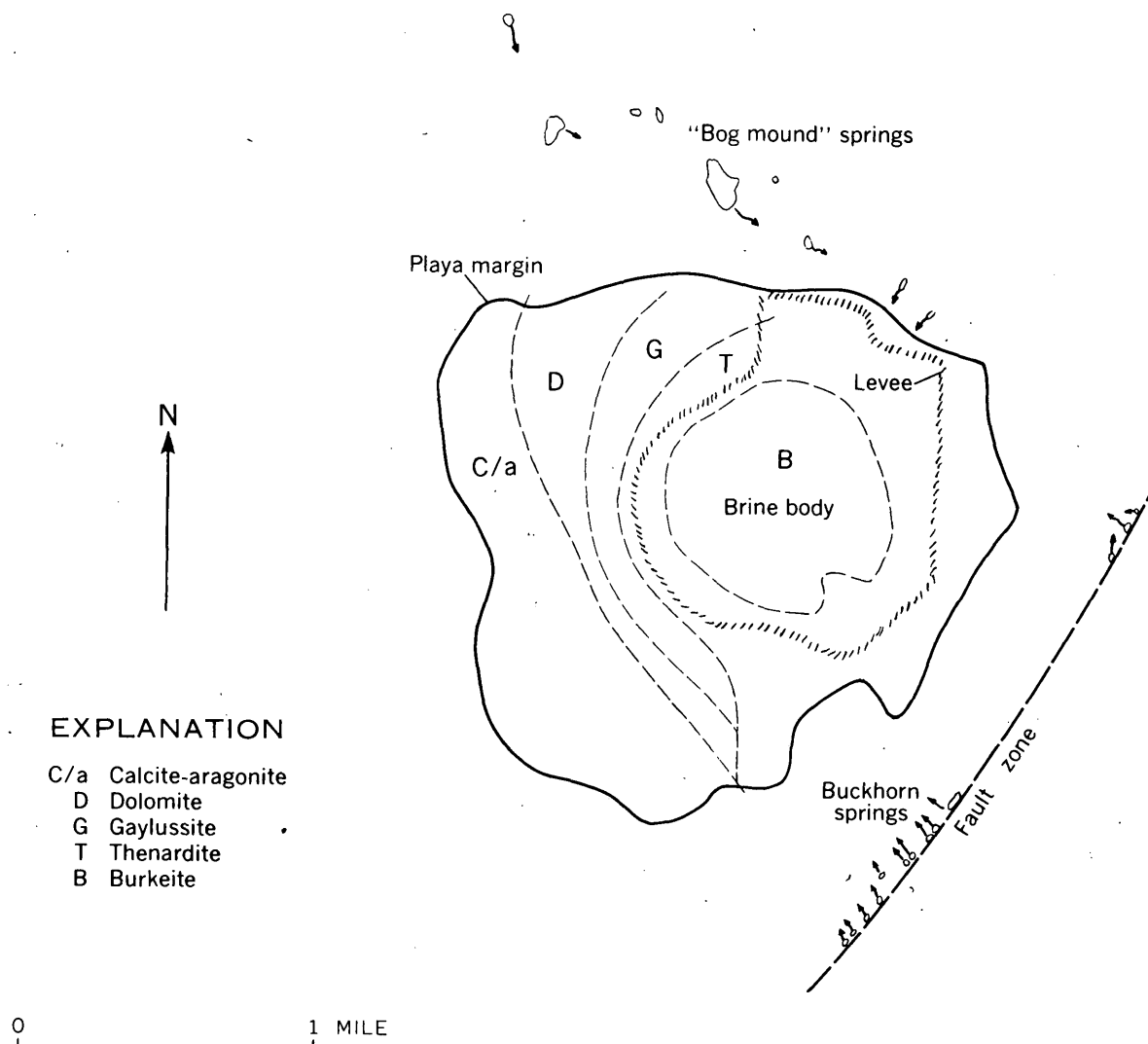
FIGURE 83.1.—Sketch map of Deep Spring Lake, Inyo County, Calif., showing mineral zoning.

few stagnant pools in the driest seasons. Normally, a standing body of saline water a few inches deep occupies a substantial part of the leveed area. In wetter seasonal cycles, the lake water extends beyond the levee. Most of the coherent saline crusts have been precipitated by evaporation of lake waters.

The waters of Deep Spring Lake are derived from (a) a series of "bog mound" springs on the north side of the lake, (b) the Buckhorn springs (which rise along a prominent fault zone on the east side of the lake), (c) direct precipitation on the lake area, (d) seepage through the lake muds from below, and (e) overland flow. The last two sources are probably minor as compared to the others. Normally the Buckhorn springs contribute by far the greatest amount of inflow to the lake at all times of the year.

The saline minerals and the general type of deposit in which they occur are listed below in approximate order of abundance:

Mineral	Occurrence
Dolomite, $CaMg(CO_3)_2$	Mud
Calcite, aragonite, $CaCO_3$	Mud
Thenardite, Na_2SO_4	Mud, saline crust, efflorescence
Halite, $NaCl$	Mud, saline crust, efflorescence
Gaylussite, $Na_2Ca(CO_3)_2 \cdot 5H_2O$	Mud
Burkeite, $Na_6(SO_4)_2CO_3$	Mud, saline crust, efflorescence
Aphthitalite, $Na_3K(SO_4)_2$	Saline crust, efflorescence
Trona, $Na_3H(CO_3)_2 \cdot 2H_2O$	Saline crust, efflorescence
Pirssonite, $Na_2Ca(CO_3)_2 \cdot 2H_2O$	Efflorescence
Nahcolite, $NaHCO$	Mud
Thermonatrite, $Na_2CO_3 \cdot H_2O$	Efflorescence
Glauberite, $Na_2Ca(SO_4)_2$	Saline crust, efflorescence
Sylvite, KCl	Saline crust, efflorescence
Bloedite, $Na_2Mg(SO_4)_2$	Saline crust

Detrital minerals, predominantly quartz and "illite" (as defined by Grim, 1953, p. 35) are also present in the muds.

Hunt (1960) has delineated mappable zones in the salt pan at Death Valley based on dominant anion composition and related to the sequence of precipitates formed on evaporation of an average brine. To provide greater detail and correlation with water composition, the zoning of the deposits at Deep Spring Lake has been worked out on the basis of saline mineralogy rather than chemical composition. This zoning is of three types: relatively regular lateral zoning of precipitate minerals in the lacustrine deposits over the entire playa area (fig. 83.1); local vertical zoning within distinct layers of saline minerals; and highly irregular and often localized zoning of saline mineral assemblages in efflorescent crusts. The first type is the only one that can be mapped.

With the exception of calcite and dolomite, zonal boundaries are drawn along the outer limit of certain key precipitate minerals on the playa. Calcite-aragonite and dolomite zones are based on the relative amounts of these minerals. The sequence of key minerals from playa margin to center is calcite and (or) aragonite, dolomite, gaylussite, thenardite, burkeite. Except for aragonite and gaylussite, all the key minerals persist from the outer limits of their occurrence to the center of Deep Spring Lake. No aragonite could be positively identified in deposits containing thenardite. Gaylussite crystals persist only into the outer reaches of the thenardite zone.

No zone based on halite can be established, inasmuch as halite crystallizes from evaporating waters over a wide area. Other saline minerals occur irregularly, or in response to conditions other than fluctuating lake levels alone.

Calcite and (or) aragonite strongly dominate over dolomite only on the playa's far western side. Typically the surficial sediments of these areas contain a high percentage of detrital material. Most of the carbonate is present as an extremely fine grained aggregate.

Dolomite is the dominant precipitate mineral of the muds throughout most of the playa. Such muds usually are extremely fine grained, smooth and even textured, plastic, and normally gray-green except near the top where they are oxided and are light brown. The dolomite-clay aggregate is commonly coated with hydrous iron oxide. It is very difficult to draw a precise zonal boundary separating areas containing mostly dolomite from those containing mostly calcium carbonate. This boundary probably is closely dependent on the microrelief of the playa surface, and lies near the highest shoreline achieved by the ephemeral lake during an average climatic cycle. Precipitation of dolomite directly from solution is suggested by the distribution of dolomite: muds within areas of relatively frequent flooding by lake waters contain the highest percentage of dolomite; and near the playa, dolomite ooze coats the bottoms of all surface inflow channels from springs.

Near the central part of the playa in an area of broad flats gaylussite occurs as clear euhedral flattened wedge-shaped crystals disseminated in a carbonate-clay matrix that is mostly dolomite, but that also contains calcite and laminae of white aragonite. The gaylussite crystals are fairly uniform in size, averaging 1 or 2 mm in maximum dimension, and are present only in permanently wet mud. They are oriented with long axes approximately parallel to traces of stratification and seem to interrupt such traces. This suggests that the gaylussite formed by reaction of calcite with sodium-rich interstitial solutions. The distribution of the crystals within the zone is quite variable; in places they make up nearly 35 percent of the total, whereas a short distance away they may be totally absent.

The playa area immediately west and south of the levee consists of a nearly monomineralic crust of thenardite overlying dolomitic mud. Enclosed in the mud are crystals of thenardite. The proportion of crystals decreases rapidly with depth. Textures suggest that the very fine grained dolomite-clay aggregate has been forced aside by the growth of the thenardite crystals.

Thenardite also is the major constituent of the saline crusts that cover nearly the whole eastern side of the playa. The upper surface of these layers is often covered with a network of skeletal powdery mirabilite ($Na_2SO_4 \cdot 10H_2O$) crystals altered to thenardite by dehydration, which indicates solution and reprecipitation of sulfate during fluctuation in lake levels.

Inside the area enclosed by the levee, crustal layers of thenardite overlying brown and green dolomitic muds grade abruptly into layers of brilliant white crust. This crust becomes thicker and the mud underneath becomes darker and more fluid in the area underlain by perennial brine. In the central part of the leveed area, the average total thickness of saline layers exceeds one foot.

Where the saline crusts exceed 2 or 3 inches in thickness, burkeite becomes a persistent component of the upper crustal layers. Thus burkeite may be considered the characteristic mineral of the central zone.

REFERENCES

Grim, R. E., 1960, Clay mineralogy: New York, McGraw Hill Book Co., 304 p.
Hunt, C. B., 1960, The Death Valley Salt Pan, a study of evaporite *in* Short papers in the geological sciences: U.S. Geol. Survey Prof. Paper 400-B; p. B456-B457.

84. EFFECTS OF RAINFALL AND GEOLOGY ON THE CHEMICAL COMPOSITION OF WATER IN COASTAL STREAMS OF CALIFORNIA

By J. H. FETH, Menlo Park, Calif.

Water flowing into the Pacific Ocean from streams originating along the California coast shows a variation between summer and winter in the concentration of dissolved solids, and between north and south in the composition of dissolved solids. The summer-winter variation has been examined on the west slope of the San Francisco Peninsula, and the north-south variation has been examined in streams north and south of the San Francisco Peninsula.

SAN FRANCISCO PENINSULA

During the summer of 1957 and again during the following winter samples of water were taken from 13 sites along 10 small streams originating on the west slope of the San Francisco Peninsula. These streams head at distances ranging from 5 to 15 miles from the coast in an area about 35 miles long. A few of the drainage basins remain in virtually a wild state; in most of the others human use, other than farming, is slight. In areas where farming is practiced irrigation is minimal, characteristically by sprinklers rather than by flooding or by ditch, hence flow returning to the streams is probably negligible. Natural influences thus dominate the chemical relations found.

The pairs of samples representing, respectively, late summer and early winter show persistent differences. Without exception the summer samples contain almost twice the concentration of dissolved solids as the winter samples. The summer samples, taken at a time of minimal flow, probably consist almost entirely of ground water discharge because summer rains are almost unknown in this area. The samples taken during the winter rainy season con-sist of both ground water and rain water and thus show the lower concentration of dissolved solids.

Because of the dilution, it is preferable to compare samples on the basis of percentage reacting values instead of concentration in parts per million. Comparison of mean values calculated for 13 sampling points indicated the following changes in percentage reacting values:

Constituent	Change, in percent, from summer (dry season) to winter (rainy season) (Mean of 13 pairs of samples)
Calcium	+1.0
Magnesium	+1.8
Sodium plus potassium	−2.8
Bicarbonate	−6.0
Chloride	−1.5
Sulfate	+7.5

Nitrate, a minor constituent of stream water not included in the table above, shows both a relative and an absolute increase in concentration in the winter samples. This increase may be attributed to the decay of plant material during the fall and the washing of the nitrogenous byproducts into the streams by the heavy winter rains.

Inasmuch as the winter rains originate over the ocean, it was expected that winter stream samples would contain appreciably larger amounts of wind-blown salts derived from the ocean than the summer samples. It was found, however, that in terms of mean percentage composition, sodium and chloride both decrease in winter. Comparison of percentage contents of chloride and of sulfate for individual samples is given in figure 84.1. This graph shows that in six streams (8 pairs of samples) the chloride percentage decreased and sulfate percentage in-

		PERCENT REACTING VALUES, IN ANIONS			
		10	20	30	40
Molino Creek at road to Swanton	S			O	×
	W			O ×	
Big Creek, 0.25 miles north of Swanton	S	O ×			
	W		O ×		
Little Creek at bridge near Swanton	S		×	O	
	W		×		O
Mill Creek, 0.25 miles southeast of Seaside School	S		O ×		
	W			O ×	
Pescadero Creek at Pescadero	S		O ×		
	W		×	O	
Pescadero Creek, 4 miles east of Pescadero	S		O ×		
	W		×	O	
San Gregorio Creek, 2 miles south of La Honda	S	×		O	
	W	×			O
Nameless Creek above Tunitas Creek	S			O ×	
	W		×	O	
Tunitas Creek above Nameless Creek	S		O		×
	W		O ×		
Tunitas Creek, 0.5 miles above mouth	S			O	×
	W			× O	
Purissima Creek, 2.5 miles above mouth	S	×	O		
	W	×	O		
Purissima Creek near mouth	S		O ×		
	W		× O		
Scott Creek at Seaside School	S		× O		
	W		× O		

FIGURE 84.1.—Graph showing percentage reacting values of chloride (×) and of sulfate (O) in summer (S) and winter (W) samples from 10 streams on the San Francisco Peninsula, Calif.

● Streams north of San Francisco
O Streams south of San Francisco

PERCENTAGE REACTING VALUES
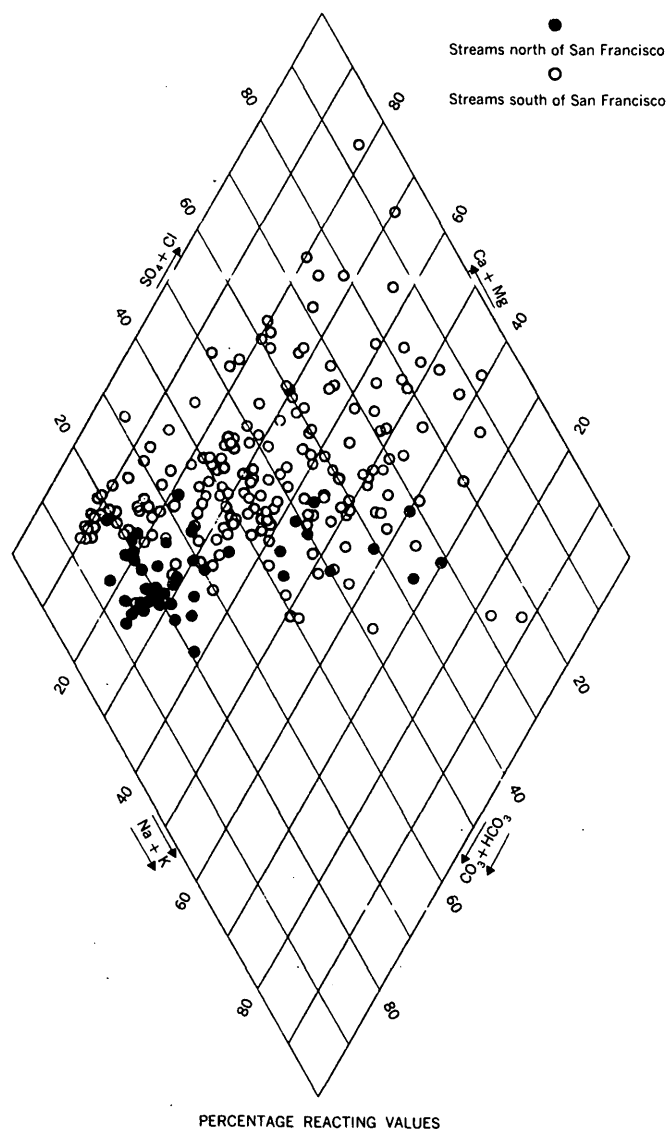
FIGURE 84.2.—Diagram showing differences in general chemical composition of water in coastal streams north and south of San Francisco.

creased in the winter samples. In four streams (5 pairs of samples) both sulfate and chloride percentages increased in winter. In no sample did chloride increase and sulfate decrease. When consideration is given to the fact that in seawater chloride is a little more than 7 times as abundant as sulfate (Clarke, 1924, p. 127), it seems clear that oceanic salts are of less influence than other factors in determining the chemical composition of waters in the 10 streams.

CALIFORNIA COAST NORTH AND SOUTH OF THE SAN FRANCISCO PENINSULA

The general chemical composition of water in 44 streams north of San Francisco and in 88 streams

south of San Francisco is shown in figure 84.2. All these streams discharge into the Pacific Ocean, all rise within 125 miles of the coast and most of them rise within 25 to 50 miles.

The solid circles, representing streams of the northern coast, indicate by their location and tight grouping the predominance of calcium magnesium bicarbonate waters. The open circles, representing streams of the southern coast, indicate by their sporadic distribution a wide variation of water types and the scatter of points toward the top of the diagram reflects the predominance of sulfate and chloride among the anions and of calcium and magnesium among the cations. These differences reflect major differences in the geologic environment and in the amount of rainfall. As previously determined for streams on the San Francisco Peninsula, windblown salts derived from the ocean are not present in significant quantities in the streams along the northern and southern coasts. As shown by the Geologic Map of California (Jenkins, 1951) much of the area along the northern coast is underlain by igneous rocks and by low-rank metamorphic rocks of the Franciscan formation. The southern coast, on the other hand, is underlain predominantly by

sedimentary rocks of diverse types and geologic age, many of which are weakly consolidated and contain readily soluble minerals. The northern coast also receives relatively large amounts of precipitation as compared to the southern coast (Dale, 1959).

The streams along the northern coast are relatively high in bicarbonate, in part (at least) because of a relative abundance of carbon dioxide in the air and soil. These streams are probably relatively low in chloride and sulfate because these substances are tied up in complex compounds in the igneous and metamorphic terrane and are not readily dissolved. Amounts that are available for solution are removed immediately and continuously by the heavier rainfall.

The streams along the southern coast contain relatively larger quantities of sulfate, chloride, calcium and magnesium derived from the loosely consolidated sedimentary rocks.

REFERENCES

Clarke, F. W., 1924, Data of geochemistry: U.S. Geol. Survey Bull. 770, 841 p.
Dale, R. F., 1959, Climate of California, in Climatography of the United States No. 60–4: U.S. Weather Bureau, 37 p.
Jenkins, O. P., 1951, Outline geologic map of California showing oil and gas fields and drilled areas: San Francisco, California Div. Mines.

⚒

85.   GROUND WATER FROM COASTAL DUNE AND BEACH SANDS

By E. R. HAMPTON, Portland, Oreg.

The coastal plain along the youthful coast of Oregon is narrow or entirely lacking (Brown and Newcomb, 1956; Hampton, 1960). The harder rocks of the cliffed headlands extend a few miles out to sea, and the interheadland bays are relatively narrow low plains underlain by windblown sand. Onshore winds prevail from the northwest in summer and from the southwest in winter; consequently, the longshore currents can feed sand to the interheadland beaches from either direction, and the baymouth bars and the beaches are tied to headlands at either or both ends. The bedrock consists almost entirely of poorly permeable sedimentary, volcanic-sedimentary, and volcanic rocks of Tertiary age.

The areas of windblown sand in the interheadland bays range in size from small pocketlike accumu-

lations to some as much as 20 miles in length and 4 miles in maximum width. The three largest areas, (fig. 85.1 A), are the Clatsop dunelands near the mouth of the Columbia River, the Florence dunelands near the town of Florence, and the Coos Bay dunelands near Coos Bay. Smaller, but important, sand areas occur at Manzanita, Newport, Sand Lake, Bandon, and Langlois.

These windblown sands lie on the westward sloping bedrock surface, as shown by figures 85.1 B and C. The thickness of the sand ranges from zero at the inland edges to a maximum of about 200 feet. The uppermost 100 feet of the sand consists largely of evenly sized, subangular to rounded grains of quartz. Samples from the top 20 feet of sand of the Coos Bay dunelands deposit contain 78 percent
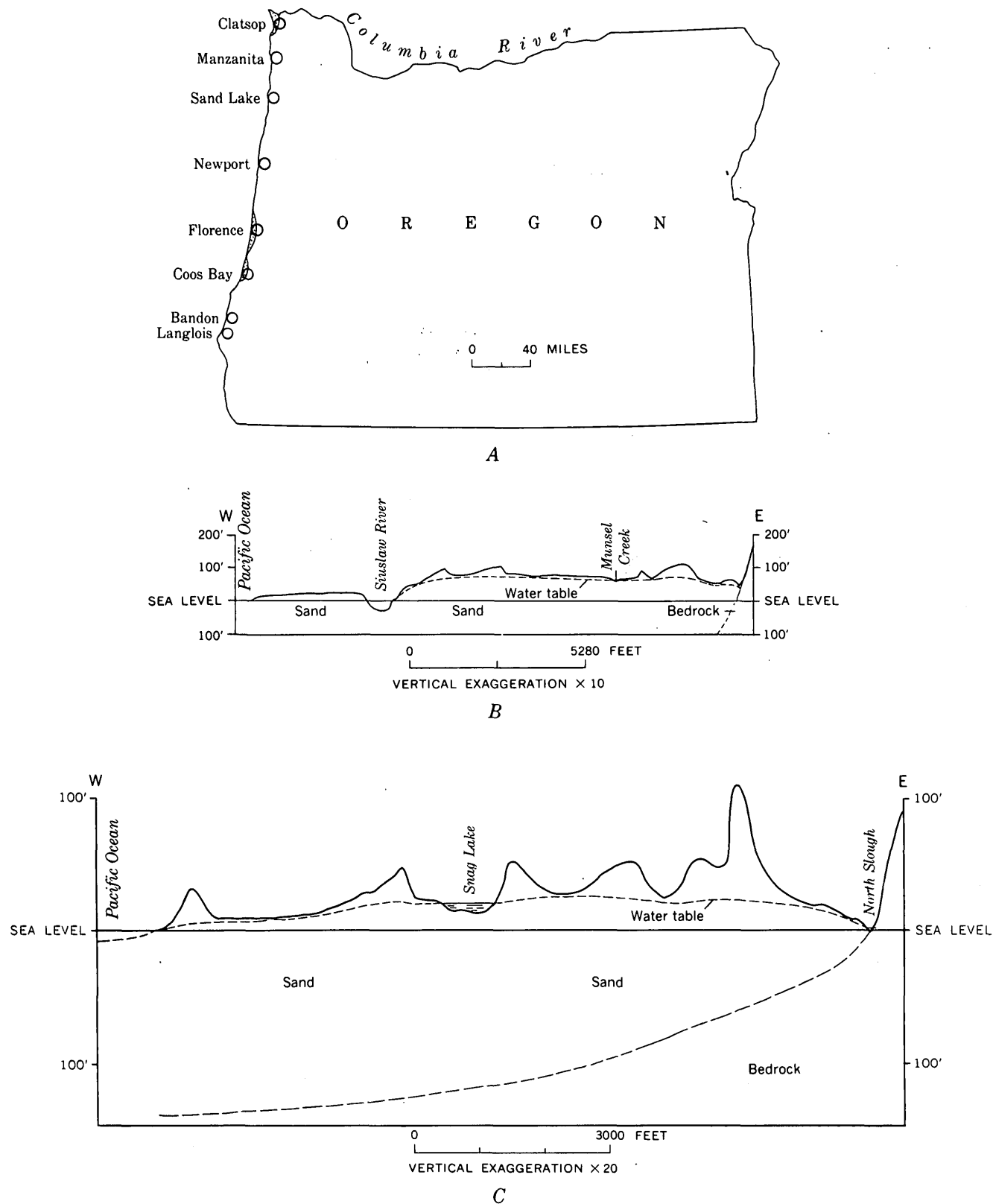
FIGURE 85.1.—Map of Oregon, and cross sections of sand deposits. *A*, map of Oregon showing location of principal coastal dune and beach sands; *B*, cross section of sand deposit north of Florence showing its surface, saturated zone, and part of the bedrock base; *C*, cross section of the sand deposit north of Coos Bay showing its surface, saturated zone, and bedrock base.

medium-grained sand and 19 percent fine-grained sand. The sand of the top 20 feet of the Florence dunelands deposit is similar but finer, containing from 50 to 80 percent fine-grained sand and 20 to 50 percent medium-grained sand.

Some sand beds are silty and clayey, and in places contain considerable peat and wood. In some deposits, as in the Coos Bay dunelands, the percentage of silt increases progressively with depth, but in others, as in the Manzanita deposit, the sand is almost uniform down to bedrock at a depth of 200 feet. These conditions suggest that the sand accumulated as a wind deposit inland from the beach as the ocean level rose 200 feet during late Pleistocene and Recent time.

The annual rainfall is 50–70 inches, but the summers are dry and the streams are very low during the summer and fall. About 75 percent of the annual precipitation sinks into the sand. Surface runoff occurs only in places where the sand has become saturated to the land surface: as in some low areas, along a few creeks, and in the ground-water discharge areas around the edge of the dunelands. Within each dune area the water table slopes outward toward its margins and is shallowest in topographic lows. During the wet winter months the water table rises from 3 to 10 feet.

Properly screened 8-inch diameter wells commonly yield 200 to 300 gpm (gallons per minute). The sand of the Coos Bay dunelands has a coefficient of transmissibility of about 50,000 gpd/ft (gallons a day per foot) and a specific yield of 35 percent. The sand of the Florence dunelands probably has about the same values.

At some places, the ground-water bodies may "float" on sea water as so-called Gyhben-Herzberg

lenses. However, at the few places where wells have completely penetrated the sand, the entire body of ground water is fresh. Apparently, infiltration from precipitation is able to move the water seaward through the sand at a rate sufficient to keep out the sea water. As a result, the water table stands remarkably high above sea level in some of the dunelands—10–30 feet in the Coos Bay dunelands, and 10–115 feet in the Florence dunelands.

Lakes occur in the dunelands wherever depressions in the land surface extend below the water table (fig. 85.1 C). Lakes as deep as 100 feet, formed by the encroachment of the sand upon the channels of marginal streams, are common at the inner edge of the dunelands, and are in hydraulic continuity with the ground-water bodies.

The ground water generally is of good chemical quality. It is soft and contains only about 20 ppm (parts per million) chloride. However, some of it has an amber color and contains enough dissolved iron, and is sufficiently acid to require treatment for some uses. Saline water has not been found above bedrock, but probably is in contact with the fresh water in the sand farther offshore. Therefore, plans for large withdrawals of fresh water should include precautions against encroachment of sea water.

These sand deposits are virtually the only natural reservoirs of fresh water along the coast, for the older rocks are relatively impermeable.

REFERENCES

Brown, S. G., and Newcomb, R. C., 1956, Ground-water resources of the coastal dune-sand area north of Coos Bay, Oregon: U.S. Geol. Survey open-file report, 27 p., 23 pls.
Hampton, E. R., 1960, Ground water in the dune-sand area near Florence, Oregon: U.S. Geol. Survey open-file report, 40 p., 15 figs.

86.   MASS BUDGET OF SOUTH CASCADE GLACIER, 1957-60

By Mark F. Meier, Tacoma, Wash.

Over a period of years, the changing mass of a glacier represents a moving average of its mass net budgets during each of these years. Considerable effort went into the measuring of net mass budgets, or volumetric changes, of typical glaciers all over

the world during the International Geophysical Year and the year following. This paper reports on one of these cooperative investigations.

Accumulation and ablation usually predominate in different seasons, so the mass of a glacier varies

with time. Considering this variation we can define the following quantities:

1. *Budget year* is the interval between the time of minimum mass in one calendar year to the time of minimum mass in the next following year.
2. *Accumulation* is the net change in mass from the value at the beginning of one budget year to the maximum value during that budget year. It is considered as a positive value.
3. *Ablation* is the net change in mass from the maximum value during a budget year to the value at the end of the same budget year, and is defined as a negative value.
4. *Net budget* is the net change from the beginning to the end of a budget year, is equal to accumulation minus ablation, and can have a positive or negative value.

These components of the mass budget can be defined for a glacier as a whole, as an area-average for a whole glacier, or at points on the glacier surface. Values are given here in cubic feet of water (density 1 gm per cubic cm) per square foot of glacier surface, reported simply as feet.

It is also instructive to determine the altitudinal gradient in the net budget. This parameter, termed here the "activity index," determines the amount of material that must be transferred from high elevations to low elevations in order to maintain a steady-state condition, and thus determines the thickness and velocity of a glacier on a given bedrock slope. The net budget as a whole describes a glacier's state of health, and the activity index describes its metabolism (Shumskii, 1947).

The Geological Survey began studies on South Cascade Glacier in 1957 (Meier, 1958). This glacier lies in the Northern Cascade Mountains of Washington, and is the source of the South Fork Cascade River, a tributary of the Skagit River. It flows toward the northwest at an average speed of about 60 feet per year. The glacier is 2.2 miles long, as much as 3,600 feet wide, ranges in altitude from 5,292 feet to about 7,300 feet, and covers an area of 1.0 square mile, not including partially or completely separated ice masses clinging to the contiguous slopes (fig. 86.1). These separated ice masses are not included in the information presented here. The glacier terminus calves into a lake, but the yearly mass lost by this means is not considered in this report.

The distribution of mass net-budget values, given in feet of water equivalent, over the surface of

South Cascade Glacier for the 1957–58 budget year is reported in figure 86.1. Note that only a very small area (3.9 percent) was included within the accumulation zone. The irregular distribution of net budget is primarily due to the effects of changes in the inclination of the surface slope (which cause erosion or augmented deposition by the wind) and the movement of accumulated snow by avalanches. The average net budget for the whole glacier was − 7.1 feet.

Firn lines for 1959 and 1960 are also shown in figure 86.1. In 1959, 66.9 percent of the whole area was included in the accumulation zone, and the average net budget was + 2.33 feet. In 1960, 48.7 percent of the area was included in the accumulation zone, and the average net budget was − 1.84 feet.

The time distribution of accumulation and ablation for a station in the middle of the glacier is shown in figure 86.2. This station is located on the flow centerline, and is located in such an area that its mass budget is closely related to the average mass budget for the whole glacier. This illustration is drawn showing true depths of the various layers of snow, and these depths must be multiplied by appropriate values of density in order to obtain values of accumulation, ablation, or mass budget. Inspection of this chart shows that—

1. The long and intense period of ablation from mid-April to mid-August 1958 not only removed the complete 1957–58 winter accumulation, but also the net snow remaining from several years before, creating a pronounced unconformity in the stratigraphic record. Another unconformity was produced in October 1960. A third pronounced unconformity, occurring at depth, was formed in 1947, 1948, or 1950. Thus a stratigraphic section taken in 1961 at this locality (P1) would contain at least three major time breaks, and it would be difficult if not impossible to reconstruct the climatic history or mass budget history from stratigraphic evidence alone.
2. The close of the budget year occurred on different dates: October 12, 1958, September 25, 1959, and October 23, 1960. The 1959–60 budget year was 394 days long whereas the 1958–59 budget year included only 348 days. It is common practice to measure the size of a glacier once a year on a fixed date to determine its growth or decline. The data given
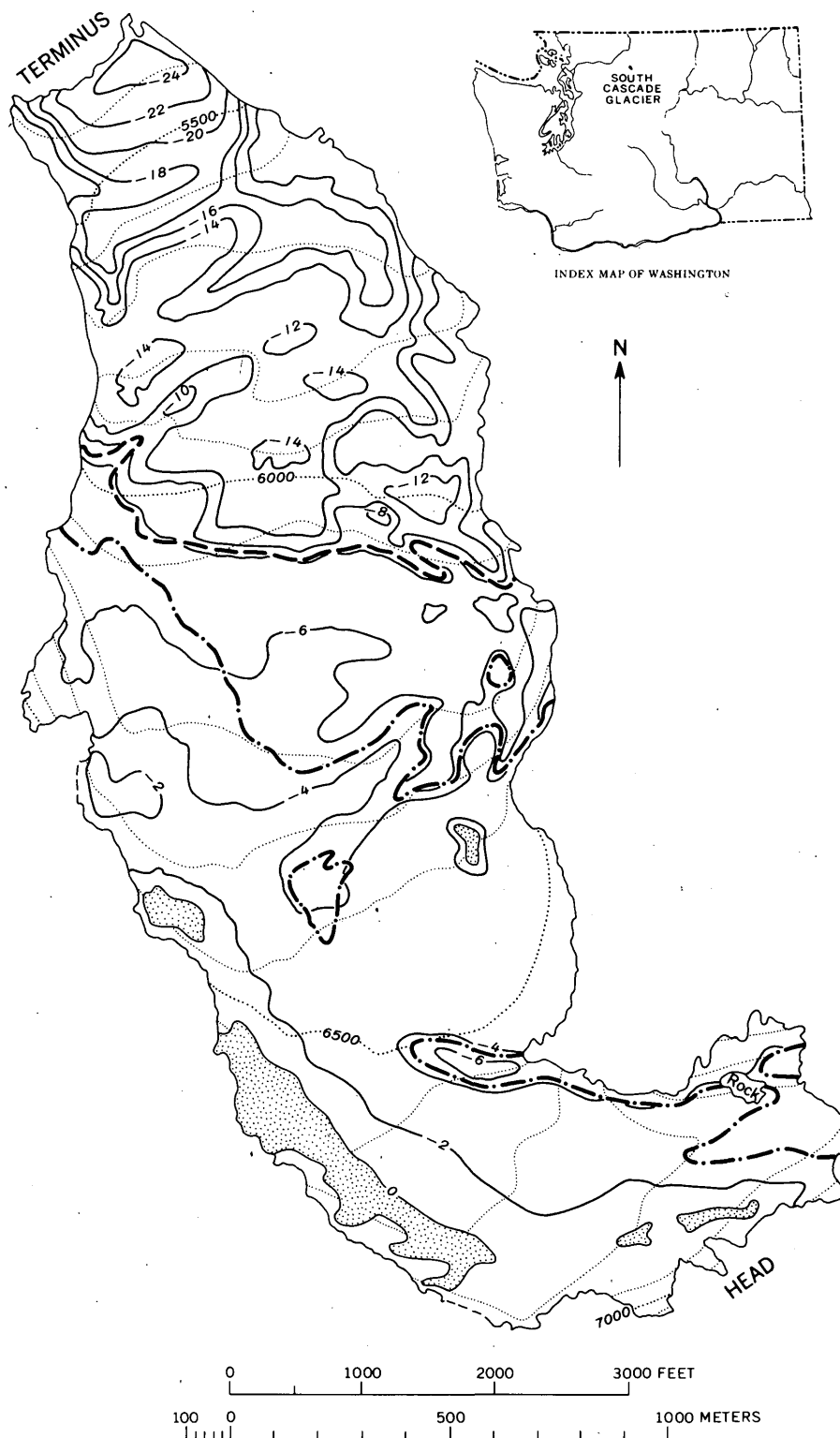
FIGURE 86.1.—South Cascade Glacier, Wash., showing distribution of net budget values
for 1957–58 budget year. The accumulation area for this budget year is indicated
by the stippled pattern; the perimeter of the stippled area is the firn line in 1958.
Interval between lines of equal net budget is 2 feet. Firn line in 1959 indicated by
heavy dashed line, and firn line in 1960 indicated by heavy dash-dot line. Topography
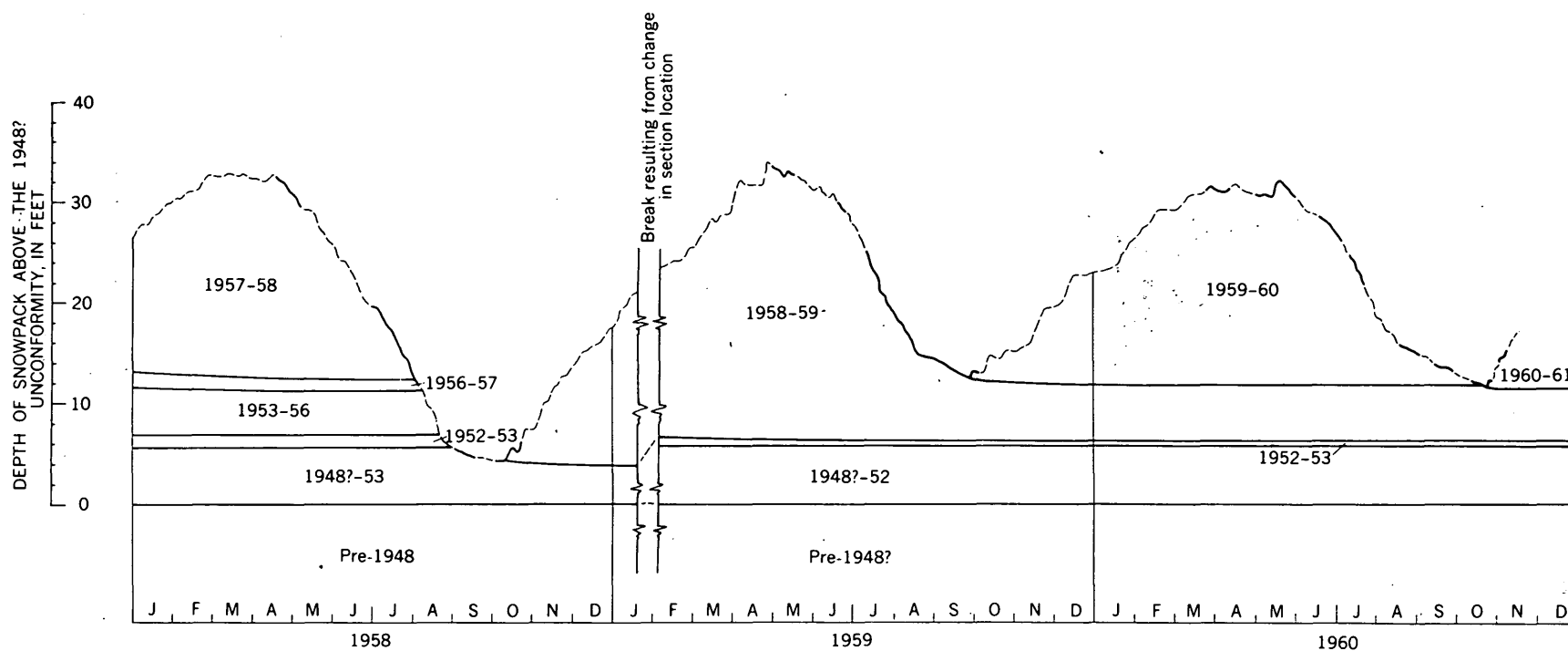indicated by dotted lines, contour interval is 100 feet.

FIGURE 86.2.—Growth and decay of the snowpack at Station P1 (6,160 feet) on South Cascade Glacier. Solid lines indicate values known by direct measurement, dashed lines indicate values estimated on basis of weather records obtained at Darrington, Wash., and streamflow records obtained at South Cascade Glacier.

below show that this practice is not likely to yield more than qualitative results.

Measurement date	Change in thickness (feet) in budget year —		
	1957–58	1958–59	1959–60
August 1................	+0.6	+12.7	+7.3
September 1.............	−6.6	+8.1	+3.3
October 1...............	−7.8	+7.0	+1.3
Actual change in thickness..	−8.0	+6.0	−0.2

This analysis ignores the fact that there is a component of flow in a vertical direction so that a zero net budget does not necessarily imply a zero net thickness change. However, locality P1 is located near the long-term average position of the firn line, at which place the vertical component is zero. The effect of vertical motion on these data would be the addition or subtraction of a constant small amount to all values.

The altitudinal variation of accumulation, ablation, and net budget is shown for each of the three years in figure 86.3. The 1957–58 curves show very large values of ablation and slightly less than average accumulation, producing a strongly negative net budget. In 1958–59 accumulation was large and ablation less than average, causing a positive net budget. The budget year 1959–60 appears to have been intermediate in its characteristics although it is interesting to note that ablation was large and accumulation was low at the lower elevations.
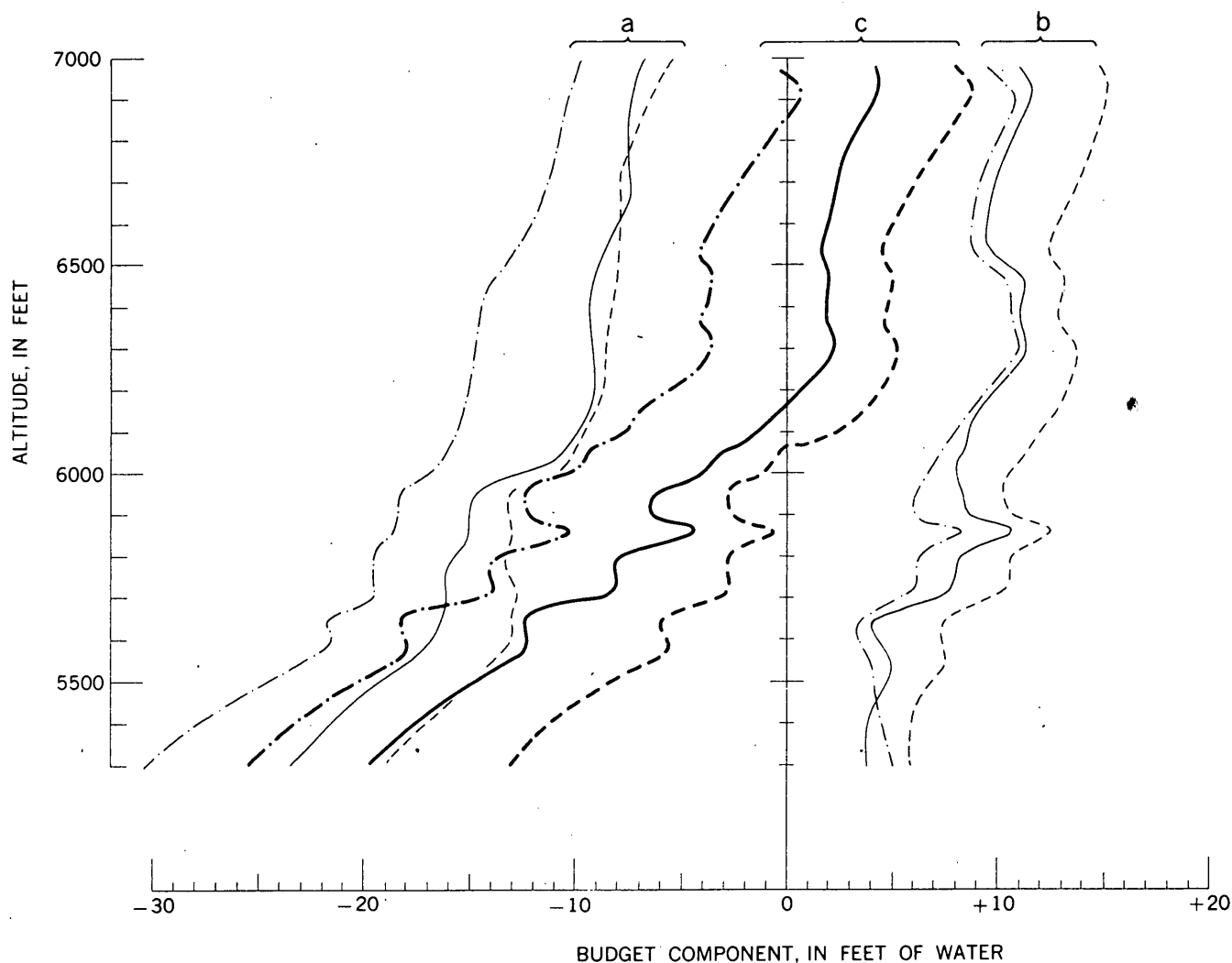
FIGURE 86.3.—Altitudinal variation in accumulation, ablation, and net budget, South Cascade Glacier, 1957–60. Light lines, a, indicate ablation; light lines, b, indicate accumulation; and heavy lines, c, indicate net budget. Budget year 1957–58 designated by dash-dot lines, 1958–59 by dashed lines, and 1959–60 by solid lines.

In analyzing a diagram such as figure 86.3, it is important to note that ablation is *not* independent of accumulation. Ablation is caused primarily by the net absorption of radiation, and thus is a sensitive function of albedo. The albedo of old firn or ice is very low compared with that of snow so that ice or old firn is capable of absorbing several times as much radiant energy as snow. A heavy winter snow accumulation will result in a snow cover persisting long into the ablation season, decreasing the amount of possible ablation.

The activity index, or vertical gradient of net budget, was relatively constant for the 3 years— 0.014 (14 mm per m). This is a high value, as high as any values quoted by Shumskii (1947, fig. 3). This activity index suggests an environment similar to that of the Blue Glacier, Olympic Mountains, Wash. (LaChapelle, 1959, p. 444-5), indicating that these glaciers occur in a maritime climate with relatively high values of winter snow accumulation and summer melt, and rapid transfer of material from high to low elevations.

REFERENCES

LaChapelle, E. R., 1959, Annual mass and energy exchange on the Blue Glacier: Jour. Geophys. Research, v. 64, no. 4, p. 443–449.

Meier, M. F., 1958, Research on South Cascade Glacier: The Mountaineer, Seattle, Wash., v. 51, p. 40–47.

Shumskii, P. A., 1947, Energiia oledeneniia i zhizn lednikov (Energy of glacierization and the life of glaciers): Moscow, Geografgiz, translated by William Mandel, the Stefansson Library, New York, 60 p.

---

87.   COMPETENCE OF A GLACIAL STREAM

By ROBERT K. FAHNESTOCK, Fort Collins, Colo.

Size measurements of boulders in transport, and measurement of associated stream velocities were made in White River below the Emmons Glacier, Mount Rainier, Wash., during a study of the processes of valley-train formation (Fahnestock, 1960). These measurements provide excellent data for the study of competence, for in White River all sizes at or near the range of competence are readily available for transport.

Size measurements were made of boulders that were either trapped in a wooden-framed sieve with 0.175-foot openings or caught by hand. Most point velocities were measured with a Price Type-A current meter set at 0.6 stream depth. Because of the large size of the particles, this depth setting provided velocity measurements in the immediate vicinity of the moving particles. Surface float velocities adjusted to 0.6 depth were used when current-meter measurements of velocity could not be made. Velocity measurements were made in the reach through which the boulders had been transported.

The relation of particle size to velocity (fig. 87.1) indicates that the boulders from White River were moving at lower stream velocities than would be predicted from the other data cited. White River data show that boulders up to 1.8 feet intermediate diameter moved in currents of about 7 fps (feet per second). For comparison, data that Nevin (1946) selected from Gilbert (1914), the U.S. Waterways Experiment Station (1935), Rubey (1937), and Nevin's own traction-tube experiments have been used to define bed velocity and critical traction velocity lines shown in figure 87.1. Projections of these lines intersect at a velocity of about 12 fps and a particle diameter of about 1.5 feet. The White River data indicate that the critical traction velocity [1] for coarse materials is closer to the velocity at 0.6 depth than to the bed velocity computed with Rubey's formula.

Parts of Hjulström's curves (1935, p. 298) which separate the zones of erosion, transportation, and deposition are also shown in figure 87.1. Most data for White River boulders in motion plot in the zone of deposition that is defined by projections of these curves. Hjulström's curves, however, were based on average velocity and uniform materials.

---

[1] Critical traction velocity (Nevin 1946, p. 665) is the velocity measured near the bed or mean velocity in shallow flow.
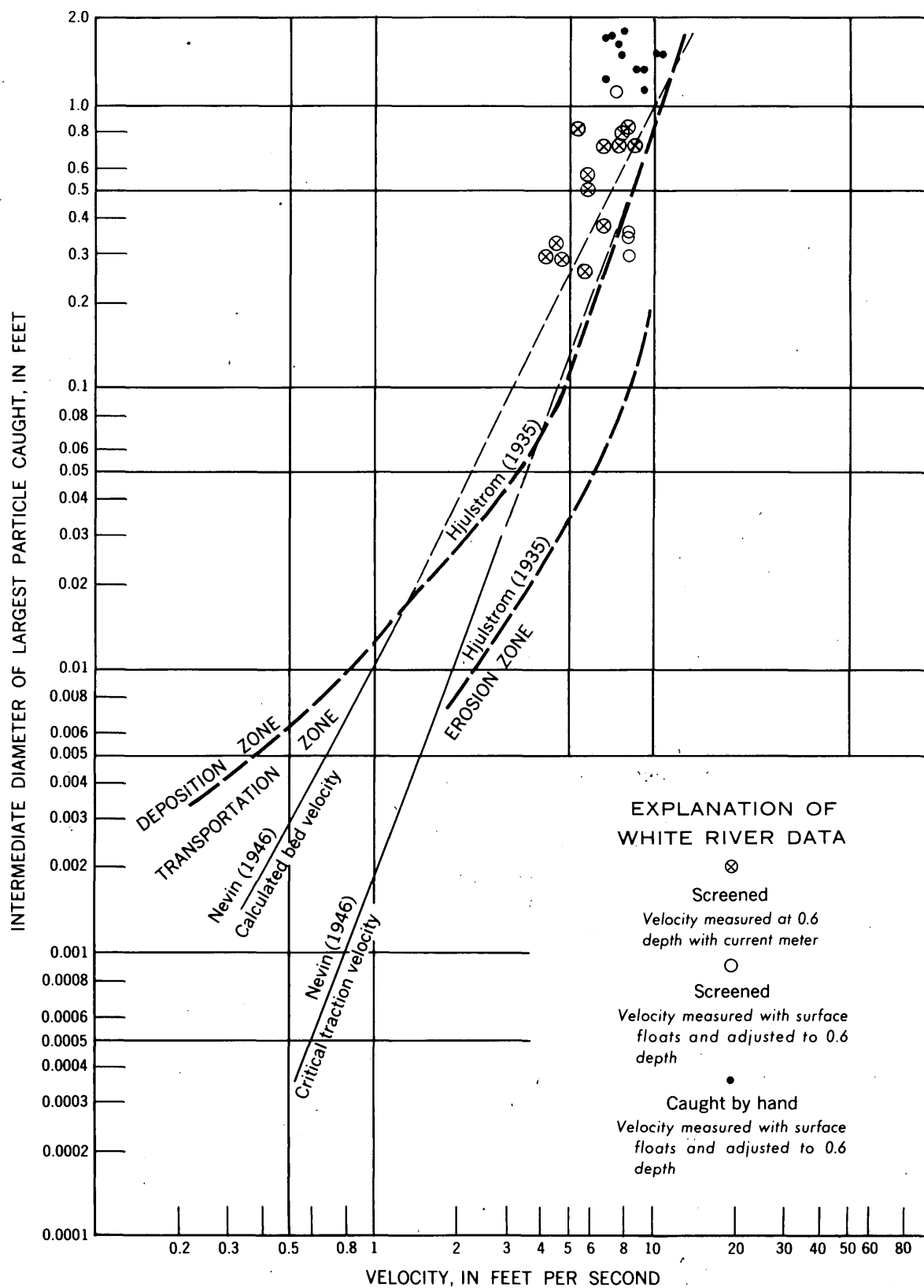
FIGURE 87.1.—Relation of particle size to velocity in White ·River.

Hjulström's curves indicate that particle size is proportional to the 2.6 power of velocity, which is the power found by Nevin (1946), who used average velocity. A line with a slope of 2.6 fits the White River data better than one with a slope of 2.0 (the "sixth power law" when particle size is expressed in terms of linear dimensions). Thus, for materials having intermediate diameters larger than 0.1 foot, streams may have greater competence than some applications of the "sixth power law" would predict.

Most experiments related to erosion and traction velocities have been made in laboratory flumes using uniform materials, mostly sand, with diameters of less than 0.1 foot. The few experiments that have been made with mixed sizes show that the mobility of such materials is quite different from that of uniform materials. Gilbert (1914, p. 173) stated that fine particles fill irregularities in a rough stream bed permitting larger particles to move more readily on the smoother bed and to continue in motion longer. Ippen and Verma (1953) noted a similar effect of bed roughness. Thus, because of the wide variation of particle sizes in the bed and banks of White River, one can expect erosion of particles larger than those predicted by formulas based on data for uniform materials. On the valley train, boulders of all sizes are readily available for movement by any current capable of eroding the finer supporting materials. Boulders on the bed were often set in motion by the blows from other boulders loosened from the banks.

Studies by White (1940) emphasize the importance of turbulence in initiation of motion of particles on the bed of natural streams. He concluded that the higher the turbulence the more effective a given mean velocity. White River's high turbulence is another factor that favors high competence.

REFERENCES

Fahnestock, R. K., 1960, Morphology and hydrology of a glacial stream [abs.]: Geol. Soc. America Bull., v. 71, no. 2, pt. 2, p. 1862.

Gilbert, G. K., 1914, The transportation of debris by running water: U.S. Geol. Survey Prof. Paper 86, 263 p.

Hjulström, Filip, 1935, Studies of the morphological activity of rivers as illustrated by the river Fyris: Univ. Upsala Geol. Inst. Bull., v. 25, p. 221–527.

Ippen, A. T., and Verma, R. P., 1953, The motion of discrete particles along the bed of a turbulent stream: Minnesota Internat. Hydraulics Convention Proc., 1953, Internat. Assoc. Hydraulic Research and Am. Soc. Civil Eng., p. 7–20.

Nevin, C. M., 1946, Competency of moving water to transport debris: Geol. Soc. America Bull., v. 57, no. 7, p. 651–674.

Rubey, W. W., 1938, The force required to move particles on a stream bed: U.S. Geol. Survey Prof. Paper 189–E, p. 121–141.

U.S. Waterways Experiment Station, 1935, Studies of river bed materials and their movement with special reference to the Lower Mississippi River: Paper no. 17, 161 p.

White, C. M., 1940, The equilibrium of grains on the bed of a stream: Royal Soc. (London) Proc., ser. A., v. 174, p. 322–338.

88. STRUCTURAL BARRIER RESERVOIRS OF GROUND WATER IN THE COLUMBIA RIVER BASALT

By R. C. Newcomb, Portland, Oreg.

A thick sequence of dark-colored lava flows, the Columbia River basalt of Miocene and early Pliocene(?), extends beneath about 50,000 square miles of the Columbia Plateaus and adjacent areas of the Pacific Northwest. In the central part of its vast areal extent the total thickness of the basalt is more than 5,000 feet and may exceed 10,000 feet. At its margins it tapers out against the pre-basalt slopes: the Okanogan Highlands at the north, the Rocky Mountains at the east, the mountains of central Oregon at the south, and the Cascade Range at the west, though it crosses through the Cascade Range at a few places (fig. 88.1 top). The individual lava flows range in thickness from about 5 to 150 feet, and average about 50 feet.

The basalt is a dense gray or black rock, composed of microcrystals in a glassy groundmass, that solidified in near horizontal position from highly fluid lava that rose along fissures. Cooling joints cracked the rock into sets of vertical columnar and cubical
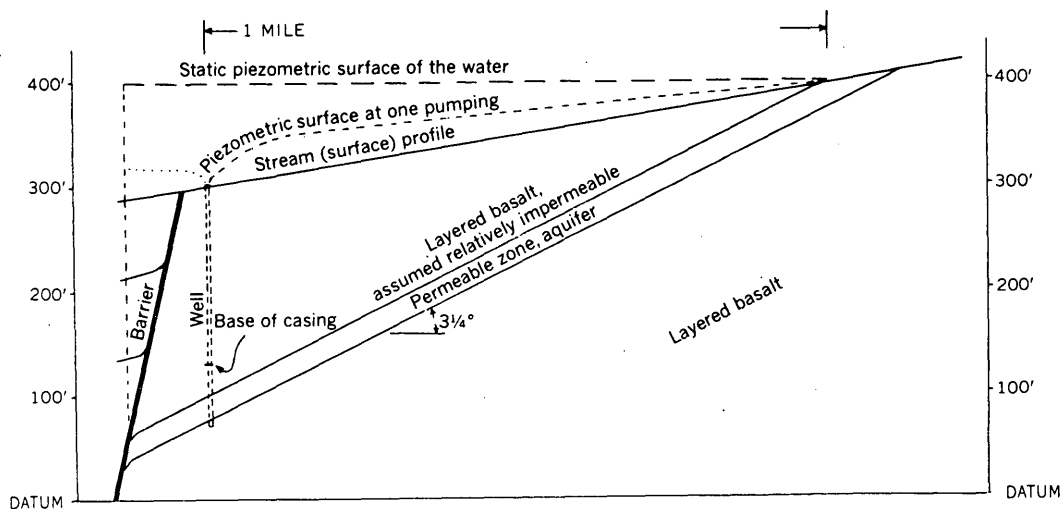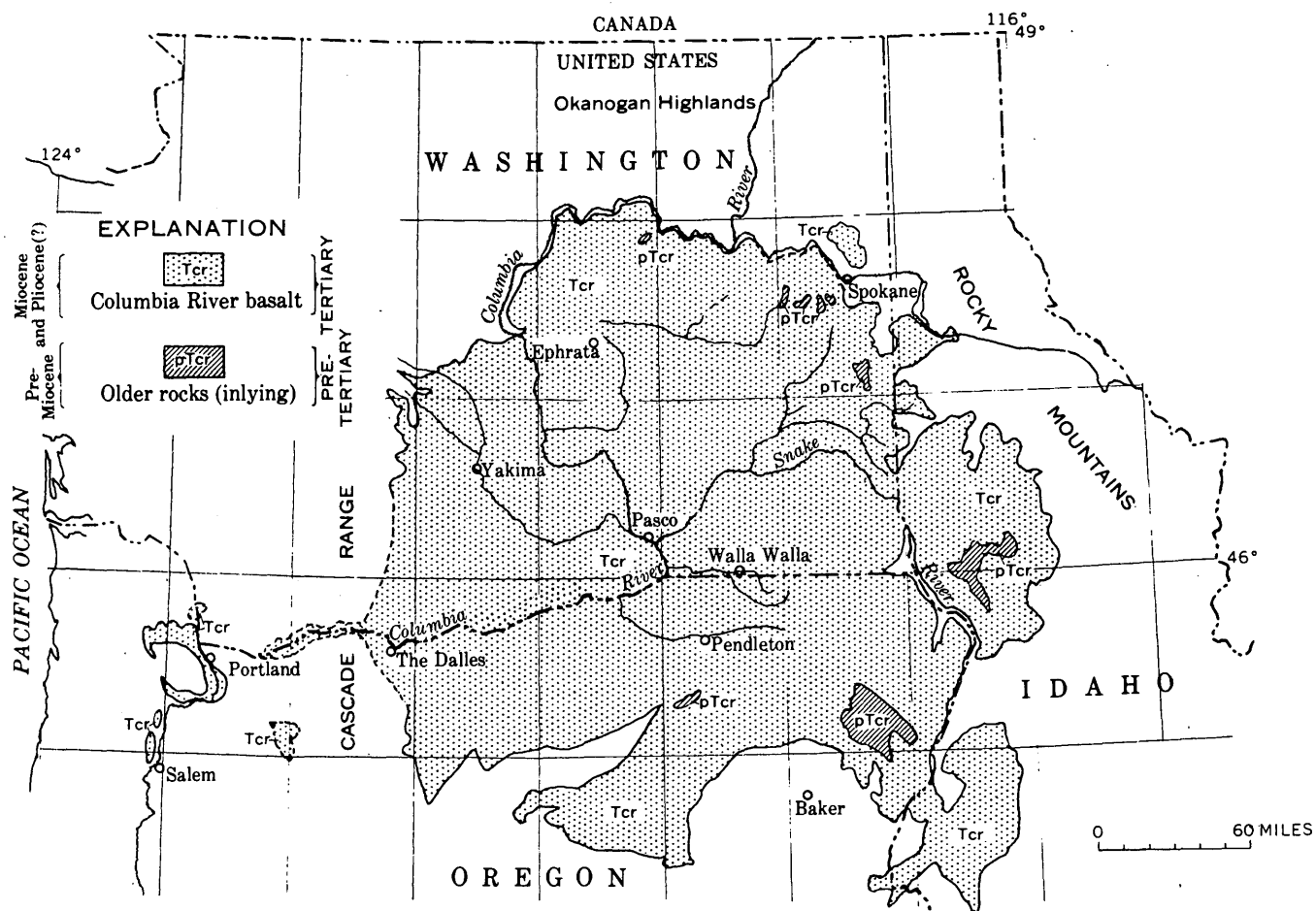
FIGURE 88.1.—Top, Generalized map of the main area underlain by the Columbia River basalt; Bottom, Diagrammatic cross section of a hypothetical ground-water withdrawal system operating on an aquifer of a barrier reservoir.

blocks and into less prominent horizontal sheeting slabs. Except for the cooling joints, most flows are rather monolithic; little breccia or fragmental lava is present. Few sedimentary interbeds are present except around the edges of the basalt unit. Most individual flows are dense and tight in their center parts, but some are vesicular, rubbly, and porous near their tops. Water percolates mainly along the porous tops of some of the lava flows. Tabular separation of the aquifers is common, and the hydraulic conditions of such occurrences vary from place to place.

The basalt has been tectonically warped into broad open folds with local areas of intense deformation. Infiltrated water moves down the dip of inclined porous flow tops so that the downwarped areas are sites of ground-water accumulation.

Locally structural deformation has sheared and crushed the rock along faults and along tight folds in which the porous tops of the flows were crushed during the interflow slippage. These zones of crushed rock obstruct the tabular percolation of ground-water

and cause impounding back to points of discharge. These ground-water reservoirs updip from structural barriers occur in and near some of the valleys and in the uplands. Notable among the barrier reservoirs now in use is one underlying the Upper Cold Creek valley northwest of Pasco, Wash., and one under the Walla Walla valley plain at College Place west of Walla Walla, Wash.

The hydraulic characteristics of a typical barrier reservoir in the basalt are illustrated in figure 88.1 (bottom). The impounded water is best tapped by wells at the barrier end of the reservoir. The perennial yield would be determined by the annual recharge and would differ from reservoir to reservoir. Withdrawals from reservoirs where flowing streams cross the intake area may decrease the streamflow; however, calculations on theoretical examples suggest this deduction in stream flow, at its maximum in late summer, would equal only a small part of the water drawn from otherwise unused storage.

✗

GEOLOGY AND HYDROLOGY OF ALASKA AND HAWAII

89.   XENOLITHIC NODULES IN THE 1800-1801 KAUPULEHU FLOW OF HUALALAI VOLCANO

By Donald H. Richter and Kiguma J. Murata, Hawaiian Volcano Observatory, Hawaii, and Washington, D. C.

Hualalai is one of the five volcanoes whose flows have built up the island of Hawaii. Now dormant, it was last active in 1800–1801 when the Kaupulehu and smaller Huehue flows were erupted from its northwest rift zone. The presence of xenolithic nodules in the Kaupulehu lavas has long been known, but only limited mention of them or of their remarkable occurrence has appeared in the literature. Stearns and Macdonald (1946) briefly described some of the physical features of the nodules and later Macdonald (1949) presented additional petrographical data. Chemical analyses of a clinopyroxene and a spinel from the Kaupulehu nodules were given, along with a discussion on the origin of dunitic inclusions, by Ross, Foster, and Myers (1954). Recent geologic studies on Hualalai Volcano have revealed some exceptional exposures of nodules which indicate a possibly greater abundance of nodules than heretofore

believed, as well as a significant difference in their aggregate composition. The possible significance which these nodules may have in regard to the genesis of the Hawaiian lavas has prompted a detailed mineralogical-chemical study, now in progress; this paper describes the geologic occurrence and physical mineralogy of the nodules.

The Kaupulehu flow, together with the Huehue flow, represents the youngest lavas of the alkalic basalt series which mantle Hualalai Volcano. On the basis of the well-established chronological succession of Hawaiian magma types, however, the main bulk of Hualalai is believed to be composed principally of basalts of the tholeiitic series. The tholeiitic rocks, characterized by a saturated groundmass, are erupted frequently and rapidly during the youthful and mature stages of volcanic activity; whereas the undersaturated alkalic basalts and their differen-
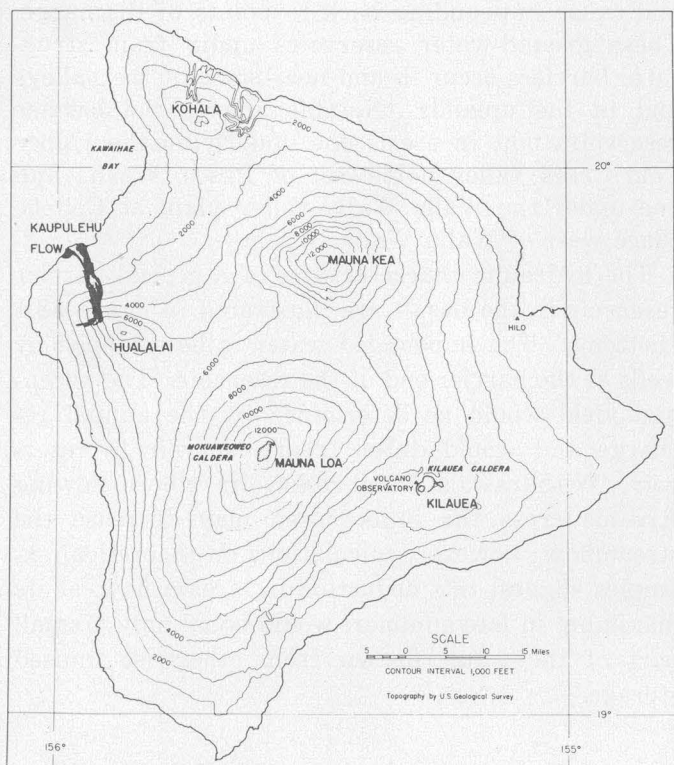
FIGURE 89.1.—Map of the island of Hawaii showing location of the 1800–1801 Kaupulehu flow on Hualalai Volcano. Outline of flow from report by Stearns and Macdonald (1949).

tiates are erupted intermittently and in minor volume during the decadent stage of volcanism. Xenolithic nodules appear to be restricted in their occurrence to these later alkalic rocks, not only on Hualalai, but on other volcanoes of the Hawaiian Islands as well.

The voluminous Kaupulehu lavas were erupted from a group of vents, between 5,500 and 6,000 feet in elevation, along the northwest rift of Hualalai, and with the exception of a few short tongues that flowed to the west, they flowed northward down the slopes of the volcano some 10 miles before entering the sea south of Kawaihae Bay (fig. 89.1). The nodule locality recently investigated is along a relatively flat bench, on the first major break in slope, 2 miles below the vent area at an elevation of about 3,250 feet.

Briefly reconstructing the history of the flow, it appears that the rapidly flowing, extremely fluid lava—heavily charged with nodules—lost velocity and carrying capacity on reaching the area of reduced gradient. Here the early flows spread out in relatively thin sheets, both on the level area and on the slopes below, depositing the nodules in well-defined layers. As lava continued to flow into the

level area a pond of considerable depth soon formed, first by surface overflow and later by lava running under the surface and floating the crust. Eventually, as the lithostatic head increased, the impounded fluid lava broke through the downslope wall of the pond and cut a deep channel through the nodule-bearing flows which had spread out earlier over the surface below the pond. As material drained out of the pond, the still fluid lava in many of the nodule zones also drained away leaving discrete nodule beds, without appreciable matrix lava. Toward the end of eruptive activity, lava domes on the surface of the pond and portions of tubes within the pond collapsed, and it is in these collapse features together with the main lava channel below the pond that the spectacular nodule beds are now exposed.

The great abundance of the nodules is well shown in the wall of the main lava channel where no less than 4 distinct nodule beds, ranging in thickness from 3 to 9 feet, are exposed (figs. 89.2 and 89.3). In fact, along one 200-foot long exposure, the nodule beds have an aggregate thickness of 26 feet and constitute more of the rock than the lava itself. In the collapsed domes and tubes on the top of the lava pond only the uppermost nodule bed is visible; and where collapse occurred prior to complete solidification of remnant matrix lava the nodules tumbled into the depressions forming an outcrop very similar in appearance to a cobble beach deposit (fig. 89.4).

In size, the nodules generally range from a fraction of an inch to more than one foot in diameter; the largest observed measured 27 inches in its greatest dimension. They are angular to subrounded in

FIGURE 89.2.—Wall of main lava channel in Kaupulehu flow showing four nodule beds (1, 2, 3, 4) each separated by several thin pahoehoe flows.

external form, although in the exposures where matrix lava has been withdrawn the thin coating of lava remaining on the nodules tends to accentuate their roundness.

The nodules consist principally of medium- to coarse-grained crystal aggregates of one or more of the following three minerals: clinopyroxene (approximately $Ca_{42}Mg_{44}Fe_{14}$), olivine (Fa_{12-18}), and plagioclase feldspar (An_{60-75}). Opaque minerals are generally present in amounts ranging from a few tenths to 2 percent. The crystals are all anhedral and form a tightly interlocked allotriomorphic granular texture. With the exception of a minute corona-like clinopyroxene growth observed around some opaques in a few specimens, the minerals do not exhibit any evidence of magmatic reaction. Some of the olivine grains, however, do show an incipient marginal alteration probably caused by the action of hot water-laden gases streaming through the nodules after the cessation of volcanic activity.

On the basis of mineralogy four general types of nodules are recognizable. These types in order of decreasing abundance, as shown by random sampling of over 200 nodules, are: clinopyroxene-olivine, olivine, clinopyroxene, and clinopyroxene-feldspar. Only a few olivine-feldspar and olivine-clinopyroxene-feldspar nodules were observed, and predominantly feldspar nodules apparently do not exist. Modal analyses of representative nodules from the different types indicate that clinopyroxene is the most abundant mineral present.

FIGURE 89.3.—Closeup view of nodule bed 2, shown in figure 89.2. Spatter from the last flows through channel is draped over some of the nodules.

FIGURE 89.4.—Loose nodules on the floor of a collapsed dome in the surface of the lava pond. Note the relatively thin lava caprock of the nodule bed.

CONCLUSIONS

Murata (1960) and Eaton and Murata (1960) support the theory that the fundamental Hawaiian magma is tholeiitic and that fractional crystallization of pyroxene is the principal mechanism for producing the undersaturated alkalic magmas. The mineralogy and abundance of the Kaupulehu nodules (together with the fact that xenolithic nodules, in general, occur only in alkalic rocks) lends additional support to this view. The nodules therefore, are interpreted to represent fragments of subterranean consolidated deposits of crystals whose precipitation has played a dominant role in affecting the fundamental change in magma type. Furthermore their angularity and lack of pronounced magmatic reaction strongly suggest that the processes of fractional crystallization occurred far above the original source of the tholeiitic magma—probably in relatively shallow magma reservoirs within the volcano.

REFERENCES

Eaton, J. P., and Murata, K. J., 1960, How volcanoes grow: Science, v. 132, p. 925–938.

Macdonald, G. A., 1949, Petrography of the Island of Hawaii: U.S. Geol. Survey Prof. Paper 214–D, p. 51–96.

Murata, K. J., 1960, A new method of plotting chemical analyses of basaltic rocks: Am. Jour. Sci., v. 258–A, p. 247–252.

Ross, C. S., Foster, M. D., and Myers, A. T., 1954, Origin of dunites and of olivine-rich inclusions in basaltic rocks: Am. Mineraloglist, v. 39, p. 693–737.

Stearns, H. T., and Macdonald, G. A., 1946, Geology and ground-water resources of the Island of Hawaii: Hawaii Div. Hydrography Bull. 9, 363 p.

90. RECONNAISSANCE OF THE KANDIK AND NATION RIVERS, EAST-CENTRAL ALASKA

By Earl E. Brabb, Menlo Park, Calif.

The purpose of this report is to describe briefly the rocks and structure along two previously unmapped rivers in east central Alaska. All localities mentioned are shown on Charley River A–2, B–1, B–2, B–3, C–1, C–2 and D–1 quadrangles, scale 1:63,360.

All of the rocks cropping out along the Kandik River are provisionally assigned to the Kandik formation of Early Cretaceous age. They are predominantly shale, mudstone, argillite, slate, and graywacke but include minor amounts of chert-pebble conglomerate, "clean" sandstone, pebbly mudstone, and cherty limestone. These rocks seem to represent one lithogenetic sequence. Graded beds and other features suggestive of turbidity current deposits are common. The rocks are intensely deformed between the mouth of the Kandik River and Easy Moose Creek and between Indian Grave Creek and the United States-Canada border. The beds have a general northeast strike and a moderate northwest dip between Easy Moose Creek and Indian Grave Creek, and an anomalous northwest strike and moderate northeast dip in the vicinity of the border. Pelecypods collected from the formation along the Kandik River about 2 miles upstream from the mouth of Big Sitdown Creek suggest an Early Cretaceous (Valanginian) age according to D. L. Jones (written communication, 1961).

Slate, shale, mudstone, argillite, and minor graywacke and quartzite cropping out along the Nation River between the mouths of Tindir and Jungle Creeks are also provisionally referred to as the Kandik formation. These rocks are moderately to intensely deformed and appear to have an anomalous northwest strike. Several minor southeastward-plunging folds in these rocks can be seen near the mouth of Ettrain Creek. Most of the rocks are not well dated but all of the fossils collected from them indicate an Early Cretaceous age. For example, Foraminifera collected from shale along the Nation River near the mouth of Tindir Creek are possibly of early Neocomian age, according to H. R. Bergquist (written communication, 1961). Megafossils collected from the same beds and from another locality nearby were identified by D. L. Jones (written communication) as *Polyptychites* and *Buchia* cf. *B. crassicollis* and are also suggestive of an early Neocomian (Valanginian) age.

The Kandik formation may be in fault contact with petroliferous shale and limestone of Triassic age, Tahkandit limestone of Permian age, and Nation River formation of Carboniferous (Pennsylvanian?) age, which crop out along the Nation River about 1 mile upstream from the mouth of Waterfall Creek. These late Paleozoic and early Mesozoic rocks have a northeast strike and, for the most part, a northwest dip. Conglomerate, sandstone, siltstone, and minor coal and "red beds" cropping out along the Nation River between Waterfall and Hard Luck Creeks are also provisionally referred to the Nation River formation. These rocks have a northeast strike and southeast dip. They are apparently in fault contact with shale and limestone about 2 miles downstream from the mouth of Hard Luck Creek. Corals from the limestone are of Silurian or Devonian age, according to W. A. Oliver, Jr. (written communication, 1961).

No oil seeps or deposits of economic interest were found.

GEOLOGY OF PUERTO RICO

91.   HYDROTHERMALLY ALTERED ROCKS IN EASTERN PUERTO RICO

By FRED A. HILDEBRAND, Denver, Colo.

Work done in cooperation with the Department of Industrial Research,
Puerto Rico Economic Development Administration

A belt of light-colored altered rocks approximately 50 km long and 5 km wide extends from the eastern coast of Puerto Rico northwest to the Cerro La Tiza area, as shown in figure 91.1. The altered belt skirts the northern edges of the San Lorenzo and Caguas plutons and lies within a broad zone of structural weakness trending about N. 70° W. across north-central Puerto Rico (Smith and Hildebrand, 1953; Hildebrand and Smith, 1959). Within the belt, exposures of hard altered quartzose rock stand in relief as ridges and knolls above the softer volcanic country rocks.

The greenish-gray volcanic country rocks consist principally of lava, tuff, tuff and volcanic breccia, and agglomerate. In general, the volcanic rocks are of borderline basaltic-andesitic composition and their age is probably Cretaceous and early Tertiary (Hildebrand, 1959).

The plutonic rocks shown on figure 91.1 consist mainly of granodiorite. Zircon age determinations indicate that the San Lorenzo pluton is of late Cretaceous or early Tertiary age. The age of the Caguas pluton has not been determined.

On the whole the altered rocks are light colored and consist of intermixed hard, massive quartzose rocks and soft, clayey, sericitic rocks composed principally of quartz, sericite, alunite, pyrophyllite, kaolinite, and halloysite. Less abundant minerals are hematite, goethite, diaspore, zunyite, jarosite, barite, sulfur, pyrite, and svanbergite.

The belt of altered rocks is not continuous but consists of elongated patches of altered rock (fig. 91.1) surrounded by unaltered country rock. Within the patches of altered rock there is no distinct zoning of rock types, however, elongated zones of hard banded quartz-alunite rocks and soft foliated, pyrophyllitic rocks commonly occur within softer, clayey sericitic rocks. At the western end of the belt, where the terrain is generally higher, the altered rocks have weathered to an earth-rock debris that has moved downslope to form extensive tongue and apron deposits over the volcanic country rocks.

The mineral assemblages at the largest and best exposed areas along the hydrothermal belt are listed in table 1. Most noteworthy observations at these areas are as follows:
1. At Cerro La Tiza and Pueblito Del Rio, alunite and quartz occur as alternating bands in finely banded and crenulated rock. The banding is believed to be inherited from the foliated structure of the volcanic host rock.
2. At Cerro La Tiza and Cerro Marquesa, kaolinite, and halloysite are more abundant at the southern margins of the altered zone. The margins of the zones in other areas are concealed.
3. Crystalline pyrophyllite and diaspore are most abundant at Cerro Marquesa.
4. Between Aguas Buenas and Gurabo the rocks are mainly silicified and sericitized volcanic host rocks. Further study of quartz-sericite rocks in this area may show that they are greisen.
5. That part of the belt richest in barite borders the north edge of the San Lorenzo pluton from Cantagallo eastward to Pueblito Del Rio.
6. Kaolinite and halloysite are generally less abundant and zunyite and jarosite more abundant toward the eastern end of the belt.

The altered rock belt shown in figure 91.1 is believed to be of hydrothermal origin; that is, the volcanic host rocks were altered by emanations from a magmatic source. The emanations probably originated in plutonic rocks that presumably underlie much of Puerto Rico (Hildebrand, 1959). The alteration processes have destroyed all primary textures of the volcanic host rocks and have caused profound compositional changes that have resulted in a completely different mineral assemblage. Calcium, magnesium, and most of the iron were removed from the host rocks, but silica, sulfur, and probably potassium were added during the alteration processes. The abundance of introduced quartz, aluminum silicates and sulfate-bearing minerals is evidence that the emanations were acid, sulfate bear-
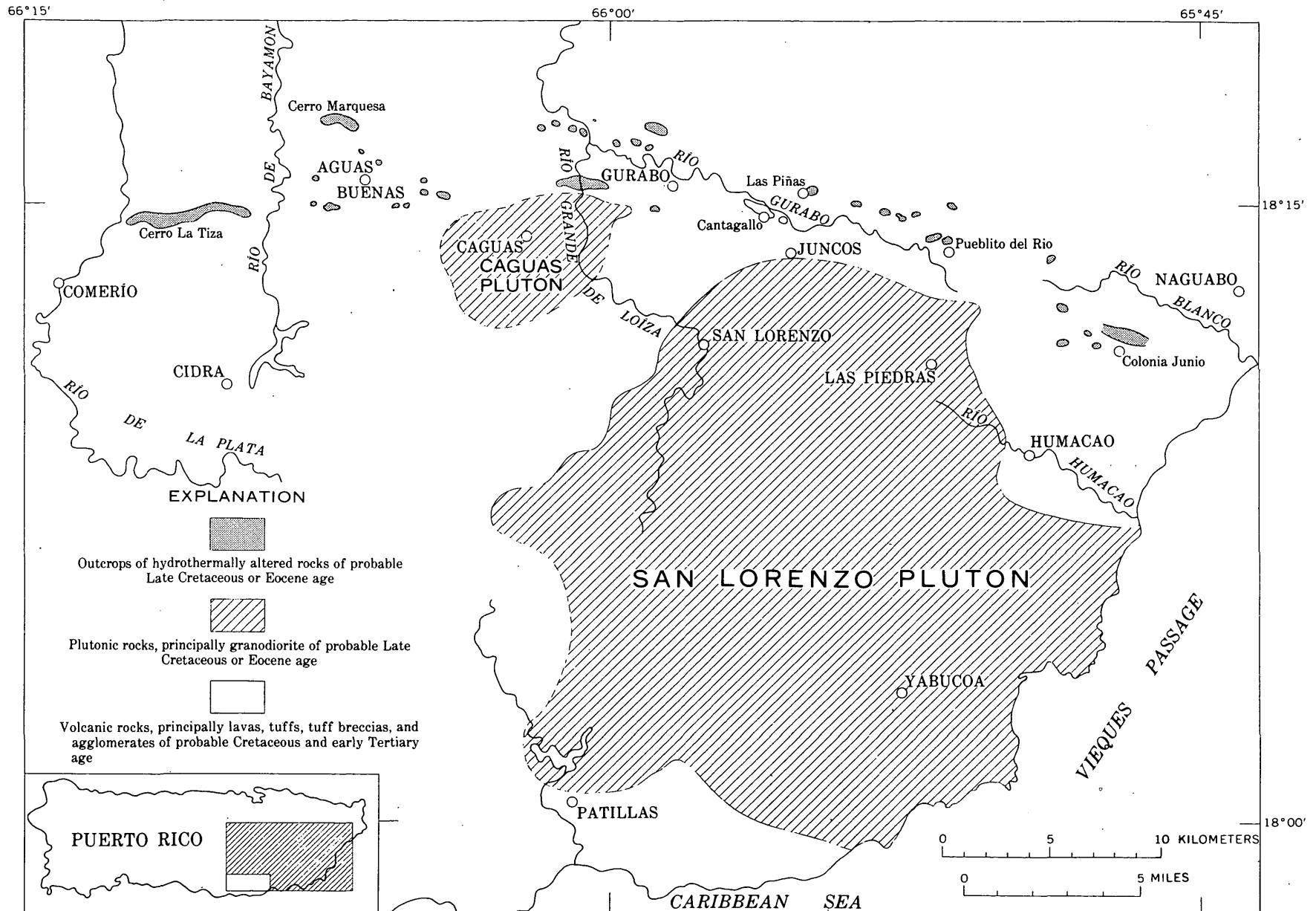
FIGURE 91.1.—Outcrop belt of hydrothermally altered rocks and their relationship to plutonic and volcanic rocks in eastern Puerto Rico.

TABLE 1.—*Mineral assemblages at prominent outcrop areas in belt of hydrothermally altered rocks shown in figure 91.1*

[Hematite and goethite occur in the altered rocks at all areas. Some hematite is believed to be of hydrothermal origin but goethite and some hematite has probably resulted from weathering of ferruginous minerals.]

			Areas		
Cerro La Tiza	Cerro Marquesa	Between Aguas Buenas and Gurabo [1]	Cantagallo and Las Pinas	Pueblito Del Rio	Colonia Junio
Quartz	Quartz	Quartz	Quartz	Quartz	Quartz.
Sericite	Sericite	Sericite	Sericite		Sericite.
Alunite	Alunite		Alunite	Alunite	Alunite.
Pyrophyllite	Pyrophyllite		Pyrophyllite	Pyrophyllite	
Kaolinite	Kaolinite	Kaolinite	Kaolinite		
Halloysite	Halloysite				
Diaspore	·Diaspore			Diaspore	
Zunyite				Zunyite	Zunyite.
Jarosite					Jarosite.
			Barite	Barite	
Sulfur					
Pyrite					
Svanbergite?					
Rutile?					

[1] The elongated outcrop area shown at the north edge of the Caguas pluton in figure 91.1 consists of greisen and is described in Art. 92 in this volume.

ing, and silica rich. This type of genesis agrees with stability relations in a similar mineral assemblage studied experimentally by Hemley (1959). The maximum temperature to permit the existence of kaolinite which is abundant in much of the belt is about 350°–400°C. In those areas where kaolinite is lacking and the assemblage sericite-pyrophyllite-diaspore predominates, the temperature was somewhat higher.

Puerto Rico is rapidly undergoing industrial expansion and is keenly interested in reducing imports of raw materials and developing its own natural resources. Alunite, which is now imported, is useful in the preparation of sulfates (Faith, Keys and Clark, 1950, p. 59–62) for use as a coagulant in water purification. The alunitic rocks of Puerto Rico might be used for this and also in the manufacture of aluminum refractory materials (Knizek and Fetter, 1950, p. 202–249). The Puerto Rico alunite probably contains too much sodium to be used for potash fertilizer.

Pyrophyllite could be used in the ceramic tile and refractory industries in the manufacture of vitreous floor tiles, which are commonly used in buildings in Puerto Rico. Pyrophyllite could also be used as a carrier for paint pigments, insecticides, and fungicides, as a filler in the preparation of soaps, and in the manufacture of porcelain, sanitary ware, artware, and hotel china (Johnstone, 1954; Mudd, 1949).

Kaolinite could be employed in Puerto Rico in the glass, ceramic, pottery, and clay pipe industries. Halloysite could be used as a porous catalyst support of high surface area in the cracking of petroleum (Emmett, 1954, p. 261).

REFERENCES

Emmett, P. H. (ed.), 1954, Catalysis: New York, Reinhold Publishing Corporation, v. 1, 394 p.

Faith, W. L., Keyes, D. B., and Clark, R. L., 1950, Industrial Chemicals: New York, John Wiley and Sons, Inc., 652 p.

Hemley, J. Julian, 1959, Some mineralogical equilibria in the system $K_2O-Al_2O_3-SiO_2-H_2O$: Am. Jour. Sci., v. 257, p. 241–270.

Hildebrand, Fred A., and Smith, R. J., 1959, Occurrence of alunite, pyrophyllite, and clays in the Cerro La Tiza area, Puerto Rico: U.S. Geol. Survey open-file report, 82 p. 6 pl.

Hildebrand, Fred A., 1959, Zones of hydrothermally altered rocks in eastern Puerto Rico [in Spanish]: Commonwealth of Puerto Rico, Dept. Indus. Inv., Econ. Devel. Adm., Tech. Inf., p. 82–96.

Johnstone, S. J., 1954, Minerals for the chemical and allied industries: New York, John Wiley and Sons, Inc., 692 p.

Knizek, J. O., and Fetter, Hans, 1950, The refractory properties of alunite: I—High alumina refractories and the genesis, occurrence and uses of alunite: British Ceramic Soc. Trans., v. 49, no. 5, p. 202–223.

Mudd, S. W., 1949, Industrial Minerals and Rocks (non-metallics other than fuels): New York, Am. Inst. Mining Metall. Engineers, 2d ed., 1156 p.

Smith, R. J., and Hildebrand, F. A., 1953, Occurrence of alunite and pyrophyllite in Puerto Rico [abs.]: Geol. Soc. America Bull., v. 64, no. 12, pt. 2, p. 1476.

92. ANDALUSITE-TOPAZ GREISEN NEAR CAGUAS, EAST-CENTRAL PUERTO RICO

By Fred A. Hildebrand, Denver, Colo.

Hydrothermally altered rocks with a greisen mineral assemblage are exposed about 3 km northeast of Caguas, P. R., in the extreme southeast corner of the Aguas Buenas quadrangle. The greisen zone lies within a larger zone of hydrothermally altered rocks of different and possibly lower temperature mineral assemblage than greisen. As shown in figure 92.1, the area described in this report embraces only a small part of this larger zone, which extends from the east coast of Puerto Rico northwest for about 50 km (30 miles) to the Cerro La Tiza area (Hildebrand, 1959).

The greisen zone and the distribution of adjacent volcanic country rocks and plutonic rocks are shown in figure 92.2. The volcanic rocks are of probable Cretaceous and early Tertiary age; the greisen zone is presumably related in origin to the Caguas pluton of undetermined age and the San Lorenzo pluton of Late Cretaceous or Eocene age (Hildebrand, 1959).

The host rocks of the greisen are metamorphosed and silicified nearly beyond recognition. By analogy to fresher rocks nearby, the host rocks are probably lavas, tuffs, tuff breccias, volcanic breccias and agglomerates of borderline andesitic-basaltic composition. They are greenish gray, moderately foliated, and contain local patches of weakly bedded siltstone or sandstone. No contacts of the country rocks with either the plutonic rocks or the greisen zone were seen.

Plutonic rocks along the south edge of the greisen zone are coarse-grained quartz diorite or granodiorite. Megascopically recognizable minerals are quartz, plagioclase feldspar, biotite, hornblende, sphene, and magnetite. Pinkish-white pegmatite dikes composed mainly of orthoclase and quartz and having a crude graphic granite texture intrude the volcanic rocks adjacent to the pluton.

The greisen zone, because of its assemblage of hard resistant minerals, stands in relief above the valley floor of the Rio Grande de Loiza, which cuts transversely across and separates the zone into two knolls (fig. 92.2). Where exposed only in these knolls, the zone is about 3 km long and ¾ km wide.

Although the edges of the greisen zone are concealed, scattered outcrops of country rock, and float blocks of border-phase rock show that the greisen probably grades through silicified, greenish-white volcanic rock to the greenish-gray unaltered country rock.

Exposures of fresh, unweathered greisen are scarce; specimens of fresh rock were found in only two shallow test pits. The fresh rock is grayish white to tannish gray and has a faint banding. Because of the scarcity of outcrops, many specimens were collected from massive, brown to brownish-red ferruginous float blocks, some of which are strongly banded and have a pronounced fluting from differential weathering of the bands. The greisen rocks have a wide range of grain size from fine-grained quartzitelike phases to coarse-grained pegmatitelike phases in which the minerals have maximum dimensions of about ½ to 1 cm. Both banded and structureless rocks contain well-distributed mica and generally the most micaceous rocks are also the most ferruginous.

The greisen mineral assemblage consists principally of muscovite, andalusite, quartz, and topaz with moderate amounts of hematite and goethite, and minor amounts of rutile and jarosite. Topaz is less abundant than andalusite, muscovite, and quartz. Quartz occurs as pods and stringerlike masses. Muscovite occurs as fine and coarse books and plates as large as 1 cm in maximum dimension that commonly contain blood-red hematite along cleavage planes, especially at the outer edges. Hematite commonly occurs in thin, black, submetallic veins less than 1 mm in thickness. Hematite is present on some vuggy vein surfaces as tiny euhedral crystals with striated faces. Some of these crystals of hematite have apparently been altered completely to goethite. Goethite most commonly occurs as thin, black to brown botryoidal coatings. In some coatings and crusts, goethite grades into hematite and appears to have been altered from it. Rutile occurs sparingly as tiny purplish-red to light-brown euhedral crystals with adamantine luster. Jarosite was observed only in the
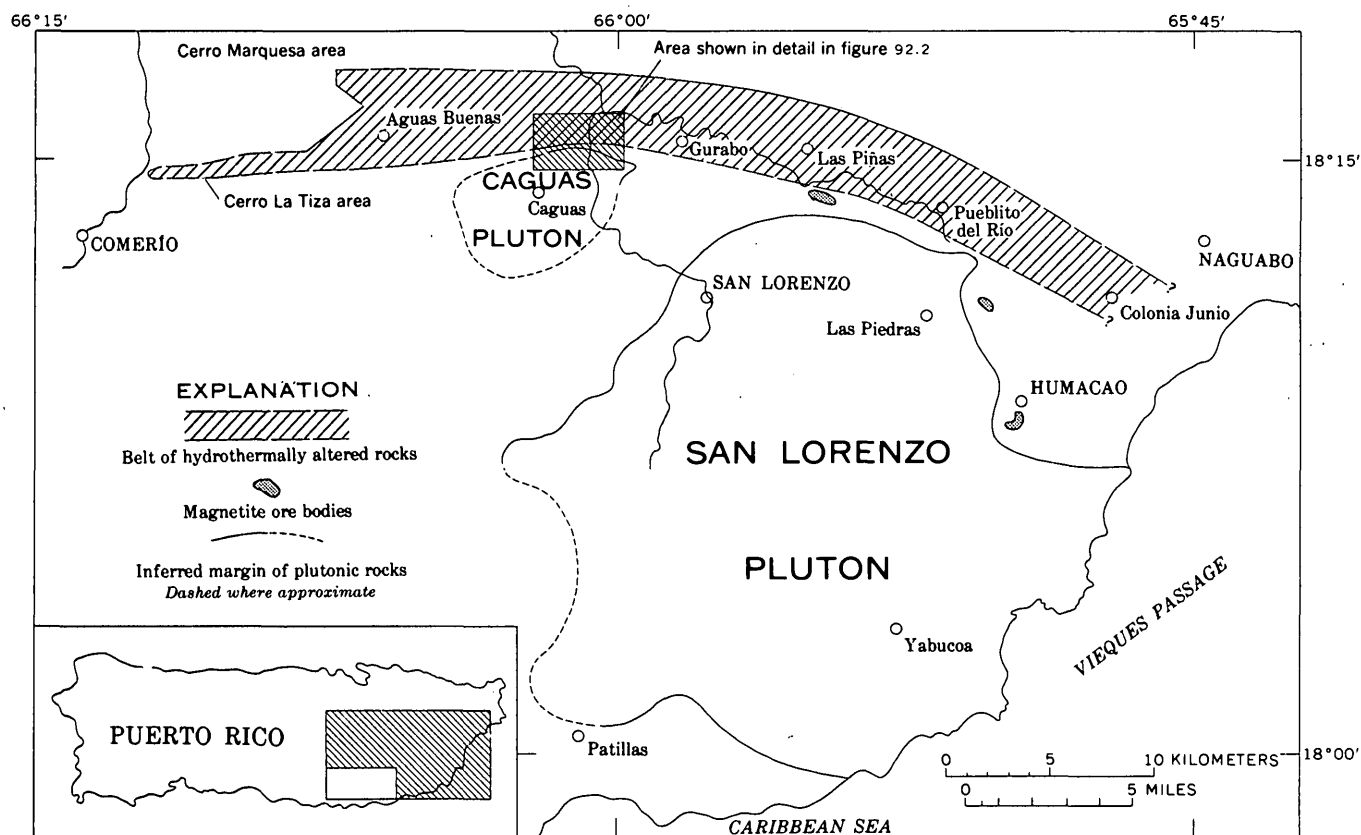
FIGURE 92.1.—Index map showing position of greisen area in the long belt of hydrothermally altered rocks and relation of greisen area to plutonic rocks and magnetite ore bodies. Area shown in details in figure 92.2 is outlined.
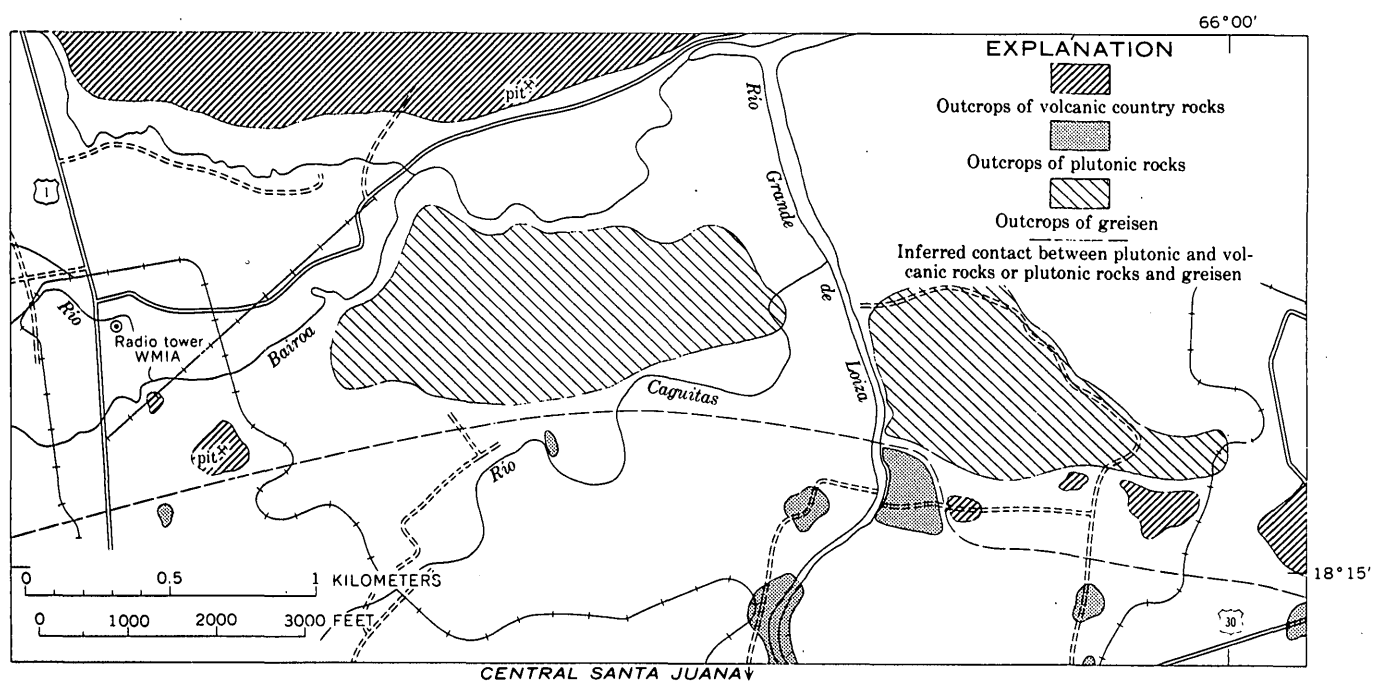
FIGURE 92.2.—Outcrop map showing relation of greisen to plutonic and country rocks.

freshest specimens as a thin yellowish-brown crust in tiny vugs and as minute colloform clusters.

The greisen probably developed from hydrothermal alteration of the volcanic country rocks by emanations from the Caguas pluton or from similar plutonic rocks at depth. The mode of origin is in agreement with stability relations among these minerals as outlined by Hemley (1959). The temperature necessary for the development of andalusite was probably above 400°C, which is too high for the development or existence of kaolinitic clays that occur elsewhere in the long, broad hydrothermally altered belt (Hildebrand, 1959)[1]. By comparison with the minerals of the volcanic host rock the abundance of muscovite, topaz, and iron minerals in the greisen indicates that potassium, silica, iron,

and fluorine were introduced into the host rocks. Because of the lack of minerals containing sodium, calcium, and magnesium, these cations must have been removed from the minerals of the host rock. The hematite in the greisen may be of hydrothermal origin but it may also have developed by alteration from magnetite. Assuming that the greisen previously contained primary magnetite that is now hematite and goethite, it seems likely that this greisen zone may be related in origin to magnetite ore bodies that occur between the hydrothermal belt and the plutonic rocks (fig. 92.1).

REFERENCES

Hemley, J. J., 1959, Some mineralogical equilibria in the system K_2O–Al_2O_3–SiO_2–H_2O: Am. Jour. Sci., v., 257, p. 241–270.

Hildebrand, F. A., 1959, Zones of hydrothermally altered rocks in eastern Puerto Rico [in Spanish]: Commonwealth of Puerto Rico, Dept. Indus. Inv., Econ. Devel. Adm., Tech. Inf., p. 82–96.

---

[1] This belt is described in article 91 of this volume. Although information on the temperature of formation of some minerals of this assemblage is lacking at this time, presumably the greisen zone was formed at a somewhat greater temperature than was the rest of the hydrothermally altered belt.

---

93. ASH-FLOW DEPOSITS, CIALES QUADRANGLE, PUERTO RICO, AND THEIR SIGNIFICANCE

By HENRY L. BERRYHILL, JR., Denver, Colo.

The only known ash-flow deposits[1] in Puerto Rico are in the north-central part of the island within and adjacent to an arcuate northwest-trending graben about 30 km long and 3 km wide (Berryhill and others, 1960). A segment of this graben crosses the southern part of the Ciales quadrangle (fig. 93.1), which was mapped in 1958–59 with the assistance of Fred A. Hildebrand. The ash-flow deposits represent a specific phase of a regional volcanic cycle.

Special thanks are extended to Ray E. Wilcox, whose knowledge of volcanic processes was freely given and extensively utilized during the study of these rocks.

---

[1] The term "ash flow" is applied here according to the nomenclature of Smith (1960, p. 800).

STRATIGRAPHY

The lower member of the Coamo formation in the Ciales quadrangle (Berryhill and others, 1960) is about 495 m thick and consists of ash-flow deposits interbedded with conglomerate, lapilli tuff, and reworked coarse and fine tuff. A reddish color distinguishes this sequence of rocks from all other volcanic rocks in north-central Puerto Rico.

Lenticular and very dense ash-flow deposits within the sequence range in thickness from 10 to 40 m and extend laterally for at least 4 km in discontinuous outcrops. The ash-flow deposits consist primarily of plagioclase crystals, devitrified glass shards, fragments of feldspathic oxidized lava, pumice, and a very fine ash matrix containing iron oxide

EXPLANATION

Quaternary deposits and middle Tertiary limestone

Lower Tertiary granodiorite and dioritic intrusive rocks

Upper Cretaceous dacitic ash flows and associated rocks

Cretaceous volcanic rocks; includes some lower Tertiary rocks

Contact
Dashed where approximately located

Fault
U, *upthrown side;* D, *downthrown side. Arrows indicate direction of strike-slip movement*

Syncline, approximately located

Strike and dip of beds

FIGURE 93.1.—Map of eastern Puerto Rico showing location of ash-flow deposits.

dust. The plagioclase crystals are highly fragmented, the microscopic glass shards are altered, mostly to quartz and clay, and the flattened pumice bombs and much of the matrix have been altered to a clay mineral (nontronite?), quartz, and zeolites. A concentration of plagioclase crystals is common at the base of the deposits.

Welding of the glass shards and fragments under intense heat and pressure at time of emplacement is a distinctive feature of the lower part of each individual ash-flow deposit. The degree of compaction and cohesion decreases from base to top. Basal parts of most deposits have vitroclastic texture, but they also have a distinct parallelism of shards and flattening of pumiceous bombs. Upper parts of flows are nonwelded tuff comprised primarily of pumiceous and feldspathic lava fragments and iron-rich chert.

The sequence of rock types and the crude zonation within an ash-flow deposit are described in the following representative section:

Section of an ash-flow deposit 200 m west of Quebrada Blacho in cliff adjacent to Rio Toro Negro, northern part of barrio Pozas, Ciales quadrangle

Top *Thickness (meters)*

6. Lapilli tuff, nonwelded except for very slight welding at base, reddish brown, compact; intermixed fragments of pumice, oxidized feldspathic lava, and iron-rich, reddish-black chert. Fine matrix

Top *Thickness (meters)*

makes up less than 20 percent of total mass, fragmented plagioclase crystals less than 15 percent. Some fragments have heat reaction rims; pumice bombs are compressed only in basal part_____ 26

5. Lapilli tuff, partially welded, reddish brown; heterogeneous mixture of partially sericitized fragmented plagioclase crystals, oxidized feldspathic lava fragments, devitrified glass shards, and compressed pumice bombs well alined parallel to stratification. Reddish, fine-grained matrix, largely altered to zeolite(?), quartz, and nontronite(?), makes up 40 percent of total mass; plagioclase crystals about 15 percent_____ 3

4. Tuff, welded, reddish-brown, with sparse fragments of feldspathic lava as much as 5 mm long, vitroclastic; abundant iron oxide dust; fragmented plagioclase crystals make up about 15 percent of mass; all pumice bombs compressed; feldspathic lava fragments have heat-reaction rims_____ 5

3. Tuff, welded, reddish-gray, vitroclastic; all pumice bombs compressed and altered to nontronite(?); fragmented plagioclase crystals comprise about 15 percent of mass_____ 0.5

2. Tuff, welded, reddish-brown, vitroclastic-fluidal texture; consists of pulverized andesine(?) crystals in a flour of quartz, iron oxide, zeolite(?), and nontronite(?); plagioclase makes up about 40 percent of mass_____ .3

1. Crystal tuff, welded, vitroclastic-fluidal texture; highly fragmented, cracked, and bent andesine(?) crystals make up about 50 percent of mass (represents sole of ash flow)_____ .07

Base of ash-flow deposit.

TABLE 1.—*Chemical and approximate mineral composition of a dacite ash-flow deposit and of granodiorite from the Ciales stock, north-central Puerto Rico*

[Analysts: P. D. Elmore, I. H. Barlow, S. D. Botts, and Gillison Chloe]

	Granodiorite	Dacite	Norms			
			Granodiorite		Dacite	
SiO_2	61.3	63.7	Q	14.9	Q	16.8
Al_2O_3	16.4	16.5	or	20.0	or	25.0
Fe_2O_3	3.0	3.7	ab	28.8	ab	36.6
FeO	2.7	1.0	an	19.5	an	10.0
MgO	2.1	1.3			c	1.3
MnO	.18	.15	wo	2.4		
CaO	5.1	2.2	en	5.2	en	3.2
Na_2O	3.4	4.2	fs	2.8		
K_2O	3.4	4.2	mt	4.4	mt	1.6
H_2O	1.1	2.2	il	1.1	il	1.1
TiO_2	.56	.74	ap	1.0	ap	1.3
P_2O_5	.40	.22			he	1.3
CO_2	.07	.06			r	.2
Total	99.61	100.17	100.1		98.4	

The age of the ash-flow deposits, based on correlation with fossil-bearing marine rocks of the Coamo formation elsewhere in Puerto Rico, is latest Cretaceous (Maestrichtian). Massive gray poorly stratified andesitic volcanic breccia and possibly reworked marine tuffs of Late Cretaceous(?) and early Tertiary age overlie the ash-flow deposits.

Chemical analyses and normative mineralogic calculations (table 1) indicate that the ash-flow deposits are dacite.

STRUCTURE

The graben that contains the ash-flow deposits is bounded on the southwest by a regional strike-slip fault and on the northeast by a fault that is subsidiary to the regional fault (fig. 93.1). The throw of the graben increases progressively toward the southeast end where the ash-flow deposits are in juxtaposition with basaltic pillow lavas that are several thousand meters stratigraphically lower than the ash-flow deposits. The rocks within the graben form a syncline, although internal faulting has segmented the graben into tilted blocks.

REGIONAL RELATIONS AND SIGNIFICANCE

Ash-flow deposits of dacitic composition on top of a pile of andesitic tuffs and basaltic pillow lavas several thousand meters thick, suggest a progressive change in the composition of magmas that supplied the Late Cretaceous volcanic materials.

Although both overlain and underlain by volcanic breccia and tuff that are obviously marine, the Coamo formation ash-flow deposits are probably subaerial in origin as shown by interlayers of fluvial gravel and nonstratified mudflow deposits, and plant-root casts. Moreover, as pointed out by Rankin (1960, p. 32), an ash flow (the specific gravity of which is well below unity) could not be propagated under water, much less become welded.

The geographic and structural position of the graben relative to plutonic intrusives (fig. 93.1) and the restricted occurrence of ash-flow deposits within and adjacent to the graben suggest that the area of accumulation was initially outlined by sagging of a crustal segment above a magma chamber. Faulting, both contemporaneous with and subsequent to ash-flow deposition, formed the graben. The chemical and mineralogical similarity (table 1) of the dacite ash-flow deposits and the granodiorite in the nearby stocks suggests that the ash-flow deposits represent expulsion of volatile-rich magmatic material from these plutonic bodies after they had moved upward into the near-surface crustal zone.

REFERENCES

Berryhill, H. L., Jr., Briggs, R. P., and Glover, Lynn, III, 1960, Stratigraphy, sedimentation, and structure of Late Cretaceous rocks in eastern Puerto Rico—preliminary report: Am. Assoc. Petroleum Geologists Bull., v. 44, no. 2, p. 137–155.

Rankin, D. W., 1960, Paleogeographic implications of deposits of hot ash flows: Internat. Geol. Cong., 21st, Copenhagen, 1960, sec. 12, pt. 12, p. 19–34.

Smith, R. L., 1960, Ash flows: Geol. Soc. America Bull., v. 71, no. 6, p. 795–846.

PALEONTOLOGY AND PLANT ECOLOGY

94.　REPLACED PALEOCENE FORAMINIFERA IN THE JACKSON PURCHASE AREA, KENTUCKY

By I. G. SOHN, S. M. HERRICK, and T. W. LAMBERT, Washington, D. C., Atlanta, Ga., and Paducah, Ky.

Abundant replaced Foraminifera were recognized by Sohn in a glauconitic sandy claystone of the Clayton(?) formation near Reidland, 8.2 miles southeast of the Paducah Court House. The fossiliferous bed is in a bank of a tributary of the Clark River, in which the following formations are exposed:

Section near Reidland, McCracken County, Ky.

(Paducah East 7½-minute quadrangle measured by T. W. Lambert)

	Feet
Paleocene.	
Porters Creek clay:	
Black claystone	10
Clayton(?) formation:	
Glauconitic claystone, sandy; Foraminifera and	
barite(?) crystals	2 to 3
Upper Cretaceous.	
Owl Creek(?) formation:	
Black claystone	6
Black glauconitic claystone	5(?)
McNairy sand:	
Interlaminated lignitic clay and fine-grained	
micaceous sandstone	15+

The bulk of the faunule is small enough to pass through a 100-mesh screen, although some large specimens also are present. The following forms were identified by S. M. Herrick:

Reophax? sp.
Textularia midwayana Lalicker, 1935
Clavulinoides midwayensis Cushman, 1936
Adhaerentia midwayensis Plummer, 1938
Robulus midwayensis (Plummer), 1927
    cf. R. rosettus (Gümbel). Cushman, 1940
Dentalina cf. D. cooperensis? Cushman. Cooper, 1944
Nodosaria latejugata Gümbel, 1870
Chrysalogonium eocenicum? Cushman and Todd, 1946
Ramulina cf. R. aculeata (d'Orbigny). Cushman, 1940
Nonionella sp.
Bolivinopsis cf. B. rosula (Ehrenberg). Cushman, 1949
Guembelina morsei Kline, 1943
Siphogenerinoides eleganta (Plummer). Cushman, 1940
Bulimina cacumenata Cushman and Parker, 1936
    (Desinobulimina) quadrata Plummer. Cushman, 1940
Bolivina midwayensis Cushman, 1936
    midwayensis Cushman, 1936
Loxostomum deadericki Cushman, 1947
    deadericki Cushman var. exilis Cushman, 1947
Ellipsonodosaria paleocenica? Cushman and Todd, 1946
Valvulineria wilcoxensis Cushman and Ponton, 1932
Gyroidina aequilateralis (Plummer). Cushman, 1944
Gyroidina subangulata (Plummer). Cushman, 1940
Siphonina prima Plummer, 1927
    wilcoxensis? Cushman, 1927
Asterigerina primaria Plummer, 1927
Alabamina wilcoxensis Toulmin, 1941
Pullenia quinqueloba (Reuss). Cushman, 1940
Globigerina pseudo-bulliodes Plummer, 1927
    triloculinoides Plummer, 1927
Anomalina midwayensis (Plummer). Cushman, 1940
    acuta Plummer, 1927
    clementiana (d'Orbigny). Franke, 1925
Cibicides alleni (Plummer). Plummer, 1933
    newmanae (Plummer). Cushman and Todd, 1942

When tested with dilute hydrochloric acid, specimens belonging in normally calcareous foraminiferal genera did not dissolve. Charles Milton determined that the foraminiferal tests are composed of a mixture consisting of hulandite and, probably barite. Crystals probably composed of barite are found with the fossils.

Switzer and Boucot (1955) record foraminiferal tests replaced by heulandite in specimens of Paleocene age from a well near Jackson, Tenn., at depths 483–509 feet. Barite has not yet been recorded as replacing foraminiferal tests, although megafossils replaced by barite are known (Ladd, 1957, p. 23).

The only other record of Tertiary Foraminifera in the Upper Mississippi Embayment is that by Cooper (1944). He described a foraminiferal assemblage of Paleocene age from the Porters Creek formation in well samples from depths of 115–135 feet at Cache, Alexander County, Ill. These fossils are calcareous.

Lamar and Sutton (1930) pointed out that absence of calcareous material is one of the outstanding features of most of the Cretaceous and Tertiary sedimentary rocks in Kentucky, Illinois, and Missouri. They suggested that the absence of fossils is due to leaching. Replaced fossils near the surface at Reidland, and unreplaced fossils at a depth of more than 100 feet in Illinois support that hypothesis.

REFERENCES

Cooper, C. L., 1944, Smaller Foraminifera from the Porters Creek formation (Paleocene) of Illinois: Jour. Paleontology, v. 18, p. 343–354, pls. 54, 55.
Ladd, H. S., 1957, Treatise on marine ecology and paleoecology: Geol. Soc. America Mem. 67, v. 2, 1077 p.

Lamar, J. E., and Sutton, A. H., 1930, Cretaceous and Tertiary sediments of Kentucky, Illinois and Missouri: Am. Assoc. Petroleum Geologists Bull., v. 14, p. 845–866, 3 figs.

Switzer, George, and Boucot, A. J., 1955, The mineral composition of some microfossils: Jour. Paleontology, v. 29, p. 525–533.

95.   COAL-BALL OCCURRENCES IN EASTERN KENTUCKY

By JAMES M. SCHOPF, Columbus, Ohio

Coal balls containing abundant petrified plant remains were found beneath the marine Magoffin beds of Morse (1931) in eastern Kentucky during field seasons of 1949, 1950, and 1951. Apparently, these are the oldest coal-ball occurrences known in North America, and the first to be found in the Appalachian province. The eastern Kentucky coal balls are intermediate in age between those known from the Lower Coal Measures of Britain and the Interior basins in the United States. Collections of this material have been studied intermittently by me since autumn 1950. I am indebted to John W. Huddle, John E. Johnston, and other U. S. Geological Survey geologists for knowledge of the Kentucky occurrences, which are listed below:

1. Shock Branch. Creek-bed outcrop half a mile above the confluence of Shock (Shack) Branch with Rockhouse Creek, about 3 miles southwest of Hyden, Leslie County, Ky.
2. Lewis Creek. Creek-bed outcrop one-fourth mile above confluence of Lewis Creek with Left Fork, about 4 miles east of Chappell townsite, Leslie County, Ky.
3. Bear Branch. Outcrop in ravine on southeast slope about three-fourths mile from the point where Bear (Briar) Branch empties into North Fork of Kentucky River, about one mile west of Cornettsville townsite (Dent), Perry County, Ky.

The Magoffin beds of Morse (1931, p. 302–303) represent one of the most widely distributed and easily identified stratigraphic "markers" of eastern coal measures. In some places, the marine beds are distinguished chiefly by impressions of invertebrate fossils in shale; in other places, they are accompanied by limestone masses of lenticular concretionary habit. A lower limestone layer a few inches thick is most persistent and, near the Lewis Creek oc-

currence, this bed thickens and resembles a coquinoid breccia. The Magoffin beds of Morse (1931) are discussed by Johnston and others (1955) in the Cornettsville area and have been widely identified by Wanless (1939, p. 53; 1946, p. 145). McFarlan (1943) also has discussed the occurrence of this marine zone in Kentucky. Wanless (1957, p. 73) indicated that the Magoffin beds of Morse (1931) were correlated with the Winefrede limestone of West Virginia, the Lower Mercer limestone of Ohio and Pennsylvania, the Minshall limestone of Indiana, the Verne limestone of Michigan, and the Curlew and Seville limestones of Illinois.

The eastern Kentucky coal balls occur close below the marine beds at Shock Branch and Lewis Creek and apparently occupy the position of the Copeland coal of Morse (1931). They evidently are within Read's (1947) *Neuropteris tenuifolia* zone of late Kanawha (Mercer) age. The relation of the Bear Branch coal balls to the principal marine zone is less definite (J. E. Johnston, written communication); they probably are slightly older than those at the other localities.

The coal balls consist of limestone having less than 10 percent included plant substance. They generally appear light buff to brown on weathered surfaces, and include whiter areas of purer calcite and darker areas due to crusts of coal. Coal balls range from the size of small pisolites to large solid aggregated masses as much as a yard thick. Coal balls characteristically are restricted to local areas in a coal bed, and, in this respect, the eastern Kentucky coal balls are typical. The coal bed beneath the limestone is not thick, and it becomes particularly inconspicuous in the presence of abundant coal-ball deposits.

Plant assemblages from coal balls at all three localities appear similar and include calamites and
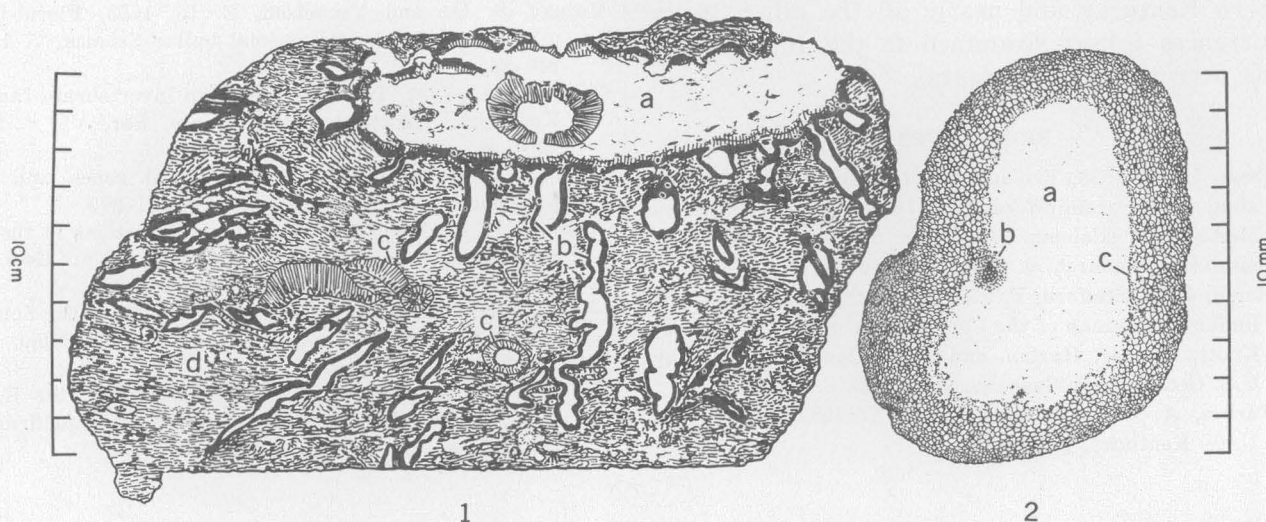
FIGURE 95.1.—1, Cross section of Bear Branch coal ball showing arrangement of peaty plant material. Stigmarian axis (a), stigmarian roots radiating from axis (b), calamite stem fragments (c), and fine vegetable debris including tiny leaves, stems, spores, and seeds (d).

2, Cross section of delicate stigmarian root from Bear Branch coal ball showing original form. Central air cavity (a), conductive strand (b), and parenchymatous outer cortex (c).

lepidophytes in abundance; *Botryopteris, Cardiocarpon, Medullosa,* and other elements may be new.

Coal balls represent petrified peat litter, or peat, of Carboniferous age. A cross section of one of the coal balls shown in figure 95.1.(1) illustrates the arrangement of peaty plant material. If it had not been petrified, this peat would have contributed a layer of coal to the thin coal bed. The brown coloration of coal-ball limestone is mostly derived from the natural color of the original peat preserved in a finely crystalline to cryptocrystalline calcite matrix. Spherulitic or concretionary bands of crystal patterns in the matrix often pass through plant fossils without notable interruption. However, tissue preservation is mostly a result of mineral infiltration and impregnation, rather than replacement. The cell walls of tissues generally are intact and mineral infiltration has been early and rapid enough to preserve even residues of protoplasmic substances inside the cells of some fossils. Preservation of delicate cytologic structures of fossil plants is not as unusual as was once supposed, but it serves to emphasize the quality of preservation in some of these coal balls. A common type of delicate tissue preservation is illustrated in figure 95.1(2) by a section of stigmarian root showing its original form. Preservation generally is poor wherever plant substance is actually replaced by mineral matter. A few vugs and veins represent a later generation of coarsely crystalline calcite within larger coal balls. Petrified tissues are interrupted in these areas.

The marine limestone associated with these coal balls is argillaceous, calcite-cemented, and contains small cavities. Weathered surfaces are mottled buff or gray. Many dissociated crinoid stem segments, worn brachiopod valves, small gastropods, bryozoan fragments, and one shark tooth have been observed. Pebbles and small cobbles of the brown coal-ball limestone also may occur within this coquinoid matrix, but these appear to be erratic, redeposited in the coquina. The surfaces of these coal-ball pebbles are rounded, with some re-entrant cavities. Some rounding may come from local transport, but the cavities suggest etching or solution. The coal balls themselves, the later generation of coarsely crystalline veins, and the coquina cement all show that excess calcium carbonate was present during petrification and early diagenesis.

Preservation of cytologic details in some of the land plant remains strongly indicates early and rapid initial precipitation of coal-ball calcite. The close association with an overlying marine limestone in eastern Kentucky is similar to relations at other coal-ball localities such as those at Berryville, Ill. and West Mineral, Kans. described by Mamay and Yochelson (1953). Henbest (1958) has discussed ecologic implications of a similar deposit in the Secor coal bed near McAlester, Okla. The marine invasion over the coal swamp evidently was so rapid that it corresponds to a "local catyclism." The same interpretation seems applicable to occurrences in

eastern Kentucky and nearly all the other 20-odd occurrences I have examined in the Interior coal fields over the past 30 years.

REFERENCES

Henbest, L. G., 1958, Ecology and life association of fossil algae and Foraminifera in a Pennsylvanian limestone, McAlester, Oklahoma: Cushman Foundation for Foraminiferal Research, v. 9, pt. 4, p. 104–111.

Johnston, J. E., Stafford, P. T., and Welch, S. W., 1955, Preliminary coal map of the Cornettsville quadrangle, Perry, Knott, Letcher, Harlan, and Leslie Counties, Kentucky: U.S. Geol. Survey Coal Inv. Map C–22.

McFarlan, A. C., 1943, Geology of Kentucky: Lexington, Univ. Kentucky, p. 105–106.

Mamay, S. H., and Yochelson, E. L., 1953, Floral-faunal associations in American coal balls: Science, v. 118, p. 240–241.

Morse, W. C., 1931, The Pennsylvanian invertebrate fauna of Kentucky: Kentucky Geol. Survey, Ser. VI, v. 36, p. 296–349.

Read, C. B., 1947, Pennsylvanian floral zones and floral provinces: Jour. Geology, v. 55, p. 271–279.

Wanless, H. R., 1939, Pennsylvanian correlations in the eastern Interior and Appalachian coal fields: Geol. Soc. America Spec. Paper no. 17, p. 1–130, 9 pls.

———— 1946, Pennsylvanian geology of a part of the Southern Appalachian coal field: Geol. Soc. America Mem. 13, p. 1–161, 40 pls.

———— 1957, Geology and mineral resources of the Beardstown, Glasford, Havana, and Vermont quadrangles: Illinois Geol. Survey Bull. 82, 233 p., 7 pls.

96.   AGE OF THE OHIO CREEK CONGLOMERATE, GUNNISON COUNTY, COLORADO

By D. L. GASKILL, Denver, Colo.

The discovery of fossil plants in the Ohio Creek conglomerate about 10 miles northwest of the type locality in the Anthracite quadrangle, Gunnison County, Colo., indicates a Paleocene age for the formation.

The Ohio Creek beds were first referred to by Hill (1890), and by Cross (1892), and mapped as the Ohio formation by Eldridge (1894). In the northwest quarter of the Anthracite quadrangle the Ohio Creek conglomerate is a light-gray to white, conglomeratic, feldspathic, quartzose sandstone unconformably overlying beds assigned to the Mesaverde formation (Lee, 1912), and unconformably overlain by the Wasatch ("Ruby") formation. The Ohio Creek beds are generally massive, conglomeratic at the base, with a few conglomeratic lenses or pebble layers above. Grain size is predominantly medium to coarse, but individual lenses range from very fine to very coarse angular-grained sandstone. Grains of quartz predominate. Weathered feldspar locally constitutes 15 to 30 percent of the matrix. Scattered grains of chert, argillite, and occasional rounded granules of chert are common constituents. Some lenses contain flakes of biotite, muscovite, and less commonly, grains of pink feldspar and hornblende.

At places, particularly at the base of the forma-tion, there is much argillaceous and carbonaceous material, including thin lenses and pellets of greenish-gray clay, thin silty shaly layers, and carbonized wood fragments. The conglomeratic lenses are composed of smooth generally well-rounded, poorly cemented pebbles and cobbles of variously-shaded gray, red, orange, yellow, or brown chert and quartzite, white quartzite, quartz, argillite, and claystone, and an occasional pebble of igneous or volcanic rock. The pebbles and cobbles range from about ¼ to 3 inches in diameter, but most of them are ½ to 1½ inches in diameter. At one locality numerous boulder-size concretions and concretionary lenses of hard dense fine-grained sandstone were found. Torrential cross-bedding commonly occurs within the individual layers. The mineral composition seems to be rather uniform, although no microscopic examinations were made. The thickness of the formation ranges from about 15 to 80 feet in this area.

Fossil plants were collected from a locality on the ridge north of Middle Anthracite Creek at an elevation of 9,100 feet in the N½ sec. 1, T. 13 S., R. 88 W., 6th P.M. From this collection, J. A. Wolfe (written communication, 1960) identified *"Juglans" rhamnoides* Lesquereux, *"Magnolia" magnifolia*

Knowlton, and *Platanus regularis* Knowlton. Wolfe states:

> The *"Juglans" rhamnoides* is known from several Paleocene floras, but has also been recorded (erroneously I think) from Late Cretaceous floras. The other two species are only known from Paleocene floras such as the Raton and Denver. This small flora is certainly of Paleocene age, and is probably correlative with the early Paleocene Raton and Denver floras * * *. The species identified are characteristic forms of the Paleocene and preclude a Cretaceous age.

REFERENCES

Cross, Whitman, 1892, Post-Laramie deposits of Colorado: Am. Jour. Sci., 3rd ser., v. 44, no. 259, p. 19–42.
Eldridge, G. H., 1894, Description of the sedimentary formations, *in* Anthracite-Crested Butte quadrangles, Colorado: U.S. Geol. Survey Geol. Atlas, Folio 9, p. 6–10.
Hill, R. C., 1890, Orographic and structural features of Rocky Mountain geology: Colorado Sci. Soc. Proc., v. 3, p. 362–458.
Lee, W. T., 1912, Coal fields of Grand Mesa and the West Elk Mountains, Colorado: U.S. Geol. Survey Bull. 510, 237 p.

97. BIOHERMS IN THE UPPER PART OF THE POGONIP IN SOUTHERN NEVADA

By REUBEN J. ROSS, JR., and HENRY R. CORNWALL, Denver, Colo., and Menlo Park, Calif.

Recent stratigraphic study in southern Nevada has led to the recognition of large bioherms of very pure limestone in the upper part of the Pogonip group (Early and Middle Ordovician). These are known at Meiklejohn Peak in the Bare Mountain quadrangle (Cornwall and Kleinhampl, 1960), southwest of Aysees Peak in the Frenchman Lake quadrangle, and probably west of Oak Spring in the northern part of the Tippipah Spring quadrangle.

In cross section these bioherms are great lens-shaped masses almost flat on the bottom and convex upward on the top. The largest, located on the west side of Meiklejohn Peak (fig. 97.1), is estimated to be 250 to 300 feet in maximum thickness and approximately ½ mile in lateral extent. All these masses are composed of light-gray aphanitic limestone of a massive nature that shows very few internal depositional structures. However, detailed petrologic work is yet to be done.

All the bioherms are in the lower part of the Antelope Valley limestone of southern Nevada. Specifically they rest almost directly on top of unit *F* of Johnson and Hibbard (1957, p. 347) and they extend upward within what those authors call unit *G*. It is of considerable importance to note that unit *G* does not increase in thickness where the bioherms are present. Its top and bottom limits remain essentially parallel.

The bed on which each bioherm rests is seemingly continuous underneath the bioherm. Surrounding beds above the base are composed mostly of impure silty and muddy limestones which are highly fossiliferous and are characterized in particular by the presence of trilobites that suggest correlation with the Kanosh shale of Hintze (1952, p. 20–23) and of the brachiopods of the *Orthidiella* zone of Nolan, Merriam, and Williams (1956, p. 28–29). Each of these surrounding beds seems to grade laterally into some portion of the upper convex side of the bioherm in which it loses its identity within a few feet. Although there is locally an appearance of "wrapping around" the upper surface of the bioherm, no single bed can be found to overlie its curved surface for an appreciable distance. At no place have we been able to find a truly distinct contact along the sloping sides of the bioherm. We infer that the surrounding muddy beds were deposited while the bioherm was growing and that its mass was not developed and then buried at a later date.

Our examination of lithologic features has been only cursory and was undertaken only at Meiklejohn Peak. There, small masses of thinly laminated limestones, in which the laminae appear complexly contorted, are present within the base of the bioherm. The boundaries of the laminae, which do not exceed 1 inch in thickness, are delineated by extensive development of secondary calcite. There are also some 6-inch to 1-foot beds composed almost entirely of the shells of small brachiopods, but these beds are exceedingly rare. On the north side of the bioherm on Meiklejohn Peak, large cephalopods are well defined in various orientations within its mass.
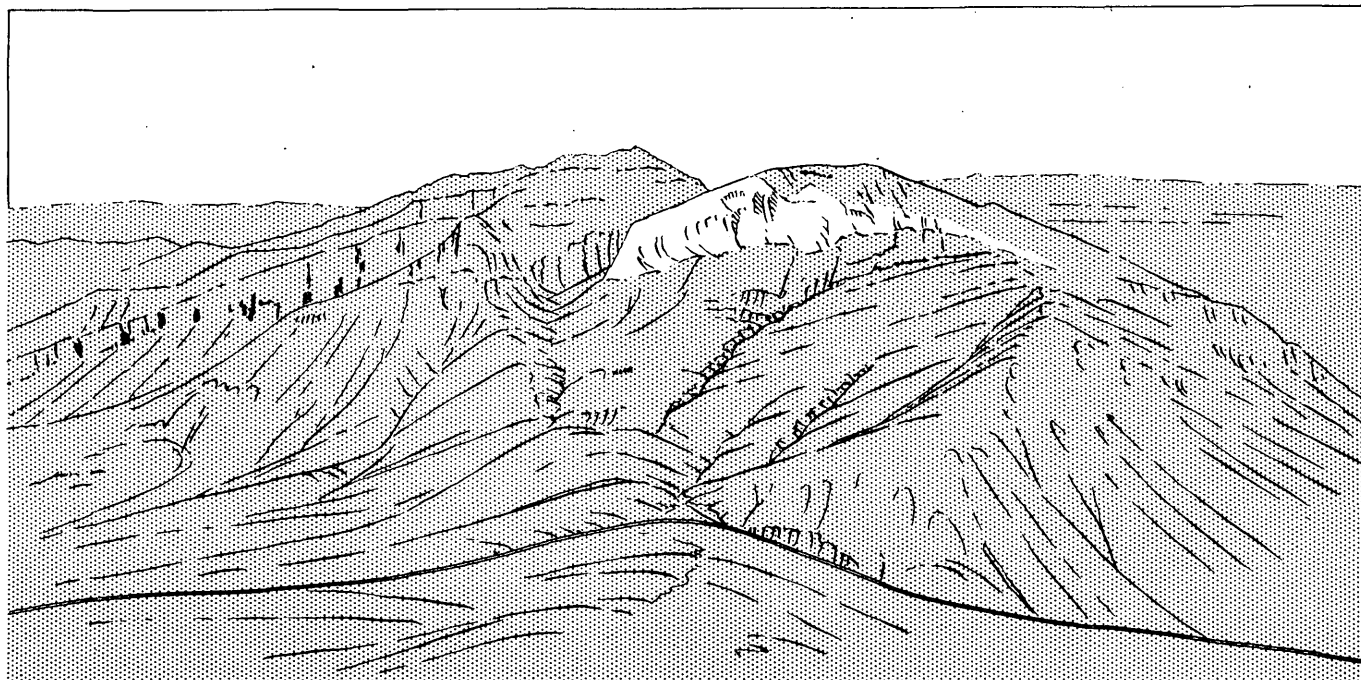
FIGURE 97.1.—Large bioherm (white area) in the Pogonip group in the southwest slope of Meiklejohn Peak is about 250 feet thick.
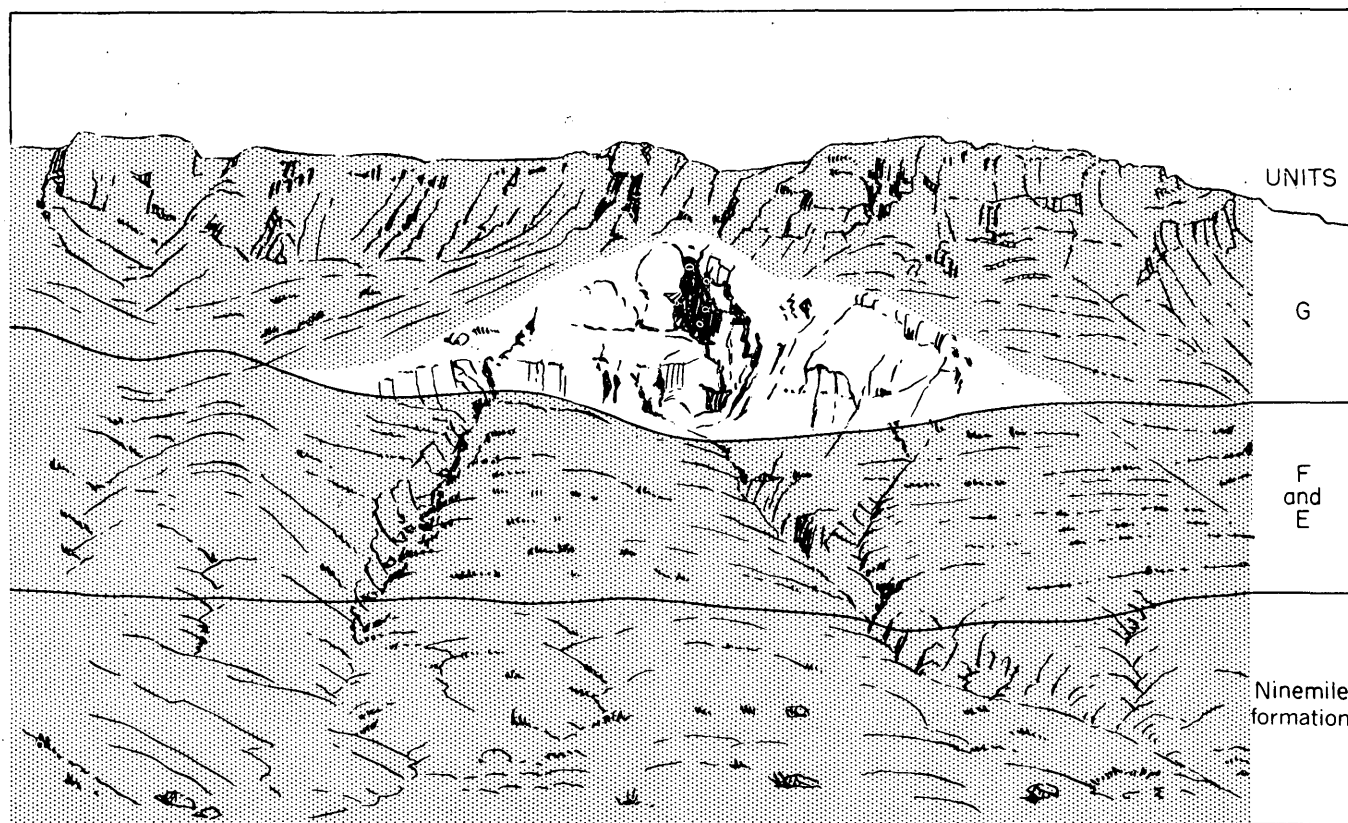
FIGURE 97.2.—Bioherm (white area) in the Pogonip group southwest of Aysees Peak, Frenchman Lake quadrangle, is 75 feet thick, rests on unit *F*, and is within lower part of unit *G* of Johnson and Hibbard (1957, p. 347).

The bioherm southwest of Aysees Peak (Nevada grid, central zone, 750,100 feet E. and 773,000 feet N., on Frenchman Lake quadrangle) (fig. 97.2) probably does not exceed 75 feet in thickness and 250 feet in width. It is located high on the east wall of a large canyon. The eroded remains of another bioherm are readily seen high above the canyon in a side draw 4,000 feet to the north-northeast (Nevada grid, central zone, 751,000 feet E., 776,700 feet N.).

A third bioherm buildup may be located west of Oak Spring in the Tippipah Spring quadrangle (Nevada grid, central zone, 674,750 feet E., 907,500 feet N.). This area on the west side of Amphitheater Valley has been mapped geologically by Houser and Poole (1960). Ross believes such a mass may be represented by the uppermost exposed unit of the Pogonip as mapped by Houser and Poole (1960, unit Opma, sheet 1) as the upper part of the Pogonip. This unit is composed of exceedingly fine grained homogenous dolomite in which bedding is either massive or very thick. The typical flat bottom and convex top cannot be demonstrated and the presence of a bioherm is therefore uncertain. We have established the presence of a fauna within the underlying unit which dates it beyond question as equivalent to the Ninemile formation and to unit D of Johnson and Hibbard (1957, p. 346) in a much dolomitized state. The stratigraphic position, homogeneous nature of the rock, and aphanitic texture of the dolomite suggest to Ross that this body is also a bioherm.

The localities mentioned here are in an area that is approximately 50 miles from east to west and 30 miles from north to south in the southern part of Nevada. To our knowledge, no algalogist has examined any of these deposits. We do not know what organisms contributed most to their construction. When detailed studies have been undertaken and completed on these and any other similar structures in the same stratigraphic position it may be possible to reach conclusions concerning their ecologic significance, and concerning the factors that caused or permitted growth of such impressive structures essentially contemporaneously in a large area of southern Nevada.

At the present time the economic significance of these buildups seems limited. They are so compact and aphanitic in texture that they probably could not themselves serve as reservoirs for petroleum. Analyses by I. C. Frost and E. J. Fennelly, U. S. Geological Survey, indicate that the single sample tested is composed 93 percent of calcite and 2.65 percent of dolomite.

REFERENCES

Cornwall, H. R., and Kleinhampl, F. J., 1960, Preliminary geologic map of the Bare Mountain quadrangle, Nye County, Nevada: U.S. Geol. Survey Mineral Inv. Field Studies Map MF-239.

Hintze, L. F., 1952, Lower Ordovician trilobites from western Utah and eastern Nevada: Utah Geol. and Mineralog. Survey Bull 48, 249 p., 28 pls.

Houser, F. N., and Poole, F. G., 1960, Preliminary geologic map of the Climax stock and vicinity, Nye County, Nevada: U.S. Geol. Survey Misc. Geol. Inv. Map I-328.

Johnson, M. S., and Hibbard, D. E., 1957, Geology of the Atomic Energy Commission, Nevada Proving Grounds area, Nevada: U.S. Geol. Survey Bull. 1021-K, p. 333-384, pls. 32, 33, fig. 57.

Nolan, T. B., Merriam, C. W., and Williams, J. S., 1956, The stratigraphic section in the vicinity of Eureka, Nevada: U.S. Geol. Survey Prof. Paper 276, 77 p., illus.

98. SOIL MOISTURE UNDER JUNIPER AND PINYON COMPARED WITH MOISTURE UNDER GRASSLAND IN ARIZONA

By R. F. MILLER, F. A. BRANSON, I. S. McQUEEN, and R. C. CULLER, Denver, Colo.

Soil-moisture movement and retention in areas under juniper and pinyon as compared with areas under grass are being investigated at selected sites on the Fort Apache Indian Reservation in Arizona to determine if a net gain of usable water can result from the eradication of juniper and pinyon and replacement with grass. Soil moisture, temperature, and moisture tension under the three types of plant cover illustrated in figure 98.1 will be measured periodically for one year starting early in 1961; prelimi-

A
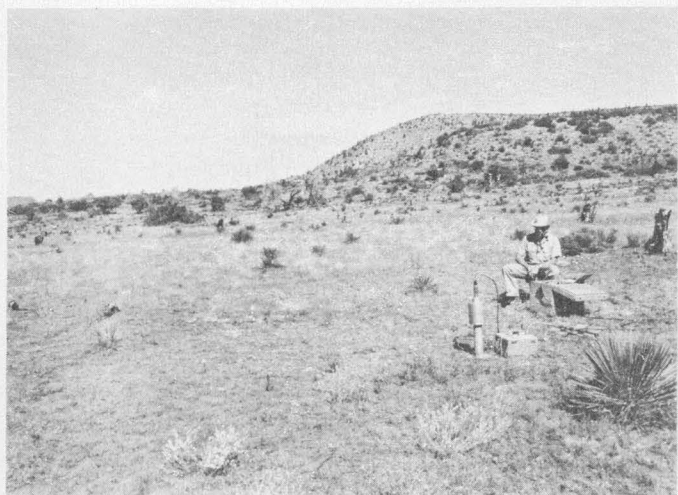
B

FIGURE 98.1.—Photographs of sites being investigated. *A*, forested area in background, sparsely vegetated area in foreground; *B*, open grassland.

nary measurements were made at these sites near the end of the 1960 growing season (late September). Information on the vegetative and aerial cover at each site is given in table 1.

TABLE 1.—*Ground and aerial cover on each of three sites sampled.*

Vegetative cover	Type of roots using water from the soil	Ground cover (percent)					Aerial cover
		Bare soil	Bare rocks	Mulch	Grass	Forbs	
Sparsely vegetated .	Grass and tree....	75.3	0.2	20.3	4.0	0.3	12
Forested..........	Tree............	0	0	100	0	0	100
Grassland........	Grass...........	48	0.8	40.1	12.2	0.9	25

Soil moisture, temperature, and moisture tension were determined at 3- to 4-inch increments down through each of the three soils (fig. 98.2). Soil samples were obtained with a 3-inch diameter barrel-type auger. Part of each sample was placed in a can with a disc of dry pentachlorophenol-treated filter paper, and sealed with elastic adhesive tape. The containers were then stored in a constant temperature chamber for 2 weeks to permit equilibration between the moisture in the soil and the moisture in the paper. Moisture contents of the filter papers and the soil samples were obtained gravimetrically. Soil moisture tension was then determined from a curve that relates the percent of moisture in the paper to soil moisture tension (Gardner, 1936). Soil temperature was determined for each sample as it was taken from the auger hole.

Moisture storage in the upper part of the soil columns was greatest under the dense stand of trees
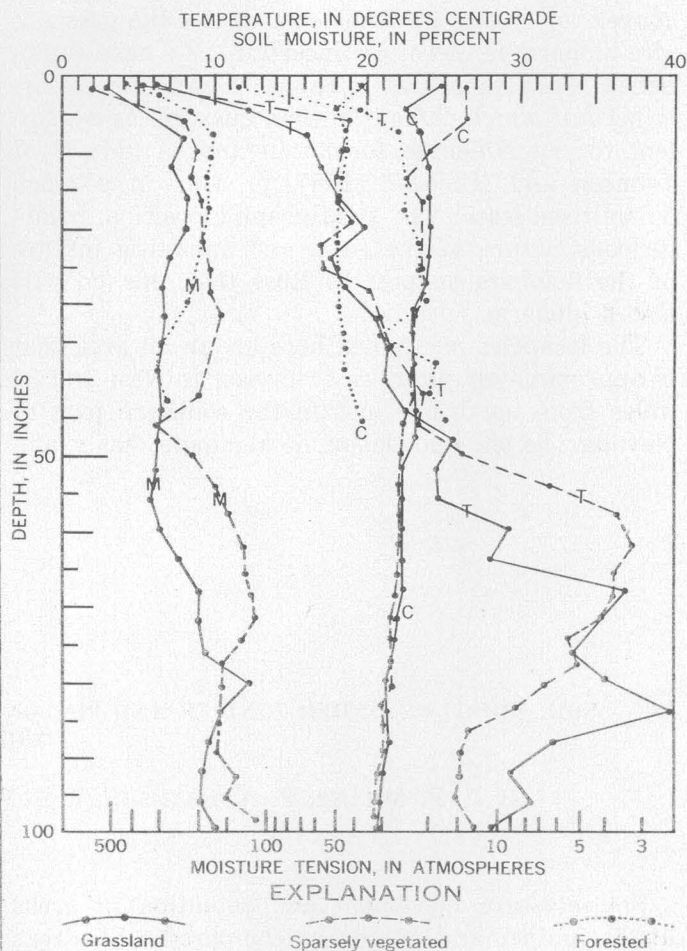
FIGURE 98.2.—Soil moisture (M), temperatures, in degrees centigrade (C), and moisture tension (T) under the three different types of plant cover illustrated in figure 98.1.

(fig. 98.2). Soil moisture under the trees, to a depth of 3 feet, was also retained at lower moisture tensions. This is apparently the combined result of lower temperatures from shading, and reduction of evaporation by a thick mulch of fallen foliage.

Soil temperatures and moisture tensions at the surface (fig. 98.2) were highest in the site with the least aerial plant cover and decreased as the cover increased.

Soil moisture in the grass-root zone (0–48 inches) of the two grassed sites was held at about the same moisture tensions down through the soil profiles. The decrease in moisture tension with depth probably reflects a decrease in the amount of grass roots with depth. The differences in moisture content between soils are apparently the result of differences in soil porosity, rather than differences in water use by the plants. Therefore, differences in water-using capabilities of trees compared to those of grass may be more adequately reflected by moisture-tension data than by soil moisture.

Throughout the profiles temperatures tend to decrease with depth in the two grass-covered soils, but to increase with depth under the trees. Thus, mois-

ture could move down by vapor diffusion in the two grass-covered soils, but would move toward the surface under the trees in response to the slight temperature gradients (Philip and Devries, 1957).

The accumulations of moisture that are indicated by zones of reduced moisture tension at several depths in each of the grass-covered soils (fig. 98.2), reflect a downward movement of water. This movement could be a response to moisture-tension gradients as well as to temperature gradients, inasmuch as capillary tension increases below each zone of moisture accumulation. Moisture tensions at depth are within the range through which Philip and Devries (1957) report a maximum of soil-moisture transfer by a combination of capillary tension and moisture diffusion in response to temperature gradients.

REFERENCES

Gardner, Robert, 1936, A method of measuring the capillary tension of soil moisture over a wide range: Soil Science, v. 43, p. 277–283.

Philip, J. R., and Devries, D. A., 1957, Moisture movement in porous materials under temperature gradients: Am. Geophys. Union Trans., v. 38, p. 222–232.

99.   CORALS FROM PERMIAN ROCKS OF THE NORTHERN ROCKY MOUNTAIN REGION

By Helen Duncan, Washington, D. C.

The seeming absence of corals in the Permian rocks of the northern Rocky Mountain region has been a faunal anomaly to stratigraphic paleontologists concerned with studies of the Phosphoria, Park City, and Shedhorn formations. Some of the sedimentary environments that prevailed in the region through much of Permian time quite obviously were unfavorable for corals, but it is difficult to explain why these organisms should not be present in carbonate facies that supported a fairly prolific fauna of bryozoans and articulate brachiopods. Solitary rugose corals normally occur in such faunal associations, and representatives of the group are found, at least sporadically, in temporally equivalent strata to the west and south.

The many reports of Girty on Permian faunas of the region contain no references to corals; moreover,

during a period of about 15 years, I had seen no corals in Permian collections made by U.S. Geological Survey geologists from the northern Rockies. It is therefore worthy of note that E. L. Yochelson's current investigations of faunas from the Phosphoria, Park City, and Shedhorn formations have disclosed the presence of horn corals in 4 collections, of which at least 2 are certainly Permian. E. R. Cressman's discovery of colonial rugose corals in strata assigned to the lower member (supposedly Grandeur equivalent) of the Park City formation in Lemhi County, Idaho, extends our data on the geographic distribution of a coral zone that is fairly widely developed in western Lower Permian rocks (Wolfcamp and early Leonard equivalents).

The material presently available is meager and very poorly preserved, but it is adequate to demon-

strate that corals are not entirely lacking in the Permian of the region. It is hoped that future collecting will provide specimens that can be used for systematic description. Known occurrences are reviewed in this paper.

MONTANA

Corals were found in two collections from tongues of the Park City that extend into the Snowcrest Range in southeast Beaverhead County, Mont. A mold of a calyx of a small horn coral was collected about the middle of the Franson tongue on Sawtooth Peak (USGS 10854–PC). The rock is composed largely of organic debris, and the coral was reworked to some extent but presumably came from essentially contemporaneous deposits. This occurrence is definitely Permian.

Two fragments of small horn corals in fine-grained siliceous rock were collected from beds considered in the field to be about the middle of the Grandeur tongue of the Park City on Hogback Mountain (USGS 11674–PC). Sections reveal that one of the specimens is probably *Lophophyllidium*. The other is a zaphrentoid coral too altered for generic identification. According to Yochelson (oral communication, 1961), the beds from which the collection came probably are older than the type Grandeur member. The corals are not of kinds that can be safely used to differentiate Permian from Pennsylvania.

WYOMING

A collection (USGS 12201–PC) from the base of the lower part of the Shedhorn sandstone on Tosi Creek, Gros Ventre quadrangle, Sublette County, Wyo., provided a mold of a small horn coral, which I suspect belongs to the lophophyllidid group. There is no good evidence from the associated fauna that the beds in question are Permian.

IDAHO

Three minute horn corals of indisputable Permian age were discovered in a collection from a limestone lens near the middle of the Rex chert member of the Phosphoria formation. This lot (USGS 19532–PC) was collected on the South Fork of Sage Creek, Stew-art Flat quadrangle, Caribou County, Idaho. The corals were obtained when rock from this locality was dissolved in acid. These silicified specimens have slightly curved ceratoid coralla, the largest being about 10 mm long, with rather conspicuous longitudinal ribbing. Evidence of internal deposits (septa, tabulae, etc.) is lacking, possibly having been destroyed by the acid treatment.

E. R. Cressman found colonial rugose corals at three localities in the Morrison Lake quadrangle, Lemhi County, Idaho. The material is recorded as coming from the lower part of the Park City formation, a unit that presumably would now be called the Grandeur member. The corals are replaced by silica, and one cannot be certain that all critical internal structures are preserved. Specimens from two of the localities, one (USGS 19302–PC) 66 feet above the base of the Park City in the Hawley Creek section and the other (USGS 19303–PC) from about the middle of the supposed Grandeur member, are dissepimented phaceloid forms. The corallites seem to have relatively short septa and slightly domed tabulae. Most individuals show no evidence of columellae or axial structures; however, traces of delicate axial rods and slightly more complicated structures were seen in a few transverse sections. It is impossible to tell whether axial structures originally were present in all corallites and largely destroyed in the course of replacement, or whether these corals represent a diphyphyllid variant of some lithostrotionoid genus.

Another genus of dissepimented phaceloid coral was collected 185 feet above the base of the Park City in the Hawley Creek section (USGS 19304–PC). The septa are persistent and relatively long, and most of the corallites exhibit an arachnoid axial structure. This form is related to *Heritschioides*.

The colonial corals obtained from the lower part of the Park City of the Morrison Lake quadrangle suggest that the beds involved are pre-Kaibab in age and somewhat older than the Grandeur member of the type area in the Wasatch Mountains. Similar corals occur rather widely in the Great Basin, commonly in the zone of *Pseudoschwagerina* and primitive *Parafusulina*.

100. OCCURRENCES OF THE PERMIAN GASTROPOD *OMPHALOTROCHUS* IN NORTHWESTERN UNITED STATES

By ELLIS L. YOCHELSON, Washington, D. C.

Omphalotrochus is a guide to the lower part of the Lower Permian (Yochelson, 1954) occurring in the type Wolfcamp formation and its equivalents. More than half a century ago George H. Girty (1905a, p. 20) wrote of an American "*Omphalotrochus* zone," and Knight (1940) discussed the stratigraphic importance of the genus in Russia.

The genus is a common, widely distributed fossil in southwestern United States (Yochelson, 1956). It is also widespread in northwestern United States but has rarely been collected, possibly because the significance of this gastropod has not been emphasized. Localities where it has been found are here documented. Because *Omphalotrochus* is easily identified in the field it has a high potential usefulness in stratigraphic investigations.

Omphalotrochus is large: specimens are seldom less than one inch across the base and may be up to 6 inches across. The base is flattened and bears a large umbilicus with nearly vertical walls. Shells are low spired, with few whorls and with a fairly simple whorl profile. Incomplete specimens and cross sections can be identified as to genus with a high degree of confidence. All known American species are illustrated by Yochelson (1956). Apertural and basal views of representative specimens are shown in figure 100.1.

Occurrences of *Omphalotrochus* in Arizona, Kansas, New Mexico, Oklahoma, and Texas are given by Yochelson (1956), and no additional records from these states are included in this review. "*Omphalotrochus*" as used by Girty for specimens from the Park City, Phosphoria, and "Embar" formations has been assigned to the genus *Babylonites* Yochelson, which is excluded. Numbers in parenthesis refer to the permanent register of U. S. Geological Survey fossil localities.

South Dakota.—In 1957, V. R. Wilmarth collected *Omphalotrochus* near Minnekahta, S. Dak., in the SW¼ sec. 27, T. 6 S., R. 4 E. Fossils were collected from the steep west wall of the unnamed canyon just east of Argyle Canyon, about 1.25 miles north of the Custer-Fall River County line. *Omphalotrochus* occurs in two zones: one is a red, fine- to medium-grained sandstone, 59 to 22 feet below the top of the Minnelusa sandstone (19152-PC); the second is a limestone breccia 96 to 84 feet below the top of the formation (USGS 19153-PC). Specimens are rare and too incomplete to be specifically identified.

Wyoming.—Thompson and Thomas (in Thomas, Thompson, and Harrison, 1953, p. 19) cite an identification by J. Brookes Knight of *Omphalotrochus* collected in 1940 by H. R. McCurdy from the upper part of the Casper formation near Farthing, Wyo. In 1959, *Omphalotrochus wolfcampensis* Yochelson was collected by the writer in abundance from a cherty limestone on the north side of a branch of Chugwater Creek in the NE¼SW¼SE¼ sec. 34, T. 19 S. 70 W., Laramie County, Wyo., as determined from Harrison's unpublished map (USGS 19820-PC). Thomas, Thompson, and Harrison (1953, pl. 9) indicate that *Omphalotrochus* occurs about 450 feet below the top of the Casper formation.

In 1922, C. R. Longwell and W. W. Rubey collected a specimen 70 feet below the top of the Minnelusa sandstone, in Fawcett Canyon, Newcastle quadrangle, Weston County, Wyo., (USGS 4397-PC). The specimen may be *O. wolfcampensis*, but additional material is needed to verify the specific identification.

Utah.—Girty (1905b, p. 391) listed *Omphalotrochus* in a fauna collected by him and J. M. Boutwell, in the Bingham mining district. His specimens came from the "upper portion of limestone," now recognized as the upper part of the Oquirrh formation, one-eighth mile west of the Dalton and Lark mine, Salt Lake County, Utah (USGS 2555 green series). In 1959, the writer, R. J. Roberts and E. W. Tooker, relocated this locality in Cooper Canyon, west of Lark, Utah, on the extreme edge of the Bingham Canyon quadrangle (USGS 18892-PC). The specimens we obtained were identified as *O. wolfcampensis*. In 1958, Roberts and Tooker collected the same species in the upper part of the Oquirrh at an elevation of 5,700 feet in Black Rock Canyon, NE¼ sec. 30, T. 1 S., R. 3 W., Garfield quadrangle, Tooele County, Utah, (USGS 18486-PC, 18893-PC).

Girty (*in* Nolan, 1935, p. 38) listed *Omphalotrochus* sp., from the "western facies" of the Oquirrh formation about ½ mile NNE of the AB Claim on the west side of Dutch Mountain in the Gold Hill mining district (USGS 6332-PC). From the "central facies" of the Oquirrh, he listed *Omphalotrochus* sp., occurring just west of the intersection of the
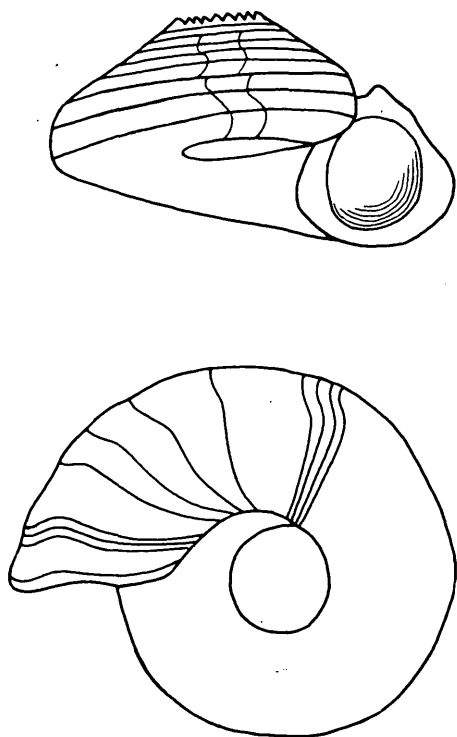
FIGURE 100.1.—Apertural and basal views of representative specimens of *Omphalotrochus*, approximately natural size.

center spur in Sheridan Canyon with the main ridge line (USGS 6362–PC), and *Omphalotrochus?* sp. from the lower slopes of the center spur in Sheridan Canyon (USGS 6360–PC). The specimens from the first two localities are *O. wolfcampensis;* that from the third locality is indeterminate. All localities were considered to be from the "higher Pennsylvanian" as used by Girty, which now refers to the lower part of the Permian.

Omphalotrochus may occur in the Silver Island Range of northwest Utah, but specimens are incomplete and locality data unsatisfactory. In faunal lists, Girty (in McKnight, 1940, p. 34) reports *Omphalotrochus?* sp. from the Rico formation in San Juan County. Unfortunately, the specimen or specimens could not be found in the collection (USGS 6036–PC), and this report cannot be substantiated.

Nevada.—Although this genus has been reported informally as being widespread and locally abundant, a brief examination of the many Survey collections from this State yielded *Omphalotrochus* from only three areas. To the best of the writer's knowledge these occurrences have not been cited heretofore.

In 1900, F. B. Weeks collected a large specimen from the southeast slope of Hamels Peak, Egan Range, 17 miles south of Ely in the gully south of Ice Creek (USGS 2702 green series); presumably

this is from the Carbon Ridge formation. Girty identified the specimen in the collection as *O. whitneyi.* This first use of the specific name for a specimen far from the type area in California probably was based on the large size of the shell, here considered to be specifically indeterminate.

In 1923, C. R. Longwell's party, mapping in the Las Vegas quadrangle, collected specifically indeterminate *Omphalotrochus* from 250 feet of "Pennsylvanian limestone and sandstone" at the top of Williams Peak in the Spring Mountains (USGS 6484–PC). Excellent *O. wolfcampensis* was collected in the quadrangle, but the locality data are poor; the specimens are from the first 30 feet of black dense limestone just below the "Supai" formation (USGS 6473–PC). Presumably both collections are from the upper part of the Bird Spring formation of current terminology.

A single small specimen of *O. wolfcampensis* was collected by H. G. Ferguson and J. S. Williams in 1940 in float from the Antler Peak limestone. It was obtained on the southeast slope of Antler Peak, near the top, in the SE¼ sec. 33, T. 31 N., R. 43 E., Antler Peak quadrangle (USGS 8730–PC).

Idaho.—In 1958, W. J. Carr and D. E. Trimble collected two specimens from approximately sec. 5, T. 12 S., R. 32 E., about 7 miles south of the southwest corner of the Arbon quadrangle on the west face of the Deep Creek Mountains, Power County, Idaho. The first specimen (USGS 19114–PC) is *O. wolfcampensis;* the second (USGS 19116–PC) is less well preserved and is specifically indeterminate. Carr and Trimble obtained one other specimen, which probably is *O. wolfcampensis,* 890 feet below the top of a measured section, ending at the top of peak 7484, Deep Creek Mountains, on the east side of the north fork of Sawmill Canyon in the NW¼ sec. 19, T. 9 S., R. 32 E., Rockland quadrangle, Power County, Idaho (USGS 19105–PC).

Oregon.—In 1908, J. T. Pardee submitted several collections from the Sumpter quadrangle to George H. Girty for identification. One collection from along the railway about 2.75 miles south of Sumpter, Baker County, Oreg., (USGS 19549–PC) contains fusulinids, echinoid spines, *Composita?* sp. indet., and a poorly preserved *Omphalotrochus.*

California.—A review of old collections has brought to light additional specimens of *Omphalotrochus,* including some from the Redding quadrangle (Diller, 1906). Some of the specimens are topotypes of *O. whitneyi* (Meek), the type of the genus, but also the least well known species. Because some *Omphalotrochus* undergo pronounced ontogen-

etic change, there has been a question of the relationship of *O. whitneyi* to better known forms. Investigation of all California specimens may result in revision of the limits of several species.

REFERENCES

Diller, J. S., 1906, Description of the Redding folio [California]: U.S. Geol. Survey Geol. Atlas, Folio 138.

Girty, G. H., 1905a, The relations of some Carboniferous faunas: Washington Acad. Sci. Proc., vol. 7, p. 1-26.

————1905b, Paleontology, p. 387-393 *in* Boutwell, J. M., Economic geology of the Bingham mining district, Utah, with a section on areal geology, by Arthur Keith, and an introduction on general geology, by S. F. Emmons: U.S. Geol. Survey Prof. Paper 38, 413 p., 49 pls.

Knight, J. B., 1940, Are the "*Omphalotrochus* beds" of the U.S.S.R. Permian?: Am. Assoc. Petroleum Geologists Bull., v. 24, p. 1128-1131, with additional discussion by C. O. Dunbar and R. B. King.

McKnight, E. T., 1940 [1941] Geology of area between Green and Colorado Rivers, Grand and San Juan Counties, Utah: U.S. Geol. Survey Bull. 908, 147 p., 13 pls.

Nolan, T. B., 1935, The Gold Hill mining district, Utah: U.S. Geol. Survey Prof. Paper 177, 172 p., 15 pls.

Thomas, H. D., Thompson, M. L., and Harrison, John W., 1953, Stratigraphy of the Casper formation, p. 1-14, pl. 9, *in* Fusulinids of the Casper formation of Wyoming: Wyoming Geol. Survey Bull. 46.

Thompson, M. L., and Thomas, H. D., 1953, Systematic Paleontology of fusulinids from the Casper formation, p. 15-56, pls. 1-8, *in* Fusulinids of the Casper formation of Wyoming: Wyoming Geol. Survey Bull. 46.

Yochelson, E. L., 1954, Some problems concerning the distribution of the late Paleozoic gastropod *Omphalotrochus*: Science, v. 120, p. 233-234.

————1956, Permian Gastropoda of the southwestern United States: 1, Euomphalacea, Trochonemataceae, Pseudophoracea, Anomphalacea, Craspedostomatacea, and Platyceratacea: Am. Mus. Nat. History Bull., v. 110, art. 3, p. 173-276.

101.   PENNSYLVANIAN ROCKS IN SOUTHEASTERN ALASKA

By J. Thomas Dutro, Jr., and Raymond C. Douglass, Washington, D. C.

The apparent scarcity of marine rocks of Pennsylvanian age in Alaska has been a stratigraphic anomaly that has puzzled geologists for nearly 50 years. In his summary of the geology of Alaska, P. S. Smith (1939, p. 26) emphasized the importance of a limestone at a single locality in Soda Bay, Prince of Wales Island, concluding:

More detailed examination of the locality will be required before this determination (Pennsylvanian?) can be regarded as definite, but should it be confirmed by that study it would be of special importance, because it would prove the presence of Pennsylvanian rocks, which are unknown not only elsewhere in southeastern Alaska but in any other part of the Territory.

PRINCE OF WALES ISLAND

Material collected from this locality is not sufficiently diagnostic to establish the precise age of the beds in question. A restudy of the coelenterates by Helen Duncan, the gastropods by Ellis Yochelson, and the foraminifers by Douglass has been inconclusive. The fossils could represent a lower Namurian fauna (highest Mississippian equivalent) which might reasonably occur above the Upper Mississip-

pian *Gigantoproductus* beds, present also at Soda Bay. On the other hand, the strata of doubtful age could correlate with the Lower Pennsylvanian beds with *Gastrioceras*, which crop out in Trocadero Bay, just to the north on the west coast of Prince of Wales Island (Gordon, 1955).

Fusuline foraminifers were listed in several collections from southeastern Alaska by G. H. Girty in Buddington and Chapin (1929, p. 112-115). Girty stated that the evidence, although not unequivocal, suggested a Mississippian age. L. G. Henbest (written communication, 1936) called Girty's attention to the significance of the Fusulinellas in a collection from northern Kuiu Island; this information, together with the evidence from crinoids and a reevaluation by Girty of the rest of the fossils, was the basis for Kirk's (1937a, p. 110) Pennsylvanian age assignment. Our detailed reexamination of this collection has resulted in a definite Middle Pennsylvanian age determination.

Field geologists should be alert to the possibility that Pennsylvanian rocks are more widespread in the area than hitherto assumed. Further study is needed to determine the areal extent of these rocks
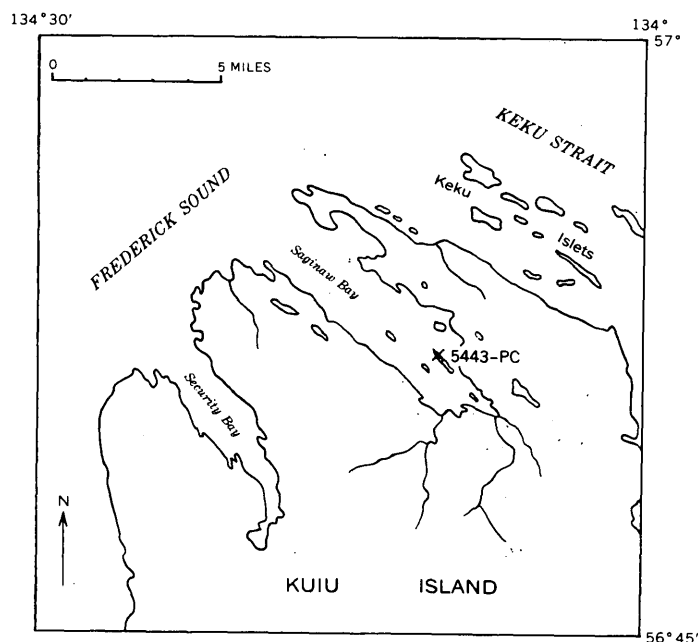
FIGURE 101.1—Locality of Middle Pennsylvanian collection (USGS 5443-PC) near the head of Saginaw Bay, northern Kuiu Island, southeastern Alaska.

and their precise stratigraphic relations with the Mississippian and Permian strata.

KUIU ISLAND LOCALITY

Collection 5443-PC came from a 40-foot thick bed of limestone, intercalated in a series of interlayered chert, quartzite, and chert-bearing limestone, at the northwest end of the long island near the head of Saginaw Bay, Kuiu Island (figure 101.1). Lithologically similar rock sequences are relatively widespread in southeastern Alaska at the top of what was considered Mississippian by Buddington and Chapin (1929, p. 110), and Pennsylvanian fossils should be sought in this part of the section during future field investigations.

Foraminifera identified in this collection (5443-PC = f2277 = Buddington field No. 930) are:

>Climacammina sp.
>endothyrid foraminifer, undet.
>Tetrataxis sp.
>Bradyina sp.
>Nummulostegina ? sp.
>Fusulinella spp.

Probably two species of Fusulinella are represented. One is a loosely coiled form with plane septa and small, nearly symmetrical chomata. This form resembles F. bocki Möller, 1878. It is smaller and shows less fluting of the septa than is shown by

forms referred to this species by Forbes (1960) from Spitzbergen. The species is quite like—and may be referable to—Fusulinella jamesensis Thompson, Pitrat, and Sanderson (1953), described from British Columbia.

The other species is more tightly coiled, fusiform to elongate, and has asymmetrical chomata extending along the septa and floors toward the poles, somewhat resembling Wedekindellina. Fusulinella iowensis Thompson (1936) is similar in many ways to the Alaskan specimens.

The foraminiferal fauna indicates an early Middle Pennsylvanian age, possibly an Atoka equivalent.

Although Girty prepared a long fossil list from this locality, many of the forms either were not determined as to species or were listed as new. A restudy of the collection has resulted in the identification of the following larger fossils:

>Clithrocrinus pyriformis Kirk
>Synbathocrinus sp.
>Delocrinus sp.
>Cyathaxonia sp.
>aulophylloid corals, genus undet.
>horn coral, undet.
>Fenestella sp.
>"Batostomella" sp.
>Cystodictya sp.
>rhomboporoid bryozoan, indet.
>multifoliate fistuliporoid, undet.
>Leioclema ? sp.
>Petrocrania? sp.
>Rhipidomella aff. R. nevadensis (Meek)
>Schizophoria aff. S. resupinoides (Cox)
>Derbyia? sp.
>Chonetes sp.
>Chonetina? sp. (compare C. flemingi crassiradiata Dunbar and Condra)
>Juresania aff. J. ovalis Dunbar and Condra
>Krotovia? sp.
>Linoproductus (sensu stricto) spp.
>dictyoclostid brachiopod, genus indet.
>"Marginifera" sp.
>Spirifer aff. S. rockymontanus Marcou
>Neospirifer sp.
>Spiriferella aff. S. texana (Shumard)
>Martinia? sp.
>Composita sp. (small)
>Crurithyris sp.
>Phricodothyris? sp.
>Stenoscisma sp.
>Hustedia sp.
>Rhynchopora cf. R. magnicosta Mather

Crenispirifer? sp.
Punctospirifer? sp.
Dielasma spp.
Aviculopecten sp.
Schizodus sp.
Platyceras sp.
cf. *Straparollus (Euomphalus?) savagei* Knight
euomphalacean gastropod, indet.
. pleurotomariacean gastropod, indet.
bellerophontacean gastropod, indet.
ostracodes, indet.

This revised list of megafossils clearly indicates a Pennsylvanian age. Several species to which the Alaskan fossils have been compared are restricted to the lower part of the Pennsylvanian, insofar as their distribution is known at present. For example, *Rhipidomella nevadensis* (Meek), *Chonetina flemingi crassiradiata* Dunbar and Condra, *Spirifer rockymontanus* Marcou, *Rhynchopora magnicosta* Mather, and *Straparollus savagei* Knight are all compatible with the early Middle Pennsylvanian age assignment suggested by the fusulines. The other fossils do not conflict with such an assignment.

REFERENCES

Buddington, A. F., and Chapin, T., 1929, Geology and mineral deposits of southeastern Alaska: U.S. Geol. Survey Bull. 800, 398 p., 22 pls., 3 figs.

Dunbar, C. O., and Condra, G. E., 1932, Brachiopoda. of the Pennsylvanian system in Nebraska: Nebraska Geol. Survey Bull. 5, second series, 377 p., 44 pls., 25 figs.

Forbes, C. L., 1960, Carboniferous and Permian Fusulinidae from Spitzbergen: Palaeontology, v. 2, pt. 2, p. 210-225, pls. 30-33, text fig.

Gordon, Mackenzie, Jr., 1955, Alaskan Carboniferous goniatites [abstract]: Geol. Soc. America Bull., v. 66, no. 12, pt. 2, p. 1565.

Kirk, E., 1937a, *Clistocrinus*, a new Carboniferous crinoid genus: Washington Acad. Sci. Jour., v. 27, no. 3, p. 105-111, figs. 1-8.

——— 1937b, *Clithrocrinus*, new name for *Clistocrinus* Kirk: Washington Acad. Sci. Jour., v. 27, no. 9, p. 373-374.

Knight, J. B., 1934, The gastropods of the St. Louis, Missouri, Pennsylvanian outlier: VII. The Euomphalidae and Platyceratidae: Jour. Paleontology, v. 8, no. 2, p. 139-166, pls. 20-26.

Moore, R. C., and others, 1944, Correlation of Pennsylvanian formations of North America: Geol. Soc. America Bull., v. 55, p. 657-706.

Muir-Wood, H., and Cooper, G. A., 1960, Morphology, classification and life habits of the Productoidea (Brachiopoda): Geol. Soc. America Mem. 81, 447 p. 135 pls., 8 figs.

Smith, P. S., 1939, Areal geology of Alaska: U.S. Geol. Survey Prof. Paper 192, 100 p., 18 pls., chart.

Thompson, M. L., 1936, Pennsylvanian fusulinids from Ohio: Jour. Paleontology, v. 10, no. 8, p. 673-683, pls. 90, 91.

Thompson, M. L., Pitrat, C. W., and Sanderson, G. A., 1953, Primitive Cache Creek fusulinids from central British Columbia: Jour. Paleontology, v. 27, no. 4, p. 545-552, pls. 57, 58.

⚒

GEOPHYSICS

102.   POISSON'S RATIO OF ROCK SALT AND POTASH ORE

By R. E. WARRICK and W. H. JACKSON, Denver, Colo.

Work done in cooperation with the U.S. Atomic Energy Commission for the Plowshare Program, Project Gnome

Measurements of elastic constants of rock salt and potash ore of the Salado formation of Permian age (Dunlap, 1951) were made in the mine of the U.S. Potash Co. near Carlsbad, N. Mex. The same constants were measured on samples in the laboratory, and Poisson's ratio determined by the different methods was found to differ. The writer is grateful for help given in the field by the management and staff of the U.S. Potash Co.

In-place measurements.—In-place measurements of elastic constants consisted of determining the velocities of compressional and shear waves in a

pillar of rock (Roller and others, 1959). Pillars representing the potash rock and the salt rock were selected. Four sites in the same horizontal plane along the pillars were chosen for instrument locations, and a matching set of four positions was surveyed directly opposite from the first set of points on the other side of the pillar. The potash pillar was 38 feet wide and 150 feet long. The salt pillar was 25 feet wide and more than 300 feet long.

The source of vibrations was a small hammer that was struck against a steel block fastened to the rock wall with an expansion bolt. Two barium-titanate accelerometers were fastened on the opposite side of the pillar with a small expansion bolt. One was mounted with its principal axis of sensitivity perpendicular to the wall, and the other with its axis parallel to the wall. The signals from the accelerometers were amplified with a wide-band preamplifier, and were displayed on a calibrated oscilloscope.

Permanent records were made by photographing the oscilloscope screen. The instant the hammer struck the anvil, the oscilloscope sweep began moving across the screen at a constant rate. The energy arriving through the pillar was detected by accelerometers and the signal that was produced was presented on this time base.

The first energy arriving at the detectors was compressional. The shear energy arrived somewhat later and could be distinguished by the change of the wave form. The velocities of both waves were determined from transit times of the waves transmitted through the pillar. All elastic constants can be derived from compressional and shear velocities and the density of the rock (Howell, 1959, p. 204). Density was determined from large samples taken from the pillars.

Spectrographic analyses of the samples, made by T. Botinelly, showed the salt was 90 to 93 percent NaCl, and included a trace of sylvite (KCl). The potash was 95 percent sylvite, and included traces of halite and polyhalite.

Laboratory measurements.—Samples from the mine pillars were sent to two laboratories for determination of the elastic constants. For one set the constants were measured by ultrasonic-pulse methods (Mason, 1958, p. 95) by E. C. Walker in the Geological Survey laboratories in Washington, D.C. For the other set the constants were measured by uniaxial compression tests through the courtesy

TABLE 1.—*Poisson's ratio determined by different techniques*

Type of rock and location of test or sample within pillar	In-place test		Ultrasonic test		Unconfined uniaxial compression test			
	Ratio	Standard deviation	Ratio	Standard deviation	600 lb. per sq. in.	1,000 lb. per sq. in.		1,600 lb. per sq. in.
					Ratio	Ratio	Standard deviation	Ratio
Potash pillar:								
North	0.32	0.03	0.35	0.05	0.16	0.17	0.02	0.23
Central	.32	.01	.24	.05	......	......	....	....
South	.29	.01	.31	.05	......	......	....	....
Salt pillar:								
North	.27	.03	.15	.04	0.14	0.19	.02	0.27
South	.24	.01	.18	.04	......	......	....	....

of O. J. Olson in the Bureau of Reclamation laboratories in Denver, Colo.

Comparison of results.—Values of Poisson's ratio determined by the three methods are shown in table 1. Poisson's ratio was selected for comparison because it is derived more directly from the measured data than other elastic constants. The values listed are mean values of the several determinations. The in-place and ultrasonic methods yielded values of Poisson's ratio that are in fairly good agreement for potash. Internally disrupted or slightly weathered samples may be the cause of lower values determined by the ultrasonic method for the salt. The salt pillar was several years older than the potash pillar, and the salt samples could not be taken as deep within the pillar as the potash samples.

Unconfined uniaxial-compression determinations did not agree with in-place and ultrasonic determinations of Poisson's ratio for potash. The compression-test values approached the in-place values as the stress increased for both potash and salt samples.

Exact correspondence of Poisson's ratio determined by the different techniques could not be expected because of the variation of elastic constants with the method of measurement. The in-place method should be preferable because the problem of altering properties through sampling is less severe.

REFERENCES

Dunlap, John C., 1951, Geologic studies in a New Mexico potash mine: Econ. Geology, v. 46, no. 8, p. 909–923.

Howell, B. F., Jr., 1959, Introduction to geophysics: New York, McGraw-Hill Book Co.

Mason, Warren P., 1958, Physical acoustics and the properties of solids: Princeton, D. Van Nostrand Co., Inc.

Roller, J. C., and others, 1959, Seismic measurements by the U.S. Geological Survey during the pre-Gnome high-explosive tests: A preliminary summary: U.S. Geol. Survey open-file report.

103.   FREQUENCY CONTENT OF SEISMOGRAMS OF NUCLEAR EXPLOSIONS AND AFTERSHOCKS

By S. W. STEWART and W. H. DIMENT, Denver, Colo., and Washington, D. C.

Work done in cooperation with the Advanced Research Projects Agency, Department of Defense

The frequency content of seismic waves is a fundamental part of the data obtained from seismograms. Reported methods for studying the frequency spectra of seismic waves have ranged from simple measurements of apparent frequency along the seismogram to elaborate cross- and auto-correlation calculations by digital or analog computers. Most of these studies have necessarily been concerned with the frequency spectrum of fairly large parts of the seismogram. However, some investigators have reported a technique of presenting a continuously changing frequency spectrum as a function of time. This technique, called here the moving-spectrum method, essentially is one of calculating the frequency spectrum of relatively small parts of the seismogram, and presenting the frequency spectra so calculated as a function of time. Ewing and others (1959) have used seismograms recorded on magnetic tape, and appropriate analog methods, to present moving-spectrum representations of seismograms of earthquakes and explosions. In this paper results are given for the calculation of moving-spectrum data by digital methods.

R. G. Henderson and H. W. Oliver helped in setting up the digitizing program. We are particularly indebted to R. G. Henderson for helping us in designing the method of analysis, and to Walter Anderson for writing the program. F. M. Valentine assisted in the seismogram digitizing and plotting of the data.

CALCULATION OF MOVING-SPECTRUM DATA

Seismograms used in this study were taken from larger groups used in studies of nuclear explosions in Nevada (Diment and others, 1961), and aftershocks of the Hebgen Lake, Mont., earthquake of August 1959 (Stewart and others, 1960). For these seismograms, frequencies were chiefly in the range 2 to 10 cycles per second, and the main part of the seismic energy had traveled past the recording station in a few tens of seconds.

The frequency content of parts of seismograms was calculated by the Fourier transform method on a Datatron 220 digital computer. The seismogram trace was prepared for input into the computer by digitizing it at intervals of 10 milliseconds, using a semi-automatic seismogram digitizer developed under the direction of Donald Rock, with assistance from E. C. Moore. Frequency spectra were calculated for 1-second segments along the trace, with the 1-second segments overlapping by ½ second. For example, spectra were calculated that covered the intervals 10.0–11.0 seconds, 10.5–11.5 seconds, 11.0–12.0 seconds, etc. Although the time associated with the spectrum covering a 1-second interval of the trace has been taken to be the time at the midpoint of the interval, it must be realized that the time of arrival of any frequency component is no more accurate than the length of this interval, or approximately $\pm$ ½ second.

Referring to figures 103.1, 103.2, and 103.3, the spectra so computed are then plotted in the form of a contour map, with the X-axis representing time along the seismic trace, the Y-axis representing frequency, and the values of the contours representing the amplitude components of the Fourier frequency spectrum calculation, referred to a maximum Fourier amplitude component of 100. Fourier amplitude components were calculated for the frequency range of 0 to 20 cycles per second, at intervals of ½-cycle per second. The Fourier amplitude components were not corrected for the frequency response characteristics of the seismic recording system. Because the seismic recording system has a peak response at about 3 cycles per second (Diment and others, 1961, p. 205, curve B), the effect of this is to make the Fourier amplitude components progressively smaller than they should be, for progressively higher frequencies. However, the qualitative nature of the contour map is preserved. Although a smaller contour interval adds greatly to the usefulness of the data, the large contour interval used in these figures is sufficient to bring out the main features of the method.

cycles per second. Taking into account the time delays associated with the shot and station locations, the observed time of arrival of this transient event is only 0.2 seconds earlier than that calculated for a P-wave reflection from the base of crustal material having a velocity of 6.15 km per sec in this region (Diment and others, 1961). The good agreement between the observed event at 13.4 seconds and the calculated time of 13.6 seconds suggests that the observed spectral broadening beginning at 13 seconds may be related to this reflection event. The effect of reciprocal spreading (Ewing and others, 1959) may account for the broad-band nature of these short-lived events.

Similar broadenings of the spectrum, beginning at 17 and 19½ seconds, are suggested in figure 103.1. These may also be caused by the appearance of short-lived but coherent transients superposed upon

FIGURE 103.1.—Moving-spectrum analysis, and tracing of seismogram for vertical component of air nuclear shot SMOKY. Distance from shot to station is 58.8 kilometers. Contours are in percent of largest Fourier amplitude component present.

RESULTS

The seismogram for air nuclear shot SMOKY (fig. 103.1) shows, just before the arrival of the initial P-wave at 10.6 seconds, a background of continual noise. The moving spectrum analysis indicates that this microseismic noise is confined to a relatively narrow frequency band centered at about 12 cycles per second, and that the amplitude of this noise is about 1 percent of the maximum amplitude recorded on the seismogram. The arrival of the initial P-wave coincides with a noticeable broadening of the frequency spectrum, both above and below this microseismic band.

The seismogram also shows a large-amplitude transient event with an arrival time of 13.4 seconds. The spectrum beginning at 13 seconds shows a noticeable broadening, the 10-percent contour lines covering the spectrum from 2 to 7 cycles per second, and the 1-percent contour lines extending up to 16.5

FIGURE 103.2.—Moving-spectrum analysis, and tracing of seismogram, for vertical component of underground nuclear shot BLANCA. Distance from shot to station is 61.2 kilometers. Contours are in percent of largest Fourier amplitude component present.
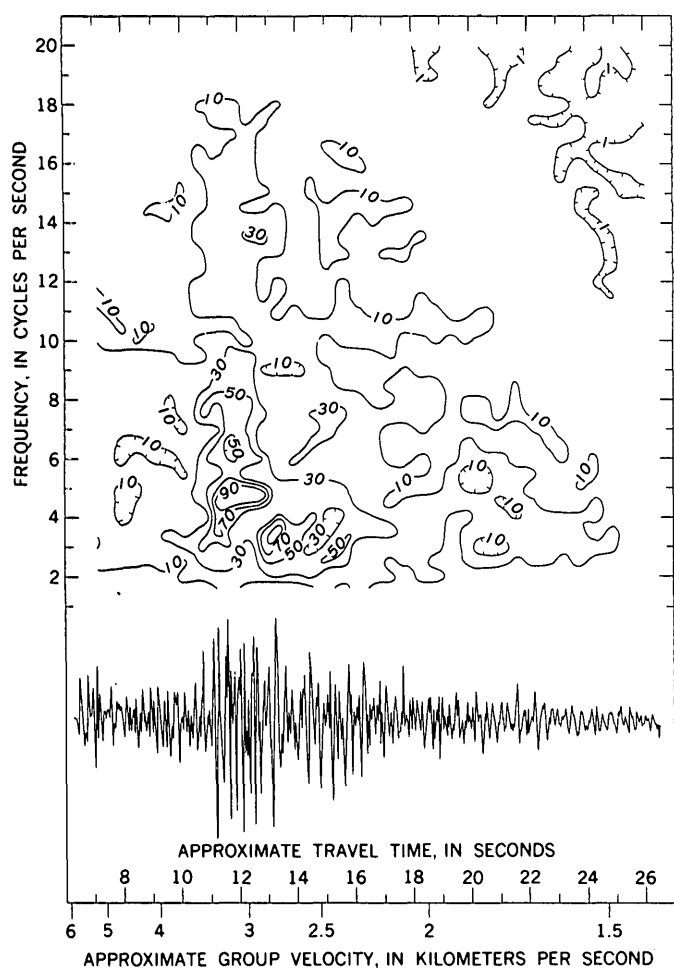
FIGURE 103.3.—Moving-spectrum analysis, and tracing of seismogram, for vertical component of an aftershock of the Hebgen Lake, Mont., earthquake of August 1959. Distance from focus to station is about 37 kilometers. Contours are in percent of largest Fourier amplitude component present.

the relative "noise" of the seismic trace, but it seems reasonable to associate the broadening of the spectrum at 19½ seconds with the onset of the large-amplitude surface waves at this time.

Because the seismic traces on figures 103.2 and 103.3 were free of noise, spectrum analyses were calculated only from the beginning of the first arrival of seismic energy. The seismogram on figure 103.2 shows a large-amplitude pulselike event arriving at about 13.3 seconds, and a noticeable broadening of the spectrum beginning at 13 seconds. The observed time of this event is only about 0.2 seconds earlier than that calculated for a P-wave reflection from the base of crustal material having a velocity of 6.15 km per sec in this region.

Although the complex nature of the near-surface geology in Nevada and the relatively high frequencies

recorded on these seismograms would complicate greatly the appearance and interpretation of seismic surface waves, it was hoped that the dispersive character, if any, of the surface waves could be displayed by this moving-spectrum technique. The best example of dispersed waves found is shown on figure 103.2, corresponding to group velocities in the range 2.3 to 2.6 km per sec, and frequencies in the range 2 to 3 cps. The dispersion is reversed, the higher frequencies having the higher group velocities.

It is instructive to compare the envelopes of the 10-percent contour lines for the moving-spectrum presentation. For the air and underground nuclear shots (figs 103.1 and 103.2) the main part of the seismic energy is below 10 cycles per second, and the envelope of the 10-percent contour decreases in frequency only gradually with time. For the aftershock (fig. 103.3) the main part of the seismic energy is in a higher part of the frequency spectrum, and the envelope of the 10-percent contour decreases more rapidly with time. This difference has been noted for most seismograms from the Nevada and Montana groups, and we attribute it primarily to differences in the near-surface geology along the propagation path and in the broad vicinity of the recording stations, rather than to differences in the source mechanism. All other conditions being essentially the same, seismograms from recording stations located within predominantly bedrock areas generally are characterized by higher frequency waves and shorter duration of the entire wave train than are seismograms from stations located within predominantly alluviated areas. Conversion and scattering of body and surface waves by changes in geology and topography along the propagation path may account for much of this effect (Tatel and Tuve, 1955).

The data presented here do not permit generalizations about the character of seismograms of natural and artificial seismic sources. However, they do suggest that the moving-spectrum method furnishes a useful way to study and characterize seismograms.

The digital method of preparing moving-spectrum diagrams, as presented here, is more time-consuming than the analog method reported by Ewing and others (1959). However, the digital method has the advantages that seismic data not on magnetic tape can be analyzed; the calculation of phase angles from the Fourier transform program is valuable (for example, Sato, 1960); and quantitative amplitude

information can be obtained. Recent developments in the preparation of seismic traces for input into digital computers (for example, Adams and Allen, 1961), and of methods for plotting large masses of data, can speed up the digital method of presentation.

In the examples presented here, nothing has been brought out by the moving-spectrum presentation, at least in a qualitative sense, that is not already apparent by examination of the seismogram itself. Presently, the chief merit of the moving-spectrum method is that it separates the various frequency components in a way that calls attention to events that might be overlooked by the observer, and it provides quantitative information on amplitudes, frequencies, and phase angles that should be helpful in describing and studying the seismogram. It remains to be seen if the fine structure and details of these presentations will provide useful information not derived directly from the seismogram.

REFERENCES

Adams, W. M., and Allen, D. C., 1961, Reading seismograms with digital computers: Seismol. Soc. America Bull., v. 51, no. 1, p. 61–67.
Diment, W. H., Stewart, S. W., and Roller, J. C., 1961, Crustal structure from the Nevada Test Site to Kingman, Arizona, from seismic and gravity observations: Jour. Geophys. Research, v. 66, no. 1, p. 201–214.
Ewing, Maurice, Mueller, Stephan, Landisman, Mark, and Sato, Yasuo, 1959, Transient analysis of earthquake and explosion arrivals: Geofisica Pura e Appl., v. 44, p. 83–118.
Sato, Yasuo, 1960, Analysis of dispersed surface waves, in Davids, N., ed., International symposium on stress wave propagation in solids: New York, Interscience Publishers, p. 303–327.
Stewart, S. W., Hofmann, R. B., and Diment, W. H., 1960, Some aftershocks of the Hebgen Lake, Montana, earthquake of August 1959, in Short papers in the geological sciences: U.S. Geol. Survey Prof. Paper 400–B, p. B219–B221.
Tatel, H. E., and Tuve, M. A., 1955, Seismic exploration of a continental crust, in Poldervaart, Arie, ed., Crust of the earth: Geol. Soc. America Spec. Paper 62, p. 35–50.

※

104. GRAVITY, VOLCANISM, AND CRUSTAL DEFORMATION IN AND NEAR YELLOWSTONE NATIONAL PARK

By L. C. PAKISER and HARRY BALDWIN, JR., Denver, Colo.

A gravity survey made during 1960 in Yellowstone National Park and adjacent parts of Idaho, Montana, and Wyoming, revealed a pronounced gravity low that coincides approximately with the late Cenozoic rhyolites of the Yellowstone Plateau. A narrow north-trending gravity low was also revealed along Madison Valley, west of the Madison Range (fig. 104.1). The area of the Yellowstone Plateau anomaly, inside the zone of steep gradients, is about 1,500 square miles. The steepest gradient, on the southeast side of the anomaly, is 7 milligals (mgals) per mile (fig. 104.1), and the maximum residual gravity relief is about 40 mgals.

Gravity was measured at 890 stations, some of them north of the area discussed in this paper. The measurements were reduced to the simple-Bouguer anomaly with respect to the International Ellipsoid (Nettleton, 1940, p. 139–143) using an assumed density above sea level of 2.67 g per cm^3, and the resulting data were then contoured at an interval of 10 mgals (fig. 104.1).

RELATIONS OF GRAVITY AND GEOLOGY

Gravity is high over (a) the pre-Tertiary rocks that form the high mountains north, south, and west of the Yellowstone Plateau, (b) the basalts of the Snake River Plain, and (c) the Tertiary volcanic breccias east of the Plateau. Gravity is relatively low over (a) the Cenozoic rhyolites of the Yellowstone Plateau and (b) the Cenozoic clastic deposits and rhyolites of Madison Valley (fig. 104.1).

The gravity low of Madison Valley probably reflects a narrow graben filled with low-density Cenozoic clastic deposits and rhyolites several thousand feet thick, bounded by high-angle faults.

A disc-shaped accumulation of rhyolite with gently tapered sides, 10,000 or more feet thick, and 0.3 g per cm^3 less dense than the surrounding rocks, could explain a major part of the Yellowstone Plateau gravity low. If the interface of density contrast is deeply buried, the disc-shaped body could have steep or even vertical sides. Using Gauss's theorem in a manner described by Yokoyama (1958), the mass

EXPLANATION

Cenozoic clastic deposits

Cenozoic rhyolite deposits and rhyolite welded tuff

Cenozoic basalt

Tertiary volcanic breccias

Pre-Tertiary rocks

Contact

— 160 —

Gravity contour
Contour interval 10 milligals

—230—

Gravity low

Lake boundary

Geology compiled from State geologic
maps of Idaho, Montana, and
Wyoming, and from Hamilton (1960)

0 5 10   20   30 MILES
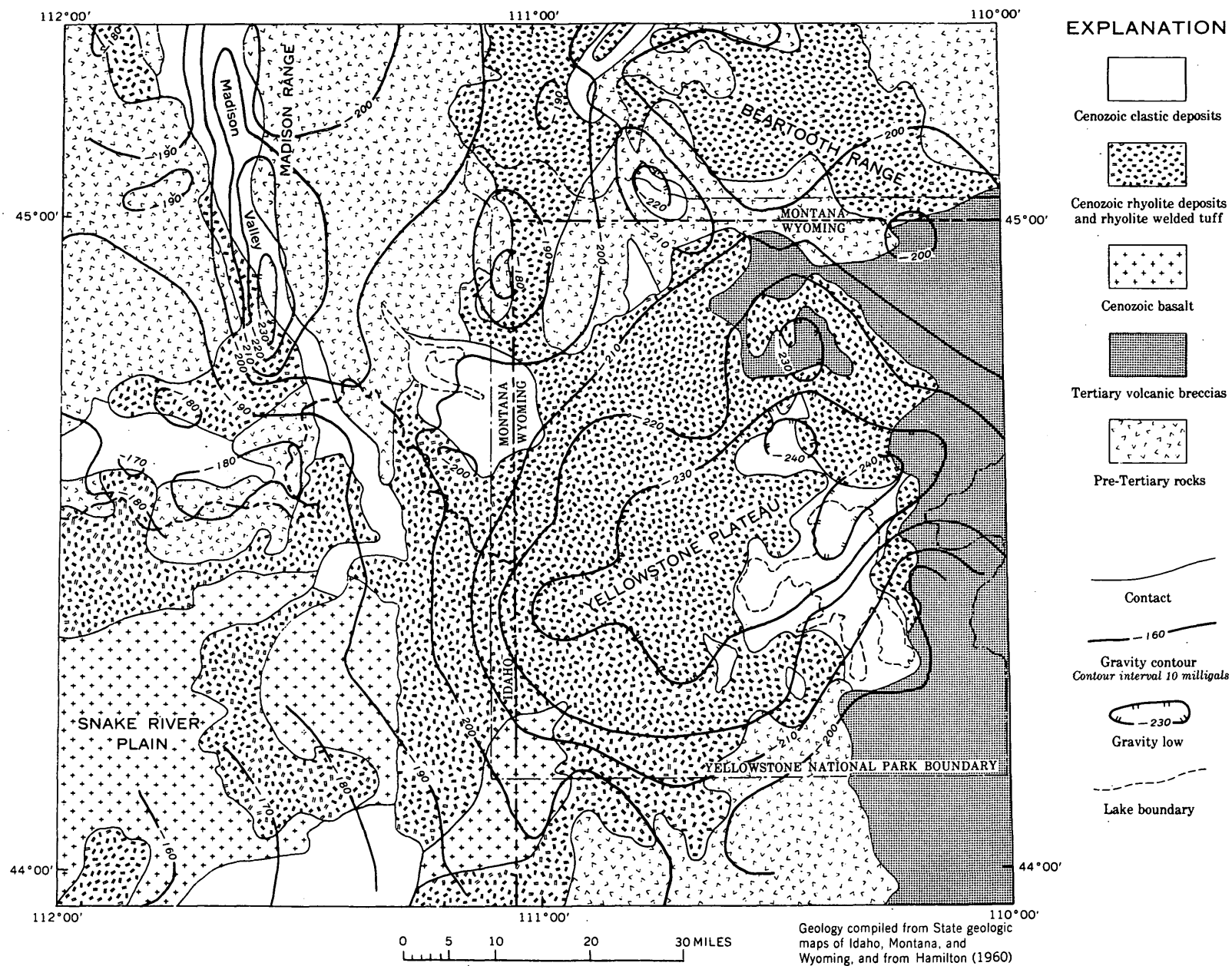
FIGURE 104.1.—Combined gravity and geologic map of the Yellowstone region, Idaho, Montana, and Wyoming.

deficiency corresponding to the gravity low was determined to be about 5×10^{18} g, which is equivalent to 4,000 cubic miles of material 0.3 g per cm^3 less dense than the surrounding material. If this volume of material is spread over a circular area 40 miles in diameter, the average thickness would be nearly 20,000 feet.

The Yellowstone Plateau gravity data could also be explained in part by (a) a thickening of the low-density silicic upper part of the earth's crust from, say, 15 to 21 km, (b) a magma chamber, or (c) a silicic batholith.

Hamilton (1959, p. 228) has suggested that the rhyolites of the Yellowstone Plateau " * * * may be the upper crust of a lopolith which has been forming with a complex history since early Pliocene time, an extrusive lopolith roofed by its own differentiates, its mafic bulk hidden beneath its felsic cover * * *". The mafic bulk of such a lopolith would presumably be dense, especially if it is the mafic fraction of which the silicic differentiate has a mass deficiency as large as 5×10^{18} g. The lack of a positive gravity expression of such a dense mass, assuming that it immediately underlies the rhyolite, must mean that the proposed lopolith does not exist. If the rhyolite differentiated from a mafic magma, it was at such a great depth that the gravity expression of the mafic fraction is overwhelmed by the gravity low of the near-surface low-density rocks of the Yellowstone Plateau. Alternatively, the rhyolites of the Yellowstone Plateau could have been formed from silicic magma generated by partial fusion of relatively shallow crustal rocks.

The gravity data are consistent both with F. R. Boyd's (written communication) conclusion that the Yellowstone Plateau marks the site of a gigantic caldera formed by collapse into a huge underlying magma chamber which may still exist, and with Daly's (1933, p. 142–143) suggestion that the rhyolite may be the foundered crust of a roofless batholith of low density, that is, a silicic batholith.

REFERENCES

Daly, R. A., 1933, Igneous rocks and the depths of the earth: New York, McGraw-Hill Book Co., 508 p.

Hamilton, Warren, 1959, Yellowstone Park area, Wyoming: a possible modern lopolith: Geol. Soc. America Bull., v. 70, p. 225–228.

Hamilton, Warren, 1960, Late Cenozoic tectonics and volcanism of the Yellowstone Region, Wyoming, Montana, and Idaho: Billings Geol. Soc. Guidebook 11, p. 92–105.

Nettleton, L. L., 1940, Geophysical prospecting for oil: New York, McGraw-Hill Book Co., 444 p.

Yokoyama, Izumi, 1958, Gravity survey on Kuttyaro Caldera Lake: Jour. Physics of the Earth, v. 6, p. 75–79.

---

105. GRAVITY, VOLCANISM, AND CRUSTAL DEFORMATION IN THE SNAKE RIVER PLAIN, IDAHO

By D. P. Hill, Harry L. Baldwin, Jr., and L. C. Pakiser, Denver, Colo.

A net of gravity recordings was established over 6,800 square miles of the Snake River Plain in southwestern Idaho during 1959 and 1960.

The western Snake River Plain is a relatively flat lava plain that trends northwest and ranges in width from 40 to 100 miles. It is bounded on the southwest by the Owyhee Mountains and on the northeast by the mountains of the Idaho batholith. The average elevation of the plain is about 3,000 feet above sea level.

The highlands immediately to the north and south of the plain are composed mainly of silicic volcanic rocks of early Pliocene age and of granite of Cretaceous age. A veneer of basalt flows of middle Pliocene age covers the silicic volcanic rocks in the lower elevations. The western Snake River Plain is a graben filled with Pliocene and Pleistocene sedimentary rocks and interbedded basalt flows to a depth of at least 3,000 feet below the surface of the plain (H. E. Malde and H. A. Powers, written communication, 1961). Subsidence of the graben took place along a series of faults trending northwest. The most prominent fault zone forms a sharp escarpment along the northern edge of the Snake River Plain. Malde (1959) estimates that the aggregate throw along this zone is at least 9,000 feet.

The net of 1,859 gravity stations has an average density of one station per 3.7 square miles. The
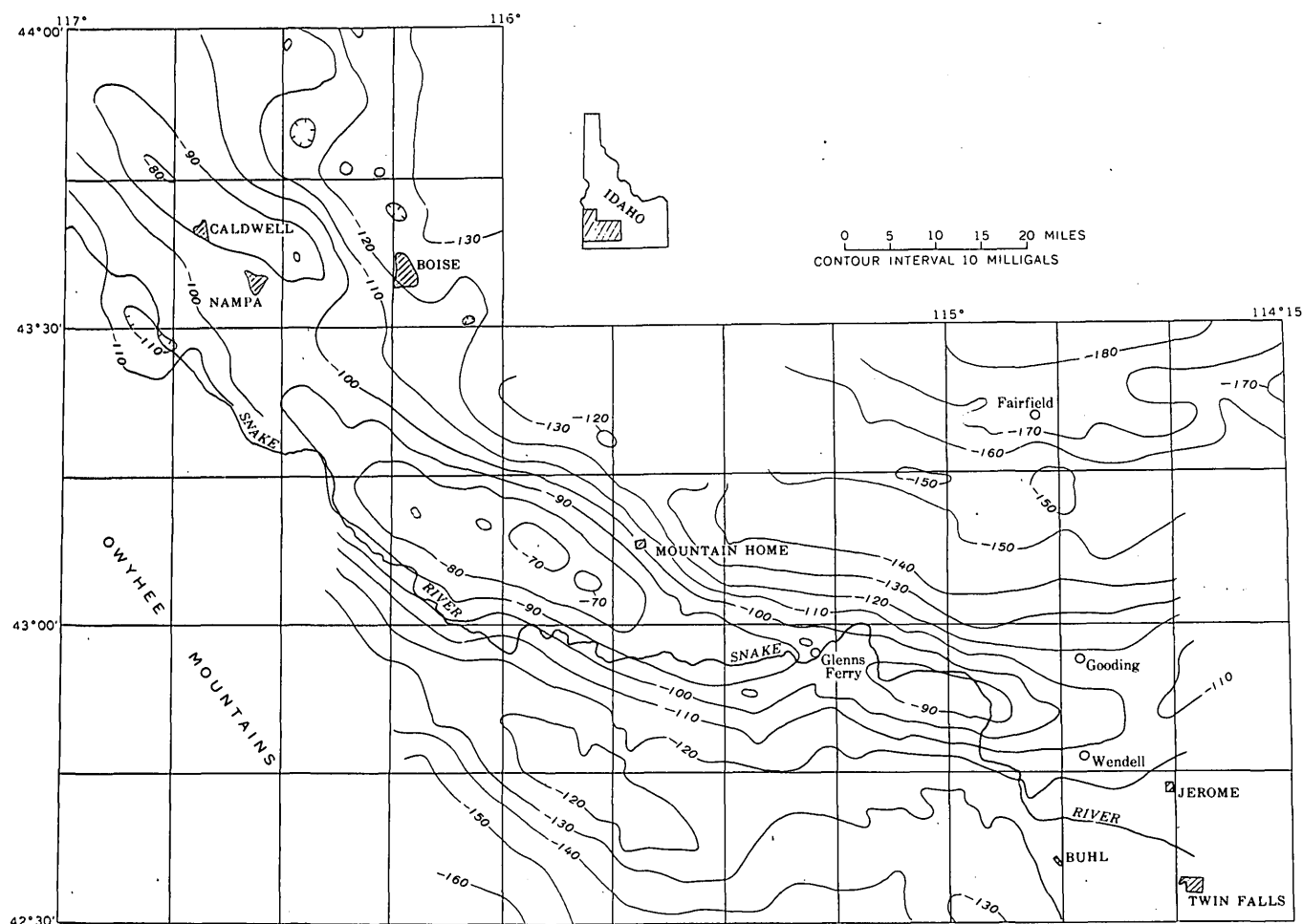
FIGURE 105.1.—Simple-Bouguer gravity map of part of the Snake River Plain, Idaho.

vertical and horizontal control for the survey was taken from Geological Survey 7½- and 15-minute topographic maps. The gravity data were reduced to simple-Bouguer values assuming a density of 2.67 grams per cm[3] down to sea level. These simple-Bouguer values are represented as gravity contours plotted at a 10-milligal contour interval on figure 105.1.

The major anomalies form three elongated, en echelon gravity highs, oriented in a northwest direction. The axes of the gravity highs are parallel to the major fault zones of the region.

The central gravity high is the largest of the three; it extends for 95 miles from Wendell northwestward to about 10 miles south of Nampa, has a maximum amplitude of about 70 mgals, and a maximum simple-Bouguer gravity of −66.5 mgals. Gradients are steepest on the northeast side of the anomaly, reaching 6 to 8 mgals per mile in places. The high is divided into two parts in the vicinity of

Glenns Ferry, Idaho. The eastern section of the high is slightly offset to the northeast with respect to the western section.

The northern and southern gravity highs are similar in outline and amplitude; both are approximately 35 miles long and have amplitudes of about 20 mgals. The northern high is offset about 15 miles northeast from the central high, and the southern high is offset about the same distance southwest from the central high.

Preliminary two-dimensional analyses, based on an assumed density contrast of 0.3 grams per cm[3], have been made along several profiles normal to the axes of the gravity highs. These analyses take into account the fact that the gravity highs are over the relatively low-density sedimentary deposits of Pliocene and Pleistocene age. The tops of the anomaly-causing bodies are at least 3,000 feet below the surface as the thickness of these sedimentary deposits is known. Results of the two-dimensional

analyses suggest that the anomaly-causing bodies extend at least 16,000 feet below sea level and may reach 60,000 feet below sea level, depending on how the shape of the bodies and the regional gravity are assumed. In the preferred interpretation the disturbing masses are approximated by tabular bodies, the largest about 90 miles long, 4 to 6 miles wide, and extending from about 5,000 to 60,000 feet below sea level.

A graphical integration using Gauss's theorem over the surface of the gravity map was used to estimate the total mass excess of the anomalous bodies. A mass excess of about 1×10^{19} grams, or 1×10^{13} tons, is obtained if the simple-Bouguer background is taken as -120 mgals. The volume of this mass excess for material 0.3 grams per cm^3 more dense than the surrounding material would be approximately 8,000 cubic miles.

Several geological hypotheses have been offered in explanation of the gravity highs. The most important of these are:

1. The Snake River Plain is a broad downwarp that has been filled with extensive basalt flows.
2. The plain is a graben bounded by faults with large vertical displacements. Volcanism has accompanied the subsidence. The resulting lava flows filled the depression, yielding thick accumulations of basalt.
3. Crustal stresses have caused large en echelon fissures under the Snake River Plain. These fissures have been injected with basalt or basalt-like material.

In light of the evidence presented in this paper, the authors believe that the anomalies are explained by a combination of the second and third hypotheses.

REFERENCE

Malde, H. E., 1959, Fault zone along northern boundary of western Snake River Plain, Idaho: Science, v. 130, no. 3370, p. 272.

106. GRAVITY, VOLCANISM, AND CRUSTAL DEFORMATION IN LONG VALLEY, CALIFORNIA

By L. C. Pakiser, Denver, Colo.

Work done in cooperation with the California Division of Mines

A gravity survey made during 1955 and 1956 in and around Long Valley, Mono County, Calif., led to the discovery of a pronounced elliptical gravity low bounded by steep gradients that coincide approximately with the margin of the basin and with the exposed boundary between Cenozoic volcanic and sedimentary rocks and pre-Tertiary crystalline rocks. The area of the anomaly inside the zone of steep gradients is about 150 square miles, the steepest gradient on the east end of the anomaly is 20 mgals per mile, and the maximum local gravity relief is 78 mgals (fig. 106.1). This is the largest local difference in gravity in the Great Basin reported to date. A prominent gravity high, only suggested at the 10-mgal contour interval of the gravity map (fig. 106.1), was found near the center of the

gravity low a short distance west of the intersection of sections A–A' and B–B'.

An aeromagnetic survey of the Long Valley area was flown in 1956.

The areal geology shown on figure 106.1 has been generalized from reports by Gilbert (1941), and Rinehart and Ross (1957), and from unpublished work between 1952 and 1959 by C. D. Rinehart, D. C. Ross, and N. K. Huber (C. D. Rinehart, written communication). I am grateful to Mr. Rinehart for permission to use the results of the geologic mapping in this study.

RELATIONS OF GRAVITY AND GEOLOGY

Gravity tends to be high over exposures of pre-Tertiary rocks and relatively low over areas where Cenozoic deposits are found at the surface (fig.

EXPLANATION

Cenozoic clastic deposits

Pleistocene Bishop tuff of Gilbert (1938)

Cenozoic rhyolite and quartz latite

Cenozoic andesite and basalt

Pre-Tertiary rocks

Vertical fault based on geophysical evidence

-250-
-260-
Gravity contour
Contour interval 10 milligals

-210
Gravity low

A⊢————————⊣A'
Location of cross section

Gilbert (1941)		37°45'
Rinehart and Huber (unpublished)	Rinehart and Ross (1957, unpublished)	37°30'

119°00'   118°30'
INDEX TO FIGURE SHOWING
GEOLOGY SOURCES

0 ½ 1 2 3 4 5 MILES
DATUM IS MEAN SEA LEVEL

FIGURE 106.1.—Combined gravity and geologic map of Long Valley, Calif., showing locations of profiles *A–A'* and *B–B'*.
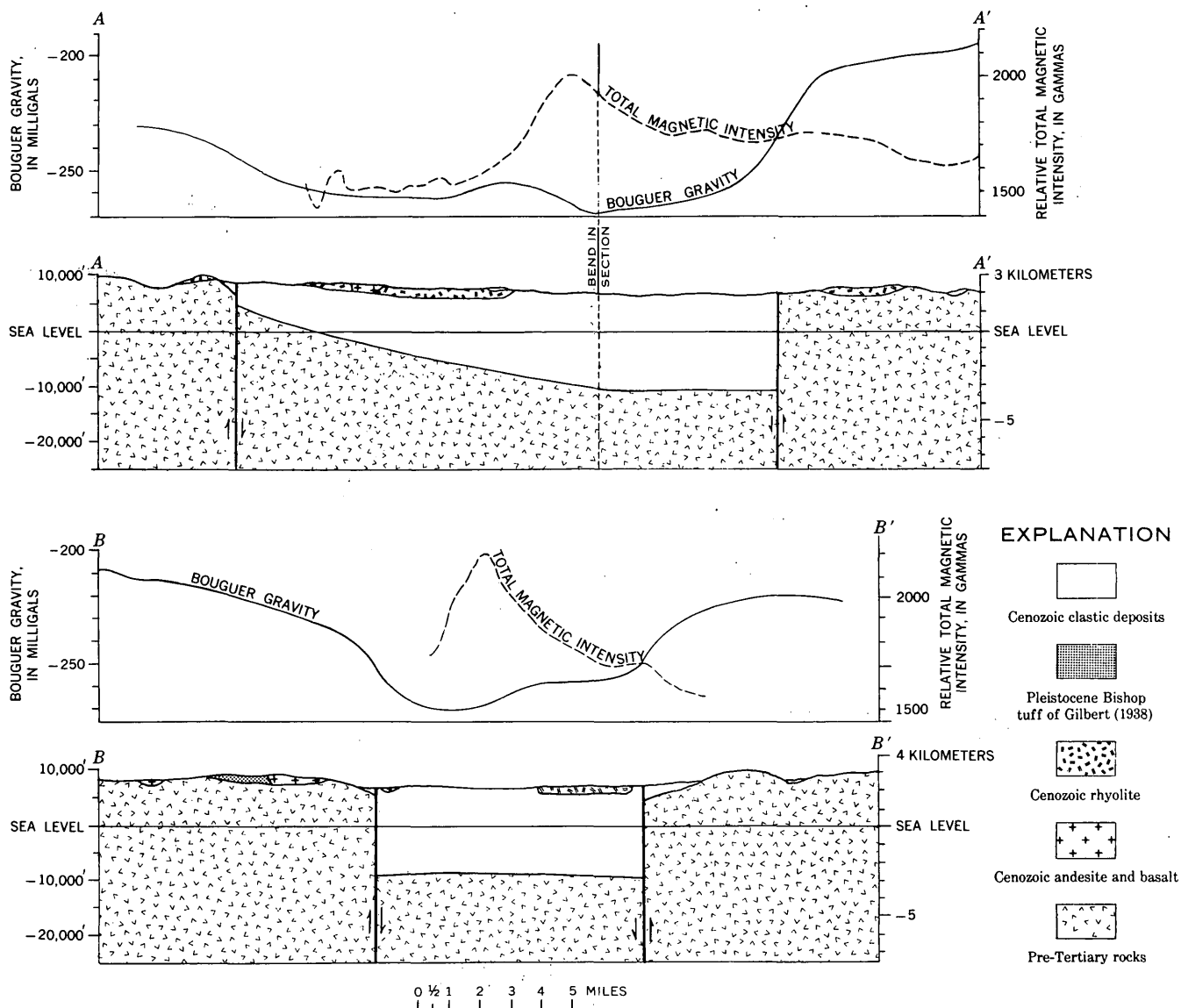
FIGURE 106.2.—Analysis of gravity and magnetic profiles.

106.1). The average density of pre-Tertiary rocks is about 2.7 g per cm³, and the average density of Cenozoic deposits is probably about 2.3 g per cm³. The correspondence of high gravity over rocks of high density and low gravity over material of low density suggests the configuration of the surface of pre-Tertiary rocks. The amplitude of negative departure of the gravity field from higher values over exposures of pre-Tertiary rocks is related to the thickness of the Cenozoic deposits, but the form of the gravity contours does not in general correspond to the actual subsurface configuration of the Cenozoic and pre-Tertiary boundary (fig. 106.2). However, the steepness of gravity gradients is a general guide to the steepness of this boundary.

By making a simple computation, using the expression for the gravity attraction of an infinite sheet and an assumed density contrast of 0.4 g per cm³ between the Cenozoic and pre-Tertiary rocks, it can be concluded that the thickness of Cenozoic deposits in Long Valley corresponding to a residual gravity low of 60 mgals is greater than 12,000 feet.

Similar relations between gravity and geology were found in the Mono Basin area just north of Long Valley (Pakiser, Press, and Kane, 1960).

ANALYSIS OF GRAVITY AND MAGNETIC PROFILES

Profiles A-A' and B-B' (fig. 106.1) were analyzed to determine a depressed structure filled with Cenozoic deposits 0.4 g per cm³ less dense than the en-

closing pre-Tertiary rocks that could account for the measured gravity anomaly (fig. 106.2). The gravity effect within the ellipse-shaped area bounded on all sides by a vertical fault zone (fig. 106.1) was computed and compared with the measured gravity along the east segment of profile $A-A'$ at 9 points by a method previously described (Pakiser, Press, and Kane, 1960, p. 424, 441, fig. 17). Using the result of this computation of gravity effect as a guide, generalized geologic cross sections were constructed along profiles $A-A'$ and $B-B'$ and compared with the measured gravity. A wedge of Cenozoic deposits bounded on all sides by a vertical fault zone and increasing gradually from a thickness of less than 5,000 feet on the west to 18,000 feet on the east can account for the gravity anomaly (fig. 106.2). The density contrast between the Cenozoic deposits and pre-Tertiary rocks may be greater or less than that assumed, so there is an uncertainty of ± 5,000 feet in the computed maximum depth of 18,000 feet.

Total-intensity aeromagnetic profiles along parts of profiles $A-A'$ and $B-B'$ reveal that the magnetic field is generally high over Long Valley, in contrast with the low gravity (fig. 106.2). However, the sharp magnetic high near the center of Long Valley corresponds very roughly with the local gravity high in the same general area. By measuring the horizontal extent of steepest gradients and using an interpretive method described by Vacquier and others (1951), Isidore Zietz (written communication) calculated the depth to the upper surface of the magnetic body to be about 3,000 feet below the surface. This is in the upper part of the Cenozoic section as determined by gravity.

DISCUSSION

The mass deficiency corresponding to the entire gravity low of the Long Valley area was determined uniquely by Gauss's theorem to be about 7.8×10^{17} g, which is equivalent to 470 cubic miles of Cenozoic deposits 0.4 g per cm^3 less dense than pre-Tertiary rocks. Yokoyama (1958) has used Gauss's theorem

to solve a similar problem. The volume of the Long Valley structural block based on the same density contrast was found by direct computation to be 375 cubic miles. Local accumulations of low-density material outside the boundaries of the Long Valley structure contribute to the gravity low and the volume determined from Gauss's theorem but not to the volume of the structure found by direct computation, so the agreement between volumes computed by the two methods is good.

The volume of clastic deposits that could have been transported to Long Valley by streams was found by a method described by Pakiser, Press, and Kane (1960, p. 444) to be only about 150 cubic miles. The discrepancy between the probable volumes of the structure and the stream-transported deposits suggests that a large proportion of the Cenozoic deposits in Long Valley is volcanic. This conclusion is supported by direct observation of volcanic rocks at the surface and by gravity and magnetic evidence of a mass of dense and magnetic material buried near the center of Long Valley.

Long Valley may be a volcano-tectonic depression caused by subsidence along faults, following extrusion of magma from a chamber at depth. A similar conclusion was reached for the origin of Mono Basin (Pakiser, Press, and Kane, 1960).

REFERENCES

Gilbert, C. M., 1938, Welded tuffs in eastern California: Geol. Soc. America Bull., v. 49, p. 1829–1862.
——— 1941, Late Tertiary geology southeast of Mono Lake, California: Geol. Soc. America Bull., v. 52, p. 781–816.
Pakiser, L. C., Press, Frank, and Kane, M. F., 1960, Geophysical investigation of Mono Basin, California: Geol. Soc. America Bull., v. 71, p. 415–448.
Rinehart, C. D., and Ross, D. C., 1957, Geology of the Casa Diablo Mountain quadrangle, California: U.S. Geol. Survey Geol. Quad. Map GQ–99.
Vacquier, V., Steenland, Clarence, Henderson, R. G., and Zietz, Isidore, 1951, Interpretation of aeromagnetic maps: Geol. Soc. America Mem. 47, 151 p.
Yokoyama, Izumi, 1958, Gravity survey on Kuttyaro Caldera Lake: Jour. Physics of the Earth, v. 6, p. 75–79.

107.   GRAVITY STUDY OF THE STRUCTURAL GEOLOGY OF SIERRA VALLEY, CALIFORNIA

By W. H. JACKSON, F. R. SHAWE, and L. C. PAKISER, Denver, Colo., Bowling Green, Ky., and Denver, Colo.

Sierra Valley is in parts of Sierra and Plumas Counties, Calif., and near the northern end of the Sierra Nevada. The valley is a flat, almost featureless plain, approximately 10 miles on a side. An arm about 4 miles wide extends south about 7 miles from the southwest corner. Mountains rise abruptly on all sides to altitudes of more than 3,000 feet above the valley floor, which has an altitude of about 4,900 feet.

During parts of 1959 and 1960 approximately 300 gravity stations were established in Sierra Valley and in the surrounding areas as a part of a long-range study of major crustal features. Data from an additional 418 stations in the valley were made available to the Geological Survey by the Division of Resources Planning of the California Department of Water Resources. The observed gravity data were corrected for latitude, elevation, and terrain effects. Terrain corrections were made through Hayford Zone "H" using the modified Hayford-Bowie charts and tables described by Swick (1942). Both terrain and elevation corrections were based on a density of 2.67 grams per cm³. The data were tied to the airport gravity control network (Woollard, 1958) at Reno, Nev., and San Francisco, Calif., contoured at a 5-milligal interval, and generalized to delete the minor irregularities (fig. 107.1).

The authors are especially indebted to Mr. Lawrence B. James, Chief Geologist of the California Department of Water Resources, and to Mr. Jerome C. Nelson, Geophysicist of the Division of Resources Planning, California Department of Water Resources, for making available geologic and gravity data for this area.

Rocks ranging in age from Precambrian(?) to Quaternary are exposed in the region surrounding Sierra Valley (fig. 107.1), although rocks of many geologic periods are missing. Most of the bedrock is composed of volcanic rocks of Tertiary age. These rocks range in composition from basalt to rhyolite; andesite predominates. The total thickness of the volcanic rocks and the thickness of the individual units vary greatly. Much of the region is covered by deposits of unconsolidated or poorly consolidated clastic sediments of Quaternary age. The age of the underlying valley deposits is not known but could possibly range from late Tertiary to Recent.

The geologic history is incompletely known. The area may have undergone diastrophism during Precambrian time; certainly the rocks were deformed prior to the intrusion of the Sierra Nevada granitoid rocks during Late Jurassic(?) to Cretaceous time. The post-Cretaceous rocks have also been deformed; both normal and strike-slip faults seem to have developed during this period of deformation, although high-angle reverse and minor thrust faults may have contributed to the present geologic configuration. Faulting that commenced with the initial uplift of the Sierra Nevada has continued intermittently to the present.

As in other areas along the Sierra Nevada front, the gravity maxima in the Sierra Valley area are generally associated with outcrops of pre-Tertiary rocks, and the gravity minima with thick deposits of Cenozoic rocks. The average density contrast between the pre-Tertiary rocks and Cenozoic rocks probably ranges from 0.3 to 0.5 grams per cm³. The largest residual gravity minimum in Sierra Valley is about −15 milligals, which for a simple approximation based on the gravity attraction of an infinite slab represents a minimum thickness of from 2,500 to 3,000 feet of Cenozoic deposits.

The prominent, elongated gravity minimum associated with the valley floor indicates a broad, deep basin with a northeasterly trend, corresponding approximately with the outline of the valley floor. Relatively steep gravity gradients on the northwest and west margins of the valley suggest steep bounding faults. The trend of the marginal faults on the west side of the valley is slightly east of north; however, an abrupt change in direction occurs near Beckwourth, where the trend is approximately northeast. The southern boundary of the valley, in the vicinity of Sierraville, may be formed by a complex

EXPLANATION

Cenozoic clastic deposits

Cenozoic volcanic rocks
Predominantly andesite

Pre-Tertiary rocks

Contact
Dashed where approximate

Inferred fault

—*-150*— Gravity contour
Contour interval 5 milligals

Closed gravity low
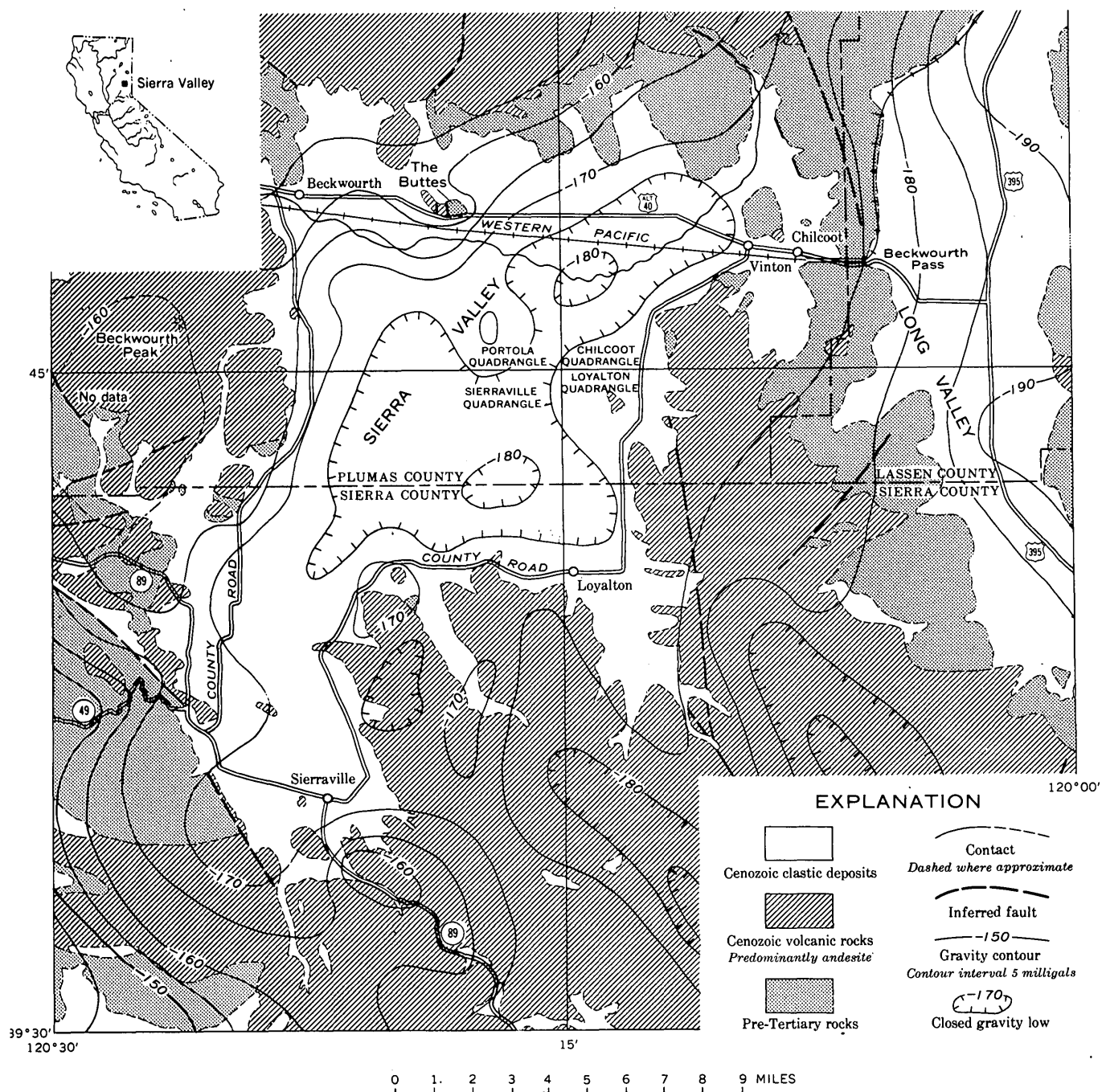
FIGURE 107.1.—Generalized geologic and gravity map of Sierra Valley, California.

pattern of faults. The gravity gradient at the northeast end of Sierra Valley near Vinton suggests a gently sloping contact between Cenozoic fill and pre-Tertiary bedrock. The margin of the valley southwest of Vinton is probably bounded by a steeply dipping faults, and the trend of the gravity field is northeast, suggesting that bounding faults on each side of the valley are parallel.

Pre-Tertiary rock is exposed on the low, rounded hills called The Buttes. This rock gives rise to the northernmost of three gravity highs that form a line trending southeastward across the valley. There is no exposed bedrock associated with the high near the center of the valley, which may represent a buried hill of pre-Tertiary rock or of dense volcanic rock. The southernmost high is relatively broad and centers near a hill of Tertiary volcanic rock. This anomaly suggests that dense volcanic rock may

extend under the alluvial cover for some distance toward the center of the valley.

The gentle gravity gradient near Beckwourth Pass indicates an easterly sloping bedrock surface beneath the light Cenozoic stream and lake deposits in Long Valley. The structural setting of Sierra Valley is similar in many respects to that of Mono Basin and Long Valley, Calif., (Pakiser, Press and Kane, 1960; Pakiser, Art. 106).

REFERENCES

Pakiser, L. C., Press, Frank, and Kane, M. F., 1960, Geophysical investigation of Mono Basin, California: Geol. Soc. America Bull., v. 71, no. 4, p. 415–448.

Swick, C. H., 1942, Pendulum gravity measurements and isostatic reductions: U.S. Coast and Geod. Survey Spec. Pub. 232, 82 p.

Woollard, G. P., 1958, Results for a gravity control network at airports in the United States: Geophysics, v. 23, no. 3, p. 520–535.

MINERALOGY, GEOCHEMISTRY, AND PETROLOGY

108.　DISTRIBUTION OF NIOBIUM IN THREE CONTRASTING COMAGMATIC SERIES OF IGNEOUS ROCKS

By David Gottfried, Lillie Jenkins, and Frank S. Grimaldi, Washington, D. C.

Because of the difficulties involved in the measurement of small concentration of niobium, little is known regarding the distribution of this element in suites of igneous rocks from the United States. Much of our present knowledge on the geochemistry of niobium in igneous rocks is based on about 80 analyses by Rankama (1948) of various igneous rocks, chiefly from localities in Europe. From this study it was shown that siliceous rocks generally contain greater amounts of niobium than the mafic rocks; but relatively few samples of a single province were analyzed to determine the distribution of niobium in an individual differentiated rock series.

This paper presents a summary of new data on the niobium content of 62 samples of related igneous rocks from three different petrographic provinces: the southern California batholith; the Shonkin Sag laccolith of Montana; and the White Mountain plutonic-volcanic series of New Hampshire.

The analyses for niobium were made by a modified niobium thiocyanate spectrophotometric procedure (Grimaldi, 1960) adapted to the determination of niobium in the parts-per-million range in rocks. The method yields results reproducible to better than ± 5 percent as determined by replicate analyses on 22 samples containing different amounts of niobium. Satisfactory agreement was obtained on the niobium content of standard granite G–1

between this method and spectrographic analyses (Ahrens and Fleischer, 1960).

SOUTHERN CALIFORNIA BATHOLITH

This batholith has been studied in great detail by Larsen (1948) both in the field and in the laboratory. The igneous rocks range in composition from calcic gabbro to granite and constitute a calc-alkalic batholith typical of the great Mesozoic batholiths of western North America. Twenty-two chemically analyzed igneous rocks were analyzed spectrophotometrically for niobium. The average niobium content for each of the major rock types is given in table 1. Figure 108.1 is a variation diagram showing the relation of niobium content of the rocks to their chemical composition. The position of each rock is calculated from its chemical analyses by the method described by Larsen (1938).

Niobium is low in the mafic rocks, averaging 4.7 ppm in the gabbros, and shows only a small upward trend in the tonalites and granodiorites, which average 5.3 and 5.6 ppm niobium, respectively. The most siliceous rocks of the batholith, the quartz monzonites and granites, average 7.4 ppm of niobium. The data show a considerable variation in niobium content for rocks of nearly the same composition. On the average, however, niobium shows an enrichment of about 1½ times in the most siliceous rocks over the gabbroic rocks.

TABLE 1.—*Niobium in igneous rocks from the southern California batholith.*

Rock types	Number of samples	Niobium (ppm)	
		Range	Average
Gabbro	6	2.2– 7.7	4.7
Tonalite	5	3.3– 6.9	5.3
Granodiorite	7	4.4– 7.5	5.6
Quartz monzonite and granite	4	4.9–10.5	7.4

THE SHONKIN SAG LACCOLITH

This laccolith provides an excellent opportunity to follow the behavior of niobium during differentiation of a subsilicic-alkalic magma. Chemically these rocks are unusually high in potassium for rocks containing from about 45 to 50 percent silica. The laccolith consists mainly of four rock types: shonkinite, syenite, aegirine syenite, and transition rock which separates shonkinite and syenite. Also present are small aplitic and minette dikelets. Fourteen samples of rocks representing successive stages of differentiation have been analyzed for niobium. The samples were provided by the Department of Mineralogy and Petrography of Harvard University. The results are given in table 2. The chilled shonkonite is represented by two samples from the lower contact. One sample contains 22 ppm niobium and another that was in contact with the underlying sandstone contains 15 ppm niobium. The mafic phonolite is transitional to the lower shonkinite, two samples of which contain 13 and 15 ppm niobium. The transition rock ranges from 17 to 23 ppm and the syenite 25 ppm niobium. The aegirine syenite is intrusive into the enclosing rocks as thin horizontal dikes. Two samples of this rock contain 28 and 56 ppm of niobium. The minette and aplitic syenite contain 23 and 43 ppm niobium respectively.
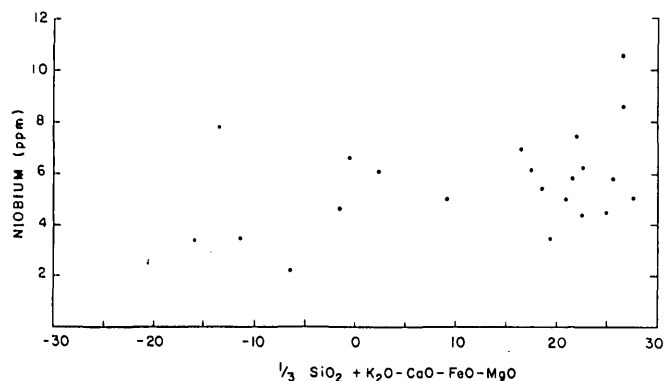
FIGURE 108.1.—Distribution of niobium in igneous rocks of the southern California batholith.

TABLE 2.—*Niobium in igneous rocks of the Shonkin Sag laccolith.*

Sample	Rock type and location [1]	Niobium (ppm)
21	Upper part of Upper shonkonite	24
450	Upper shonkonite	15
15	Syenite	25
1044	Aegirine syenite	28
1067	Aegirine syenite	56
1065	Minette (3 inches thick)	23
1066	Aplitic syenite	43
a [1]	Transition rock	17
a	Transition rock	20
451	Transition rock	23
b	Lower shonkinite	13
1008	Lower shonkinite	15
415	Basal mafic phonolite	22
1081	Basal mafic phonolite next to contact with sandstone.	15

[1] Samples are listed in approximate order from top to bottom of the laccolith.

According to Hurlbut (1939), most of the rocks of the laccolith were derived from a magma which differentiated in place. The niobium content of the initial magma, based on the niobium content from the chilled mafic phonolite, is probably about 15 to 20 parts per million. There is a small increase in niobium in the transition rocks and syenite, and a relatively large increase of niobium in the latest differentiates. Our data on niobium distribution are as yet too few to use the distribution guide to support or reject Hurlbut's (1939) proposal of differentiation in place.

WHITE MOUNTAIN PLUTONIC-VOLCANIC SERIES

This series contains a considerable variety of plutonic rocks which have definite alkalic characteristics (Chapman and Williams, 1935). The plutonic rocks (in order of decreasing age) consist of gabbro, diorite, nepheline syenite, syenite, quartz syenite, and a variety of amphibole and biotite granite. The syenite and granitic rocks are predominant. Quartz is a late mineral in the series and is important only in the quartz syenites and granites. Chemically these rocks are relatively high in Na_2O and low in CaO and MgO.

Twenty-six samples of some of the plutonic rocks were analyzed for niobium. These samples were made available by Arthur P. Butler of the U.S. Geological Survey. The results (table 3) show that the plutonic rocks of this province contain much more niobium than the rocks of southern California. The granitic rocks from the main intrusive mass average about 100 ppm niobium and those from the outlying masses contain about 80 ppm niobium. Only a few of the other rock types were analyzed. The gabbro contains 55 ppm and the nepheline

TABLE 3.—*Niobium content of plutonic rocks of the White Mountain plutonic-volcanic series.*

Rock types	Number of samples	Niobium (ppm)	
		Range	Averages
Gabbro	1	....	55
Monzodiorite	1	....	119
Nepheline syenite	1	....	179
Syenite	1	....	120
Quartz syenite	1	....	102
Biotite granites (main intrusive mass)	8	70–148	105
Amphibole granites (main intrusive mass)	4	72–126	101
Biotite granites (outlying masses)	8	46–120	82

syenite 179 ppm of niobium. One sample not included in the table, a riebeckite granite cut by veinlets, contains 330 ppm niobium. The composition of the veinlets is as yet unknown.

DISCUSSION

Just as each of the petrographic provinces discussed here has distinct mineralogic and chemical characteristics, the niobium content of each province is distinctly different. From the available data, there is very little overlap in the niobium content of the rocks of one suite as compared to another. The lowest niobium content in the rocks of the southern California batholith is in a gabbro which contains 2.2 ppm niobium. The maximum content is 10.5 ppm in a granite. In the Shonkin Sag laccolith the minimum value is 13 ppm in the mafic shonkonite and the maximum is 56 ppm in the aegirine syenite. Except for two samples of granite from outlying masses, the gabbro of the White Mountain plutonic-volcanic series contains 55 ppm of niobium and most of the late differentiates contain more than 100 ppm. The results also indicate that, on the average, niobium is concentrated in the later differentiates of each of the series.

Of the three provinces discussed, only the rocks of the southern California batholith can be consid-ered typical major crustal igneous masses. Hence, it is of interest to compare the niobium content of this batholith with the estimates of the average abundance of niobium in igneous rocks. According to Rankama the average niobium content of igneous rocks is 24 ppm, whereas the average niobium content of the southern California batholith is probably between 5 and 6 ppm. Assuming that this divergence is not due to analytical procedures, either the batholith of southern California is abnormally low in niobium, or, as pointed out by Fleischer and Chao (1960), estimates of the abundance of many elements, including niobium, are of questionable value unless regional variations are taken into account.

REFERENCES

Ahrens, L. H., and Fleischer, Michael, 1960, Report on trace constituents of the granite G-1 and the diabase W-1, *in* Stevens, R. E., and others, Second report on a cooperative investigation of the composition of two silicate rocks: U.S. Geol. Survey Bull. 1113, p. 83–1113.

Chapman, R. W., and Williams, C. R., 1935, Evolution of the White Mountain magma series: Am. Mineralogist, v. 20, p. 502–530.

Fleischer, Michael, and Chao, E. C. T., 1960, Some problems in the estimation of the abundances of elements in the earth's crust: Internat. Geol. Cong., 21st, Copenhagen, 1960, pt. I, p. 141–148.

Grimaldi, F. S., 1960, Determination of niobium in the parts per million range in rocks: Anal. Chemistry, v. 32, p. 119–121.

Hurlbut, C. S., Jr., 1939, Igneous rocks of the Highwood Mountains, Montana, pt. I, The laccoliths: Geol. Soc. America Bull., v. 50, p. 1043–1112.

Larsen, E. S., Jr., 1938, Some new variation diagrams for groups of igneous rocks: Jour. Geology, v. 46, p. 505–520.

——— 1948, Batholith and associated rocks of Corona, Elsinore, and San Luis Rey quadrangles, southern California: Geol. Soc. America Mem. 29, 182 p.

Rankama, Kalervo, 1948, On the geochemistry of niobium: Acad. Sci. Fennicae Annales, ser. A, III. Geol.-geog., no. 13, p. 1–57.

109.   BERYLLIUM CONTENT OF CORDIERITE

By WALLACE R. GRIFFITTS, and ELMO F. COOLEY, Denver, Colo.

The abundance of information about the beryllium contents of many rock-forming minerals contrasts sharply with the lack of data on the beryllium content of cordierite. This is especially odd in view of the structural similarity between cordierite and beryl, and the occurrence of cordierite in contact metamorphic rocks, pegmatites, and veins, all of which are types of deposits that may contain beryllium minerals. We have made beryllium determinations on 16 cordierite specimens, both fresh and altered, from several geologic environments. The beryllium contents of these specimens range from less than one to 2,000 parts per million (table 1).

The well-known abundance of beryllium in some pegmatites needs no discussion. The veins that contain beryllium-rich cordierite are in pegmatite districts, though not necessarily districts of beryl-bearing pegmatites; they may represent deposits from solutions that escaped from the pegmatite magmas. Igneous and sedimentary rocks rich enough in magnesium to yield cordierite-bearing gneisses by isochemical metamorphism are unlikely to contain much beryllium, because beryllium and magnesium tend to be separated by either magmatic or sedimentary processes. Formation of gneiss in which cordierite is rich in beryllium, thus would require an introduction of beryllium before or during metamorphism.

TABLE 1.—*Beryllium content of cordierite.*

[Sample 262664 analyzed by J. C. Hamilton, all others by E. F. Cooley]

Laboratory No.	Beryllium content (parts per million)	Type of occurrence	Locality
	[1] 2,000	Pegmatite......	Colorado.
	[1] 2,000	....do..........	Do.
60-4013.....	2,000	Quartz vein or pegmatite.	Connecticut.
262664......	1,500	Quartz vein.....	South Dakota.
60-4007.....	[1] 1,500	Pegmatite......	Finland.
	1,000	Quartz vein.....	Colorado.
60-4017.....	700	....do..........	Do.
60-4015.....	50	Pegmatite.......	Norway.
60-4003.....	30	Gneiss.........	New Hampshire.
60-4008.....	30	....do..........	Finland.
60-4004.....	20	....do..........	Sweden.
60-4005.....	15	....do..........	Norway.
60-4006.....	10	....do..........	Wyoming.
60-4014.....	10	....do..........	Czechoslovakia.
60-4016.....	1.5	Vein..........	Colorado.
60-4011.....	[1] <1	Hornfels........	Japan.

[1] Cordierite that has been altered to micaceous minerals.

110.   GERMANIUM CONTENT OF ENARGITE AND OTHER COPPER SULFIDE MINERALS

By MICHAEL FLEISCHER, Washington, D. C.

The principal source of germanium has for many years been as a byproduct of zinc smelters, although some has been recovered in England from flue dusts from the burning of coal, and germanium has been produced in recent years as a byproduct of copper ores at Tsumeb, South West Africa, and at Kipushi, Congo. At these mines, much of the germanium is present as germanite, probably $Cu_3(Fe,Ge)S_4$, and the related mineral renierite, perhaps $(Cu,Fe)_3(Fe,Ge)S_4$.

It has long been known (Papish, Brewer, and Holt, 1927; Goldschmidt and Peters, 1933; Noddack and Noddack, 1931) that appreciable amounts of germanium may be present in other copper sulfide minerals, and especially in enargite, but very little work seems to have been done on the possibility of recovering germanium as a byproduct of the smelting of such ores.

The U.S. Geological Survey has been interested in analyzing such ores, especially those rich in enargite. In 1954, Earl M. Irving, then with the U.S. Geological Survey at Manila, obtained from Mr. C. B. Foster, Superintendent, Lepanto Consolidated Mining Co., a suite of ores from the Lepanto mine, where

TABLE 1.—*Spectrographic analyses of ores from Lepanto Consolidated Mines, Philippines*

Sample No. [1]	Ge (ppm)	Sn (ppm)	Ag (percent)	Sb (percent)	Bi (percent)
1........	30	90	0.00X	X.	0.X
2........	0	20	.0X	0	.X
3........	20	200	.0X	X.	.X
4........	100	300	.0X	X.	.X
5........	40	90	.0X	X.	.X
6........	40	200	.0X	X.	.X
7........	60	80	.0X	X.	.X
8........	0	500	.00X	X.	.0X
9........	0	2000	.0X	X.	.0X
10........	0	800	.0X	X.	.0X

[1] (1) Enargite and luzonite, hanging wall, 1030 level; (2) chalcocite with luzonite, hanging wall, 1030 level; (3) luzonite, enargite, and chalcocite, hanging wall, 1030 level; (4) enargite, hanging wall, 1000 level; (5) enargite with luzonite, footwall, 1070 level; (6) luzonite with enargite, footwall, 1070 level; (7) enargite, footwall, 950 level; (8) enargite, footwall branch vein, 1030 level; (9-10) luzonite, footwall branch vein, 1030 level.

the ore consists predominantly of enargite and luzonite (Gonzales, 1956). These were analyzed quantitatively for germanium and tin, and semiquantitatively for other elements by Harry Bastron, and the results are given in table 1.

All samples contained major Cu, and all but No. 2 (0.X percent As) contained major As. Nos. 7 and 9 contained Au; Nos. 3, 7, and 9 contained Pb; No. 7 contained Zn X. percent and Fe X. percent. Gallium was not found in any.

It will be noted that antimony, arsenic, tin, germanium, and silver are present in nearly every sample. The presence of such large amounts of tin had not been noted previously in enargite or luzonite. The germanium contents are lower than in most samples of enargite analyzed (table 2); data are as yet too scattered to permit any generalizations between germanium content and geological conditions of formation of enargite.

Table 2 is a summary of available analyses, including some unpublished determinations, of the germanium content of some sulfides. Those for sphalerite, wurtzite, and chalcopyrite are mainly from Fleischer (1955), plus later data, especially by Burnham (1959), El Shazly and others (1957), and Haranczyk (1957). The distribution of the germanium contents in sphalerite, enargite, and chalcopyrite is shown graphically in figure 110.1.

Other copper sulfides that have been reported to contain germanium include chalcocite (secondary?) up to 300 ppm Ge, colusite (up to 200 ppm), covellite (up to 60 ppm), stannite (up to 50 ppm), tetrahedrite (up to 200 ppm), and chalcostibite (0.5-1 percent). It is possible that germanite or renierite might have been present in some of these samples.

Except for the samples analyzed by Burnham
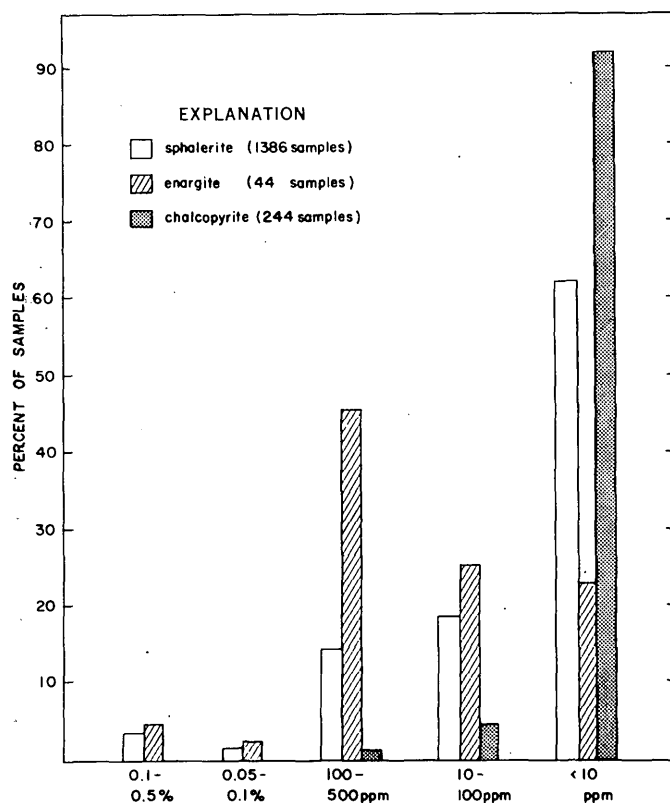
FIGURE 110.1.—Distribution of germanium content of sphalerite, enargite, and chalcopyrite.

(1959), only a few of the analyses summarized in table 2 refer to coexisting minerals, and therefore do not indicate the preferential takeup of germanium by one mineral or another. Burnham's analyses show clearly that germanium is much more concentrated in sphalerite than in chalcopyrite from the same deposit. A few analyses indicate that enargite and luzonite contain more germanium than sphalerite from the same deposit, and analyses by Arsenijevic (1959) show higher contents of germanium in bornite than in enargite from the Bor deposit, Yugoslavia.

It is evident that further study should be made of the distribution of germanium among the minerals of major deposits containing enargite and bornite. Scattered analyses have been published of material from Butte, from Bor, and from Tsumeb, but no data have been published for the remaining major deposits. Studies of the fate of germanium during the smelting of such ores are also needed; analyses by Arsenijevic (1959) showed contents of 150 to 860 ppm germanium in various flue dusts obtained during the smelting of ore from Bor.

I thank Harry Bastron for the spectrographic analyses, Mr. C. B. Foster of the Lepanto Consoli-

TABLE 2.—*Summary of data on germanium content of various sulfides*

Mineral	Maximum (ppm)	Number of samples reported in each concentration range										Total number of samples
		1 percent or more	5000-9999 (ppm)	1000-4999 (ppm)	500-999 (ppm)	200-499 (ppm)	100-199 (ppm)	50-99 (ppm)	10-49 (ppm)	<10 (ppm)	Not found	
Sphalerite	1000	....	....	50	19	97	105	121	132	86	776	1386
Wurtzite	5000	....	1	6	1	2	1	....	2	5	3	21
Chalcopyrite	200	....	....	....	....	1	2	3	7	18	213	244
Enargite	>1000	....	....	2	1	12	8	5	6	2	8	44
Bornite	1000	....	....	1	2	2	1	1	1	....	6	14

dated Mining Co., who furnished the samples, and Mr. V. E. Lednicky, President, Lepanto Consolidated Mining Co., who kindly gave permission to publish the results.

REFERENCES

Arsenijevic, M., 1959, Germanium in the Bor copper mines: Srpskog geol. Drushtva, Zapisnici for 1957, p. 149-151.

Burnham, C. W., 1959, Metallogenetic provinces of the southwestern United States and northern Mexico: New Mexico Bur. Mines and Mineral Resources Bull. 65, p. 1-76.

El Shazly, E. M., Webb, J. S., and Williams, David, 1957, Trace elements in sphalerite, galena, and associated minerals from the British Isles: Inst. Mining and Metallurgy Trans., v. 66, p. 241-271.

Fleischer, Michael, 1955, Minor elements in some sulfide minerals: Econ. Geology, 50th anniversary Volume, p. 970-1024.

Goldschmidt, V. M., and Peters, Cl., 1933, Zur Geochemie des Germaniums: Gesell. Wiss. Gottingen Nachr., Math.-phys. Kl., Heft 2, p. 141-166.

Gonzales, Arsenio, 1956, Geology of the Lepanto copper mine, Mankayan, Mountain Province, *in* Copper Deposits of the Philippines, Part 1, Text: Manila, Philippine Bur. Mines, Spec. Projects Ser., Pub. No. 16, p. 17-50.

Haranczyk, Czeslaw, 1957, Trace elements in ore minerals from Silesian Cracovian zinc lead deposits: Inst. geol. (Poland), Buil. 115, p. 63-126 (Polish with English summary).

Noddack, Ida, and Noddack, Walter, 1931, Die Geochemie des Rheniums: Zeitschr. physikal. Chemie, v. 154 A, p. 207-244.

Papish, Jacob, Brewer, F. M., and Holt, D. A., 1927, Germanium, XXV, Arc spectrographic detection and estimation of germanium. Occurrence of germanium in certain tin minerals. Enargite as a possible source of germanium: Am. Chem. Soc. Jour., v. 49, p. 3028-3033.

111.   CHLORINE AND FLUORINE IN SILICIC VOLCANIC GLASS

By Howard A. Powers, Denver, Colo.

The chlorine and fluorine content of 120 samples of silicic volcanic glass is plotted on figure 111.1[1]. Five of the samples are matrix glass separated from blocks of vitrophyric pumice, and 115 samples are vitric shards from beds of volcanic ash. The chlorine content differs from ash bed to ash bed independently of the fluorine content, and differences in both chlorine and fluorine content have no apparent relation to geologic age. The Galata ash in Montana and Alberta (Horberg and Robie, 1955, p. 949) is postglacial, the Pearlette ash in Kansas (Carey and others, 1952, p. 13) is late Kansan, the Reager and Reamsville ash beds in the central Great Plains (Swineford and others, 1955, p. 254), the Peters Gulch and the Narrows ash layers in Idaho (Powers and Malde, Art. 70), the Wray ash in Colorado, and five beds labeled "X" on figure 111.1 are all of Pliocene age from the Snake River Plain, Idaho. The content of Cl and F is fairly constant in different samples from the same ash bed except in those from the Pearlette; 14 samples from the type Pearlette localities range in Cl from 0.12 to 0.15 percent and in F from 0.13 to 0.17 percent. Even greater ranges are found in samples of the glass from three blocks of pumice collected by R. L. Smith and R. A. Bailey from different parts of the Bandelier tuff from the

---

[1] Chlorine content was determined by a method described by Peck and Tomasi (1959).

FLUORINE, IN PERCENT

0.15

0.10

0.05

0.05   0.10   0.15   0.20   0.25

CHLORINE, IN PERCENT

2. Pearlette

5 Peters Gulch

EXPLANATION

+

Sample known to be from named ash bed

O

Sample similar physically and chemically to named ash bed

▲

Isolated sample known to be different from other known beds

●

Sample of unknown relation

□

Pumice from Bandalier rhyolite tuff (Smith, 1938)

Known individual ash beds

1 Galata	5 Peters Gulch
2 Pearlette	6 Narrows
3 Reager	7 Wray
4 Reamsville	8 Sand Point
9 Recent pumice, Saint Helens	
X Unnamed ash bed of Pliocene age	

FIGURE 111.1.—Chlorine and fluorine content in silicic volcanic glass.

Valles caldera in New Mexico (R. L. Smith and R. A. Bailey, oral communication, 1960); these samples contain Cl 0.20 and F 0.14, Cl 0.09 and F 0.05, and Cl 0.14 and F 0.04 percent, respectively. In contrast, 2 samples of glass from blocks of Recent pumice from St. Helens volcano in the Washington Cascades (D. R. Mullineaux, oral communication, 1961) are very similar in their content, Cl 0.07 and F 0.03 and Cl 0.08 and F 0.03 percent, respectively.

More data are available from U.S. Geological Survey analytical laboratories on fluorine content than on chlorine. The fluorine content of 555 samples (including the 120 mentioned above) of silicic volcanic glass of late Cenozoic age collected from many places in the western United States is summarized as follows:

Percent F:	0.01	.02–.06	.07–.08	.09–.12	.13–.17	.19–.30
No. of samples:	20	295	40	105	80	15

The source area from which many of these samples were erupted is known, and some of the data support the conclusion of R. R. Coats (1956, p. 76) that the abundance of fluorine, and of several other elements present in trace amounts, differs in different igneous provinces. For instance, 75 samples known to be

from the High Cascade volcanoes range from 0.005 to 0.065 percent F; 30 samples of early Pliocene age from a province overlapping the Idaho-Nevada border range from 0.065 to 0.14 percent F; and 7 samples of the younger silicic tuffs in the Thomas Range in west-central Utah (M. H. Staatz, written communication, 1960) range from 0.14 to 0.32 percent F in contrast to 4 samples of the older series of rhyolite-latite rocks that contain from 0.04 to 0.07 percent F. However, the different content of fluorine in the 3 blocks of pumice from the Bandelier rhyolite tuff does not support the generalization.

Friedman and Harris (written communication, 1961) have determined that hydration of volcanic glass does not drive out a measurable part of the fluorine contained in the original glass, but no similar tests have been made in respect to chlorine.

REFERENCES

Carey, J. S., Frye, J. C., Plummer, N., and Swineford, Ada, 1952, Kansas volcanic ash resources: Kansas State Geol. Survey Bull. 96, pt. 1, p. 1–68.
Coats, R. R., 1956, Uranium and certain other trace elements in felsic volcanic rocks of Cenozoic age in western United States, in Contributions to the geology of uranium and thorium by the United States Geological Survey and Atomic Energy Commission for the United Nations International Conference on Peaceful uses of atomic energy, Geneva, Switzerland, 1955: U.S. Geol. Survey Prof. Paper 300, p. 75–78.
Horberg, Leland, and Robie, R. A., 1955, Postglacial volcanic ash in the Rocky Mountain Piedmont, Montana and Alberta: Geol. Soc. America Bull., v. 60, p. 949–956.
Peck, L. C., and Tomasi, E. J., 1959, Determination of chlorine in silicate rocks: Anal. Chemistry, v. 31, p. 2024–2026.
Swineford, Ada, Frye, J. C., and Leonard, A. B., 1955, Petrography of the late Tertiary volcanic ash falls in the central Great Plains: Jour. Sed. Petrology, v. 25, p. 243–261.

112.   ELECTRONPROBE ANALYSIS OF SCHREIBERSITE (RHABDITE) IN THE CANYON DIABLO METEORITE

By I. ADLER and E. J. DWORNIK, Washington, D. C.

Work done in cooperation with the National Aeronautics and Space Agency

The problem of the mode of formation of metallic meteorites requires thorough and detailed knowledge of their composition. The many existing analyses made by conventional methods are essentially analyses of composites; many problems, however, such as the distribution of nickel and cobalt between two different phases in contact, require analyses of specific localized areas definable only under high magnification. For example, analyses exist of kamacite (alpha-Ni-Fe), taenite (gamma-Ni-Fe), schreibersite (Fe,Ni)$_3$P and cohenite (Fe,Ni)$_3$C from meteorites, but nearly all of them represent composite samples. It is of great interest to analyze individual grains to determine the constancy or variation in composition of each phase, and the constancy or variation of ratios of elements (such as Ni:Fe) in two adjacent phases. Such studies could yield valuable information on whether equilibrium conditions prevailed.

The electronprobe is ideally suited to this type of analysis as it can be used to provide point by point analysis of microscopic volumes of the order of several cubic microns which in the ideal case correspond to absolute amounts of 10^{-11} to 10^{-12} grams of an element.

The electronprobe microanalyzer was developed in France by Castaing (1951, Application of electron probes to local chemical and crystallographic analysis, Paris Univ. Thesis). This device has been described in a number of reports dealing in the main with metallurgical applications.

A particularly appealing feature is the nondestructive nature of the technique which enables the researcher to reexamine the specimen in the light of the compositional data obtained. The tedious preparation of any constituent phase for analysis by conventional methods can be circumvented.
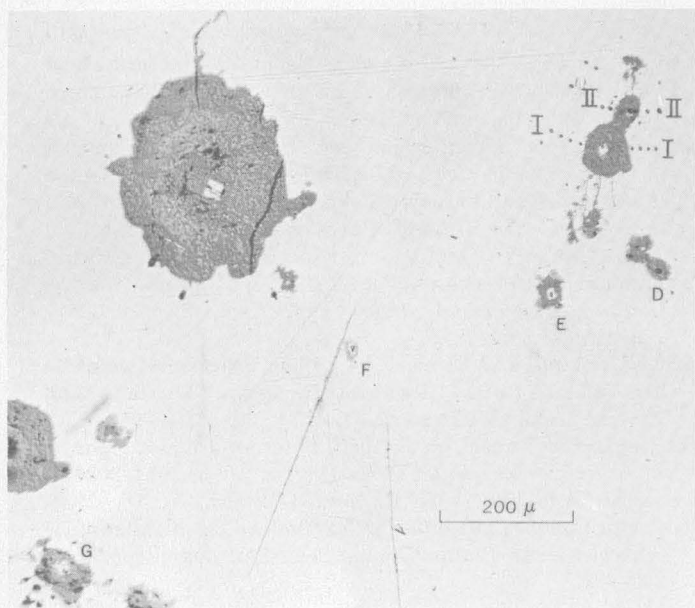
FIGURE 112.1.—Photomicrograph of polished specimen of Canyon Diablo meteorite. Rhabdite grains, E, D, F, and G.

Briefly, in principle, a focused beam of electrons is made to impinge on a selected area of the specimen. The X-rays which are excited are diffracted by analyzers, which are various single crystals with characteristic interplanar spacings to cover the range of elements of atomic number 12 and greater. The intensity of the X-radiation is measured by radiation detectors such as Geiger or proportional counters and scalers. The intensities measured are compared with those given by standards, and corrections are made for fluorescence and absorption in order to relate the intensities to concentration. A probe similar in principle to the Castaing probe, but somewhat modified in design, is now in operation in the U.S. Geological Survey laboratories.

Maringer, Richard, and Austin (1959) have studied the Widmanstätten structure in the Grant meteorite from New Mexico with an electronprobe and reported on the nickel-iron content of kamacite, taenite, and plessite—a fine-grained mixture of both phases. David B. Wittry (written communication, 1959), using the electronprobe, reported on the nickel-iron content of kamacite and taenite in the Canyon Diablo meteorite. He also described an individual crystal within a taenite band and tentatively identified it as $Ni_3Fe_2P_2$. Presumably, this is similar to the rhabdite rhombs of this study.

A one-quarter by one-eighth inch fragment was carefully removed from the edge of the Canyon Diablo meteorite specimen 841, generously provided
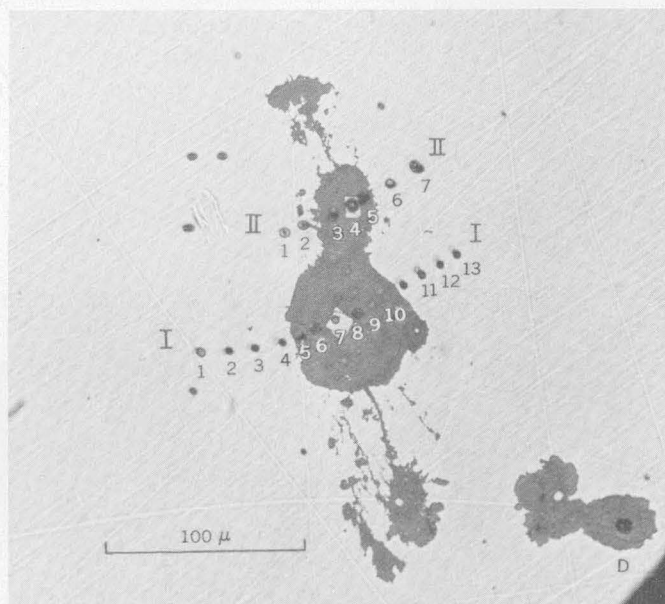
FIGURE 112.2.—View enlarged from figure 112.1 to show point-by-point traverses I and II.

TABLE 1.—Analytical results for traverses I and II

[In percent; precision of measurements approximately 5 percent of the amount present]

		Traverse I					Traverse II		
	Spot	Ni	Fe	Ni+Fe		Spot	Ni	Fe	Ni+Fe
Kamacite......	1	7.8	88	96	Kamacite......	1	6.5	89	96
	2	7.9	88	96		2	6.6	90	97
	3	7.9	91	99					
	4	7.4	86	93					
Gray phase....	5	1.4	48	49	Gray phase....	3	3.1	46	49
	6	2.0	46	48					
Rhabdite......	7	38	40	78	Rhabdite......	4	42	43	85
Gray phase....	8	2.5	41	44	Gray phase....	5	3.9	40	44
	9	1.4	46	47					
	10	2.4	47	49					
Kamacite......	11	7.4	90	97	Kamacite......	6	7.2	90	97
	12	7.6	89	97		7	7.2	89	96
	13	7.2	89	96					

TABLE 2.—*New analyses of rhabdites, Canyon Diablo meteorite*

[In percent; precision of measurements approximately ± 5 percent of the amount present]

Grain	Size (microns)	Ni	Fe	Ni+Fe	Ni:Fe (ratios)
A	10	22	63	85	.34
B	31	41	46	87	.89
C	21	37	42	79	.88
D	5	48	36	84	1.33
E	20	45	39	84	1.15
F	18	44	39	83	1.12
G	35	44	38	82	1.15

by E. P. Henderson of the U.S. National Museum, and the fragment was prepared for examination in the conventional bakelite polished-section mount.

Fragments of pure iron, pure nickel, and stainless steel (National Bureau of Standards standard sample no. 101d) were also mounted for use as reference standards. Figure 112.1 illustrates the general area studied. The various phases present, as described in metallographic studies of meteoritic irons by Perry (1944), include a kamacite matrix, irregularly shaped gray bodies (probably iron oxides with some carbon in the form of graphite), and schreibersite, an iron-nickel phosphide, $(Fe,Ni)_3P$, as rhombs or squares and referred to as rhabdites.

The gourd-shaped gray mass in the upper right of figure 112.1 is the site of two separate point by point traverses for which analytical data are given in table 1. The small regularly spaced spots on a line through the area are contamination spots formed by the electron beam. The spots are normally of the order of 1 to 3 microns but appear somewhat enlarged because of prolonged exposure to the beam. In figure 112.2 these spots are numbered so that the analyses can be related to the particular area. Also shown in figure 112.1 are 4 of the 7 additional rhabdites for which Ni-Fe contents were determined (table 2). Appreciable amounts of phosphorus in these rhabdite grains were demonstrated by spectrometer traces but the element was not determined quantitatively. The theoretical content of phosphorous for $(Fe,Ni)_3P$ with Fe:Ni = 1:1 is 15.27 percent.

The magnetism of the meteorite made it necessary to recenter the beam with respect to the optical microscope in moving from point to point and accounts for the unnumbered beam spots appearing in the micrographs. The rhabdite grain D (figs. 112.1 and 112.2), approximately 5 microns across and the smallest of the 9 crystals analyzed, has been concealed by the contamination spot.

No clear-cut chemical relationship between the rhabdites and the surrounding gray areas could be established. The total Ni + Fe in rhabdite grain F, exhibiting virtually no oxide halo, corresponds closely to the total in other rhabdites. Grains A and D, which show the maximum variation in Ni and Fe content, both show good agreement with the formula $(Ni,Fe)_3P$ used by Perry (1944) for schreibersite. Henderson and Monnig (1956), analyzed rhabdite needles removed from the Richland, Tex., and Coahuila, Mex., meteorites by dissolving the kamacite matrix in dilute hydrochloric acid. They report 33.17 and 31.71 percent Ni, respectively. The average nickel content of the 9 rhabdites analyzed in this study is 40.1 percent.

The present study clearly demonstrates the variation in content of iron and nickel in rhabdites in one single meteorite specimen. The nickel in these rhabdites ranges from 22 percent in grain A to 48 percent in grain D; the Ni:Fe ratios range from 0.34 to 1.33. The sum of the weight percents of nickel and iron range from 79 to 87 percent. Two analyses of schreibersite from the Canyon Diablo meteorite are given by Palache, Berman, and Frondel (1944, p. 125) as follows: Fe 58.54, Ni 26.08, and Ni:Fe 0.44 percent; and Fe 54.34, Ni 31.48, and Ni:Fe 0.57 percent.

Eleven analyses of the kamacite phase adjacent to the gourd-shaped area show average contents of 7.3 percent nickel and 89 percent iron; the range in composition is strikingly less than in the rhabdites, namely, Ni 6.5 to 7.9 and Fe 86 to 91 percent. The gray phase has the lowest nickel content, 1.4 to 3.1 percent; its iron content is 46 to 48 percent.

REFERENCES

Henderson, E. P., and Monnig, O. E., 1956, The Richland, Navarro County, Texas, meteorite (CN=0964,319)—A new hexahedrite: Meteoritics, v. 1, no. 4, p. 459–467.

Maringer, R. E., Richard, N. A., and Austin, A. E., 1959, Microbeam analysis of Widmanstätten structure in meteoritic iron: Am. Inst. Mining Metall. Engineers, Metall. Soc. Trans., v. 215, p. 56–68.

Palache, Charles, Berman, Harry, and Frondel, Clifford, 1944, The system of mineralogy of James Dwight Dana and Edward Salisbury Dana, Volume 1, Elements, sulfides, sulfosalts, oxides. 7th ed.: New York, John Wiley and Sons, 834 p.

Perry, S. H., 1944, The metallography of meteoric iron: U.S. Natl. Mus. Bull. 184, 206 p.

113.   THE SYNTHESIS OF LARGE CRYSTALS OF ANDERSONITE

By ROBERT MEYROWITZ and DAPHNE R. ROSS, Washington, D. C.

Andersonite, $Na_2CaUO_2(CO_3)_3 \cdot 6H_2O$, was first synthesized by Axelrod and others (1951) from a solution containing uranyl nitrate, potassium carbonate, sodium nitrate, and calcium nitrate. Microscopic crystals were formed by allowing the solution to evaporate at room temperature. The procedure described below was developed to prepare large crystals (0.5 to 1 mm and occasionally some slightly larger) of synthetic andersonite.

An aqueous solution (10 ml) containing 7.53 g $UO_2(NO_3)_2 \cdot 6H_2O$ (0.015 mol UO_3) is added slowly with constant stirring (magnetic stirrer) to an aqueous solution (100 ml) containing 4.77 g anhydrous Na_2CO_3 (0.045 mol CO_2). An aqueous solution (10 ml) containing 3.54 g $Ca(NO_3)_2 \cdot 4H_2O$ (0.015 mol CaO) is added slowly with constant stirring to the uranyl carbonate solution. Dilute sodium carbonate is added dropwise with constant stirring until the pH of the solution is 8.0. The solution is allowed to stand after sealing the beaker with plastic film so that no evaporation takes place. The crystals which form on standing are detached from the sides and bottom of the beaker and washed by decantation with water. Most of the excess water is removed by rolling the crystals on absorbent paper. The crystals are then allowed to air dry. They were identified as andersonite by their powder X-ray diffraction patterns (Axelrod and others, 1951).

The help of Alan L. Meyrowitz is acknowledged.

REFERENCE

Axelrod, J. M., Grimaldi, F. S., Milton, C., and Murata, K. J., 1951, The uranium minerals from the Hillside Mine, Yavapai County, Arizona: Am. Mineralogist, v. 36, p. 1–22.

114.   UNIT-CELL DIMENSION VERSUS COMPOSITION IN THE SYSTEMS:
PbS-CdS, PbS-PSe, ZnS-ZnSe, and $CuFeS_{1.90}$-$CuFeSe_{1.90}$

By PHILIP M. BETHKE and PAUL B. BARTON, JR., Washington, D. C.

As part of an extensive experimental investigation of the distribution of minor elements between coexisting sulfide minerals (Bethke and Barton, 1959), the relationship between unit-cell edge and composition was established with high precision for PbS-PbSe and ZnS-ZnSe solid solutions and cadmium-bearing galenas. The relationship between a and composition for $CuFeS_{1.90}$–$CuFeS_{1.90}$ solid solution was also established, but with less precision.

Shirley K. Mosburg made and measured a number of the X-ray diffraction runs. Jean Bethke measured and computed all the PbS–PbSe diffraction patterns.

SAMPLE PREPARATION

Pure PbS, PbSe, ZnS, ZnSe, and CdS were prepared from high-purity elements. The metals were heated for several days at about 750°C in evacuated silica glass tubes with a slight excess of sulfur (or selenium) over the stoichiometric proportions. Excess sulfur or selenium was removed by repeated washing with warm carbon disulfide in a soxhlet extractor.

Solid solutions of various compositions were prepared by sintering mechanical mixtures of the above end members in evacuated silica glass tubes until a single homogeneous phase was formed. $CuFeS_{1.90}$–$CuFeSe_{1.90}$ solid solutions were prepared directly from mixtures of the elements.

The iron, zinc, and sulfur are the same reagents used by Skinner, Barton, and Kullerud (1959). The sources and analyses of the selenium, cadmium and lead used in this study are given in table 1.

Reagents were weighed to ± 0.05 mg and the total weight of the charges ranged between 100 and 500 mg.

X-RAY DIFFRACTION TECHNIQUES

All X-ray diffraction data were gathered on a Norelco diffractometer using copper radiation ($\lambda = 1.54050A$). The ZnS–ZnSe and PbS–CdS systems were analyzed at our laboratory in Washington using the counting rate computer. The bulk of the PbS–PbSe data were gathered at the Missouri School of Mines and Metallurgy at Rolla, Mo., using an oscillating technique. The chalcopyrite data were gathered in Washington, also by the oscillating technique. In all cases the peaks of the samples were measured against those of various internal standards that had been mutually calibrated against silicon powder supplied by Dr. Gunnar Kullerud of the Geophysical Laboratory, Carnegie Institution of Washington. The cell edge of $a = 5.4301A$ for silicon, given by Swanson and Fuyat (1953), was used. Precision of measurement by either method was ± 0.005° 2θ, and various checks indicate that data gathered by either method, in Washington or Rolla, are mutually comparable, within the limit of precision of measurement.

Diffraction slides were prepared by evaporating a slurry of the sample and internal standard in amyl acetate onto a microscope slide. Oscillation tracings were made at a scanning rate of ¼° 2θ per minute with a chart speed of half an inch per minute. The step scan interval was 0.01° 2θ. Two sets of measure-ments were made for each sample, the slide being rotated 180° in its own plane between each set. At least three complete oscillations were made in each set when using the oscillation technique. Measurements were made at 25 ± 2°C. The values of the cell edges given are numerical averages of all measurements on a given sample. The plus or minus attached to the cell edges is the standard deviation computed from the deviations from the average values for all the samples in a given system, regardless of composition.

Because galena deforms on grinding, giving rise to diffuse X-ray reflections, the galena crystals were reduced in size by giving them several sharp "raps" with a pestle. The sample was then sized and only those fragments smaller than 200 mesh used to prepare the slide. The galena reflections were very sharp, even at high angles, using this procedure.

CELL EDGES OF PbS, ZnS, PbSe, AND ZnSe

The cell edges of pure PbS, PbSe, ZnS, and ZnSe were determined from a large number of individual measurements, all from oscillation tracings. These values, together with the peaks measured, internal standards used, and number of measurements made are given in table 2. The plus-minus attached to each value is the standard deviation computed from all the measurements.

The value of a for ZnS determined in this study is in exact agreement with that reported by Skinner and Barton (1960) and Skinner, Barton, and Kullerud (1959). Our value of 5.9358 ± 0.0002 A for PbS is in excellent agreement with that of Wasserstein (1951) (5.9360 ± 0.0004 A[1]) and of Swanson and Fuyat (1953) (5.9362). Our value of 6.1255 ± 0.0004 A for the cell edge of PbSe is in only fair agreement with that of 6.1243 A reported by Swanson and others (1955), but is much more consistent with our data on PbS–PbSe solid solutions. Our value of 5.6685 ± 0.0004 A for ZnSe is in good agreement with the less precise value of 5.667 A

TABLE 1.—*Spectrographic analyses of reagents (in weight percent)*

[N.D., looked for but not detected; . . . not specifically looked for; V.F. Tr., very faint trace.]

Element	Lead [1]	Cadmium [2]	Selenium [2]
Ag	0.001	0.0001	N.D.
Al	N.D.	. . . .	N.D.
As	N.D.	N.D.	0.0001
Bi	0.0003	0.001	N.D.
Ca	N.D.	N.D.	N.D.
Cd	N.D.	([3])	N.D.
Cr	N.D.	N.D.	N.D.
Cu	0.003	0.001	V.F. Tr.
Fe	0.001	0.001	N.D.
Hg	N.D.	N.D.	N.D.
In	N.D.	0.001	N.D.
Mg	0.00003	0.00001	N.D.
Mn	N.D.	N.D.	N.D.
Na	N.D.	. . . .	N.D.
Ni	0.001	N.D.	N.D.
Pb	([3])	0.003	N.D.
Sb	N.D.	N.D.	N.D.
Si	N.D.	N.D.	N.D.
Se	. . . .	. . . .	([3])
Sn	N.D.	0.0001	N.D.
Te	N.D.	N.D.	0.0001
V	0.0001	. . . .	. . . .
Zn	N.D.	N.D.	N.D.

[1] National Bureau of Standards melting point standard 49d. Semi-quantitative spectrograph analysis by K. V. Hazel, U.S. Geological Survey.
[2] Spectrographic analysis by supplier: American Smelting and Refining Co.
[3] Major constituent.

TABLE 2.—*Cell edges of PbS, PbSe, ZnS, and ZnSe*

Compound	Average a in A	Standards used	Reflections measured	Number of measurements
PbS	5.9358 ±0.0002	CaF$_2$	(600)(620)(533)(444)	141
PbSe	6.1255 ±0.0004	CaF$_2$ and PbS	(620)(640)(711)	128
ZnS	5.4093 ±0.0002	CaF$_2$	(620)	30
ZnSe	5.6685 ±0.0004	CaF$_2$	(620)	33

[1] Converted from kX units by the kX/A conversion factor of 1.00202.
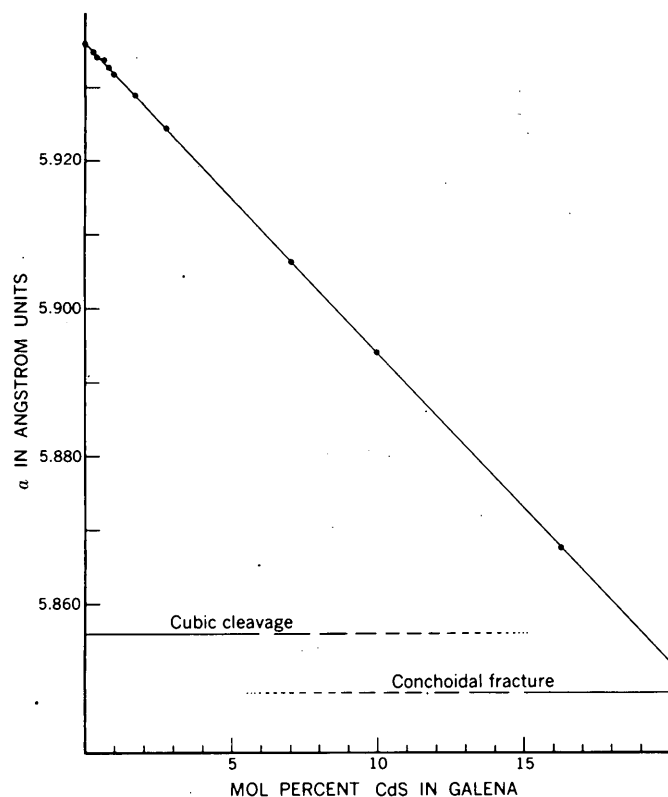
FIGURE 114.1.—*a* versus composition for cadmium-bearing galenas. Size of circle equals 2 times standard deviation of individual *a* determinations.

reported by Swanson and others (1954). Again our value is entirely consistent with our data on ZnS–ZnSe solid solutions.

PbS-CdS SOLID SOLUTIONS

A series of solid solutions in the system PbS–CdS was prepared from the pure end members by holding carefully weighed mixtures of the end members at 860°C for a period of two weeks. The limit of solid solution at this temperature is approximately 17.5 mol percent CdS. The cell edges determined for these compositions are given in table 3. The relationship

TABLE 3.—*Cell edges of cadmium-bearing galenas*

Mol percent CdS	α measured ± 0.0002A	α calculated	Difference
0	5.9358	5.9359	−0.0001
.28	5.9347	5.9347	.0000
.40	5.9340	5.9342	− .0002
.64	5.9336	5.9332	+ .0004
.80	5.9327	5.9325	+ .0002
.98	5.9317	5.9318	− .0001
1.67	5.9289	5.9289	.0000
2.77	5.9244	5.9243	+ .0001
7.06	5.9063	5.9063	.0000
9.98	5.8942	5.8941	+ .0001
16.27	5.8676	5.9677	− .0001

TABLE 4.—*Cell edges of ZnS-ZnSe solid solutions*

Mol percent ZnSe	α measured ±0.0004A	Linear cell edge assumption		Linear cell volume assumption	
		α calculated	Difference	α calculated	Difference
0	5.4093	....	....	....	....
7.72	5.4290	5.4293	−0.0003	5.4302	−0.0012
14.30	5.4458	5.4464	− .0006	5.4479	− .0021
30.04	5.4865	5.4872	− .0007	5.4898	− .0033
33.35	5.4939	5.4957	− .0018	5.4985	− .0046
49.84	5.5375	5.5385	− .0010	5.5415	− .0040·
69.22	5.5870	5.5887	− .0017	5.5415	− .0044
77.11	5.6096	5.6092	+ .0004	5.6113	− .0017
100.00	5.6685	....	....	....	....

of cell edge to composition is illustrated in figure 114.1.

The best fitting straight line determined by least squares analysis of the solid solution data intersects the *a* axis at a value of $a = 5.9359$ A, almost exactly that determined for pure PbS. The equation of this line is

$$a = 5.9359 - 0.004194 \text{ mol percent CdS}$$

where *a* is in A units. The standard deviation of the measured values of *a* of PbS–CdS solid solutions from those calculated through the above relationship is less than ± 0.0002 A. The extrapolated value of *a* for a hypothetical pure CdS having the galena structure is 5.516 A.

An interesting feature of the PbS–CdS solid solutions is the relationship between cleavage and (or) fracture and composition. Low cadmium-bearing galenas retain a cubic cleavage and break along this cleavage almost exclusively. At compositions above about 6 mol percent CdS, however, a conchoidal fracture appears in addition to the cubic cleavage. With increasing CdS content the number of cleavage surfaces seen in a crushed sample decreases, until for CdS concentrations over 15 mol percent only the conchoidal fracture is seen. These comments are

TABLE 5.—*Cell edges of PbS-PbSe solid solutions*

Mol percent PbSe	α measured ±0.0004A	Linear cell edge assumption		Linear cell volume assumption	
		α calculated	Difference	α calculated	Difference
0	5.9358	....	−0.0002	....	−0.0007
10.06	5.9547	5.9549	−0.0002	5.9554	−0.0007
20.70	5.9758	5.9751	+ .0007	5.9761	− .0003
30.15	5.9941	5.9930	+ .0011	5.9943	− .0002
39.83	6.0126	6.0114	+ .0012	6.0128	− .0002
60.10	6.0507	6.0498	+ .0009	6.0512	− .0005
79.08	6.0871	6.0858	+ .0013	6.0868	+ .0003
90.72	6.1079	6.1079	.0000	6.1084	− .0005
100.00	6.1255	....	....	....	....

based on observation of the spacing curve runs as well as others prepared for other purposes.

ZnS-ZnSe AND PbS-PbSe SOLID SOLUTIONS

Complete series of ZnS–ZnSe and PbS–PbSe solid solutions were prepared from mixtures of the end members at 900°C and 750°C, respectively. The ZnS–ZnSe runs equilibrated in one month, the PbS–PbSe in two weeks. The cell edge data for these series are given in tables 4 and 5.

The ZnS–ZnSe data fall slightly below a straight line drawn between the values of a for the pure end members. Least squares analysis of the solid solution data yields a linear relation between cell edge and composition essentially parallel to the line drawn between the pure end members. This least squares line extrapolates to values of $a_{ZnS} = 5.4086$ A and $a_{ZnSe} = 5.6679$ A. Because of the larger number of measurements used in calculating the cell edges of the end members and because of the minimum compositional uncertainty, a linear relationship between cell edge and composition passing through the a values of pure ZnS and ZnSe is preferred. The equation of such a line is—

$$a = 5.4093 + 0.002592 \text{ mol percent ZnSe}$$

where a is in Angstrom units. The small deviation of the solid solution data from this relationship is not considered significant.

In contrast, the cell edges of PbS–PbSe solid solutions are not linear functions of composition. Rather, they indicate a linear relationship between *cell volume* and composition. The differences between measured values of a and those calculated as-
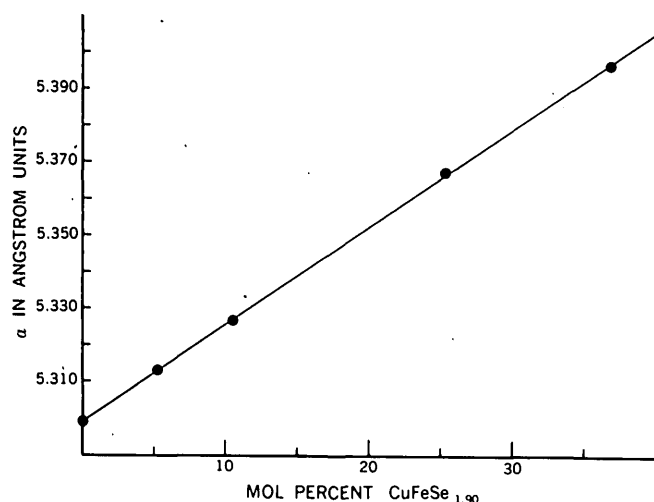
FIGURE 114.2.—a versus composition for CuFeS$_{1.90}$–CuFeSe$_{1.90}$ solid solutions. Size of circle equals standard deviation of individual a determinations.

TABLE 6.—a of $CuFeS_{1.90}$-$CuFeSe_{1.90}$ solid solutions

Mol percent CuMeSe$_{1.90}$	$a + 0.0015A$	Calculated	Difference
0	5.298$_7$	5.2988	−0.0001
5.26	5.313$_0$	5.3128	+.0002
10.53	5.326$_5$	5.3269	−.0004
25.32	5.367$_2$	5.3664	+.0008
36.84	5.396$_6$	5.3971	−.0005

suming both linear cell edge and linear cell volume relationships are given in tables 4 and 5 for both ZnS–ZnSe and PbS–PbSe data. It is immediately obvious from these differences that a linear volume assumption much better describes our data for PbS–PbSe solid solutions, whereas a linear cell edge assumption much better describes our data for ZnS–ZnSe solid solutions. The relationship adopted between cell edge and composition for the PbS–PbSe solid solution is—

$$a = 3\sqrt{209.140 + 0.20699 \text{ mol percent PbSe}},$$

where a is the cell edge in Angstrom units.

Earley (1950) found an apparently linear relationship between cell edge and composition for the PbS–PbSe series. Earley's study was of broad scale and neither his cell edge measurements nor compositional control were of sufficient precision to differentiate between a linear cell volume or linear cell edge relationship with composition.

Coleman (1959) has determined the cell edges of 20 analyzed galena-clausthalite solid solutions, mostly from the Colorado Plateau. His objective was to establish the existence of such a series in nature, and his data seem to confirm such a conclusion. However, the wide scatter of his data allow only the most general conclusions as to the way in which cell dimension varies with composition.

Bloss (1952) and Zen (1956) have emphasized that for ideal solid solutions partial molar volumes are additive. Thus, a linear relationship between cell volume and composition would be predicted, were the solid solutions ideal. Our work on the distribution of selenium between sphalerite and galena (Bethke and Barton, 1959) strongly indicates that at least above 740°C both ZnS–ZnSe and PbS–PbSe solid solutions behave ideally. The cell edge measurements reported in this study were made at approximately 25°C, however, and it is possible that the PbS–PbSe solid solutions are ideal, or nearly so, at this temperature, whereas ZnS–ZnSe solid solutions are not.

A great deal of precision of measurement was necessary to establish the additivity of cell volumes for PbS–PbSe solid solutions as opposed to the additivity of cell edges (Vegard's Law) for ZnS–ZnSe compounds, even though the difference in molar volumes of the end members is very large. Most measurements made on solid solutions are not this precise and few complete solid solution series exhibit such a large volume difference. Further, most naturally occurring solid solutions contain other elements as structural impurities in sufficient concentrations to mask the detailed relations between cell edge and concentrations of the major components. Finally, almost all precise lattice parameter measurements are made at room temperature where it is quite likely that solid solutions, although possibly ideal under the conditions of their formation, may show a measurable departure from ideality. For most systems the difference between Vegard's Law (additive cell edge) and ideal behavior (additive cell volume) is too small to be detectable by standard procedures.

CuFeS$_{1.00}$ — CuFeSe$_{1.90}$ SOLID SOLUTIONS

Solid solutions up to 36.8 mol percent CuFeSe$_{1.90}$ were prepared in 2 weeks at 600°C starting directly from the elements. Runs with higher selenium content produced spurious phases. The poor quality of the X-ray diffraction patterns of chalcopyrite at high angles, particularly with copper radiation, necessitated the use of low-angle lines in establishing the relationship between cell edge and composition for selenium-bearing chalcopyrites. Correspondingly, the precision of measurement was much lower, in terms of cell edge, than for the above-described systems. Although the chalcopyrites measured were tetragonal, only the a dimension, as computed from the (220) reflection is reported here. It should be noted that the chalcopyrite solid solutions were specifically prepared to be anion deficient and with a 1:1 Cu:Fe ratio in order that they would be within their compositional stability ranges under the conditions of the distribution experiments. The results of our study are, therefore, not directly comparable to those obtained on chalcopyrites of different cation: anion or Cu:Fe ratios.

The cell edge and compositional data are listed in table 6 and illustrated in figure 114.2. Within the limits of precision, the a dimension of chalcopyrite is seen to be a linear function of selenium content. The data are not sufficiently precise to define the details of the relationship, but it is approximately given by the expression—

$$a = 5.298_8 + 0.00266_8 \text{ mol percent CuFeSe}_{1.90}$$

where a is in Angstrom units.

REFERENCES

Bethke, P. M., and Barton, P. B., Jr., 1959, Trace-element distribution as an indicator of pressure and temperature of ore deposition [abs.]: Geol. Soc. America Bull., v. 70, no. 12, pt. 2, p. 1569.

Bloss, F. D., 1952, Relationships between density and composition in mol percent for some solid solution series: Am. Mineralogist, v. 37, p. 966–981.

Coleman, R. G., 1959, The natural occurrence of galena-clausthalite solid solution series: Am. Mineralogist, v. 44, p. 166–175.

Earley, J. W., 1950, Description and synthesis of the selenide minerals: Am. Mineralogist, v. 35, p. 337–364.

Skinner, B. J., and Barton, P. B., Jr., 1960, The substitution of oxygen for sulfur in wurtzite and sphalerite: Am. Mineralogist, v. 45, p. 612–625.

Skinner, B. J., Barton, P. B., Jr., and Kullerud, Gunnar, 1959, Effect of FeS on the unit-cell edge of sphalerite. A revision: Econ. Geology, v. 54, p. 1040–1046.

Swanson, H. E., and Fuyat, R. K., 1953, Standard X-ray diffraction powder patterns: U.S. Natl. Bur. Standards Circ. 539, v. 2, p. 6–9, 18–19.

Swanson, H. E., Fuyat, R. K., and Ugrinic, G. M., 1954, Standard X-ray diffraction powder patterns: U.S. Natl. Bur. Standards Circ. 539, v. 3, p. 23.

Swanson, H. E., Gilfrich, N. T., and Ugrinic, G. M., 1955, Standard X-ray diffraction powder patterns: U.S. Natl. Bur. Standards Circ. 539, v. 5, p. 38–39.

Wasserstein, B., 1951, Precision lattice measurements of galena: Am. Mineralogist, v. 36, p. 102–115.

Zen, E-an, 1956, Validity of "Vegard's Law": Am. Mineralogist v. 41, p. 523–524.

115.   UNIT-CELL EDGES OF COBALT- AND COBALT-IRON-BEARING SPHALERITES

By Wayne E. Hall, Washington, D. C.

Pure ZnS, "CoS", and FeS were prepared by combining high-purity elements in sealed, evacuated silica glass tubes. The iron, zinc, and sulfur are the same reagents used by Skinner, Barton, and Kullerud (1959). The cobalt reagent was obtained from Johnson, Matthey and Co., Ltd., catalogue no. J. M. 870, who supplied the following spectrographic analysis:

	Percent			Percent
Ag	<0.0001		Mg	<0.0001
Al	....		Mn	....
As	....		Mo	....
Ba	....		Na	.0001
Bi	....		Ni	....
Ca	.0002		Pb	....
Co	Major		Sb	....
Cr	....		Si	.0002
Cu	< .0001		Sn	....
Fe	.0005		V	....
Ge	....		Zn	....

ZnS was prepared by heating zinc with sulfur in slight excess of stoichiometric proportions for 10 days at 650°C. Excess sulfur was removed by washing with carbon disulfide. FeS and "CoS" were prepared by combining stoichiometric mixtures at 650°C for at least 7 days. Stoichiometric CoS was not formed, but the resulting intergrowth of $Co_{1-x}S$ and probably Co_9S_8 was so fine and uniform that it had the bulk composition CoS in the quantities used for individual runs. Definite identification of the two phases has not been completed, and the intergrowth will be referred to hereafter as "CoS".

All X-ray data were obtained using Ni-filtered $CuK_{\alpha 1}$ radiation ($\lambda = 1.54050A$). An oscillation technique was used, and all peaks were repeated at least 4 times at a scanning speed of $\frac{1}{4}°$ 2θ per minute and a chart speed of half an inch per minute. The peaks were measured against those of the same CaF_2 or NaCl internal standards used by Bethke and Barton (Art. 114). Several checks were made by using a counting-rate computer at a step-scanning rate of 0.01° 2θ, and the unit-cell edge measurements by both techniques are comparable. Shirley K. Mosburg made most of the X-ray diffraction patterns and calculated the unit-cell edges.

The unit-cell edge of ZnS determined as 5.4093A in this investigation is the same as that determined by Skinner and others (1959, p. 1043), Skinner and Barton (1960), and Bethke and Barton (Art. 114).

COBALT-BEARING SPHALERITE

A series of cobalt-bearing sphalerites was prepared from "CoS" and pure ZnS by holding known proportions of the two at 850°C for 21 days. At the end of one week the silica glass tubes were opened and the samples reground in acetone. The charge was then reheated at 850°C until homogeneous.

The cell edges of the cobalt-bearing sphalerites are listed in table 1, and the relation of cell edge to composition is shown in figure 115.1. The relation is linear, and the best fitting straight line by least squares analysis intersects the a axis for pure ZnS at 5.4093A. The equation for the line is:

$$a = 5.4093 - 0.00700Y \text{ where } Y \text{ is the mol percent "CoS".}$$

The maximum amount of CoS that can substitute in ZnS is 33 mol percent at 850°C. The precision given for each unit-cell edge measurement is the maximum deviation from the numerical average of 4 to 6 repeated measurements. A comparison of the measured and calculated unit-cell edges based on a linear relationship between a and composition is also given in table 1. The standard deviation of the measured values of a and those calculated by the above formula is 0.0003A.

COBALT-IRON-BEARING SPHALERITES

A series of cobalt-iron-bearing sphalerites were prepared from known proportions of pure ZnS, FeS, and "CoS", and were heated at 850°C for 4 weeks.
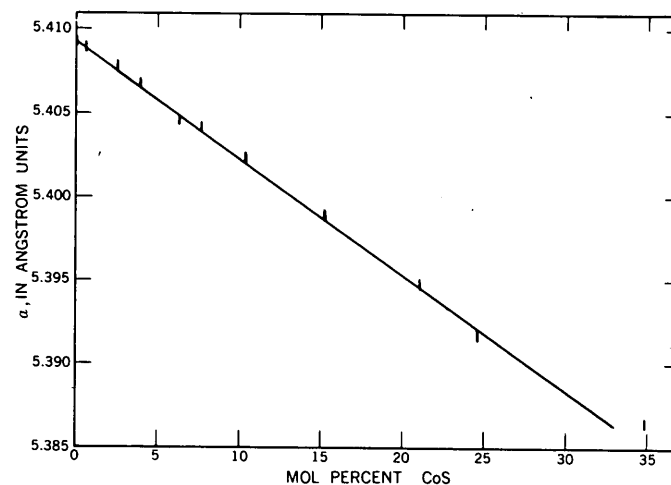
FIGURE 115.1.—Relation of a and composition in cobalt-bearing sphalerites.

TABLE 1.—*Unit cell edges of cobalt-bearing sphalerite*

CoS content		Unit-cell edge in A (measured)	Unit-cell edge in A (calculated)	Difference
Weight percent	Mol percent			
0.57....	0.60	5.4090 ±0.0003	5.4089	−0.0001
2.21....	2.36	5.4078 ± .0002	5.4076	− .0002
3.70....	3.95	5.4068 ± .0003	5.4065	− .0003
5.90....	6.28	5.4045 ± .0003	5.4049	+ .0004
7.23....	7.70	5.4042 ± .0004	5.4039	− .0003
9.75....	10.36	5.4025 ± .0005	5.4020	− .0005
14.34....	15.19	5.3990 ± .0002	5.3987	− .0003
19.94....	21.05	5.3948 ± .0002	5.3946	− .0002
23.32....	24.56	5.3918 ± .0003	5.3921	+ .0003

The charges were reground in acetone after 2 weeks. The measured unit-cell edges are listed in table 2. These are compared with a calculated unit-cell edge based on a linear relation between a of cobalt-bearing sphalerite and a of iron-bearing sphalerite. The effect of FeS on the unit-cell edge of sphalerite was investigated by Kullerud (1953) and by Skinner and others (1959). The latter derived the linear function:

$$a = 5.4093 + 0.000456X \text{ (where } X \text{ is the mol percent FeS and } a \text{ is in Angstrom units).}$$

This equation was combined with the one determined in this investigation for cobalt-bearing sphalerite to give the a for cobalt-iron-bearing sphalerites as follows:

$$a = 5.4093 + 0.000456X - 0.000700Y$$

The relation between a and composition of cobalt-iron-bearing sphalerite is shown in figure 115.2.
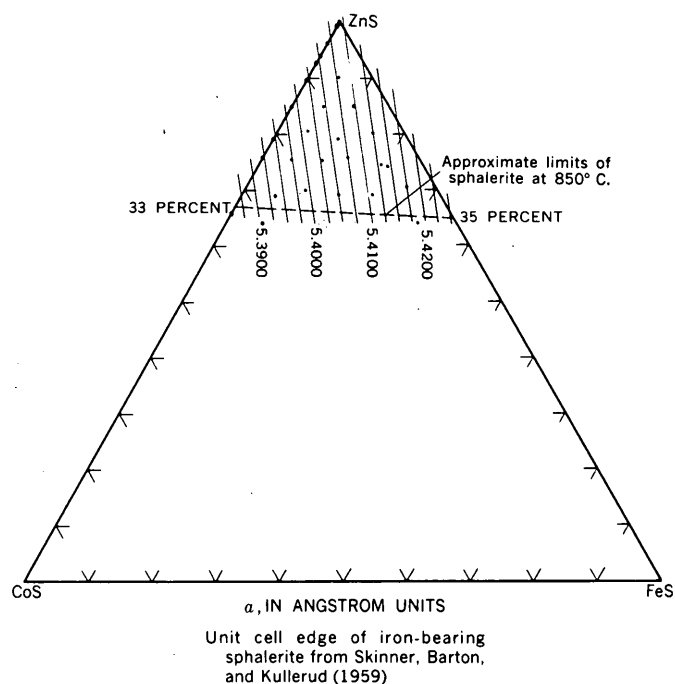
FIGURE 115.2.—Relation of a (in angstrom units) and composition (mol percent) of cobalt-iron-bearing sphalerites.

The unit-cell edges are approximately additive, but the calculated unit-cell edges tend to be slightly smaller than measured ones in cobalt-iron-bearing sphalerites containing more than 75 mol percent ZnS, and larger in ones containing 65 to 75 mol percent ZnS.

The a is one parameter used by the writer in conjunction with an Fe:Zn ratio to determine composi-

TABLE 2.—*Unit-cell edges of cobalt-and-iron-bearing sphalerites*

Composition of sphalerite						a, in angstrom units (measured)	a, in anstrom units (calculated)	Difference
Weight percent			Mol percent					
ZnS	CoS	FeS	ZnS	CoS	FeS			
90.87	4.63	4.50	90.15	4.91	4.94	5.4084 ±0.0002	5.4082	0.0002
86.30	4.60	9.10	85.19	4.86	9.95	5.4109 ± .0002	5.4104	− .0005
85.98	9.43	4.59	85.00	9.98	5.02	5.4042 ± .0003	5.4046	+ .0004
82.01	13.68	4.31	80.85	14.44	4.71	5.4014 ± .0002	5.4013	− .0001
81.66	4.51	13.83	80.22	4.74	15.04	5.4130 ± .0003	5.4129	− .0001
80.82	9.91	9.27	79.47	10.43	10.10	5.4069 ± .0005	5.4066	− .0003
76.81	18.70	4.49	75.45	19.66	4.89	5.3977 ± .0002	5.3977	.0000
76.76	14.24	9.00	75.28	14.95	9.77	5.4030 ± .0003	5.4033	+ .0003
76.75	9.47	13.78	75.13	9.92	14.95	5.4084 ± .0003	5.4092	+ .0008
76.20	5.52	18.28	74.44	5.77	19.79	5.4134 ± .0007	5.4143	+ .0009
72.34	4.30	23.36	70.35	4.47	25.18	5.4169 ± .0006	5.4177	+ .0008
71.64	19.19	9.17	70.00	20.07	9.93	5.3992 ± .0003	5.3998	+ .0006
71.26	9.60	19.14	69.35	10.00	20.65	5.4113 ± .0005	5.4117	+ .0004
71.06	14.76	14.18	69.15	15.37	15.28	5.4046 ± .0005	5.4055	+ .0009
70.60	24.40	5.00	69.03	25.55	5.41	5.3928 ± .0007	5.3939	+ .0011
65.77	28.82	5.41	64.09	30.07	5.84	5.3903 ± .0002	5.3910	+ .0007

tion of cobalt-iron-bearing sphalerites in the phase studies.

REFERENCES

Kullerud, Gunnar, 1953, The FeS–ZnS system. A geological thermometer: Norsk geol. tidsskr., v. 32, p. 61–147.

Skinner, B. J., Barton, P. B., Jr., and Kullerud, Gunnar, 1959, Effect of FeS on the unit-cell edge of sphalerite. A revision: Econ. Geology, v. 54, p. 1040–1046.

Skinner, B. J., and Barton, P. B., Jr., 1960, The substitution of oxygen for sulfur in wurtzite and sphalerite: Am. Mineralogist, v. 45, p. 612–625.

---

116.   X-RAY DIFFRACTOMETER METHOD FOR MEASURING PREFERRED ORIENTATION IN CLAYS

By ROBERT H. MEADE, Menlo Park, Calif.

The preferred orientation of clay minerals is a key to the understanding of the deposition and compaction of clayey sediments. This orientation is not always susceptible to measurement by optical means because (a) individual clay-mineral particles are generally too small to be studied, and (b) many clays, particularly those rich in montmorillonite, have swelling properties that make the preparation of thin sections difficult. X-ray diffraction provides a way to overcome these difficulties.

X-ray diffractometer methods of petrofabric study have been described by Higgs and others (1960), Silverman and Bates (1960), and Kaarsberg (1959, p. 453–454). The method to be described in this article is similar to the one used by Kaarsberg. Its main advantage over previously described methods is that a numerical index is obtained that can be used to compare the orientation of different phyllosilicate minerals in rock specimens from different terranes.

BASIS OF METHOD

The use of X-ray diffraction in petrofabric study depends on the fact that the intensity of the reflection from any crystallographic plane varies directly with the mass of material oriented so that the plane reflects X-rays according to the Bragg relation. This is illustrated by X-ray diffraction patterns from two specimens of the same clay-mineral fraction (fig. 116.1). The first specimen was prepared by allowing the clay-mineral particles to settle out of suspension and lie with their basal planes parallel; the preferred orientation of these clay particles is nearly perfect. All the peaks in the diffraction pattern from this specimen (lower pattern, fig. 116.1)

represent reflections from basal planes. In the other specimen, prepared with random rather than preferred orientation of the clay minerals, the reflections from the basal planes are less intense. Other crystallographic planes within the minerals reflect X-rays, and their peaks also appear in the pattern (upper pattern, fig. 116.1).

In the pattern from the specimen that has preferred orientation, the (001) reflection from basal planes of montmorillonite (at 15 A) is much enhanced and the (020) reflection from planes perpendicular to the basal planes (at 4.4 A) is absent. On the other hand, in the pattern from the specimen that is oriented at random, the 4.4–A peak is nearly as high as the one at 15 A. These two peaks are the ones whose heights are used to measure the preferred orientation of montmorillonite particles. Because montmorillonite is the most abundant clay mineral in the sediments that were examined by this method, this article will describe the measurement of its preferred orientation. The same principle, however, can be used to measure the preferred orientation of other clay minerals.

The samples illustrated in figure 116.1 were taken from a clay-mineral fraction that is especially rich in montmorillonite. The X-ray patterns are ideally simplified because most of the nonclay minerals have been removed, and the orientation of the clay particles was produced artificially. Patterns from natural sediments are not so well defined.

PREPARATION AND X-RAY DIFFRACTION

From a block of air-dried sample, three small cylinders are cut in such a way that their circular ends
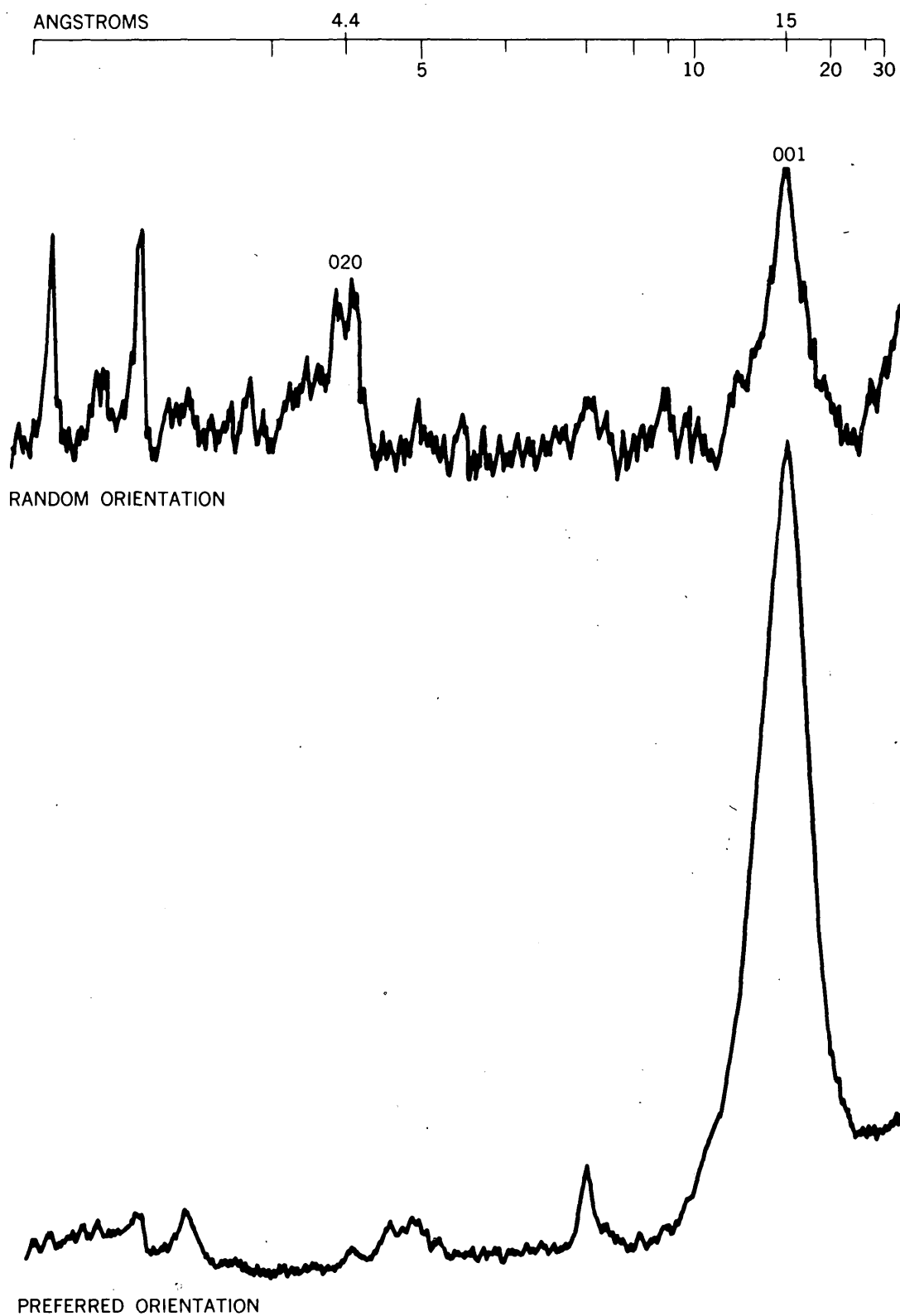
FIGURE 116.1.—Effects of particle orientation on X-ray diffraction patterns of clay minerals.
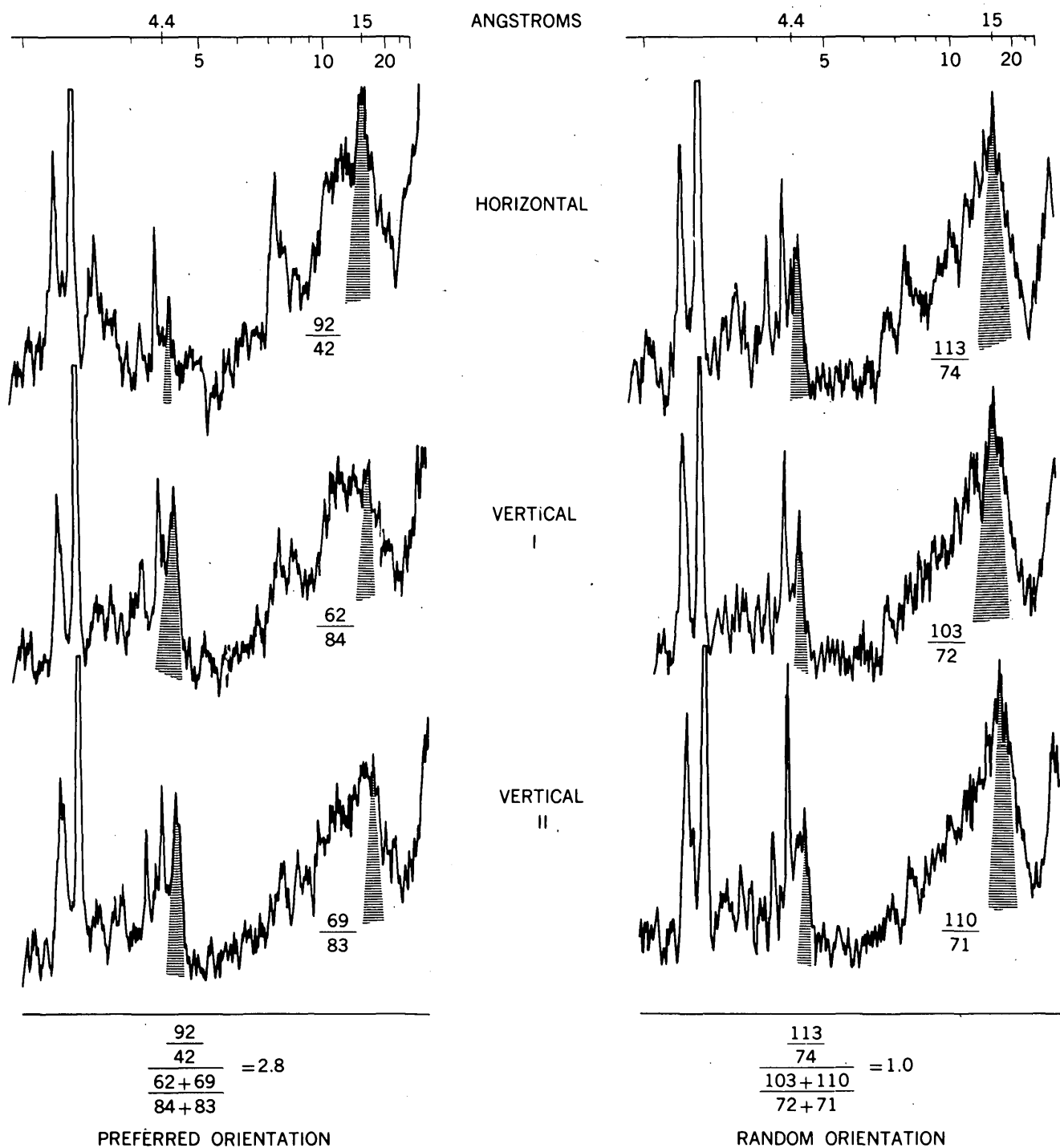
FIGURE 116.2.—Measurement of horizontal preferred orientation by comparison of X-ray diffraction peak heights.

form mutually perpendicular planes, one horizontal (parallel to the bedding) and two vertical. The cylinders have diameters of about 2 cm so that they fit snugly into a low-angle rotating specimen holder (Norelco type 52184–A) on the Norelco X-ray diffractometer. The plane sections are polished on progressively finer frosted-glass plates without added abrasives as suggested by Weatherhead (1940,

p. 530). The polished specimens are then placed in the rotating specimen holder, which is mounted on a wide-range goniometer, and exposed to radiation.

ORIENTATION RATIO

For each section, the (001) and (020) reflections are recorded three times, and average values are used for the peak heights. From the average values the ratio between the heights of the 15–A peak and 4.4–A peak is computed for each section. The peak-height ratio for the horizontal section is then divided by an average ratio for the two vertical sections. The quotient is taken as a measure of the horizontal orientation of the basal planes of montmorillonite, and is called the orientation ratio. Other factors that affect the intensities of X-ray reflections —particle size, chemical composition, degree of crystallinity—are cancelled out of the orientation ratio when the horizontal peak-height ratio is divided by the vertical peak-height ratios.

Figure 116.2 shows the measurement of the orientation ratio in two samples, one having preferred orientation and the other having random orientation. In contrast with those in figure 116.1, the patterns are complicated by reflections from illite, chlorite, and by stronger reflections from quartz and feldspar. The peak heights of montmorillonite have been adjusted ("noise corrected") to eliminate the effects of background reflections. Peak-height ratios are given for each section, and the orientation ratios are computed from them. An orientation ratio of 1.0 indicates completely random orientation with respect to the horizontal; clays having preferred horizontal orientation have orientation ratios larger than 1.0. The orientation ratios given in figure 116.2 measure only the preferred orientation parallel to the bedding. The planes may be adjusted, however, to measure the orientation in any directions— parallel to cleavage, schistosity, or other planar elements.

The most precise measurements of the orientation ratio are obtained from materials in which one phyllosilicate predominates over all others to the extent that X-ray reflections from the other minerals do not interfere seriously with the reflections from the principal mineral. Reflections from montmorillonite, for example, can be masked or modified by (020) reflections from illite at 4.4 A or by (001) reflections from chlorite at 14 A. This method, therefore, should be applied cautiously to rocks that contain heterogeneous mixtures of clay minerals and other layer silicates.

REFERENCES

Higgs, D. V., Friedman, Melvin, and Gebhart, J. E., 1960, Petrofabric analysis by means of the X-ray diffractometer, in Rock deformation (a symposium): Geol. Soc. America Mem. 79, p. 275–292.

Kaarsberg, E. A., 1959, Introductory studies of natural and artificial argillaceous aggregates by sound-propagation and X-ray diffraction methods: Jour. Geology, v. 67, p. 447–472.

Silverman, E. N., and Bates, T. F., 1960, X-ray diffraction study of orientation in the Chattanooga shale: Am. Mineralogist, v. 45, p. 60–68.

Weatherhead, A. V., 1940, A new method for the preparation of thin sections of clays: Mineralog. Mag., v. 25, p. 529–533.

117. MOLYBDENUM CONTENT OF GLACIAL DRIFT RELATED TO MOLYBDENITE-BEARING BEDROCK, AROOSTOOK COUNTY, MAINE

By F. C. CANNEY, F. N. WARD, and M. J. BRIGHT, JR., Denver, Colo.

A recent survey by Riddell (1960) of the experience of 24 Canadian companies engaged in mineral exploration disclosed a lack of unanimity of opinion concerning the usefulness of soil-sampling techniques in glaciated areas. Although widely used, opinion on the value of applied geochemistry ranged from "extremely useful and valuable tool" to "no value whatsoever." At least part of the negative attitude is attributed to the scarcity of published studies that provide useful data for guiding mineral exploration programs in glaciated areas. The molybdenum anomaly described in this paper provides
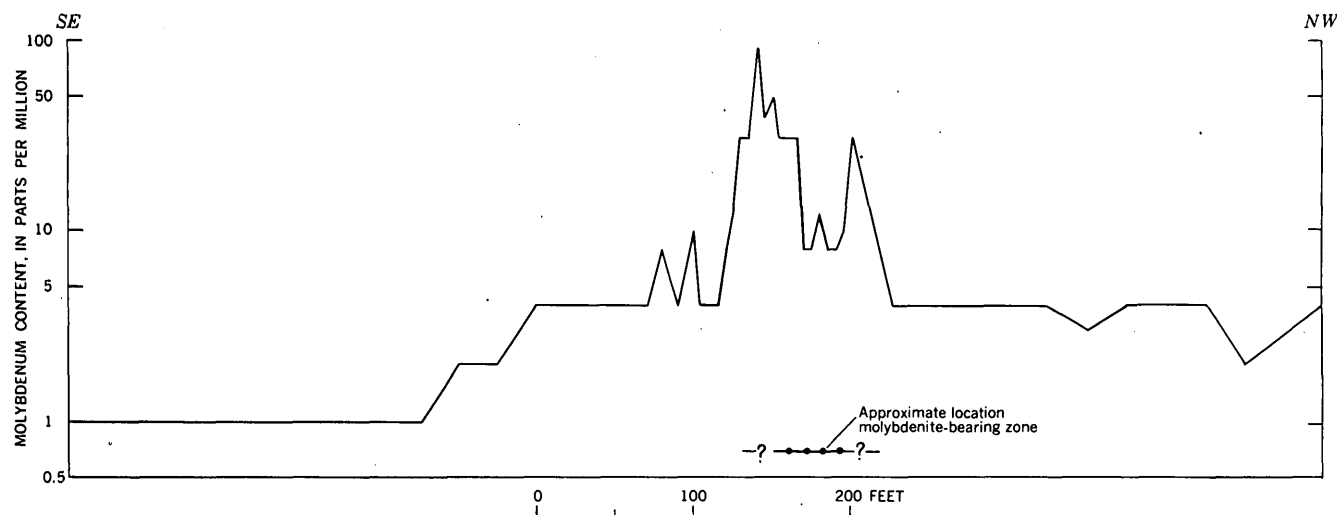
FIGURE 117.1.—Geochemical profile showing lateral distribution of molybdenum in glacial drift over molybdenite-bearing zone. Land surface along sample traverse is nearly level.

another positive illustration of the usefulness of geochemical prospecting techniques in a glaciated area.

A zone of silicified limestone containing easily visible but sparse molybdenite as flakes and thin seams is poorly exposed in a group of prospect pits about 6 miles north-northeast of Houlton, Maine. Detailed mapping by Louis Pavlides (oral communication, 1960) in the Houlton quadrangle has shown this zone to be satellitic to a small intrusive plug of granite. The bedrock in this test area is almost completely covered with glacial ground moraine, 6 to 24 inches thick. Although glacial-fluviatile deposits are very common in the Houlton quadrangle, the available exposures were insufficient for us to classify the cover as till or stratified drift. The brief investigation described here was designed to determine whether anomalous amounts of molybdenum occurred in the soil in the vicinity of this metallized zone.

A line 800 feet long was surveyed across the projected trend of the mineralized zone. Soil samples were collected along this line at intervals of 5 feet above and near the suboutcrop of the zone and the spacing between samples was increased progressively to 50 feet as the distance from the deposit increased. The samples were taken from a depth of 8 to 12 inches below the land surface. Because the area had once been cultivated, no original soil profile is present, but we believe that the samples were from undisturbed soil below plow depth. Most of the 49 samples collected along this line contained a large percentage of material in the silt- and clay-size range.

All samples were dried and sieved through a 100-mesh sieve, and the fines analyzed for molybdenum by a geochemical prospecting field method utilizing a carbonate fusion to decompose the sample (Ward, 1951).

The molybdenum contents of the soil samples (fig. 117.1) show that the soil both over and on either side of the exposed part of the mineralized zone contains anomalous amounts of molybdenum (background in this area is 1 to 2 ppm molybdenum). For a distance of more than 80 feet the soil contains more than 8 ppm, and the soil contains 30 ppm or more in one stretch of 35 feet. The soils containing the most molybdenum occur just to the southeast of the exposed zone. Because this zone, which seems to trend northeasterly, is exposed in only a few small trenches, its maximum dimensions as well as the possible presence of other molybdenite-bearing zones are unknown. The rather abrupt decrease in a southeasterly direction from the peak value of 90 ppm to background in less than 150 feet suggests little, if any, glacial drag. In this part of Maine the ice movement was probably in a south-southeasterly direction. If the anomaly were formed by diffusion of soluble molybdenum upward into the glacial cover after retreat of the ice, no asymmetry due to ice movement would be present.

The form in which the molybdenum occurs in the

soil is not known. Several samples containing anomalous amounts of molybdenum were leached with hot water, but no molybdenum was found in the leachate; this apparent lack of water-soluble molybdenum could be interpreted as weak evidence that this anomaly is not a superimposed diffusion pattern.

Although certain questions about the genesis of this particular anomaly remain unanswered, the point of greatest significance to those engaged in mineral exploration is that this is another example of the usefulness of soil sampling techniques in the search for mineral deposits concealed beneath a thin cover of glacial materials.

REFERENCES

Riddell, J. F., 1960, Geochemical prospecting methods employed in Canada's glaciated Precambrian terrains: Mining Eng., v. 12, no. 11, p. 1170–1172.

Ward, F. N., 1951, Determination of molybdenum in soils and rocks: Anal. Chemistry, v. 23, p. 788.

⚒

118. ANOMALOUS HEAVY MINERALS IN THE HIGH ROCK QUADRANGLE, NORTH CAROLINA

By Amos M. White and Arvid A. Stromquist, Washington, D. C., and Denver, Colo.

Work done in cooperation with North Carolina Division of Mineral Resources

---

Heavy-mineral concentrates obtained by panning alluvial sediment from streams in the High Rock 7½-minute quadrangle, North Carolina, contain minerals anomalous to the known bedrock of the quadrangle. The area investigated lies west of the Atlantic Coastal Plain in Davidson, Rowan, Stanly, and Montgomery Counties, N. C., and is underlain by rocks of the so-called Carolina slate belt, a volcanic and sedimentary sequence probably of Precambrian and Paleozoic ages in the eastern part of the North Carolina Piedmont (fig. 118.1).

Geologic mapping of the area has established for the first time a stratigraphic sequence for the Carolina slate belt (Stromquist and Conley, 1959). Outcropping rocks in the High Rock quadrangle are largely tuffaceous argillite interbedded with and unconformably overlain by metamorphosed tuffs, lapilli tuffs, and minor flows, all of rhyolitic to andesitic composition. Diabase dikes and dacitic(?) to gabbroic intrusive bodies are also present. Regional metamorphism of these rocks is low grade, nowhere exceeding the greenschist facies. Metamorphic grade increases west of the slate belt in rocks comprising the adjoining Charlotte, Kings Mountain, and Inner Piedmont belts (King, 1955, p. 346–356).

Forty-pound samples of sand and gravel deposited by the modern streams were collected at 57 localities in the High Rock quadrangle. Each sample was collected from the channel of a stream having a drainage area of 2 square miles or less, and was collected at a point outside the flood plain of the present Yadkin River, the major stream in the quadrangle (fig. 118.1). All the concentrates contain one or more minerals characteristic of the almandine-amphibolite facies of regional metamorphism (Fyfe, Turner, and Verhoogen, 1958, p. 228–232). These minerals are staurolite, kyanite, sillimanite, and garnet. Kyanite is present in 55 of the concentrates, staurolite is in 47 concentrates, and sillimanite or probable sillimanite is in 23. Garnet is present in 48 concentrates and is abundant in many of these. Relatively coarse-grained zircon, much of which shows some degree of rounding, is present in 35 of the concentrates. At least 13 concentrates contain monazite or probable monazite. In general, the concentrates with the largest suites of anomalous minerals are from streams in the west half of the quadrangle.

Most of the kyanite shows some degree of rounding, and the monazite is well rounded, which suggests transport from some fairly remote source.
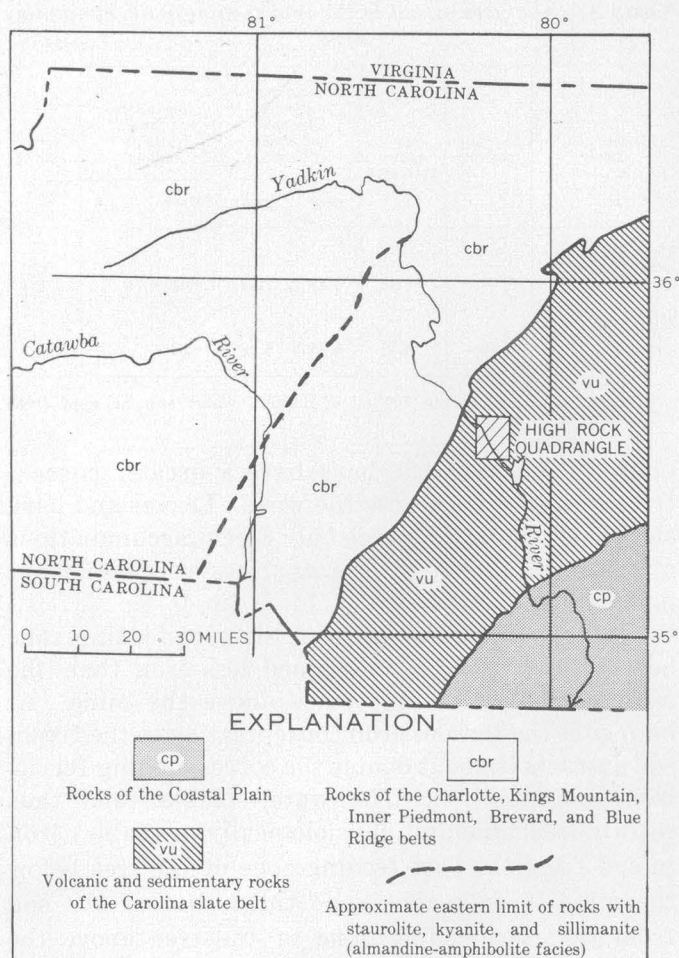
FIGURE 118.1.—Index map of west-central North Carolina showing location of the High Rock quadrangle. Geology generalized from King (1955) and from the geologic map of North Carolina (Stuckey and Conrad 1958).

Rounded detrital kyanite denotes a stream of low velocity according to Krumbein and Pettijohn (1938, p. 436), but many of the streams from which the concentrates were obtained have steep gradients and are relatively short and fast moving, particularly those draining the highest points in the quadrangle.

The nearest known occurrence of rocks of the almandine-amphibolite metamorphic facies is approximately 30 miles to the northwest, and the Yadkin is the only stream in the area that extends westward to these rocks (fig. 118.1). Presumably the higher grade metamorphic minerals were deposited in sediments along former courses of the Yadkin, possible remnants of which are now preserved on topographically high surfaces in the quadrangle. The small streams in eroding these surfaces pick up the anomalous minerals and redeposit them at lower elevations. The presence of heavy minerals in the surficial materials in the High Rock quadrangle suggests that regional studies of heavy mineral distribution would provide data for tracing the former major drainage systems in the region.

REFERENCES

Fyfe, W. S., Turner, F. J., and Verhoogen, John, 1958, Metamorphic reactions and metamorphic facies: Geol. Soc. America Mem. 73, 259 p.

King, P. B., 1955, A geologic section across the southern Appalachians—an outline of the geology in the segment in Tennessee, North Carolina, and South Carolina, *in* Russell, R. J., ed., Guides to southeastern geology: Geol. Soc. America, p. 332–373.

Krumbein, W. C., and Pettijohn, F. J., 1938, Manual of sedimentary petrography: New York, Appleton-Century-Crofts, Inc., 549 p.

Stromquist, A. A., and Conley, J. F., 1959, Geology of the Albemarle and Denton quadrangles, North Carolina: Carolina Geol. Soc. Field Trip Guidebook, Oct. 24, 1959, Div. Mineral Resources, Raleigh, N. C., 36 p.

Stuckey, J. L., and Conrad, S. G., 1958, Explanatory text for geologic map of North Carolina: North Carolina Dept. Cons. and Devel., Div Mineral Resources, Bull. 71, p. 3–51, map.

119.   IRON CONTENT OF SOILS AND TREES, BEAVER CREEK STRIP MINING AREA, KENTUCKY

By EUGENE T. OBORN, Denver, Colo.

In the Beaver Creek strip mining area, Kentucky, trees growing on the soil through which the mine waters percolate extract iron from the drainage water. This is shown by samples of soil from the root feeding zone and samples of vegetation collected at two locations, one upslope and one downslope from a strip mine opened in May 1955.

Sampling of vegetation was restricted to the white

TABLE 1.—*Analyses of white oak plant parts, strip-mine area*

Location of tree sampled	Material analyzed	Iron per gram dry matter (milligrams)	Iron in ash (percent)
Above mine	Leaves...................	0.07	0.11
Do...................	Trunk before 1955........	.05	1.72
Do...................	Trunk 1955–60...........	.07	1.25
Do...................	Bark....................	.13	.13
Below mine	Leaves...................	.29	.47
Do...................	Trunk before 1955........	.04	1.40
Do...................	Trunk 1955–60...........	.10	1.79
Do........●..........	Bark....................	.32	.35

TABLE 2.—*Analyses of soil in the root feeding zone, strip mine area*

Location of sample	Moisture (percent)	Organic matter (percent)	Total iron content of dry soil (milligrams per gram)		Iron in fresh soil extract [1] (parts per million)		pH of extract
			62°C	575°C	Fe^{+2}	Fe^{+3}	
Above mine, in treeroot feeding zone...........	6.0	6.13	6.81	7.28	0.11	0.07	6.7
Below mine, in treeroot feeding zone...........	9.6	5.37	5.96	6.28	.04	.02	4.3

[1] Extract made by mixing 100 ml of distilled water and 1.0 g of fresh soil. Filtered after 1 hour.

oak, *Quercus alba* L. Wood and bark were sampled in duplicate with a large-diameter increment borer. Analyses of the samples are given in tables 1 and 2; the results are summarized below.

Iron content, on a dry-matter basis, in the wood of trees growing both upslope and downslope from the mine is greater in wood produced from 1955 to 1960 than in wood produced earlier. The iron content is greatest in the 1955 to 1960 wood of the downslope tree which received drainage from the mine. The iron content in ash of the wood from the tree above the mine is greater for the period preceding 1955 than it is for the period 1955 to 1960. The reverse is true for the downslope tree. These data indicate that from 1955 to 1960 iron was more readily available and absorbed by the downslope tree than was the case with the upslope tree.

As determined by analyses of the dry matter, in the downslope trees the iron content of the leaves is four times, and the bark is more than two times, the iron content of the corresponding parts of the upslope trees. Analyses of the ash of the leaves and bark also shows a greater concentration of iron in the ash of these parts of the downslope trees than in the upslope trees. It is usually true in woody plants that leaves and bark have a greater concentration of iron than does the wood. Leaves and bark slough off regularly, hence only recent accumulations of iron are shown by the analyses of these plant parts.

The soil sample taken from the root feeding zone below the strip mine contained less iron than the sample taken from the slope above the mine. At both sites the ferrous-iron concentration in the fresh-soil extracts is about double the corresponding ferric-iron concentration. The water-soluble (and thus readily leachable and physiologically available) iron in soil from the root feeding zone of the tree below the mine is only about one third that of the soil from the root-feeding zone of the tree above the mine. This was true in spite of the fact that the extract of soil from below the mine had a pH of 4.3 whereas the soil extract from above the mine had a pH of 6.7. The moisture content of the soil sample taken below the mine was greater than that of the sample taken from the upslope location.

120.   MINERALOGY OF THE OLIVE HILL CLAY BED, KENTUCKY

By JOHN W. HOSTERMAN and SAM H. PATTERSON, Beltsville, Md.

Work done in cooperation with the Kentucky Geological Survey

The Olive Hill clay bed of Crider (1913) in northeastern Kentucky contains three types of clay—flint, semiflint, and plastic—in irregular lenses of variable thicknesses. Boundaries between types of clay are usually sharp and well defined, and the clay bed is nonbedded except for the superposition of one

type of clay above the other. Typically, the flint clay overlies the semiflint clay, but at many places this order is reversed. Where plastic clay is present it is usually in the lower part of the bed, but there are exceptions.

Much of the clay is medium gray to brownish gray, but colors may range from very light gray to almost black. The darker gray colors are due to carbonaceous material of fossil roots, and occur at the top of the clay bed which underlies a thin coal bed. The lighter colors occur toward the base of the bed. Reddish-brown staining of iron oxides along joints is quite common.

Flint clay in the Olive Hill clay bed is hard, resistant, and nonplastic. It possesses the flintlike characteristics of almost complete homogeneity and conchoidal fracture. Oolites are very abundant in some of the flint clays. The flint clay weathers to shardlike fragments having sharply curved knife edges and pointed corners. It is composed of more than 85 percent kaolinite and less than 15 percent illite and mixed-layer clay minerals. Boehmite has been found in the flint clay at only one locality.

Plastic clay in the Olive Hill clay bed is quite plastic after it has been exposed to weathering for a short time, but the fresh clay requires grinding before maximum plasticity is developed. Abundant slickensides are present in the fresh plastic clay, but after the clay weathers the slickensides become sealed and disappear and the clay becomes a homogeneous mass. The plastic clay is composed of less than 60 percent kaolinite; illite and mixed-layer minerals make up the balance.

Semiflint clay is intermediate between flint and plastic clay in physical properties and mineral composition. Nearly all semiflint clays contain abundant randomly oriented slickensides along which partings may occur. When exposed to the weather, semiflint clay breaks down into rubble of irregular polyhedra having a slickenside surface on each face. Semiflint clay consists of 60 to 85 percent of kaolinite; illite and mixed-layer minerals form the balance.

The sedimentary nonclay minerals are quartz, tourmaline, garnet, ilmenite, and magnetite. Authigenic minerals are siderite and pyrite. Fine-grained anatase is also present, but the time of its formation is not known.

The mineralogy of the Olive Hill clay bed has been interpreted primarily from X-ray diffraction traces supplemented by differential thermal analysis and petrographic microscope studies. The diffraction traces of oriented and random specimens of several
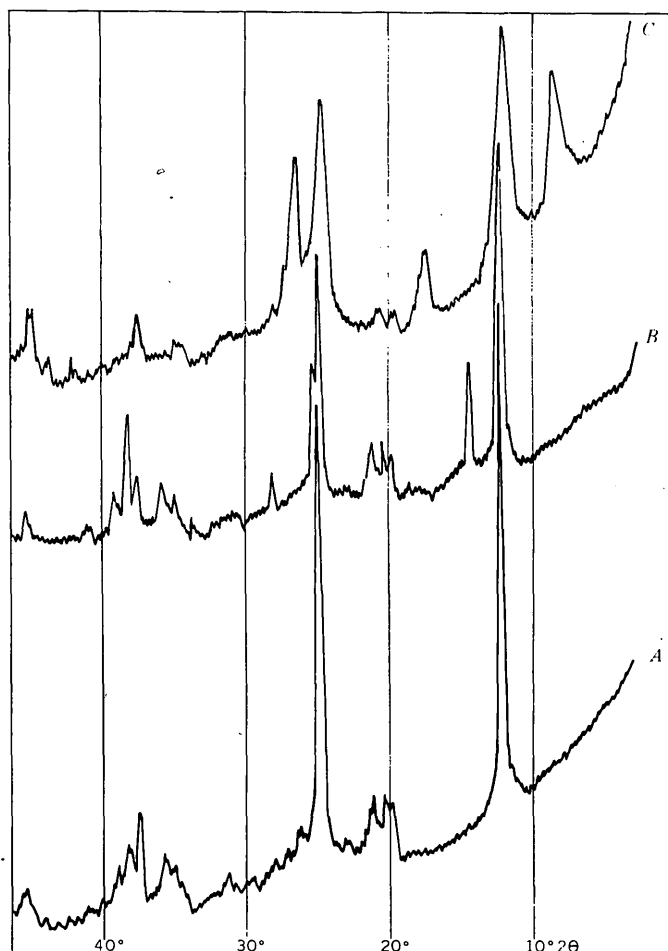
FIGURE 120.1.—X-ray diffraction traces using CuK$_\alpha$ radiation. A, well-crystallized kaolinite in flint clay; B, kaolinite and boehmite in flint clay; and C, poorly crystallized kaolinite and illite in plastic clay.

samples were obtained using CuK$_\alpha$ radiation. Oriented specimens were heated to 550°C for 30 minutes, heated to 300°C for 30 minutes, treated with ethylene glycol, and X-ray dried.

Kaolinite in the Olive Hill clay bed ranges from well crystallized in the flint clay to poorly crystallized in the plastic clay, with intermediate stages of crystallinity in the semiflint clay. Well-crystallized kaolinite has a narrow basal (001) peak, which has an area-to-height ratio that approaches 1 in the X-ray diffraction trace at 7.14A (fig. 120.1A). Poorly crystallized kaolinite or "fireclay" (Brindley and Robinson, 1947) has a broad basal (001) reflection at about 7.20A and the area-to-height ratio of the peak is almost 2 in the X-ray diffraction trace (fig. 120.1C). The well-crystallized kaolinite occurs in samples having a small amount of other clay minerals, and the poorly crystallized kaolinite is
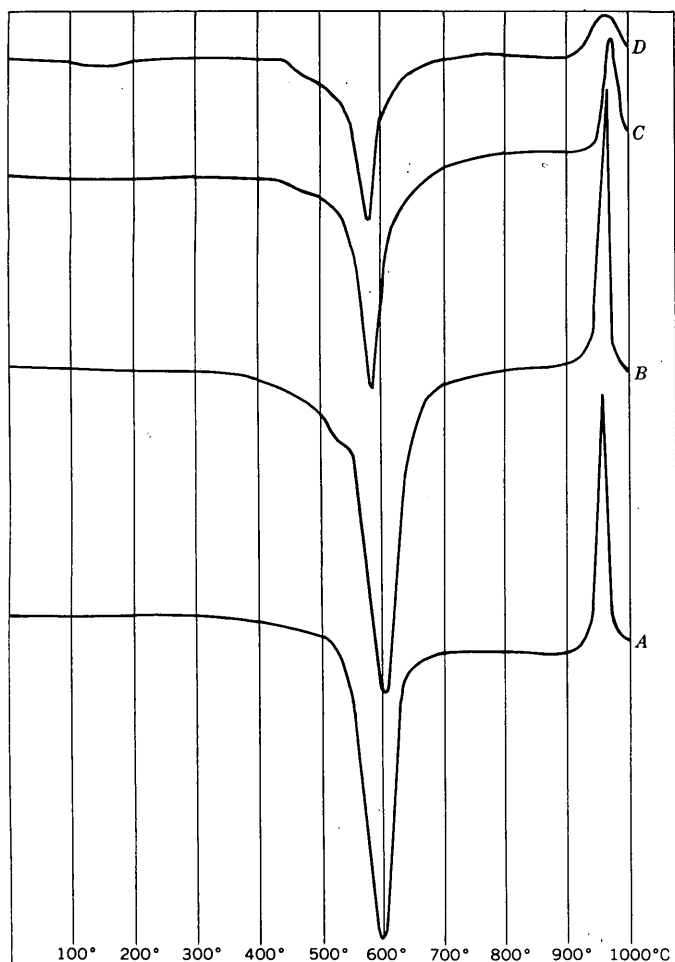
FIGURE 120.2.—Differential thermal-analysis curves. A, well-crystallized kaolinite in flint clay; B, kaolinite with boehmite in flint clay; C, medium-crystallized kaolinite in semiflint clay; and D, poorly crystallized kaolinite in plastic clay.

associated with abundant illite and mixed-layer clay minerals.

Differential thermal-analysis curves support the above determinations of the kaolinite. The endothermic peak of kaolinite occurs at approximately 600°C for flint clay (fig. 120.2A) and at about 580°C for plastic clay (fig. 120.2D). Also, the exothermic reaction at about 975°C occurs over a 25° interval for flint clay and over a 75° interval for plastic clay. The differential thermal curve for semiflint clay is intermediate between flint and plastic clay (fig. 120.2C). The temperature of the endothermic peak indicates that more energy is required to break the

hydroxyl ion bonds in the flint clay than in the plastic clay. The exothermic peak suggests that the strength of the bonds holding the final structure of the kaolinite is more uniform and tends to release suddenly in the flint clay but not in the plastic clay.

Boehmite, a mineral usually found in bauxite, but also found in the flint clays of central Pennsylvania (Bolger and Weitz, 1952), has been recognized in two samples taken from the strip mine on Grassy Creek about 1 mile west of Kehoe, Greenup County, Ky. It occurs as nodules ½ to 1 millimeter in diameter in a matrix of flint clay. The major X-ray diffraction peaks of boehmite (fig. 120.1B) are 6.23A, 3.53A, 3.16A, and 2.34A. The differential thermal-analysis curve (fig. 120.2B) shows a single endothermic peak at 525°C.

Illite is the second most common clay mineral in the Olive Hill clay bed. The amount ranges from a trace in the flint clay to about 40 percent in the plastic clay. Illite is recognized on the X-ray diffraction traces by its basal (001) peak at about 10A (fig. 120.1C). Only the clay mineral that gives this sharp peak and does not expand when treated with ethylene glycol is considered to be illite. The presence of illite is shown on the differential-thermal-analysis curves by the broad weak endothermic reaction between 100°C and 200°C and by the small endothermic reaction beginning at 450°C (fig. 120.2D).

Mixed-layer clay minerals consist of a heterogeneous mixture of illite, montmorillonite, chlorite, and probably some vermiculite. X-ray diffraction traces of these minerals have a broad diffuse peak in the 10A to 14A range, and the position of this peak is changed very little with ethylene glycol or heat treatments. These mixed-layer clay minerals are present in all types of clay but are most abundant in the plastic and semiflint clay.

REFERENCES

Bolger, R. C., and Weitz, J. H., 1952, Mineralogy and origin of the Mercer fire clay of north-central Pennsylvania, in Problems of Clay and Laterite Genesis: Am. Inst. Mining Metall. Engineers Symposium, p. 81–93.

Brindley, G. W., and Robinson, K., 1947, An X-ray study of some kaolinitic fire clays: British Ceramic Soc. Trans., v. 46, p. 49–62.

Crider, A. F., 1913, The fire clays and fire clay industries of the Olive Hill and Ashland districts of northeastern Kentucky: Kentucky Geol. Survey, ser. 4, v. 1, pt. 2, p. 592–711.

121.   FOUR ENVIRONMENTS OF THORIUM-, NIOBIUM-, AND RARE-EARTH-BEARING MINERALS IN THE POWDERHORN DISTRICT OF SOUTHWESTERN COLORADO

By D. C. HEDLUND and J. C. OLSON, Denver, Colo.

Geologic mapping and radioactivity investigations in the Powderhorn district, Gunnison County, Colo., show that the thorium, rare earths, and niobium deposits of the district are related to alkalic intrusive rocks, probably of Precambrian age, that cut diverse Precambrian rocks. The alkalic rock complex of Iron Hill, which has been mapped and described by Larsen (1942), occupies an elliptical area of about 12 square miles and is economically the most important intrusive body in the district. The rocks in the complex from oldest to youngest are pyroxenite, uncompahgrite, ijolite, diverse hybrid pyroxenite-syenite rocks, nepheline syenite, gabbro, and carbonatite. Locally at the borders of the complex is a syenite that is interpreted to be fenite, or metasomatically altered granite. The carbonatite, the youngest rock of the intrusive series, underlies an area of 2 by 1¼ miles at Iron Hill. Many carbonatite dikes radiate from the main carbonatite mass and cut all the other rock types of the complex.

Four rock types in the Powderhorn district (fig. 121.1) that have radioactivities appreciably higher than background and contain thorium, niobium, or rare earths in abnormal amounts are (a) carbonatite, (b) magnetite-ilmenite-perovskite bodies, (c) thorite veins, and (d) trachyte porphyry dikes.

Carbonatite dikes are the most radioactive rocks within the alkaline complex of Iron Hill. Of 214 carbonatite dikes examined; 132 have radioactivities ranging from 0.05 – 0.70 mr per hr or 2 to 35 times background. These more radioactive dikes generally contain layers of siderite or ankerite alternating with layers of dolomite, calcite, or biotite. They also contain pyrite and moderate to very minor amounts of barite, apatite, monazite, quartz, bastnaesite, and synchisite, and commonly weather to a chocolate-brown color. In contrast, the less radioactive carbonatite dikes, with radioactivity less than twice background, generally are homogeneous, contain dolomite, quartz, calcite, and biotite with only sparse pyrite and apatite, and weather to buff or rusty yellow colors. The thorium in the carbonatite is, in part at least, in reddish-brown monazite which has an equivalent thoria content of 0.5 – 0.6 percent. Rare earths occur as monazite, as the fluocarbonates synchisite and bastnaesite, and substitute for calcium in the apatite. Analyses of the carbonatites are summarized in figure 121.2.

The carbonatite stock of Iron Hill is less radioactive than the carbonatite dikes and has a maximum radioactivity of about 0.10 mr per hr, or 5 times background. The radioactivity is due chiefly to thorium in monazite(?), pyrochlore, and perhaps other minerals.

The magnetite-ilmenite-perovskite veins, dikes, and segregations make up a very small percentage of the total outcrop area in the pyroxenite, ijolite, and uncompahgrite of the alkaline complex of Iron Hill, chiefly in the parts of the complex north of Iron Hill. The magnetite-ilmenite-perovskite veins and dikes are discontinuous and generally occur in swarms; most are less than 2 feet thick but some are as much as 150 feet thick. The magnetite, ilmenite, and perovskite also occur as disseminated discrete grains within the pyroxenite, ijolite, and uncompahgrite and are generally more abundant in the coarser grained rocks.

The radioactivity of the magnetite-ilmenite-perovskite bodies at 128 localities ranges from 0.05 to 0.25 mr per hr or 2 to 12 times background. This radioactivity is attributable to thorium in the perovskite, concentrates of which have an equivalent thoria content of 0.12 to 0.15 percent. In transmitted light the perovskite is dusky purple, strongly twinned, and anisotropic. The perovskite content of the magnetite-ilmenite-perovskite bodies is highly variable and locally is as much as 50 percent.

The thorite veins, which occur outside the complex of Iron Hill, constitute the third and most radioactive type of rare-metal concentration in the Powderhorn district. About 217 thorium-bearing veins have been examined, and 96 of these veins have radioactivities in the range of 0.15 to 5.0 mr per hr or 5 to 250 times background. These veins cut the amphibolite, quartz-biotite schist, granite, and other Precambrian rocks outside of the complex of Iron Hill and tend to be more abundant in the vicinity of the complex and outlying syenitic bodies. The thorite veins are generally less than a foot thick and commonly occur in anastomosing shear or breccia zones up to 10 feet wide. The veins are discontinuous, rarely as much as 3,500 feet long, and preferentially strike N. 45°–60° W. and N. 60°–80° E.
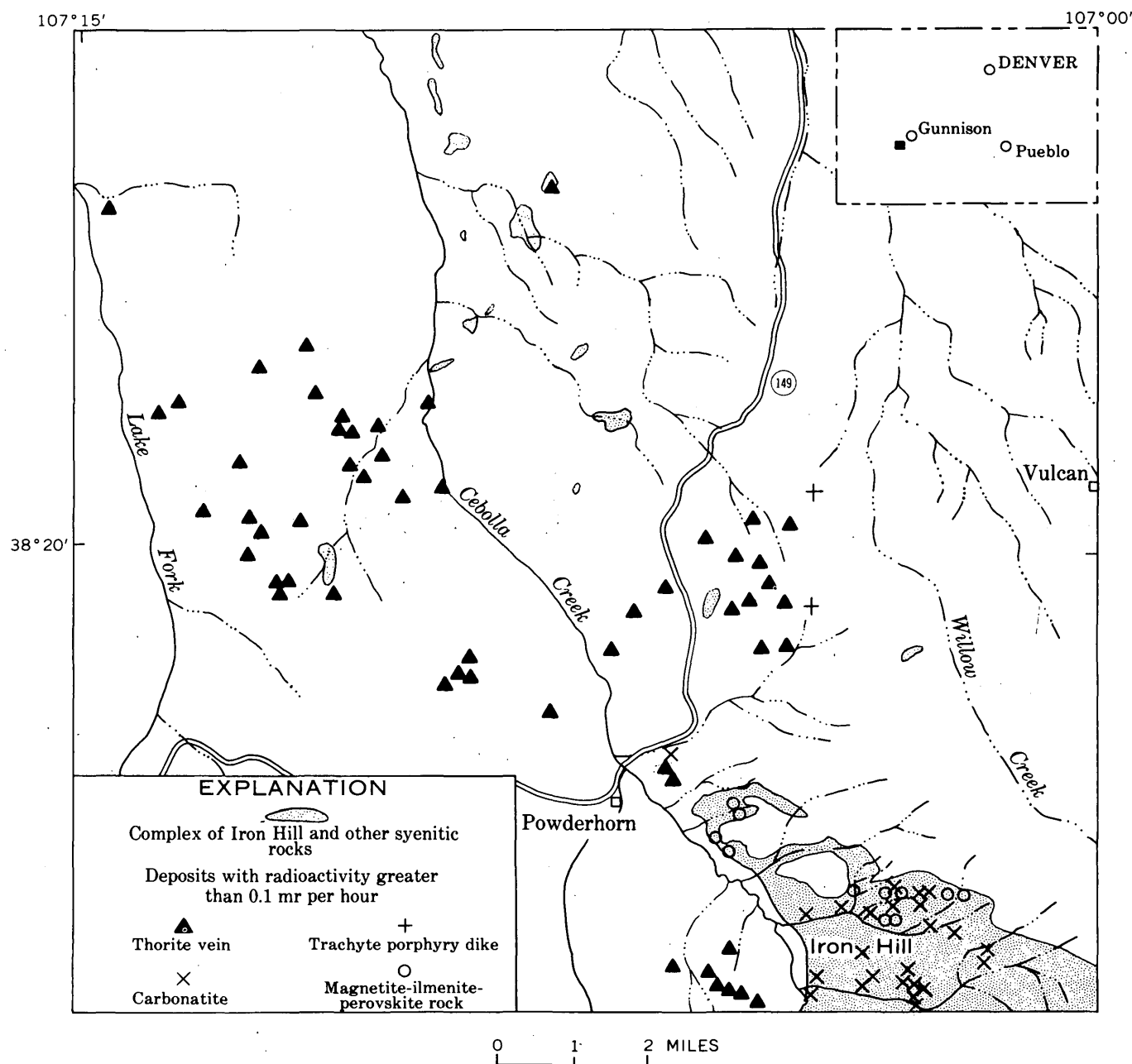
FIGURE 121.1.—Generalized map of part of Powderhorn district, Colorado, showing locations of thorium-bearing deposits.

The thorium-bearing veins consist of orthoclase, quartz, barite, specular and earthy hematite, goethite, thorite, thorogummite, calcite, dolomite, fluorite, biotite, sodic amphibole, pyrite, chalcopyrite, galena, and sphalerite. Commonly the wall rocks have been partly replaced by orthoclase, and fragments of the resulting syenitic rock have locally been incorporated in the veins. From the analyses (fig. 121.2B) it is apparent that the thorite veins are characterized by relatively large amounts of Th, Ba, Sr, rare earths, Nb, and alkalies, an assemblage that is also characteristic of the radioactive minerals of the alkalic rock complex of Iron Hill.

The fourth type of radioactive deposit consists of pink to red fine-grained trachyte porphyry dikes which also cut various Precambrian rocks of the district outside the complex of Iron Hill. About 100 dikes have been mapped, chiefly in the vicinity of the complex. The dikes, which are generally less than 50 feet thick but locally as much as 75 feet thick, are discontinuous, branching, and locally follow joint planes in the country rock. The trachyte

Rare-earth elements

PERCENT

M
7
3
1.5
0.7
0.3
0.15
0.07
0.03
0.015
0.007
0.003
0.0015
0.0007
0.0003
0.00015

	Na	Mg	P	K	Ca	Ti	Fe	Sr	Y	Nb	Ba	La	Ce	Pr	Nd	Sm	Eu	Gd	Tb	Dy	Ho	Er	Tm	Yb	Lu	$eThO_2$
Atomic No.	11	12	15	19	20	22	26	38	39	41	56	57	58	59	60	62	63	64	65	66	67	68	69	70	71	

A. CARBONATITES FROM IRON HILL COMPLEX (21 ANALYSES)

Rare-earth elements

PERCENT

M
7
3
1.5
0.7
0.3
0.15
0.07
0.03
0.015
0.007
0.003
0.0015
0.0007
0.0003
0.00015

	Na	Mg	P	K	Ca	Ti	Fe	Sr	Y	Nb	Ba	La	Ce	Pr	Nd	Sm	Eu	Gd	Tb	Dy	Ho	Er	Tm	Yb	Lu	$eThO_2$
Atomic No.	11	12	15	19	20	22	26	38	39	41	56	57	58	59	60	62	63	64	65	66	67	68	69	70	71	

B. THORIUM-BEARING VEINS (47 ANALYSES)

FIGURE 121..2—Distribution of semiquantitive spectographic analyses and radiometric ($eThO_2$) analyses of carbonatite (A) and thorium-bearing veins (B) from Powderhorn district, Colo. The numbers indicate the number of analyses in which a given element is present in the percentage shown. The approximate limit of detection by this analytical method is shown by a horizontal dash, although a few determinations were made below this limit; the number of samples in which percentages are below this threshold amount and too low to determine is indicated by number in circle. Equivalent thoria was determined radiometrically and adjusted to scale of percentages used for spectrographic data.

porphyry dikes are generally radioactive with readings of 0.04 – 0.08 mr per hr or 2 to 4 times background. About 20 of the dikes have radioactivities between 0.05 and 0.3 mr per hr, and one has as much as 5.0 mr per hr. In the rock studied, the radioactivity is concentrated in hematite pseudomorphs after pyrite pyritohedrons and may be due to extremely fine-grained intergrown thorogummite.

Features that characterize most of the four types of radioactive deposits and indicate their genetic relation include (a) the amounts of such elements as Th, rare earths, Nb, Ba, Sr, which are well above that of most igneous rocks; (b) the spatial relation to the environs of the complex of Iron Hill and smaller bodies of syenitic rock in the district; (c) a fetid odor like garlic that locally characterizes freshly broken rock from thorite veins, trachyte dikes, and fenitic rocks; and (d) alkali metasomatism or replacement of wall rocks by orthoclase, which is especially characteristic of the thorite veins and less so of the trachyte dikes. Along the borders of the alkaline complex of Iron Hill the granitic country rocks are locally feldspathized to form soda syenite (fenite), implying the introduction of Na rather than K.

The four types of thorium-rare-earth-niobium concentrations are thought to have been formed during the late stages of emplacement of the Iron Hill stock and related syenitic rocks. Within the complex of Iron Hill, the magnetite-ilmenite-perovskite bodies are among the youngest rocks, and the stock and dikes of carbonatite are the youngest. Inasmuch as the thorite veins and trachyte dikes are known only outside the complex, their age in relation to the main mass of the complex is uncertain, but the similar features mentioned above suggest they also formed late in the sequence of the alkalic rocks.

REFERENCE

Larsen, E. S., Jr., 1942, Alkalic rocks of Iron Hill, Gunnison County, Colorado: U.S. Geol. Survey Prof. Paper 197–A, p. 1–64.

122.   RHENIUM IN PLANT SAMPLES FROM THE COLORADO PLATEAU

By A. T. MYERS and J. C. HAMILTON, Denver, Colo.

In a recent review of the geochemistry of rhenium, Fleischer (1959) pointed out that our present knowledge rests almost entirely on the work of the Noddacks (1931), with the exception of new analyses of molybdenite and a few other determinations. He pointed out that no mineral other than the molybdenum minerals, molybdenite and wulfenite, has been reported to contain as much as 2 ppm (parts per million) rhenium. The close association of rhenium with molybdenum is further confirmed by the fact that in nearly 1,000 analyses of ores and smelter products, Kaiser, Herring, and Rabbitt (1954) found rhenium in only three, all of which were molybdenite ores or concentrates.

Rhenium was discovered for the first time in uranium ore from Triassic sedimentary rocks of the Colorado Plateau by Peterson, Hamilton, and Myers (1959); it was associated with the molybdenum minerals jordisite(?) and ilsemannite. Helen Cannon (oral communication, 1960) had noted that *Astragalus* and other plants from the Yellow Cat area of Grand County, Utah, contained relatively large amounts of molybdenum, in addition to toxic amounts of selenium. These are the so-called "indicator" plants used by her as a prospecting guide to uranium mineralization. With the above geochemical association in mind, several plants from soils rich in uranium and molybdenum were analyzed and found to contain rhenium in the ash. This is the first time rhenium has been found in plants.

Helen Cannon provided many plant samples she collected from the Yellow Cat area in Utah. Other plant samples were collected by P. F. Narten, C. M. Mobley, Frank Kleinhampel, Fred Ward, Harry Nakagawa, and Henry Bell, III. A preliminary statement of the results presented below has been published (Myers and Hamilton, 1960).

The analyses, reported by numbers on a semiquantitative basis, were obtained by the method of Myers

TABLE 1.—*Rhenium and some other elements in plant ash* [1]

[In parts per million; ..., not looked for; d, detected, but concentration uncertain]

Laboratory No.	Plant	Plant part	Ash (percent)	Re	Mo	Cu	Ni	V	U	Se	Locality
Yellow Cat area, Grand County, Utah											
56-2308	*Grindelia fastigiata* (gum weed)...	Tops...	8.2	150	1500	150	7	30	10	100	McCoy group (schroeckingerite deposit).
56-2309	....do........	Roots..	6.4	<50	1500	300	15	150	......	......	Do.
59-317B	*Astragalus preussi* (poisonvetch)..	Tops...	......	150	700	150	15	70	......	......	Do.
57-1811	*Astragalus pattersoni* (locoweed)..	..do....	21.8	70	300	70	30	70	61	1500	Do.
32-60	*Ephedra viridis* (Mormon tea)....	..do....	9.6	150	150	15	15	70	......	......	Do.
33-60	*Atriplex confertifolia* (shadscale salt bush)...............	..do....	26.3	300	300	15	15	30	......	......	Do.
Gypsum Valley, Montrose County, Colo.											
D-71417	*Astragalus pattersoni* (locoweed)..	Tops...	18.7	70	30	70	7	70	4	400	Gypsum claim.
D-71419	....do........	..do....	15.2	70	7	70	7	70	1	400	Do.
D-71420	....do........	..do....	18.4	300	7	70	7	70	2	1900	Do.
D-71438	....do........	..do....	28.6	d	300	70	15	300	33	1800	Terrible claim.
DD-71441	....do........	..do....	16.8	70	70	70	15	30	4	36	Do.
D-71435	*Eriogonum inflatum* (desert trumpet)................	..do....	7.4	70	15	150	15	70	3	0.5	Do.
D-71436	....do........	..do....	6.2	150	15	150	15	70	3.2	1.0	Do.
D-71437	....do........	..do....	7.5	70	15	150	7	30	4	28	Do.
Grants area, Grant County, N. Mex.											
D-71142...	*Astragalus confertiflorus* (?)......	Tops...	8.9	d	30	150	15	70	2.5	560	
D-71146	*Mentzelia pumilis* (stickleaf)......	..do....	13.4	d	15	300	30	300	25.2	100	
D-71147	*Onothera caespitosa* (primrose)....	..do....	17.6	150	70	300	30	300	33.6	300	

[1] Semiquantitative spectographic analyses, J. C. Hamilton, analyst, method of Myers and others (1961). Chemical analysis for U, E. Fennelly, G. Burrow, and C. Huffman, analysts; method of Grimaldi and others (1954, p. 195). Chemical analysis for Se reported on a dry weight basis, H. Crow, C. Thompson, E. Smith, W. Bowles, Jr., G. Burrow, and W. Meadows, analysts; methods of Association of Official Agricultural Chemists (1950, p. 416-419).

and others (1961). The plant samples were originally ashed overnight in a muffle furnace at 550°C. Ashing experiments made on a number of plant samples for a shorter time interval (3 hours instead of overnight) indicated very little if any loss by the longer ashing period. Analyses of the rhenium-bearing samples are listed on table 1.

Mr. J. D. Stephens, Kennecott Copper Corp., Salt Lake City, Utah, has advised us (written communication, 1960) that rhenium oxide begins to volatilize at 375°C. Therefore, it is possible that there may be a slight loss of rhenium during the ashing process at 550°C if it is present as the oxide. When the ashing temperature was lowered to 450°C for one hour, the final result for rhenium content showed little if any change.

Spectrographic and chemical results are shown on table 1 for 5 different plant samples, including 4 different plant species, growing in a small schroeckingerite deposit in the Yellow Cat area of Utah. Rhenium was detected in all 5 different plant tops and 4 different plant species; it was detected in the tops,

but was not detected in the roots of 1 sample of *Grindelia* (gum weed). The rhenium content ranges from about 50 to 500 ppm in the ash of these plants. An *Atriplex* (shadscale salt bush) plant contains about 300 ppm rhenium. The data show little apparent correlation of rhenium content with other elements listed on table 1.

Analyses are shown on table 1 for 8 plants, including 5 *Astragalus* and 3 *Eriogonum*, growing in uraniferous ground in the Gypsum Valley area of Colorado. The rhenium content ranges from about 50 to 500 ppm in the ash of these plants. One *Astragalus pattersoni* plant contained about 300 ppm in the ash. There is no apparent correlation of rhenium with any of the other elements listed on table 1. With the exception of one *Astragalus* sample (D-71438), the plants all contained significantly less molybdenum than the plants that grew in the schroeckingerite deposit in the Yellow Cat area.

Table 1 shows analyses for three rhenium-rich plants growing in mineralized ground in the Grants area, New Mexico. These samples, like the Gypsum

TABLE 2.—*Samples in which rhenium was not detected*
[Rhenium less than 50 parts per million]

Number of analyses	Area
Uranium-mineralized ground (105 plants analyzed)	
6 plants (5 species)	Yellow Cat area, Grand County, Utah.
73 plants (7 species)	Gypsum Valley, San Miguel and Montrose Counties, Colo.
17 plants (11 species)	Grants area, McKinley County, N. Mex.
3 plants (3 species)	Paradox Valley, Montrose County, Colo.
3 plants (1 species)	Marysvale, Piute County, Utah.
3 plants (1 species)	Elk Ridge, San Juan County, Utah.
Barren ground (39 plants analyzed)	
34 plants	Death Valley, Inyo County, Calif.
3 plants (2 species)	Southern Black Hills, Fall River County, S. Dak.
2 plants (2 species)	Paradox Valley, Montrose County, Colo.

Valley plants, contained significantly less molybdenum than the plants from the schroeckingerite deposit.

Samples that contained no detectable rhenium are grouped on table 2 according to locality. Six plants that are listed as growing in uranium-mineralized ground at the Yellow Cat area were not growing over the schroeckingerite deposit; plant species analyzed in this group included *Astragalus confertiflorus*.

Rhenium could not be detected in 73 plants from mineralized areas at Gypsum Valley (table 2). Included in these plants were 7 different species including *Astragalus* from the following claims: Pooch, Pay Day, Terrible, Rambler, Gypsum, and American Eagle.

In order to test the repeatability of both the ashing and spectrographic method, four of the plant samples were reashed and analyzed a second time for Re, Mo, Cu, V, and Ni. The results are shown in table 3 for samples 56–2308, 59–317B, D–71417, and D–71438.

TABLE 3.—*Comparison of results from duplicate ashing of plant samples*
[In parts per million; ... not looked for; d, detected but concentration uncertain]

Sample No.	Ash (percent)	Re	Mo	Cu	Ni	V
56–2308A	8.2	150	1500	150	7	30
56–2308B	8.5	150	1500	150	7	30
59–317BA	....	150	700	150	15	70
59–317BB	11.3	150	700	300	15	70
D–71417A	18.7	70	30	70	7	70
D–71417B	19.8	d	30	150	7	30
D–71438A	27.3	d	300	70	15	300
D–71438B	....	d	300	70	15	300

The data so far gathered seem to indicate that the plant tops (or leaves) are more likely than the stems or roots to show the presence of rhenium in mineralized soil.

REFERENCES

Association of Official Agricultural Chemists, 1950, Official methods of analysis, 7th ed.: Washington, D. C., 910 p.

Grimaldi, F. S., and others, compilers, 1954, Collected papers on methods of analysis for uranium and thorium: U.S. Geol. Survey Bull. 1006, 184 p.

Fleischer, Michael, 1959, The geochemistry of rhenium with special reference to its occurrence in molybdenite: Econ. Geology, v. 54, p. 1406–1413.

Kaiser, E. P., Herring, B. F., and Rabbitt, J. C., 1954, Minor elements in some rocks, ores, and mill and smelter products: U.S. Geol. Survey TEI–415, 119 p., issued by U.S. Atomic Energy Comm. Tech. Inf. Serv., Oak Ridge, Tenn.

Myers, A. T., Havens, R. G., and Dunton, P. J. 1961, A, spectrochemical method for the semiquantitative analysis of rocks, minerals, and ores: U.S. Geol. Survey Bull. 1084–I.

Myers, A. T., and Hamilton, J. C., 1960, Rhenium in plant samples from the Colorado Plateau [abs.]: Geol. Soc. America Bull., v. 71, p. 1934.

Noddack, Ida, and Noddack, Walter, 1931, Die Geochemie des Rheniums: Zeitschr. phys. Chemie, v. A154, p. 207–244.

Peterson, R. G., Hamilton, J. C., and Myers, A. T., 1959, An occurrence of rhenium associated with uraninite in Coconino County, Ariz.: Econ. Geology, v. 54, p. 254.

123. CLASSIFICATION OF ELEMENTS IN COLORADO PLATEAU URANIUM DEPOSITS AND MULTIPLE STAGES OF MINERALIZATION

By A. T. Miesch, Denver, Colo.

Chemical elements in sandstone-type uranium deposits of the Colorado Plateau have been classified into two broad groups: (a) dominantly intrinsic elements, or elements whose presence in the deposits is largely unrelated to the process of uranium mineralization, and (b) dominantly extrinsic elements, or elements whose presence in the deposits is largely a result of uranium mineralization or related processes (Shoemaker and others, 1959, p. 35). Elements that are dominantly intrinsic and those that are dominantly extrinsic can generally be distinguished empirically by their relative abundances in uranium ore and unmineralized sedimentary host rocks. Extrinsic components of various elements were introduced into the host sandstone and mudstone to form the present deposits epigenetically, but were not necessarily introduced at the same time nor by exactly the same process. Elements that are dominantly intrinsic in uranium deposits in the Salt Wash member of the Morrison formation include silicon, aluminum, calcium, magnesium, sodium, potassium, antimony, boron, beryllium, carbon, chlorine, chromium, fluorine, gallium, manganese, phosphorus, scandium, strontium, and titanium. Dominantly extrinsic elements in these deposits, in addition to uranium, include arsenic, cobalt, copper, molybdenum, nickel, lead, selenium, silver, vanadium, yttrium, and zinc. Several elements, including iron, barium, and zirconium, seem to be about equally intrinsic and extrinsic in deposits in the Salt Wash member.

Examination of the co-variation of extrinsic elements among uranium deposits in the Salt Wash member shows that they may be classified further into geochemically coherent groups and subgroups (fig. 123.1). Deposits rich in one of the elements tend to be rich in the other elements of the same subgroup. The classification of extrinsic elements into coherent groups and subgroups has been accomplished through computation of linear correlation coefficients between logarithms of element concentrations in samples from 215 deposits. Every element within a subgroup has a moderate or higher correlation with each of the other elements in the subgroup (fig. 123.1). Elements in the same group, but in different subgroups, have moderate or weaker correlations with each other. All correlations between elements in different groups are less than moderate. Elements in Group I (fig. 123.1) have moderate or nearly moderate correlations with iron, and none has a moderate or higher correlation with aluminum. Elements in Group II have moderate or nearly moderate correlations with aluminum, but their correlations with iron are lower than moderate. Elements in Group III and IV, yttrium and uranium respectively, do not have moderate or higher correlations with any of the other dominantly extrinsic

Very high correlation (r>0.75)

High correlation (0.75>r>0.50)

Moderate correlation (0.50>r>0.35)
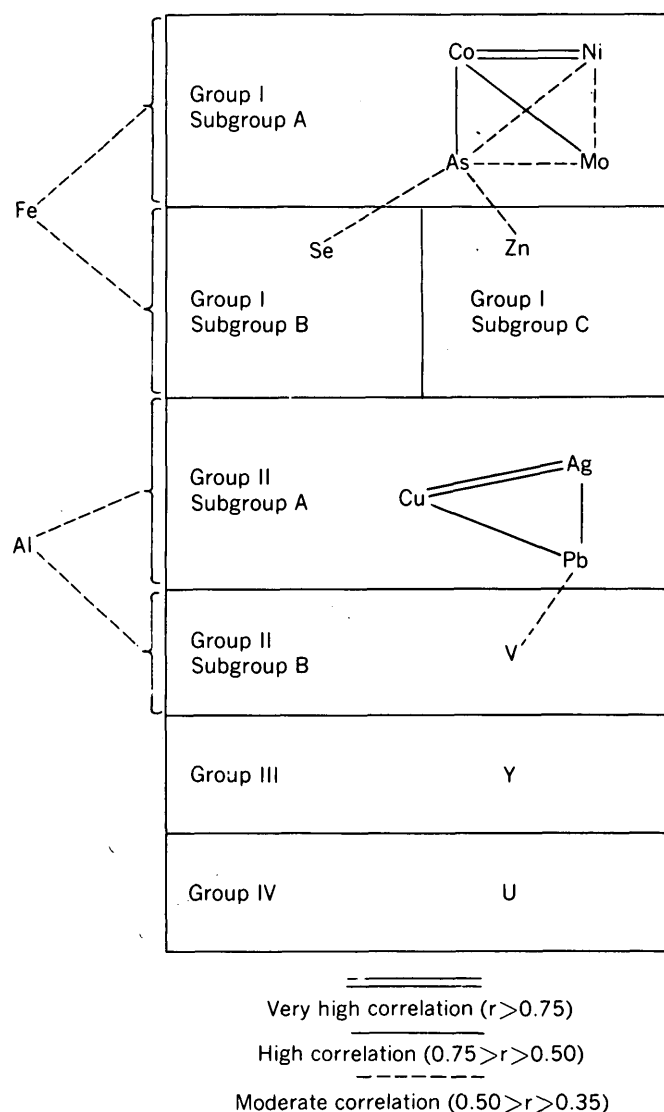
FIGURE 123.1.—Groups of coherent elements in uranium ores from the Salt Wash member of the Morrison formation.

elements studied. Examination of the low correlation coefficients, however, indicates that both yttrium and uranium in the deposits have greater affinities for the Group I elements than for the Group II elements.

All elements in Group I, in addition to iron, tend to be more highly concentrated in uranium deposits of the Salt Wash member of the Morrison formation on the western and northwestern parts of the Colorado Plateau, and in this respect their distributions correspond to the distribution of tuffaceous materials in unmineralized sandstone of the Salt Wash, as determined from lithologic data of R. A. Cadigan (written communication, 1958). Copper, silver, and lead, in Group II, are distinctly more highly concentrated in uranium deposits in the structurally deformed region of the salt anticlines in western Colorado and eastern Utah, a region where vein-type copper-silver deposits are known to occur and where the sandstone of the Salt Wash member tends to contain more copper (and possibly other elements) than sandstone of the same unit elsewhere on the Plateau. Zinc, in addition to being more highly concentrated in deposits on the western and northwestern parts of the Plateau, also tends to be highly concentrated in deposits within the salt anticline region. Vanadium is, in general, more highly concentrated in deposits on the eastern part of the Plateau. The regional distribution of uranium in the deposits has not been determined; the samples which were studied are biased with respect to uranium grade, and the distribution of uranium assays on a map appears random.

Recent study of the abundances and distributions of the elements in uranium deposits and in the altered sandstone that encloses the deposits in a typical mining district (Legin area, San Miguel County, Colo.) shows that the amount of each element added to the deposits, except uranium and vanadium, could have come from the altered sandstone, without the sandstone having had unusually high original concentrations of the elements. However, the regional distributions of the elements in uranium deposits of the Salt Wash member, considered together with the hydrologic and structural history of the Salt Wash and the occurrence of some elements in veins, indicate that sources external to the Salt Wash host rock contributed some elements, and that at least two periods of mineralization occurred.

The broad features of the regional distribution of elements in uranium deposits of the Salt Wash member of the Morrison formation might be explained by the hypothesis outlined below.

After burial of the Salt Wash member by the Brushy Basin member of the Morrison formation, ground water within the Salt Wash was confined and discharge probably minor. As a result, the ground water became nearly stagnant. It is postulated that precipitation of iron and minute amounts of other elements near carbonaceous material caused concentration gradients to be established within the stagnant ground water, and diffusion of iron and other elements toward the carbonaceous material began in response to the gradients. In the chemical environments likely to occur near carbonaceous material (Hostetler and Garrels, written communication), the solubility of iron is highly sensitive to Eh and pH differences. This implies that the concentration gradients of iron in solution were steep and that diffusion of iron may have been relatively rapid. Boundaries or interfaces between nearly stagnant solutions near and more distant from carbonaceous material were established owing to contrasting chemistry of the solutions, and could have remained relatively stable because of the nearly stagnant ground-water conditions. The interfaces were marked by the precipitation of pyrite and other sulfides; these formed roll-type structures. Iron and most other Group I elements that accumulated during this early stage of mineralization could have been derived from devitrification of tuffaceous material in the sandstone within a few hundred feet of the deposits. Deposits on the western part of the Plateau may be richer in these elements because the sandstone there contained more tuff.

At a later stage in the history of the deposits, structural deformation of the Salt Wash and associated rocks occurred on a regional scale in the Salt Valley region of western Colorado and eastern Utah. Numerous northwest-trending faults were developed on the flanks and crests of the anticlines, and the rocks of Early Cretaceous and older age were intruded by laccoliths which are now partially exposed in the La Sal Mountains. The structural deformation opened channels of recharge and discharge and activated ground-water flow within the Salt Wash member. Solutions bearing copper, silver, lead, and zinc (Fischer, 1936, p. 575) deposited these elements as sulfides in several formations along faults in the salt anticline region, and may have enriched the ground waters in these elements. Enrichment of ground water in the Salt Wash member by addition of solutions from an external source may account for the relative high copper content of sandstones

from the Salt Wash in this region, and may also explain why the uranium ores from the Salt Wash member in the salt anticline region contain more copper, silver, lead, and zinc than ores from the Salt Wash in other areas.

Inasmuch as uranium and vanadium could not have been derived from altered sandstone adjacent to the deposits, they must have been derived from more distant sources, and the transporting mechanism was probably flowing solutions, rather than diffusion. Uranium and vanadium may have been deposited during the second stage of mineralization, along with copper, lead, silver, and some of the zinc, but this is uncertain. According to this hypothesis, the forms of the deposits were established by the first stage of mineralization, when pyrite and other sulfides of Group I elements accumulated in roll-structures. Uranium may have been precipitated from solution by the reduction of hexavalent uranium in a complex carbonate ion by the earlier formed

pyrite, thereby preserving the roll-structures as uraniferous ore bodies. In the laboratory, uraninite has been precipitated from aqueous solutions by the reduction of uranium with pyrite (Vickers, 1956). This mechanism explains the common abundance of limonite adjacent to uraniferous ore bodies.

REFERENCES

Fischer, R. P., 1936, Peculiar hydrothermal copper-bearing veins of the northeastern Colorado Plateau: Econ. Geology, v. 31, no. 6, p. 571–599.

Shoemaker, E. M., Miesch, A. T., Newman, W. L., and Riley, L. B., 1959, Elemental composition of the sandstone-type deposits, in Geochemistry and mineralogy of the Colorado Plateau uranium ores, compiled by R. M. Garrels and E. S. Larsen, 3d: U.S. Geol. Survey Prof. Paper 320, p. 25–54.

Vickers, R. C., 1956, Syntheses of pitchblende, in Geologic investigations of radioactive deposits—Semiannual progress report, June 1 to November 30, 1956: U.S. Geol. Survey TEI–640, p. 305, issued by U.S. Atomic Energy Comm. Tech. Inf. Service, Oak Ridge, Tenn., p. 305.

124.   HYDROGEOCHEMICAL ANOMALIES, FOURMILE CANYON, EUREKA COUNTY, NEVADA

By R. L. Erickson and A. P. Marranzino, Denver, Colo.

Results of analyses of spring waters in Fourmile Canyon, Cortez quadrangle, Eureka County, Nev., show marked metal anomalies in a little-prospected area. Spring waters near the head of the canyon are acid sulfate waters that contain as much as 300 ppb (parts per billion) heavy metals (Zn, Cu, Pb); waters near the mouth of the canyon are slightly alkaline bicarbonate-sulfate waters that contain as much as 60 ppb molybdenum.

The springs occur in siliceous clastic rocks of Silurian age in the upper plate of the Roberts Mountains thrust fault (James Gilluly, oral communication, 1960). A quartz monzonite mass intrudes the clastic rocks near the head of the canyon and the strongest base-metal anomaly occurs in springs near the contact of quartz monzonite and clastics (fig. 124.1). Sufficient water issues from these springs to maintain permanent flow a few hundred yards downstream. Between sample localities W–52 and W–52B the pH and heavy metal content of the water were determined at 100-foot intervals; the pH ranges from

4 to 5, sulfate is the principal anion, and the heavy metal content determined with dithizone ranges from 100 to 300 ppb (background in Fourmile Canyon is less than 20 ppb). Spectrographic analyses of the residue after evaporation of the waters show that the chief heavy metal is zinc, but that manganese, nickel, copper, and cobalt are also anomalously high. Coatings of red iron oxide on stream-bottom sediments contain as much as 1,500 ppm arsenic and 20 ppm molybdenum. The source of the acid, high sulfate, and high base metal content of the springs and also the high arsenic content of the iron-oxide precipitate on the stream bottom probably is a concealed oxidizing sulfide deposit.

Bicarbonate-sulfate spring water contains 60 ppb molybdenum at locality W–50 and 15 to 20 ppb molybdenum in adjacent springs (background in Fourmile Canyon is about 2 ppb). There are no rock exposures in the vicinity of W–50 and the source of the molybdenum is unknown.
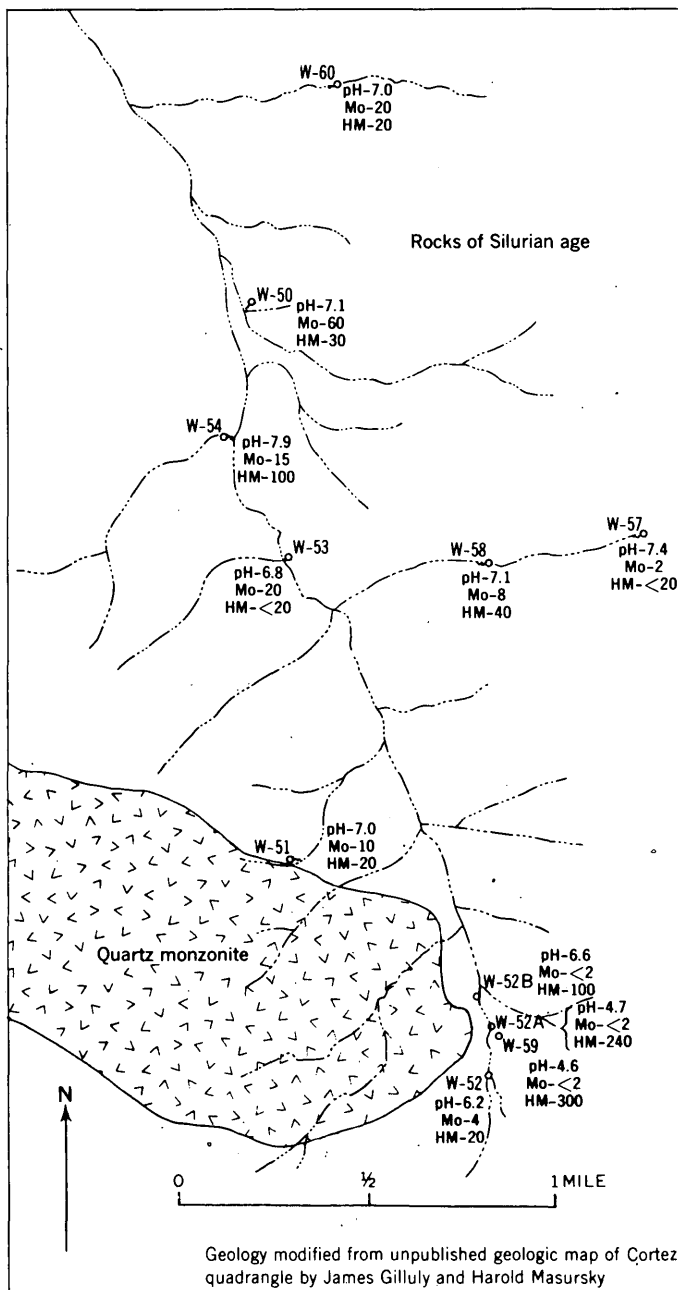
FIGURE 124.1.—Map showing sample locality (W), pH, molyb-
denum (Mo) and heavy metal (HM) content, in parts per
billion, of some spring waters in Fourmile Canyon, Eu-
reka County, Nev.

125. GRANTSITE, A NEW HYDRATED SODIUM CALCIUM VANADYL VANADATE FROM NEW MEXICO AND COLORADO—A PRELIMINARY DESCRIPTION

By A. D. WEEKS, M. L. LINDBERG, and ROBERT MEYROWITZ, Washington, D. C.

Grantsite, a new hydrated sodium calcium vanadyl vanadate, is a dark olive-green to greenish-black mineral which occurs in fibrous aggregates that coat fractures or form thin seams in sandstone or limestone in vanadiferous uranium ores of the Colorado Plateau. It very rarely forms microscopic bladed single crystals. It is soft and smears easily when rubbed—a characteristic of most of the vanadyl vanadate minerals or "corvusite" group to which it belongs.

A small amount of this mineral was first found in an ore sample collected in 1952 by T. W. Stern from an early prospect of the F–33 mine (Anaconda Company, Sec. 33, T. 12 N., R. 9 W.) in Valencia County, near the town of Grants, N. Mex. It comes from the Todilto limestone of Late Jurassic age. Grantsite was also collected in 1954 by A. D. Weeks, R. B. Thompson, and R. F. Marvin from the La Salle Mining Company's shaft on Club Mesa, Montrose County, Colo. and in 1956 by A. D. Weeks and A. H. Truesdell from the Golden Cycle mine on Atkinson Mesa, near Uravan in Montrose County, Colo. The two Colorado samples are from the Salt Wash sandstone member of the Morrison formation of Late Jurassic age. In 1957 during a detailed study of the F–33 mine near Grants, N. Mex., Weeks and Truesdell found much more material and observed the paragenesis and oxidation sequence, which will not be discussed here.

Grantsite is monoclinic with the elongation of the fibers parallel to the b-axis. It usually forms aggregates of extremely fine fibers or narrow blades, similar in habit to the hewettite group of vanadates which are also elongated parallel to the b-axis. Its luster is silky or pearly to subadamantine. The optical properties cannot be determined accurately or completely because of its very fine grain size and high refraction and absorption. The blades or fibers are "length slow." The indices of refraction are α between 1.81 and 1.83, $\beta > 2.0$, and $\gamma > 2.0$. The orientation and pleochroism are X normal to the blade, green, Y parallel to the intermediate dimension of the blade, greenish brown, and Z = b parallel to the length of the blade, brown. The absorption is Z > Y > X. The mineral is biaxial negative.

The strongest lines of the X-ray diffraction powder pattern for sample AW–43–56, Golden Cycle mine, with Cr-radiation, V-filter ($K\alpha_1 = 2.2897$) are as follows in order of decreasing d-spacings in Angstrom units and intensity given as strong S, medium strong MS, and medium M: 12.4 MS, 8.7 S, 4.34 M, 3.719 M, 3.607 MS, 3.008 MS, 2.866 M, 2.715 M, 2.275 M, and 2.240 M. A partially completed set of single-crystal precession and rotation patterns indicates grantsite is monoclinic: $a = 17.54$, $b = 3.60$, $c = 12.45$; $\beta = 95°15'$; unit cell volume = 781A³. The b-axis is the fiber axis; individual fibers are tabular parallel to (100).

Chemical analyses have been completed on sample AW–47–54 from the La Salle mine, AW–43–56 from the Golden Cycle mine, and AW–20–57 from the F–33 mine. All are essentially hydrated sodium calcium vanadyl vanadates but the amount of calcium and V^{+4} varies slightly in the samples. The ratio of the oxides is close to $2Na_2O \cdot CaO \cdot V_2O_4 \cdot 5V_2O_5 \cdot 8H_2O$. The gram-formula-weight as derived from the unit cell volume and the observed density of 2.94 gcm³ is 1383. This corresponds closely to the weight of the oxides as derived from the chemical analysis and equals 1400.

The name grantsite is for the town of Grants, N. Mex., near which the mineral was discovered and later found more abundantly in partly oxidized vanadiferous uranium ore.

126.   INSOLUBLE RESIDUES AND Ca:Mg RATIOS IN THE MADISON GROUP, LIVINGSTON, MONTANA

By Albert E. Roberts, Denver, Colo.

The Madison group is exposed prominently in the lower canyon of the Yellowstone River near Livingston, Mont. It includes the Lodgepole limestone, which is partly Kinderhook and partly Osage in age, and the overlying Mission Canyon limestone, which is partly Osage and partly Meramec in age. Age assignments are similar, in part, to those suggested by Sloss and Moritz (1951, p. 2155) and Sando and Dutro (1960, p. 118). The Lodgepole is 575 feet thick; the Mission Canyon is subdivided into a lower member 330 feet thick, and an upper member 325 feet thick.

Generally, the limestone in the Madison group is massive to thick bedded, finely to coarsely crystalline, light olive gray (5Y5/2)[1], fossiliferous, oolitic, and contains less than 5 percent insoluble residues. The dolomite is generally medium to thin bedded, micro-crystalline, variable in color, but usually light olive gray (5Y6/1) to yellowish brown (10YR6/2), commonly brecciated, and contains more than 5 percent insoluble residues. A few dolomite units are fossiliferous, but most of the fossils are in limestone units. Oolites occur only in massive limestone containing very little insoluble residues. The lithology of the formation is shown on figure 126.1.

Chert is common throughout the carbonate sequence in thin layers along bedding planes or, less commonly, in nodules or lenses. The thin layers have irregular shapes in cross section and they stand out in etched relief on weathered surfaces. The relative amounts of chert and insoluble residues in individual stratigraphic units have no apparent relation.

Dolomite beds in the Madison group include some intraformational breccias and some local breccias caused by readjustment during folding. Laterally persistent breccia beds in the Mission Canyon limestone may be solution breccias resulting from removal of soluble minerals such as anhydrite or gypsum. Similar laterally continuous breccia beds in the Mission Canyon have been described by McMannis (1955, p. 1400) in the Bridger Range, and by Klepper, Weeks, and Ruppel (1957, p. 19) in the Elkhorn Mountains. A bed 5½ feet thick of limestone conglomerate forms the base of the upper member of the Mission Canyon at Livingston. A similar conglomerate is found at the same stratigraphic horizon in the Gallatin Basin, Mont. (Laudon, 1948, p. 295; Andrichuk, 1955, p. 2179) and a breccia zone is found at this horizon in north-central Wyoming (Denson and Morrissey, 1952, p. 40) and in western Wyoming (Strickland, 1956, p. 54).

Calcium-magnesium ratios and percentages of insoluble residues are given on figure 126.1. The Lodgepole limestone has relatively few dolomite or dolomitic limestone strata; the Mission Canyon has considerable dolomite and dolomitic limestone. The Ca:Mg molal ratio curve illustrates a cyclic alternation of carbonate rocks of varying $CaCo_3$–$MgCo_3$ composition. The cycles are imperfect or are not apparent in the lower part of the Lodgepole but become better defined in the Mission Canyon, and in the upper member of the Mission Canyon they are easily demonstrated. The intimate interlayering of dolomite and limestone, as well as the finer crystallinity of the dolomites and a larger content of insoluble residues in the dolomites relative to the limestones are systematic variations that seem most easily explained if most of the limestone and dolomite was deposited directly from sea water. Cyclic deposition of limestone and dolomite in Mississippian rocks is excellently illustrated by Laudon and Severson (1953, p. 509–512) in the Bridger Range, Mont., and cyclic deposits of this age at Logan, Mont., have been observed by G. D. Robinson (1961, oral communication). The fossil assemblages in these rocks indicate normal marine benthonic faunas that probably lived in relatively shallow, well-aerated waters on extensive shelves or in epeiric seas (Dutro, Sando, and Yochelson, 1958, written communication).

The percent-carbonate curve (fig. 126.1) shows, in general, an increase of insoluble residues in the dolomite compared to the limestone. Recent studies by Roy and others (1955), Fairbridge (1957), Dunbar and Rodgers (1957), and Bisque and Lemish (1959) discuss or demonstrate this same relation for dolomites in general.

Insoluble residues in the Madison group at Livingston consist predominantly of clay minerals, fossil fragments, quartz, feldspar (mostly microcline), and chert, and lesser amounts of pyrite, magnetite, tourmaline, zircon, garnet, biotite, and sphene. The clay minerals, identified by X-ray diffraction, are illite,

[1] Designation as shown on the Rock-Color Chart of the National Research Council, 1948.
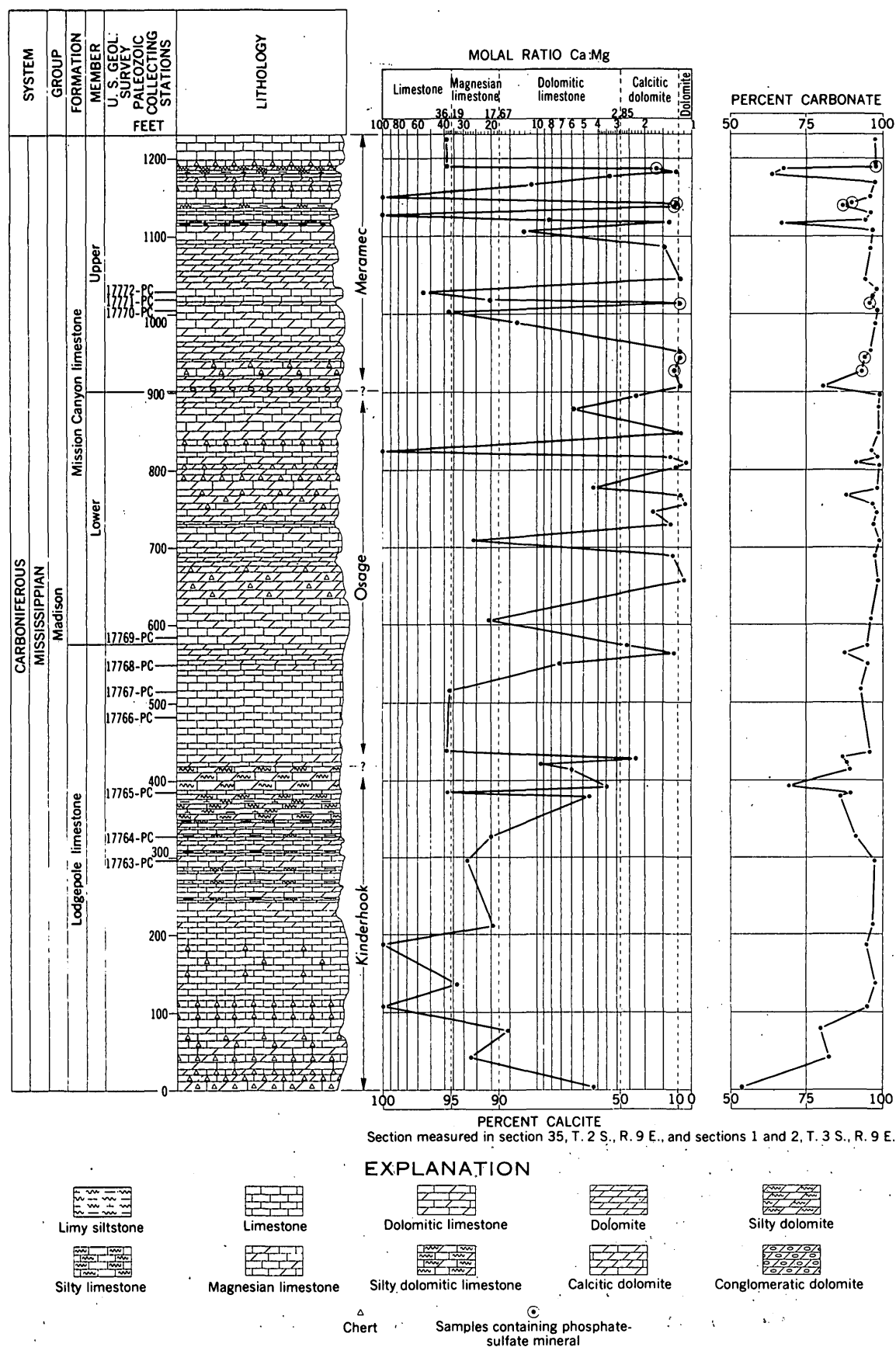
FIGURE 126.1.—Stratigraphic section of the Madison group near Livingston, Mont.

kaolinite, and mixed clays. Illite ranges from 60 to 100 percent of the total clay minerals and averages approximately 90 percent. A few insoluble residues contain as much as 30 percent kaolinite, but most contain 10 percent or less. About half the insoluble residues from the Mission Canyon limestone contain mixed clays (illite and montmorillonite), ranging from a trace to as much as 20 percent. Only one insoluble residue from the Lodgepole limestone contained mixed clays. In the upper member of the Mission Canyon six insoluble residues contained an unidentified hydrous double salt (probably of the beudantite group) very similar to woodhousite [Ca Al$_3$ (PO$_4$) (SO$_4$) (OH$_6$)]. This mineral was found in the dolomites or calcitic dolomites that contained less than 15 percent insoluble residues. Samples containing this mineral generally were rich in kaolinite or mixed clays and poor in illite. Phosphate and sulfate radicals in this mineral suggest incipient deposition of evaporites. The solution-breccia zones and presence of this mineral are consistent with a tentative correlation of the upper member of the Mission Canyon limestone at Livingston with interbedded carbonates and evaporites that elsewhere in Montana make up the Charles formation.

REFERENCES

Andrichuk, J. M., 1955, Mississippian Madison group stratigraphy and sedimentation in Wyoming and southern Montana: Am. Assoc. Petroleum Geologists Bull., v. 39, no. 11, p. 2170–2210.

Bisque, R. E., and Lemish, John, 1959, Insoluble residue— magnesium content relationship of carbonate rocks from the Devonian Cedar Valley formation: Jour. Sed. Petrology, v. 29, no. 1, p. 73–76.

Denson, M. E., Jr., and Morrissey, N. S., 1952, The Madison group (Mississippian) of the Big Horn and Wind River Basins, Wyoming, in Wyoming Geol. Assoc. Guidebook, 7th Ann. Field Conf., p. 37–43.

Dunbar, C. O., and Rodgers, John, 1957, Principles of stratigraphy: New York, John Wiley and Sons, Inc., 356 p.

Fairbridge, R. W., 1957, The dolomite question, in Le Blanc and Breeding, eds., Regional aspects of carbonate deposition—a symposium: Soc. Econ. Paleontologists and Mineralogists Spec. Pub. no. 5, p. 125–178.

Klepper, M. R., Weeks, R. A., and Ruppel, E. T., 1957, Geology of the southern Elkhorn Mountains, Jefferson and Broadwater Counties, Montana: U.S. Geol. Survey Prof. Paper 292, 82 p.

Laudon, L. R., 1948, Osage-Meramec contact, in Weller, J. M., ed., Symposium on problems of Mississippian stratigraphy and correlation: Jour. Geology, v. 56, no. 4, p. 288–302.

Laudon, L. R., and Severson, J. L., 1953, New crinoid fauna, Mississippian, Lodgepole formation, Montana: Jour. Paleontology, v. 27, no. 4, p. 505–536.

McMannis, W. J., 1955, Geology of the Bridger Range, Montana: Geol. Soc. America Bull., v. 66, no. 11, p. 1385–1430.

Roy, C. J., Thomas, L. A., Weissmann, R. C., and Schneider, R. C., 1955, Geologic factors related to quality of limestone aggregates: Highway Research Board Proc., v. 34, p. 400–412.

Sando, W. J., and Dutro, J. T., Jr., 1960, Stratigraphy and coral zonation of the Madison group and Brazer dolomite in northeastern Utah, western Wyoming, and southwestern Montana, in Wyoming Geol. Assoc. Guidebook, 15th Ann. Field Conf., p. 117–126.

Sloss, L. L., and Moritz, C. A., 1951, Paleozoic stratigraphy of southwestern Montana: Am. Assoc. Petroleum Geologists Bull., v. 35, no. 10, p. 2135–2169.

Strickland, J. W., 1956, Mississippian stratigraphy, western Wyoming, in Wyoming Geol. Assoc. Guidebook, 11th Ann. Field Conf., p. 51–57.

127.   MANGANESE OXIDE MINERALS AT PHILIPSBURG, MONTANA

By WILLIAM C. PRINZ, Washington, D. C.

The Philipsburg district is underlain by sedimentary and metamorphic rocks of Precambrian and early Paleozoic age that have been intruded by a granodiorite batholith of Tertiary age. The sedimentary rocks consist of limestone, dolomitic and calcitic marble, shale, and quartzite that have been folded into a broad north-plunging anticline (Goddard, 1940, pl. 26). Hydrothermal veins containing quartz, sphalerite, galena, silver- and copper-bearing sulfides, barite, and late rhodochrosite cut both the granodiorite and the sedimentary rocks. These veins strike west or northwest and have steep southerly dips or are vertical. Late hydrothermal rhodochrosite has partly replaced some favorable limestone and marble beds adjacent to some veins. In thin limestone or marble beds, the replacement deposits

follow bedding closely and form tabular ore bodies. In massive or thick-bedded marble they tend to be irregular vertical pipes that swell in more favorable beds and pinch in less favorable ones. Sphalerite, some silver, and sparse galena accompany rhodochrosite in the primary replacement deposits in parts of the district.

Oxidation of rhodochrosite by ground water has produced various manganese oxide minerals. The following have been identified by X-ray and microscopic techniques:

Todorokite $((Ca,Na,Mn^{II},K) (Mn^{IV},Mn^{II},Mg)_6O_{12} \cdot 3H_2O)$ until recently was considered rare as it had been observed only at its type locality in Japan, but in the last year it has been identified at numerous localities. At Philipsburg it is widely distributed in the oxidized replacement deposits where it forms aggregates of irregular or fibrous grains. It is commonly pseudomorphous after carbonate minerals or in bands with cryptomelane, gamma-MnO_2, or pyrolusite.

Cryptomelane $(KR_8O_{16}, R = Mn^{II},Mn^{IV})$ was first identified in the Philipsburg oxide ore by Richmond and Fleischer (1942, table 1). It is probably one of the more abundant oxide minerals in the district, but to date I have done little chemical work on the mineral and some of the material that I have identified as cryptomelane may be one of the other members of the psilomelane group. Cryptomelane and gamma-MnO_2 comprise the bulk of the material called "psilomelane" in hand specimen.

Gamma-MnO_2 is hard (about 6), anisotropic, and white with a faint cream tint in polished section. It gives X-ray patterns similar to those of synthetic gamma- and rho-MnO_2 and is probably the same mineral described by Sorem and Cameron (1960) as Nsuta MnO_2. It is in bands with cryptomelane and todorokite, forms pseudomorphs after carbonate minerals, and is in late veinlets that cut earlier formed manganese oxides.

Pyrolusite (MnO_2) is commonly a late mineral that lines vugs in quartz or earlier formed oxide minerals. Some also formed with the other oxides and has a habit similar to theirs.

Chalcophanite $((Mn^{II}, Zn)Mn^{IV}_2O_5 \cdot 2H_2O)$ is commonly late and fills vugs, but it is also in bands with cryptomelane, in tiny prisms in a fine-grained matrix of todorokite, and in stalactites with hetaerolite and todorokite.

Hetaerolite $(ZnMn_2O_4)$ was found in only a few samples from oxidized veins where it is associated with chalcophanite.

Manganite $(Mn_2O_3 \cdot H_2O)$ is rare. In one place it formed early and is cut by later manganese oxide minerals; in another it was formed late and lines vugs in earlier formed oxides.

Wad, the soft, dark brown to black earthy material, was shown by X-ray analysis to consist of one or more of the following minerals: todorokite, cryptomelane, chalcophanite, pyrolusite, or goethite.

Cryptomelane, todorokite, gamma-MnO_2, and pyrolusite are the most abundant manganese oxide minerals at Philipsburg (probably in that order), chalcophanite is locally abundant, hetaerolite and manganite are rare. Todorokite is restricted to the oxidized replacement deposits, probably because of the availability of calcium in these deposits and its absence in the veins. The zinc-bearing manganese oxides, chalcophanite and hetaerolite, are found in or adjacent to oxidized veins or in oxidized replacement deposits only in areas where the primary rhodochrosite is accompanied by sphalerite. These two minerals may prove to be valuable guides to the exploration for deeper primary rhodochrosite deposits that also contain sphalerite.

The depth of oxidation ranges from as little as 100 feet in some impure limestone beds to more than 850 feet in massive coarse-grained marble where open cavities and water courses are common. Unoxidized remnants of rhodochrosite are preserved within some oxidized ore bodies or below impermeable beds.

I agree with the suggestion of Pardee (1921, p. 155) that the formation of the manganese oxide minerals was accompanied by only limited migration and secondary concentration of manganese.

REFERENCES

Goddard, E. N., 1940, Manganese deposits at Philipsburg, Granite County, Montana: U.S. Geol. Survey Bull. 922–G, p. 157–204.

Pardee, J. T., 1921, Deposits of manganese ore in Montana, Utah, Oregon, and Washington: U.S. Geol. Survey Bull. 725–C, p. 141–177.

Richmond, W. E., and Fleischer, M., 1942, Cryptomelane, a new name for the commonest of the "psilomelane" minerals: Am. Mineralogist, v. 27, p. 607–610.

Sorem, R. K., and Cameron, E. N., 1960, Manganese oxides and associated minerals of the Nsuta manganese deposits, Ghana, West Africa: Econ. Geology, v. 55, p. 278–310.

128.   URANIUM AND RADIUM IN GROUND WATER FROM IGNEOUS TERRANES OF THE PACIFIC NORTHWEST

By FRANKLIN B. BARKER and ROBERT C. SCOTT, Denver, Colo.

Water samples from the igneous terranes of the Pacific Northwest were collected and analyzed for uranium and radium as part of a study of the geochemistry of radioelements. For this work these igneous terranes were divided into those developed on the Idaho batholith (silicic intrusive terrane), Columbia River basalt, Snake River basalt, and silicic-subsilicic volcanic rocks. The data on radium and uranium concentrations in water from each terrane were analyzed statistically so that characteristic parameters could be obtained and compared.

The concentrations of uranium in water from each terrane except the Snake River basalt are in excellent agreement with log-normal distributions. The samples from the Snake River basalt showed a uranium-concentration distribution that was skewed to the left (lower concentration). The concentrations of radium in all of these terranes were so low that only small portions of the distribution curves were above the detection limit, 0.1 pc/1 (picocuries per liter; 1 pc = 10^{-12} curies), and could readily be examined. In all instances, however, these portions were found to agree with log-normal distributions; therefore, these distributions have been assumed to be valid for the entire range of concentrations. The statistical parameters applicable to the radium and uranium concentrations in water from the various terranes are given in table 1. The geometric means are those obtained from the assumed log-normal distributions. No value is reported for the geometric mean of uranium concentrations in water from the Snake River basalt because a log-normal distribution does not fit the data.

TABLE 1.—*Statistical parameters relating to concentrations of uranium and radium in water from igneous terranes*

Terrane	Number of samples	Uranium μg/l[1]			Radium pc/1		
		Range	Median	Geometric mean	Range	Median	Geometric mean
Silicic-subsilicic rocks.........	73	<0.1–10	0.2	0.3	<0.1–62	0.1	0.1
Idaho batholith..	41	<0.1–13	.1	.07	<0.1–6.0	<.1	.03
Snake River basalt..	82	<0.1–2.6	1.4	....	<0.1–17	<.1	.03
Columbia River basalt.........	30	<0.1–0.6	.1	.1	<0.1–10	<.1	<.01

[1] μg/l = micrograms per liter or (approximately) parts per billion.

The relative abundances of uranium in igneous rocks are generally in the order: silicic extrusive > silicic intrusive > basic extrusive. The relative abundance of radium should roughly parallel the abundances of uranium. The concentrations of uranium in the water samples were in the order: Snake River basalt > silicic-subsilicic volcanic rocks > Columbia River basalt ≈ Idaho batholith; the concentrations of radium, on the basis of the estimated geometric means, were in the order: silicic-subsilicic volcanic rocks > Idaho batholith ≈ Snake River basalt > Columbia River basalt. The apparent disorder of concentrations of uranium in water with respect to the abundances of uranium in rocks has been attributed partly to climatological and topographical factors for the Idaho batholith, and to man's agricultural developments on the Snake River Plain.

The Idaho batholith is a mountainous region that receives much more precipitation than the other terranes, with an annual average of more than 20 inches over the entire area, compared with less than 10 inches for most of the area underlain by the silicic-subsilicic volcanic rocks and the Snake River basalt (Visher, 1954). Except for joints and other fractures, the permeability and porosity of the rocks of the batholith are lower than those of the other terranes. Thus, as ground water moves more rapidly through the jointed granitic rocks it has only a limited degree of rock-water contact, and, hence, has less opportunity to dissolve mineral matter. The concentrations are further reduced by dilution with the relatively large quantities of recharge resulting from the high precipitation rates. The flushing action of the large volumes of flow also contributes to the low concentrations in that much of the readily soluble material has already been dissolved and carried out of the area. As might be expected on the basis of this reasoning, the concentrations of all dissolved matter tends to be lower than in water from the other terranes. Variations in composition of the rocks probably contribute also to the observed differences in uranium concentrations.

The Snake River Plain, which includes most of the area of the Snake River basalt, has been developed agriculturally in many areas, and both ground water and surface water are used extensively for irrigation. Irrigation water dissolves ad-

ditional mineral matter from the soil and is further concentrated by evapotranspiration during its use; the unconsumed water then returns to the ground-water reservoir as a more concentrated solution. Much of the water tributary to the Snake River Plain originates in the adjacent silicic volcanic rock terranes, thus the recharge to the Snake River basalt has uranium concentrations greater than would be expected to be derived from the basalt. Another factor that, possibly, contributes uranium to solution is that small amounts of uranium are present in some commercial high-phosphate fertilizers. The skewness of the observed distribution could have arisen if a few of the samples were from low-uranium water, representing a normal basalt terrane, and if a larger number of samples were from sources affected by one or more of those factors leading to abnormal concentrations of uranium. The water samples from the Columbia River basalt probably are more representative of the normal uranium content in ground water from basalt terranes.

The concentrations of radium in water from the Idaho batholith are less than those in water from the silicic-subsilicic volcanic rock terrane in about the same ratio as the differences in uranium concentrations. This phenomenon might be explained partly by the large differences in annual precipitation; however, variations in composition of the rocks may also contribute to the differences in concentrations.

The concentrations of radium in water from the Snake River basalt are higher than those from the Columbia River basalt, but they are not so anomalous as the uranium concentrations in water from the Snake River basalt. Radium is subject to the same concentrating processes as uranium, but it has not been enriched in the water of the Snake River basalt to the same extent as uranium. The basalt underlying the Snake River plain contains many intercalated lacustrine and other sedimentary beds of clastic material. Clays in this sedimentary material may have adsorbed some of the radium by cation exchange, thus reducing its concentration. The uranium, which probably exists in solution as an anionic uranyl carbonate complex, is not adsorbed effectively by this mechanism. Removal of radium from solution in this or some other manner would partly compensate for the factors tending to cause enrichment.

The observations discussed in this report are not definitive; however, they do indicate some general trends regarding the concentrations of uranium and radium to be expected in water from igneous terranes. More detailed examination of possible interrelations, both among samples from individual terranes and among parameters characteristic of the different terranes, may define better the roles of various geologic, hydrologic, and geochemical factors in controlling the occurrence of uranium and radium in water.

REFERENCE

Visher, S. S., 1954, Climatic atlas of the United States: Cambridge, Mass., Harvard Univ. Press, p. 197.

129.   SBORGITE IN THE FURNACE CREEK AREA, CALIFORNIA

By JAMES F. MCALLISTER, Menlo Park, Calif.

Work done partly in cooperation with the California Division of Mines

Sborgite ($Na_2O \cdot 5B_2O_3 \cdot 10H_2O$), which Cipriani (1957) described as a new mineral from Larderello, Italy, has been found in a different environment in the Furnace Creek area, Death Valley region, California. The sborgite at Larderello is in fine-grained mixtures of borax and thenardite that encrust artificial conduits for natural steam; samples were recovered from depths between 104 and 256 meters some time after eruption of steam at 180° to 200°C had ceased (Cipriani, 1957, p. 520). In contrast, sborgite in the Furnace Creek area is unrelated to steam vents or thermal springs, but forms virtually at the surface

by common processes that redistribute constituents of borate minerals under the control of the present desert climate. At three separate places near the Twenty Mule Team Canyon road, sborgite has been found locally concentrated within a few centimeters of the surface of the ground in debris weathered from the underlying Furnace Creek formation. In the Widow No. 3 mine [1], 10 miles southeast of Twenty Mule Team Canyon, sborgite is a constituent of small stalactites on an ore chute near the surface.

At two localities near the Twenty Mule Team Canyon road, concentrations of sborgite are localized in surficial debris around weathering colemanite and priceite veins in altered fragmental basalt. The veins lie stratigraphically above a zone that contains commercial deposits of colemanite and ulexite. Relationships of other borate minerals in the varied assemblages associated with sborgite and derived from the same veins have been briefly described (Erd, McAllister, and Vlisidis, 1961). Sborgite, like sassolite or ginorite, generally is distributed farther from the decomposing vein, whereas meyerhofferite, gowerite, and nobleite generally remain nearer the vein. No other hydrous sodium borate mineral has been identified in these assemblages, which contain minerals consisting of boric acid or a hydrous borate of calicum, sodium-calcium, calcium-magnesium, or magnesium.

Concentrations of sborgite at the third locality are limited to a strip about a meter wide along the strike of tilted beds of saline, tuffaceous siltstone and sandstone. Much of this sborgite is associated with halite and thenardite in a layer as much as 15 cm thick that lies on bedrock. Above the bottom layer, a conspicuous efflorescence of thenardite, like that left by the dessication of mirabilite, makes an incoherent but more persistent layer about 8 cm thick, which in turn is covered by a thin crust of very fine-grained debris. The underlying siltstone and sandstone, in contrast to the basaltic rocks, do not contain veins of colemanite and priceite or other obvious accumulations of borate minerals. The source of the sborgite, thenardite, and halite seems to be minerals disseminated in the clastic rocks and secondarily encrusted on minor joint surfaces.

Stalactites that contain sborgite were formed at the foot of an ore chute in the Widow No. 3 mine about 25 meters below the surface where storm water could seep down through colemanite ore in

[1] Property of the United States Borax & Chemical Corp., Los Angeles, Calif., which owns also the other specified sites within the boundary of Death Valley National Monument.

TABLE 1.—*Comparison of X-ray diffraction data for sborgite from California and Italy*

[Only reflections having d-spacings between 10.0 and 2.000 A and having intensities greater than 1/2 are listed]

Furnace Creek, chart X-923 [1] sborgite		Synthetic Na₂O·5B₂O₃·10H₂O (Cipriani, 1957)		Larderello, Italy; sample 10; sborgite, borax, and thenardite (Cipriani, 1957)	
d-spacing (A)	Intensity	d-spacing (A)	Intensity[2]	d-spacing (A)	Intensity[2]
8.59	2	8.62	2	8.58	2
8.19	2	8.22	2	8.21	2
....	....	....	....	7.79	1
....	....	....	....	7.14	2
6.86	2	6.88	4	6.84	2
6.24	2	6.24	1	6.23	2
6.11	1	6.12	1	....	....
....	....	....	....	5.97	1
....	....	....	....	5.69	3
....	....	....	....	5.37	1
....	....	....	....	5.15	1
5.11	2	5.10	1	5.11	1
4.80	1	4.81	1	4.84	5
4.60	10	4.60	10	4.59	10
4.35	2	4.35	2	4.34	2
4.29	3	4.29	3	4.28	3
4.11	2	4.11	1	4.09	1
....	....	....	....	3.93	2
....	....	....	....	3.83	2
3.74	5	3.74	2	3.73	4
3.56	3	3.56	4	3.55	3
3.52	3	3.54	4	3.52	4
....	....	....	....	3.44	1
3.33	1	3.35	2	3.34	1
3.30	8	3.30	8	3.29	8
3.20	7	3.20	8	....	....
3.18	5	....	....	3.18	7
3.12	1	3.13	1	3.13	2
....	....	....	....	3.07	5
3.04	2	3.04	2	3.04	3
2.95	2	2.95	1	2.94	2
2.93	3	2.93	2	2.92	3
2.86	2	2.865	2	2.827	4
....	....	....	....	2.784	5
....	....	2.676	2	2.669	1
2.64	1	....	....	2.646	3
2.57	2	2.572	4	2.564	5
2.40	1	2.409	1	2.406	1
2.35	1	2.350	1	....	....
....	....	....	....	2.329	2
....	....	2.274	1	....	....
2.25	1	2.253	1	2.253	1
2.21	1	2.215	2	2.210	2
2.17	1	2.177	1	....	....
....	....	2.169	1	2.173	1
2.14	1	2.139	1	2.140	2
2.09	1	2.090	1	2.085	1
....	....	....	....	2.073	1
....	....	....	....	2.064	1
....	....	....	....	2.037	1
....	....	2.025	2	....	....

[1] CuK α (Ni filter), λ = 1.5418A
[2] Intensities recorded by Cipriani have been rounded to the nearest whole number, maximum 10.

the chute. Several nearby openings to the surface on the same level as the stalactites provided good circulation of desert air for evaporating the saline solution that deposited a highly soluble fine-grained mixture of thenardite, sborgite, and halite. These

minerals go into solution readily in water at 26°C. The largest stalactite is 20 mm in diameter; a slender one, ovate in section, is from 5 to 10 mm in diameter. The stalactites consist of a shell of sborgite, thenardite, and some halite, from a fraction of a millimeter to about 3 mm thick, that encloses a more friable mixture of thenardite, halite, and an unidentified borate. The rate of growth is not known, but the age is no more than 35 years, which is the length of time since mining stopped in the mid-1920's.

The sborgite occurs in sugary-textured crystal aggregates and mesh-work in loosely coherent weathered materials. Anhedral to euhedral crystals are colorless and generally 0.05 to 0.2 mm in diameter, but some are nearly 1 mm. The following combination of optical properties distinguishes sborgite from other known borate minerals: biaxial positive, moderately small optic angle, lowest measured index of refraction 1.432 ± 0.002, and highest measured index of refraction 1.488 ± 0.003. R. C. Erd (written communication, 1958) has provided X-ray powder diffraction data given on table 1, and pointed out the close similarity to data for sborgite and synthetic $Na_2O \cdot 5B_2O_3 \cdot 10H_2O$ as reported by Cipriani (1957, table 1).

REFERENCES

Cipriani, Curzio, 1957, Un nuovo minerale fra i prodotti boriferi di Larderello: Accad. naz. Lincei, Atti, classe sci. fis., mat. e nat., Rend., v. 22, p. 519–525.

Erd, R. C., McAllister, J. F., and Vlisidis, A. C., 1961, Nobleite, another new hydrous calcium borate from the Death Valley region, California: Am. Mineralogist, v. 46, p. 560–571.

GEOLOGY AND HYDROLOGY APPLIED TO ENGINEERING AND PUBLIC HEALTH

130. ECONOMIC SIGNIFICANCE OF A BURIED BEDROCK BENCH BENEATH THE MISSOURI RIVER FLOOD PLAIN NEAR COUNCIL BLUFFS, IOWA

By Robert D. Miller, Denver, Colo.

Industrial plants are beginning to dot the flood plain of the Missouri River in ever-increasing numbers since the completion of several flood-control dams along the Missouri River north of Omaha, Nebr. and Council Bluffs, Iowa. Availability of large tracts of level land, ample cheap water for industrial uses, and access to transportation are major factors in building on the flood plain. Absence of bedrock near the surface of the flood plain can, at places, require costly types of foundation construction.

Bedrock configuration was studied as part of an investigation of the geology of the Omaha-Council Bluffs area. In most places bedrock is more than 100 feet below the flood plain. Southeast of Council Bluffs, however, a well-defined bedrock bench lies within 100 feet of the surface. The northern edge of the bench is about 3 miles southeast of Council Bluffs, about 1½ miles east of Lake Manawa, and about 1 mile east of the channel of the Missouri River (fig. 130.1). The bench underlies the southern part of sec. 20, and all of sec. 29 and 32, T. 74 N., R. 43 W., and sec. 5 and part of sec. 8, T. 73 N., R. 43 W. This bench is more than 3 miles long and 1 mile wide, is 80 to 90 feet below the flood plain, and has a nearly level surface. On the west the bench slopes gradually to depths of about 130 and 141 feet.

The bedrock surface east of the bench proper is lower—more than 95 feet below the surface—which may indicate the presence of an old channel. The channel (?) may cross the northern part of sec. 20, T. 74 N., R. 43 W., but this is not definitely established. Bedrock is only 80 feet below the surface in the southeastern part of sec. 17, T. 74 N., R. 43 W.; bedrock at this depth suggests that there may be a northern remnant, or perhaps an extension, of the bedrock bench. Bedrock in the northern part of sec. 17, T. 74 N., R. 43 W. is more than 95 feet below the surface of the flood plain.
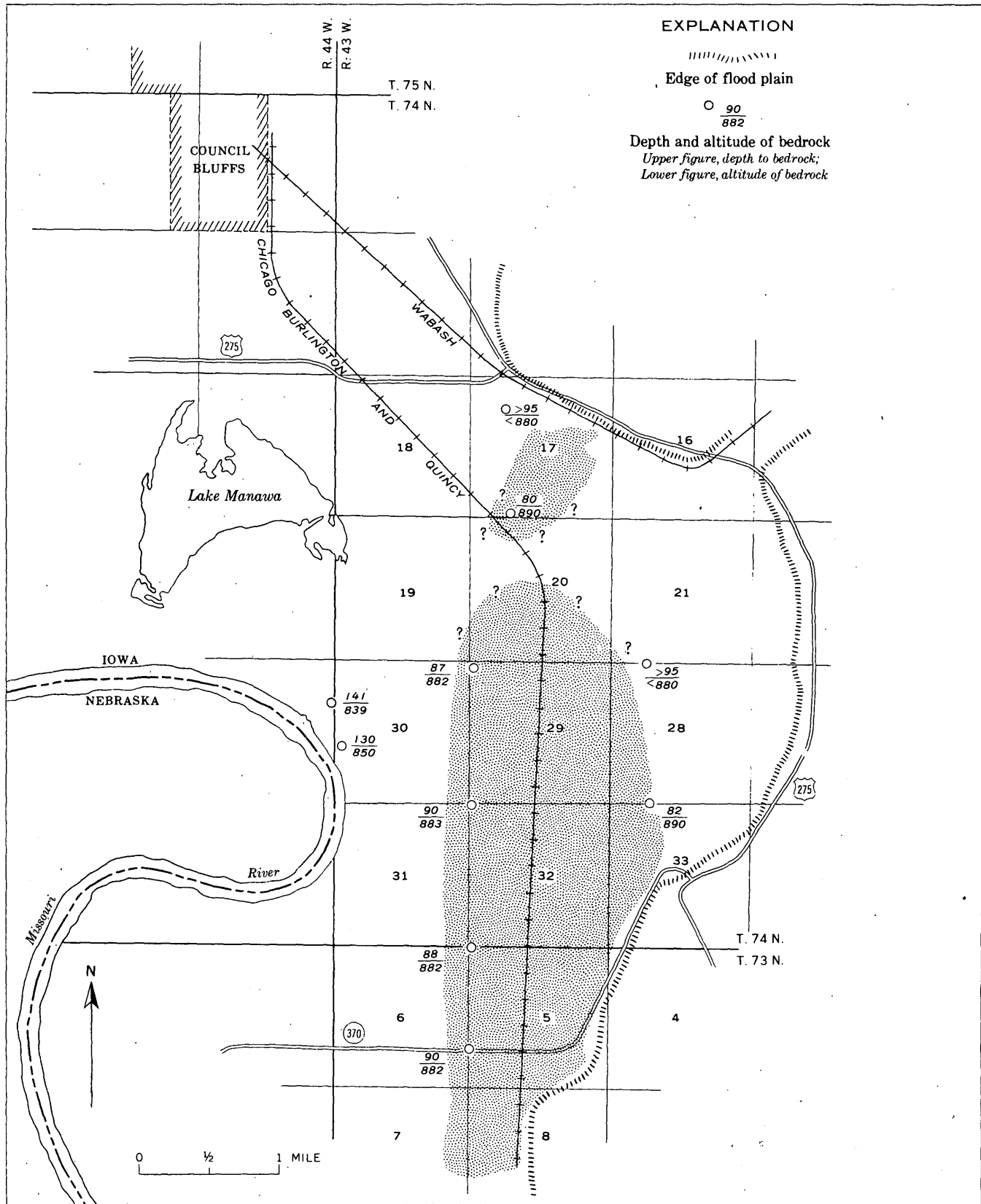
FIGURE 130.1.—Map showing location of area underlain by bedrock bench near Council Bluffs, Iowa.

The bedrock bench consists of limestone of Pennsylvanian age that would provide a stable foundation for piles. Water-saturated alluvium overlies the bench and consists of fine, medium, and coarse sand, as well as layers of fine to medium gravel; no consolidated layer intervenes between the bedrock bench and the ground surface. Access to the bench area is provided by U.S. Highway 275, Iowa State Road 370, and the Chicago, Burlington, and Quincy Railroad.

Suitable foundation conditions, good accessibility into the area, and ample water from the underlying alluvium indicate this area to be a potential industrial site.

⚒

131. RELATION OF SUPPORTS TO GEOLOGY IN THE HAROLD D. ROBERTS TUNNEL, COLORADO

By E. E. WAHLSTROM, L. A. WARNER, and C. S. ROBINSON, University of Colorado, Boulder, Colo., and Denver, Colo.

Geologic conditions played an important part in the location and engineering of the Harold D. Roberts Tunnel, which extends for 23.3 miles from near Dillon to near Grant, Colo. (fig. 131.1). Among the engineering problems directly due to the geologic conditions was the use of supports during construction of the tunnel.

The purpose of the tunnel, which holed through in February 1960, is to bring water from the Blue River on the western side of the Continental Divide to the Platte River on the eastern side where it will be utilized as part of the water supply of Denver and environs. Construction was by the Blue River Constructors, Inc., under the supervision of Tipton and Kalmbach, Inc., for the Board of Water Commissioners of the City and County of Denver.

The regional geology in the vicinity of the tunnel has been described by T. S. Lovering (1935). Geologic investigations from 1943 to 1960 (prior to and during construction of the tunnel) were made by E. E. Wahlstrom assisted by L. A. Warner and V. Q. Hornback. In 1960 the U.S. Geological Survey established a project to compile and publish the geology as related to the engineering. This article is a preliminary report of that project.

GENERAL GEOLOGY

The geology of the Roberts Tunnel, as it affects engineering problems, can be divided into five sections: (a) a section of sedimentary rocks between the west portal and the Williams Range thrust, (b) the Williams Range thrust plate, (c) the sedimentary rocks between the Williams Range thrust and the Montezuma stock, (d) the Montezuma quartz monzonite stock, and (e) the Precambrian rocks between the Montezuma stock and the east portal. Figure
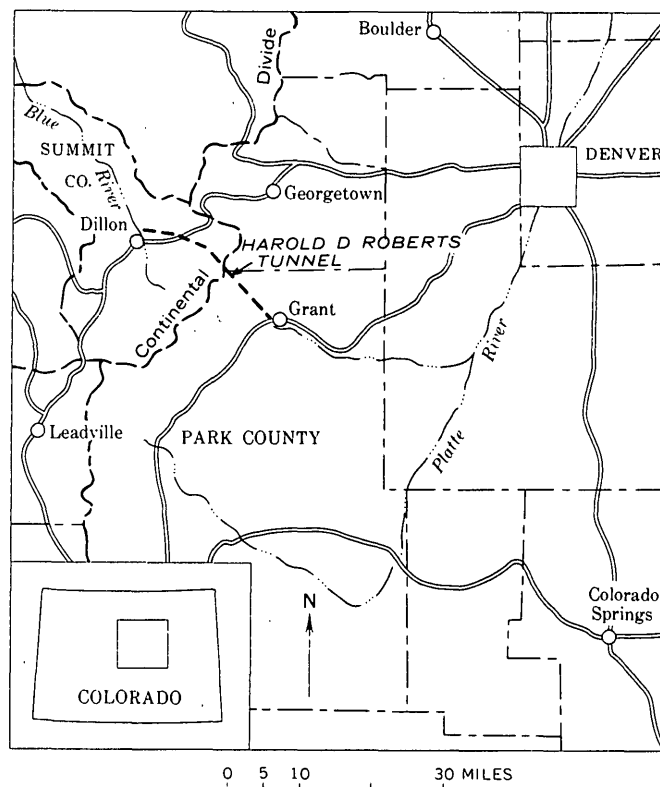
FIGURE 131.1.—Index map showing location of the Harold D. Roberts Tunnel.
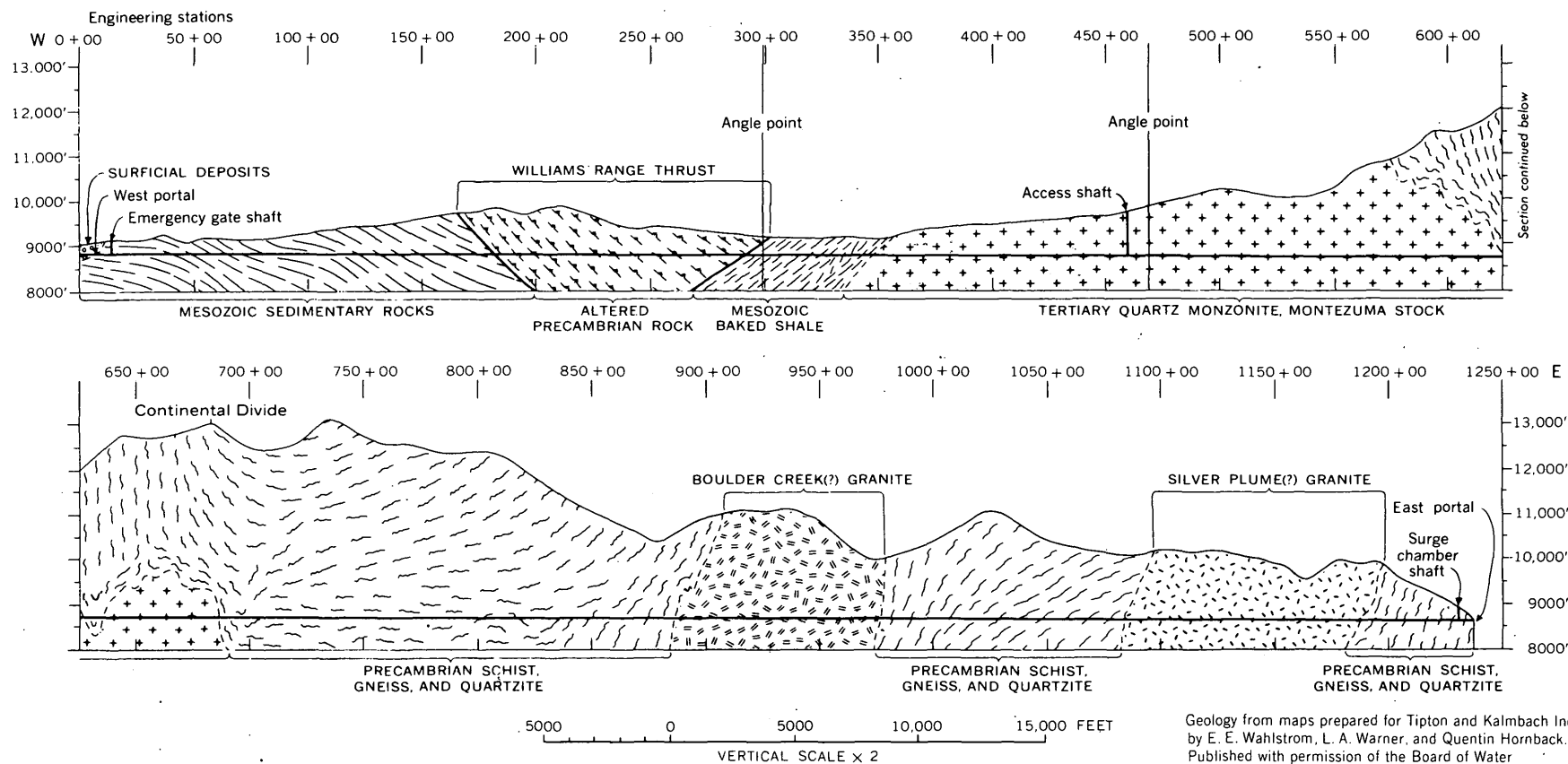
FIGURE 131.2.—Generalized geologic section through the Harold D. Roberts Tunnel.

131.2 is a geologic section through the tunnel showing the distribution of the principal rock types.

The shale, sandstone, and limestone of Mesozoic age between the west portal and the Williams Range thrust have been extensively folded and faulted. The Williams Range thrust plate is brecciated Precambrian rock of uncertain original composition that was silicified and later extensively faulted. The metasedimentary rock east of the Williams Range thrust plate probably is equivalent to some part of the section west of the thrust plate, but it has been baked to a black brittle hornfels by the intrusion of the Montezuma stock. The Montezuma stock consists of fine- to medium-grained locally porphyritic biotite quartz monzonite, which probably was intruded during the Laramide orogeny. The Precambrian schist, gneiss, quartzite, and lime-silicate rocks between the Montezuma stock and the east portal are complexly interlayered and injected with large and small bodies of granite, granodiorite, pegmatite, and aplite. The rock of one of the larger plutons resembles the Boulder Creek granite (Lovering and Goddard, 1950, p. 25-27). Near the east portal is granitic rock, containing many bodies of schist and gneiss, similar to the Silver Plume granite (Lovering and Goddard, 1950, p. 28).

SUPPORTS IN RELATION TO GEOLOGY

The geologic factors that influenced the use of supports are layering in the rock, spalling and popping rock, faults and joints, and squeezing and swelling rock. Table 1 summarizes the relation between supports and geology.

The supports used are 6- and 8-inch steel horseshoe-shaped H ribs supported on wooden footblocks, with struts across the tunnel invert where necessary. Tie rods were used between ribs, and wooden lagging and wedges were placed above and on the sides of the ribs as required. The steel supports will be left in the tunnel as part of the reenforcing for the concrete lining.

LAYERING IN ROCK

Two types of layering contributed to the need for supports—stratification in the sedimentary rocks and layering in the schist and gneiss.

The sedimentary rocks west of the Williams Range thrust (fig. 131.2) dip northeast at angles ranging from a few degrees to 30°. Consequently, the beds, especially in the shaly rocks, were flat enough in the tunnel arch to tend to break away from bedding planes if unsupported. Sets on 5-foot centers gen-

TABLE 1.—*Summary of relation of tunnel supports to geology*

Section (stations)	Percent supported	Average spacing of sets (in feet)	Remarks
9+46 (west portal) to 43+14............	75.5	4.9	Mesozoic sedimentary rocks. Unsupported section in quartzite of Dakota group only.
43+14 to 180+20......	100	3.9	Mesozoic sedimentary rocks below Williams Range thrust. Mostly shales, limy shales, and sandy shales.
180+20 to 291+50.....	100	2.5	Highly fractured and altered Precambrian schist, gneiss, and aplite in plate above Williams Range thrust.
291+50 to 339+75.....	100	4.2	Baked shale below Williams Range thrust.
339+75 to 347+50.....	60.9	5.0	Mixed quartz monzonite and baked shale in border zone of Montezuma stock.
347+50 to 625+00.....	88.0	4.7	Quartz monzonite of Montezuma stock.
625+00 to 636+85.....	58.6	5.0	Quartzite roof pendant in Montezuma stock.
636+85 to 686+50.....	72.4	5.0	Quartz monzonite of Montezuma stock.
686+50 to 886+20.....	69.9	4.5	Precambrian schist, gneiss, and quartzite with minor aplite, pegmatite, and granite.
886+20 to 977+00.....	52.3	5.1	Boulder Creek(?) granite (granodiorite) with minor inclusions of metamorphic rocks.
977+00 to 1084+00....	48.9	4.8	Precambrian schist and gneiss with minor aplite, pegmatite, and granite.
1084+00 to 1187+50...	24.0	4.8	Silver Plume(?) granite with numerous inclusions of schist, gneiss, and quartzite.
1187+50 to 1238+58 (east portal)........	7.3	4.5	Precambrian schist, gneiss, and lime silicates injected by granite and pegmatite.

erally proved adequate to prevent detachment of slabs. The only section of sedimentary rock west of the Williams Range thrust that did not require support was massive quartzite of the Dakota group near the west portal. The stratification of the metasedimentary rock east of the Williams Range thrust was largely obliterated and therefore little support was needed.

The layering in the schist and gneiss between the Montezuma stock and the east portal is commonly contorted, and the attitude of this layering in relation to the bearing of the tunnel determined to a large extent whether or not supports were needed. Where the layering dips steeply, few or no supports were required, but where the layering is flat, supports were required, usually on 5- or 6-foot centers. The schist and gneiss in the Williams Range thrust plate were silicified so layering in these rocks was not a factor in the need for support.

SPALLING AND POPPING ROCK

Spalling and popping rock, although not a serious problem, was encountered chiefly in that part of the tunnel extending southeast from station 595 + 00 in the Montezuma stock into the Precambrian rock at about station 965 + 00 (fig. 131.2). The thickness of cover in this portion of the tunnel ranges from about 1,500 to 4,500 feet. Spalling in parts of the tunnel continued for several hours after the rock was exposed and supports were used to enable safe advance of the heading.

The spalling or popping rock generally was fresh, brittle, competent rock, such as granite or quartz monzonite, or unaltered schist or gneiss in flat layers. Some of the popping and spalling sections were between less competent rock, or were bounded by faulted or fractured rock masses. The popping and spalling are attributed to the tendency of some of the rocks to establish a more stable arch; to the release of asymmetric stresses in rigid rock masses subjected to unequal loading by incompetent, plastically behaving, surrounding rock masses; and, possibly, to residual stresses in rigid rock masses.

FAULTS AND JOINTS

The west portion of the tunnel, from the portal eastward to the west contact of the Montezuma stock, exposed jointed rock and numerous faults (fig. 131.2), including the Williams Range thrust. Faults in the Montezuma stock are not extensive, but locally they contributed to the development of several intersecting joint systems. Southeast of the Montezuma stock, faults of large displacement are uncommon, but locally many small faults and complex joint systems are present.

The faults causing the most difficulty in the tunneling operation were flat lying, contained considerable thicknesses of wet gouge, or were accompanied by hydrothermally altered zones. Especially bad tunneling conditions prevailed where these con-

ditions combined. Closely spaced joints, or closely spaced faults and joints, generally produced blocks that required support. Joints, particularly in the Montezuma stock, also localized hydrothermal alteration, which produced incompetent rock.

SQUEEZING AND SWELLING ROCK

Squeezing and swelling rock, which generally occurs in areas of extensive faulting and fracturing, caused considerable difficulty in several sections of the tunnel. Many faults, such as the Williams Range thrust, contain gouge that, where saturated with water, created heavy loads on the tunnel supports. Some of the faults, especially in the plate over the Williams Range thrust and in the Montezuma stock, were channelways for montmorillonitic alteration, which resulted in slow swelling of the rock on exposure to moisture. This swelling tendency required installation of considerable additional support and realinement of tunnel supports in several sections of the tunnel behind the headings.

REFERENCES

Lovering, T. S., 1935, Geology and ore deposits of the Montezuma quadrangle, Colorado: U.S. Geol. Survey Prof. Paper 178, 119 p.
Lovering, T. S., and Goddard, E. N., 1950, Geology and ore deposits of the Front Range, Colorado: U.S. Geol. Survey Prof. Paper 223, 319 p.

⚒

132. LANDSLIDES ALONG THE UINTA FAULT EAST OF FLAMING GORGE, UTAH

By WALLACE R. HANSEN, Denver, Colo.

Several factors in combination have produced abundant landslides along the Uinta fault east of Flaming Gorge, Utah, in the Antelope Flat-Clay Basin area. The Uinta fault is a large south-dipping high-angle thrust that trends east-northeast from the vicinity of Flaming Gorge toward and beyond the Utah-Colorado State line. Precambrian rocks form the hanging wall; Mississippian to Tertiary rocks form the footwall. Drag has steepened and overturned the bedding as much as a mile or more from the fault trace, especially in the footwall.

Landslides are common along or near the Uinta fault on north-facing slopes of relatively high relief; examples are on the northeast slope of Boars Tusk, near the east end of Dutch John Mountain, and along the north slopes of Goslin Mountain, Mountain Home, and Bender Mountain (fig. 132.1). Slides in these areas range from small discrete slump blocks a few yards across to large complex masses of jumbled earth and rock covering hundreds of acres. Most of them appear to be relatively inactive or stabilized at the present time, although some show
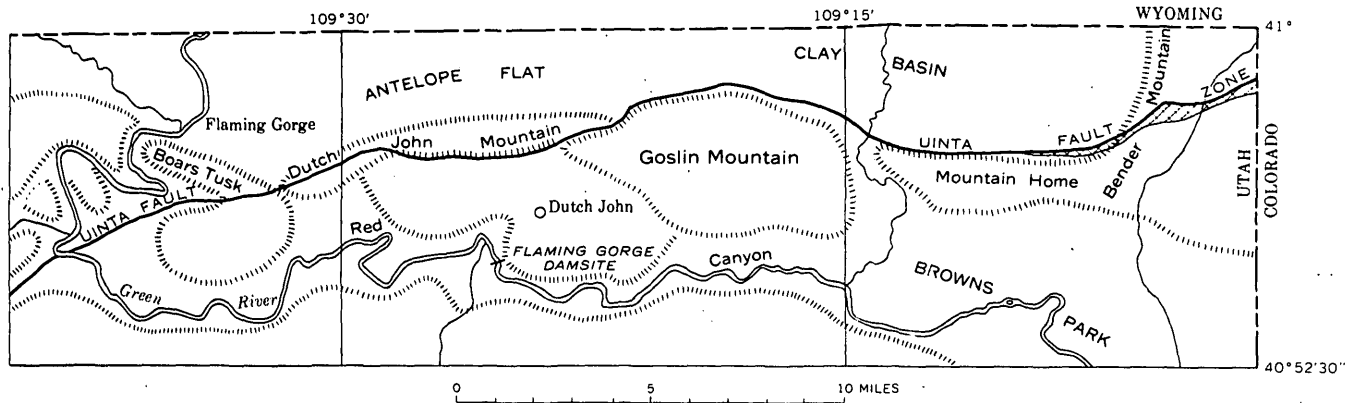
FIGURE 132.1.—Index map of Flaming Gorge area.

evidence of recent movement such as headward scarplets and disarranged vegetation. Some older slides are much dissected and evidently have ceased moving. Locally, large boulders of resistant rock far removed from their source formations are all that remain of ancient slides.

Landslides are most common where competent rocks, such as the Precambrian Uinta Mountain

FIGURE 132.2.—Factors leading to slope failure along trace of Uinta fault (1) competent quartzite overlies incompetent steeply dipping shale; (2) oversteepened slope caused by differential erosion causes potential instability; (3) northerly exposure minimizes insolation, resulting in (4) rank growth of vegetation and (5) rapid infiltration of moisture, which promotes sliding.

group or the Red Creek quartzite, have overridden incompetent rocks, such as the Cretaceous Hilliard shale (fig. 132.2). At such localities differential erosion along the fault trace has locally produced high, steep north-sloping faultline scarps that are topographically unstable. Most important, the northerly exposure of slopes minimizes insolation and promotes a rank growth of vegetation, which encourages and is encouraged by infiltration of moisture from rainfall and snowmelt. The larger amount of water in the north-facing slopes is a major factor in causing slides.

Saturated conditions on the slopes along the Uinta fault are indicated by many small springs. Most of these springs are mere seeps, but some of them, such as Ford Spring, Edith Aspden Spring, and Fighting Spring, 11, 15, and 25 miles, respectively, east of Flaming Gorge, yield several gallons of water per minute.

Virtually all landslides in the Flaming Gorge area are on northward-facing slopes—a few rockfalls excepted. Otherwise similar, southward-facing slopes are stable and lack landslides. In the Mesaverde formation, for example, where south-facing cliffs of competent sandstone overlie steep slopes of incompetent Hilliard shale, intense direct insolation stabilizes the slopes by drying the shale, inhibiting the growth of vegetation, and promoting rapid runoff.

EXPLORATION AND MAPPING TECHNIQUES

---

133.   GEOCHEMICAL PROSPECTING FOR COPPER DEPOSITS HIDDEN BENEATH ALLUVIUM IN THE PIMA
DISTRICT, ARIZONA

By Lyman C. Huff and A. P. Marranzino, Denver, Colo.

That important mineral deposits lie hidden beneath alluvium in the Basin and Range Province was convincingly demonstrated in 1951 by the discovery of the Pima copper deposit near Tucson, Ariz. Since this discovery other important ore deposits have been found hidden beneath alluvium in the Pima district and exploration activity has markedly increased throughout the Great Basin where many potential host rocks are covered by only a thin alluvial cover. The studies described here were made to determine what chemical techniques can be of use in this exploration.

GEOLOGIC SETTING

The Pima mining district is in Pima County about 15 miles southwest of Tucson, Ariz., in the northeastern foothills of the Sierrita Mountains—a low, maturely dissected range bounded on all sides by an extensive alluvium-covered pediment.

The ore deposits are on the northeast margin of a large batholithic intrusion of granodiorite of Laramide age which forms the core of the Sierrita Mountains. Near these deposits the marginal zone consists of sedimentary rocks of Paleozoic and Mesozoic age that are metamorphosed, folded, complexly faulted, and intruded by various kinds of igneous rocks among which are small bodies of quartz monzonite porphyry believed to be genetically related to the ore deposits (Cooper, 1960, p. 74). The Pima ore deposit was found beneath about 200 feet of alluvium by exploratory drilling following magnetic surveys and geologic study (Heinrichs and Thurmond, 1956). The ore of this mine and that of the nearby Banner and Mission deposits consists of disseminated chalcopyrite and molybdenite in metasediments and hydrothermally altered porphyry. It is similar in many respects to other deposits of porphyry copper type of the Southwest except for its alluvial cover.

SAMPLING AND ANALYSIS

To indicate whether geochemical anomalies were present in the vicinity of these concealed ore bodies, samples were collected of surface soil, surface alluvium, a carbonate-cemented zone at the base of the alluvium, ground water, and vegetation. The soil and the alluvium samples were sieved to minus 80 mesh when collected and the fines were used for analysis. The carbonate-cemented alluvium required crushing before sieving. Samples of these materials were obtained from the land surface, the open pit of the Pima mine, drill holes, and wells. The deeper zones of the alluvium and ground water throughout much of the area of interest are not accessible for sampling.

The samples were analyzed in the field or in a temporary field laboratory by standard geochemical prospecting tests. Copper determinations were made using the biquinoline test and molybdenum using the thiocyanate test. The field results were checked subsequently both with a spectrograph and by using standard wet laboratory methods.

DISPERSION OF COPPER AND MOLYBDENUM

Most of the samples of alluvium and alluvial soil collected at the land surface have copper contents ranging from 10 to 100 ppm (parts per million). Modern alluvium near the Pima and Mission ore bodies has a higher-than-average copper content, but these high values can be traced along washes upstream past the buried ore bodies to exposed copper mines and prospects closer to the Sierrita Mountains. The distribution of copper-rich float and of copper in the modern alluvium, which is not described in detail here, is interpreted as being due primarily to mechanical erosion from the exposed copper deposits and as having no relation to the buried ore bodies.

The carbonate-cemented zone at the base of the alluvium locally contains very high concentrations of copper. The samples highest in copper are at the extreme base of the alluvium. An area where the copper content ranges from 200 to 1,000 ppm can be traced for 2 or 3 miles to the northeast and down the pediment from the ore bodies (fig. 133.1). Because most of the copper is in the carbonate matrix of the alluvium it is believed that most of the
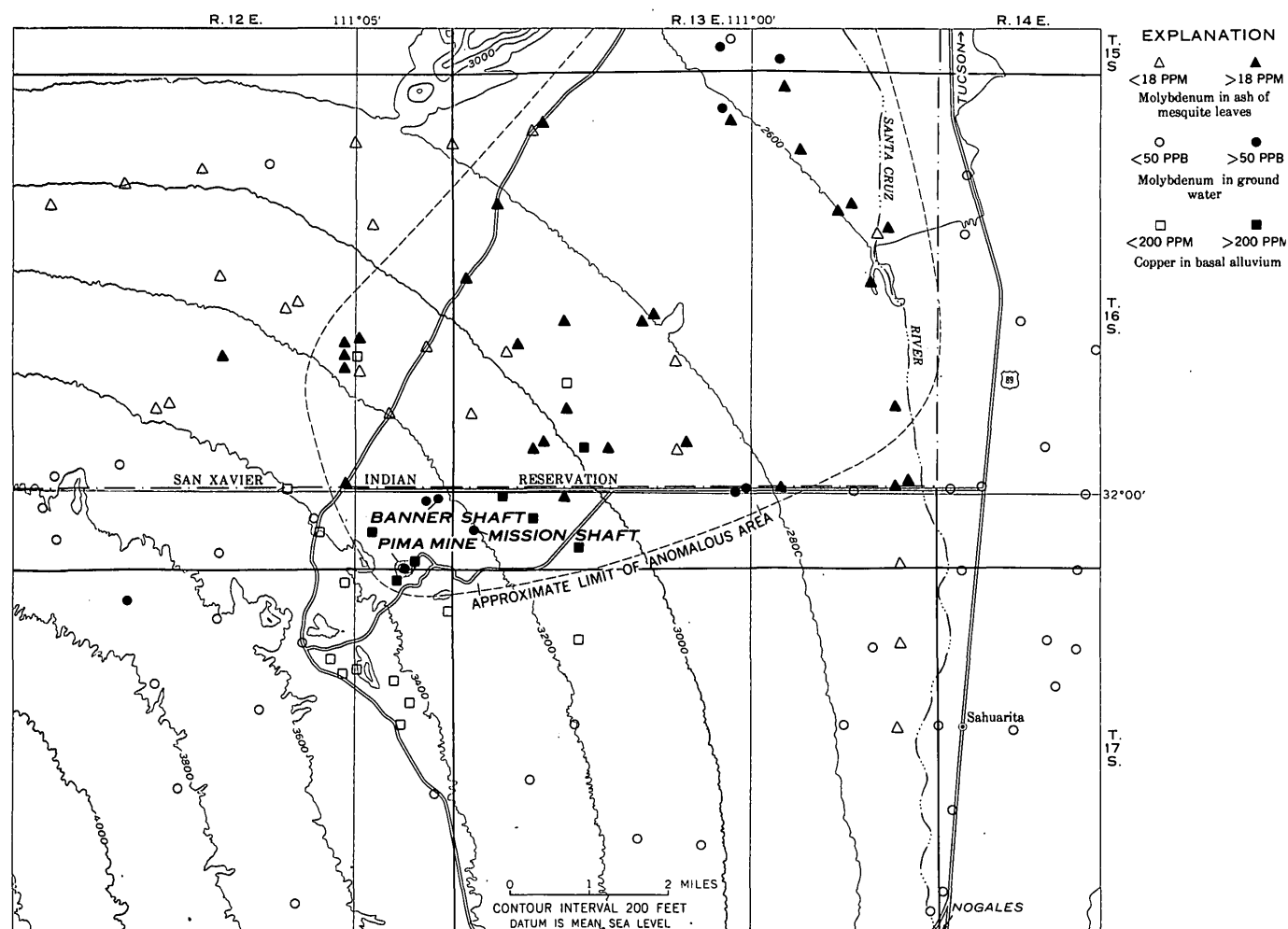
FIGURE 133.1.—Geochemical map showing anomalies resulting from dispersion of ore metals in ground water, Pima district, Arizona.

copper is a chemical precipitate from the ground water and is not detrital.

The molybdenum content of the ground water ranges from less than 6 ppb (parts per billion) to over 200 ppb. Within the limitations imposed by distribution of wells, anomalous concentrations of molybdenum were traced from the mining area to a point about 8 miles northeast (fig. 133.1). The greater solubility of molybdenum in the ground water as compared to that of copper apparently permits it to be traced for a much greater distance.

The molybdenum content of the plant samples ranges from about 10 ppm (parts per million in ash) to about 50 ppm. Among the species compared, molybdenum is highest in mesquite, a deep-rooted phreatophyte. The highest values were found in leaves of mesquite growing in the general area where ground water has a high molybdenum content (fig. 133.1), and we believe that most of the molybdenum content of the mesquite is derived chiefly from the ground water and not from the alluvium in which it grows.

APPLICATION TO PROSPECTING

Tracing the dissolved ore metals in ground water appears to have more significance in prospecting than the other methods tried. Molybdenum in the ground water and in mesquite fed by ground water can be traced over 8 miles from the ore. The mobility of molybdenum observed here confirms the

results of earlier studies in Russia (Ginzburg, 1960, p. 204). Copper deposited by ground water in the basal alluvium can be traced 2 to 3 miles from the ore. In the search for similar deposits, reconnaissance studies along major drainage routes apparently can be used to locate large areas with an anomalously high molybdenum content. Widely spaced core drilling and chemical study of the basal alluvial conglomerate within these areas may be a useful local guide for buried ore.

REFERENCES

Cooper, J. R., 1960, Some geologic features of the Pima Mining District, Pima County, Arizona: U.S. Geol. Survey Bull. 1112–C, p. 63–103.
Ginzburg, I. I., 1960, Principles of geochemical prospecting (English translation of Russian original): Pergamon Press, 311 p.
Heinrichs, W. E., Jr., and Thurmond, R. E., 1956, A case history of the geophysical discovery of the Pima Mine, Pima County, Arizona: Geophysical Case Histories, v. 2, p. 600–612.

134. MEASUREMENT OF BULK DENSITY OF DRILL CORE BY GAMMA-RAY ABSORPTION

By Carl M. Bunker and Wendell A. Bradley, Denver, Colo.

The bulk density of drill-core samples can be determined by a nuclear irradiation technique involving gamma-ray absorption. Comparative data on a series of samples show that the gamma-ray absorption method is much faster and has about the same accuracy as fluid immersion methods for determining the bulk density of homogeneous core samples.

EQUIPMENT

The equipment for measuring bulk density of core samples (fig. 134.1) consists of the following:

1. A 1-millicurie barium-133 source which emits gamma radioactivity having an energy of 0.36 million electron volts (Mev).
2. A sample holder for collimating the radiation from the source through the sample and into the gamma-ray detector in a beam 1.6 centimeters in diameter. The sample holder is split and hinged to facilitate loading the samples.
3. A scintillation-type detector consisting of a sodium iodide crystal optically coupled to a photomultiplier tube.
4. Electronic circuitry consisting of a high-voltage power supply, a linear pulse amplifier, a discriminator circuit, and a ratemeter.

A gamma-ray spectrum of the barium-133 source (fig. 134.2) was obtained to determine the pulse-height voltage that corresponds to the known energy peak of barium (0.36 Mev). The discriminator cir-

cuit is adjusted to accept gamma-ray energies that are within a 20-volt range, about ± 10 pulse-height volts, of the determined voltage at the energy peak to eliminate the measurement of scattered radiation and minimize the effect of natural background radio-
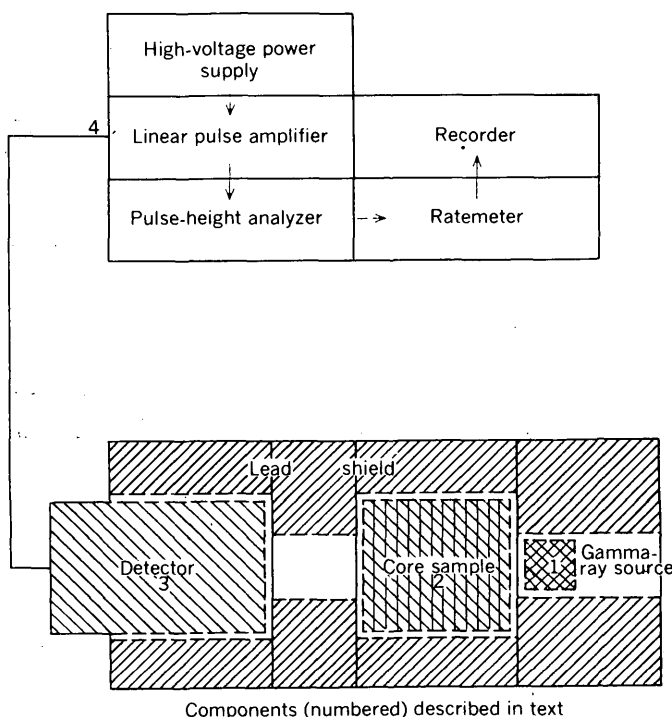
Figure 134.1.—Diagrammatic sketch of instruments for measuring bulk density of core samples.
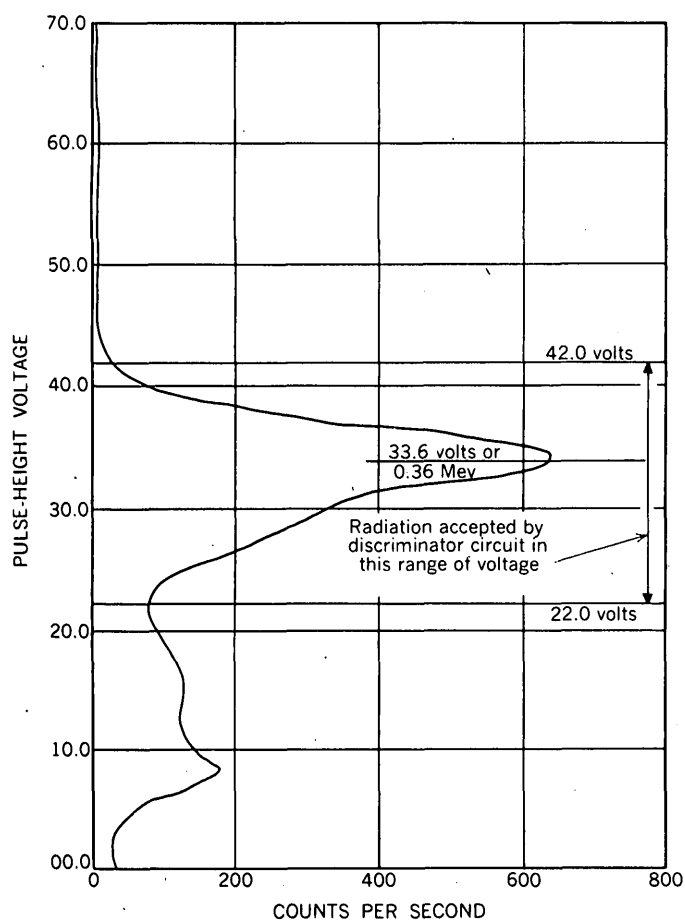
FIGURE 134.2.—Gamma-ray spectrum of barium-133 and energy range used for bulk-density measurements.

activity in the samples. The gamma-ray source, sample holder, and detector are enclosed in a cylindrical lead shield (fig. 134.1), 15.2 cm in diameter, to minimize the radiation hazard to the operator and to reduce the effect of background radioactivity.

The source-to-detector spacing without a sample in the sample holder is adjusted to yield a counting rate of 6,400 counts per second and the circuit is adjusted to accept photopeak pulses. This basic counting rate is used for determining the absorption in the samples. Because of drift in instrument response, slight adjustments in the nominal spacing, about 6.5 centimeters, are sometimes required to maintain the count rate.

The average count rate for about a 1-minute interval is obtained to reduce the statistical error to less than 10 counts per second, which is the accuracy of reading the ratemeter and recorder. Repeated readings at successive 1-minute intervals show that the reproducibility of readings is within these limits throughout the count-rate range observed during

the investigation. This small error in measurement does not affect the interpretation of density.

METHOD

The instrument was calibrated by determining the relation between percent of gamma radiation absorbed by the sample, sample length, and bulk
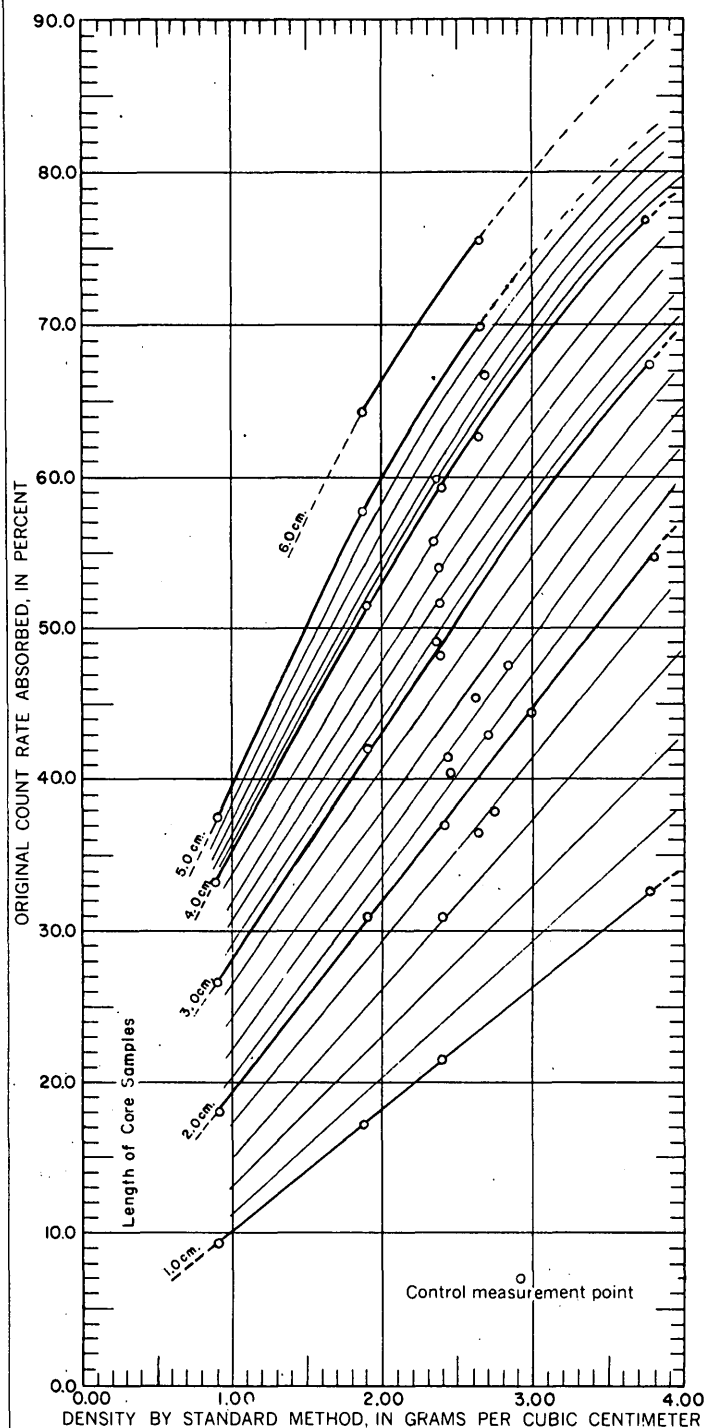
FIGURE 134.3.—Calibration chart relating bulk density, sample length, and percent of radiation absorbed by core samples.

TABLE 1.—*Summary of rock types and experimental data*

[Analysts: R. W. Babcock and G. R. Johnson]

Sample	Rock type	Core diameter (inches)	Length of sample (centimeters)	Absorption (percent)	Standard bulk density	Gamma-ray absorption method bulk density	Remarks
CZ-5	Siltstone	1⅝	5.62	68.6	2.40	2.38	
6	....do	do	3.33	51.6	2.38	2.40	
7	....do	.do	6.14	71.4	2.62	2.35	Sample fractured and vuggy.
8	....do	.do	3.61	54.0	2.38	2.39	
9	....do	.do	3.12	49.2	2.36	2.34	
10	....do	.do	5.62	68.0	2.35	2.38	Fractures and vugs.
11	....do	.do	5.62	68.7	2.38	2.37	
12	....do	.do	3.83	55.9	2.35	2.36	
13	....do	.do	5.83	68.4	2.31	2.32	
14	....do	.do	4.70	61.7	2.28	2.29	
15	....do	.do	4.72	62.5	2.34	2.34	
16	Oxidized iron formation	.do	4.30	59.5	2.38	2.35	Iron formation seams through sample.
17	....do	.do	3.22	48.9	2.30	2.30	
18	....do	.do	4.60	66.7	2.69	2.69	
20	....do	.do	4.51	68.3	2.84	2.83	
21	....do	.do	2.27	43.8	2.64	2.72	Fractures and vugs.
22	....do	.do	4.65	60.8	2.31	2.30	
24	Ferruginous chert	.do	3.75	57.1	2.58	2.50	Fractures and vugs.
L-69	Dolomite	1	2.45	46.9	2.81	2.79	
70	....do	.do	2.43	44.5	2.64	2.63	
71	Quartzite	.do	2.50	45.3	2.62	2.60	
72	Dolomite	.do	1.92	39.2	2.77	2.73	
73	....do	.do	2.43	47.3	2.84	2.83	
74	Quartzite	.do	2.42	44.5	2.61	2.62	
75	Dolomite	.do	2.02	40.9	2.76	2.70	Fractured.
76	....do	.do	2.42	46.1	2.75	2.74	
77	Quartzite	.do	1.85	36.7	2.62	2.59	
78	Dolomite	.do	2.42	47.7	2.85	2.85	
79	....do	.do	2.48	46.9	2.73	2.75	
80	....do	.do	2.51	48.5	2.81	2.83	
81	Quartzite	.do	2.45	45.3	2.63	2.63	
82	Dolomite	.do	2.43	47.7	2.85	2.85	
83	....do	.do	2.43	44.5	2.62	2.63	
84	Quartzite	.do	1.89	37.9	2.75	2.72	
85	Dolomite	.do	2.37	41.4	2.42	2.44	
87	....do	.do	2.25	40.6	2.44	2.46	
88	....do	.do	1.60	31.1	2.40	2.40	

density. The samples used for calibration were analyzed for bulk density by routine laboratory (fluid immersion) methods. The calibration was limited to sample sizes and densities normally processed by the mass physical-properties laboratory of the U. S. Geological Survey in Denver, Colo. Core-sample diameters of 1 inch and 1⅝ inches, lengths from 1.0 to 6.0 cm in increments of about 1 cm, and densities from 0.92 to 3.78 gm per cc were used for calibration. Sample lengths were determined by making several measurements at the ends of the sample in the area penetrated by the collimated beam of gamma rays. Each of the core samples was placed in the sample holder in the collimated beam of gamma radiation, and the percent reduction in radiation as a result of gamma-ray absorption was determined.

The absorption, in percent, of the gamma radiation passing through the samples was plotted as a function of sample length and density on a calibration chart (fig. 134.3).

RESULTS

The calibration chart was used to compare bulk density measurements obtained by standard laboratory (fluid immersion) methods (table 1) with bulk-density measurements obtained by the nuclear irradiation technique. The standard laboratory measurements were assumed to be correct for this comparison. The results are given on figure 134.4. Samples containing visible fractures or vugs were not used because preliminary measurements showed that the nuclear irradiation technique may give erroneous results for these types of samples. These samples can usually be recognized from outward appearances and are set aside for analysis by standard methods, which give more reliable results for this type of sample because of the larger volume of rock used for the measurement.

Changes in counting rate related to density changes of as little as 0.01 gm per cc can be observed easily on the ratemeter or recorder. Interpretation
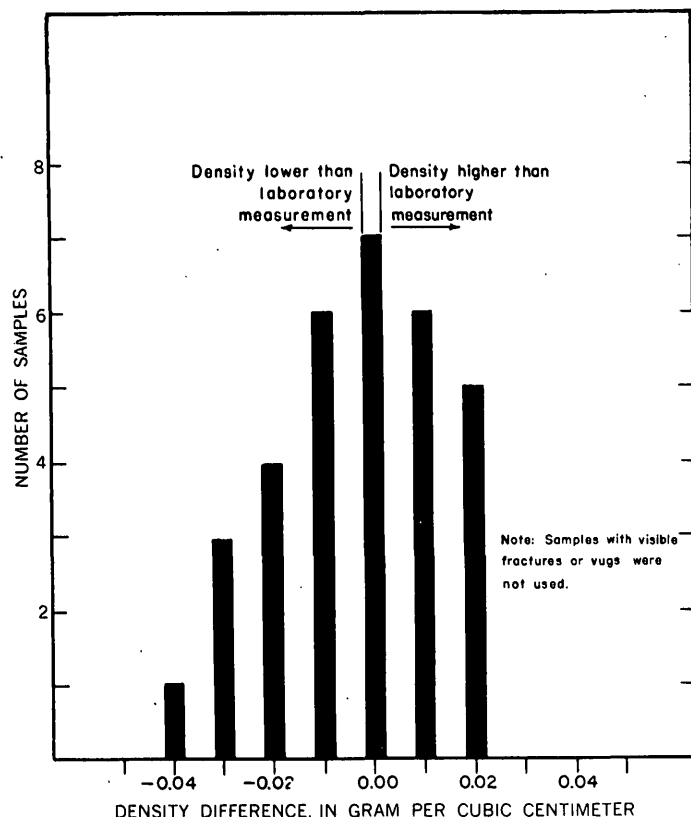
FIGURE 134.4.—Comparison of bulk density measurements determined by gamma-ray absorption method and by standard laboratory methods.

from the calibration chart is less accurate because some bulk density values must be interpolated from the curves.

The measurement of bulk density by the nuclear irradiation technique—including the time required to obtain an accurate reading on the ratemeter, measure of the sample length, calculate the percent absorption, and interpret the density with these data —requires only 2 or 3 minutes. The standard laboratory procedure requires from about 4 to 20 minutes for the same analysis, depending on the method used.

Although this investigation was limited to sample lengths between 1.0 and 6.0 centimeters, diameters up to $1\frac{5}{8}$ inch, and densities from 0.92 to 3.78 gm per cc, the method can be adapted easily to other sample sizes and densities.

The equipment is portable and can be transported to field offices or well sites. Bulk density measurements of drill core can be completed within a few minutes after core is recovered from a drill hole. A major advantage of gamma-ray absorption method for field use is that it requires neither laboratory conditions nor laboratory apparatus such as analytical balances, water, or mercury, which are inconvenient to use in the field.

135.   MECHANICAL CONTROL FOR THE TIME-LAPSE MOTION-PICTURE PHOTOGRAPHY OF GEOLOGIC PROCESSES

By ROBERT D. MILLER, ERNEST E. PARSHALL, and DWIGHT R. CRANDELL, Denver, Colo.

A minute-to-minute, hour-to-hour, or day-to-day photographic record can be made of certain geologic processes by the use of a mechanically controlled time-lapse motion-picture camera. Some of the processes that are particularly suited for such a study are glacier motion (Miller and Crandell, 1959), mass wasting (Crandell and Varnes, Art. 57), and erosion of streams and beaches. Time-lapse cameras having an electronic interval-circuit and timer, operated by a solenoid-type plunger, have been used to study stream braiding and stream flow (Fahnestock, 1959). A major advantage of a mechanically con-

trolled timing device is that the battery drain is so negligible that the camera can be left unattended for several months.

Unfortunately, the camera shutter cannot be tripped by a simple lever attached to a clock. Instead, provisions must be made to (a) operate the exposure meter circuit for only a short time in order to prolong battery life, (b) protect the shutter from damage by harsh tripping, and (c) reset the timing mechanism to insure the proper interval between exposures.

In order to accomplish these things, the shutter

Battery

Motor and gear reducer

Timing

Cycle

Reset

Timing cam as shown is on a 2:1 gear reduction; 1 revolution in 24 hours

Single-pole double-throw microswitches throughout; refer to circuit diagrams

Radio spaghetti-tubing of suitable diameter used to seal clock

6-volt automobile clock, hands and face removed

Extended winding handle to clear counter

Gear and friction spline

8-tooth

10-tooth

Rotary counter

Camera tripping lever

Timing cam cut from blank diameter blank

Set time

Suitable bracket to support counter in correct location

Tripping lever

Small 6-volt automobile heater motor-mount to suit

3600:1 reduction gear case

Pressure release bar

Sponge rubber

3 No. 8-32 screws

2 11/16"

Cycle cam

Reset cam

Activating lever

Second hexagonal brass spacer here

Shelter box

2½"²

0.70"

1⅛"

1⅜" hexagonal brass

Activating cam

Ratchet counter

18"

9⅛"

4½"

½" thick base

7½"

15¼"

11"

All cams are ³/₁₆ plexiglass drilled and tapped for small set screws

Cycle and reset cams: 1" across points, ⅝" minimum diameter

3600:1 reduction gear assembly

A complete gear assembly from a 1-RPM motor; rotor rings removed from high speed shaft. Mounted in a brass shell, the inside diameter to clear gear assembly, outside diameter approximately ¼ in. larger; gear assembly mounted on a round brass plate; diameter same as outside diameter of shell with a shoulder to match inside diameter. Hole center-bored in alinement with and as bearing for ⅛ in. diameter slow speed shaft; back plate is the same except drilled for bearing of small high speed shaft. Gear case shell is of minimum length to allow maximum projections of shafts thru forward and rear plates. Motor shaft turned down to approximately ⅛ in. diameter, coupled to gear shaft with flexible radio spaghetti-tubing.

Cam shaft, ¼ in. diameter, drilled to receive ⅛ in. shaft; drilled and tapped for set screws, and mounted on slow speed shaft.

Oil filler hole and plug provided. Entire assembly held together by flat, hard aluminum plates and 3 equally spaced bolts.

Seal gear case with liquid gasket material.

Design and prototypes by E. E. Parshall

FIGURE 135.1.—Mechanical time-lapse control for motion-picture photography.

of the time-lapse camera is tripped by an arrangement of cams and levers activated by a 6-volt electric motor (fig. 135.1). Two 6-volt "hot-shot" batteries in parallel provide power for both the motor and a 6-volt magnetically wound, spring-operated automobile clock used as a timer. The clock is geared from the hour hand so that a shaft rotates once every 24 hours. A timing cam placed on this shaft can vary the range of the exposure interval in hours, or a cam placed directly on the minute hand can vary the tripping interval in minutes. Projections on the timing cam close a single-pole, double-throw microswitch that starts the electric motor. The motor drive shaft is attached to a gear reduction assembly taken from a 1-rpm motor. Snug-fitting tubing is telescoped to couple the gear shaft to the motor. Clamping is not necessary if the fit is snug. The motor must rotate at about 3,600 rmp in order to be reduced in the gear box to slightly more than 1 rpm. Leading out of the gear assembly is a shaft to which are fixed an activating cam, a reset cam, and a cycle cam (fig. 135.1). As the activating cam turns, it lifts the activating lever, to which are fastened a tripping lever and a pressure-release bar.

The shape of the activating cam causes the activating lever to rise slightly and to push the tripping lever and, in turn, the camera tripping lever toward the camera. This inward movement closes the camera's photoelectric cell circuit and operates a motor in the camera that opens or closes the camera lens opening in response to light conditions in front of it. Following closure of the photoelectric cell circuit for about 10 seconds, the activating lever is raised further, pushing the tripping lever upward and tripping the camera shutter. Continued rotation of the cam shaft lowers the activating lever and turns the reset cam, which opens the clock microswitch circuit and shuts off the electric motor. The timing cam on the clock continues to turn until the microswitch lever is released; this closes the reset circuit and causes the cam shaft to rotate until the cycle cam opens the adjacent microswitch and breaks the circuit. The activating cam has now rotated 180° and is in position for the next exposure cycle.

Damage to the shutter by excessive inward movement during the operation of the photoelectric cell circuit is prevented by adjustment of the upright position of the tripping lever by means of the adjustable bolt on the activating lever. The pressure-release bar is fastened to the tripping lever by an adjustable coil spring that absorbs excessive movement of the activating lever. Detailed dimensions of the activating mechanism are shown in figure 135.2 (see p. B–316).

Two frame counters provide cross checks for coordinated operation of the activating lever and camera shutter. One, a ratchet counter, is attached by a metal strip and spring to the activating lever; the other, a rotary counter, is attached by a gear and friction spline to the shutter mechanism of the camera.

The camera and timing mechanism are fastened to a magnesium plane table board. A protective aluminum cover with a slanted polished plate-glass window is bolted to the edges of the board. Sponge-rubber gaskets keep the cover tight and dustproof; the cover and plate can be fitted with latches for padlocks.

The planetable board is screwed and bolted to a planetable tripod head. The head is brazed to a tube, the sides of which are cut out to permit access to wingnuts on the underside of the tripod head. The tube slips over a slightly smaller tube which can be placed in the ground and embedded in concrete. While the upper tube is raised, the camera and planetable board can be adjusted to the desired viewing angle, and the wingnuts tightened. When the tube is lowered, the tripod head and wingnuts are within it and cannot be reached. A latch fastens the tubes together and a padlock prevents tampering.

The camera is operated by a spring-wound motor. The winding handle is extended in order to clear the rotary frame counter attached to the camera. The spring motor will expose about 1,200 frames after one full winding. We have found that new 6-volt batteries will run the electric motor in the timing mechanism unit at least 4 months, and probably longer, exposing 2 frames each day.

REFERENCES

Fahnestock, R. K., 1959, Dynamics of stream braiding as shown by means of time-lapse photography [abs.]: Geol. Soc. America Bull., v. 70, no. 12, p. 1599.
Miller, R. D., and Crandell, D. R., 1959, Time-lapse motion-picture technique applied to the study of geological processes: Science, v. 130, no. 3378, p. 795-796.

6-volt   Motor

Timing

Cycle

Reset

CIRCUIT DIAGRAM

Hole A

½″ $^{19}/_{32}$″

Hole B

Camera tripping lever

5½″

Bearing, to suit

No. 1–56 screw with locknut

No. 3–56 screws

$1^{17}/_{32}$″

1″

¼″
square brass

Hard aluminum plate, .070″

$^{1}/_{16}$″ x ¼″ brass

Hole A

¾″ x ¾″ x ⅛″ aluminum angle

No. 4–40 screw with locknut

1¼″

1″

2 $^{7}/_{16}$″

5½″

Hole B

⅜″ diameter
brass roller

Flat

No. 3–56 screw

90°

$1^{1}/_{16}$″   ½″

¾″

Counter linkage requires some
overtravel (absorbed by spring)

All pivot points have small shouldered
bushings clamped by screws

Ratchet counter

FIGURE 135.2.—Detail of activating and tripping mechanism of time-lapse control.

136.   LIQUID-LEVEL TILTMETER MEASURES UPLIFT PRODUCED BY HYDRAULIC FRACTURING

By FRANCIS S. RILEY, Sacramento, Calif.

Work done in cooperation with the U.S. Atomic Energy Commission

In September 1960 the Oak Ridge National Laboratory conducted an experiment to test the feasibility of disposing of radioactive wastes by injecting them into deep artificial fractures in nearly impermeable shale. The vehicle for the simulated wastes was a cement-bentonite grout, which was pumped down an injection well into fractures created by the hydraulic-fracturing technique that is used to improve the yields of oil wells.

At the suggestion of Wallace de Laguna (written communication, 1960), geologist with the Oak Ridge National Laboratory, three liquid-level tiltmeters of the kind described by Riley and Davis (1960) were used to detect land-surface uplift during the hydraulic fracturing and grout injection.

INSTRUMENTATION

The tiltmeter measures differential changes in elevation of the land surface, by reference to a liquid surface that provides a level datum. This is accomplished by measuring water-level changes in two identical cylindrical pots commonly set 100 to 200 feet apart, and connected by two hoses. One hose, filled with water, is connected to the bottom of each pot, permitting the water surfaces in the two pots to seek a common level. The other hose connects the air spaces above the water in the pots. Differential uplift, or tilting, causes a decline of the water level in the rising pot, and an equal rise of water level in the other pot. In these basic principles the instrument is similar to the tiltmeters used by Eaton (1959), Green (Green and Hunt, 1960), and others in investigations of volcanic and tectonic tilting. It differs from these instruments in that measurements in both pots are obtained indirectly from a centrally located displacement device, consisting of a cylinder and micrometer-actuated piston connected at the middle of the water hose. By using a relatively small piston a magnification factor of about 20 is introduced, thus making the smallest readable division on the displacement micrometer (0.0001 inch) equivalent to a water-level change of approximately 0.000005 inch in the pots.

In the Oak Ridge test three tiltmeters were set up at different distances from the injection well (fig. 136.1), along lines approximately following the topographic contours. As much as 18 inches of cut and fill was required to provide level lines on which to lay the hoses. The pots rested on concrete piers imbedded 5 to 7 feet in the ground.

For each tiltmeter the data were analyzed by plotting a pair of curves showing water-level change with time in each of the pots. When the water levels were influenced only by temperature-induced volume changes the curves remained parallel. Divergence from parallelism indicated tilting. Graphs of differential uplift with time were obtained by plotting the differences between the two water-level curves.

GROUT INJECTION

Two batches of grout were injected into the Cambrian Conasauga shale, near Oak Ridge, Tenn. Around the injection site the shale on the average dips 20° southeast, but locally the beds are overturned (Wallace de Laguna, written communication, 1960).

The fractures were initiated by a high-pressure sand jet that was slowly rotated so as to erode a horizontal slot through the well casing and cement liner and a short distance into the surrounding shale. Before the grout was injected, fractures were extended some distance away from the well by pumping water at well-head pressures of 1,350 to 2,500 psi. Pertinent data on the injections (Wallace de Laguna, written communication, 1961) are summarized in the table on the following page.
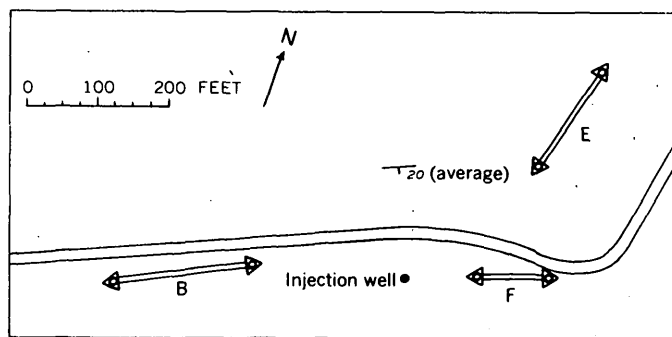
FIGURE 136.1.—Sketch map of injection site showing layout of tilt-meters along lines *B*, *E*, and *F*.

| Date (1960) | Depth of injection (feet) | Injected fluid | | Total volume injected (gallons) | Well-head pressure (pounds per square inch) | Injection rate (gallons per minute) |
		Composition	Volume percent			
Sept. 3	934	Water	100.0	1,200	1,350-1,500	80
		Grout:		91,567	1,700-2,000	125-156
		Water	81.9	....	....	139 [1]
		Cement	17.5			
		Bentonite	0.6			
9	694	Water	100.0	16,000	1,700-2,500	280 [1]
10	694	Water	100.0	4,000	....	250
		Grout:		132,770	2,000-2,300	?-280
		Water	76.8	....	....	208 [1]
		Cement	22.6			
		Bentonite	0.6			

[1] Average rate.

OBSERVED UPLIFT

The differential uplift between the tiltmeter pier closer to the injection well and the one farther away is plotted against time for each tiltmeter (figs. 136.2 and 136.3). On figure 136.3 the slight eastward tilting along the B and F lines before the start of the grout injection at 1100 hours apparently is a regional effect unrelated to the test and presumably due, at least in part, to earth tides. Minor tilting away from the well seems to have begun within 10 to 20 minutes after the start of grouting at 1100 hours, but the major effect, presumably representing the arrival of one or more grout sheets beneath the closer piers, was delayed 95 to 110 minutes. The pronounced downward inflection (westward tilting) of the F line at 1405 hours may represent passage of the edge(s) of the grout sheet(s) beneath the farther pier.

When injection of the second batch of grout was begun (fig. 136.2), all three tiltmeters indicated almost immediate uplift of the closer piers, the most distant of which was 243 feet from the injection well. This may have been due to the existence of one or more extensive fracture planes created by injecting large quantities of water the day before. The absence of strong downward inflections of the curves (fig. 136.2) in the early part of the experi-
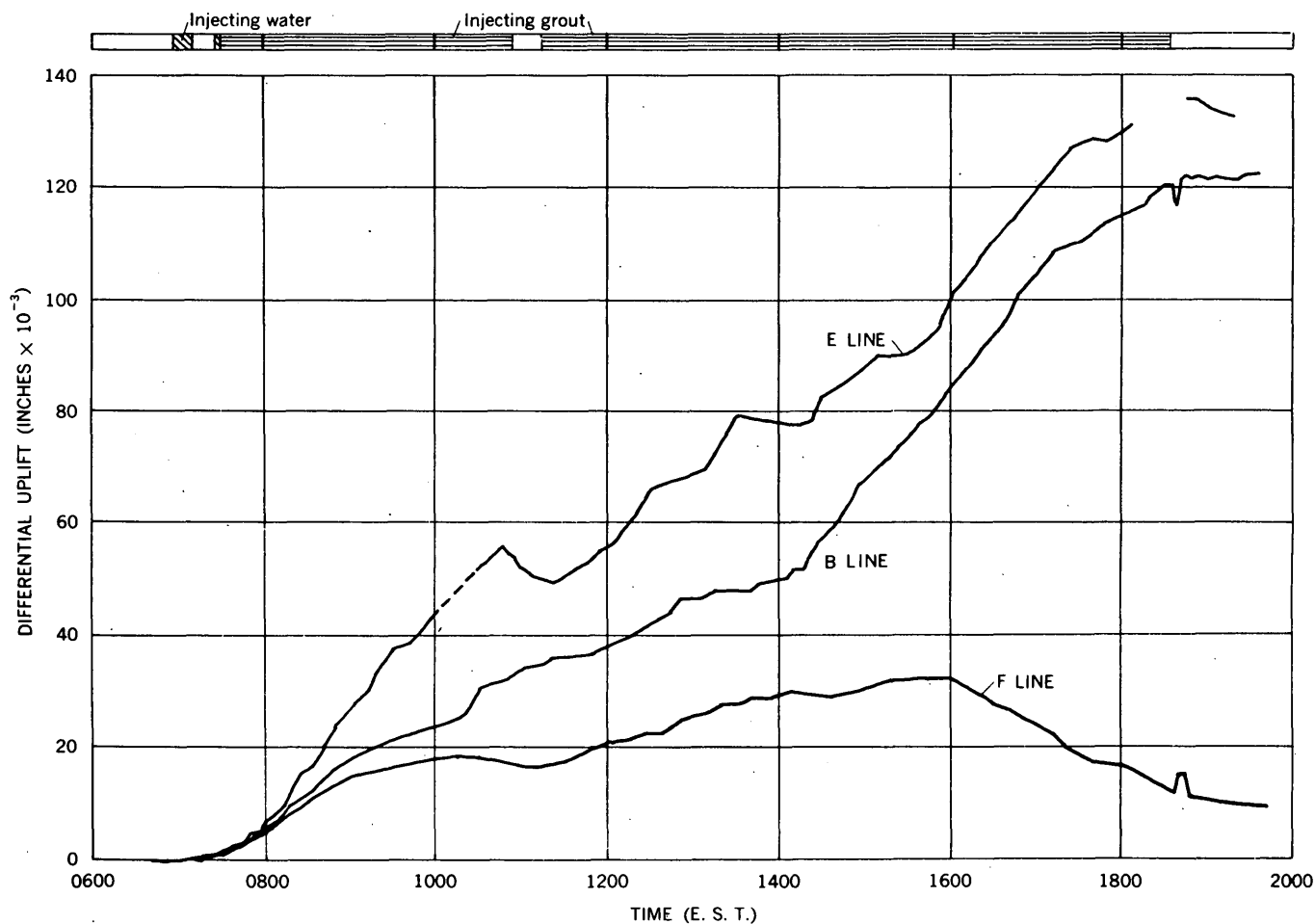
FIGURE 136.2.—Graph showing uplift of closer piers relative to more distant piers, September 10, 1960.
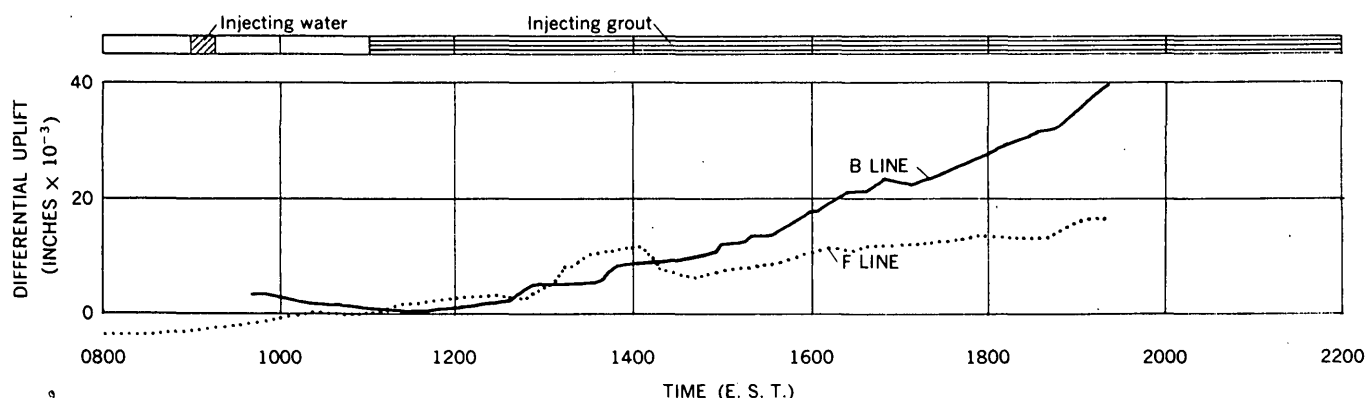
FIGURE 136.3.—Graph showing uplift of closer piers relative to more distant piers, September 3, 1960.

ment suggests that the more distant piers on all three lines also may have started to rise almost immediately, perhaps through the action of water trapped in the fractures ahead of the advancing grout.

The observed tilting seems consistent with the asumption that the grout spread out as one or several thin, sill-like sheets moving through and generating fractures that mostly tended to follow bedding planes.

REFERENCES

Eaton, J. P., A portable water-tube tiltmeter: Seismol. Soc. America Bull., v. 49, no. 4, p. 301–316.

Green, G. W., and Hunt, C. B., 1960, Observations of current tilting of the earth's surface in the Death Valley, California, area: U.S. Geol. Survey Prof. Paper 400–B, art. 124, p. B275, B276.

Riley, F. S., and Davis, S. N., 1960, A tiltmeter to measure surface subsidence around a pumping artesian well [abs.]: Jour. Geophys. Research, v. 65, no. 5, p. 1637.

137.   A METHOD OF RECORDING AND REPRESENTING GEOLOGIC FEATURES FROM LARGE-DIAMETER DRILL HOLES

By ELMER H. BALTZ and JAMES E. WEIR, JR., Albuquerque, N. Mex.

Work done in cooperation with the U.S. Atomic Energy Commission

The Geological Survey is currently studying ground-water conditions and disposal of radioactive waste in the vicinity of Los Alamos, N. Mex., in support of activities on the Los Alamos Scientific Laboratory. As part of this work the writers examined the geologic features on the walls of large-diameter holes drilled in the Bandelier tuff of Pleistocene age. The holes, which were drilled with a bucket auger, ranged from 3 to 6 feet in diameter and from 49 to 108 feet in depth. The methods and geological equipment described in this report were devised by the writers for quickly recording and representing features such as joints, cavities, and lithologic units.

The drill holes were examined from a metal personnel cage (fig. 137.1) that was lowered and raised by a powered crane. The cage is 2 feet in diameter and is equipped with electric lights and a two-way portable radio for communication with the surface. Air circulation in the holes was maintained by an exhaust fan at the surface connected to a flexible tube extending nearly to the bottom of the holes.

The writers decided that the geologic features exposed in the walls of the holes would be most easily recorded and most useful if they were plotted on diagrams representing cores from the holes, rather
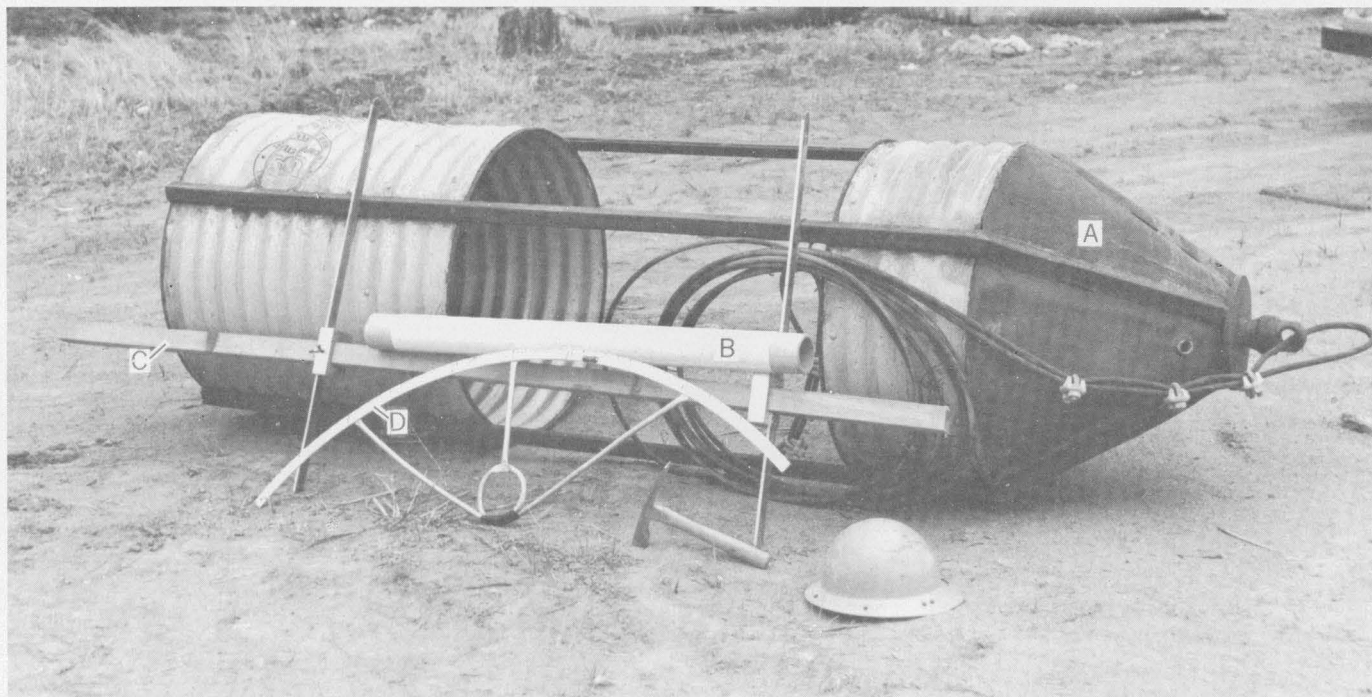
FIGURE 137.1.—Equipment used in recording geologic features in large-diameter drill holes. *A*, personnel cage; *B*, cardboard tube with graph paper attached; *C*, sighting bar; *D*, arc scale with bubble level. Photo by Roy Stone.

than on flat diagrams representing the walls of the holes. For this purpose cardboard mailing tubes with outer diameters of 1.5, 2, and 3 inches were used to correspond to drill holes with diameters of 3, 4, and 6 feet, respectively. Printed semitransparent graph paper, ruled in inches and tenths of inches, was fastened to the tubes with rubber cement or drafting tape. The line on the tube diametrically opposite the joint line of the paper was designated as north and was used as the reference from which all measured points were plotted. The north, south, east, and west lines were marked on the graph paper, and intervals of depth from the surface were marked to scale. Scale is automatically determined by ratio of the diameter of the tube to that of the hole. Thus, if the tube is 3 inches in diameter and the hole is 6 feet in diameter, the scales, both circumferential and vertical, are automatically 1 inch equals 2 feet.

A sighting bar (fig. 137.1) and a Brunton pocket transit were used to determine the north and south points of the holes. Lower extensions of the metal leaves of the sighting bar fit into the hole; the leaves slide on the wooden bar and are adjustable to fit holes of different diameters. The north and south sides of the hole were determined by orienting the bar with the aid of a Brunton pocket transit.

A steel tape, weighted at the end, was secured at the north point at the top of the hole and hung as a pendulum to the bottom of the hole. The tape was used as the north reference on the wall of the hole, and also for depth determinations. In some drill holes additional tapes were hung at the south, east, and west points of the holes.

During the first "run" down the drill hole in the personnel cage the wall of the hole was marked with carpenter's crayon at standard intervals of depth. Measuring, recording, and plotting of data usually were done bottom to top as the cage was raised. Most of the work was done by a two-man crew; one geologist plotted on the graph paper of the tube, while the other geologist measured and described geological features observed on the wall of the hole. A two-man crew proved to be considerably more efficient than one man. In the 3- and 4-foot diameter holes, measurements were made with a flexible 6-foot metal tape —but this was impractical in the 6-foot diameter holes because the distance to the wall from the cage suspended in the middle of the hole was too great. A graduated aluminum arc scale with a bubble level (fig. 137.1) was built to measure circumferential distances in these larger holes. The curvilinear length of the scale is 5 feet, and the radius of the arc is 3 feet. To avoid confusion the observer gave all measurements to the plotter in terms of feet east or west of the north line at each station within the hole.
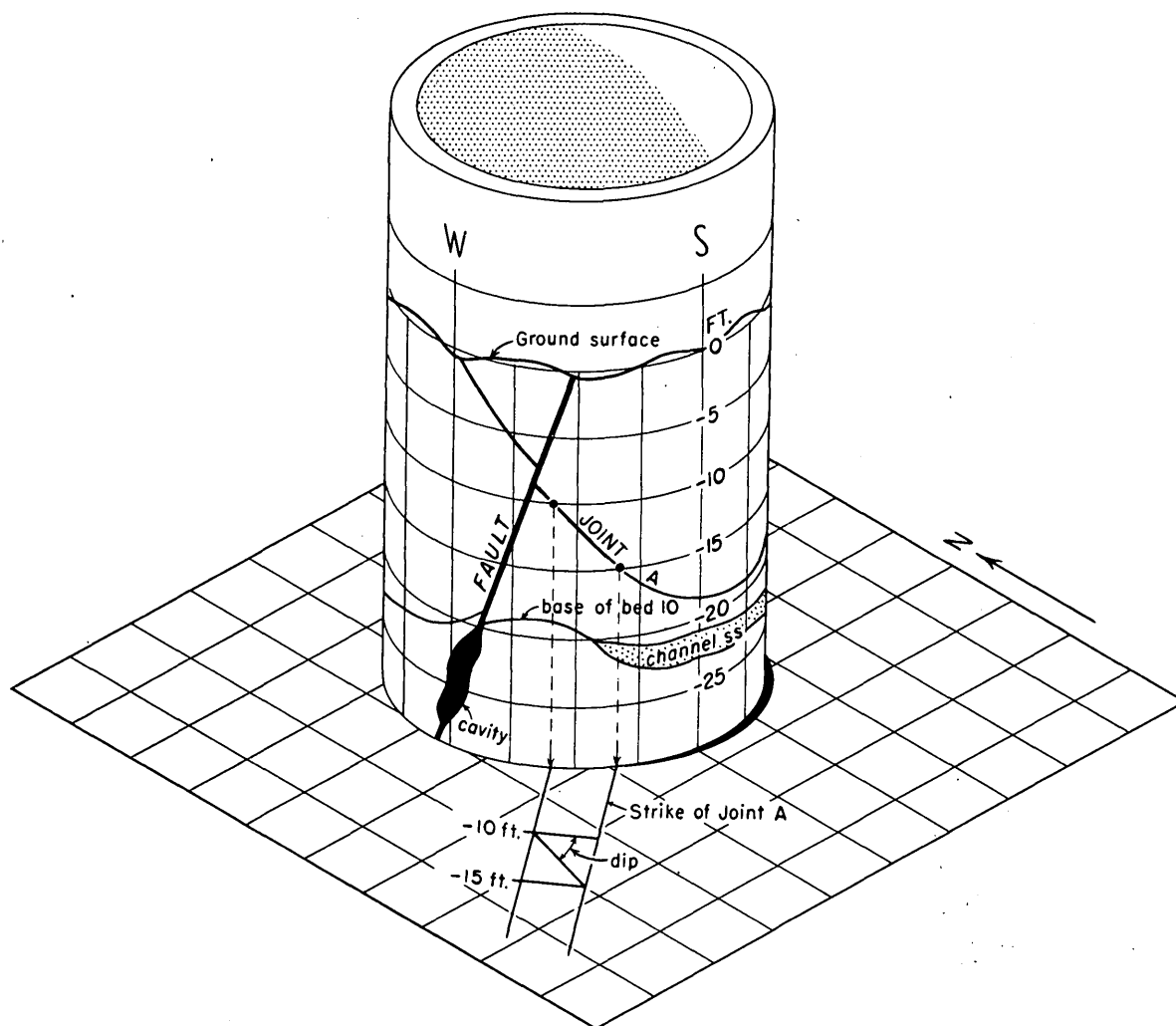
FIGURE 137.2.—Sketch of core diagram showing methods of determining strike and dip of joints.

The completed plot of geologic features is a three-dimensional representation of a core of the rock penetrated by the drill hole. Strike of bedding, joints, veins, fissures, and other features may be obtained by orienting the tube on a flat piece of graph paper. Two points of equal depth on the geologic feature are projected down the ruled lines of the tube to the graph paper (fig. 137.2). The strike is determined with a protractor from a line drawn through the points on the flat paper. If a third point on the feature at a different depth is projected down the tube to the flat paper, the dip can be determined

graphically, or trigonometrically by means of a 3-point equation. Probably this method of three-dimensional representation is applicable to other geologic and engineering problems.

The diagrams of the cores can be drafted and reproduced flat so that they can be rolled and held together by paper clips or tape. If a flat representation of the wall of the hole is needed, the semitransparent graph paper is simply turned over and a tracing is made of the reverse side. The latter form of representation shows the wall of the hole as seen by a person inside the hole.

ANALYTICAL AND PETROGRAPHIC METHODS

138.   METHODS FOR DECOMPOSING SAMPLES OF SILICATE ROCK FRAGMENTS

By JOHN C. ANTWEILER, Denver, Colo.

Three procedures are given below for the decomposition of silicate rock samples that have been neither crushed nor ground. In minor element analyses, crushing, grinding, sieving, and splitting procedures can introduce the following types of inaccuracies: (a) Errors of selective subtraction owing to loss of air-borne dust and spatter particles which may be greatly enriched in certain minor elements; (b) errors of addition from abrasion of grinding equipment, exposure to atmospheric dust, and handling; (c) chemical changes such as loss of sulfur from sulfides and oxidation of iron or copper to a higher valence state; and (d) inhomogeneities caused by unequal distribution and segregation of particles having different densities. Some of these errors can affect the accuracy of analyses for major elements (Hillebrand and others, 1953, p. 811; Kolthoff and Sandell, 1952, p. 242), but they may affect the accuracy of analyses for minor and trace constituents much more. To minimize some of these uncertainties, G. J. Neuerburg prompted the author to devise techniques for decomposition of 4-gram, or larger, fragments of rock. Many profitable suggestions were received from L. C. Peck during the work. The procedures explained here lessen chances for selective subtraction and addition caused by grinding; they fail to lessen most of the errors of chemical change; they eliminate segregation and improper representation in a specific sample, but emphasize inhomogeneities in a series of samples. The procedures are useful for certain studies such as trace element distribution; they are not intended to replace standard rock sampling and analytical procedures.

Several standard methods for silicate decomposition will eventually decompose a 4-gram rock fragment, but reagent and time requirements generally are excessive. The hydrofluoric acid procedure and two fusion procedures described below readily decompose 4-gram fragments of rock in reasonable time and require only moderate quantities of reagents. The acid procedure has been used to decompose 50-gram and larger pieces of rock. Consumption of reagents per gram of rock in most cases is no greater than that required for a powdered sample.

The final solution obtained by use of the three decomposition procedures described is designed for determination of uranium as uranyl nitrate. Determinations of some minor elements are preferably made from chloride or sulfate solutions. If such determinations are contemplated, modification in the solution procedures after decomposition is complete can readily be made. For example, in the hydrofluoric acid procedure the dry fluorides can be converted to sulfates by fuming with sulfuric acid, or they can be converted to chlorides by fuming with perchloric acid followed by solution in hydrochloric acid.

HYDROFLUORIC ACID PROCEDURE

The decomposition of finely divided silicates by HF is an extremely vigorous reaction. It is usually moderated by water and one or more strong acids such as HNO_3, H_2SO_4, HCl, or $HClO_4$. On the other hand, the decomposition of rock chips by HF is a quiet reaction and other acids are preferably omitted. For example, a 4-gram diabase chip was completely decomposed in 6 hours by 75 ml HF; a similar chip was not entirely decomposed in 4 days by the same volume of HF plus an equal volume of HNO_3.

Place a weighed rock fragment in a vessel resistant to HF, add 10 to 15 ml concentrated HF (48 percent or stronger) for each gram of rock. Place a close-fitting cover over the vessel, and digest its contents 24 hours at steam bath temperature (~85°C). After digestion remove the cover, stir occasionally, and evaporate to dryness. Add for each gram of sample about 30 ml of 50 percent (v/v) nitric acid; digest the covered mixture, stirring occasionally, for 2 hours at steam bath temperature, then evaporate to dryness. Again add nitric acid, and repeat the digestion and evaporation procedures. Dissolve the nitrates in 25 ml of $7\frac{1}{2}$ percent (v/v) HNO_3 per gram of rock and filter. If any rock remains, repeat the hydrofluoric acid decomposition procedure. If the residue consists only of zircon or other HF-insoluble

fine-grained minerals, fuse it with potassium pyrosulfate or sodium carbonate by conventional silicate analytical procedures.

Decomposition of chip samples by HF is usually preferable to decomposition by fluxes because (a) much larger samples can be handled and (b) greater concentration of minor elements in the analytical solution is possible; only volatile reagents are added and silicon is removed as gaseous tetrafluoride. It is therefore sometimes possible to lower the limit of detection of minor elements, and to improve the precision of their determination.

It is not always possible to use the HF procedure because fluorine (which is probably never completely removed) interferes in some analytical schemes; rocks, of course, cannot be analyzed for trace elements that form volatile fluorides.

Addition of boric acid after the evaporation of HF somewhat facilitates conversion of fluorides to nitrates through formation of volatile BF_3. Excess boron can subsequently be removed as methyl borate formed by the addition of methyl alcohol.

Platinum, gold, polyethylene, and glassware lined with commercial wrapping plastics (A. P. Marranzino, written communication, 1961), can be used for the HF decomposition. Plastic-lined containers are not suitable, however, for conversion of fluorides to sulfates, perchlorates, or nitrates.

SODIUM PEROXIDE FUSION PROCEDURE

Sodium peroxide is a powerful rock disintegrator, but at high temperature it also attacks most of the materials used in the manufacture of laboratory crucibles. Platinum and gold cannot be used, and nickel is far from satisfactory for rock fragment fusion. Zirconium, however, resists sodium peroxide for prolonged periods of time at temperature of as much as 900°C.

Weigh about 15 grams of sodium peroxide into a zirconium crucible, place a rock fragment weighing as much as 5 grams on top of the peroxide, and then sprinkle in enough additional peroxide to cover the sample completely. Cover the crucible and contents, heat over an open burner, slowly at first, and finally at red heat until the fragment is dissolved (usually ½ to 1 hour). Carefully add water to the cooled melt in a covered beaker. After subsidence of the vigorous reaction, dilute with enough water to make a volume of 100 ml per gram of rock. Quickly add enough concentrated nitric acid to yield a solution that has a nitric acid strength of 7½ percent by volume. Rapid addition of all the acid required eliminates effervescence, inhibits formation of gelatinous silica, and

yields a solution that is readily and quickly filtrable (L. C. Peck, oral communication, 1957). Add 0.1 grams sodium nitrite to reduce manganese which is often present in sufficient quantities to cause turbidity. Filter the solution and repeat the procedure on any undissolved residue.

One zirconium crucible will last for at least 150 sodium peroxide fusions (D. W. Richardson, written communication, 1956). Iron crucibles may be used for sodium peroxide fusions, but they introduce considerable iron to the sample, and they are not generally suitable for re-use.

SODIUM CARBONATE-BORIC ACID PROCEDURE

A carbonate-boric acid flux prepared as outlined below is more effective for silicate decomposition than either sodium carbonate, or boric acid alone, or mechanical mixtures of borax or boric acid and sodium carbonate (L. C. Peck, oral communication, 1957). Prepare the flux by melting 3 parts by weight of sodium carbonate together with 1 part of boric acid. Break the cooled melt into pieces weighing 2 to 4 grams. Preheat the weighed rock sample to 650°C to remove water. After cooling, add to the crucible containing the rock sample about 4 grams of flux for each gram of rock. Heat the crucible and contents rapidly to 900°C, and maintain this temperature for 1½ hours. If frothing occurs, lower the temperature until frothing subsides. Dissolve the cooled melt by digestion for 3 hours at steam bath temperature in 75 ml of 7½ percent (v/v) HNO_3. If there is any turbidity or rock residue, filter the solution, decompose the residue by standard analytical procedures, and add the solution to the above filtrate.

This fusion procedure is fast, economical, and effective on many kinds of rocks. Loss of samples through intumescence is its greatest shortcoming; constant attention during the fusion is necessary. The method should be tested on each new rock type before using samples that cannot be replaced or duplicated. The interference of boron in some analytical schemes is an important consideration before using this procedure.

All three of the foregoing procedures have been successfully used to decompose rocks as different in composition as basalt and granites. Their application and usefulness to diabasic rocks is reported by Neuerburg and Granger (1960, p. 780–782). The HF procedure usually is preferable to the others unless the analyses are being made in the field, or unless subsequent analytical procedures will be hampered by the presence of fluorine. The sodium peroxide procedure is best in the field because it is

the fastest, and is less apt to cause difficulty through intumescence. The sodium carbonate-boric acid procedure usually is preferable to sodium peroxide fusion in a laboratory because fusion conditions can be controlled to prevent intumescence, and complete decomposition is more likely to be obtained with the first fusion. Reagent purification, which is essential in minor element analyses, is much simpler for the HF method than it is for the fusion methods.

REFERENCES

Hillebrand, W. F., Lundell, G. E. F., Bright, H. A., and Hoffman, J. I., 1953, Applied inorganic analysis: New York, John Wiley and Sons, Inc., 1034 p.
Kolthoff, I. M., and Sandell, E. M., 1952, Textbook of quantitative inorganic analysis: New York, The Macmillan Co., 759 p.
Neuerburg, G. J., and Granger, H. C., 1960, A geochemical test of diabase as an ore source for the uranium deposits of the Dripping Spring district, Arizona: Neues Jahrb. Mineralogie Abh., v. 94, Festband Ramdohr, p. 759–797.

139.   FATIGUE IN SCINTILLATION COUNTING

By Francis J. Flanagan, Washington, D. C.

Work done in cooperation with the U.S. Atomic Energy Commission

When National Bureau of Standards radium gamma-ray standards (Mann, 1956) were counted as reference points for normalizing data, variations were noted in the counting rates. It was soon established that the variations were due to photomultiplier fatigue, and that radium from other sources caused similar effects. Although many papers on photomultiplier fatigue have been published, neither the primary cause of the fatigue nor a method of avoiding it have been discussed. Caldwell and Turner (1954) suggest, however, that the effect may be due to the low-energy gamma radiation of the radium series.

To determine the effect of gamma radiation a 2-microgram ampoule of radium was placed for 1 hour on a 2 inch by 2 inch crystal of sodium iodide coupled to a 6292 photomultiplier. The photomultiplier output was fed into a 100-channel analyzer whose gain was set so that the complete spectrum was taken in 55 channels. A 1-minute count was made during the first minute of each 1-minute interval for 1 hour, the counts obtained being recorded on tape. The initial counting rate for each channel is shown in figure 139.1, and the losses for each channel in 1 hour, expressed as percent of the first count in the channel, in figure 139.2.

Losses occur in all channels except 53, and these losses (except for irregularities between channels

45 and 55 due to low counting rates) increase with decreasing energy and with increasing counting rates. The relative error, however, decreases in most counting experiments with increasing counting rates.

To decide whether the variations in the counting rates were significant, a statistical technique was selected in preference to some arbitrary percentage loss or gain not to be exceeded. The Poisson distribution, whose mean and variance are equal, is commonly used in radioactivity counting. The initial count in any channel can represent both the mean and variance of an infinite number of observations if no changes take place in the counting conditions. If changes do occur, as they do in the present study, the variance for any channel can be calculated and then compared with that expected if there were no change. The comparison is made by the statistic χ^2/df (chi squared over degrees of freedom), which is equal to the computed variance divided by the initial count. The computed values of the statistic, together with the upper limits for the 95-percent and the 99.95-percent probability level, are shown in figure 139.3.

The computed statistic for only 8 of the channels is below the allowable limit for the 95-percent level, and hence the computed variances are not significantly greater than the Poisson variances. The
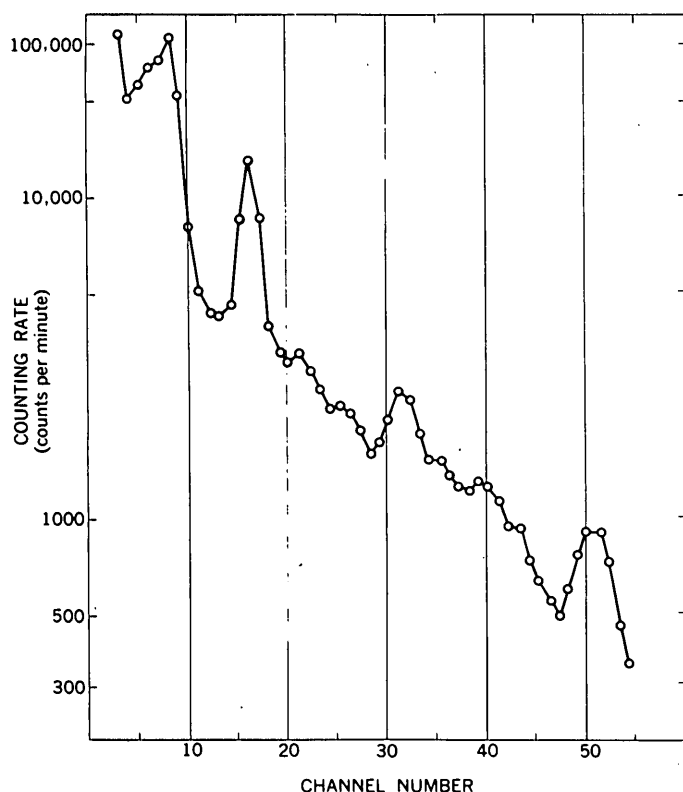
FIGURE 139.1.—Initial counting rate per channel.

statistic for 30 of the 43 channels exceeds the allowable value at the 99.95-percent level. This plot, like the one for counting-rate losses, shows that the most significant variations in counting rates occur in the low-energy part of the spectrum.

CHARACTER OF THE SOURCES

Of the gamma sources used in preliminary tests in this investigation (Co^{60}, Cs^{137}, and radium solutions) only the radium sources cause significant
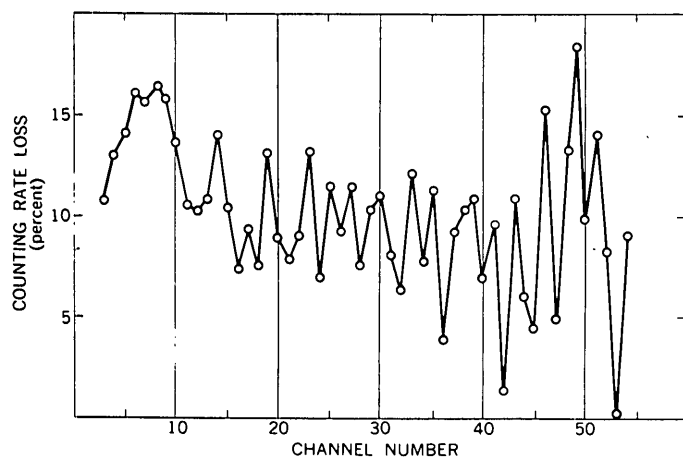
FIGURE 139.2.—Counting rate loss per channel.

losses and emit the low-energy gammas proposed by Caldwell and Turner (1954) as a possible cause of photomultiplier fatigue. If the effect is due to these gammas, it should be noticeable when counting a radium-DEF solution, since Pb^{210} is a source of low-energy gammas. One milliliter of a DEF solution was counted, but no loss was noted for this aliquot, which counted about 10,000 cpm under the same conditions that yielded 4,000 cpm for the 0.1 microgram of radium. The main solution from which this aliquot was taken was then counted with similar results. These low-energy gammas, therefore, cannot be the sole cause of fatigue.
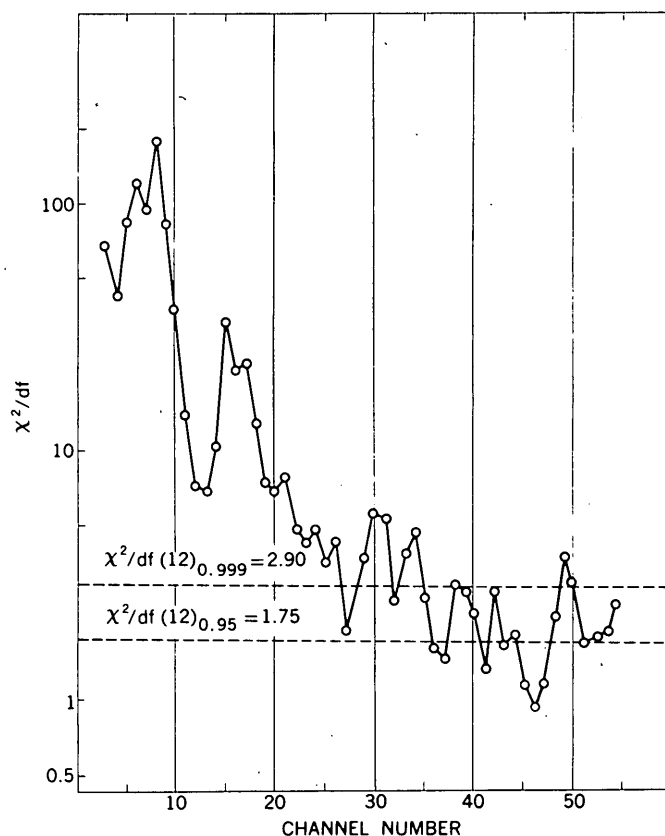
FIGURE 139.3.—Variation of counting rate per channel.

On reexamining the character of the sources used, one sees that each was contained in glass and emits beta radiation, but that the radium solutions emit the largest number. The question then arises whether bremsstrahlung, resulting from the interaction of the beta-rays with glass, could be responsible for the fatigue.

BREMSSTRAHLUNG FROM BETA PARTICLES

Two "gamma-free" beta-ray sources were available for testing this hypothesis. When a two-ounce

glass jar containing nickel sulfate recrystallized with Ni [63] ($E\beta = 0.063$ Mev) was counted with a crystal coupled to a 6342 photomultiplier, a loss of 0.7 percent of the initial counting rate of 268,000 cpm was obtained. When a Tl [204] source in the original bottle shipped from Oak Ridge National Laboratory was placed on the same crystal-tube combination, it lost 11.4 percent of its original counting rate (350,000 cpm) in one hour. The same bottle, at a different time, lost 26 percent in one hour with the 6342 photomultiplier, and gained 9 and 12 percent with a 6292 and 5819, respectively. Cathey (1958) attributes gains and losses for different photomultipliers to the amount of cesium on the dynodes.

As a further test, one ml of an uncalibrated Co [60] source was placed in a vial and counted, using the same 6342 photomultiplier; this gave 360,000 cpm with no noticeable loss in an hour. An aliquot of a solution of Tl[204], a pure beta emitter, was added to the cobalt source in the vial. This addition increased the activity of the source by 35,000 cpm, and this mixed source lost 0.8 percent of its total counting rate in one hour. When a second equal aliquot of the thallium was added, the source lost 2.3 percent in one hour. Another equal aliquot of the thallium source, dried on cellophane and placed on the same crystal, yielded 12,000 cpm with no noticeable loss.

If bremsstrahlung can cause fatigue, X-rays should have similar effects. A solid uncalibrated Co[60] source taped to a crystal yielded 130,000 counts in 16 seconds. The crystal was then exposed to white X-rays with a peak at about 10 Kev for ten seconds. When the X-ray source was removed and the cobalt counted immediately, it yielded 63,700 counts—a loss in counting rate of 51 percent. After 15 minutes the photomultiplier had recovered so much that the loss in counting rate was only 12 percent.

The hypothesis ascribing fatigue to bremsstrahlung therefore appears tenable, and since bremsstrahlung and X-rays are similar, it is consistent with the observation of Marshall and others (1947) that "the presence of fatigue is a serious defect" in the use of photomultipliers as X-ray detectors.

From these experiments it may be inferred that the photomultiplier fatigue may be primarily caused by bremsstrahlung resulting from the interaction of beta particles with the glass ampoules.

REFERENCES

Caldwell, R. L., and Turner, S. E., 1954, Gain variation of photomultiplier tubes: Nucleonics, v. 12, no. 12, p. 47–48.

Cathey, L., 1958, Fatigue in photomultipliers, in Scintillation Counter Symposium, 6th Washington, 1958, Proc: I R E Trans on Nuclear Sci., v. NS–5, no. 3, p. 109–114.

Mann, W. B., 1956, The preparation and maintenance of standards of radioactivity: Internat. Jour. Applied Radiation and Isotopes, v. 1, p. 3–23.

Marshall, F. H., Coltman, J. W., and Hunter, L. P., 1947, The photomultiplier X-ray detector: Rev. Sci. Instruments, v. 18, p. 504–513.

---

140. A SIMPLIFIED METHOD OF CONCENTRATING AND PREPARING CARBONATE SHELLS FOR C[14] AGE DETERMINATIONS

By Thomas C. Nichols, Jr., Denver, Colo.

Because handpicking of carbonate shells from a field sample is laborious and time consuming, a simpler method of concentrating and preparing these shells for C[14] age determinations was developed using already existing equipment and reagents of the U.S. Geological Survey Laboratory at Denver. Three steps are involved: determining the feasibility of removing shell material from the sample matrix, disaggregating the sample and concentrating the shell material, cleaning the shell material. All reagents and containers coming in contact with the shells must be free of contaminating carbon.

FEASIBILITY OF REMOVING SHELLS FROM SAMPLE

The feasibility of removing shells from a sample depends upon the size and condition of the shells and also the condition, texture, and composition of the matrix. It is difficult and tedious to process

shells smaller than 420 microns—but if necessary, a modified procedure will reclaim some of the smaller ones. The matrix must be reasonably free of ferruginous, siliceous, and carbonate cementing materials. These materials, if present in large quantities, are difficult to remove without destroying the shells. The size and sorting of the matrix are of concern only in actual separation techniques.

SEPARATING SHELLS FROM MATRIX

The sample is presoaked for 16 hours in a 3.5 percent solution of sodium polyphosphate in distilled water to disperse the clays and other fine materials which tend to cement the matrix together. These dispersed fine materials are discarded first by wet screening the sample through a U.S. Standard No. 200 screen. The disaggregated portion remaining on the screen is dried and passed through a U.S. Standard No. 40 screen, thus concentrating the larger shells with the coarse fraction of the sample. The —40-mesh fraction is set aside in a closed container for possible further processing. The +40-mesh fraction is now examined for sorting of grains rather than sorting for shells and shell fragments. Most of the shells and shell fragments are in the same size range as the accompanying sand grains and cannot be isolated by screening, but there are usually some large shells which can be isolated. Therefore, the +40-mesh fraction is sized with appropriate screens to isolate the larger shells and to divide the remaining portion into well-sorted fractions containing the smaller shells and shell fragments. At this point, there might be a sufficient quantity of isolated shells for age determination. If not, it is necessary to isolate shell material from the finer of the +40-mesh fractions.

By taking advantage of their shapes and relatively light densities, shells and shell fragments can be rapidly and completely separated from the heavier more equidimensional sand grains by air elutriation. A large elutriation apparatus similar to that described by Frost (1959, p. 886) is effective.

Light-mineral impurities such as gypsum will separate with the shells, but these can be eliminated by elutriating a second time, and readjusting the air stream velocity. Fractionation of shell material from the minus 40-mesh fractions by air elutriation is impractical because of the static electricity generated. This problem is overcome if distilled water is used as an elutriating medium.

CLEANING SHELL MATERIAL FOR C^{14} DETERMINATIONS

The concentrated shell material from the different fractions can now be added together and more closely scrutinized for impurities. There will probably still be clay imprisoned within the shells, and possibly some secondary lime encrustations on the outer surfaces. At this point, the shells should be gently fractured, but not pulverized, in a mortar with a pestle. The shells are placed in a beaker and allowed to soak in 3.5 percent solution of sodium polyphosphate in distilled water for 1 to 2 hours; then they are processed in an ultrasonic transducer for about 15 minutes or until the shells appear to be clean. The ultrasonic transducer is very effective in breaking up clays and secondary encrustations ordinarily immune to other treatment. Very fragile shells must be treated sparingly in the ultrasonic transducer as they tend to disintegrate. After this treatment, repeated washing and decanting with distilled water will remove impurities present as suspended fines. The clean shells remaining in the beaker are covered with a watch glass and allowed to dry slowly under a heat lamp. The dry shells are suitable for a C^{14} age determination.

There will be many problems peculiar to individual samples. The above procedure is meant to be a general outline and can be revised to meet the demands of any individual sample.

REFERENCE

Frost, I. C., 1959, An elutriating tube for the specific gravity separation of minerals: Am. Mineralogist, v. 44, p. 886–890.

141. COLORIMETRIC DETERMINATION OF IRON IN SMALL SAMPLES OF SPHALERITE

By Leonard Shapiro and Martha S. Toulmin, Washington, D. C.

The increased use of the "sphalerite geothermometer" (Kullerud, 1953, and Barton and Kullerud, 1958) that correlates the temperature of formation of the sphalerite with the amount of iron substituting for zinc in the crystal structure, has developed a need for a simple, rapid, and reliable procedure for determining the amount of iron in sphalerite. Because natural sphalerite is commonly fine grained and/or compositionally zoned, the analytical method used should be suitable for small samples, preferably single small fragments. The method described here has been utilized to trace changes in composition from the center to the margin of zoned sphalerite crystals.

A method adapted (Yoe and Jones, 1944) to meet these requirements is based on the use of disodium–1,2–dihydroxybenzene–3,5–disulfonate (Tiron). It is a simple but flexible procedure, being suitable for visual estimation for greatest simplicity, or measurement in a photometer for increased accuracy. Samples from 0.6 to 30 mg have been used, and iron contents ranging from 0.1 to about 20 percent have been determined. The procedure is described for a 10 mg sample for the range 0 to 1.1 percent iron. Smaller size sample may be used if necessary, and small aliquots of solutions may be used where iron concentrations are high.

The sphalerite is decomposed with aqua regia in a test tube, heated to drive off oxides of nitrogen and sulfur that may have been formed, and the remaining salts taken back into solution with hydrochloric acid. Tiron and a buffer are added, and the purple color produced is compared with a set of standard iron solutions, either visually or in a photometer using a wave length of 550μ.

REAGENTS

1. Standard iron solution. Dissolve 121 mg $FeCl_3$ •$6H_2O$ in water containing a few ml of hydrochloric acid and dilute to 250 ml in a volumetric flask.
2. Buffer solution. Dilute 80 g of ammonium acetate and 30 ml of acetate acid to 2 liters.
3. Tiron. Pure powdered disodium–1,2–dihydroxybenzene–3,5–disulfonate.
4. Concentrated hydrochloric acid. Contained in a dropping bottle.
5. Concentrated nitric acid. Contained in a dropping bottle.
6. Zinc chloride solution. Dilute 210 mg of $ZnCl_2$ to 100 ml in a volumetric flask.

PREPARATION OF STANDARDS

To a series of 22 × 175 mm test tubes add: 0.0, 0.1, 0.3, 0.5, 0.7, 0.9, and 1.1 ml of the standard iron solution with a graduated pipette. Add 6.7 ml of zinc chloride solution, 3 drops of concentrated hydrochloric acid, and 10 to 20 mg Tiron to each tube. With a graduate add 20 ml of the buffer solution to each tube, and add water to make the volumes equal to 30 ml. Invert to mix. The resulting solutions correspond to 0.0, 0.1, 0.3, 0.5, 0.7, 0.9, and 1.1 percent iron when a 10 mg sample is used, and are stable for a few days.

PROCEDURE

1. Crush a small crystal of sphalerite with a mortar and pestle.
2. Weigh 10 mg of the sample and transfer to a dry test tube.
3. Add about 6 drops of concentrated nitric acid and 6 drops of concentrated hydrochloric acid.
4. Evaporate to dryness over a Bunsen burner, then heat with the full flame of the burner for 10 to 20 seconds.
5. Allow to cool for several minutes.
6. Add 3 drops of hydrochloric acid and wet the bottom of the test tube by rotation, then add 1.1 ml of water.
7. Add 10 to 15 mg of Tiron powder.
8. Add 20 ml of buffer solution and water to 30 ml. Mix by inversion.
9. Compare with the set of standards. A visual comparison can be made to obtain a value to the nearest 0.1 percent, or better results can be obtained by comparison in a photometer at a wave length of 550μ.

The procedure may be modified by using smaller samples or by dilution of the sample after step 6 and use of a portion of the diluted solution. If single fragments of 0.5 to 2 mg are used, it may be necessary to repeat steps 3 and 4 to obtain complete decomposition.

DISCUSSION AND RESULTS

Accuracy and precision of the procedure were studied using 1 to 2 mg of five synthetic sphalerites of known composition. The samples were analyzed at four different times to provide reproducibility data, and the averages obtained were compared with the known iron content. The samples also

TABLE 1.—*Determinations of percent iron in synthetic sphalerite*

Sample	Proposed colorimetric method				Average	Known content	Conventional ceric titration
	1	2	3	4			
55.........	4.5	5.0	4.9	5.0	4.9	4.7	4.7
56.........	7.8	9.2	8.6	9.4	8.7	8.6	8.5
59.........	2.4	2.5	2.8	2.2	2.5	2.6	2.6
101........	15.1	15.9	20.7	17.4	17.3	17.7	17.6
109........	13.8	12.3	13.1	13.3	13.1	14.4	14.2

were analyzed by C. A. Kinser with a conventional ceric sulfate titration procedure as an additional basis of comparison. The results are shown in table 1.

Samples of approximately 1 to 2 mg were weighed directly into the decomposition test tubes. Such weighings may be expected to have an accuracy of about 10 percent. The replication of results shows a spread of about 10 percent from the known iron concentration, but deviations of the averages from the known are generally better, indicating that chance variations such as weighing errors can be reduced by replication, or the use of larger samples.

Manganese, sometimes present in significant amounts, was found to introduce no error up to 10 percent manganese. Copper present in amounts greater than those found in natural sphalerites also had no effect.

The ability to use very small samples, especially small single fragments, plus the simplicity of the procedure, provide a useful tool for determination of the iron content of sphalerite. The method is readily adaptable to use in the field.

REFERENCES

Barton, P. B., Jr., and Kullerud, Gunnar, 1958, The FeS–ZnS–S system: Carnegie Inst. Washington, Ann. Rept. Director, Geophys. Lab., Paper 1289, p. 227–229.

Kullerud, Gunnar, 1953, The FeS–ZnS system, a geological thermometer: Norsk geol. tidsskr., v. 32, no. 2–4, p. 61–147.

Yoe, J. H., and Jones, L. A., 1944, Colorimetric determination of iron with disodium-1,2-dihydroxybenzene-3,5-disulfonate: Anal. Chemistry, v. 16, p. 111–115.

142.   INDIRECT SEMIAUTOMATIC DETERMINATION OF ALUMINA WITH EDTA

By J. I. DINNIN and C. A. KINSER, Washington, D. C.

In the course of investigating the application of EDTA (disodium ethylenediaminetetraacetate dihydrate) titrations to the determination of alumina in geological materials, a new indirect titration system has been developed. Because of the uncertainty of most of the methods available for alumina it is useful to have auxiliary procedures, as different in nature as possible, by which to check results.

The new method involves the addition of a controlled excess of EDTA and titration of the excess with ferric chloride solution using Tiron (disodium 1,2–dihydroxybenzene 3,5–disulfonic acid) as an indicator. The Tiron-ferric chloride titration system has been used for the direct determination of iron (Haberli, 1954) and the indirect determination of zirconium (Manning, Meyer, and White, 1955) but as far as is known it has not previously been used for the determination of alumina.

Other EDTA titration systems for aluminum tested in this laboratory have been unsatisfactory. Indirect titration with cupric sulfate using Pyrocatechol Violet as indicator (Suk and Malat, 1956) gives excellent results with pure aluminum solutions. The system is extremely susceptible to changes in the chemical environment however, and its use must be rigorously restricted. In titrations performed in pyridine-acetate buffered solutions, the presence of moderate concentrations of phosphate or sulfate prevent the formation of an end point; perchlorate or chloride have significant effects on the location of the end point. Indirect titrations with ferric chloride using salicylic acid (Milner and Woodhead, 1954) or sulfosalicylic acid (Patrovsky and Huka, 1957) as indicators give indistinct end points under the conditions of the tests.

The Tiron-ferric chloride titration system is less subject to interferences than the Pyrocatechol Violet-cupric sulfate system and appears to have several

advantages over other methods proposed for the determination of alumina with EDTA. The reaction appears to be stoichiometric, the solution does not have to be boiled, and the end point is very sharp. The sharpness of the end point can be ascribed in part to the use of elevated temperatures, but the use of an automatic colorimetric recording titrator is also a major contributing factor.

The recording colorimetric titrator used in this investigation is similar to one described by Shapiro and Brannock (1955) but differs in several features. The titrating solution is fed by a motor-driven syringe rather than by gravity. The light beam from a tungsten lamp, after being collimated by a plano-convex lens, passes through the sample solution, then through a narrow band interference filter with a transmission peak at 620 mu; it is detected by a barrier layer photocell. The output from the photocell is fed through a voltage dividing potentiometer to a recorder. A low value resistance in series with the voltage divider is electrically removed from the circuit by the same switch that starts the syringe drive motor. This effectively increases the input to the recorder by a small increment, causing a fiducial mark from which to measure the duration of the titration.

The recording titrator affords a higher sensitivity than can be attained by visual titration. The effects of minor changes in titration conditions, not discernible by visual titration, can readily be ascertained by the titrator. The precision of the motor-driven syringe, based on weight of solution delivered during varying distances of chart travel, was better than one part in two thousand.

REAGENTS FOR TITRATION OF ALUMINA

Alumina standard solution: 1.00 mg Al_2O_3 per ml in 2 percent hydrochloric acid.
EDTA solution: 0.0100 M.
Phenolphthalein solution: 0.1 percent in ethyl alcohol.
Ammonia solution: 1 + 1 (v + v).
Acetate buffer: 140 g sodium acetate and 60 ml acetic acid (conc.) per liter.
Tiron solution: 2 percent in water.
Ferric chloride solution: 0.2 mg iron per ml in water.

PROCEDURE

In a 400 ml beaker, treat a sample solution containing no more than 2.0 mg alumina as follows:
Add 10.00 ml EDTA solution. Using several drops phenolphthalein solution as indicator, adjust the pH of the solution to alkaline (pink) with ammonia. Add 25 ml of acetate buffer, 1 ml of Tiron solution, and sufficient hot water (80°–90°C) to make a total volume of 300 ml. Titrate excess EDTA with ferric chloride solution.

STANDARDIZATION PROCEDURE AND CALCULATION

Titrate three solutions containing (1) 0 mg, (2) 1.00 mg, and (3) 2.00 mg of alumina by the same procedure used for the samples. The titer of solution (1) furnishes the base value for 10.00 ml of EDTA solution. Subtract titer (2) from titer (1); this is the equivalent titer for 1.00 mg of alumina. Subtract titer (3) from titer (1); this is the equivalent titer for 2.00 mg of alumina. Calculate the titration factor by dividing the mg of alumina in solutions (2) and (3) by their respective equivalent titers.

Subtract the titers of each of the sample solutions from the titer of solution (1). The net titer represents the EDTA complexed by alumina in each solution.

Calculate the percent Al_2O_3 as follows:

$$\text{percent } Al_2O_3 = \frac{\text{titration factor} \times \text{net titer} \times 100}{\text{mg sample}}$$

DISCUSSION

The intermediate stability constant of the aluminum-EDTA complex (log K=16.1) allows the use of a rather low pH (3.7) for the titration. This precludes interference by elements such as the alkalies and alkaline earths, which are complexed at high pH only. However, this still leaves a major portion of the elements in the periodic table free to interfere by consuming EDTA. These elements must be separated if they are present in significant concentration.

Among the anions, perchlorate interferes with the end point. Its effect in moderate concentration however, can be overcome by the addition of sodium sulfate. Phosphates must be absent.

The method has thus far been applied to the determination of alumina in chromite and chrome ore. A mercury cathode electrolysis was used to separate chromium, iron, and nickel; a cupferron separation was used to separate titanium and vanadium when present in significant concentrations. Excess cupferron had to be destroyed completely with sulfuric and nitric acids before proceeding with the titration. The results given by the titration procedure were in good agreement with results obtained by a colorimetric procedure. Good agreement with the certified analyses was obtained in the analysis of standard samples of chrome ore.

REFERENCES

Haberli, E., 1954, A method for the titrimetric determination of iron in blood by means of complexon: Experientia, v. 10, p. 34–35.

Manning, D. L., Meyer, A. S., Jr., and White, J. C., 1955, The compleximetric titration of zirconium based on the use of ferric iron as the titrant and Tiron as the indicator: U.S. Atomic Energy Commission ORNL–1950, 15 p.

Milner, G. W. C., and Woodhead, J. L., 1954, The volumetric determination of aluminum in non-ferrous alloys: Analyst, v. 79, p. 363–367.

Patrovsky, V., and Huka, M., 1957, Complexometric titration

XXI. Volumetric determination of iron, aluminum, and titanium in silicates: Coll. Czechoslov. Chem. Commun., v. 22, p. 37–42.

Shapiro, L., and Brannock, W. W., 1955, Automatic photometric titrations of calcium and magnesium in carbonate rocks: Anal. Chemistry, v. 45, p. 725–728.

Suk, V., and Malat, M., 1956, Pyrocatechol Violet; indicator for the EDTA titration: Chemist-Analyst, v. 45, p. 61–62.

143.   DETERMINATION OF COPPER IN PLANT ASH WITH NEO-CUPROINE

By Claude Huffman, Jr., and Dwight L. Skinner, Denver, Colo.

Smith and McCurdy (1952) first investigated neo-cuproine (2,9–dimethyl–1, 10–phenanthroline) as a new and more specific chelating reagent for copper. Neo-cuproine reacts with a cuprous copper solution buffered with acetic acid to form a yellow-orange chelate extractable with water-immiscible alcohols at pH 7 or less. Since Smith and McCurdy's report, many applications of neo-cuproine to determinations of copper in diverse materials have been made, for example, for copper in uranium ores (Skinner and Goss, oral communication), for copper in germanium and silicon (Luke and Campbell, 1953), for copper in steels (Gahler, 1954), and for copper in titanium ore (Andrew and others, 1957). Thus the neo-cuproine reagent has become increasingly popular for the determination of copper in complex materials because of its unique specificity, stability, and sensitivity with copper. The method described here is an application of neo-cuproine to the determination of copper in plant ash. In developing this method analyses were made of plant samples collected by F. J. Kleinhampl and field party from the following areas: Circle Cliffs, Garfield County, Utah; Grants district, McKinley County, N. Mex.; and Elk Ridge, San Juan County, Utah.

REAGENTS AND EQUIPMENT

Neo-cuproine solution. 1.085 g neo-cuproine is dissolved in 333 ml ethyl alcohol and diluted to 500 ml with water.

Sodium citrate solution. 3 percent (w/v) solution in water.

Sodium acetate solution. 20 percent (w/v) solution in water.

n-hexyl alcohol, Eastman practical grade. This reagent can be reused after recovery by distillation.

Hydroxylamine sulfate solution: 1 percent (w/v) solution in water, freshly prepared.

Sodium hydroxide solution. 40 percent (w/v) in water.

Standard copper solution. Stock solution 1 ml = 0.1 mg Cu. Dissolve 0.3929 g of clear unfloresced crystals of $CuSo_4 \cdot 5H_2O$ in water, add 10 ml of hydrochloric acid and dilute one liter. Dilute solution 1 ml = 0.005 mg Cu. Dilute 50 ml of the stock solution to one liter with water.

Absorption cells, matched, 1 cm.

Beckman D. U. spectrophotometer.

PREPARATION OF SAMPLE

Dry and grind the plant material. Ash off 10 g of the ground vegetation at 550°C in a tared porcelain dish. Calculate the ash content. Thoroughly mix the ash and reserve for analysis.

PROCEDURE

Accurately weigh about 100 mg of plant ash and transfer to a test tube (16 by 150 mm). Add 5 ml (1+4) hydrochloric acid and boil for one minute. Filter the solution through a retentive 9 cm filter paper into a 60 ml separatory funnel. Wash the residue four times with demineralized water. Add 5 ml of 3 percent sodium citrate solution to the filtered solution to complex the iron, then add 5 ml of 20 percent sodium acetate solution. Mix thoroughly. Add 5 ml of freshly prepared one percent hydroxylamine sulfate solution to reduce the cupric ion; adjust the solution to pH 5 with approximately 10 drops of 40 percent sodium hydroxide solution, and mix again. Add 4 ml of neo-cuproine solution and mix the contents of the funnel again. Add 10.0 ml of n-hexyl alcohol, stopper the separatory funnel and shake for 30 seconds. Allow the solution to stand for 5 minutes until the two immiscible solutions separate. Drain the aqueous layer and discard.

Draw off a portion of the n-hexyl alcohol into a 1-cm cell and measure the absorbance with the spectrophotometer at 454μ, using a reagent blank carried through the entire procedure as a reference.

STANDARDIZATION

Portions of the standard solution containing 1, 3, 5, 10, 20, 30, 40 micrograms copper and one reference solution (reagent blank) were carried through the entire procedure to establish a working curve. A plot of data from the standards above gives a satisfactory working range of 10 to 400 parts per million copper based on a 100-milligram sample of plant ash.

REMARKS

The neo-cuproine reagent is unique because it is specific for copper (Smith and McCurdy, 1952). The absence of interference by 56 metal ions at the 50-microgram level was shown by Luke and Campbell (1953). Tests for interference from 15 mg amounts of iron (III), aluminum, chromium (III), manganese (II), molybdenum (VI), and vanadium (IV), showed that they could be tolerated except for the chromium. Only about 2 mg of chromium can be tolerated (Andrew and others, 1957). The interference from anions can be significant because they form a tighter complex with copper than does neo-cuproine. Gahler (1954) has shown that trace amounts of cyanide, sulfide, and large amounts of phosphate must be removed to prevent their serious interference. No interference from chromium or phosphate occurs in the analysis of plant ash be-

TABLE 1.—*Summary of 82 plant samples used in the precision study*

Plant species	Number of samples	Average ash (percent)	Copper (ppm)	
			Range	Average
Juniper	35	5.3	15–120	60
Pinon pine	38	3.3	50–200	125
Ponderosa pine	9	3.0	65–150	108

TABLE 2.—*Comparison of copper values determined by the neo-cuproine method and the biquinoline method*

[Analysts: neo-cuproine method, Claude Huffman, Jr.; biquinoline method, J. H. McCarthy]

Sample	Ash (percent)	Copper in ash (ppm)		
		Neo-cuproine	Biquinoline	Difference
236762	8.6	15	15	none
236763	4.8	75	80	−5
236764	5.7	30	25	+5
236765	6.0	65	55	+10
236766	5.1	30	25	+5
236767	2.9	90	80	+10
Average		51	47	6

cause the concentration of both elements is well below the interference levels established by the above authors.

The precision of the determination of copper by the method described was calculated from paired data (Youden, 1951, p. 17) using replicated determinations on 82 samples of plant ash. The standard deviation of the determination is 9.6 ppm copper. The 82 samples used in the precision study consisted of branch tips from 35 juniper, 38 piñon pine, and 9 ponderosa pine. A summary of the 82 samples is shown in table 1.

Table 2 compares the neo-cuproine method and the biquinoline method for the determination of copper in six plant ash samples. The agreement between methods is about the same as the standard deviation of the determination.

REFERENCES

Andrew, J. F. Goulstone, A. B., and Deacutis, A. A., 1957, Spectrophotometric determination of copper in titanium: Anal. Chemistry, v. 29, p. 750–753.

Gahler, A. R., 1954, Colorimetric determination of copper with neo-cuproine: Anal. Chemistry, v. 26, p. 577–578.

Luke, C. L., and Campbell, M. E., 1953, Determination of impurities in germanium and silicon: Anal. Chemistry, v. 25, p. 1588–1593.

Smith, G. F., and McCurdy, W. H., 1952, 2,9-dimethyl-1,10-phenanthroline, new specific in spectrophotometric determination of copper: Anal. Chemistry, v. 24, p. 371–373.

Youden, W. J., 1951, Statistical methods for chemists: New York, John Wiley and Sons, Inc., p. 125.

144.   DIRECT-READING SPECTROMETRIC TECHNIQUE FOR DETERMINING MAJOR CONSTITUENTS IN NATURAL WATER

By JOSEPH HAFFTY and A. W. HELZ, Washington, D. C.

Methods used by the Geological Survey for determining major cations and silica in natural water entail in most instances five separate determinations employing titrimetric, spectrophotometric, and flame-photometric procedures. The use of optical emission spectrography with multiplier phototubes to measure the radiant energy of the spectral lines can quickly establish the concentrations of the major constituents in one operation. The procedure is simple in that no complicated preparation of sample or standards is necessary. It is designed to determine the elements and compounds listed on table 1 in the ranges of concentration indicated. A spectographic-residue method for determining minor elements in waters has been described previously (Haffty, 1960).

Potassium was not included in the list of elements determined because a red-sensitive tube for measuring the very sensitive 7800 A (Angstrom units) line was not available. However, the writers feel that no difficulty would be encountered if this element were to be determined, as the behavior of potassium in the spark is analogous to that of sodium. The present work was exploratory, and was done on a spectrometer set up specifically for the analysis of major elements of rocks rather than natural waters.

Standard solutions were prepared as follows: Calcium carbonate was dissolved in dilute nitric acid; sodium and potassium were added as the chlorides; magnesium added as the oxide was dissolved by addition of sulfuric acid; and silica was introduced by boiling commercial silica gel in distilled water, filtering, diluting the filtrate slightly and reboiling for a total time of four hours. All of the above substances, except silica gel, were of "specpure" grade. R. O. Fournier prepared the silica solution, and Leonard Shapiro and J. J. Rowe analyzed it.

J. I. Dinnin made flame-photometric determinations for calcium and sodium in the water samples tested. The procedure consists of mixing 9 parts by

TABLE 1.—*Spectrum lines and concentration ranges*

Element or compound	Wavelength (A)	Concentration range (parts per million)
Calcium	3179.33	3 to 316
Sodium	5889.95	1 to 316
Magnesium	2802.70	0.3 to 100
Silica	2881.58	3 to 31.6
Lithium	3232.61	Reference line
Mercury	5460.74	Monitor line
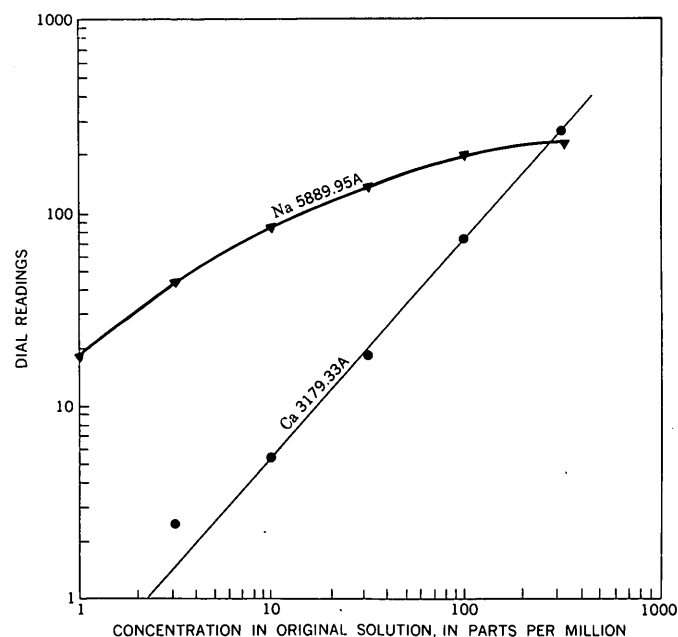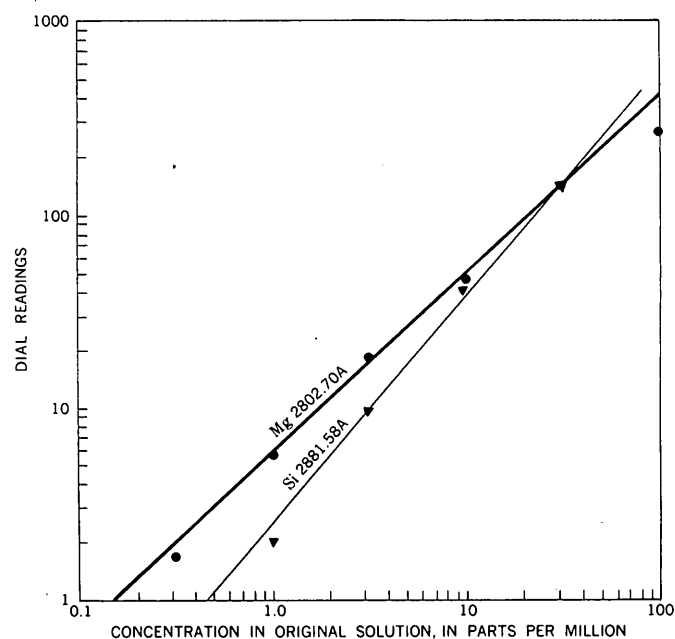
FIGURE 144.1.—Working curves used for obtaining concentrations of major constituents in natural water.

volume of water sample with 1 part of a lithium solution, prepared by dissolving lithium carbonate in dilute nitric acid. Lithium is used as the reference element, and in the final mixture it is equivalent to 1 gram per liter. The mixture is then poured into a porcelain boat and excited directly using the rotating disk method. The standards are treated in the same way as the unknown samples. The radiant energy is measured by multiplier phototubes placed in back of slits so located as to select lines of wavelengths indicated in table 1. The output of the multiplier phototubes activate amplifiers which record the intensity of light on the tubes. The length of a "run" is determined by the output of the phototube for lithium. The response is adjusted to give a 60-second run by setting the dc (direct current) supply voltage for the "lithium" multiplier phototube. The analytical range for the elements sought is subsequently adjusted by setting the corresponding dc supply voltages. Working curves are constructed from the standard solutions by plotting parts per million of the element or compound versus the dial readings on log-log paper. Examples of such curves are shown on figure 144.1. The concentrations of the elements in the unknown samples are read from the working curves.

The excitation source is a low-voltage underdamped repetitive discharge having a sparklike character. The circuit parameters of a satisfactory unit used for this work are: capacitance, 14 microfarads; inductance, residual; resistance, residual; discharge-point control, 30°; and output voltage,

940. A 3-mm spark gap is maintained between an upper pointed graphite electrode ¼-inch in diameter and a lower graphite disk, ½-inch in diameter, which is partly immersed in the sample and rotated at a speed of 10 rpm.

Sparse comparative data with chemical and flame-photometric methods indicate that acceptable agreement has been obtained for the elements determined in the lower range of concentrations. However, the calcium line seems to be enhanced in higher concentrations (about 35 ppm and higher). The working curve for sodium shows that self-reversal of the 5890A line takes place, but acceptable agreement with flame-photometric results was realized in the range 2 to 10 ppm. Good comparisons were obtained for magnesium in the range 2 to 25 ppm and silica in the range 3 to 30 ppm.

Dilution of the sample may solve the difficulties indicated above for calcium and sodium. However, this requires additional operations that defeat the purpose of the procedure. Further work may disclose that there are more suitable additives to the solutions, or that a selection of other spectral lines is necessary to determine accurately the concentrations of these elements. Our experience indicates that within a few minutes the procedure will provide determinations of the major constituents in natural waters.

REFERENCE

Haffty, Joseph, 1960 Residue method for common minor elements: U.S. Geol. Survey Water-Supply Paper 1540–A.

145. RAPID QUANTITATIVE ESTIMATES OF QUARTZ AND TOTAL IRON IN SILICATE ROCKS BY X-RAY DIFFRACTION

By D. B. TATLOCK, Menlo Park, Calif.

The relationships between diffraction, absorption, fluorescence, and density allow for rapid and reasonably accurate quantitative estimates of quartz and total iron in most holocrystalline silicate rocks, both fresh and altered, from X-ray diffraction patterns of whole-rock powders. Diffraction analysis has proved indispensable in the study of cryptocrystalline metasomatized rocks not amenable to

modal analysis by microscopic examination. No attempt is made in this short paper to present details of instrumentation or of sample preparation.

The reproducibility of quartz peak heights in quantitative diffraction work has been well demonstrated by many investigators (Klug and Alexander, 1954, and Weiskirchner, 1960). Only a few (Black, 1953, and v. Engelhardt and Haussühl, 1960), how-
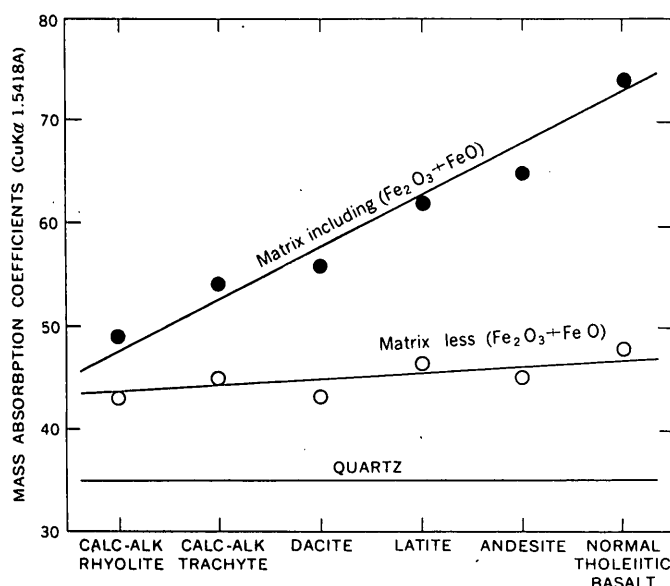
FIGURE 145.1.—Mass absorption coefficients of matrices of average igneous rocks with and without (Fe_2O_3 + FeO) and exclusive of normative quartz.

ever, have applied diffraction to modal analysis of the common silicate rocks on a mass production basis, owing to the seemingly adverse effects of absorption and fluorescence. In comparing diffraction patterns of quartz-bearing whole-rock powders ranging from felsic to mafic in composition, absorption effects are present that usually prevent a direct comparison of the quartz peak heights (Leroux, Lennox, and Kay, 1953). Specifically, when a mixture contains both a weak and a strong absorber, peaks of the weakly absorbing component appear weaker, and those of the strongly absorbing component stronger, than expected from a linear relationship for each component (Klug and Alexander, 1953, p. 411). In determining the quartz content of a whole-rock powder, the powder may be regarded as consisting of just two components, the quartz, and the sum of the other minerals which may be designated the matrix. Figure 145.1 shows that the mass absorption coefficients of the matrix portion of average igneous rocks (Nockolds, 1954), exclusive of the iron oxides and normative quartz, are nearly constant, ranging from 43 for rhyolite to 48 for basalt. With iron oxides included in the matrix, however, the mass absorption coefficients range from 49 for rhyolite to 74 for basalt. Hence, iron is shown to be the element chiefly responsible for appreciable differences in absorption in the matrix component of the common silicate rocks.

Iron, also, is the only relatively abundant common rock-forming element whose fluorescence under copper radiation affects appreciable differences in background. The greater the iron content of a whole-rock powder, the greater the background intensity of its diffraction pattern. This relationship allows for an estimation of the total iron in a sample by reading the background at a given angle 2θ after the diffraction unit has been calibrated. In figure 145.2 the total iron, calculated from chemical analyses of metasomatized rhyolitic and andesitic rocks and Franciscan graywackes, has been plotted against background intensities at the 4.26A quartz line as recorded on diffraction patterns of splits of the chemically analyzed powders. The background intensity is the average of measurements on both sides of the selected line (Carl, 1947). Such a curve can easily be extended for rapid and reasonably accurate analysis of low-grade iron ores by preparing mixtures of quartz and hematite or magnetite; accuracy is within 10 percent of the amount of iron present in concentrations greater than 20 percent.

Referring again to figure 145.1, the slightly strongly absorptive character of the matrix component (less iron) in mafic rocks relative to felsic rocks, and its consequent depressant effect on quartz
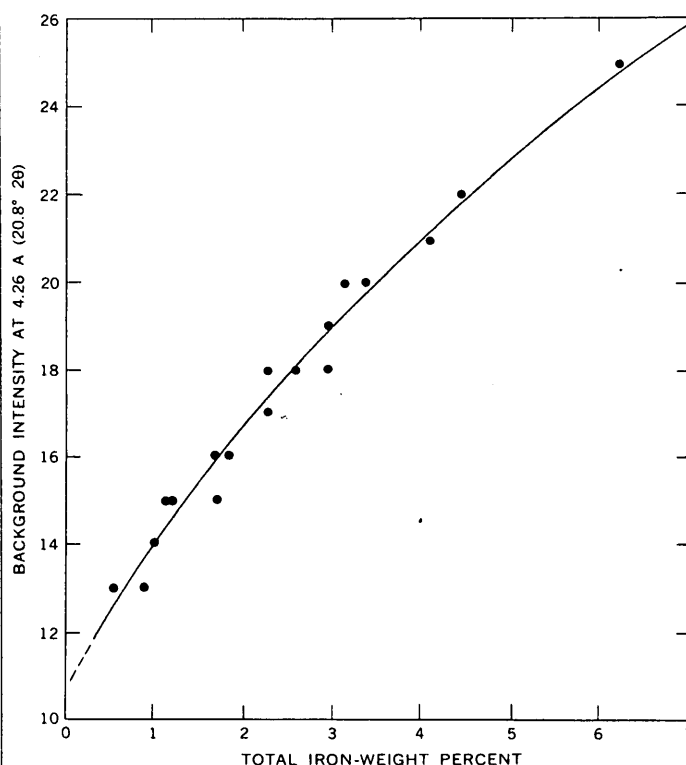
FIGURE 145.2.—Total iron, calculated from chemically analyzed rocks, plotted against background intensity of 20.8°2θ (CuKα; nickel filter).
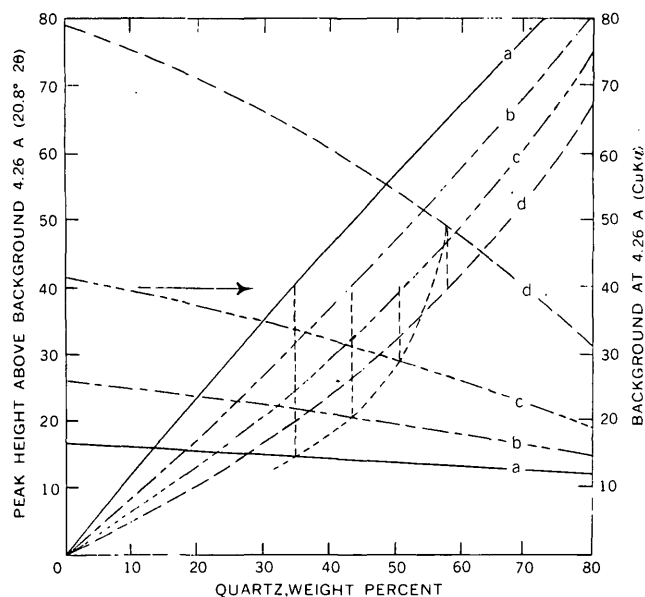
FIGURE 145.3.—Peak height curves and corresponding background curves for quartz mixed with materials having different mass absorption coefficients resulting chiefly from differences in iron content. Construction of interpolation curve is illustrated.
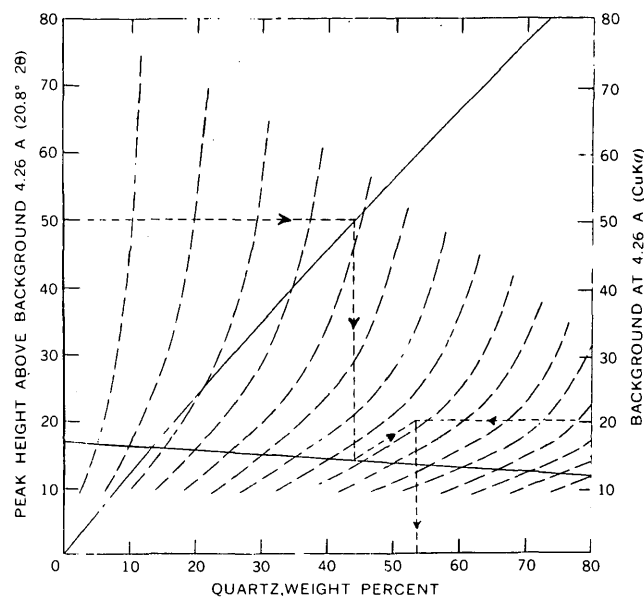
FIGURE 145.4.—Peak height and background curve-set, with interpolation curves, for determining weight percent of quartz in silicate matrices containing 0 to 72.4 percent iron.

peak intensities, is roughly compensated by density differences in quartz (2.65) and *total* matrix (basalt 2.97). This is because of the greater volume percent (and hence, greater percent of the surface exposed to radiation) of quartz relative to its weight percent when mixed with a denser material. This density-absorption compensation permits an almost direct comparison of quartz peak intensities regardless of the matrix—except for the effects of iron.

To compensate for the absorption and fluorescence effects of iron when analyzing for quartz, four peak height curves and their corresponding background curves were established from prepared powders of quartz mixed, in order of increasing absorptive strengths, with (a) natural pinite (muscovite), (b) biotite-actinolite greenstone, (c) chlorite, and (d) magnetite; the letters correspond with the curve-sets in figure 145.3. The curves are based on the diffraction intensity of copper radiation from the (100) plane of quartz (Weiskirchner, 1960) and the background intensity in the immediate vicinity of the same line (4.26A or 20.8°2θ) at a scanning speed of 2° 2θ per minute. Slower scanning speeds may be used, but with only slightly better accuracy. Differences in the mass absorption coefficients of matrices have been shown to be chiefly a function of iron content, and iron content is expressed by background intensity. As iron content increases, background intensity increases, and so, too, does

the absorptive strength of the matrix which has the effect of depressing the peak height curve. Using this relationship, the quartz content of a rock-powder can be determined from any combination
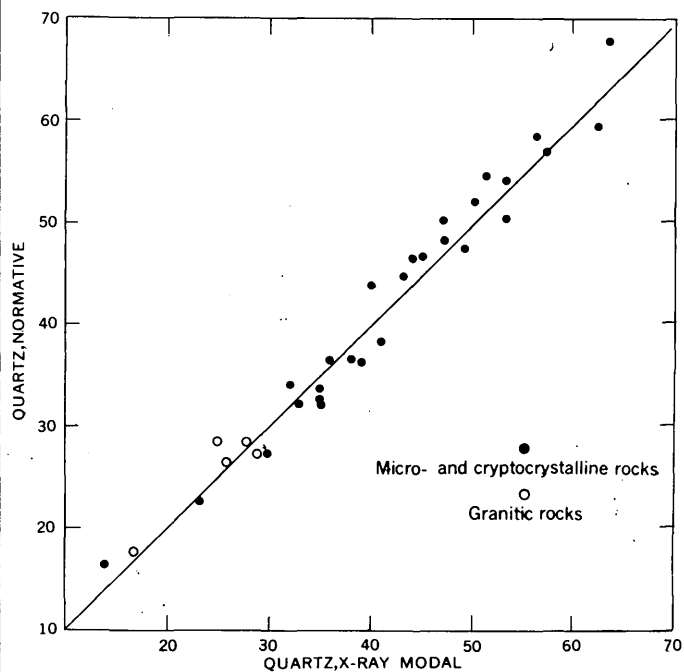
FIGURE 145.5.—Weight percent of quartz determined from diffraction patterns of splits of 32 chemically analyzed samples plotted against normative quartz. Scanning speed: 2°2θ per minute.

of peak height (above background) and background (above base line) by interpolating between established sets of peak height and background curves. The greater the mass absorption coefficient of the matrix (as a function of iron, and expressed by background) the greater the quartz content for a given peak height. For example, in figure 145.3, at a peak height above background of 40, the quartz content of a powder having the absorption characteristics of curve-set (a) would be 35 percent, of curve-set (b) 43 percent, of curve-set (c) 51 percent, and of curve-set (d) 58 percent. This relationship establishes a so-called interpolation curve, the construction of which is illustrated in figure 145.3. A series of interpolation curves is shown in figure 145.4, in conjunction with a peak height and background curve-set. Actually, any one of the sets of curves in figure 145.3 showing peak height and corresponding background intensity could be used in conjunction with the interpolation curves in preparing figure 145.4. To illustrate how the weight percent of quartz is determined from figure 145.4, assume a peak height above background of 50 and a background of 20; both are read in the same units on the ordinate scale. By following the dotted lines, the quartz content for this combination of diffraction and background intensities is shown to be 53 percent.

To substantiate the reliability of the curves established with prepared powder mixtures, the normative quartz values of 5 granitic rocks and 27 metasomatized rhyolitic and andesitic rocks, with iron contents ranging from 0.2 to 6.2 percent, were plotted against quartz determined from diffraction patterns of splits of the chemically analyzed powders (fig. 145.5). The standard deviation of the modal quartz from the normative quartz is 2.2 percent.

Similar curves have been established for determining amounts of feldspar, muscovite, andalusite, pyrophyllite, and chlorite, but in general these are applicable only to rocks of a given type from a given area. Curves for quartz and total iron, however, appear to work well with almost all the common holocrystalline silicate rocks, both fresh and altered, regardless of rock type or source area, and they can be readily established for use with any recent model diffractometer.

REFERENCES

Black, R. H., 1953, Analysis of bauxite exploration samples by X-ray diffraction: Anal. Chemistry, v. 25, p. 743–748.

Carl, H. F., 1947, Quantitative mineral analysis with a recording X-ray diffraction spectrometer: Am. Mineralogist, v. 32, p. 508–517.

Engelhardt, W. von, and Haussühl, S., 1960, Röntgengraphische Phasenanalyse grobcrystalliner Gesteine: Chem. Erde, v. 20, no. 3, p. 155–161.

Klug, H. P., and Alexander, L. E., 1954, X-ray diffraction procedures for polycrystalline and amorphous materials: New York, John Wiley and Sons, 716 p.

Leroux, Jean, Lennox, D. H., and Kay, Kingsley, 1953, Direct quantitative X-ray analysis by diffraction-absorption technique: Anal. Chemistry, v. 25, p. 740–743.

Nockolds, S. R., 1954, Average chemical compositions of some igneous rocks: Geol. Soc. America Bull., v. 65, p. 1007–1032.

Weiskirchner, W., 1960, Untersuchungen zur quantitativen Bestimmung der Phasen mit Hilfe von Röntgenstrahlen: Soc. mineralog. italiana, v. 16, p. 363–378.

146.   THE KOBERG-DAUM WIND-DIRECTION AND WIND-VELOCITY RECORDER

By G. E. KOBERG and C. R. DAUM, Denver, Colo.

The conventional instruments for recording wind direction generally require four event markers or pens to record wind directions to 8 points of the compass, although one type of commercially available recorder has a single pen. Some recorders use electrically controlled event markers which tick at regular intervals of time, and the marker that makes the tick is selected by a switch attached to the wind vane. If wind direction is sampled once each minute, the desirable chart speed to insure legibility of the record is 3 inches per hour.

The Koberg-Daum wind-direction and wind-velocity recorder uses a single pen to record wind direction to 8 points of the compass, and for an 8-inch circular chart a chart speed of one revolution per week generally is suitable. The recorder, including

anemometer, costs about $350 to make, which is much less than the cost of most commercially available instruments. Other advantages are portability and ease of installation. All of these features make this an instrument to be used in preference to the conventional recording system.

The Koberg-Daum recorder has a variable radius cam on the vertical shaft supporting the wind vane, so that the angular position of the cam is controlled by the vane. The variable radius cam is divided into 8 segments, each representing 40 degrees of the compass with 5 degree transition zones between segments. Each segment has a different radius. The transition zone is provided so that a roller pressed against the cam by a spring and held in place by an arm can move from one segment to the next with minimum friction. The variable-radius cam, through a suitable mechanical linkage, positions a stylus on a circular chart so that the distance from the center of the chart indicates the wind direction. The stylus uses an electric arcing system to burn a series of small holes in the surface of the chart paper, thus providing a legible trace. The chart paper is made specifically for this purpose; one side being impregnated with an electrically conducting material. If the wind direction should fluctuate rapidly, for example between southwest and northwest, three directions will be recorded, namely southwest, west, and northwest.

A noteworthy feature of this recorder is that during the transition from one segment to the next, a trace is not recorded because a switching device shuts off the marking device during transition. This feature prevents the recording of an unintelligible trace during periods of rapidly fluctuating wind direction.

The speed of the wind is recorded on the margin of the chart by an ink pen. Individual ticks are usually distinguishable if the event marker is regulated to record every 10 miles of wind.

Koberg-Daum recorders now being used have a spring-wound 8-day clock to turn the circular chart. The torque needed to overcome the friction created by the marking devices on the chart is so slight that very little trouble is experienced from clock stoppage. The drain on the batteries that supply power for the marking device is negligible.

A patent application has been made for the Koberg-Daum recorder, with all rights reserved for the Government.

SUBJECT INDEX

[Numbers refer to articles; finding list of article page numbers follows author index]

A

	Article
Abnormal bedding, sandstone and shale......	49
Age determinations. *See particular method.*	
Alabama, Birmingham area, structural geology	43
Tallapoosa River, hydrology.....................	42
Alaska, Kandik River, paleontology and stratigraphy......................	90
Kuiu Island, paleontology and stratigraphy	101
Nation River, paleontology and stratigraphy	90
Prince of Wales Island, paleontology and stratigraphy	101
Alluvial fans, compaction...................................	77
tectonic significance	75
Alluvium, copper deposits beneath..................	133
heavy-mineral studies	118
Alteration, hydrothermal, clay minerals	91
greisen	92
iron ores...	35
relation to metals in lithosols	58
supergene, iron ores.	35
Alumina, determination of with EDTA.......	142
Alunite, Puerto Rico...................................	91
Analog, electric, of liquid flow...............	28
Andersonite, synthesis	113
Anthozoa, Pennsylvanian, Alaska..	101
Appalachians, fracture systems......	43
Triassic dikes	41
See also specific States.	
Archeology, use in Recent stratigraphy........	81
use of desert varnish in dating..............	80
Arizona, Bisbee quadrangle, stratigraphy..	53
Fort Apache Indian Reservation, soil-moisture studies	98
Pima mining district, geochemical prospecting	133
See also Colorado Plateau.	
Aroostook limestone, age.....................................	.30
Arsenic, in soils..	58
Ash, volcanic. *See Volcanic ash.*	

B

Barite replacement, Foraminifera	94
Basalt, ground-water barriers	88
petrology, Hawaii	89
Beach sands, ground water..............................	85
Belt series, Idaho-Montana..............................	67
Beryllium, in cordierite...................................	109
Bicarbonate, in surface water.........................	84
Bioherms, Mississippian, Kentucky...............	39
Ordovician, Nevada	97
Bliss sandstone, stratigraphic relations......	51
Boggy shale, abnormal bedding......................	49
Borate minerals, Furnace Creek area, California	129
Brachiopoda, Pennsylvanian, Alaska	101
Brazil, Serra de Jacobina, uranium	4
Bremsstrahlung	139

	Article
Brachiopoda, Pennsylvanian, Alaska...........	101
Bulk density, measurement by gamma-ray absorption	134

C

Calcium,	
in limestone	126
in soils	22
in surface water..	84
California, Coast Ranges, stratigraphy	78
Death Valley, climate...............	79
Deep Spring Lake, mineralogy..............	83
Furnace Creek area, mineralogy............	129
Long Valley, geophysical investigations	106
Mojave Desert, structural geology..........	82
paleontology	100
Palo Alto, hydrology 22,	76
Sacramento Valley, stratigraphy............	78
San Francisco Peninsula, hydrology......	84
San Joaquin Valley, geomorphology....	75
hydrology 24–26,	77
Sierra Valley, geophysical investigations	107
southern California batholith, geochemical investigations	108
Canyon Diablo meteorite, analysis...............	112
Carbonatites, radioactive and rare-earth minerals	121
Carboniferous. *See Mississippian; Pennsylvanian.*	
Carbon-14 age determinations, carbonate shells	140
peat	65
Carolina Piedmont, Paleozoic history..........	45
Cation exchange, in soils....................................	22
Catskill formation, unconformity...................	38
Cephalopoda, Pennsylvanian, Alaska............	.101
Chalcopyrite, germanium content...................	110
X-ray diffraction studies..........................	114
Channels. *See Streams.*	
Chinle formation, cross-strata, origin.............	54
Chloride, in surface water.................................	84
Chlorine, in silicic volcanic glass......................	111
Clausthalite, X-ray diffraction studies..........	114
Clay minerals, effect on compaction	77
hydrothermal alterations	91
Olive Hill clay bed, Kentucky.................	120
preferred orientation	116
Climax stock, Nevada, age relations.............	73
Coal, pH of mine water.......................................	37
Coal balls, Kentucky...	95
Coamo formation, ash-flow deposits..............	93
Coffinite, paragenesis	2
Collapse structures, Ogallala formation, New Mexico	52
Spanish Valley, Utah....................................	72
Yellowstone Plateau	104
Colorado, Arkansas Valley, geomorphology and glacial geology......................	56
Badger Wash, hydrology.............................	59
Colorado River, geomorphology..............	60

	Article
Colorado—Continued	
DeBeque, stratigraphy	61
Front Range, mineral deposits.................	1, 2
Gunnison County, paleobotany...............	96
Gunnison River, geomorphology.............	60
Lake City, geomorphology..........................	57
Leadville district, geomorphology and glacial geology	56
paleontology	99
Piceance Creek basin, stratigraphy......	61
Powderhorn district, mineralogy............	21
Prairie Divide, mineral deposits............	1
Red Mountain area, geochemical investigations	58
Roberts Tunnel, engineering geology....	131
Unaweep Canyon, geomorphology........	60
Uravan, mineralogy	125
See also Colorado Plateau.	
Colorado Plateau, geochemical investigations 122,	123
paleobotany	55
stratigraphy	54
See also specific States.	
Colorimetric method, determination of iron in sphalerite	141
Columbia River basalt, barrier reservoirs....	88
Compaction, of aquifers 23, 25,	26
recorder	24
Conductivity bridge, direct-reading...............	29
Copper, deposits beneath alluvium.................	133
in plant ash..	143
in soils	58
Corals, Devonian, Alaska...................................	90
Permian, Colorado	99
Silurian, Alaska	90
Cordierite, beryllium content...........................	109
Cretaceous, Alaska, east-central	90
Arizona, Mural Hill......................................	53
California, Coast Ranges	78
Sacramento Valley	78
Idaho, Clark Fork..	67
Montana, Clark Fork....................................	67
Puerto Rico, east-central.............................	92
eastern	91
north-central	93
Tennessee, Highland Rim............................	40
Utah, Spanish Valley....................................	72
Wyoming, Black Hills...................................	66
Crinoidea, Pennsylvania, Alaska......................	101
Cross-strata, origin	54
Crustal deformation, California, Long Valley	106
Idaho, Snake River Plain	105
Yellowstone National Park	104

D

Depressions, closed...	52
thaw	65
Desert varnish, origin..	80

AUTHOR INDEX

INDEX

FINDING LIST OF ARTICLE PAGE NUMBERS